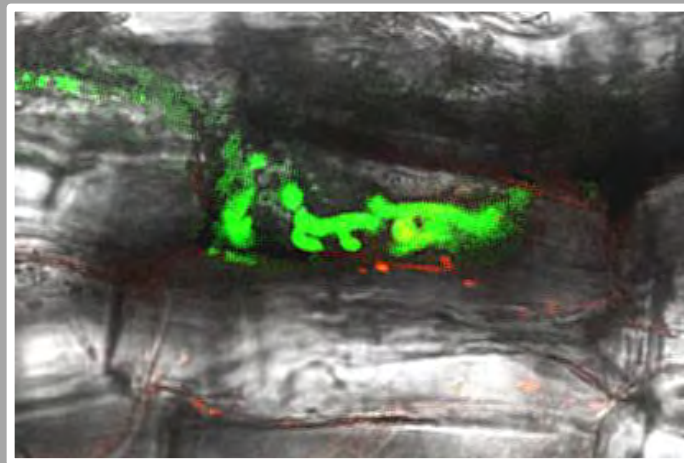


University of Thessaly

Department of Biochemistry & Biotechnology

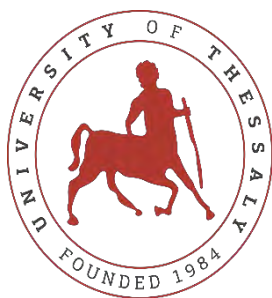
**Colonization of legumes by an endophytic *Fusarium solani* strain K.
Early-stage molecular signaling and sub-cellular responses**



Vasiliki Skiada

PhD Dissertation

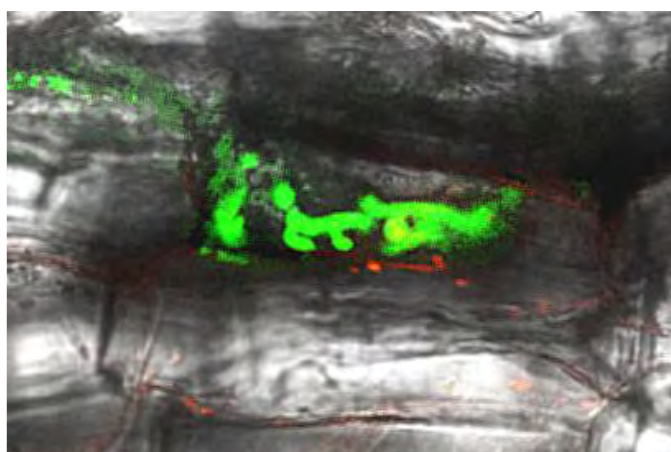
September 2019



Πανεπιστήμιο Θεσσαλίας
Τμήμα Βιοχημείας & Βιοτεχνολογίας

Πρότυπα αποικισμού ψυχανθών από τον ενδοφυτικό μύκητα *Fusarium solani* στέλεχος K.

Μοριακή σηματοδότηση και υπο-κυτταρικές αποκρίσεις στα πρώιμα στάδια της αλληλεπίδρασης



Βασιλική Γ. Σκιαδά
Διδακτορική διατριβή

Σεπτέμβριος 2019



Examination committee (seven members)

Advisory Committee:

Papadopoulou K. Kalliope (University of Thessaly)

Ehaliotis Constantinos (Agricultural University of Athens)

Karpouzas Dimitrios (University of Thessaly)

Examining Committee:

Bonfante Paola (University of Turin)

Ehaliotis Constantinos (Agricultural University of Athens)

Karamanoli Aikaterini (Aristotle University of Thessaloniki)

Karpouzas Dimitrios (University of Thessaly)

Kavroulakis Nektarios (National Agricultural Research Foundation, Crete)

Papadopoulou K. Kalliope (University of Thessaly)

Tsikou Daniela (University of Thessaly)

The present PhD thesis was conducted in the 'Plant and Environmental Biotechnology Laboratory', Department of Biochemistry & Biotechnology, University of Thessaly, Larissa, Greece, under the supervision of Associate Professor Kalliope Papadopoulou.

Part of the thesis was conducted in the 'Plant-Microbe Interactions' and in the 'Advanced Microscopy Laboratory', Department of Life Sciences and Systems Biology, University of Turin, Italy, under the supervision of Professor Paola Bonfante and Associate Professor Andrea Genre, respectively.

The COST Actions FA1206 and FA1405 are acknowledged for the two Short Term Scientific Mission Grants given to Vasiliki Skiada to travel and perform research in the above mentioned laboratories in Italy.

Abstract

Legumes interact with a plethora of microbes in their root system ranging from beneficial symbionts to pathogens. Symbiont recognition initiates at the pre-contact level, with typical symbiotic rhizobial Nod- and the putative glomeromycetes Myc-Factors (LCOs, and mix of COs/LCOs, respectively) identified via LysM-receptor like kinases at the plant cell Plasma Membrane (PM). This triggers a so-called common symbiotic signaling pathway (CSSP), including the induction of nuclear calcium spiking in legume root epidermis. At the post-contact level, legumes colonization by symbionts is well described, with similarities to infestation by pathogenic fungi. On the other hand, plant cellular responses to endophytic fungi are relatively underreported.

The aim of the present work, was to investigate the early stages of interaction of an endophytic fungal isolate, *Fusarium solani* strain K (FsK), with the model legume *Lotus japonicus*, at the molecular and at the cellular level.

Commonalities arose with symbiont recognition at the molecular level, as FsK induced the expression of LysM receptors for chitin-based molecules, CSSP members and CSSP-dependent genes in *L. japonicus*. Activation of defense genes also occurred. In addition, FsK exudates, comprising heat labile, and/or chitinase sensitive molecules, induced nuclear calcium spiking at the epidermis of *M. truncatula* Root Organ Cultures (ROCs) harboringameleon reporters, and this response was proven to be CSSP-dependent. This response was, furthermore, recorded in response to other fungal exudates, derived from mutualistic or pathogenic fungi. Results were complemented by mutant analysis: FsK intraradical progression was stimulated in LysM mutants examined, whereas in CSSP mutants it was dependent on genes acting downstream the Ca²⁺ spiking response (*LjCCaMK*, *LjCYCLOPS*). It was therefore shown through this work that the CSSP is a more common pathway than previously envisaged.

To study the interaction at the cellular level, either *L. japonicus* whole plants or *M. truncatula* ROCs (labelled for specific cellular compartments, thus allowing a more detailed investigation), were employed. Optical, confocal, and TEM microscopy revealed a polarized reorganization of the legume root cell: endoplasmic reticulum and cytoplasm accumulation and nuclear placement at contact sites, occasional development of papillae underneath hyphopodia and membranous material rearrangements towards penetrating hyphae. Cell death was recorded during colonization process, and fungal hyphae were observed within the vascular bundle of the plant. FsK proceeds in the aerial part of the plant, where it grows epiphytically and endophytically. Differentiated round structures, of unknown function, were also recorded in the stem in epidermal/upper cortical cells. It was therefore pointed through this work that the establishment of FsK within legume tissues requires fungal growth adaptations and plant cell-autonomous responses, known to occur during both symbiotic and pathogenic plant-fungal interactions. Unique responses were also observed, worth of additional investigation.

To further gain insight on FsK-*Lotus* interaction, the lifecycle of inoculated plants was followed, and no apparent phenotypic defects or growth promotion traits were recorded in comparison to controls, under the normal conditions examined. Furthermore, the ability of the endophyte to complete its lifecycle in association with its host was examined by measuring conidiation events in the substrate. Propagule formation recorded was independent of the plant, at least up to the last time point examined.

Results at the molecular level, were furthermore complemented with transcriptome profiling of FSK-inoculated *L. japonicus* plants, at early stages of the interaction. A large repertoire of the legume host transcripts is differentially expressed: genes coding for proteins involved in membrane transport, hormonal regulation, lipid metabolism, cell modifications, defense are activated, indicating the molecular and cellular alterations necessary for recognition and accommodation of another eukaryotic organism within the plant cell.

Περίληψη

Ένα μεγάλο εύρος μικροοργανισμών αλληλεπιδρούν με το ριζικό σύστημα των φυτών της οικογένειας των ψυχανθών, συνάπτοντας με αυτά από αμοιβαία επωφελείς έως και παρασιτικές σχέσεις. Τα ψυχανθή αντιλαμβάνονται τους συμβιωτικούς μικροοργανισμούς (ριζόβια, δενδρόμορφοι μυκορριζικοί μύκητες) προτού να έλθουν σε επαφή με αυτούς, μέσω αναγνώρισης της έκκρισης των μικροβιακών παραγόντων Nod, και των μέχρι σήμερα μη αναγνωρισμένων/ μη χαρακτηρισμένων παραγόντων Myc (λιποχιτοολιγοσακχαρίτες, και μίγμα χιτοολιγοσακχαριτών/λιποχιτοολιγοσακχαριτών, αντίστοιχα). Η αναγνώριση πραγματοποιείται στην πλασματική μεμβράνη των ριζικών κυττάρων μέσω των υποδοχέων LysM που φέρουν δραστικότητα κινάσης. Ακολουθώς ενεργοποιείται ένα μονοπάτι σηματοδότησης, γνωστό ως Common Symbiotic Signaling Pathway (CSSP), το οποίο μεταξύ άλλων περιλαμβάνει την επαγωγή ενδοπυρηνικών ταλαντώσεων ασβεστίου στην επιδερμίδα της ρίζας. Ο αποικισμός της ρίζας των ψυχανθών από επωφελείς συμβιώτες είναι καλά μελετημένος, και είναι γνωστό πως παρουσιάζει μια σειρά από ομοιότητες με τα πρότυπα αποικισμού της ρίζας από παθογόνους μικροοργανισμούς. Εντούτοις, ο αποικισμός από ενδοφυτικούς μύκητες, καθώς και οι υποκυττάρειες αλλαγές που αυτός περιλαμβάνει, χρήζουν περαιτέρω μελέτης.

Ο σκοπός της παρούσας εργασίας ήταν η μελέτη των πρώιμων σταδίων της αλληλεπίδρασης ενός ενδοφυτικού μυκητιακού στελέχους, του *Fusarium solani* στέλεχος K (FsK), με το φυτό μοντέλο *Lotus japonicus*, τόσο σε μοριακό όσο και σε κυτταρικό επίπεδο.

Όσον αφορά στους μοριακούς μηχανισμούς αναγνώρισης του ενδόφυτου από το φυτό, παρατηρήθηκαν ομοιότητες με τους καλά μελετημένους μηχανισμούς αναγνώρισης των συμβιωτικών μικροοργανισμών από τα ψυχανθή. Πιο συγκεκριμένα, ο FsK επήγαγε την έκφραση των LysM υποδοχέων που αναγνωρίζουν μόρια με σκελετό χιτίνης, καθώς και την έκφραση γονιδίων που ανήκουν στο CSSP, και γονιδίων που εξαρτώνται από- και δρουν κατάντη του CSSP. Επιπλέον, ο μύκητας επήγαγε την έκφραση γονιδίων που σχετίζονται με την άμυνα του φυτού. Προχωρώντας ένα βήμα παραπέρα, αποδείχθηκε πως εξωκυτταρικές ενώσεις του FsK, οι οποίες αποτελούνται τόσο από θερμοευαίσθητα όσο και από μόρια επιρρεπή στη δράση χιτinasών, φέρουν την ικανότητα επαγωγής ταλαντώσεων ασβεστίου εντός του πυρήνα των επιδερμικών κυττάρων ριζικών οργάνων *M. truncatula*, σημασμένων με το μοριακό δείκτη *cameleon*. Για την επαγωγή τέτοιων ταλαντώσεων ασβεστίου, είναι γνωστό ότι ένα λειτουργικό μονοπάτι σηματοδότησης CSSP είναι απαραίτητο. Η απόκριση αυτή των επιδερμικών κυττάρων παρατηρείται όχι μόνο έπειτα από διέγερση αυτών με εξωκυτταρικές ενώσεις του FsK, αλλά και έπειτα από διέγερση με μια σειρά άλλων εκκριμάτων, προερχόμενα από μύκητες που συνάπτουν είτε σχέσεις αμοιβαιότητας είτε σχέσεις παθογένειας.

Η ανάλυση μιας σειράς μεταλλαγμένων φυτών *L. japonicus* οδήγησε στη συμπλήρωση των παραπάνω αποτελεσμάτων. Πιο συγκεκριμένα, καταγράφηκε προχωρημένος ενδορριζικός αποικισμός από τον FsK σε μεταλλάγματα γονιδίων που κωδικοποιούν για ορισμένους υποδοχείς LysM, ενώ περιορισμένος αποικισμός σημειώθηκε σε μεταλλάγματα γονιδίων που δρουν κατάντη των ενδοπυρηνικών ταλαντώσεων ασβεστίου (*LjCCaMK*, *LjCYCLOPS*). Είναι εμφανές, λοιπόν, με βάση τα παραπάνω αποτελέσματα, πως μέσω του μονοπατιού σηματοδότησης CSSP αναγνωρίζονται από το φυτό και άλλοι μικροοργανισμοί πλην των συμβιωτικών ριζοβίων και δενδρόμορφων μυκορριζικών μυκήτων.

Προκειμένου να μελετηθεί η αλληλεπίδραση φυτού-μύκητα εντός του φυτικού κυττάρου, χρησιμοποιήθηκαν είτε ολόκληρα φυτά *L. japonicus* είτε καλλιέργειες ριζικών οργάνων *M. truncatula* που είναι σημασμένα για συγκεκριμένα οργανίδια, επιτρέποντας έτσι λεπτομερείς παρατηρήσεις σε υποκυτταρικό επίπεδο. Μια πολωμένη αναδιοργάνωση του κυττάρου της ρίζας καταγράφηκε με τη χρήση οπτικού, συνεστιακού, ηλεκτρονικού μικροσκοπίου διέλευσης. Παρατηρήθηκε συσσώρευση ενδοπλασματικού δικτύου και κυτοπλάσματος, πυρηνική μετατόπιση στα σημεία επαφής του μύκητα στο κύτταρο, εκάστοτε ανάπτυξη θηλής (προεκβολής) στο εσωτερικό τμήμα του φυτικού κυττάρου, ακριβώς κάτω από το σημείο επαφής με υποπόδια, καθώς και μετακινήσεις μεμβρανικών υλικών προς το σημείο διάτρησης του κυττάρου από τις διερχόμενες υφές. Επίσης σημειώθηκαν φαινόμενα κυτταρικού θανάτου στο φυτό-ξενιστή, ενώ υφές παρατηρήθηκαν και εντός του αγωγού συστήματος της ρίζας. Ο FsK μετακινήθηκε προς το υπέργειο τμήμα του φυτού, στο οποίο μάλιστα αναπτύχθηκε τόσο επιφυτικά όσο και ενδοφυτικά. Σε τομές του βλαστού πλησίον της βάσης της ρίζας, εντός επιδερμικών / κυττάρων του άνω φλοιού, καταγράφηκαν διαφοροποιημένες δομές στρόγγυλου σχήματος μυκητιακής προέλευσης. Συμπερασματικά, η εγκαθίδρυση του FsK στους ιστούς των ψυχανθών, απαιτεί μια σειρά αλλαγών που αφορούν προσαρμογές στην ανάπτυξη του μύκητα αλλά και αυτόνομες αποκρίσεις των φυτικών κυττάρων. Οι περισσότερες από αυτές τις αλλαγές έχουν περιγραφεί τόσο για συμβιωτικές όσο και για σχέσεις παθογένειας μεταξύ φυτών και μικροοργανισμών. Διακριτές αλλαγές, όμως, επίσης λαμβάνουν χώρα και είναι άξιες περαιτέρω διερεύνησης.

Μελετήθηκε επίσης ο κύκλος ζωής των εμβολιασμένων με μύκητα φυτών, προκειμένου να αποκτηθεί μια πληρέστερη εικόνα της σχέσης FsK-*Lotus*. Διαφαίνεται πως η ανάπτυξη του μύκητα εντός του φυτού δεν είναι ούτε επιβαρυντική αλλά ούτε και ευεγερτική, κάτω από φυσιολογικές συνθήκες ανάπτυξης και δίχως εφαρμογή καταπόνησης. Επιπρόσθετα διερευνήθηκε η ικανότητα του ενδόφυτου να ολοκληρώσει τον κύκλο ζωής του σε συνάρτηση με το φυτό-ξενιστή, μέσω παρακολούθησης της ικανότητάς του για κονιδιογένεση στη ριζόσφαιρα. Τουλάχιστον ως και το τελευταίο χρονικό σημείο του πειράματος, η ικανότητα του μύκητα να δημιουργεί νέες μονάδες πολλαπλασιασμού ήταν ανεξάρτητη της παρουσίας του φυτού.

Τέλος, όλα τα παραπάνω αποτελέσματα συμπληρώθηκαν με τη μελέτη του μεταγραφικού προφίλ των εμβολιασμένων με FsK φυτών, στα πρώιμα στάδια της αλληλεπίδρασης. Ένας μεγάλος αριθμός μεταγραφημάτων εντοπίστηκε ως διαφορεικά εκφραζόμενος, συμπεριλαμβανομένων γονιδίων που κωδικοποιούν πρωτεΐνες που εμπλέκονται στη (δια)μεμβρανική μεταφορά, στην ορμονική ρύθμιση, στο μεταβολισμό λιπιδίων, σε κυτταρικές τροποποιήσεις, στην άμυνα· καταδεικνύοντας τις μοριακές και κυτταρικές αλλαγές που απαιτούνται από το φυτό για την αναγνώριση και φιλοξενία ενός άλλου ευκαρυωτικού οργανισμού εντός των κυττάρων του

Abbreviations

Abbreviations

AM, Arbuscular Mycorrhizal
AU, airy units
CA, cytoplasmic aggregation
CB, chlorazol black
CFUs, colony forming units
CLSM, Confocal Laser Scanning Microscopy
CO5, pentameric chito-oligosaccharide
CSSP, Common Symbiosis Signalling Pathway
CWAs, cell wall appositions
DE, differential expression
DEGs, differentially expressed genes
dpi, days post inoculation
ER, endoplasmic reticulum
Fom, *Fusarium oxysporum* f. sp. *medicaginis*
FsK, *Fusarium solani* strain K
FsK, *Fusarium solani* strain K
FSSC, *Fusarium solani* species complex
GFP, green fluorescent protein
IT, infection thread
LCOs, lipo-chitooligosaccharides
Lj, *Lotus japonicus*
LyM, Lysin-motif
Mt, *Medicago truncatula*
MVBS, multi-vesicular bodies
Mya, Million years ago
NF, Nod Factor
PI, propidium iodide
PM, Plasma Membrane
PM, plasma membrane
PPA, prepenetration apparatus
RLK, receptor-like kinase
RLS, rhizobium-legume symbiosis
ROCs, root organ cultures
ROCs, Root Organ Cultures
ROI, region of interest
TB, trypan blue
TEM, transmission electron microscopy
wt, wild-type

Table of Contents

1	Introduction	14
1.1	Legumes.....	14
1.1.1	The family of legumes	14
1.2	Symbiotic interactions of legumes.....	17
1.2.1	The Legume Rhizobium Symbiosis (LR symbiosis)	17
1.2.2	The Arbuscular Mycorrhizal Symbiosis (AM symbiosis)	19
1.3	Interactions of fungi with plants.....	19
1.3.1	Mycorrhizal associations	19
1.3.2	Endophytes	23
1.3.3	Parasites	26
1.4	The genus <i>Fusarium</i>	27
1.4.1	The <i>Fusarium solani</i> species complex (FSSC).....	29
1.5	Signaling in recognition and accommodation of PMIs	31
1.5.1	Pattern Recognition Receptors (PRRs)	31
1.5.2	Perception of N-acetyl-glucosamine derivatives	32
1.5.3	The role of LysM receptors	33
1.5.4	Other symbiotic signals	35
1.5.5	The Common Symbiosis Signaling Pathway (CSSP)	35
1.5.6	Genes downstream the CSSP	37
1.6	Calcium, a versatile secondary messenger	38
1.6.1	Role of calcium oscillations in biotic interactions of plants	39
1.7	Commonalities in PMIs	41
1.7.1	Cellular level.....	41
1.7.2	Molecular level	43
1.8	Legume mutants as a useful tool to investigate PMIs	44
1.9	References	47
2	Assessing the impact of different nutrient sources and abiotic factors on growth and reproduction of <i>Fusarium solani</i> strain K.....	61
2.1	Introduction.....	61
2.1.1	Physiology of filamentous fungi	61
2.1.2	Nutrient uptake/assimilation	63
2.1.3	Elements required for fungal growth	65
2.1.4	Other major nutrients	68

Contents

2.1.5	Abiotic (environmental factors) influencing fungal physiology	71
2.1.6	Factors influencing sporulation	73
2.2	Materials and methods	75
2.2.1	Fungal material	75
2.2.2	Effect of different temperatures on FsK mycelium growth	75
2.2.3	Effect of pH adjustment on FsK conidia production and mycelium dry weight	75
2.2.4	Effect of growth medium composition on FsK mycelium growth	76
2.2.5	Effect of different carbon sources on FsK conidia production and mycelium dry weight	77
2.2.6	Effect of different nitrogen sources on FsK conidia production and mycelium dry weight	77
2.2.7	Statistical analysis	78
2.3	Results	79
2.3.1	Effect of temperature on FsK mycelial colony growth	79
2.3.2	Effect of pH values on FsK sporulation and mycelial growth	80
2.3.3	Effect of different media on FsK mycelial growth	82
2.3.4	Effect of various carbon sources on FsK sporulation and mycelial growth	84
2.3.5	Effect of various nitrogen sources on FsK sporulation and mycelial growth	86
2.4	Discussion	89
2.5	References	94
2.6	Appendix of Chapter 2: Statistical analysis	98
2.6.1	Effect of temperature on FsK mycelial growth	98
2.6.2	Effect of different growth media on FsK mycelial growth	98
2.6.3	Effect of different carbon sources in FsK conidia production	99
2.6.4	Effect of different carbons sources in FsK mycelium dry weight	99
2.6.5	Effect of different nitrogen sources in FsK conidia production	100
2.6.6	Effect of different nitrogen sources in FsK mycelium dry weight	101
3	Colonization of legumes by an endophytic <i>Fusarium solani</i> strain K reveals common features to symbionts or pathogens	103
3.1	Introduction	104
3.2	Materials and methods	106
3.2.1	Plant and fungal material	106
3.2.2	<i>Agrobacterium tumefaciens</i> mediated transformation of FsK	106
3.2.3	Quantification of fungal colonization by qPCR	107
3.2.4	Monitoring the life cycle of <i>L. japonicus</i> during its interaction with FsK	107
3.2.5	Monitoring of asexual structures formation (conidiation) in the rhizosphere	108
3.2.6	<i>Lotus japonicus</i> root inoculation with FsK for microscopy	109
3.2.7	<i>Medicago truncatula</i> ROCs inoculation with FsK for microscopy	109

Contents

3.2.8	Confocal microscopy	109
3.2.9	Electron microscopy	110
3.2.10	Light microscopy	111
3.3	Results	112
3.3.1	FsK colonizes <i>L. japonicus</i> without adversely affecting its growth	112
3.3.2	FsK progressively colonizes <i>L. japonicus</i> root system and subsequently migrates to the stem	113
3.3.3	FsK exhibits plasticity in its colonization mode of <i>L. japonicus</i> root tissues	114
3.3.4	Membrane dynamics at penetration sites	116
3.3.5	FsK colonizes the root system of <i>Medicago truncatula</i> and promotes distinct sub-cellular responses	118
3.3.6	Ultrastructural evidence for membrane trafficking and defence activation during the fungal penetration attempts	122
3.4	Discussion	125
3.4.1	FsK exhibits plasticity upon engagement with legumes	127
3.4.2	Assigning common sub-cellular responses to plant-fungal interactions	129
3.4.3	Conclusions.....	130
3.5	References	132
3.6	Appendix of Chapter 3	137
3.6.1	Supplementary material	137
4	Symbiotic signaling is at the core of an endophytic <i>Fusarium solani</i> -legume association	147
4.1	Introduction.....	148
4.2	Materials and methods.....	150
4.2.1	Plant materials	150
4.2.2	Fungal materials.....	150
4.2.3	Experimental setup for gene expression analysis and phenotypic screening of <i>L. japonicus</i> mutants	150
4.2.4	DNA isolation	151
4.2.5	RNA isolation	151
4.2.6	Gene expression analysis.....	151
4.2.7	Quantification of fungal colonization in <i>L. japonicus</i> wt, CSSP, <i>LysM</i> mutant lines .	152
4.2.8	Preparation of fungal exudates and root treatment	152
4.2.9	Assays performed on fungal exudates and COs	152
4.2.10	Confocal microscopy for calcium spiking measurements in <i>M. truncatula</i> ROC epidermis.....	153
4.2.11	Statistical analysis.....	153
4.3	Results	154

4.3.1	FsK inoculation affects the expression of CSSP members and CSSP-regulated genes	154
4.3.2	FsK colonization is reduced in CSSP mutants compared to wt plants	154
4.3.3	Fungal exudates trigger nuclear calcium spiking in wt <i>M. truncatula</i> ROC epidermis	155
4.3.4	Nuclear calcium spiking is abolished in <i>Mtdmi2-2</i> but not in <i>Mtdmi3-1</i> epidermis ...	159
4.3.5	The biological activity of <i>Fusarium</i> exudates is affected by chitinase and heat treatment	160
4.3.6	Reaching the pathway backwards: involvement of LysM-RLKs in <i>Lotus japonicus</i> response	161
4.4	Discussion	163
4.4.1	Intraradical accommodation of an endophytic fungus is controlled by multiple LysM receptors	163
4.4.2	A very common symbiosis signaling pathway	163
4.4.3	Conclusion	167
4.5	References	168
4.6	Appendix of Chapter 4	176
4.6.1	Supplementary material	176
5	Activation of chitin-induced, defense genes in <i>L. japonicus</i> -FsK interaction.....	188
5.1	Introduction.....	188
5.2	Materials and methods.....	189
5.2.1	Plant materials	189
5.2.2	Experimental setup for gene expression analysis	189
5.2.3	Statistical analysis.....	189
5.3	Results	190
5.4	Discussion	192
5.5	References	193
5.6	Appendix of Chapter 5	195
6	Differential expression analysis of <i>Lotus japonicus</i> genes at early stages of <i>Lotus</i> -FsK interaction using an RNA sequencing approach	197
6.1	Introduction.....	197
6.1.1	Background on transcriptomics analysis	197
6.1.2	RNA sequencing technology and benefits	199
6.1.3	Main steps in an RNA sequencing experiment.....	201
6.1.4	RNA seq data analysis (pipeline for DE analysis)	202
6.1.5	Packages used for analysis of RNA sequencing data	204
6.1.6	Applications of RNA seq technology.....	206

Contents

6.1.7	Gene expression analysis and RNA sequencing techniques application in studying PMIs	207
6.2	Materials and methods	211
6.2.1	Plant and fungal material	211
6.2.2	Experimental setup and sample collection for RNA sequencing analysis.	211
6.2.3	RNA isolation	212
6.2.4	Library construction and Illumina sequencing.....	212
6.2.5	Mapping of sequenced reads, assessment of gene expression and differential gene expression analysis.....	212
6.2.6	Gene annotation.....	212
6.3	Results and discussion	214
6.3.1	Input data and preparations	214
6.3.2	Data exploration and quality assessment	214
6.4	References	282
6.5	Appendix of Chapter 6	286
7	Concluding remarks.....	288
7.1	References	294
	Acknowledgments	295

Chapter 1

Introduction

1 Introduction

1.1 Legumes

1.1.1 The family of legumes

Legumes are defined by their unusual flower structure, podded fruit, and the ability of 88% of species examined to date to form nodules with nitrogen fixing soil bacteria, known as rhizobia (Graham and Vance, 2003). The family of legumes (Leguminosae or Fabaceae) consists of approximately 700 genera and 18000 species and is the third largest family of Angiosperms, after Orchids and Compositae (daisies). This plant family comprises of three subfamilies, *Papilionoideae*, *Caesalpinioideae*, and *Mimosoideae* (Stougaard, 2013). Common legume plant species include alfalfa (*Medicago sativa*), common bean (*Phaseolus vulgaris*), pea (*Pisum sativum*), soybean (*Glycine max*), peanut (*Arachis hypogaea*), lentil (*Lens culinaris* Med), chickpea (*Cicer arietinum*). Most are important crop plants, mainly cultivated for their high in protein and oil content seeds. Other species are cultivated as ornamentals, vegetables, pulses, and pasture crops, or for production of protein, oil, and pharmaceuticals. Their seeds contain 20 to 30% protein and are lysine (Lys) rich, therefore complementing the nutritional profiles of cereals and tubers in the diet. Legumes are on the other hand poor in sulfur amino acids (Graham and Vance, 2003). They provide essential minerals required by humans, produce health promoting secondary metabolites (isoflavones) that can protect against human cancers and lower cholesterol, but also protect the plant against pathogens and pests. Legumes are included in the diet of insulin-dependent diabetics (Gepts et al., 2005).

As mentioned above, most legumes develop root nodules in symbiosis with rhizobia. Specific rhizobia species develop associations with certain legume species, consisting the legume-rhizobia interaction selective. The hallmark of legumes is that nodulated plants can use atmospheric dinitrogen as their sole nitrogen source (Stougaard, 2013). Nitrogen is the key element to protein-rich seed/forage and rhizobial symbiosis. The nitrogen-rich life style of legumes can at least partially explain the success and diversity of this important crop family (Gepts et al., 2005). Their symbiotic abilities play an important role in colonization of disturbed ecosystems, including those that are fire prone (Graham and Vance, 2003). Only a small group of plants limited to four orders (Fagales, Fabales, Rosales and Cucurbitales) are able to form nitrogen-fixing root nodule symbiosis in association with soil bacteria. This group comprises most legume species and a few species of *Parasponia* (Cannabaceae) able to interact with Gram-negative proteobacteria, collectively called rhizobia; and actinorhizal plants able to interact with Gram-positive filamentous actinobacteria *Frankia*. Phylogenetic analysis places all plants involved in rhizobial or actinorhizal symbiosis in the same clade (Fabid) (Svistonoff et al., 2013)

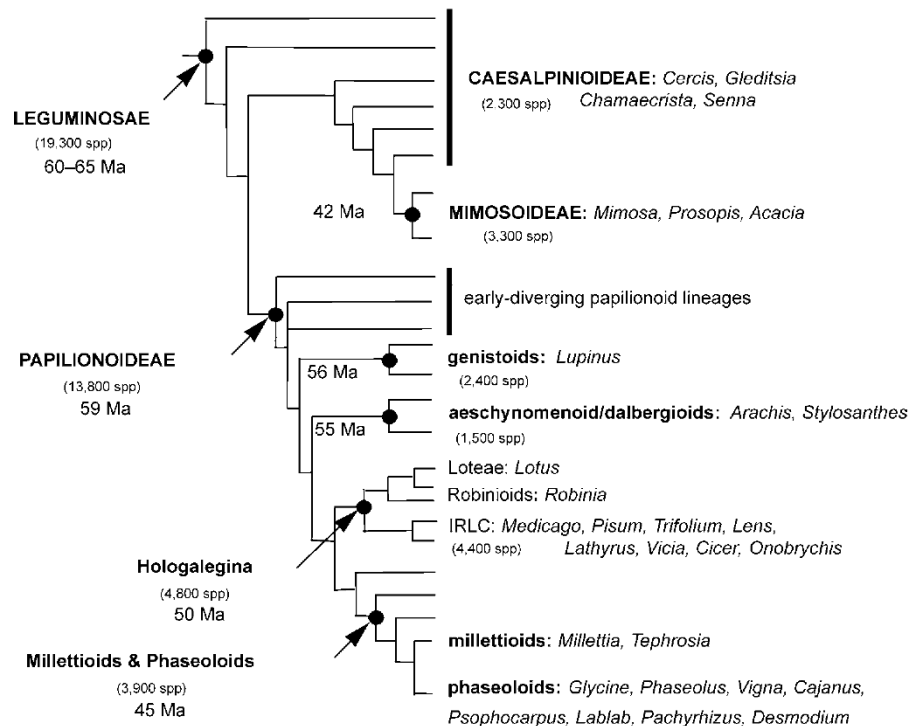


Figure 1-1 Schematic tree of legume family. The 3 subfamilies (*Caesalpinioideae*, *Mimosoideae*, *Papilionoideae*) are shown in capital bold letters. Both *Lotus* and *Medicago* genera belong to *Papilionoideae* subfamily. From (Gepts et al., 2005)

Symbiotic N fixation mediated by legume plants is of great importance, not only because it acts as a source of protein N in the diet, but also due to the economic impact in agriculture: N from legume fixation is “free” N for use by the host plant or by associated or subsequent crops. The fertilizer N used instead, is not only expensive, but also frequently unavailable to farmers (Graham and Vance, 2003).

Research has focused over the years on development of resources and information for two model legume species *Medicago truncatula* and *Lotus japonicus*, and soybean, a legume of great economic importance. In comparison with other families with model species, legumes are a large family: Gramineae have ~10000 species, and Brassicaceae ~3500 (Gepts et al., 2005).

1.1.1.1 The model legume *Lotus japonicus*

Lotus japonicus is a model plant of the legume family. It originates from East Asia and the species is distributed over the Japanese islands, the Korean Peninsula, east and central parts of China, and there are also reports from northern India, Pakistan and Afghanistan. Two ecotypes, Gifu and Miyakojima (MG-20), have been chosen for model studies. *L. japonicus* is a close relative of the tetraploid ($2n=24$) herbaceous perennial legume *Lotus corniculatus* (birds foot trefoil). Phylogenetically, it belongs to the largest subfamily of legumes, the *Papilionoideae* (tribe *Loteae*).

Concerning its morphological characteristics, *L. japonicus* is a small, perennial, self-fertile plant. The best conditions for its cultivation are temperatures between 18–22 °C, and humidity 70% in order to avoid seedpod dehiscence (spontaneous opening at maturity). *Lotus* grows slowly the first weeks after

germination, but the mature plant has a bushy growth with many branches and leaves. The mature plant shows indeterminate flowering, with yellow flowers usually arranged in pairs. The plant has a small size and a short life cycle of ca. three months. Fertilization and seed set occur without manipulation of the flowers. Pod formation in fertilized flowers occurs within 3-4 days. Pods are straight, cylindrical and contain up to 20 seeds. The plant is therefore characterized by a large seed set, and mature seed weight is ~ 1.0-1.2 mg. Hand pollination can be achieved relatively easy on *Lotus* plants. Vegetative propagation can also easily occur from nodal cuttings with a rooting frequency of 90%, even in the absence of hormones. As far as its genome characteristics are concerned, it is a diploid ($2n=12$), with a relatively small genome size (ca. 450 Mb). It is amenable to efficient plant transformation with *A. tumefaciens* and *A. rhizogenes*, leading to regeneration of transgenic plants (Pajuelo and Stougaard, 2005).

L. japonicus develops effective symbiotic association with the fast growing *Mesorhizobium loti* and *Rhizobium* sp. NGR 234, which have a broad host range. Symbiotic association leads to formation of determinate root nodules. Slow growing *Bradyrhizobium* sp. also nodulate *L. japonicus*, but nodules formed are ineffective. *Rhizobium etli* also nodulates *Lotus*, but nitrogen fixation in nodules is poor and nodules senesce rapidly. The plant species develops association with the ancient symbiotic Arbuscular Mycorrhizal (AM) fungi (Pajuelo and Stougaard, 2005) (Stougaard, 2013).

The whole genome structure and the annotated sequence of *L. japonicus* was first presented by (Sato et al., 2008). (Mun et al., 2016) presented 'Lotus base', a web-based database that hosts the two latest versions of *L. japonicus* genome assembly, v 2.5 and v 3.0. Both versions of the genome comprise 6 chromosomes and a single artificial chromosome 0 containing unassembled contigs¹.

1.1.1.2 The model legume *Medicago truncatula*

M. truncatula Gaertner (common name barrel medic) is a plant of Mediterranean origin, well adapted to semi-arid conditions. As *L. japonicus*, it belongs to the subfamily Papilionoideae of the legume family. There are several reported ecotypes of *M. truncatula*, including Jemalong, Cyprus, R108, and Ghor. It is a close relative to an important forage legume, the tetraploid *M. sativa* (common name alfalfa), and has been chosen together with *L. japonicus* as a model legume species due to its small, diploid genome, short generation time, self-fertility and high transformation efficiency (Barker et al., 1990) (Bell et al., 2001). It is an annual, autogamous (self-fertile) species. It is an opportunistic plant, which has become naturalized in other regions of the world following European migrations. The optimal temperature for *M. truncatula* cv. Jemalong germination is 20 °C. The plant demonstrates an indeterminate pattern of development: it can simultaneously produce vegetative and reproductive organs. Its leaves are trifoliate. It bears small inflorescences, bearing 1 to 5 yellow flowers. As an autogamous plant, it sets seeds efficiently in the absence of insect pollination. Its seeds have morphological features typical of dicotyledons, and are born in a spine-covered spiral pod. The pod provides protection during seed development, it is a source of nutrients, and possibly contributes to maintenance of dormancy. Its life cycle is short, lasting approximately three months. (Moreau, 2006) (Gallardo et al., 2006).

¹ Contig: a group of clones representing overlapping regions of the genome. A set of overlapping DNA segments that together represent a consensus DNA region.

As a legume, it establishes symbiotic relationships with nitrogen fixing rhizobia. *M. truncatula* cv. Jemalong is efficiently nodulated by the strain *R. meliloti* 2011, leading to formation of indeterminate root nodules. *M. truncatula* is also colonized by beneficial AM fungi (Bell et al., 2001).

The plant is easily transformed with *A. tumefaciens* and *A. rhizogenes*, leading to regeneration of transgenic plants. It is a diploid ($2n=16$), and, as *L. japonicus*, its genome size is ~ 500 Mb. Its genome has been sequenced (Young et al., 2011) (Sato et al., 2008).

1.2 Symbiotic interactions of legumes

The term symbiosis was first introduced by (De Bary, 1879) and can be defined as: the stable association between two or more distinct organisms, at least for a fraction of their lifestyle (Rai and Agarkar, 2014). As mentioned above, legumes establish two types of symbiosis, the Arbuscular Mycorrhizal, and the Legume Rhizobium (LR) symbiosis. AM symbiosis originated ~400 Million years ago (Mya); LRS is more recent, it dates back ~60-65 Mya. It has been postulated that the latter originated from the former. In the following section I present the main features of the LR symbiosis. Despite the fact that legumes engage with AM fungi as well, this endosymbiosis is presented in the section 1.3.1.2 of the present chapter due to the fact that it is not a sole feature of legumes, on the contrary most land plants engage into this type of symbiosis.

1.2.1 The Legume Rhizobium Symbiosis (LR symbiosis)

There are no eukaryotic enzymes able to break the triple bond of N_2 . The reduction of N_2 to NH_3 (nitrogen fixation) is limited to prokaryotes and is catalyzed by nitrogenase enzyme. Nitrogenase activity is responsible for most of the nitrogen that enters the biosphere. In this respect, plants that associate with nitrogen-fixing bacteria have a selective advantage under nitrogen limiting conditions (Downie, 2014). Legumes are among the plants that enter into symbiosis with N_2 -fixing rhizobia. This symbiosis is one of the best studied plant-microorganism interactions. Rhizobia are oligotrophic Alpha- or Betaproteobacteria, and are common members of the community in most soils, regardless of the presence of a legume plant. After establishment of the symbiosis, both partners receive benefits, and therefore the association is mutualistic: plants provide carbon and energy in the form of dicarboxylic acids to the bacteria, and in return, bacteria secrete ammonia, which the plant uses to synthesize amino acids. As mentioned above, the interaction is selective: most rhizobia have a narrow host range. A few rhizobia though have a quite broad host range, like the case of *Sinorhizobium fredii* NGR234, which infects 112 genera (Poole et al., 2018).

Nodulation and nitrogen fixation is controlled by the host plant. Successful symbiosis is established after bacterial entrapment within nodules. There, rhizobia produce NH_3 , but they cannot use it for growth because they inactivate their glutamine synthase, the primary enzyme for ammonia assimilation (Downie, 2014). On the other hand, rhizobia possess a series of genes in their chromosomes or plasmids that are important for endosymbiosis: *nod* genes encode for proteins involved in lipochitooligosaccharide (LCO) signaling to stimulate nodule formation; *nif* genes encode proteins essential for N_2 fixation; *fix* genes encode proteins specifically required by rhizobia for N_2 fixation.

The main steps of nodulation/rhizobial infection can be described as follows:

- Plants release flavonoids that induce *nod* genes in rhizobia. Rhizobia synthesize and secrete LCOs, also known as Nod Factors (NFs).
- Rhizobia attach to root hairs, root hairs curl and entrap rhizobia, leading to formation of an infection pocket.
- Bacteria secrete a cellulase that creates a hole in the root hair. Rhizobia enter through this hole into the root hair and proceed along a plant derived infection tube, the so called infection thread (IT), that separates them from the plant cell. Bacteria therefore remain in the extracellular space. Besides infection through root hairs, infection through epidermal cracks is also possible.
- Concomitantly, nodule meristem development initiates in the plant cortex. The nodule meristem contains dividing cells.
- As the nodule develops, the ITs branch and carry rhizobia into the developing nodule.
- Bacteria are released and are engulfed by nodule cells in a process involving endocytosis. Bacteria, therefore, enter the cytoplasm of nodule cells.
- In the nodule cells, bacteria differentiate into bacteroids, the N_2 -fixing form of rhizobia.
- Bacteroids, together with bacterial and plant-derived membranes, form the symbiosome (Oldroyd et al., 2011) (Poole et al., 2018).

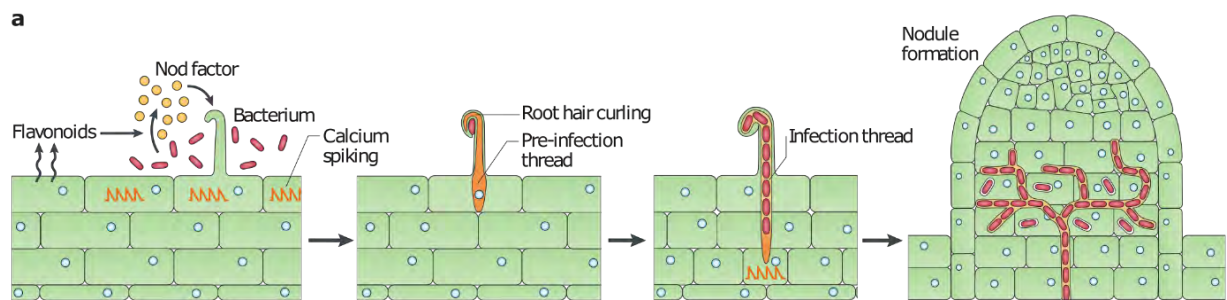


Figure 1-2 Main steps in rhizobial colonization. From (Oldroyd, 2013).

In the nodule, low oxygen concentration allows nitrogenase to reduce N_2 to ammonia. There are two types of nodules: a) determinate nodules, developed in beans, soybeans and *L. japonicus*, b) indeterminate nodules, developed in *M. truncatula*, alfalfa, peas. In the first type, the meristem dies, and all cells senesce while being at the same developmental stage. Nodules grow larger by cell expansion; each cell contains several bacteroids enclosed by a single symbiosome membrane. In the indeterminate type of nodules, the meristem persists, and this leads to development of zones in nodules. Usually symbiosomes contain a single bacteroid in indeterminate nodules. 4 distinct zones are observed: zone I contains the nodule meristem; zone II contains ITs full of bacteria, so infection and differentiation occurs in this zone; in the interface between zone II and III, bacteria are released from ITs and engulfed by plant cells; zone III contains the mature N_2 -fixing bacteroids; in zone IV bacteroids senesce (Poole et al., 2018).

Behind the cellular modifications occurring during legume-rhizobial symbiosis, lies a tight and coordinated regulation of nodulation and successful establishment of endosymbiosis at the molecular

level. Gene expression coupled with hormonal signaling are involved in the process. Molecular signaling involved in Root Nodule Symbiosis is described later in the present Chapter.

1.2.2 The Arbuscular Mycorrhizal Symbiosis (AM symbiosis)

Arbuscular mycorrhizas represent a unique interaction between two eukaryotes – an obligate biotrophic fungus and its host plant – leading to a bilateral improvement of the fitness of both interacting partners. AM fungi belong to the phylum Glomeromycota. These fungi have coevolved with plants for the last 400 million years, and it is believed to have aided the transition of plants to the dry lands, and colonization of the harsh terrestrial environment by higher plants (Bonfante and Genre, 2008). For more information, refer to section 1.3.1.2 of the present chapter.

1.3 Interactions of fungi with plants

1.3.1 Mycorrhizal associations

Mycorrhizal fungi can be divided in two major groups: aseptate² endophytes such as Glomeromycota, or septate Asco- and Basidiomycota. Mycorrhiza classifications can also reflect anatomical aspects and two broad categories can be identified: ectomycorrhizas (EMs) and endomycorrhizas, depending on whether the fungus colonizes the root intercellular spaces or develops inside cells. Endomycorrhizas are further divided into orchid, ericoid, and arbuscular mycorrhizas (Bonfante and Genre, 2010).

1.3.1.1 Ectomycorrhizae (ECM)

ECM fungi are mainly Basidiomycetes and to a lesser extent Ascomycetes that interact with trees of the families Pinaceae, Fagaceae, Dipterocarpaceae, and Caesalpinoidaceae which are found in many forests. These fungi contribute to tree nutrition via mineral weathering and mobilization of nutrients from organic complexes. Through them, carbon is delivered to the soil and contribute to forest soil carbon fluxes (Anderson and Cairney, 2007). These fungi colonize the roots of these trees by creating a sheath: a fungal mantle covers the root tip, and intercellular hyphae surround the epidermal and outer cortical cells by creating a so called Hartig net. EM fungi are also free-living fungi; they can grow in the absence of a plant host. They have a dual lifestyle: they live as symbionts with plant roots and as facultative saprotrophs in soil (Bonfante and Genre, 2010). The plant-fungus interface formed by the Hartig net in the ECM root, is critical to the mutualism, as across this interface nutrients and carbon are transferred between the two partners. ECM fungi produce also mycelia that extent from the mantle into the surrounding soil. These soil extending mycelia are important to the mutualism as they seek and translocate nutrients and water. They can also proceed and infect short lateral roots from other plants forming a mycelial network that facilitates carbon and nutrient movement among trees (Anderson and Cairney, 2007).

² Aseptate endophytes: Plant colonizing fungi that develop syncytial hyphae that lack transversal walls (septa).

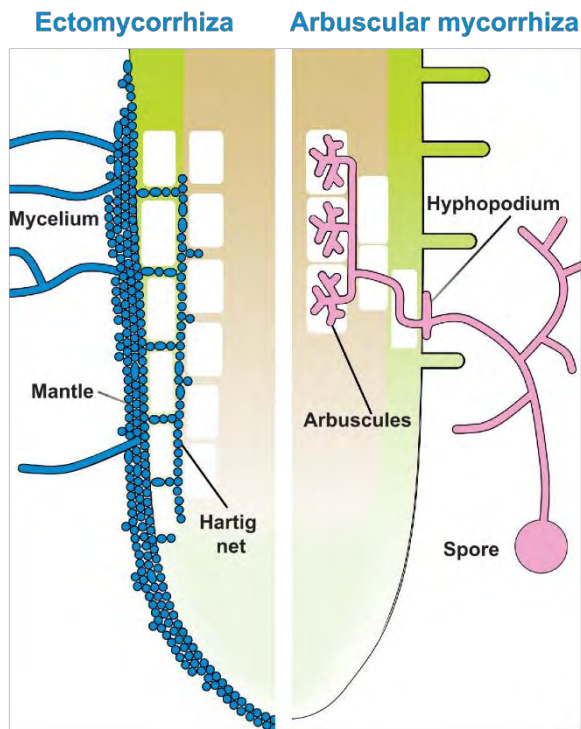


Figure 1-3 Illustration of root colonization structures in ectomycorrhizal and AM interactions. From (Bonfante and Genre, 2010).

Genome sequencing of EM fungi, such as the Basidiomycete *Laccaria bicolor* (Martin et al., 2008) and the Ascomycete *Tuber melanosporum* (Martin et al., 2010) gave insight into the life strategies of EM fungi. These fungi possess a relatively small number of genes encoding for enzymes that target plant cell wall components (like pectinases), and these genes are mainly regulated during establishment of the symbiosis, when the fungus develops inside plant tissues, indicating a strategy towards limitation of host damage (Bonfante and Genre, 2010).

As previously stated, EM interactions are mutualistic interactions; there is a bidirectional benefit between the two hosts. The EM fungus takes up carbon from their living host plant in exchange for nutrients. *L. bicolor*, for example, possesses genes coding for hexose transporters, many of them are upregulated during symbiosis. Interestingly, there is no invertase gene in the *L. bicolor* genome, implying that this fungus is unable to use sucrose directly from the plant, and perhaps relies on the host plant for breakdown of sucrose into glucose and fructose (Martin et al., 2008). In exchange of carbon, the fungus provides the plant with soil-acquired phosphorus and nitrogen.

1.3.1.2 Endomycorrhizae

As mentioned, endomycorrhizae develop intracellularly in the root system of the host plant and can be divided into arbuscular, orchid and ericoid mycorrhizas. For the purposes of this dissertation, only the first type of endomycorrhizae will be described.

The AM Symbiosis is the association of members of the fungi belonging to the Glomeromycota phylum and roots of the majority of terrestrial plants. Despite the fact that mycorrhizal fungi can spend part of their life cycle as free-living organisms, they always associate with the roots of higher plants (Bonfante and Genre, 2010). AM relies on an evolutionary ancient program. It dates back to early land plants, and

is assumed to have aided the transition of plants from the aquatic environment to land. The AM symbiosis is a mutualistic symbiosis as both engaged partners receive nutritional benefits. The AM connects plants to the hyphal network of fungi, which is specialized for nutrient (phosphate predominantly), and water uptake. In return for this supply, AM fungi obtain carbohydrates from plants (Parniske, 2008).

Although spores of AM fungi can germinate in the absence of host plants, they are obligate biotrophs, depending on their living photoautotrophic partner to complete their life style and produce the next generation of spores. The development of an AM symbiosis is characterized by distinct steps: presymbiotic communication between the two partners, contact and penetration through the root epidermis, outer cortex invasion, arbuscule formation, vesicle and spore formation. Despite the fact that intraradical colonization steps occur consecutively in a single infection site, when we refer to the whole root level AM development is a nonsynchronous process, as all steps occur concomitantly during root colonization (Choi et al., 2018). The steps for successful establishment of an AM symbiosis can be described as follows:

- Presymbiotic communication: both organisms release diffusible signals to achieve chemical communication. Plants release strigolactones³ (SLs) into the soil, whereas fungi release oligosaccharides. SLs activate AM fungal metabolism, inducing fungal hyphal branching, therefore increasing the chance for the fungus to encounter the plant host. Fungal oligosaccharides trigger nuclear calcium spiking in the root epidermis, activating the so called Common Symbiotic Signaling Pathway (the CSSP is discussed later in the present chapter).
- Contact and penetration: fungal attachment structures resembling a foot, the so called hyphopodia, attach on the root surface. On the same time, the host cell produces the pre-penetration apparatus (PPA), which serves to accommodate the incoming fungus (Genre et al., 2005). Once PPA is formed, local softening of the plant cell wall is assumed to occur, which allows the fungal hypha to enter the plant cell, while kept excluded from the host cell cytoplasm.
- Outer cortex invasion: following epidermal penetration fungal hyphae proceed towards the inner cortex either inter- or intracellularly. When inside the plant cell the fungus is always excluded from the plant cell cytoplasm.
- Arbuscule formation: when the inner cortex is reached, the fungus develops the arbuscules: highly branched, tree-shaped feeding structures. An increase in ploidy levels anticipates fungal colonization and is limited in arbusculated and neighboring cells in the cortical tissue (Carotenuto et al., 2019). Successful arbuscule formation enables carbon uptake (by the fungus) in exchange for mineral nutrients (delivered by the fungus to the plant). Arbuscules are ephemeral structures though, they have a life span of only a few days.
- Vesicle and spore formation: after successful arbuscule setting, the fungus produces lipid storage vesicles. These are thick-walled, irregular lobes that are formed either within or between host cells by most orders of Glomeromycota fungi, except the Gigasporales. If the fungus is appropriately nourished by the plant, it then produces asexual spores. Both spores

³ Strigolactones: carotenoid-derived plant hormones, that enable root parasitic plants and symbiotic fungi to detect their host plant.

and nuclei contain storage lipids to support spore germination and asymbiotic germ-tube growth (Choi et al., 2018).

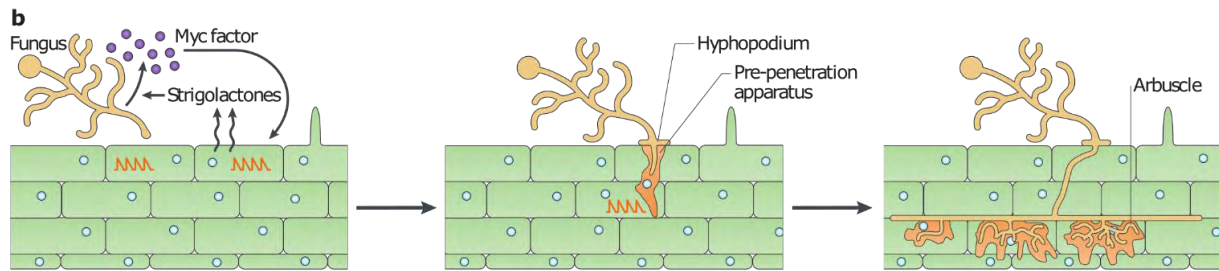


Figure 1-4 Main steps in mycorrhizal colonization (pre-contact to arbuscule establishment). From (Oldroyd, 2013).

The great importance of the AM symbiosis lies in the bidirectional exchange of nutrients between the two partners. The AM fungus receives soil-derived phosphate and nitrogen and provides it to the plant in exchange for carbon. More specifically, polyphosphates are translocated in the intraradical fungal structures, they are hydrolysed into their inorganic form, and are released into the periarbuscular interface⁴ (PAI). Plant symbiosis specific phosphate transporters (like *MtPT4*) acquire the phosphate form the periarbuscular membrane (PAM). Nitrogen derived from the soil, arrives in the arbuscule in the forms of amino acids (glutamate and arginine), which are converted into urea and ammonia, and released again in the PAI. Plant ammonium specific transporters (like *MtAMT2;4*) take up ammonium from the PAM. The plant on the other hand, provides the fungus with photosynthates in two forms: sugars and lipids. In the PAI, sucrose is broken down to hexose, and glucose is the main carbohydrate taken up by the fungus. Since AM fungi lack the genes for long-chain fatty acid (FA) biosynthesis, they depend on the host plant for FA acquisition. FA biosynthesis occurs in arbusculated cells by expression of several FA biosynthetic genes. The plant provides the fungus with long chain FA which are converted into storage forms or converted for immediate use in fungal growth and development [references within (Choi et al., 2018)].

⁴ Periarbuscular Interface (PAI): The periarbuscular membrane, which is continuous with the plant plasma membrane of the cortical cell containing the arbuscule.

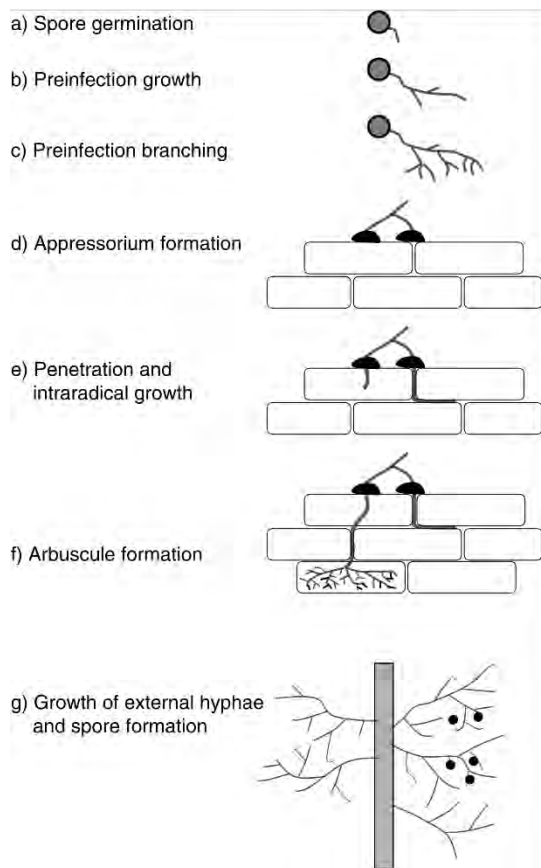


Figure 1-5 Stages of AM development. (a, b) Spore germination and limited hyphal growth occur in the absence of the plant root, (c) extensive preinfection branching and sustained hyphal growth require the presence of host plant roots, (d) Upon contact with the root epidermis, hyphal tips swell and form appressoria, (e) penetration of the root and the proliferation of intraradical hyphae. Cortical cells are subsequently penetrated and arbuscules develop, (f) colonization of the root promotes extensive growth of external hyphae.

This scheme represents the 'Arum'⁵ type of AM. This type is formed on the model plant species *M. truncatula*. Under natural conditions infections do not need to originate from germinating spores, but occur predominantly from previously infected root segments covered with external hyphae. From (Marsh and Schultze, 2001).

1.3.2 Endophytes

Unlike mycorrhizal fungi that colonize plant roots and grow into the rhizosphere, typical endophytes reside entirely within plant tissues and may grow within roots, stems and/or leaves, and sporulate at plant or host-tissue senescence (Rodriguez et al., 2009). Two major groups of endophytic fungi have been recognized previously:

Clavicipitaceous endophytes (C-endophytes) or class 1 endophytes that infect some grasses. They are ascomycetous fungi and comprise of free-living and symbiotic species. *Epichloe* species (anamorphs: *Neotyphodium*) which are endophytic symbionts of cool-season grasses belong in this class.

Non-clavicipitaceous endophytes (non-clavicipitaceous endophytes; NC-endophytes), represent the largest group of fungal symbionts and are thought to colonize all plants in natural ecosystems. These endophytes can be recovered from asymptomatic tissues of nonvascular plants, ferns and allies, conifers and angiosperms. NC-endophytes can be furthermore divided in three functional classes (class 2, 3, 4) based on colonization patterns, mechanisms of transmission between host generations, *in planta* biodiversity levels, and ecological function. Class 2 comprises a diversity of species, all of which

⁵ Depending on the plant species two major morphological types of AM are observed. In the 'Paris' type, hyphae grow relatively slowly and primarily intracellularly. Intracellular coiled hyphae are formed with intercalary arbuscules. The 'Arum' type is characterized by the rapid growth of intercellular hyphae followed by extensive formation of the intracellular arbuscules which are terminal (Marsh and Schultze, 2001).

are members of the Dikarya⁶ (Ascomycota or Basidiomycota). Most belong to Ascomycota and only a minority in Basidiomycota. Some of their distinct traits are: they colonize roots, stems, and leaves; they extensively infect plant tissues, they can be transmitted vertically or horizontally⁷. Class 3 endophytes comprises member of the Dikarya (Asco- and Basidiomycota), with a special representation by Ascomycota. They occur primarily on above ground tissues; they are transmitted horizontally; they form highly localized infections. Class 4 endophytes are the dark septate endophytes, and are distinguished by presence of darkly melanized septa. They are primarily ascomycetous fungi, with little host specificity (broad host range); they colonize only the root; they show extensive in planta colonization; they are transmitted horizontally (Rodriguez et al., 2009).

Endophytes can confer various benefits to their hosts in contrast to parasites, which cause disease. Benefits provided to the plant by endophytic fungi are well documented. These fungi can provide fitness in their hosts upon biotic or abiotic stress. Many endophytic fungi have been reported to confer resistance to plants against pathogens.

A well-studied paradigm of a beneficial endophytic fungus is *Piriformospora indica* (*Serendipita indica*), isolated from an AM (*Glomus mosseae*) spore from a desert soil in India (Verma et al., 1998). *P. indica* is a member of the basidiomycetous order Sebaciniales (Basidiomycota: Agaricomycetes). The case of *P. indica* is intriguing. The fungus shows growth-promoting effects in a wide range of monocotyledonous and dicotyledonous plant species, including maize, tobacco, poplar (Varma et al., 1999), *Arabidopsis thaliana* (Peškan-Berghöfer et al., 2004) (Abdelaziz et al., 2017), and increased grain yield effects in barley (Waller et al., 2005) (Achatz et al., 2010).

The fungus confers resistance to biotic and abiotic stress: it has been reported to confer in barley plants tolerance to mild salt stress and resistance against the root necrotrophic fungus *Fusarium culmorum* and the leaf biotrophic fungus *Blumeria graminis* (Waller et al., 2005). Its colonization success relies on suppression of plant innate immunity (Schäfer et al., 2009) (Jacobs et al., 2011). *P. indica* shows a versatile lifestyle highly depending on the plant host. In barley, it was shown that the endophyte interferes with the host cell death program to establish a mutualistic interaction with the plant. More specifically, (Deshmukh et al., 2006) showed that the fungus colonizes barley root system, proliferates inter- and intracellularly and produces chlamydospores in dead root tissue. The authors calculated the fungus to plant DNA ratio to check growth of *P. indica* within barley roots, and found that the fungus grows moderately at the beginning, subsequently induces plant growth, and finally reaches a steady-state level of fungal structures in the plant root. The highest fungal biomass during colonization was found in the differentiation and root hair zones, whereas the meristematic zone was less colonized. After symbiosis establishment, the fungus confers improved growth, disease resistance and tolerance to abiotic stress to the host plant (Deshmukh et al., 2006).

⁶ Dikarya: a subkingdom containing the largest extant clade of fungi. They do not have any flagellated life stages. Their name comes from dikaryons, a life stage containing two genetically distinct nuclei. They are divided into two phyla, Basidiomycota and Ascomycota.

⁷ Horizontal transmission: the spread of an infectious agent from one individual to another. Acquired from the environment with each new generation.

Vertical transmission: transmission from one generation to another. In plants from generation to generation via seed.

P. indica cell death associated colonization does not lead to necrotization as seen for hemi-biotrophic or necrotrophic fungi. It was therefore proposed that the term ‘necrotrophy’ is misleading, and ‘cell-death dependent colonization’ is a more precise description for this interaction phase (Schäfer et al., 2009). In *Arabidopsis*, successful colonization by *P. indica* is dependent in endoplasmic reticulum (ER) stress-induced cell death (Qiang et al., 2012b). It was later shown by cytological and transcriptomic analysis that the fungus switches life styles depending on the host plant: in *Arabidopsis* the fungus establishes a biotrophic relationship within living epidermal cells, whereas in barley the fungus switches to saprotrophy by producing secondary thinner hyphae in dead plant cortical cells (Lahrman et al., 2013).

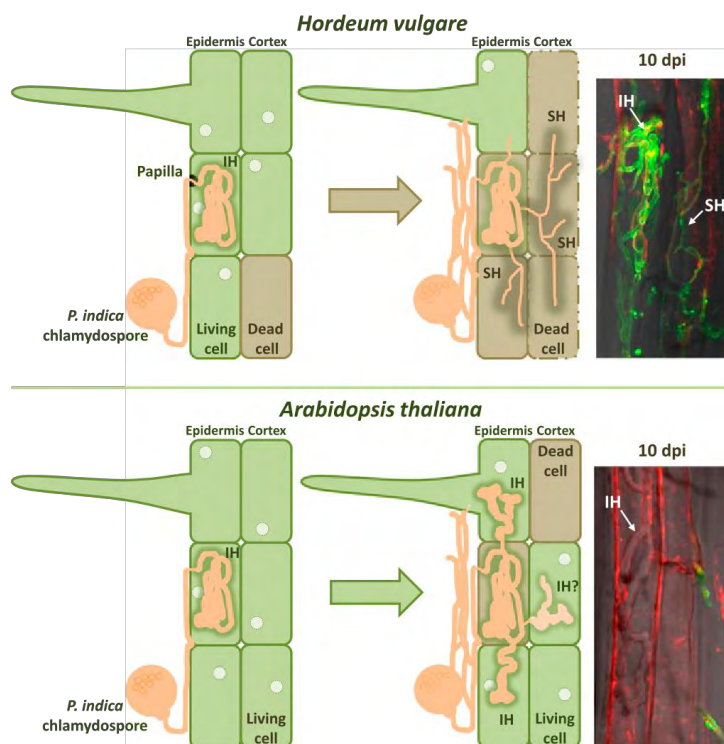


Figure 1-6 *P. indica* colonization strategies at different symbiotic stages in barley and *Arabidopsis*. Invasive hyphae (IH) and secondary thin hyphae (SH) are observed in barley dead cells (10 dpi). From (Lahrman et al., 2013).

Colletotrichum sp constitute another excellent paradigm of fungi capable of lifestyle transitions. These fungi are mainly known as fungal pathogens that devastate crop plants worldwide. Host infection is characterized as a multistage hemibiotrophy and involves: differentiation of specialized cell types that are associated with penetration (dome shaped appressoria); bulbous biotrophic hyphae growing inside living host cells (biotrophy); and tissue destruction by fast growing hyphae (necrotrophy). Genome and transcriptome analysis of two *Colletotrichum* species (*C. higginsianum* infecting *Arabidopsis* and *C. graminicola* infecting maize) revealed that this transition of lifestyles during infection process is also reflected in the expression profile of the species with specific genes being transcribed in successive waves during infection: effectors and secondary metabolism enzymes induced prior to penetration and during biotrophy, whereas hydrolases and transporters at later stages during necrotrophy (O'Connell et al., 2012). Despite the fact that a large number of *Colletotrichum* species has been reported as pathogens, (Hiruma et al., 2016) described *C. tofieldiae* (Ct) as an endophyte of natural populations of

A. thaliana growing in central Spain. The authors describe that the fungus penetrates the rhizodermis via undifferentiated hyphae, which they ramify through the root cortex inter- and intracellularly, and occasionally move towards the shoot via the root central cylinder, without causing visible symptoms. In epidermal cells a host plasma membrane (PM) invaginates around the hyphae and the fungus establishes a biotrophic interaction with living host cells. However, soon after penetration, the plant cells lose viability, although adjacent more recently colonized cells remained alive, suggesting a transient initial biotrophic interaction of intracellular hyphae with root epidermal cells. The endophyte promotes plant growth and fertility under phosphate deficient conditions and mediates the translocation of phosphate in the shoots, as shown by ^{33}P radiotracer experiments (Hiruma et al., 2016). The authors furthermore showed that tryptophan derived metabolites are required for restricting the endophyte colonization, as mutants depleted in production of these metabolites demonstrate increased fungal biomass. Genome and transcriptome comparative analysis of five endophytic *C. tofieldiae* isolates with one pathogenic relative *C. incanum* (Hacquard et al., 2016), revealed that an altered gene expression pattern during colonization, rather than extensive remodeling of the gene repertoire, provides an alternative and probably transient adaptation to a beneficial endophytic lifestyle. The authors report no obvious common genomic signatures to indicate the convergent evolution⁸ of an endophyte toolkit (Hacquard et al., 2016).

Besides benefits provided from the endophytes to the host, the fungus also profits from the association: the host plant provides to the fungus organic nutrients, protective shed, and guaranteed transmission to the next host generation. Endophytic fungi can be transmitted in two ways: vertical (systemic) transmission occurs via seeds, whereas horizontal (non-systemic) transmission occurs via spores. The mode of transmission has been linked with virulence, with vertical transmitting endophytes showing tendency for mutualism (Rai and Agarkar, 2014).

The term endophyte has been controversial ever since its appearance, and there are various reports in the literature for endophytes that can switch lifestyle and turn into parasites under certain conditions. The range of symbiotic lifestyle expression from mutualism to parasitism has been described as the symbiotic continuum (Rodriguez and Redman, 2008). Examples can be found within the genera *Epichloe* and *Colletotrichum*. Other genera also demonstrate the capability of switching lifestyles. For example, asymptomatic colonization of hosts has also been reported for *Fusarium* genus (Bacon and Yates, 2006). The *Fusarium* genus is more explicitly described below.

1.3.3 Parasites

Focussing on fungi, parasitic ones infect plant tissues and cause disease. Plant pathogenic fungi are primarily categorized into three main groups based on their lifestyle and nutritional needs:

- Biotrophs: they rely on the living host plant, and they develop an intimate relationship with their host. They are characterized by a total dependency on the host to complete their life cycle. Biotrophic pathogens form haustoria to absorb nutrients: a short or long simple unbranched projection from an intracellular hypha, which extend into living plant cells. Haustoria are not

⁸ Convergent evolution: the independent evolution of similar features in species of different lineages.

really intracellular as they breach the cell wall only, and a newly formed host plasma membrane (the extrahaustorial membrane surrounds them (Mendgen et al., 2000). Examples of biotrophic pathogenic fungi are the rust fungi (Basidiomycota) and the powdery mildew fungi (Ascomycota).

- Hemibiotrophs: They act as biotrophs at the initial stage of infection, and later on they act as necrotrophs. Typical examples of hemibiotrophs are the rice interacting fungi *Magnaporthe grisea* and *M. oryzae* (the blast fungus), as well as *Colletotrichum lindemuthianum* which interacts with bean plants (Masurkar et al., 2018) (Mendgen and Hahn, 2002).
- Necrotrophs do not possess specialized infection structures, and do not have a biotrophic state. They derive nutrients from dead matter. Shortly after penetration, they cause cell lysis and death of host cells (Divon and Fluhr, 2007). Both necrotrophic and hemibiotrophic fungi trigger cell death to subsequently feed as saprotrophs. Characteristic examples of necrotrophic fungi include *Botrytis cinerea* and *Sclerotinia sclerotiorum*.

1.4 The genus *Fusarium*

The genus *Fusarium* constitutes a large monophyletic⁹ group of several hundred species of filamentous fungi. It is one of the most important groups of plant pathogenic fungi affecting a huge diversity of crops in all climatic zones across the globe. It is also an animal and human pathogen, mainly affecting immunocompromised patients. *Fusarium* species produce active secondary metabolites, known as mycotoxins, such as trichothecenes and fumonisins, which have negative impact on animal production and possible deleterious effect on human health (Summerell, 2019). Plant infections by *Fusarium* can occur at all developmental stages, from germinating seeds to mature vegetative tissues, depending on the host plant and *Fusarium* species involved (Moretti, 2009). As a plant pathogen it causes some of the most important plant diseases: Panama disease of bananas, cotton wilt, *Fusarium* wilt of tomatoes (Summerell, 2019).

The genus *Fusarium* belongs to the Ascomycota phylum (Sordariomycetes: Hypocreales: Nectriaceae). The phylogenetic analysis performed by (O'Donnell et al., 2013) reports on a monophyletic group that encompasses all economically important *Fusarium* species. Most species are spread around 20 monophyletic species complexes that consist of as many as 60 species (Ma et al., 2013). The term species complex implies a grouping of species with shared morphological characteristics and phylogenetic markers, and some level of cryptic speciation (Summerell, 2019). Alternative generic names have been linked to sexual stages of species (e.g. *Gibberella*, *Nectria*), but to avoid confusion only the name *Fusarium* should be used (Ma et al., 2013). Within the genus there are currently more than 300 phylogenetically distinct species the majority of which lacks formal names (Geiser et al., 2013). *Fusarium* is hypothesized to have originated ~91.3 Mya, an indication that its diversification coincided with that of flowering plants (Ma et al., 2013).

The main approach for classification of isolates into the *Fusarium* genus was first introduced by (Link, 1809): classification is achieved by morphology and the main trait used is the occurrence of the asexual

⁹ Monophyletic group: includes a group of organisms descended from a single (common) ancestor, whereas a polyphyletic taxon comprises unrelated organisms descended from more than one ancestor.

spores, the distinctive banana-shaped macroconidia. *Fusarium* species produce three types of spores: macroconidia, microconidia, chlamydospores. Septated macroconidia can be produced on monophialides and polyphialides in the aerial mycelium, but also on short monophialides in specialized structures called sporodochia. A monophialide is a conidiation cell with a unique pore from which the endoconidia are released; a polyphialide can possess several such openings. Microconidia can vary in shape and size, and are produced in the aerial mycelium in clumps or chains, both on monophialides and polyphialides. Chlamydospores are resistance structures with thickened walls, and high lipid content. They can form in the middle of the hyphae or at their termini. The different shape of macroconidia is the main taxonomic feature for distinguishing among species. Other traits also contribute to distinguishing species, such as: presence/absence of chlamydospores, the characteristics of the micro- and macro-conidiogenous cells. Cultures derived from a single spore isolation should be used for species identification (Moretti, 2009). Nowadays, molecular approaches have been developed, and *Fusarium* species interacting with well-known hosts or in culture collections are more thoroughly documented with DNA-based technology. Direct sequencing of one or more genes is now the standard methodology to make or confirm species assignments. One (or more preferably more) genes are amplified and sequenced. Some of the more commonly used genes for *Fusarium* include translocation elongation factor-1a (*tef-1a*)¹⁰, RNA polymerase 1 and 2 (*RPB1* and *RPB2*), β -tubulin (*tub*), and histone (*his*). The sequence is then compared with similar sequences from strains in related species deposited in public databases. Limitations of this analysis are: the cost, and the availability of sequence data from reference strains in accessible data banks to allow for comparisons. *tef-1a* gene is recommended as the routine barcode for *Fusarium* identification. The standard DNA barcode for fungi, the internal transcribed spacer region of the ribosomal gene (*ITS*), is not informative for a large number of *Fusarium* species and is not recommended for species identification in this genus (Summerell, 2019).

The genome of this complex fungus is compartmentalized into core and adaptive regions that encode functions mostly associated with primary growth versus adaptation to specific niches (e.g. virulence on specific hosts, growth in specific environments). Among the completely sequenced *Fusarium* genomes are *F. graminearum*, *F. oxysporum* f. sp.¹¹ *lycopersici*, *F. pseudograminearum*, *F. solani* f. sp. *pisi*, *F. verticillioides*. Their genomes vary greatly in size and content within the genus. For example, *F. graminearum* has a 36 Mb genome, whereas *F. oxysporum* f. sp. *lycopersici* has a genome of 61 Mb. Mechanisms that could decrease genome size include: unequal crossover that induces localized deletions of individual or multiple genes, or other types of chromosomal rearrangement that could induce large-scale deletions. Mechanisms that could increase genome size include gene duplication, whole or partial genome duplication, hybridization between species, and/or horizontal transfer. *Fusarium* genome has been affected by localized and large-scale deletions, as well as counterbalancing gene duplications. The acquisition of foreign DNA (xenologs) can be achieved through the transfer of an entire plasmid, or chromosome, or may be integrated into the chromosomal complement of a species. Chromosomes that contain horizontally acquired genes are supernumerary or conditionally

¹⁰ Translation elongation factor (*tef-1a*): proteins that play two important roles during the elongation cycle of protein biosynthesis on the ribosome.

¹¹ *Forma specialis* (f. sp.): artificial taxonomic grouping based on ability to cause disease on a specific plant host (Ma et al., 2013).

dispensable chromosomes. They are usually small (<2 Mb) and are required for survival under standard conditions. Supernumerary chromosomes share certain features that can result from horizontal transfer: (a) lack of housekeeping genes involved in primary metabolism, (b) a high level of G+C content (relative to the normal chromosomal complement), (c) a lack of synteny¹² with related species, and (d) the presence of a large number of transposable elements. Supernumerary chromosomes contribute significantly to genome evolution of species, and are linked to genome compartmentalization into two components: a core component that encodes functions necessary for growth and secondary metabolites, and an accessory component that encodes pathogenicity (or virulence factors) and secondary metabolites (Ma et al., 2013). Experiments on tomato have confirmed the 'transfer' of pathogenicity via in vitro transfer of supernumerary chromosomes between strains of *F. oxysporum* (Ma et al., 2010).

Fusarium spp strains have been also described as non-pathogenic/biocontrol agents, including several *F. oxysporum* isolates effective in suppressing *Fusarium* wilt in watermelon (Larkin et al., 1996), and tomato (Larkin and Fravel, 1998). A well-studied endophytic strain is *F. oxysporum* 47 (Fo47) (Aimé et al., 2013).

1.4.1 The *Fusarium solani* species complex (FSSC)

The ascomycetous fungus *Nectria haematococca* (asexual name *Fusarium solani*), is a member of a monophyletic group of at least 60 species known as the '*Fusarium solani* species complex' (FSSC). Members of the complex adapt to a plethora of environments, reflecting their plasticity and metabolic diversity. *F. solani* was among the fungal species recovered from the inner parts of the damaged nuclear reactor in Chernobyl. They can be saprobes, pathogens causing disease in > 100 genera of plants, animal and human pathogens causing opportunistic infections like keratitis especially in immunocompromised patients (Coleman et al., 2009) (Coleman, 2016).

F. solani is the only species within the FSSC. Members of the complex have been subdivided into *formae speciales* based on host specificity. They represent a diverse set of self-fertile (homothallic) and self-sterile (heterothallic) species, and sexual cycles are only known for some of the species. FSSC members have been divided into seven mating populations (MP) based on their ability to mate with one another, thus constituting the same biological species. Based on molecular phylogenetic analysis, the FSSC comprises three major clades; clade 3 encompasses all of the isolates formerly characterized as *N. haematococca*. In addition to *N. haematococca*, other teleomorphic names have been assigned to these seven MPs among them '*Hypomyces solani*' and '*Haematonectria haematococca*'. Nowadays the usage of teleomorph names has been abandoned (Coleman, 2016).

The most extensively studied member of the complex is MP VI of *N. haematococca*, also known as *Haematonectria haematococca*. These fungi possess genes controlling the ability of isolates to colonize specific habitats (Coleman et al., 2009). The extra genes are located on conditionally dispensable (CD) chromosomes, and the latter term reflects that they can be lost with no alteration in growth under

¹² Synteny: describes the distribution pattern of genes on a chromosome. This pattern of gene locations can be conserved such that genes positioned near each other on the genome in one species are likely to be found close to each other on a single chromosome in evolutionarily related species.

laboratory conditions; they are however able to broaden the habitat of the fungus when present. CD chromosomes were first described in fungi and more specifically in *N. haematococca* in 1991 (Miao et al., 1991). The extra genes may have occurred through gene duplication events or may have been acquired by horizontal gene transfer (Coleman, 2016). *N. haematococca* which possesses a relatively large genome (~51.3 Mb, 15707 protein genes, 17 chromosomes), possesses three such chromosomes (chromosomes 14, 15, 17), containing functional genes for pathogenicity, antibiotic resistance, and the utilization of unique carbon/nitrogen sources. Two classes of genes contribute to gene expansion: a) specific genes that are not found in other fungi, and b) genes that are present as multiple copies in *N. haematococca* but commonly occur as a single copy in other fungi (Coleman et al., 2009).

Members of the FSSC are important pathogens of a number of agriculturally important crops and are known to cause root rot on several plants. Agronomically important plant diseases caused by members of the FSSC may include: sudden death syndrome in soybean (Aoki et al., 2003), root rot in pea (Ondrej et al., 2008) (Hamid et al., 2012), crown disease in oil palm (Hafizi et al., 2013). The association of a pathogenic *F. solani* isolate with the model legume *L. japonicus* has been previously investigated (Takeuchi et al., 2007a). Notably, non-pathogenic and/or biocontrol agents have been reported as well: *F. solani* isolates are able to reduce *Fusarium* wilt of tomato plants (Larkin and Fravel, 1998), while the non-pathogenic *F. solani* 5 (Fs5) strain is able to suppress root-knot nematode in the same plant species (Siddiqui and Shaukat, 2003), an endophytic *F. solani* with antimicrobial properties was isolated from the conifer *Taxus baccata* (Tayung et al., 2011), and *F. solani* endophytes were isolated from the stems of tomato plants (Imazaki and Kadota, 2015).

1.4.1.1 The fungal isolate *Fusarium solani* strain K

Fusarium solani strain K was primarily isolated from the roots of tomato plants (Kavroulakis et al., 2007) grown on a compost with abilities to suppress root and foliar pathogens (Kavroulakis et al., 2006). FsK was able to colonize the root system of tomato plants and to grow endophytically. The fungus reached the root cortex at 15 days post inoculation and formation of round bodies of unknown function was observed. FsK proliferated in the vascular system of the plant, colonization extended to the root crown, but not to the stem and leaf tissues. No apparent growth effect was detected on FsK-plants, which nonetheless demonstrated resistance against crown and root rot caused by *F. oxysporum* f. sp. *radicis-lycopersici* (FORL). The fungus also conferred systemic protection against the foliar pathogen *Septoria lycopersici*, as indicated by the fewer lesions on plant leaves. FsK also reduced the expression of certain pathogenesis-related (PR) genes (PR1, PR5, P69/PR7), that were previously shown to be induced in tomato plants grown on the compost used for the experiments (Kavroulakis et al., 2006), whereas genes encoding for chitinases or glucanases were unaffected by FsK presence.

FsK needs a functional ethylene pathway in order to confer resistance against the root pathogen FORL, as indicated by analysis of mutant lines deficient in ethylene production (either ethylene insensitive or ethylene overproducing). On the other hand, FsK protected tomato mutant lines deficient in jasmonic acid biosynthesis against FORL disease occurrence, indication that this hormone is not necessary for resistance conferred by the endophyte.

FsK is also capable of protecting tomato plants by increasing the plant resilience to drought abiotic stress, as shown by (Kavroulakis et al., 2018). FsK basically ameliorates the physiological status of the plant under deficient irrigation conditions: plants restore levels of net photosynthesis rate, maximal potential yield of PSII (Photosystem II), and relative water content, display increased stomatal conductivity, and a large decrease in proline levels which are known to rise in plant tissues in cases of drought stress. The authors advocate that the endophyte promotes a shift to the plant towards an anisohydric type of response to water stress, and reduces stomatal closure which would be the expected response to drought. They furthermore hypothesize that the improved water acquisition could be due to water translocation from the surrounding medium to the plant's xylem through the extraradical fungal mycelium (Kavroulakis et al., 2018).

FsK may also be regarded as a biocontrol agent as shown in the recent publication of (Garantonakis et al., 2018). The capability of FsK to protect tomato plants against the zoophytophagous predator *Nesidiocoris tenuis* was assessed, by measuring necrotic rings caused by the arthropod on tomato stems and leaves. FsK plants demonstrated significantly lower number of necrotic rings in comparison to non-inoculated plants. The endophyte necessitates a functional ethylene signaling and jasmonic acid biosynthesis to confer protection to the plant against the predator, as indicated by analysis of the ethylene perception-deficient *Nr* mutant and the jasmonic-deficient *def-1* mutant. As mentioned above, ethylene was also shown to be important for FsK-mediated resistance against root pathogens (Kavroulakis et al., 2007).

Finally, the potential role of FsK as a biocontrol agent was furthermore assessed by examining its ability to protect the plant against the spider mite *Tetranychus urticae* again in tomato. FsK presence affected in both direct and indirect ways tomato defenses against the arthropod. Differential defense gene expression was recorder for FsK inoculated and spider mite infested plants, and the same trend was observed in the plant volatiles emitted. In the presence of the endophyte, spider mite performance and feeding damage on the plant were negatively affected, and FsK demonstrated a clear positive effect on plant biomass, as shown in both spider mite infested and clean plants (Pappas et al., 2018).

1.5 Signaling in recognition and accommodation of PMIs

1.5.1 Pattern Recognition Receptors (PRRs)

Plants encounter a plethora of microorganisms, particularly at the root-soil interface, that can invade their tissues leading to detrimental or beneficial associations. When in their vicinity, plants recognize microbial molecules, which leads to mutualism or immunity (Zipfel and Oldroyd, 2017). Recognition of these signals occurs via receptor like kinases (RLKs), or receptor-like proteins (RLPs). RLKs comprise a ligand-binding ectodomain and an intracellular serine/threonine kinase domain, whereas receptor-like proteins, have no known intracellular signaling domain (Macho and Zipfel, 2014).

Among the most studied plant receptor-like kinases are those with (a) leucine-rich repeat (LRR) domains, and (b) lysine-motif (LysM) domains. Plant RLKs involved in immunity are so-called pattern recognition receptors (PRRs), able to detect pathogen-associated molecular patterns (PAMPs), which are their cognate elicitors. Broader terms, to include a wider range of microbial signals are: MAMPs,

microbial-associated molecular patterns, and DAMPs, damage-associated molecular patterns (Greeff et al., 2012). Symbiotic signals are also recognized by PRRs. MAMPs are conserved microbial signatures that are not specific to pathogens but are also present in beneficial microbes. Typical fungal MAMPs are chitin and its derivatives, typical bacterial MAMPs are the peptidoglycan (PGN) fragments; many other MAMPs do not contain N-acetyl-glucosamine molecules¹³ (GlcNAc), like bacterial flagellin and its various peptides, like flg22 (Buendia et al., 2018).

Following PAMP recognition, a set of defense responses termed PAMP-triggered immunity (PTI) initiates. Features of PTI include: reactive oxygen species (ROS) production, callose deposition, generation of secondary messengers and defense gene expression (Greeff et al., 2012).

1.5.2 Perception of N-acetyl-glucosamine derivatives

Recognition of microbes by plants occurs via perception of main components of their cell wall. Chitin is a primary structural polysaccharide in the fungal cell wall (Gow et al., 2017). β -glucans constitute the major component of oomycetes¹⁴ cell wall (Mélida et al., 2013), and it was recently shown that these plant pathogens (non-true fungi) possess chitin synthase enzymes and produce short chitooligosaccharides (Fuechtbauer et al., 2018) (Gibelin-Viala et al., 2019). Chitin oligosaccharides (COs) are β -1,4-linked polymers of GlcNAc with various degrees of polymerization, which can be synthesized anew, or produced through enzymatic cleavage of the long-crystalline chitin.

Symbiotic signals that are necessary for the establishment of AM (Myc Factors) and LR symbiosis (NFs, NFs) are derivatives of chitin oligosaccharides. NFs differ from other COs in that they contain lipid decorations on their chitooligosaccharidic backbone, which transforms them into lipo-chitooligosaccharides (LCOs). Rhizobia produce various modified Nod-LCOs that differ in the length of their chito-oligosaccharidic chain, lipid acylation, and the presence of modifications such as sulfation, acetylation and fucosylation. These decorations probable contribute to plant host specificity (Zipfel, 2008). Myc Factors on the other hand, are probably a mixture of LCO and chitin oligosaccharide molecules (Maillet et al., 2011) (Genre et al., 2013). Both Myc (CO4/CO5) and NFs are responsible for induction of calcium spiking in the nucleus of root cells of host plants (NFs, CO4/CO5: *M. sativa*, *M. truncatula*, *L. japonicus*; CO4: rice) (Ehrhardt et al., 1996) (Sieberer et al., 2009) (Genre et al., 2013) (Carotenuto et al., 2017) (Zipfel and Oldroyd, 2017).

Chitin oligomers with a relatively high degree of polymerization (hexamers or octamers) are potent inducers of immune responses (Stacey and Shibuya, 1997) (Kouzai et al., 2014) (Liang et al., 2014). The similarities between long-chain chitin, peptidoglycan, symbiotic chitin oligosaccharides and LCOs raise questions about how plant distinguish friend from foe: molecules that trigger immunity from molecules that trigger symbiosis (Zipfel and Oldroyd, 2017).

¹³ N-acetyl-glucosamine: a monosaccharide. The monomeric unit of polymer chitin.

¹⁴ Oomycetes: a phylogenetically distinct lineage of fungus-like eukaryotic microorganisms.

1.5.3 The role of LysM receptors

LCOs, COs, and PGN, the three types of GlcNAc-containing molecules produced by microorganisms are perceived by LysM-RLKs/RLPs in plants, that contain 3 extracellular LysMs. A LysM is a protein domain of about 40 aa found in most living organisms except Archaea. Its name originates from its identification in bacterial autolysin proteins that hydrolyze bacterial PGN and lead to cell lysis. Based on their kinase domains, two types of LRs can be distinguished: a) LYK, which has a kinase domain showing *in vitro* autophosphorylation activities, and b) LYR which carries an aberrant kinase and does not exhibit *in vitro* auto-phosphorylation or trans-phosphorylation activities (Buendia et al., 2018).

In *M. truncatula* and *Lotus japonicus*, receptor complexes comprising both a LYR gene (*MtNFP* or *LjNFR5*) and a LYK gene (*MtLYK3* or *LjNFR1*) are required for NF perception and NF-dependent nodulation and infection (Amor et al., 2003) (Limpens et al., 2003) (Arrighi et al., 2006) (Madsen et al., 2003) (Radutoiu et al., 2003) (Buendia et al., 2018). NFP/LYK3 are orthologous¹⁵ to NFR5/NFR1, respectively. NFR5 and NFP do not contain functional kinases in their intracellular domain, indication that they require NFR1/LYK3 for intracellular signal transduction (Zipfel and Oldroyd, 2017). Recently, another receptor NFR1 (LYS1) was reported to also perceive NFs in *L. japonicus*. NFR1 has an active intracellular kinase domain, induces *NIN* (Nodule Inception)¹⁶ gene expression in epidermal cells, and is required for normal nodulation (the mutant forms fewer nodules). It was proposed that NFR1 contributes to NFR1/NFR5 mediated signaling, by keeping epidermal cells in an idling state, tuned in to rhizobia (Murakami et al., 2018).

Myc Factors comprise a mixture of LCOs and COs and the identification of their receptors has not proven to be straight forward thus far. Given their structural similarity with NFs and the fact that AM and LRS share a signaling pathway (CSP), it was anticipated that similarities would lie also in the perceiving receptors (Zipfel and Oldroyd, 2017). Mutants of *MtNFP* and *MtLYK3* are not altered in mycorrhiza formation (Amor et al., 2003) (Maillet et al., 2011), so they might not be suitable candidates for receptors. Nevertheless NFP perceives Myc signals in a manner, as it is involved in Myc-LCO-induced lateral root formation (Maillet et al., 2011).

The ortholog of *MtNFP/LjNFR5* in tomato (*SILYK10*), but not their ortholog in rice (*OsNFR5/OsRLK2*) (Miyata et al., 2016), seems required for successful AM colonization (Buendia et al., 2016). NFP, NFR5, RLK2 have several paralogs¹⁷ in their respective species (*Medicago*, *Lotus*, rice), and the lack of clear phenotype in the respective mutants might be due to genetic redundancy (Zipfel and Oldroyd, 2017). Among these paralogs, in *M. truncatula* LYR1 and LYR3 are potential candidates for the Myc-LCO receptors as LYR1 is upregulated during mycorrhization, and LYR3 has high affinity for LCOs (Fliegmann et al., 2013) and interacts with the NF-receptor LYK3 in response to LCOs (Fliegmann et

¹⁵ Orthologs are genes in different species that evolved from a common ancestral gene by speciation. Normally orthologs retain the same function in the course of evolution.

¹⁶ Nodule Inception (*NIN*) gene: a transcriptional regulator. In *M. truncatula*, the gene is not essential for early NF signaling but is required for bacterial entry and autoactive CCaMK-induced nodule organogenesis. *MtNIN* also plays a role in restricting the spatial pattern of nodulin gene expression (Marsh et al., 2007). In *L. japonicus* *NIN* is a bifunctional transcription factor that negatively regulates infection but positively regulates nodule organogenesis during the course of symbiosis (Yoro et al., 2014)

¹⁷ Paralogs are genes related by duplication within a genome. Orthologs retain the same function in the course of evolution, whereas paralogs evolve new functions.

al., 2016). Taking the above into consideration, several receptor complexes might be involved in Myc-LCO perception and no definitive candidates for the Myc-LCO receptors have yet emerged. The mixed nature of Myc-Factors comprising both COs and Myc-LCOs might add complexity on the subject (Zipfel and Oldroyd, 2017).

L. japonicus LysM family comprises 17 members (including the NF receptors NFR1 and NFR5). Information on some of them is presented in the lines that follow, with a main focus on those examined in the subsequent chapters of the present dissertation.

LjLys6 demonstrates the highest similarity to LjNFR1 (61% full length amino acid sequence identity). The gene shows no regulation upon symbiont (rhizobia or AMF), NF, CO₄/CO₈ treatment. Lys6 receptor protein shows specificity for chitin, but is not involved in the perception of symbiotic LCOs. Mutant analysis demonstrated that *Ljlys6* mutants are impaired in defense responses elicited in wild plants by COs of various degree of polymerization. Furthermore, *Lys6* has a role in limiting pathogens, as the corresponding mutant shows increased susceptibility to *Botrytis cinerea*. In contrast, the mutant develops a normal nodulation phenotype. In all, Lys6 is a chitin-binding receptor kinase, has a putative role in limiting pathogen proliferation, but has no effects on interaction with symbionts (Bozsoki et al., 2017).

LjLys7 is related to LjNFR1, with which it demonstrates 51% full length amino acid sequence identity (Lohmann et al., 2010).

Lys11 is the closest paralog to LjNFR5. It is not regulated nor is essential during nitrogen-fixing symbiosis (Gomez et al., 2009). Lys11 is upregulated in inner cortical root cells of mycorrhized plants (either arbusculated cells, or cells in close vicinity). It is not expressed in roots exposed to isolated fungal signals, an indication that an intraradical signal produced upon fungal accommodation drives the gene's activation in the inner cortex (Rasmussen et al., 2016). Lys11 acts as an AM-inducible gene, possibly to fine-tune later stages of the interaction. Lys11 can perceive LCOs and initiate intracellular signaling, but has different requirements and a different expression pattern compared to NFR5. Lys11 is transcriptionally regulated during intraradical accommodation of AMF, and downstream of symbiotic genes and spatio-temporal profile showed that it is activated in the cells with arbuscules, or in their close proximity (Rasmussen et al., 2016).

LjLys12 is the ortholog of *MtLyr3*. Together with *LjLys13* it is highly regulated upon *L. japonicus* treatment with the oomycete pathogen *Phytophthora palmivora*. Lys12 is a PM receptor expressed in *P. palmivora*-infected root zones. The protein lacks a kinase domain as also reported for NFR5 (Fuechtbauer et al., 2018)

Three members of this family (*LjLys13*, *LjLys14*, *LjLys20*) have been characterized as chitin regulated in both shoots and roots in *L. japonicus*, with *Lys13* being highly upregulated upon chitin elicitation in root tissues. Lys13 and Lys14 protein sequences are very similar (92% amino acid identity): they have identical LysM domains, whereas their kinase domains slightly differ. Sequence similarity among Lys13 and Lys14 suggest the recognition of very similar to identical ligands. Lys20 kinase domain shows 70% similarity to plant cell wall associated kinases involved in resistance to pathogens (Lohmann et al., 2010).

Moving away from legumes, surprising findings link immunity and symbiosis at the level of microbial molecules recognition by LysM receptors. OsCERK1 receptor in rice and its homolog in Arabidopsis AtCERK1 were identified originally for their role in mediating chitin perception (Miya et al., 2007) (Wan et al., 2008) (Shimizu et al., 2010). The LysM membrane protein OsCEBiP acts as a co-receptor to OsCERK1 and is essential for defense-related chitin perception (Kaku et al., 2006) (Shimizu et al., 2010). Mutant analysis revealed that an *OscebiP* mutant successfully establishes AM symbiosis (Miyata et al., 2014), thus uncoupling OsCEBiP from both chitin-triggered immunity and mycorrhizal symbiotic responses, and suggesting that another OsCERK1 co-receptor might be involved in enabling AM symbiosis. OsCERK1 was later identified to also play a role in AM symbiosis as it mediates the perception of fungal spore exudates and short-chain COs in rice (Carotenuto et al., 2017), and *Oscerk1* mutants demonstrate reduced mycorrhizal colonization levels (Miyata et al., 2014) (Zhang et al., 2015a). This revealed a dual function of the receptor in mediating both chitin triggered immunity to restrict the growth of fungal pathogens and in promoting colonization by AM fungi (MacLean et al., 2017).

1.5.4 Other symbiotic signals

In legumes, besides symbiotic COs and LCOs, other oligosaccharides, including lipopolysaccharides, exopolysaccharides, cyclic β -glucans and peptidoglycans are also known to contribute to establishment of root-nodule symbiosis. Surface polysaccharides of rhizobia are crucial for establishment of successful symbiosis. Unlike nod genes, most of the genes involved in polysaccharide synthesis are located outside of symbiosis island/plasmid (Kucho et al., 2010). Exopolysaccharides can contribute to host specificity. A LysM receptor in *Lotus*, EPR3, mediates recognition of exopolysaccharides from compatible rhizobia and is induced upon perception of Nod-LCO (Kawaharada et al., 2015) (Zipfel and Oldroyd, 2017).

1.5.5 The Common Symbiosis Signaling Pathway (CSSP)

Perception of symbiotic signals by plant cells has been hypothesized to activate a core set of plant genes, a so-called Common Symbiotic Signaling Pathway (CSSP), activated both during AM and LR symbiosis. Initially, seven genes were identified as CSSP components (Kistner et al., 2005). Based on recent evidence, in *L. japonicus* CSSP gene products include: the receptor-like kinase SYMRK (MtDMI2, also known as NORK); three nucleoporins (NUP85, NUP133, and NENA); CASTOR and POLLUX (MtDMI1, Does Not Make Infections 1), cationic channels located on the inner nuclear envelope; a nuclear calcium and calmodulin-dependent kinase CCaMK (MtDMI3); and a CCaMK substrate, CYCLOPS (MtIPD3) (Oldroyd, 2013). HMGR1, a key component of the mevalonate biosynthetic pathway¹⁸ (Kevei et al., 2007), and MCA8, a sarco/endoplasmic reticulum calcium ATPase (SERCA) and putative calcium pump (Capoen et al., 2011), are also considered members of the CSSP in *M. truncatula* (Genre and Russo, 2016).

In *M. truncatula*, *DMI1*, *DMI2*, and *DMI3* are essential components of the CSSP, as the respective mutants are defective for both symbioses (Venkateshwaran et al., 2015).

¹⁸ Mevalonate biosynthetic pathway: or isoprenoid pathway, leads to synthesis of sterols and isoprenoids.

In *L. japonicus* as well, *SYMRK*, *CASTOR*, *POLLUX*, *NUP85*, *NUP133*, *CCaMK*, *CYCLOPS* are also essential components of the CSSP, as the respective mutants are defective for both symbioses [references within (Parniske, 2008)].

The signaling initiates by perception of Nod- and Myc-Factors at the host cell PM, transmission of the signal from the PM to the nucleus, leading to activation of regulatory proteins and symbiosis related gene expression (MacLean et al., 2017). Signal perception initiates with the PM receptor like kinase SYMRK, an essential protein required for both bacterial and fungal endosymbiosis (Stracke et al., 2002). SYMRK interacts with the NFR1 and NFR5 (Ried et al., 2014), and is presumed to act in complex with the NF receptors during NF signaling. Since it is required for mycorrhizal establishment it is also thought to function as co-receptor to the yet unidentified Myc-Factor receptor.

MtDMI2 (NORK) also interacts in vitro with the enzyme 3-hydroxy-3-methylglutaryl CoA reductase 1 (Mt HMGR1), one of the key enzymes of the mevalonate biosynthetic pathway, which is also required for nodule development, thus linking Nod- and Myc- Factor perception with the mevalonate pathway (Kevei et al., 2007). HMGR1 is required for Ca^{2+} spiking initiation, and the direct product of its activity, mevalonate induces nuclear calcium spiking in wt and *dmi2* mutants, but not in *dmi1* (Venkateshwaran et al., 2015). It is hypothesized that HMGR1 has an early role in the CSSP, and mevalonate acts as a secondary messenger transmitting the symbiotic factors perception from the PM to the cell nucleus (Venkateshwaran et al., 2015).

The cationic channels CASTOR and POLLUX (MtDMI1) are preferentially located in the nuclear envelope (Charpentier et al., 2008) and both proteins are required for generation of calcium oscillations in the nucleus (Miwa et al., 2006b). They are nonselective ion channels showing preference for potassium over ions (Charpentier et al., 2008). It is hypothesized that the release of Ca^{2+} from the nuclear envelope lumen is counterbalanced by the opposite flow of potassium ions (K^+) through CASTOR/POLLUX, in a charge compensation mechanism (Genre and Russo, 2016).

In *M. truncatula* MCA8 (the SERCA-type ATPase, nuclear calcium pump) localizes to the nuclear envelope (inner and outer nuclear membrane) and ER. The K^+ -permeable channel DMI1 and MCA8 are necessary for symbiotic calcium oscillations. It was proposed that symbiotic calcium changes (release of calcium) occur in the inner nuclear membrane, and this release allows targeted release of the ER calcium store. Reloading of this calcium store necessitates capture of calcium from the nucleoplasm and nuclear-associated cytoplasm (Capoen et al., 2011).

Cyclic nucleotide-gated channels encoded by CNGC15, and located at the nuclear envelope, were later shown to act as Ca^{2+} -permeable channels responsible for targeted Ca^{2+} release from the nuclear envelope-ER stores to the nucleus. *cngc15* mutants show reduced nodulation and mycorrhization phenotype as well as defected symbiotic gene expression, thus it was presumed to function early in the establishment of both associations (Charpentier et al., 2016).

Three nucleoporins, NUP85, NUP133, and NENA (Kanamori et al., 2006) (Saito et al., 2007) (Groth et al., 2010), are part of the nucleopore scaffold¹⁹ (Alber et al., 2007) and are required for symbiotic Ca^{2+} oscillations. The main function of the nucleopore complex is to mediate macromolecular transport, such as mRNA export and protein import across the nuclear envelope. A putative role for these nucleoporins

¹⁹ Nucleopore scaffold: a complex of proteins (nuclear pore complex) that spans the nuclear envelope.

in nuclear Ca^{2+} spiking could be their implication in the diffusion of a symbiotic signal from the PM to the nucleus in order to activate the spiking response (Charpentier and Oldroyd, 2013).

A nuclear localized calcium and calmodulin-dependent protein kinase (CCaMK) perceives the Ca^{2+} signal and translates it into phosphorylation events (Yano et al., 2008). Nuclear Ca^{2+} spiking induces association of Ca^{2+} -calmodulin with CCaMK, promoting a conformational change in the kinase that stimulates phosphorylation of a target protein, CYCLOPS (Yano et al., 2008) (Miller et al., 2013). *CYCLOPS*, encodes a coiled coil protein required for both AM and rhizobial infection (Yano et al., 2008). It was also shown that *CYCLOPS* is a DNA-binding transcriptional activator, that binds DNA in a sequence specific and phosphorylation-dependent manner, trans-activating the *NODULE INCEPTION* (*NIN*) gene, and initiating gene expression leading to nodule organogenesis (Singh et al., 2014) (MacLean et al., 2017).

1.5.6 Genes downstream the CSSP

Downstream the CSSP lie genes with specific activity in AM or LR symbiosis, or both. Among the genes acting downstream the CSSP are *NSP1*, *NSP2*, and *RAM1* coding for GRAS type transcription factors (TFs). *NSP1* and *NSP2* (Nodulation Signaling Pathway 1 and 2) are essential for all NF-induced changes in gene expression, and they act downstream of DMI3 (Smit et al., 2005) (Kalo et al., 2005). *NSP2* interacts with *NSP1* and promotes the activation of symbiotic markers such as *ENOD11* (Hirsch et al., 2009). *NSP2* and *RAM1* are also involved in the mycorrhiza signaling pathway (Maillet et al., 2011) (Gobbato et al., 2012) (Lauressergues et al., 2012). *RAM1* plays a role in mycorrhization similar to *NSP1* during nodulation by interacting with *NSP2* and activating symbiotic gene expression (Gobbato et al., 2012). Due to their role in both AM and LR symbiosis, *NSP2* and *RAM1* have been proposed to be members of the CSSP (Venkateshwaran et al., 2013).

The fact that *NSP1* was originally described as essential for rhizobial, but not fungal colonization (Catoira et al., 2000) (Smit et al., 2005), and lateral root formation in *M. truncatula* in response to Myc-LCOs was shown to be independent of *NSP1*, (Maillet et al., 2011) suggested that *NSP1* might not be involved in the mycorrhiza signaling pathway. Later on it was shown that *NSP1* is also essential for AM symbiosis: *nsp1* mutants show defects in mycorrhiza formation (Delaux et al., 2013).

IPN2 is a MYB coiled TF that interacts with *NSP2* and also plays a role in nodulation. More specifically, the GRAS domain of *NSP2* interacts with the coiled-coil domain of *IPN2*. *IPN2* shows a strong transcription activation activity, and binds directly to the *NIN* promoter. *IPN2* gene shows elevated expression during nodule development and this coincides with increased *NSP2* gene expression during nodule organogenesis. *IPN2* shows specificity for LRS, as *rnai* knockdown of *IPN2* expression only affected rhizobial infection and nodule formation and not mycorrhizal development. In all, it is hypothesized that *IPN2* forms a TF complex with *NSP2* to promote the expression of a specific set of genes essential for nodule development (Kang et al., 2014).

Other genes that act downstream the CSSP are early nodulin genes, like *ENOD2* and *ENOD40*, possibly linking the pathway with hormonal regulation and organogenesis. Early nodulin genes are so called because they are already expressed at early stages of root nodule development well before the

onset of nitrogen fixation, in contrast to late nodulin genes which are first expressed around the onset of nitrogen fixation, after a complete nodule structure has been formed (van de Wiel et al., 1990).

ENOD40 is an early nodulin gene induced in legume tissues upon NF (Minami et al., 1996), cytokinin (van Rhijn et al., 1997), chitin pentamer treatment (Minami et al., 1996), during nodule organogenesis in both determinate and indeterminate nodules (Yang et al., 1993) (Crespi et al., 1994), in spontaneous nodules (Crespi et al., 1994), during AM infection (van Rhijn et al., 1997). There are at least two distinct *ENOD40* genes in *Lotus japonicus*, *ENOD40-1* and *ENOD40-2*, expressed in symbiotic, non-symbiotic, and embryonic tissues. Both *ENOD40* genes are induced upon *M. loti* treatment or treatment with purified NFs (Flemetakis et al., 2000). *LjENOD40-1* is abundantly expressed at very early stages of rhizobium infection, whereas *LjENOD40-2* is only expressed in mature nodules (Kumagai et al., 2006). *ENOD2* is a (hydroxyl) proline-rich cell wall protein. It is an early nodulin gene expressed in legumes during nodule morphogenesis (Franssen et al., 1987), upon LCO treatment in the LCO-induced nodule primordia which develop into empty (incomplete) nodules (Niwa et al., 2001), by cytokinin (van Rhijn et al., 1997), during rhizobial infection (Franssen et al., 1987) (van de Wiel et al., 1990), during AM infection, but not upon fungal pathogen infection (van Rhijn et al., 1997). *LjENOD2* is induced by NFs, *M. loti* inoculation, and at late stages of nodulation (Takeda et al., 2005).

1.6 Calcium, a versatile secondary messenger

Calcium (Ca^{2+}) is a versatile secondary messenger²⁰ controlling many of the diverse signal-transduction pathways of plants in response to extracellular stimuli.

A question rises, as to how the plant cell discriminates among the various stimulus-induced Ca^{2+} signals to generate specific responses. Information might be encoded within the Ca^{2+} oscillations, thus providing signal specificity. To this respect, in response to individual stimuli, plant cells generate elevations in Ca^{2+} levels that are unique, in terms of their spatio-temporal characteristics. Therefore, information can be encoded in both the amplitude and frequency of the spikes. Ca^{2+} signatures are generated in the cytosol, and in non-cytosolic regions of the cell such as the nucleus and the chloroplast, through coordinated Ca^{2+} influx and efflux pathways (McAinsh and Hetherington, 1998a) (McAinsh and Pittman, 2009).

Cytoplasmic calcium oscillations constitute a general plant cell response to abiotic and biotic stimulation (Knight et al., 1997) (Aldon et al., 2018). Stimulus-induced changes in cytosolic Ca^{2+} concentrations are reported for a diverse range of abiotic factors such as salinity and drought signals (Knight et al., 1997), oxidative stress (Evans et al., 2005), touch, cold (Knight et al., 1991) (van der Luit et al., 1999), plant hormones such as abscisic acid (ABA) (Allen et al., 2001). Nuclear Ca^{2+} elevations are considered a more specific response, and have also been reported upon abiotic stimulation such as wind (van der Luit et al., 1999).

In plant cells, evidence for information encryption through the spatiotemporal dynamics of subcellular Ca^{2+} concentrations originate from studies in stomatal guard cells and the well-known symbiotic associations of legumes (McAinsh and Pittman, 2009). Changes in the cytosolic Ca^{2+} concentrations of

²⁰ Second messenger: a molecule inside cells that acts to transmit signal from a receptor to a target.

guard cells are observed in a wide range of stimuli and constitute a key component in the guard cell signaling pathway maintaining stomatal closure. In *Arabidopsis*, ABA, oxidative stress, extracellular Ca^{2+} concentrations, have been shown to induce Ca^{2+} oscillations in guard cells, resulting in a 'Ca²⁺-programmed' closure of stomata (Allen et al., 2001).

In contrast to the animal field, nuclei of plant cells can produce cell autonomous Ca^{2+} responses and nuclear Ca^{2+} events have distinct roles from those regulated by cytosolic Ca^{2+} release (Charpentier and Oldroyd, 2013).

1.6.1 Role of calcium oscillations in biotic interactions of plants

1.6.1.1 Cytoplasmic calcium oscillations

Rhizobium LCOs have been reported to induce changes in cytoplasmic free calcium in *M. sativa* root hairs and this response was considered a specific plant cell response to NFs as it did not occur in the non-legume tomato. It was also considered an early signal response as a non-nodulating mutant of alfalfa did not exhibit changes in cytosolic Ca^{2+} (Ehrhardt et al., 1996). Rapid and transient elevations in cytosolic free Ca^{2+} has also been reported in culture cells of soybean in response to AMF spores culture medium. The fungal molecules eliciting the response were heat stable and partially lipophilic. The response was considered specific, as the nonhost plant *A. thaliana* did not exhibit the Ca^{2+} response (Navazio et al., 2007).

Cytosolic calcium elevations do not only occur at early steps upon perception of symbiotic molecules. They have also been recorded upon perception of fungal elicitors like chitin and β -glucans (Mithöfer et al., 1999), cell wall fractions and exudates of endophytic fungi (Vadassery et al., 2009) (Johnson et al., 2018), fungal elicitors known to induce phytoalexin²¹ production in plant cells (Knight et al., 1991).

1.6.1.2 Nuclear calcium oscillations

The best studied inducers of nuclear Ca^{2+} responses are the symbiotic signals produced by rhizobial bacteria and AM fungi. These oscillations in the calcium ion are mostly referred to as 'Ca²⁺ spiking': a sharp periodic increase in Ca^{2+} concentration around and in the nucleus of symbiotically stimulated root cells. The plant cell storage that provides Ca^{2+} cations in the nucleus has been a subject of debate. Findings on the localization of cation channels (LjCASTOR/LjPOLLUX, MtDMI1), of a Ca^{2+} -ATPase (MCA8), and of cyclic nucleotide-gated channels acting as putative Ca^{2+} permeable channels at the nuclear envelope (Charpentier et al., 2008) (Capoen et al., 2011) (Charpentier et al., 2016), as well as the spatiotemporal analyses showing the emergence of Ca^{2+} oscillations at the periphery of the nucleus (Sieberer et al., 2009) (Capoen et al., 2011) (Chabaud et al., 2011), as well as the continuity of the nuclear envelope with the ER, corroborate that ER is an ideal Ca^{2+} store for symbiotic signaling (Charpentier and Oldroyd, 2013).

As mentioned above, nuclear oscillations induced by symbionts are cell autonomous, as verified by the generation of nonsynchronous Ca^{2+} spiking between adjacent cells. (Ehrhardt et al., 1996) injected

²¹ Phytoalexin: Phytoalexins are antimicrobial substances produced by plants in response to infection by a pathogen or elicitation by abiotic agents.

multiple alfalfa root hair cells with dextran-linked calcium-selective dyes²² and showed that adjacent cells responding to NF elicitation did not show the same cytosolic spiking patterns and appeared to respond independently. (Miwa et al., 2006a) screened simultaneously adjacent *M. truncatula* root hair cells, and always found that the NF-induced Ca^{2+} spiking mostly associated with the cytoplasm around the nucleus, was a cell-autonomous event: the lag phase to induction and the frequency of the spikes differ. The cell-autonomous nature of NF-elicited calcium spiking within the nuclear compartment was shown by (Sieberer et al., 2009) which screened adjacent growing root hairs of *M. truncatula*. (Chabaud et al., 2011) reported on cell autonomy of nuclear Ca^{2+} spiking responses in adjacent *M. truncatula* and carrot root organ cultures (ROCs) epidermal cells upon elicitation with germinated AM spore exudates. Outer cortical cells adjacent to epidermals responded with low-frequency Ca^{2+} spiking. Irregularity of the oscillatory signal among cells was also shown upon hyphopodium contact, where adjacent epidermal cells showed different response, and the highest oscillatory frequency was observed in cells exhibiting nuclear movement towards the site of hyphopodium contact (Chabaud et al., 2011).

AMF and rhizobia utilize the same signaling pathway for activation of Ca^{2+} oscillations and downstream responses that lead to successful symbiont accommodation. Despite similarities in signaling, specificity must be maintained to ensure an appropriate response to each symbiont. Such specificity of signaling could be encoded within Ca^{2+} oscillations, could be a function of an unknown parallel signaling, could be due to the different cell types that the symbionts use for initial penetration, as rhizobia use root hair cells, while AMF use atrichoblasts (Charpentier and Oldroyd, 2013).

(Kosuta et al., 2008) report on differential calcium responses to NFs and mycorrhizal fungi in *M. truncatula*, and are among the first to report on signal specificity in symbiotic associations of legumes. Differences were reported in the duration of spikes, with the mycorrhiza-induced spike being shorter (major peaks at 30 sec duration) than a NF-induced spike (major peaks at 90 sec duration). The authors suggest that NF-induced and mycorrhiza-induced calcium oscillations are near-periodic and chaotic in nature, thus keeping the response flexible, and easily adaptable.

Therefore, despite the utilization of the same pathway, some sort of discrimination takes place, as various studies have pointed differences in rhizobial-induced and mycorrhizal-induced Ca^{2+} spiking. In root hairs, Ca^{2+} oscillations are induced after a lag period of 6-20 min post NF addition, and show a regular frequency (~100 sec between each spike) after an initial burst of high frequency oscillations (Ehrhardt et al., 1996) (Miwa et al., 2006a) (Sieberer et al., 2009). COs (CO4) on the other hand, produced by AMF elicit irregular and lower-frequency, in comparison to NFs, Ca^{2+} oscillations (Genre et al., 2013). However, when *M. truncatula* outer cortical cells initiating either rhizobial or AM infection where compared with typical spiking responses of NF-elicited root hair nuclei, results were similar among all comparisons: low frequency Ca^{2+} spiking prior to colonization, followed by high frequency Ca^{2+} spiking with similar spike width and periodicity, as those observed for NFs (Sieberer et al., 2012). (Russo et al., 2013) performed a waiting time autocorrelation analysis of NF and AM-exudate induced Ca^{2+} spiking in *M. truncatula* ROC epidermal cells and found that a regular peak to peak interval

²² Dextran-linked calcium-selective dyes remain in the cytosol without compartmentalization or leakage, and show affinity for Ca^{2+} . They can be used for ratiometric measurements of Ca^{2+} flux in cells after microinjection with the dye.

characterizes response to NFs (long and short waiting times followed by long and short waiting times), in contrast to a non-regular pattern in CO₄-induced Ca²⁺ spiking (most cells alternate short and long waiting times).

Studies on the topic point out that Myc and NFs trigger diverse Ca²⁺ signaling responses, and the pattern of these responses, estimated through the periodicity and the shape of the oscillatory response, is dependent on the concentration of symbiotic factors and probably the mix of Myc factors (Charpentier and Oldroyd, 2013).

It is of interest that upon presence of either symbiont (not isolated symbiotic signals) the pathway of the infection process is guided by the Ca²⁺ spiking response itself: the cells exhibiting high-frequency Ca²⁺ oscillations are the ones that 'await' and undergo the appropriate reprogramming associated with imminent penetration (Sieberer et al., 2012).

1.7 Commonalities in PMIs

Similarities in recognition of symbiotic and pathogenic fungi reveal an at least partially common set of responses at the cellular and molecular level. Here, I discuss in brief the main commonalities reported over the years by the plant-microbe interactions community with an emphasis in plant-fungal associations:

1.7.1 Cellular level

At the subcellular level plant cells undergo a reprogramming when in contact with a microbe. Similarities are well reported in the AM and LR symbiosis, but certain features are also shared by other types of plant-interacting fungi. The cytoskeleton of the plant cell plays an important role in the preparation of the plant cell to accommodate another organism (either prokaryotic or eukaryotic). Main common features are:

- Cytoplasmic aggregation (CA): a cytoskeleton-driven accumulation of organelles, including the nucleus, at contact sites. CA at plant-microbe contact site was first described many years ago, and has been observed in various interactions. Some of these cases are cited herein: (Tomiya, 1957) reported an acceleration of cytoplasmic movements upon contact of resistant potato varieties by the pathogenic oomycete *Phytophthora infestans*. During this phase of infection initiation, a migration of nuclei towards the infected part and a protoplasmic streaming around the infected part occur. These cytoplasmic movements decrease and finally disappear as the host cell dies. (Gross et al., 1993) reported also a rapid translocation of plant cell cytoplasm and nucleus to the fungal penetration site in a parsley-*P. infestans* pathogenic interaction. Translocation was dependent on intact actin filaments. (Takemoto et al., 2003) investigated pathogenic and non-pathogenic *Arabidopsis*-oomycete interactions and reported that cytoplasmic strands of actin microfilaments, ER, and Golgi bodies aggregate at penetration site, indication of active production and secretion of plant materials at contact site. (Koh et al., 2005a) investigated a compatible *A. thaliana*-*Erysiphe cichoracearum* (powdery mildew fungus) interaction and reported that at early stages cytoplasm and organelles (nucleus and

peroxisomes) moved towards penetration sites and accumulated near penetration pegs²³. (Genre et al., 2005) described the prepenetration apparatus (PPA), a nucleus-directed cytoskeletal/ER assembly within the *M. truncatula* epidermal cell in response to the AM fungus *G. margarita* appressorium formation. PPA is rich in cytoskeleton and secretory endomembranes. In a following study, (Genre et al., 2009) showed that PPA formation occurs only in association with an AM symbiont, whereas CA correlates with the contact by compatible fungi as it occurred in *Medicago* ROC epidermal cells whether in contact with a symbiont or a pathogen. On the other hand, nucleus migration was considered a more general, non-specific response to physical stimulation, which can be uncoupled from CA. Also in LR symbiosis, upon contact with rhizobia, a broad cytoplasmic column is progressively formed (the IT) in a root hair cell. The nucleus migrates close to the infection focus, and the cytoskeleton within the root hair aligns along the length of the root hair, forming a pre-IT structure. This serves to guide the inward growth of the IT initiated from the infection focus (Oldroyd et al., 2011).

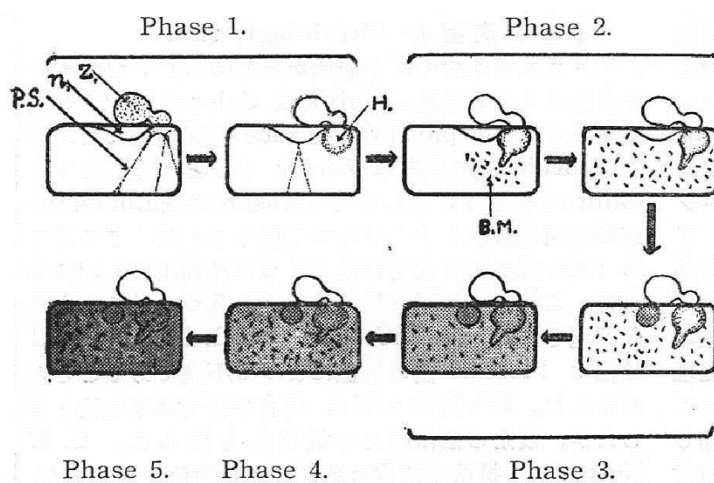


Figure 1-7 An old sketch from (Tomiya, 1957) nicely describing the degeneration process in the cells of a highly resistant potato variety infected by the oomycete *P. infestans*. Note the cytoplasmic accumulation (resembling a column) and nuclear migration at infection site during phase 1.

Phase 1: nuclei and protoplasmic strands around the infected part. Phase 2: granules in Brownian motion appear around the hyphae. Phase 3: the host cell dies and the cell content becomes yellowish. Phase 4: the cell content turns pale brown. Phase 5: the cell content finally turns blackish.

P.S., protoplasmic strands; n, nucleus; Z, zoospore and appressoria; H, infecting hyphae.

- Membrane dynamics and formation of plant-derived apoplastic compartments: steady plant derived infection compartments persisting throughout the infection and colonization process in all infected plant cells have been described only for the AM and LRS. In AM symbiosis, the AM fungus is well-confined and cytosol-excluded throughout the infection and colonization process. In LR symbiosis, the progressively grown tubular structure (IT) provides the cell machinery for tip growth, involving targeted exocytosis of membrane and extracellular materials to the growing

²³ Penetration peg: a thin hypha extending from the base of an appressorium and perforates the host surface.

apex of the IT. The growing tip of this apoplastic infection compartment is connected via a cytoplasmic bridge to the migrating nucleus of the root hair. This cytoplasmic bridge is considered equivalent to the PPA formed at the onset of AM fungal infection (Fournier et al., 2015). Ephemeral compartments have been described for other biotrophic interactions. For example, (Kankanala et al., 2007b) report that during the biotrophic state of the rice blast fungus (*Magnaporthe oryzae*) dynamic plant derived membranes surround the invasive hyphae of the fungus, and have multiple connections to peripheral rice cell membranes. While cell invasions were initially biotrophic, cell viability was lost when the fungus moved into adjacent cells. The endophytic plant growth promoting fungus *P. indica*, was also shown to be cytosol excluded and surrounded by an intact plant-derived membrane throughout intracellular growth in living barley root cells (Zuccaro et al., 2011). Another similar case is the interaction of the endophytic fungal isolate *C. tofieldiae* with *A. thaliana*: at the beginning of the interaction fungal cells that enter the root epidermal cells are enveloped by the host PM, indicating that the fungus establishes a biotrophic interaction with living host cells. Epidermal cells die soon after penetration, but adjacent recently colonized cells retain viability (Hiruma et al., 2016). Intense membrane dynamics is a common feature of PMIs, but the outcome of the association is 'judged' by the 'timeframe' during which a steady biotrophic interaction is maintained within plant cells, ensured only by the successful construction of an apoplastic compartment that will hold the 'microbial intruder' cytosol excluded.

1.7.2 Molecular level

With this section I aim to describe reports on the utilization of the CSSP and nuclear Ca^{2+} oscillations by other plant-interacting microbes. Many research groups have investigated the potential implication of this common set of genes, in their interaction systems.

A partial involvement of the pathway was shown in roots of non-symbiotic associations of *M. truncatula*, and more specifically, in its interaction with the rhizobacterium *Pseudomonas fluorescens*. Ten genes highly regulated in this interaction, are also regulated in interaction of *M. truncatula* with the AM fungus *Glomus mosseae*, and this induction in both interactions is *DMI3*-dependent, as verified by analysis of the corresponding mutant. One gene out of the ten, was a Ca^{2+} and calmodulin-dependent protein kinase, which was the only gene induced by *P. fluorescens* in the *dmi3* mutant background, indicating that calcium plays a role in the association. None of the genes was induced upon inoculation with the rhizobial microsymbiont of *M. truncatula* *S. meliloti* (Sanchez et al., 2005).

In interactions of legumes with parasites, a partial involvement of the pathway was shown in an association of *L. japonicus* with plant-parasitic root-knot nematodes. It was shown that *Lotus* root hairs respond to nematodes with a cytoskeletal response similar to that seen in response to NFs (root hair waviness and branching). These responses as well as the nematodes' ability to establish feeding sites and reproduce are *NFR1*, *NFR5*, and *SYMRK* dependent, as verified by analysis of the corresponding mutants (Weerasinghe et al., 2005).

In interactions of legumes with parasitic plants, (Fernandez-Aparicio et al., 2010) showed that *DMI2* and *DMI3* genes negatively control the infection of *M. truncatula* and pea by the parasitic plant

Orobancha crenata, by limiting the number of infection events. Mutant analysis showed either increase in the number of germinated seeds contacting the host root, or increase in the parasitic nodule establishment.

RAM2, the TF acting downstream Ca^{2+} spiking events in AM symbiosis, and controls the appropriate establishment of symbiosis, was also shown to control the infection of *M. truncatula* by oomycetes. Mutants of *RAM2* show defects in colonization by the oomycete pathogen *Phytophthora palmivora*, and more specifically absence of appressoria formation (Wang et al., 2012).

(Zgadza et al., 2015) investigated endophytic bacteria that utilize the infection route (IT) used by rhizobia, to effectively colonize the interior of *L. japonicus* root nodules. Analysis of symbiotic mutants of *Lotus* in genes involved in control of IT initiation and elongation, showed reduced colonization capabilities of the nodule inhabiting endophytic bacterium to infect nodule primordia, indication that symbiotic genes are necessary for successful infection of the IT by the endophytic bacterium. The authors conclude that the legume host controls the access into nodules for both symbionts and endophytes when ITs are used as entry routes.

At the root microbiota communities level, the structure of bacterial and fungal communities in the roots of *L. japonicus* mutants defected in key symbiotic genes was investigated. Major community shifts were observed: bacterial taxa were affected in *nfr1* and *nfr5* mutants, fungal taxa were affected in *ram1* mutants, members of both microbial kingdoms were affected in *symRK* and *ccamk* mutants. The authors concluded that symbiosis genes structure the root microbiota in *L. japonicus* (Zgadza et al., 2019).

(Gherbi et al., 2008) showed that the receptor kinase SYMRK is also required for actinorhiza formation and establishment of AM symbiosis in the tree *Casuarina glauca* (Fagales). The authors recorded reduced nodulation in *rnai* hairy roots of *Casuarina glauca* showing reduced expression levels of *CgSYMRK*. These lines when inoculated with *Glomus intraradices* they showed very weak levels of AM colonization. A conserved role for SYMRK, in both legumes and actinorhiza-forming Fagales, was pinpointed through this study.

Similar to results concerning SYMRK gene in actinorrhizal plants (Gherbi et al., 2008), CCaMK gene was also shown to be necessary for successful actinorhiza formation (nodulation by *Frankia* bacteria) and interaction with AM fungi in the actinorrhizal tree *Casuarina glauca*. Autoactive CgCCaMK lacking the autoinhibitory CaM domain, was able to induce spontaneous nodulation in the absence of *Frankia* bacteria in two actinorrhizal species, as previously shown for CCaMK in LR symbiosis (Gleason et al., 2006) (Tirichine et al., 2006), further corroborating the recruitment of similar genetic machineries in rhizobial and *Frankia* nodule organogenesis (Svistonoff et al., 2013).

1.8 Legume mutants as a useful tool to investigate PMIs

One of the interests of the PMIs community is the use of *L. japonicus* to dissect the genetic background of symbiosis. For this purpose, tools for molecular analysis were developed. Several methods have been used to establish *L. japonicus* mutant lines: (a) Insertion mutagenesis using T-DNA or the maize transposon Ac, (b) Chemical mutagenesis with Ethyl methanesulfonate (EMS), (c) The TILLING method (targeting-induced local lesions in genomes) allowed for generation of a TILLING population for reverse

genetics (Perry et al 2003), (d) the large LORE1 insertion population was generated via an endogenous retrotransposon LORE1, which generates independent new insertions in the pollen germ line of regenerated plants. In this manner both forward genetics (screening for interesting phenotypes) and reverse genetics (identification of insertion mutants in genes of interest) can be achieved.

Deficiencies occurring in nodulation mutants can be saved by providing sufficient nitrogen on the substrate. In this manner, developmental control genes implicated in other organogenetic processes besides nodulation and that would compromise development of the plant and completion of its life cycle, can thus be identified by using nodulation mutant plants. More than 40 symbiotic loci have been identified by screening EMS, T-DNA, LORE1, and Ac populations of *L. japonicus*. 3 classes of developmental plant mutants are identified by these screening: a) non-nodulating mutants arrested in bacterial recognition or nodule initiation, b) nodule development mutants arrested in consecutive stages of the organogenetic process, c) autoregulatory mutants where the plant control of root nodule numbers is nonfunctional, and d) spontaneous nodulating plant mutant developing root nodules in the absence of the rhizobial microsymbiont.

Loss-of-function and gain-of-function mutants allowed to investigate the role of individual genes in the highly synchronized infection and organogenetic pathways which lead to functional nitrogen fixing root nodules. By combining loss-of-function and gain-of-function mutations in synthetic mutants it was shown that *L. japonicus* possess three different infection routes for bacterial entry (single-cell peg entry, crack entry, and infection thread formation), providing evidence for the evolution of rhizobial invasion in the following order: direct intercellular epidermal invasion, crack entry, root hair invasions, as the latter is mostly encountered in extant legume species (Stougaard, 2013).

Towards the characterization of processes occurring during AM symbiosis at the molecular level, abnormal AM phenotypes have been identified in mutant plant lines, most frequently developed in legumes. The knowledge on common steps in AM and LRS at the molecular level, is mainly due to plant mutants affected in both LR and mycorrhiza development. Screenings for mutants affected in AM symbiosis have been most exclusively performed in mutants originally characterized as deficient in root nodule formation (Nod-) or function (Nod+/Fix-), providing us with mutants altered in both types of symbiosis (Marsh and Schultze, 2001).

In the present dissertation various mutants were screened. I provide details for some of these mutants in order to assist further reading.

In the Table I-1 characteristics of mutants in main components of the CSSP are presented. For simplification, the main symbiotic phenotype is reported, and no details on the different alleles of the mutant are included.

Table 1-1 Overview of some of the CSSP mutants and their corresponding phenotypes.

AM CSSP mutant phenotypes: Type I, impaired epidermal opening; Type II, impaired intracellular passage through the outer cell layer (or layers); Type III, impaired arbuscule formation.

Non-nodulating type II: Root-hair swelling and branching occurs after inoculation with *Mesorhizobium loti*, but neither infection threads nor nitrogen-fixing nodules are formed.

Modified from (Parniske, 2008) and updated herein, references within the cited article.

Gene	Mutants		Phenotypes of <i>Lotus</i> mutants		Ca ²⁺ spiking	Predicted function
	<i>L. japonicus</i>	<i>M. truncatula</i>				
SYMRK	<i>symrk</i> (<i>sym2</i>)	<i>dmi2</i> and <i>M. sativa nork</i>	Type II	non-nodulating II	No	Leucine-rich repeat receptor kinase
CASTOR	<i>castor</i> (<i>sym4</i> and <i>sym71</i>)	Unknown	Types II, III	non-nodulating II	No	Cation channel
POLLUX	<i>pollux65</i> (<i>sym23</i> and <i>sym86</i>)	<i>dmi1</i>	Type II	non-nodulating II	No	Cation channel
CCaMK	<i>ccamk</i> (<i>sym15</i> and <i>sym72</i>)	<i>dmi3</i>	Types I, II, III	non-nodulating II	Yes	Calcium and calmodulin-dependent protein kinase
CYCLOPS	<i>cyclops</i> (<i>sym6</i> , <i>sym30</i> and <i>sym82</i>)	<i>ipd3</i>	Types II, III	Small, non-infected nodules	Yes	Phosphorylation substrate of CCaMK – DNA binding TF

1.9 References

- Abdelaziz ME, Kim D, Ali S, Fedoroff N V., Al-Babili S. 2017.** The endophytic fungus *Piriformospora indica* enhances *Arabidopsis thaliana* growth and modulates Na⁺/K⁺ homeostasis under salt stress conditions. *Plant Science* **263**: 107–115.
- Achatz B, Kogel KH, Franken P, Waller F. 2010.** *Piriformospora indica* mycorrhization increases grain yield by accelerating early development of barley plants. *Plant Signaling and Behavior* **5**: 1685–1687.
- Aimé S, Alabouvette C, Steinberg C, Olivain C. 2013.** The Endophytic Strain *Fusarium oxysporum* Fo47: A Good Candidate for Priming the Defense Responses in Tomato Roots. *Molecular Plant-Microbe Interactions* **26**: 918–926.
- Aldon D, Mbengue M, Mazars C, Galaud JP. 2018.** Calcium signalling in plant biotic interactions. *International Journal of Molecular Sciences* **19**: 1–19.
- Allen GJ, Chu SP, Harrington CL, Schumacher K, Hoffmann T, Tang YY, Grill E, Schroeder JI. 2001.** A defined range of guard cell calcium oscillation parameters encodes stomatal movements. *Nature* **411**: 1053–1057.
- Amor B Ben, Shaw SL, Oldroyd GED, Maillet F, Penmetsa RV, Cook D, Long SR, Dénarié J, Gough C. 2003.** The NFP locus of *Medicago truncatula* controls an early step of Nod factor signal transduction upstream of a rapid calcium flux and root hair deformation. *Plant Journal* **34**: 495–506.
- Anderson IC, Cairney JWG. 2007.** Ectomycorrhizal fungi: exploring the mycelial frontier. *FEMS Microbiol Rev* **31**: 388–406.
- Aoki T, Donnell KO, Homma Y, Lattanzi AR. 2003.** Sudden-death syndrome of soybean is caused by two morphologically and phylogenetically distinct species within the *Fusarium solani* species complex — *F. virguliforme* in North America and *F. tucumaniae* in South America. *Mycologia* **95**: 660–684.
- Arrighi J-F, Barre A, Amor B Ben, Bersoult A, Soriano LC, Mirabella R, de Carvalho-Niebel F, Journet E-P, Gherardi M, Huguet T, et al. 2006.** The *Medicago truncatula* Lysine Motif-Receptor-Like Kinase Gene Family Includes *NFP* and New Nodule-Expressed Genes. *Plant Physiology* **142**: 265–279.
- Bacon CW, Yates IE. 2006.** Endophytic Root Colonization by *Fusarium* Species: Histology, Plant Interactions, and Toxicity. In: B.J.E. S, C.J.C. B, T.N. S, eds. *Microbial Root Endophytes*. Soil Biology, vol 9. Springer, Berlin, Heidelberg.
- Barker DG, Bianchi S, Blondon F, Duc G, Essad S, Flament P, Gdnier G, Guy P, Muel X, Ddnarid J, et al. 1990.** *Medicago truncatula*, a model plant for studying the molecular genetics of the Rhizobium-Legume Symbiosis. *Plant Molecular Biology Reporter* **8**: 40–49.
- De Bary A. 1879.** *Die erschenung symbiose*. (Verlag von Karl J. Trubner, Ed.). Strassburg.
- Bell CJ, Dixon RA, Farmer AD, Flores R, Inman J, Gonzales RA, Harrison MJ, Paiva NL, Scott AD, Weller JW, et al. 2001.** The *Medicago* Genome Initiative: a model legume database. *Nucleic Acids Research* **29**: 114–117.
- Bonfante P, Genre A. 2008.** Plants and arbuscular mycorrhizal fungi: an evolutionary-developmental perspective. *Trends in Plant Science* **13**: 492–498.
- Bonfante P, Genre A. 2010.** Mechanisms underlying beneficial plant-fungus interactions in mycorrhizal symbiosis. *Nature communications* **1**: 48.

- Bozsoki Z, Cheng J, Feng F, Gysel K, Vinther M, Andersen KR, Oldroyd G, Blaise M, Radutoiu S, Stougaard J. 2017.** Receptor-mediated chitin perception in legume roots is functionally separable from Nod factor perception. *Proceedings of the National Academy of Sciences* **114**: E8118–E8127.
- Buendia L, Girardin A, Wang T, Cottret L, Lefebvre B. 2018.** LysM receptor-like kinase and lysM receptor-like protein families: An update on phylogeny and functional characterization. *Frontiers in Plant Science* **871**: 1–25.
- Buendia L, Wang T, Girardin A, Lefebvre B. 2016.** The LysM receptor-like kinase SILYK10 regulates the arbuscular mycorrhizal symbiosis in tomato. *New Phytologist* **210**: 184–195.
- Capoen W, Sun J, Wysham D, Otegui MS, Venkateshwaran M, Hirsch S, Miwa H, Downie JA, Morris RJ, Ané J-M, et al. 2011.** Nuclear membranes control symbiotic calcium signaling of legumes. *Proceedings of the National Academy of Sciences of the United States of America* **108**: 14348–14353.
- Carotenuto G, Chabaud M, Miyata K, Capozzi M, Takeda N, Kaku H, Shibuya N, Nakagawa T, Barker DG, Genre A. 2017.** The rice LysM receptor-like kinase OsCERK1 is required for the perception of short-chain chitin oligomers in arbuscular mycorrhizal signaling. *New Phytologist* **214**: 1440–1446.
- Carotenuto G, Volpe V, Russo G, Politi M, Sciascia I, de Almeida-Engler J, Genre A. 2019.** Local endoreduplication as a feature of intracellular fungal accommodation in arbuscular mycorrhizas. *New Phytologist* **223**: 430–446.
- Catoira R, Galera C, de Billy F, Penmetsa RV, Journet E-P, Maillet F, Rosenberg C, Cook D, Gough C, Denarie J. 2000.** Four Genes of *Medicago truncatula* Controlling Components of a Nod Factor Transduction Pathway. *The Plant Cell* **12**: 1647–1665.
- Chabaud M, Genre A, Sieberer BJ, Faccio A, Fournier J, Novero M, Barker DG, Bonfante P. 2011.** Arbuscular mycorrhizal hyphopodia and germinated spore exudates trigger Ca²⁺ spiking in the legume and nonlegume root epidermis. *New Phytologist* **189**: 347–355.
- Charpentier M, Bredemeier R, Wanner G, Takeda N, Schleiff E, Parniske M. 2008.** *Lotus japonicus* CASTOR and POLLUX are ion channels essential for perinuclear calcium spiking in legume root endosymbiosis. *The Plant Cell* **20**: 3467–79.
- Charpentier M, Oldroyd GED. 2013.** Nuclear Calcium Signaling in Plants. *Plant Physiology* **163**: 496–503.
- Charpentier M, Sun J, Martins TV, Radhakrishnan G V, Findlay K, Soumpourou E, Thouin J, Véry A, Sanders D, Morris RJ, et al. 2016.** Nuclear-localized cyclic nucleotide-gated channels mediate symbiotic calcium oscillations. *Science* **352**: 1102–1106.
- Choi J, Summers W, Paszkowski U. 2018.** Mechanisms Underlying Establishment of Arbuscular Mycorrhizal Symbioses. *Annual Review of Phytopathology* **56**: 135–160.
- Coleman JJ. 2016.** The *Fusarium solani* species complex: ubiquitous pathogens of agricultural importance. *Molecular Plant Pathology* **17**: 146–158.
- Coleman JJ, Rounsley SD, Rodriguez-Carres M, Kuo A, Wasmann CC, Grimwood J, Schmutz J, Taga M, White GJ, Zhou S, et al. 2009.** The Genome of *Nectria haematococca*: Contribution of Supernumerary Chromosomes to Gene Expansion. *PLoS Genetics* **5**: e1000618.
- Crespi MD, Jurkevitch E, Poiret M, D'Aubenton-Carafa Y, Petrovics G, Kondorosi E, Kondorosi A. 1994.** enod40, a gene expressed during nodule organogenesis, codes for a non-translatable RNA

involved in plant growth. *The EMBO journal* **13**: 5099–5112.

Delaux P-M, Becard G, Combier J-P. 2013. NSP1 is a component of the Myc signaling pathway. *New Phytologist* **199**: 59–65.

Deshmukh S, Hückelhoven R, Schäfer P, Imani J, Sharma M, Weiss M, Waller F, Kogel K-H. 2006. The root endophytic fungus *Piriformospora indica* requires host cell death for proliferation during mutualistic symbiosis with barley. *Proceedings of the National Academy of Sciences of the United States of America* **103**: 18450–18457.

Divon HH, Fluhr R. 2007. Nutrition acquisition strategies during fungal infection of plants. *FEMS Microbiology Letters* **266**: 65–74.

Downie JA. 2014. Legume nodulation. *Current Biology* **24**: R184–R190.

Ehrhardt DW, Wais R, Long SR. 1996. Calcium spiking in plant root hairs responding to rhizobium modulation signals. *Cell* **85**: 673–681.

Evans NH, McAinsh MR, Hetherington AM, Knight MR. 2005. ROS perception in *Arabidopsis thaliana*: The ozone-induced calcium response. *Plant Journal* **41**: 615–626.

Fernandez-Aparicio M, Rispaill N, Prats E, Morandi D, Garcia-Garrido JM, Dumas-Gaudot E, Duc G, Rubiales D. 2010. Parasitic plant infection is partially controlled through symbiotic pathways. *Weed Research* **50**: 76–82.

Flemetakis E, Kavroulakis N, Quaedvlieg NE, Spaink HP, Dimou M, Roussis A, Katinakis P. 2000. *Lotus japonicus* contains two distinct ENOD40 genes that are expressed in symbiotic, nonsymbiotic, and embryonic tissues. *Molecular plant-microbe interactions : MPMI* **13**: 987–94.

Fliegmann J, Canova S, Lachaud C, Uhlenbroich S, Gasciolli V, Pichereaux C, Rossignol M, Rosenberg C, Cumener M, Pitorre D, et al. 2013. Lipo-chitooligosaccharidic Symbiotic Signals Are Recognized by LysM Receptor-Like Kinase LYR3 in the Legume *Medicago truncatula*. *ACS Chemical Biology* **8**: 1900–1906.

Fliegmann J, Jauneau A, Pichereaux C, Rosenberg C, Gasciolli V, Timmers ACJ, Burlet-Schiltz O, Cullimore J, Bono JJ. 2016. LYR3, a high-affinity LCO-binding protein of *Medicago truncatula*, interacts with LYK3, a key symbiotic receptor. *FEBS Letters* **590**: 1477–1487.

Fournier J, Teillet A, Chabaud M, Ivanov S, Genre A, Limpens E, Carvalho-niebel F De, Barker DG. 2015. Remodeling of the Infection Chamber before Infection Thread Formation Reveals a Two-Step Mechanism for Rhizobial Entry into the Host Legume Root Hair. *Plant Physiology* **167**: 1233–1242.

Franssen HJ, Nap J-P, Gloudemans T, Stiekema W, Van Dam H, Govers F, Louwerse J, Van Kammen A, Bisseling T. 1987. Characterization of cDNA for nodulin-75 of soybean: A gene product involved in early stages of root nodule development. *Proceedings of the National Academy of Sciences* **84**: 4495–4499.

Fuechtbauer W, Yunusov T, Bozsóki Z, Gavrin A, James EK, Stougaard J, Schornack S, Radutoiu S. 2018. LYS12 LysM receptor decelerates *Phytophthora palmivora* disease progression in *Lotus japonicus*. *Plant Journal* **93**: 297–310.

Gallardo K, Lesignor C, Darmency M, Burstin J, Thompson R. 2006. Seed biology of *Medicago truncatula*. In: U M, EP J, LW S, eds. *Medicago truncatula* handbook.

Garantonakis N, Pappas ML, Varikou K, Skiada V, Broufas GD, Kavroulakis N, Papadopoulou

- KK. 2018.** Tomato Inoculation With the Endophytic Strain *Fusarium solani* K Results in Reduced Feeding Damage by the Zoophytophagous Predator *Nesidiocoris tenuis*. *Frontiers in Ecology and Evolution* **6**: 126.
- Geiser DM, Aoki T, Bacon CW, Baker SE, Bhattacharyya MK, Brandt ME, Brown DW, Burgess LW, Chulze S, Coleman JJ, et al. 2013.** One Fungus, One Name: Defining the Genus *Fusarium* in a Scientifically Robust Way That Preserves Longstanding Use. *Phytopathology* **103**: 400–408.
- Genre A, Chabaud M, Balzergue C, Puech-Pagès V, Novero M, Rey T, Fournier J, Rochange S, Bécard G, Bonfante P, et al. 2013.** Short-chain chitin oligomers from arbuscular mycorrhizal fungi trigger nuclear Ca^{2+} spiking in *Medicago truncatula* roots and their production is enhanced by strigolactone. *New Phytologist* **198**: 190–202.
- Genre A, Chabaud M, Timmers T, Bonfante P, Barker DG. 2005.** Arbuscular mycorrhizal fungi elicit a novel intracellular apparatus in *Medicago truncatula* root epidermal cells before infection. *The Plant Cell* **17**: 3489–3499.
- Genre A, Ortu G, Bertoldo C, Martino E, Bonfante P. 2009.** Biotic and abiotic stimulation of root epidermal cells reveals common and specific responses to Arbuscular Mycorrhizal Fungi. *Plant physiology* **149**: 1424–1434.
- Genre A, Russo G. 2016.** Does a common pathway transduce symbiotic signals in plant-microbe interactions? *Frontiers in Plant Science* **7**: 96.
- Gepts P, Beavis WD, Brummer EC, Shoemaker RC, Stalker HT, Weeden NF, Young ND. 2005.** Legumes as a Model Plant Family. Genomics for Food and Feed Report of the Cross-Legume Advances through Genomics Conference. *Plant Physiology* **137**: 1228–1235.
- Gherbi H, Markmann K, Svistoonoff S, Estevan J, Autran D, Gabor G, Auguy F, Peret B, Laplaze L, Franche C, et al. 2008.** SymRK defines a common genetic basis for plant root endosymbioses with arbuscular mycorrhiza fungi, rhizobia, and Frankia bacteria. *PNAS* **105**: 4928–4932.
- Gibelin-Viala C, Amblard E, Puech-Pages V, Bonhomme M, Garcia M, Bascaules-Bedin A, Fliegmann J, Wen J, Mysore KS, le Signor C, et al. 2019.** The *Medicago truncatula* LysM receptor-like kinase LYK9 plays a dual role in immunity and the arbuscular mycorrhizal symbiosis. *New Phytologist* **0**.
- Gleason C, Chaudhuri S, Yang TB, Munoz a, Poovaiah BW, Oldroyd GED. 2006.** Nodulation independent of rhizobia induced by a calcium-activated kinase lacking autoinhibition. *Nature* **441**: 1149–1152.
- Gobbato E, Marsh JF, Vernié T, Wang E, Maillet F, Kim J, Miller JB, Sun J, Bano SA, Ratet P, et al. 2012.** A GRAS-type transcription factor with a specific function in mycorrhizal signaling. *Current Biology* **22**: 2236–2241.
- Gomez SK, Javot H, Deewatthanawong P, Torres-Jerez I, Tang Y, Blancaflor EB, Udvardi MK, Harrison MJ. 2009.** *Medicago truncatula* and *Glomus intraradices* gene expression in cortical cells harboring arbuscules in the arbuscular mycorrhizal symbiosis. *BMC Plant Biology* **9**: 1–19.
- Gow NAR, Latge J-P, Munro CA. 2017.** The Fungal Cell Wall: Structure, Biosynthesis, and Function. *Microbiol Spectrum* **5**: FUNK-0035-2016.
- Graham PH, Vance CP. 2003.** Update on Legume Utilization Legumes: Importance and Constraints to

Greater Use. *Plant Physiology* **131**: 872–877.

Greeff C, Roux M, Mundy J, Petersen M. 2012. Receptor-like kinase complexes in plant innate immunity. *Frontiers in Plant Science* **3**: 1–7.

Gross P, Julius C, Schmelzer E, Hahlbrock K. 1993. Translocation of cytoplasm and nucleus to fungal penetration sites is associated with depolymerization of microtubules and defence gene activation in infected, cultured parsley cells. *The EMBO Journal* **12**: 1735–1744.

Groth M, Takeda N, Perry J, Uchida H, Dräxl S, Brachmann A, Sato S, Tabata S, Kawaguchi M, Wang TL, et al. 2010. NENA, a *Lotus japonicus* homolog of Sec13, is required for rhizodermal infection by arbuscular mycorrhiza fungi and rhizobia but dispensable for cortical endosymbiotic development. *The Plant cell* **22**: 2509–2526.

Hacquard S, Kracher B, Hiruma K, Münch PC, Garrido-Oter R, Thon MR, Weimann A, Damm U, Dallery JF, Hainaut M, et al. 2016. Survival trade-offs in plant roots during colonization by closely related beneficial and pathogenic fungi. *Nature Communications* **7**.

Hafizi R, Salleh B, Latiffah Z. 2013. Morphological and molecular characterization of *Fusarium solani* and *F. oxysporum* associated with crown disease of oil palm. *Brazilian Journal of Microbiology* **44**: 959–968.

Hamid A, Bhat NA, Sofi TA, Bhat KA, Asif M. 2012. Management of root rot of pea (*Pisum sativum* L.) through bioagents. *African Journal of Microbiology Research* **6**: 7156–7161.

Hirsch S, Kim J, Munoz A, Heckmann AB, Downie JA, Oldroyd GED. 2009. GRAS Proteins Form a DNA Binding Complex to Induce Gene Expression during Nodulation Signaling in *Medicago truncatula*. *The Plant Cell* **21**: 545–557.

Hiruma K, Gerlach N, Sacristán S, Nakano RT, Hacquard S, Kracher B, Neumann U, Ramírez D, Bucher M, O’Connell RJ, et al. 2016. Root endophyte *Colletotrichum tofieldiae* confers plant fitness benefits that are phosphate status dependent. *Cell* **165**: 464–474.

Imazaki I, Kadota I. 2015. Molecular phylogeny and diversity of *Fusarium* endophytes isolated from tomato stems. *FEMS Microbiology Ecology* **91**: 1–16.

Jacobs S, Zechmann B, Molitor A, Trujillo M, Petutschnig E, Lipka V, Kogel K-H, Schäfer P. 2011. Broad-spectrum suppression of innate immunity is required for colonization of *Arabidopsis* roots by the fungus *Piriformospora indica*. *Plant physiology* **156**: 726–740.

Johnson JM, Ludwig A, Furch ACU, Mithöfer A, Scholz S, Reichelt M, Oelmüller R. 2018. The Beneficial Root-Colonizing Fungus *Mortierella hyalina* Promotes the Aerial Growth of *Arabidopsis* and Activates Calcium-Dependent Responses That Restrict *Alternaria brassicae*-Induced Disease Development in Roots. *Molecular Plant-Microbe Interactions* **32**: 351–363.

Kaku H, Nishizawa Y, Ishii-minami N, Akimoto-tomiyama C, Dohmae N, Takio K, Minami E, Shibuya N. 2006. Plant cells recognize chitin fragments for defense signaling through a plasma membrane receptor. : 1–6.

Kalo P, Gleason C, Edwards A, Marsh J, Mitra RM, Hirsch S, Jakab J, Sims S, Long SR, Rogers J, et al. 2005. Nodulation Signaling in Legumes Requires NSP2, a Member of the GRAS Family of Transcriptional Regulators. *Science* **308**: 1786–1789.

Kanamori N, Madsen LH, Radutoiu S, Frantescu M, Quistgaard EMH, Miwa H, Downie JA, James

- EK, Felle HH, Haaning LL, et al. 2006.** A nucleoporin is required for induction of Ca²⁺ spiking in legume nodule development and essential for rhizobial and fungal symbiosis. *Proceedings of the National Academy of Sciences of the United States of America* **103**: 359–64.
- Kang H, Chu X, Wang C, Xiao A, Zhu H, Yuan S, Yang Z, Ke D, Xiao S, Hong Z, et al. 2014.** A MYB coiled-coil transcription factor interacts with NSP2 and is involved in nodulation in *Lotus japonicus*. *New Phytologist* **201**: 837–849.
- Kankanala P, Czymmek K, Valent B. 2007.** Roles for Rice Membrane Dynamics and Plasmodesmata during Biotrophic Invasion by the Blast Fungus. **19**: 706–724.
- Kavroulakis N, Doupis G, Papadakis IE, Ehaliotis C, Papadopoulou KK. 2018.** Tolerance of tomato plants to water stress is improved by the root endophyte *Fusarium solani* FsK. *Rhizosphere* **6**: 77–85.
- Kavroulakis N, Ntougias S, Zervakis GI, Ehaliotis C, Haralampidis K, Papadopoulou KK. 2007.** Role of ethylene in the protection of tomato plants against soil-borne fungal pathogens conferred by an endophytic *Fusarium solani* strain. *Journal of Experimental Botany* **58**: 3853–3864.
- Kavroulakis N, Papadopoulou KK, Ntougias S, Zervakis GI, Ehaliotis C. 2006.** Cytological and other aspects of pathogenesis-related gene expression in tomato plants grown on a suppressive compost. *Annals of Botany* **98**: 555–564.
- Kawaharada Y, Kelly S, Nielsen MW, Hjuler CT, Gysel K, Muszyński A, Carlson RW, Thygesen MB, Sandal N, Asmussen MH, et al. 2015.** Receptor-mediated exopolysaccharide perception controls bacterial infection. *Nature* **523**: 308–312.
- Kevei Z, Loughon G, Mergaert P, Horvath G V, Kereszt A, Jayaraman D, Zaman N, Marcel F, Regulski K, Kiss GB, et al. 2007.** 3-hydroxy-3-methylglutaryl coenzyme A reductase1 interacts with NORK and is crucial for nodulation in *Medicago truncatula*. *Plant Cell* **19**: 3974–3989.
- Kistner C, Winzer T, Pitzschke A, Mulder L, Sato S, Kaneko T, Tabata S, Sandal N, Stougaard J, Webb KJ, et al. 2005.** Seven *Lotus japonicus* Genes Required for Transcriptional Reprogramming of the Root during Fungal and Bacterial Symbiosis. *The Plant Cell* **17**: 2217–2229.
- Knight MR, Campbell AK, Smith SM, Trewavas AJ. 1991.** Transgenic plant aequorin reports the effects of touch and cold-shock and elicitors on cytoplasmic calcium. *Nature* **352**: 524–526.
- Knight H, Trewavas AJ, Knight MR. 1997.** Calcium signalling in *Arabidopsis thaliana* responding to drought and salinity. *Plant Journal* **12**: 1067–1078.
- Koh S, André A, Edwards H, Ehrhardt D, Somerville S. 2005.** *Arabidopsis thaliana* subcellular responses to compatible *Erysiphe cichoracearum* infections. *Plant Journal* **44**: 516–529.
- Kosuta S, Hazledine S, Sun J, Miwa H, Morris RJ, Downie JA, Oldroyd GED. 2008.** Differential and chaotic calcium signatures in the symbiosis signaling pathway of legumes. *Proceedings of the National Academy of Sciences of the United States of America* **105**: 9823–8.
- Kouzai Y, Nakajima K, Hayafune M, Ozawa K, Kaku H, Shibuya N, Minami E, Nishizawa Y. 2014.** CEBiP is the major chitin oligomer-binding protein in rice and plays a main role in the perception of chitin oligomers. *Plant Mol Biol* **84**: 519–528.
- Kucho KI, Hay AE, Normand P. 2010.** The determinants of the actinorhizal symbiosis. *Microbes and Environments* **25**: 241–252.
- Kumagai H, Kinoshita E, Ridge RW, Kouchi H. 2006.** RNAi knock-down of ENOD40s leads to

significant suppression of nodule formation in *Lotus japonicus*. *Plant and Cell Physiology* **47**: 1102–1111.

Lahrman U, Ding Y, Banhara A, Rath M, Hajirezaei MR, Döhlemann S, von Wirén N, Parniske M, Zuccaro A. 2013. Host-related metabolic cues affect colonization strategies of a root endophyte. *Proc Natl Acad Sci USA* **110**: 13965–13970.

Larkin RP, Fravel DR. 1998. Efficacy of Various Fungal and Bacterial Biocontrol Organisms for Control of Fusarium Wilt of Tomato. *Plant Disease* **82**: 1022–1028.

Larkin RP, Hopkins DL, Martin FN. 1996. Suppression of Fusarium wilt of watermelon by nonpathogenic Fusarium oxysporum and other microorganisms recovered from a disease-suppressive soil. *Phytopathology* **86**: 812–819.

Lauressergues D, Delaux PM, Formey D, Lelandais-Brière C, Fort S, Cottaz S, Bécard G, Niebel A, Roux C, Combier JP. 2012. The microRNA miR171h modulates arbuscular mycorrhizal colonization of *Medicago truncatula* by targeting NSP2. *Plant Journal* **72**: 512–522.

Liang Y, Tóth K, Cao Y, Tanaka K, Espinoza C, Stacey G. 2014. Lipochitooligosaccharide recognition: an ancient story. *The New phytologist* **204**: 289–296.

Limpens E, Franken C, Smit P, Willemse J, Bisseling T, Geurts R. 2003. LysM Domain Receptor Kinases Regulating Rhizobial Nod Factor-Induced Infection LysM Domain Receptor Kinases Regulating Rhizobial Nod Factor – Induced Infection. *Science* **302**: 630–633.

Link H. 1809. Observationes in ordines plantarum naturalis. Dissetatio I. *Magazin Ges. Nat.Freunde Berlin* **3**: 3–42.

Lohmann GV, Shimoda Y, Nielsen MW, Jørgensen FG, Grossmann C, Sandal N, Sørensen K, Thirup S, Madsen LH, Tabata S, et al. 2010. Evolution and Regulation of the *Lotus japonicus* LysM Receptor Gene Family. *Molecular Plant-Microbe Interactions* **23**: 510–521.

van der Luit AH, Olivari C, Haley A, Knight MR, Trewavas AJ. 1999. Distinct Calcium Signaling Pathways Regulate Calmodulin Gene Expression in Tobacco. *Plant Physiology* **121**: 705 LP – 714.

Ma LJ, Van Der Does HC, Borkovich KA, Coleman JJ, Daboussi MJ, Di Pietro A, Dufresne M, Freitag M, Grabherr M, Henrissat B, et al. 2010. Comparative genomics reveals mobile pathogenicity chromosomes in *Fusarium*. *Nature* **464**: 367–373.

Ma L, Geiser DM, Proctor RH, Rooney AP, Donnell KO, Trail F, Gardiner DM, Manners JM, Kazan K. 2013. *Fusarium* Pathogenomics.

Macho AP, Zipfel C. 2014. Plant PRRs and the activation of innate immune signaling. *Molecular Cell* **54**: 263–272.

MacLean AM, Bravo A, Harrison MJ. 2017. Plant signaling and metabolic pathways enabling arbuscular mycorrhizal symbiosis. *The Plant Cell*: tpc.00555.2017.

Madsen EB, Madsen LH, Radutoiu S, Olbryt M, Rakwalska M, Szczyglowski K, Sato S, Kaneko T, Tabata S, Sandal N, et al. 2003. A receptor kinase gene of the LysM type is involved in legume perception of rhizobial signals. *Nature* **425**: 637–640.

Maillet F, Poinot V, André O, Puech-Pagès V, Haouy A, Gueunier M, Cromer L, Giraudet D, Formey D, Niebel A, et al. 2011. Fungal lipochitooligosaccharide symbiotic signals in arbuscular mycorrhiza. *Nature* **469**: 58–63.

- Marsh JF, Rakocevic A, Mitra RM, Brocard L, Sun J, Eschstruth A, Long SR, Schultze M, Ratet P, Oldroyd GEDD. 2007.** Medicago truncatula NIN is essential for rhizobial-independent nodule organogenesis induced by autoactive Calcium/Calmodulin-Dependent Protein Kinase. *Plant physiology* **144**: 324–335.
- Marsh JF, Schultze M. 2001.** Analysis of arbuscular mycorrhizas mutants. *New Phytologist* **150**: 525–532.
- Martin F, Aerts A, Ahrén D, Brun A, Danchin EGJ, Duchaussoy F, Gibon J, Kohler A, Lindquist E, Pereda V, et al. 2008.** The genome of Laccaria bicolor provides insights into mycorrhizal symbiosis. *Nature* **452**: 88.
- Martin F, Kohler A, Murat C, Balestrini R, Coutinho PM, Jaillon O, Montanini B, Morin E, Noel B, Percudani R, et al. 2010.** Périgord black truffle genome uncovers evolutionary origins and mechanisms of symbiosis. *Nature* **464**: 1033.
- Masurkar P, Bajpai R, Sahu V, Kumar M, Rajput RS. 2018.** Invasion and Nutrient Acquisition Strategies of Phytopathogens: Fungi, Bacteria and Viruses. *International Journal of Current Microbiology and Applied Sciences* **7**: 3132–3146.
- McAinsh MR, Hetherington AM. 1998.** Encoding specificity in Ca²⁺ signalling systems. *Trends in Plant Science* **3**: 32–36.
- McAinsh MR, Pittman JK. 2009.** Shaping the calcium signature. *New Phytologist* **181**: 275–292.
- Mélida H, Sandoval-Sierra J V., Diéguez-Urbeondo J, Bulone V. 2013.** Analyses of Extracellular Carbohydrates in Oomycetes Unveil the Existence of Three Different Cell Wall Types. *Eukaryotic Cell* **12**: 194–203.
- Mendgen K, Hahn M. 2002.** Plant infection and the establishment of fungal biotrophy. *Trends in Plant Science* **7**: 352–356.
- Mendgen K, Struck C, Voegelé RT, Hahn M. 2000.** Biotrophy and rust haustoria. *Physiological and Molecular Plant Pathology* **56**: 141–145.
- Miao V, Covert S, Vanetten HD. 1991.** A fungal gene for antibiotic resistance on a dispensable (“B”) chromosome. *Science* **254**: 1773–1776.
- Miller JB, Pratap A, Miyahara A, Zhou L, Bornemann S, Morris RJ, Oldroyd GED. 2013.** Calcium/calmodulin-dependent protein kinase is negatively and positively regulated by calcium, providing a mechanism for decoding calcium responses during symbiosis signaling. *Plant Cell* **25**: 5053–5066.
- Minami E, Kouchi H, Cohn JR, Ogawa T, Stacey G. 1996.** Expression of the early nodulin, ENOD40, in soybean roots in response to various lipo-chitin signal molecules. *Plant Journal* **10**: 23–32.
- Mithöfer A, Ebel J, Bhagwat AA, Boller T, Neuhaus-Url G. 1999.** Transgenic aequorin monitors cytosolic calcium transients in soybean cells challenged with β -glucan or chitin elicitors. *Planta* **207**: 566–574.
- Miwa H, Sun J, Oldroyd GED, Allan Downie J. 2006a.** Analysis of calcium spiking using aameleon calcium sensor reveals that nodulation gene expression is regulated by calcium spike number and the developmental status of the cell. *Plant Journal* **48**: 883–894.
- Miwa H, Sun J, Oldroyd GED, Downie JA. 2006b.** Analysis of Nod-Factor-Induced Calcium Signaling

in Root Hairs of Symbiotically Defective Mutants of *Lotus japonicus*. *Molecular plant-microbe interactions : MPMI* **19**: 914–923.

Miya A, Albert P, Shinya T, Desaki Y, Ichimura K, Shirasu K, Narusaka Y, Kawakami N, Kaku H, Shibuya N. 2007. CERK1 , a LysM receptor kinase , is essential for chitin elicitor signaling in Arabidopsis. **104**.

Miyata K, Hayafune M, Kobae Y, Kaku H, Nishizawa Y, Masuda Y, Shibuya N, Nakagawa T. 2016. Evaluation of the role of the LysM receptor-like kinase, OsNFR5/OsRLK2 for AM symbiosis in rice. *Plant and Cell Physiology* **57**: 2283–2290.

Miyata K, Kozaki T, Kouzai Y, Ozawa K, Ishii K, Asamizu E, Okabe Y, Umehara Y, Miyamoto A, Kobae Y, et al. 2014. The Bifunctional Plant Receptor , OsCERK1 , Regulates Both Chitin-Triggered Immunity and Arbuscular Mycorrhizal Symbiosis in Rice. **55**: 1864–1872.

Moreau D. 2006. Morphology, development and plant architecture of *M. truncatula*. In: Mathesius U, EP J, LW S, eds. *Medicago truncatula handbook*.

Moretti A. 2009. Taxonomy of *Fusarium* genus: A continuous fight between lumpers and splitters. *Proc. Nat. Sci, Matica Srpska Novi Sad*: 7–13.

Mun T, Bachmann A, Gupta V, Stougaard J, Andersen SU. 2016. Lotus Base: An integrated information portal for the model legume *Lotus japonicus*. *Scientific Reports* **6**: 1–18.

Murakami E, Cheng J, Gysel K, Bozsoki Z, Kawaharada Y, Hjuler CT, Sørensen KK, Tao K, Kelly S, Venice F, et al. 2018. Epidermal LysM receptor ensures robust symbiotic signalling in *Lotus japonicus*. *eLife* **7**: e33506.

Navazio L, Moscatiello R, Genre A, Novero M, Baldan B, Bonfante P, Mariani P. 2007. A Diffusible Signal from Arbuscular Mycorrhizal Fungi Elicits a Transient Cytosolic Calcium Elevation in Host Plant Cells. *Plant Physiology* **144**: 673 LP – 681.

Niwa S, Kawaguchi M, Imaizumi-Anraku H, Chechetka SA, Ishizaka M, Ikuta A, Kouchi H. 2001. Responses of a Model Legume *Lotus japonicus* to Lipochitin Oligosaccharide Nodulation Factors Purified from *Mesorhizobium loti* JRL501. *Molecular Plant-Microbe Interactions* **14**: 848–856.

O’Connell RJ, Thon MR, Hacquard S, Amyotte SG, Kleemann J, Torres MF, Damm U, Buiaite EA, Epstein L, Alkan N, et al. 2012. Lifestyle transitions in plant pathogenic *Colletotrichum* fungi deciphered by genome and transcriptome analyses. *Nature Genetics* **44**: 1060–1065.

O’Donnell KO, Rooney AP, Proctor RH, Brown DW, McCormick SP, Ward TJ, Frandsen RJN, Lysøe E, Rehner SA, Aoki T, et al. 2013. Phylogenetic analyses of RPB1 and RPB2 support a middle Cretaceous origin for a clade comprising all agriculturally and medically important fusaria. *Fungal Genetics and Biology* **52**: 20–31.

Oldroyd GED. 2013. Speak, friend, and enter: signalling systems that promote beneficial symbiotic associations in plants. *Nature reviews. Microbiology* **11**: 252–63.

Oldroyd GED, Murray JD, Poole PS, Downie JA. 2011. The Rules of Engagement in the Legume-Rhizobial Symbiosis. *Annual Review of Genetics* **45**: 119–144.

Ondrej M, Dostalova R, Trojan R. 2008. Evaluation of Virulence of *Fusarium solani* Isolates on Pea. *Plant Protect. Sci.* **44**: 9–18.

Pajuelo E, Stougaard J. 2005. *Lotus japonicus*’s a model system. In: *Lotus Japonicus Handbook*.

Springer, Dordrecht, 3–24.

Pappas ML, Liapoura M, Papantoniou D, Avramidou M, Kavroulakis N, Weinhold A, Broufas GD, Papadopoulou KK. 2018. The Beneficial Endophytic Fungus *Fusarium solani* Strain K Alters Tomato Responses Against Spider Mites to the Benefit of the Plant. *Frontiers in Plant Science* **9**: 1603.

Parniske M. 2008. Arbuscular mycorrhiza: the mother of plant root endosymbioses. *Nature Reviews Microbiology* **6**: 763.

Peškan-Berghöfer T, Shahollari B, Pham HG, Hehl S, Markert C, Blanke V, Kost G, Varma A, Oelmüller R. 2004. Association of *Piriformospora indica* with *Arabidopsis thaliana* roots represents a novel system to study beneficial plant-microbe interactions and involves early plant protein modifications in the endoplasmic reticulum and at the plasma membr. *Physiologia Plantarum* **122**: 465–477.

Poole P, Ramachandran V, Terpolilli J. 2018. Rhizobia: from saprophytes to endosymbionts. *Nature Publishing Group*.

Qiang X, Zechmann B, Reitz MU, Kogel K-H, Schafer P. 2012. The Mutualistic Fungus *Piriformospora indica* Colonizes *Arabidopsis* Roots by Inducing an Endoplasmic Reticulum Stress-Triggered Caspase-Dependent Cell Death. *the Plant Cell Online* **24**: 794–809.

Radutoiu S, Madsen LH, Madsen EB, Felle HH, Umehara Y, Grønlund M, Sato S, Nakamura Y, Tabata S, Sandal N, et al. 2003. Plant recognition of symbiotic bacteria requires two LysM receptor-like kinases. *Nature* **425**: 585–592.

Rai M, Agarkar G. 2014. Plant – fungal interactions: What triggers the fungi to switch among lifestyles? *Critical Reviews in Microbiology* **42**: 428–438.

Rasmussen SR, Füchtbauer W, Novero M, Volpe V, Malkov N, Genre A, Bonfante P, Stougaard J, Radutoiu S. 2016. Intraradical colonization by arbuscular mycorrhizal fungi triggers induction of a lipochitooligosaccharide receptor. *Scientific Reports* **6**: 1–12.

van Rhijn P, Fang Y, Galili S, Shaul O, Atzmon N, Wininger S, Eshed Y, Lum M, Li Y, To V, et al. 1997. Expression of early nodulin genes in alfalfa mycorrhizae indicates that signal transduction pathways used in forming arbuscular mycorrhizae and *Rhizobium*-induced nodules may be conserved. *Proceedings of the National Academy of Sciences of the United States of America* **94**: 5467–5472.

Ried MK, Antolín-Ilovera M, Parniske M. 2014. Spontaneous symbiotic reprogramming of plant roots triggered by receptor-like kinases. *elife* **3**: e03891.

Rodriguez R, Redman R. 2008. More than 400 million years of evolution and some plants still can't make it on their own: Plant stress tolerance via fungal symbiosis. *Journal of Experimental Botany* **59**: 1109–1114.

Rodriguez RJ, White Jr JF, Arnold AE, Redman RS. 2009. Fungal endophytes: diversity and functional roles. *New Phytologist* **182**: 314–330.

Russo G, Spinella S, Sciacca E, Bonfante P, Genre A. 2013. Automated analysis of calcium spiking profiles with CaSA software: two case studies from root-microbe symbioses. *BMC plant biology* **13**: 224.

Saito K, Yoshikawa M, Yano K, Miwa H, Uchida H, Asamizu E, Sato S, Tabata S, Imaizumi-Anraku H, Umehara Y, et al. 2007. NUCLEOPORIN85 Is Required for Calcium Spiking, Fungal and Bacterial Symbioses, and Seed Production in *Lotus japonicus*. *the Plant Cell Online* **19**: 610–624.

- Sanchez L, Weidmann S, Arnould C, Bernard AR, Gianinazzi S, Gianinazzi-Pearson V. 2005.** *Pseudomonas fluorescens* and *Glomus mosseae* Trigger DMI3-Dependent Activation of Genes Related to a Signal Transduction Pathway in Roots of *Medicago truncatula*. *Plant Physiology* **139**: 1065 LP – 1077.
- Sato S, Nakamura Y, Kaneko T, Asamizu E, Kato T, Nakao M, Sasamoto S, Watanabe A, Ono A, Kawashima K, et al. 2008.** Genome structure of the legume, *Lotus japonicus*. *DNA Research* **15**: 227–239.
- Schäfer P, Pfiffi S, Voll LM, Zajic D, Chandler PM, Waller F, Scholz U, Pons-Kühnemann J, Sonnewald S, Sonnewald U, et al. 2009.** Manipulation of plant innate immunity and gibberellin as factor of compatibility in the mutualistic association of barley roots with Piriformospora indica. *Plant Journal* **59**: 461–474.
- Shimizu T, Nakano T, Takamizawa D, Desaki Y, Ishii-minami N, Nishizawa Y, Minami E, Okada K, Yamane H, Kaku H, et al. 2010.** Two LysM receptor molecules, CEBiP and OsCERK1, cooperatively regulate chitin elicitor signaling in rice. *Plant Journal* **64**: 204–214.
- Siddiqui IA, Shaukat SS. 2003.** Factors influencing the effectiveness of non-pathogenic *Fusarium solani* strain Fs5 in the suppression of root-knot. *Phytopathol. Mediterr.* **42**: 17–26.
- Sieberer BJ, Chabaud M, Fournier J, Timmers ACJ, Barker DG. 2012.** A switch in Ca²⁺ spiking signature is concomitant with endosymbiotic microbe entry into cortical root cells of *Medicago truncatula*. *Plant Journal* **69**: 822–830.
- Sieberer BJ, Chabaud M, Timmers AC, Monin A, Fournier J, Barker DG. 2009.** A nuclear-targetedameleon demonstrates intranuclear Ca²⁺ spiking in *Medicago truncatula* root hairs in response to rhizobial nodulation factors. *Plant Physiology* **151**: 1197–1206.
- Singh S, Katzer K, Lambert J, Cerri M, Parniske M. 2014.** CYCLOPS, A DNA-binding transcriptional activator, orchestrates symbiotic root nodule development. *Cell Host and Microbe* **15**: 139–152.
- Smit P, Raedts J, Portyanko V, Debellé F, Gough C, Bisseling T, Geurts R. 2005.** NSP1 of the GRAS Protein Family Is Essential for Rhizobial Nod Factor-Induced Transcription. *Science* **308**: 1789–1791.
- Stacey G, Shibuya N. 1997.** Chitin recognition in rice and legumes. *Plant and Soil* **194**: 161–169.
- Stougaard J. 2013.** *Lotus japonicus*: A Model Plant for the Legume Family. In: Brenner's Encyclopedia of Genetics: Second Edition. 274–276.
- Stracke S, Kistner C, Yoshida S, Mulder L, Sato S, Kaneko T, Tabata S, Sandal N, Stougaard J, Szczyglowski K, et al. 2002.** A plant receptor-like kinase required for both bacterial and fungal symbiosis. *Nature* **417**: 959–962.
- Summerell BA. 2019.** Resolving *Fusarium*: Current Status of the Genus . *Annual Review of Phytopathology* **57**: 1–17.
- Svistoonoff S, Benabdoun FM, Nambiar-Veetil M, Imanishi L, Vaissayre V, Cesari S, Diagne N, Hoche V, de Billy F, Bonneau J, et al. 2013.** The Independent Acquisition of Plant Root Nitrogen-Fixing Symbiosis in Fabids Recruited the Same Genetic Pathway for Nodule Organogenesis. *PLOS ONE* **8**: e64515.
- Takeda N, Okamoto S, Hayashi M, Murooka Y. 2005.** Expression of LjENOD40 genes in response to

symbiotic and non-symbiotic signals: *LjENOD40-1* and *LjENOD40-2* are differentially regulated in *Lotus japonicus*. *Plant and Cell Physiology* **46**: 1291–1298.

Takemoto D, Jones DA, Hardham AR. 2003. GFP-tagging of cell components reveals the dynamics of subcellular re-organization in response to infection of *Arabidopsis* by oomycete pathogens. *The Plant Journal* **33**: 775–792.

Takeuchi K, Tomioka K, Kouchi H, Nakagawa T, Kaku H. 2007. A novel pathosystem to study the interactions between *Lotus japonicus* and *Fusarium solani*. *Journal of General Plant Pathology* **73**: 336–341.

Tayung K, Barik B, Jha D, Deka D. 2011. Identification and characterization of antimicrobial metabolite from an endophytic fungus, *Fusarium solani* isolated from bark of Himalayan yew. *Mycosphere* **2**: 203–213.

Tirichine L, Imaizumi-Anraku H, Yoshida S, Murakami Y, Madsen LH, Miwa H, Nakagawa T, Sandal N, Albrechtsen AS, Kawaguchi M, et al. 2006. Deregulation of a Ca^{2+} /calmodulin-dependent kinase leads to spontaneous nodule development. *Nature* **441**: 1153–6.

Tomiyama K. 1957. Cell physiological studies on the resistance of potato plant to *Phytophthora infestans*. *Japanese Journal of Phytopathology* **22**: 129–133.

Vadassery J, Ranf S, Drzewiecki C, Mithofer A, Mazars C, Scheel D, Lee J, Oelmu R. 2009. A cell wall extract from the endophytic fungus *Piriformospora indica* promotes growth of *Arabidopsis* seedlings and induces intracellular calcium elevation in roots. *The Plant Journal* **59**: 193–206.

Varma A, Verma S, Sudha, Sahay N, Bütehorn B, Franken P. 1999. *Piriformospora indica*, a cultivable plant-growth-promoting root endophyte. *Applied and Environmental Microbiology* **65**: 2741–2744.

Venkateshwaran M, Jayaraman D, Chabaud M, Genre A, Balloon AJ, Maeda J, Forshey K, den Os D, Kwiecien NW, Coon JJ, et al. 2015. A role for the mevalonate pathway in early plant symbiotic signaling. *Proc Natl Acad Sci U S A* **112**: 9781–9786.

Venkateshwaran M, Volkening JD, Sussman MR, 1 J-MA. 2013. Symbiosis and the social network of higher plants. *Current Opinion in Plant Biology* **16**: 118–127.

Verma S, Varma A, Rexer K, Hassel A, Kost G, Sarbhoy A, Bisen P, Butehorn B, Franken P. 1998. *Piriformospora indica*, gen. et sp. nov., a new root-colonizing fungus. *Mycologia* **90**: 896–903.

Waller F, Achatz B, Baltruschat H, Fodor J, Becker K, Fischer M, Heier T, Hückelhoven R, Neumann C, von Wettstein D, et al. 2005. The endophytic fungus *Piriformospora indica* reprograms barley to salt-stress tolerance, disease resistance, and higher yield. *Proceedings of the National Academy of Sciences of the United States of America* **102**: 13386–13391.

Wan J, Zhang X, Neece D, Ramonell KM, Clough S, Kim S, Stacey MG, Stacey G. 2008. A LysM Receptor-Like Kinase Plays a Critical Role in Chitin Signaling and Fungal Resistance in *Arabidopsis*. *The Plant Cell* **20**: 471–481.

Wang E, Schornack S, Marsh JF, Gobbato E, Schwessinger B, Eastmond P, Schultze M, Kamoun S, Oldroyd GED. 2012. A common signaling process that promotes mycorrhizal and oomycete colonization of plants. *Current Biology* **22**: 2242–2246.

Weerasinghe RR, Bird DM, Allen NS. 2005. Root-knot nematodes and bacterial Nod factors elicit

common signal transduction events in *Lotus japonicus*. *Proceedings of the National Academy of Sciences* **102**: 3147–3152.

van de Wiel C, Scheres B, Franssen H, van Lierop MJ, van Lammeren A, van Kammen A, Bisseling T. 1990. The early nodulin transcript ENOD2 is located in the nodule parenchyma (inner cortex) of pea and soybean root nodules. *The EMBO Journal* **9**: 1–7.

Yang W-C, Katinakis P, Hendriks P, Smolders A, de Vries F, Spee J, van Kammen A, Bisseling T, Franssen H. 1993. Characterization of *GmENOD40*, a gene showing novel patterns of cell-specific expression during soybean nodule development. *The Plant Journal* **3**: 573–585.

Yano K, Yoshida S, Mueller J, Singh S, Banba M, Vickers K, Markmann K, White C, Schuller B, Sato S, et al. 2008. CYCLOPS, a mediator of symbiotic intracellular accommodation. *Proceedings of the National Academy of Sciences of the United States of America* **105**: 20540–20545.

Yoro E, Suzaki T, Toyokura K, Miyazawa H. 2014. A Positive Regulator of Nodule Organogenesis , NODULE INCEPTION , Acts as a Negative Regulator of Rhizobial Infection in *Lotus japonicus*. *Plant Physiology* **165**: 747–758.

Young ND, Debellé F, Oldroyd GED, Geurts R, Cannon SB, Udvardi MK, Benedito VA, Mayer KFX, Gouzy J, Schoof H, et al. 2011. The Medicago genome provides insight into the evolution of rhizobial symbioses. *Nature* **480**: 520.

Zgad Zaj R, James EK, Kelly S, Kawaharada Y, de Jonge N, Jensen DB, Madsen LH, Radutoiu S. 2015. A Legume Genetic Framework Controls Infection of Nodules by Symbiotic and Endophytic Bacteria. *PLoS Genetics* **11**: 1–21.

Zgad Zaj R, Thiergart T, Bozsoki Z, Garrido-Oter R, Radutoiu S, Schulze-Lefert P. 2019. *Lotus japonicus* symbiosis signaling genes and their role in the establishment of root-associated bacterial and fungal communities. *bioRxiv* **547687**.

Zhang X, Dong W, Sun J, Feng F, Deng Y, He Z, Oldroyd GED, Wang E. 2015. The receptor kinase *CERK1* has dual functions in symbiosis and immunity signalling. *Plant Journal* **81**: 258–267.

Zipfel C. 2008. Pattern-recognition receptors in plant innate immunity. *Current Opinion in Immunology* **20**: 10–16.

Zipfel C, Oldroyd GED. 2017. Plant signalling in symbiosis and immunity. *Nature* **543**: 328.

Zuccaro A, Lahrmann U, Güldener U, Langen G, Pfiffi S, Biedenkopf D, Wong P, Samans B, Grimm C, Basiewicz M, et al. 2011. Endophytic life strategies decoded by genome and transcriptome analyses of the mutualistic root symbiont *Piriformospora indica*. *PLoS Pathogens* **7**: e1002290.

Chapter 2

Assessing the impact of different nutrient sources and abiotic factors on growth and reproduction of *Fusarium solani* strain K

2 Assessing the impact of different nutrient sources and abiotic factors on growth and reproduction of *Fusarium solani* strain K

2.1 Introduction

2.1.1 Physiology of filamentous fungi

Fungi are among the most important organisms in nature, as they contribute immensely in litter decomposition and the biogeochemical cycling of carbon, due to their ability to decompose organic materials. They contribute to soil tilth and structure, and they bind soil particles through their hyphal network (Klein and Paschke, 2004). They furthermore contribute to the mobilization of nutrients, thus affecting and altering the physicochemical environment. They interact with a plethora of organisms, associating with them as mutualists, symbionts, pathogens, saprotrophs. The term 'fungal physiology' refers to current knowledge concerning the nutrition, metabolism, growth, reproduction, and death of fungal cells (Walker and White, 2017). Fungal growth cannot be easily defined though, because it can either refer to the increase in the mass, or in the number of cells (Cochrane, 1958).

The visible structures of both macro and micro fungi²⁴ comprise of hyphae (singular hypha): long, aggregated, branching tubular-like threads, which extend and branch within the supporting substrate forming the fungal mycelium. Hyphae support spores for reproduction and dissemination. The defining feature of filamentous fungi is the hypha. They are called 'filamentous' because their vegetative²⁵ state of growth comprises of these walled tubular structures, which extend at one end (apical growth) by incorporation of new cell wall material (Weber and Pitt, 2001). Hyphal growth provides the means for: colonization of the surrounding substrate, secretion of hydrolytic enzymes, assimilation of nutrients, regulation of morphogenesis, sensing of environmental signals. Hyphae act as gametes in sexual reproduction in many fungi, and differentiate into a variety of structures, including the infectious structures of pathogenic fungi such as appressoria and haustoria²⁶ (Roberson et al., 2010).

The apical extension of hyphae can continue endlessly, on condition that the organism is supported with the appropriate nutrients, and the environmental conditions are suitable for its growth. In this respect, eucarpic²⁷ fungi are indeterminate organisms both in time and space, and unlike other organisms (animals, plants, other microbes), they have no predetermined maximum size and age (Walker and White, 2017). This indeterminate growth of filamentous fungi constitutes direct measures of fungal biomass or evaluation of individuals difficult or impossible (Anderson and Kohn, 1998).

²⁴ Micro-fungi are distinguished from macro-fungi by the absence of a large, multicellular fruiting body.

²⁵ Fungi in their vegetative state consist of a tangle of thread-like hyphae, whereas their reproductive stage is usually more obvious.

²⁶ Appressoria are specialized infection hyphal cells developed in many plant pathogenic fungi. Biotrophic and hemibiotrophic filamentous pathogens enter the host plant tissues by direct penetration through the cuticle and the cell wall using either melanized or non-melanized appressoria, or through stomata, often using non-melanized appressoria (Giraldo and Valent, 2013).

Haustroria are feeding structures developed by plant pathogenic fungi. Some plant pathogens grow from one plant cell to the next as extracellular hyphae that insert haustoria (terminal feeding structures) inside host cells (Giraldo and Valent, 2013).

²⁷ In holocarpic fungi, the entire thallus is differentiated into a reproductive cell when mature; in eucarpic fungi the thallus is differentiated into vegetative and reproductive regions.

A filamentous fungus comprises of two major vegetative components: a) the network of hyphae, and b) the cytoplasm that can move in this network. The hyphal network has no particular pattern or structure, it is influenced by nutrient availability and distribution. The cytoplasm in the hyphal network is maintained if nutrients are available. When the fungus is not able to support active growth, due to nutrient depletion, the cytoplasm is transported to other sites of active growth or even degraded. Resources are then used to support the synthesis of resting sexual and asexual propagules (Klein and Paschke, 2004). Fungi are able to translocate cytoplasmic constituents or the products of their autolysis from older to younger sites of the colony/hyphal network. In this respect they can support growth in extreme carbon: nitrogen ratios (e.g. wood with a ratio of 1600:1) for a considerable amount of time, and this is achieved through reutilization of fractions of their own mycelium as the sole nitrogen source (Griffin, 1985). Fungi that colonize substrates rich in nutrients tend to branch frequently, therefore producing dense mycelia for resource exploitation. On the other hand, fungi that colonize nutrient poor substrates, branch less frequently, producing effuse mycelia which are appropriate for resource exploration (Walker and White, 2017).

The ultrastructural organization of hyphae from all forms of fungi is similar: the polarized form of hyphal growth also entails a polarized distribution of most organelles. Secretory vesicles, sheets of rough endoplasmic reticulum, mitochondria, nuclei, vacuoles, occupy the space in the apical dome of the growing hypha (Weber and Pitt, 2001). In a filamentous fungus, single cell identification is not completely clear. The apical compartments are usually multinucleate, and in a duplication cycle nuclear replication and segregation occur in a newly extended septated²⁸ hyphal compartment. Behind the leading, growing hyphal tip, hyphae branch, and this usually occurs behind a septum. A Spitzenkörper²⁹ usually appears at the site of tip emergence and extension (Walker and White, 2017).

Hyphal growth is based on nutrition by secretion of enzymes extracellularly, and afterwards extracellular digestion of the substrate. Fungi thrive on soil, where they act as skillful decomposers of difficult-to-digest substrates like cellulose and lignin, and as skillful 'collectors' of nutrients. All the above are attributed to the characteristics of their growth: extension and secretion of exoenzymes through the hyphal apex, formation of branches, nutrient translocation from mature hyphal segments. Their success in colonizing soil is reflected in that most terrestrial plants have recruited filamentous fungi as their mycorrhizal partners (Weber and Pitt, 2001).

In the laboratory, fungi can be routinely cultured in solid or liquid media. Three phases are usually observed if we follow the temporal growth of a filamentous fungus in liquid media: a) a phase of no apparent growth which is characterized by a genuine lag phase prior to spore germination, and a phase in which growth is occurring but is undetectable by the methods used, b) a phase of rapid and approximately linear growth, and c) a phase where no net growth occurs or autolysis takes place and therefore a decline in dry weight is observed. During the phase of rapid growth, a series of chemical events take place, i.e. utilization of carbohydrates, nitrogen, phosphate. The respiratory activity is also at a maximum. As mentioned above, mycelial growth occurs at the hyphal tips. Cells located at the

²⁸ Septum: cross-walls, usually perforated by pores, which divide hyphae into cells. Pores of septa allow passage of ribosomes, mitochondria, and sometimes nuclei between cells.

²⁹ Spitzenkörper: an aggregate of secretory vesicles at the growing hyphal tip.

inner part of the mycelium do not normally contribute to the new growth directly but mostly via supplementing nutrients to the aerial structures of the mycelium (Cochrane, 1958). The ability of filamentous fungi to translocate substances from sites of absorption to sites of utilization (i.e. the newest part of the mycelium) is identified in the ability of hyphae to grow into air, basically away from the nutrient substrate (Griffin, 1985).

The *in vitro* requirements of fungi are in general minimal. Many non-obligate biotrophs can be grown axenically in minimal media supplemented with only a simple carbohydrate source, nitrogen (in the form of nitrate), phosphate and trace metals. Obligate biotrophs cannot, by definition, be grown in culture. For example, obligate symbionts such as the Arbuscular Mycorrhizal Fungi require growth of a plant partner for cultivation. Providing complex nutrient sources in the cultivation substrate does not enable growth of such fungi in most cases. It seems that the regulation of nutrient assimilation transporters and enzymes, recruited during fungal nutrition, is dependent on factors or signals produced by the plant. In obligate pathogenic fungi, fungal specialized structures, known as haustoria, are responsible for uptake of nutrients (Solomon et al., 2003).

2.1.2 Nutrient uptake/assimilation

Fungi are non-motile organisms, and their immobility has, in many aspects, defined their physiology. They are saprotrophic³⁰ (and sometimes parasitic³¹), chemo-organotrophic³² organisms. They are in general simple in their nutritional requirements. They need a source of organic nutrients to supply their energy and to acquire carbon skeletons for cellular synthesis. Provided they are given a simple energy source such as glucose, they synthesize their cellular components from inorganic sources, like ammonium or nitrate ions, phosphate ions and trace levels of other minerals such as calcium, potassium, magnesium and iron. As heterotrophs, they need to capture nutrients from the surrounding environment (Deacon, 2006).

Nutrients required for (not only) fungal growth are divided into two broad categories: a) Macronutrients: they are supplied at millimolar concentrations and they comprise of sources of carbon, nitrogen, oxygen, sulfur, phosphorus, potassium and magnesium, b) Micronutrients: they are supplied at micromolar concentrations and they comprise of trace elements such as calcium, copper, iron, manganese and zinc (Walker and White, 2017).

Feeding by absorption is a hallmark of filamentous fungi and yeasts. Free-living saprotrophs detect available carbon and nitrogen compounds in the environment through their growing hyphae on substrates like soil or dead wood. Secretion of appropriate enzymes is necessary to depolymerize and/or mobilize such compounds, and uptake and metabolism of the resulting liberated substrates (such as simple sugars and amino acids). Global carbon and nitrogen regulators ensure the preferential utilization of certain carbon sources (such as glucose and ammonium) and repression of genes responsible for utilization of less favored ones (such as xylose and nitrate). Moreover, pathway-specific

³⁰ Saprotrophic are organisms that live and feed on dead organic matter.

³¹ Parasitic are organisms that live on another organism; they depend on the other organism without providing an adequate return.

³² Chemo-organotrophs are organisms that obtain energy from the oxidation of reduced organic compounds. Organic sources are used as sources of electrons and carbon at the same time.

regulators ensure that genes involved in a specific catabolic pathway are only expressed in the presence of the appropriate inducer (Fernandez et al., 2014). The genetic control of nutrient acquisition occurs not only in free-living fungi growing on complex substrates, but also in fungal plant pathogens, where homologous regulatory systems control carbon and nitrogen metabolism in host cells (Fernandez et al., 2014).

The fungal cell wall comprises of fibrous and gel-like carbohydrate polymers forming a tensile and robust core scaffold, to which a variety of proteins and other superficial components are added, and altogether make a strong, but flexible and chemically diverse cell wall. The inner cell wall is mostly composed of branched β -(1,3): β -(1,6) glucan, linked to chitin with intra-chain hydrogen bond. The branched glucan is bound to proteins and other polysaccharides, whose composition may vary, depending on the fungal species (Gow et al., 2017). The (relatively) rigid cell wall of fungi does not allow engulfment of food particles, so fungi absorb simple, soluble nutrients through the wall and Plasma Membrane (PM) (Deacon, 2006). The hyphae involved in the exploration of the substrate are responsible for nutrient uptake through a mechanism of transport across their PM. An important aspect of the acquisition process is the breakdown of substrate molecules, especially of those which are insoluble or have the wrong molecular size (i.e. their molecular size does not allow simple entry into the hypha) (Jennings, 1990). Degradation of complex polymers is usually achieved by release of depolymerase enzymes and the degradation products are later on absorbed (Deacon, 2006).

During nutrient uptake by fungal cells, a series of cellular envelope barriers should be overcome: the cell wall, the periplasm and the cell membrane. Molecules up to 300Da pass through the fungal cell walls, though molecules greater than 700Da will be retained. The PM constitutes the major selective barrier during nutrient entry and metabolite exit (Walker and White, 2017). Certain solutes may simply diffuse into the fungal hypha. Typically, fungi absorb only small soluble nutrients such as monosaccharides and amino acids. Membrane transport systems are in general responsible for nutrient uptake, and the majority of nutrients will enter the fungal cytoplasm by crossing the PM via protein carriers (Jennings, 1990). Several modes of passive and active uptake occur at the PM: free diffusion, facilitated diffusion, diffusion channels, active transport. As mentioned above, nutrient uptake takes place at the hyphal tips, and from there fresh nutrients are supplied to the rest of the mycelium. Mitochondria localized at the apical dome supply ATP (adenosine triphosphate) to support the ion pump and generate proton motive force (Walker and White, 2017). For example, transport systems are responsible for carrying amino acids through the PM (Chalot and Brun, 1998).

Current knowledge on fungal nutrition and membrane transport systems in fungi mostly originate from studies on model species: *Saccharomyces cerevisiae* (known as the baker's yeast, Division: Ascomycota), *Aspergillus nidulans* (Division: Ascomycota), and *Neurospora crassa* (Division: Ascomycota) (Divon and Fluhr, 2007) (Chalot and Brun, 1998).

2.1.3 Elements required for fungal growth

2.1.3.1 Carbon Sources

Sugars are widely used for fungal growth. They can range from simple hexoses like glucose to polysaccharides like starch and cellulose. Typical examples of carbon sources used by fungi is presented in Table 2-1. Fungi can assimilate all forms of carbon resources, from dead matter to living tissues (Watkinson, 2016). These sources provide fungi with carbon and energy. Fungi that use plant remains for carbon acquisition contain multiple genes encoding carbohydrate-active enzymes (the CAZymes). Fungi secrete these enzymes to extracellularly break down polymeric organic compounds prior to utilization of monomers as carbon and energy sources. These enzymes are assembled by the Golgi and transported in vesicles to sites of cell growth (mainly the extending hyphal tips), from where they are secreted (Walker and White, 2017).

Table 2-1 Carbon sources used by yeasts and fungi. Adapted from (Walker and White, 2017)

Carbon Source	Typical example
Hexose sugars	D-glucose, D-galactose, D-fructose, D-mannose
Pentose sugars	L-arabinose, D-xylose, D-xylulose, L-rhamnose
Disaccharides	Maltose, sucrose, lactose, trehalose, melibiose, cellobiose, melezitose
Trisaccharides	Raffinose, maltotriose
Oligosaccharides	Maltotetraose, maltodextrins
Polysaccharides	Starch, inulin, cellulose, hemicellulose, chitin, pectic substances
Lower aliphatic alcohols	Methanol, ethanol
Sugar alcohols	Glycerol, glucitol
Organic acids	Acetate, citrate, lactate, malate, pyruvate, succinate
Fatty acids	Oleate, palmitate

Fungi are well equipped for obtaining sugar. Both active and passive transport systems contribute to sugar uptake. Most culturable fungi will rapidly assimilate common monosaccharides and disaccharides from solution. A global transcriptional regulator, CreA, is responsible for control of carbon assimilation in fungi. CreA regulates the expression of whole suite of genes encoding catabolic and anabolic pathways of carbon metabolism, as well as cell membrane transporters (Watkinson, 2016). Fungi usually have a constitutive transport protein for glucose. The protein is responsible for transport of glucose in preference to other sugars in mixture, but it has low transport specificity, so in the absence of glucose, it will transport other sugars. When the disaccharide lactose is the sole carbon source, fungi will use a wall-bound enzyme, β -galactosidase, to break down lactose to glucose and galactose. Then the fungus takes up the glucose preferentially. When glucose is depleted, a galactose protein carrier will be synthesized, and galactose will be used as a substrate now. When sucrose is provided, it will be cleaved to glucose and fructose by the wall-bound enzyme invertase, and then the glucose is taken up before fructose. Fungi that do not produce invertase, cannot use sucrose as a substrate.

Polymeric forms of carbon are cellulose and lignocellulose. Cellulose is a relatively simple polymer, it is ubiquitous in plants, it is the primary constituent of plant cell walls, and the most common carbon compound on the planet. Fungi are the primary decomposers of cellulose; most saprotrophic fungi use it as a carbon source. In its naturally occurring form it is insoluble, fibrous, strong, resistant to hydrolysis. It consists of β -(1,4)-linked glucan chains, which are held in parallel alignment by hydrogen bonding, forming long, crystalline bundles. The bundles are aligned to microfibrils, forming a closely packed structure which protects the glycosidic bonds from hydrolysis. So the physical structure of cellulose renders the enzymatic access to the substrate problematic. Enzymes with specific activities are necessary to breakdown crystalline cellulose and fungi that are able to digest this substrate synthesize these enzymes (Deacon, 2006) (Watkinson, 2016). More specifically, cellulolytic fungi secrete hydrolytic enzymes, the cellulases.

Lignocellulose is the most durable source of cellulose and is found in wood. Decomposition of wood by fungi plays an essential role in ecosystem and global carbon cycling. Wood contains 40-45 % cellulose, which is embedded in lignin, a hydrophobic phenolic polymer that is resistant to microbial attack and cannot be utilized by fungi, therefore transforming lignocellulose decomposition to a slow process. Fungi are distinguished into white and brown rot, based on their preferred way of decomposing lignocellulose (Watkinson, 2016).

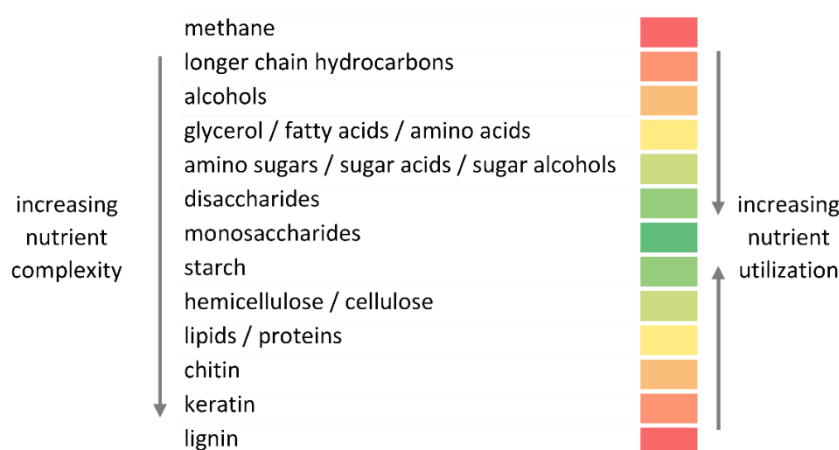


Figure 2-1 Major carbon substrates of fungi and their complexity. Free modification from (Deacon, 2006).

In general, secretion of specific enzymes is required for degradation of complex polymeric forms of carbon. Fungi can also use starch by producing amylases, lipids by producing lipases, proteins by producing proteases (Deacon, 2006). A heatmap connecting the complexity of carbon sources used by fungi and the frequency of their use is illustrated in Figure 2-1.

Ectomycorrhizal (ECM) fungi, which form symbiotic associations with fine roots of forest trees, acquire much of the carbon they need for growth from the host trees. Sucrose (the main carbon compound of phloem sap) is believed to be the primary source of carbon for ECM fungi, which is hydrolyzed to glucose and fructose by a plant derived invertase in ECM symbiosis (Ito and Reshi, 2014) (Nehls and Hampp, 2000). Soil organic sources can be used by ECM fungi when plant photosynthates are low or unavailable. Mycorrhizal fungi also obtain carbon directly from soil through decomposition of soil organic

matter. A significant amount of carbon in both mycorrhizal and ECM fungi is gained through simple organic compounds such as amino acids (Itto and Reshi, 2014). ECM fungi might also demonstrate a saprotrophic activity, acquiring carbon directly from the soil organic matter, during winter, where photosynthesis is inactive during the loss of leaves in the host (Buée et al., 2007).

2.1.3.2 Nitrogen Sources

Besides the importance of an adequate carbon source, fungi also require nitrogen for biomass formation (Fleck et al., 2011). Fungi, unlike many prokaryotes, are non-diazotrophic organisms, that is they cannot fix nitrogen, and need to be supplied with nitrogenous compounds, either in inorganic form such as ammonium salts or in organic form such as amino acids (Walker and White, 2017).

Nitrogen is a limiting nutrient in terrestrial ecosystems. Soil ammonium and nitrate, which are easily available to plants and microbes as they are not very tightly held on soil colloids, constitute a small fraction of total soil nitrogen (Chalot and Brun, 1998). The largest proportion of soil N is bound to organic molecules, in proteins and other organic nitrogen compounds. These are tightly bound to recalcitrant forms of organic matter, or chemically fixed in clays, therefore not easily exposed to microbial degradation. Soil nitrogen usually undergoes many transformations before it is removed. For example, ECM fungi, symbiotically associated with the roots of many woody plants, are directly involved in mobilization of nitrogen from organic matter. Hydrolytic enzymes responsible for making nitrogen available from organic matter have been identified in ericoid and ectomycorrhizal fungi. These extracellularly secreted enzymes possess protease activities that cleave proteins, produce oligopeptides, and release low molecular-mass compounds (Chalot and Brun, 1998). ECM fungi are able to use both organic and inorganic forms of nitrogen in natural conditions and in the laboratory (Rangel-Castro et al., 2002) (Itto and Reshi, 2014).

Commonly used nitrogen sources are ammonium sulphate, which also provides sulfur, besides nitrogen. Many fungi use nitrate, and perhaps nitrite. Nitrate reductase, followed by nitrite reductase, are the enzymes responsible for converting nitrate to ammonia. All fungi can use amino acids as nitrogen source. Often they only need to be supplied with only one amino acid such as glutamic acid or glutamine. From these amino acids they can produce all other essential amino acids by transamination reactions (Deacon, 2006). Intake of amino acids is a way to combine the simultaneous uptake of carbon and nitrogen sources. The largest proportion of amino acids though is fixed in host proteins, therefore, their uptake requires the production of proteolytic enzymes. Urea, a nitrogenous compound containing a carbonyl group attached to two amine groups ($\text{CO}(\text{NH}_2)_2$), is also a source of nitrogen for most fungi (Fleck et al., 2011).

Ammonia or ammonium can be used as nitrogen sources for many fungi. After their assimilation, they are combined with organic acids, glutamic acid is produced (from α -ketoglutaric acid) or aspartic acid, and from there the other amino acids can be formed by transamination reactions. However, ammonia/ammonium are usually taken in exchange for protons (H^+), which can rapidly lower the pH of a culture to 4 or less, therefore inhibiting the growth of the fungus. This constitutes these compounds not ideal as nitrogen sources in culture media for many fungi (Deacon, 2006).

Fungi share most pathways related to amino acid metabolism and protein synthesis with other eukaryotes, including animals. They are able to synthesize their own amino acids and therefore protein, by using soil nitrate and ammonia, on condition they are provided with a carbon source. Therefore, unlike animals, they do not depend on amino acid assimilation from the environment. Saprotrophic fungi can utilize dead wood and other nitrogen poor - carbohydrate rich plant remains to form proteins (Watkinson, 2016).

Fungi have a preference over ammonium, when various nitrogen sources are available in the growing substrate. When ammonium, or glutamine (one of the first amino acids formed from ammonium) are present, the synthesis of membrane-uptake proteins from other nitrogen sources, and furthermore the synthesis of enzymes involved in nitrate utilization are prevented (Deacon, 2006).

The mechanisms of transport of organic N by pure culture fungi depend on the type of the nitrogenous compound that is transported. Transport systems are responsible for carrying amino acids through the PM. (Chalot and Brun, 1998).

2.1.4 Other major nutrients

2.1.4.1 Phosphorus (macro element)

Phosphorus is among the primary elements limiting plant productivity. Since it is not easily available in soil, most plants associate with mycorrhizal fungi to gain access to it. It is a component of nucleic acids and cell membranes. It functions in many processes: energy generation, synthesis of nucleic acids and membranes, glycolysis, respiration, nitrogen fixation, photosynthesis, enzyme activation/inactivation (Vance et al., 2003). It is an essential element for plant nutrition and can only be taken in the form of inorganic orthophosphate (Pi), either as H_2PO_4^- or HPO_4^{2-} , depending on the pH of the soil solution. The inorganic orthophosphate (Pi) is in low concentrations in soil, whereas high P concentrations are found in the not so easily available forms of insoluble mineral P and organic P. Since free phosphate levels are low (less than 10 μM) in soils with no prior cultivation practice, fungi scavenge phosphorus from insoluble minerals like apatite, organic compounds and complexes. Mycorrhizal fungi are highly efficient in that task: hyphae solubilize phosphate by lowering the pH in their vicinity, through proton release, and further secretion of oxalic, citric and malonic acid from hyphal tips/hyphae (Watkinson, 2016). Mycorrhizal fungi achieve this task through: a) P mobilization from mineral P, b) P mobilization from organic P, c) soil exploration and P uptake (Plassard et al., 2011).

Phosphate in soils can be precipitated with calcium, iron or aluminium to form phosphate minerals. Depending on the soil pH, different minerals predominate. For example, in soils with basic pH, calcium phosphates are dominant, whereas in acidic soils, iron and aluminium phosphates are the dominant forms [references within (Plassard et al., 2011)]. Pi release from these minerals may be influenced by the presence of organic compounds, either of high (e.g. humic acid, fulvic acid) or low molecular weight organic ions (e.g. oxalate) (Hunt et al 2007). These organic compounds interact with mineral surfaces resulting in positive effects in Pi availability. ECM fungi produce low molecular weight organic ions, thus playing an important role in Pi release from phosphate minerals (Plassard et al., 2011).

A high amount of P is contained in organic compounds in the form of organic P. Much of the organic P is present as phosphate esters (C-O-P bonds) either as phosphate monoesters (such as inositol phosphates), or phosphate diesters (such as nucleic acids and phospholipids). The phosphate group of the organic P compounds must be released from the ester bond linking it to carbon by enzymes. These enzymes are phosphatases (either phosphomonoesterases or phosphodiesterases, depending on the substrate). ECM fungi are known to release phosphatases (Plassard et al., 2011).

P should be provided in a continuous mode for fungal growth. Since it is not easily available in the environment, as stated above, fungi have developed highly adapted phosphorus uptake systems. Proton coupled symporters in the cell membrane are responsible for assimilation of phosphate ions from solution and soil. Phosphate transporters are well studied in mycorrhizal fungi due to their efficient scavenging of this nutrient from the soil and subsequent provision to their plant partner, in exchange for carbon (Watkinson, 2016). A phosphate transporter has been reported to be expressed in the extraradical mycelium of the AM fungus *Glomus intraradices*, during mycorrhizal association with carrot or *Medicago truncatula* roots, in response to environmental Pi concentrations, indicating that the mycorrhizal fungus perceives and responds to phosphate levels surrounding the extra-radical mycelium (Maldonado-Mendoza et al., 2007). After intracellular uptake, phosphorus is accumulated in vacuoles in the form of inorganic phosphate, and stored as polyphosphate. It is mobilized under conditions of phosphate starvation (Weber and Pitt, 2001).

2.1.4.2 Sulfur (macro element)

Sulfur is essential for life. It is found in several biomolecules: the amino acids methionine and cysteine, the methylation donor S-adenosyl methionine, the redox regulator glutathione, the cofactors biotin, coenzyme A, lipoic acid, thiamine. These sulfur-containing compounds, especially the first three reported above, are essential for the growth and activities of all cells. Methionine initiates the synthesis of nearly all proteins in all organisms, cysteine is important for the structure, stability and catalytic function of many proteins, S-adenosylmethionine plays an important role in methyl group transfer and in polyamine biosynthesis (Marzluf, 1997). Fungi are capable of accumulating sulfur in a variety of compounds that are metabolically useful. After uptake, the acquired sulfur is transformed into a reduced state (sulfide) allowing for the production of sulfur-containing amino acids (Paietta, 2010).

Inorganic sulfate is an important source of sulfur, which is assimilated in the form of sulphate (SO_4^{2-}). Sulfate is assimilated by a well-defined pathway in *Neurospora crassa*, *Aspergillus nidulans*, yeast, as well as in other fungi and plants. Membrane sulphate transporters are implicated in its uptake in fungal cells (Marzluf, 1997). Other inorganic sources of S are (inorganic) sulfite, sulfide, and thiosulfide.

Inorganic species of sulfur are nonetheless not predominant in terrestrial soils. The main portion of sulfur in terrestrial ecosystems is in the form of high-molecular weight organosulfur compounds such as (organic) sulfides, sulfoxides, sulfones, sulfonates, and sulfate esters, glucose-6-sulfate, tyrosine-O-sulfate. Desulfurization of several of these alternative organic sulfur sources also takes place through the action of fungi (Linder, 2018). Sulfatases, such as arylsulfatases, mediate the uptake. Arylsulfatases catalyze the release of sulfate from aromatic sulphate compounds (Paietta, 2010).

Another source of sulfur for fungi are the released cysteine and methionine from exogenous proteins. Proteases are involved in this process, as revealed through work on *N. crassa*. The peptides produced contain residues of methionine and cysteine, and these (or free methionine, cysteine amino acids), supply the fungus with the necessary sulfur (Hanson and Marzluf, 1975).

Sulphate permeases mediate the acquisition of sulphate in fungal cells. Knowledge on sulfur transport in fungi originates through work on *S. cerevisiae*, *N. crassa*, *A. nidulans* (Marzluf, 1997). Sulphate permeases are widely distributed in fungi, with homologues present in a number of fungi including *F. oxysporum*, *Ustilago maydis*, *Cryptococcus neoformans* (Paietta, 2010).

Association of plants with mycorrhizal fungi alters the response of plants to sulfate uptake from soil, enhances xylem loading, and xylem transport of sulfate to leaves. The fungal partner in mycorrhizal symbiosis contributes to the regulation of sulfate uptake by the host plant (Rennenberg, 1999).

The AM fungus *Glomus intraradices* was shown to take up sulfate and transfer it to mycorrhizal carrot roots, increasing root S contents. Genes putatively involved in S assimilation were identified in this system (Allen and Shachar-Hill, 2009).

Fungi respond to sulfur limitation, and for example in *N. crassa* a number of sulfur related genes respond to limiting concentrations of sulfur in the medium. These genes encode proteins involved in the transport or hydrolysis of sulfur-containing compounds. Encoding of these proteins ensures provision in the fungal cell of an adequate sulfur supply. Under sulfur-sufficient conditions the regulatory system is under repression (Paietta, 2004).

2.1.4.3 Iron (micro element)

The element of iron is needed in relatively small amounts for fungal metabolism. It is important due to its contribution as a donor and acceptor of electrons in cellular processes (e.g. the cytochrome system in aerobic respiration). Iron normally occurs in the oxidized ferric (+3 oxidation state: Fe^{3+}), or in its ferrous state (+2 oxidation state: Fe^{2+}). It demonstrates a reduced bioavailability as it is often insolubilized in an oxidized ferric state (in the form of ferric oxides or hydroxides). Fungi have developed versatile strategies to obtain sufficient amounts of this limiting nutrient. Fungi also have mechanisms for regulation of iron uptake and storage, as high iron concentrations may lead to generation of reactive oxygen species.

Iron acquisition can occur as follows: Extracellular ferric iron is reduced to ferrous iron by metalloreductases, a high-affinity system (a ferroxidase and iron permease) that permits uptake. Under high iron conditions, a low-affinity system is responsible for uptake of the ferrous iron (Paietta, 2010).

Iron is also taken up by fungi in a different process in comparison to other elements. Iron-chelating compounds, known as siderophores, are released into the environment, the ferric ion is chelated by these compounds, which are reabsorbed through a specific membrane protein, ferric iron (Fe^{3+}) is reduced to ferrous iron (Fe^{2+}) within the cell, where it is released by the siderophore. The siderophore has a lower specificity for Fe^{2+} than for Fe^{3+} . The siderophore can be exported again to capture a further ferric ion. Siderophores are widespread in ascomycetes and basidiomycetes (Watkinson, 2016). Siderophore transporters represent a protein family that is unique to fungi (Paietta, 2010).

Filamentous fungi (except Zygomycetes) use intracellular siderophores for iron storage. As mentioned above, environmental iron is chelated by extracellularly secreted siderophores, then it is taken up by specific transporters or directly transported as ions. The majority of iron in the fungal cells is either used in metabolic processes directly, or stored using intracellular siderophores (Paietta, 2010).

2.1.4.4 Vitamins and growth factors

As growth factor can be considered any substance required for small amounts and not used for energy. This broad definition includes amino acids, purines and choline (Cochrane, 1958). Vitamins such as thiamine and biotin are necessary for some fungi. Sterols may also be necessary, fatty acids, purines and pyrimidines and inositol (Watkinson, 2016).

Table 2-2 Elements required for fungal cell growth, their source, as well as their main function within the fungal cell. Adapted from (Walker and White, 2017).

Element	Common sources	Cellular functions
Carbon	Sugars	Structural element of fungal cells in combination with hydrogen, oxygen and nitrogen. Energy source.
Hydrogen	Protons from acidic environments	Transmembrane motive force is vital for fungal nutrition. Intracellular acidic pH (around 5-6) is necessary for fungal metabolism
Oxygen	Air, O ₂	Substrate for respiratory and other mixed-function oxidative enzymes. Essential for ergosterol and unsaturated fatty acid synthesis
Nitrogen	NH ₄ ⁺ salts, urea, amino acids	Structurally and functionally as organic amino nitrogen in proteins and enzymes
Phosphorus	Phosphates	Energy transduction, nucleic acid and membrane structure
Potassium	K ⁺ salts	Ionic balance, enzyme activity
Magnesium	Mg ²⁺ salts	Enzyme activity, cell and organelle structure
Sulfur	Sulfates, methionine	Sulfhydryl amino acids and vitamins
Calcium	Ca ²⁺ salts	Possible second messenger in signal transduction
Copper	Cupric salts	Redox pigments
Iron	Ferric salts. Fe ³⁺ is chelated by siderophores and released as Fe ²⁺ within the cell	Heme-proteins, cytochromes
Manganese	Mn ²⁺ salts	Enzyme activity
Nickel	Ni ²⁺ salts	Enzyme activity
Molybdenum	Na ₂ MoO ₄	Nitrate metabolism, vitamin B12

2.1.5 Abiotic (environmental factors) influencing fungal physiology

A series of abiotic factors influence the physiology of fungi among them being: temperature, pH, oxygen, light.

2.1.5.1 Temperature

Temperature is an important abiotic factor that determines the growth and lifestyle of filamentous fungi. Microbes are usually divided into four (and potentially five) broad categories based on their preferences concerning the abiotic factor temperature: a) psychrophiles: they grow optimally at 16 °C, and their maximum growth is achieved at around 20 °C. In many cases they grow at 4 °C or lower, b) mesophiles: they grow at moderate temperatures. They commonly grow at 10-40 °C. In the laboratory, these fungi are usually grown at room temperature (22-25 °C), c) thermophiles: their optimum growth temperature is 20 °C or above, and their maximum growth occurs at 50 °C or above. They grow optimally within the range of 40-50 °C, d) hyperthermophiles, e) psychrotolerants: they can grow at low temperatures but prefer more moderate temperatures.

Most fungi are mesophiles, and relatively few can grow at or above 37 °C, or even above 30 °, in contrast, to many bacteria. The upper limit for growth for any fungus is 62 °C, while some bacteria thrive at 70-80 °C, and some archaea can grow at over 100 °C.

Temperature sets limits in growth of different organisms, including fungi. The limit is usually set by the first cellular process or component that breaks down. At low temperatures chemical reactions are slowed down, cellular water demonstrates increased viscosity, cellular ions concentrate and lead to protein inactivation. At increased temperatures (45-55 °C), fungi can synthesize heat shock proteins at elevated levels, stress proteins that act like chaperones, ensuring that the cell proteins are correctly folded and that damaged proteins are destroyed (Deacon, 2006).

Fungi have no means of internal temperature regulation, so the higher the external temperature, the greater the cellular damage, and cell viability declines as temperature exceeds optimal growth ranges (Walker and White, 2017).

2.1.5.2 pH

The pH of a fungal culture medium influences fungal physiology: growth, reproduction, metabolite production. Routinely prepared media used for re-culturing fungi in the laboratory, as well as for taxonomic and physiological studies of fungi (such as Czapek-Dox, malt, potato dextrose, Sabouraud agar) possess relatively low buffering capacity (Child et al., 1973). To this respect, when studying fungal responses to pH alterations, it should be taken into consideration that the pH of the medium can rapidly change, due to selective uptake or exchange of ions by fungi. For this purpose, it is a common practice the use of solutions with buffering capacity (common buffering solutions are KH_2PO_4 or K_2HPO_4) (Deacon, 2006).

Caution must be taken when performing and interpreting *in vitro* experiments for studying the effects of pH on fungal growth. Results can be affected by: duration of growth in the medium, the nitrogen source added in the medium, and other factors. Comparison of results from different research groups reveals differences between species or isolates within the same species that are attributed to experimental treatment, and not to inherent differences (Hung and Trappe, 1983).

Many fungi grow within the pH range of 4-8.5, or sometimes 3-9. They show a relatively broad pH optimum of about 5-7, with individual species showing variability within this normal range. Several fungi

are acid tolerant. Certain fungi are also able to grow in strongly alkaline environments, with a pH of about 10. Filamentous fungi that can colonize these environments include species of *Cladosporium*, *Fusarium*, *Penicillium*. While having the ability to grow at extreme pH values, these fungi have an internal cytosolic pH of about 7.

The fungal cytosol has strong buffering capacity. Even when the pH in the surrounding environment changes over several units, the cytosolic pH changes by at most, 0.2-0.3 units. This pH homeostasis of fungal cells can be achieved by several ways: a) by pumping H^+ ions out through the cell membrane to counteract the inflow of H^+ in acidic environments, b) by exchange of materials between the cytosol and the vacuoles (which normally have acidic contents), c) by interconversion of sugars and polyols such as mannitol, which involves the sequestering or release of H^+ . Even small changes in the well regulated cytosolic pH lead to differentiation or change to growth polarity of the hypha.

pH as a growth determining factor, is not unitary, i.e. a change of pH can affect many different factors and processes. Changes in pH can cause: a) change in the net charge on membrane proteins, with potential consequences for nutrient uptake, b) change in the degree of dissociation of mineral salts, and the balance between dissolved carbon dioxide and bicarbonate ions.

Fungi are able to modify the pH of their surrounding environment and, therefore, create their own microenvironment. For example, the form of available nitrogen plays significant role in the pH values of the surrounding environment. If nitrogen is available as NH_4^+ ions, then H^+ ions are released in exchange for NH_4^+ and the external pH can be lowered to a value of 4 or less. This can lead to growth inhibition of pH sensitive fungi such as *Pythium* spp. If nitrogen is available in the form of NO_3^- , its uptake can cause the external pH to rise by about 1 unit. Fungi, also, release organic acids that can lower the external pH. Some aggressive pathogens of plants can secrete oxalic acid in plant tissues, lowering the pH to about 4. Secretion of oxalic acid, in combination with secretion of pectic enzymes with acidic pH optima, contribute to pathogenicity. Oxalic acid can combine with Ca^{2+} in plant tissues, removing Ca^{2+} from pectin in plant cell walls, so the walls are more easily degraded by pectic enzymes (Deacon, 2006).

Fungal growth can be influenced and controlled by relatively minor pH changes. For example, several plant pathogens infect through stomata and they can be guided by topographical signals, including pH changes around leaf stomata. For example, pH gradient of more than one unit has been found around closed stomata, but little or no gradient has been detected around open stomata. Germ-tubes of the rust fungus *Uromyces viciae-fabae* use pH gradient as a means of locating stomata. These germ-tubes terminate over open stomata but not over closed ones (Edwards and Bowling, 1986).

2.1.6 Factors influencing sporulation

Fungal spores are specialized cells that function as resting or dispersal propagules. They may be organs of sexual or asexual reproduction, and they are involved in dispersal and survival (Webster and Weber, 2007). Sporulation and spore germination are frequently considered as a single process, which is sometimes interrupted by a quiescent or dormant period. Much of the information concerning fungal sporulation originate from studies on fungal germination. Fungal sporulation is a complex process that is influenced by environmental and endogenous biological rhythms (Su et al., 2012). Among the factors

that influence fungal sporulation are: light, humidity, aeration, pH, injury to the culture, nutrient type and composition. Conditions that favor rapid mycelial growth hamper sporulation and spore formation occurs when the growth rate is reduced (Dahlberg and Etten, 1982).

Sporulation denotes the completion of the life cycle of pathogenic fungi. Many nutritional factors determine fungal sporulation (carbon source, nitrogen source, microelements), and some fungi exhibit specific carbon and nitrogen requirements for sporulation. Other fungi sporulate only during starvation or depletion of nutrients (Dahlberg and Etten, 1982). Based on *in vitro* studies, sporulation can be triggered by exhaustion of nitrogen and carbon sources. Nutrient limitation triggers fungal sporulation, so that fungi survive in the adverse condition (Masurkar et al., 2018). Signaling mechanisms implicated in sporulation induction under nutrient depletion are not well understood, and a possible explanation is the existence of sensors that signal the environmental nutrient status to the fungal cell (Su et al., 2012). When working with fungi under laboratory conditions, a common issue is the inability of certain fungal isolates (endophytic, pathogenic etc.) to sporulate on artificial media. Modifications in artificial media to provide a low nutrient concentration induce sporulation. Low nutrient media include water agar media, half or ¼ strength PDA, synthetic nutrient-poor agar medium [(Su et al., 2012) and references within]. Slide cultures³³ have been used, for example, to induce appressoria and conidiophores in *Colletotrichum* (Cai et al., 2009) (Su et al., 2011).

Since pathogenic fungi tend to sporulate on host tissues, it is anticipated that some particular plant tissues are effective in inducing sporulation. For example, autoclaved pine needles have been reported to promote sporulation. Perhaps the biotin in plant tissues may alter the cell wall polysaccharides synthesis and oleic acid and thus trigger the selective expression of genes involved in sporulation (Crous et al., 2006) (Su et al., 2012). Chemical supplements also promote sporulation: CaCO₃ induced sporulation of some *Alternaria* (Ascomycota) species. The externally bound calcium has been reported to be involved in the induction step (Su et al., 2012).

The abiotic factor light also plays a role in sporulation induction. It is considered an important stimulus for conidial production. Three factors influence the photo-conidiation of fungi: a) the wavelength of the light used, b) the intensity and duration of the illumination, and c) intervals between individual illuminations. For example, the photo-induced properties of conidiation have been studied in *Trichoderma viride* (Betina, 1995). Conidiation in this fungus can be induced in two ways: a) when colonies are grown in the dark, conidiation can be induced by starvation, b) conidiation can also be induced when the fungus is grown in the dark, and pulses of light are given. *T. viride* reacts to near ultraviolet (UV) radiation (300-380 nm) and to blue light (430-490 nm) (Betina, 1995).

³³ Slide culture is a rapid method of preparing fungal colonies for examination. The fungus grows directly on the slide on a thin film of agar. The advantage of the technique is the small chance of damaging fungal structures (e.g. spore-bearing structures), that would otherwise be damaged through transfer of a portion of a previous culture of the fungus to the slide. From <https://vlab.amrita.edu>

2.2 Materials and methods

2.2.1 Fungal material

Fusarium solani strain K (FsK) (Kavroulakis et al., 2007) was used in all experiments. FsK was routinely cultured on Potato Dextrose Agar (PDA) at 26° C, in the dark.

Fungal conidia were isolated as follows: FsK was routinely cultured on potato dextrose broth (PDB) at 26 °C for 5 d in the dark. Following removal of mycelium fragments by sieving through sterile cheesecloth, conidia were recovered from the filtrate by centrifugation at 6500 rpm. Conidia were diluted in a known volume of 0.85% NaCl and counted using a haemocytometer to determine their concentration.

2.2.2 Effect of different temperatures on FsK mycelium growth

FsK was grown on PDA containing Petri dishes (90mm diameter). A 5 mm FsK plug cut with a cork borer from a previous FsK culture on water agar was used as inoculum and placed at the center of the Petri dish. Cultures were incubated in growth chambers set at the following temperatures: 18, 22, 26, 28, 30, 37 °C. The radius of the fungal colony was recorded on a daily basis for an experimental period of 14 days. The experiment ended when the fungal colony reached the plate edge. 4 or 5 biological replicates were examined for each temperature. 4 radius measurements were averaged per Petri dish for each biological replicate.

Fungal colony radius values (y) over time (x) were fit into a linear regression model, and slopes were estimated for each temperature. Slope values corresponded to the linear velocity growth (mm/day) of the fungal colony at the various temperatures.

2.2.3 Effect of pH adjustment on FsK conidia production and mycelium dry weight

Potato Dextrose Broth medium was prepared in 0.1 M Potassium Phosphate Buffers of various pH, to generate PDB media with desired pH values. After the addition of PDB in the Potassium Phosphate Buffers the pH of the media was adjusted as follows: 5.45, 5.7, 6.15, 6.8, 7.14, 7.5.

A 5 mm FsK plug cut with a cork borer from a previous FsK culture on water agar was used as inoculum for each flask. Cultures were placed on a rotary shaker and incubated for 5 days (180 rpm, 28 °C). The incubation temperature was chosen based on optimal growth temperature findings derived from the above described experiment. At the end of the experimental period, conidia were harvested and their concentration was estimated using a haemocytometer. Mycelium was also collected, dried in an oven (70 °C, 2 days), and mycelium dry weight was determined.

Potassium Phosphate Buffer (0.1M, 1L, various pH) was prepared as described in Table 2-3:

Table 2-3 Preparation of Potassium Phosphate Buffer

Desired pH	pH after PDB addition	Volume of 1M K ₂ HPO ₄ (ml)	Volume of 1M KH ₂ PO ₄ (ml)
5.8	5.4	8.50	91.50
6.0	5.7	13.20	86.80
6.4	6.1	27.80	72.20
7.0	6.8	61.50	38.50
7.4	7.1	80.20	19.80
7.8	7.5	90.80	9.20

Dilute the combined 1M stock solution to 1L with distilled H₂O.

2.2.4 Effect of growth medium composition on FsK mycelium growth

0.1 M Potassium Phosphate buffer (pH 5.8) was used to prepare 3 different media instead of water: water agar, complete yeast medium, Brock's medium. The incubation temperature was chosen based on optimal growth temperature findings derived from the above described experiment. The pH value of the buffer was chosen based on optimal FsK growth results at different medium pH values derived from the previously described experiment. All media maintained a pH value of ~5.8 after ingredients addition. A 5 mm FsK plug cut with a cork borer from a previous FsK culture on water agar was used as inoculum and placed at the center of the Petri dish. Cultures were incubated in a growth chamber set at 28 °C. The radius of the fungal colony was recorded on a ~ daily basis for an experimental period of 9 days. The experiment ended for the different media when the fungal colony reached the Petri dish edge. 4 biological replicates were examined for each medium. 4 radius measurements per Petri dish were averaged for each biological replicate.

Fungal colony radius values (y) over time (x) were fit into a linear regression model, and slopes were estimated for each medium. Slope values corresponded to the linear velocity growth (mm/day) of the fungal colony at the different media.

Potassium phosphate buffer was prepared as described in Table 2-3.

Complete yeast medium and Brock's medium composition is described in Table 2-4 and 2-5, respectively:

Table 2-4 Composition of Complete Yeast Medium (1L)

Component	Weight (g)
Glucose	20.00
Peptone	2.00
Yeast Extract	2.00
MgSO ₄ ·7H ₂ O	0.50
KH ₂ PO ₄	0.46
K ₂ HPO ₄	1.00

Table 2-5 Composition of Brock's Medium (1L)

Component	Weight (g)
Glucose	30.00
NaNO ₃	1.50
MgSO ₄ ·7H ₂ O	0.50
FeSO ₄ ·7H ₂ O	0.01
K ₂ HPO ₄	1.00

2.2.5 Effect of different carbon sources on Fsk conidia production and mycelium dry weight

0.1 M Potassium Phosphate buffer (pH=5.8) was used to prepare Brock's medium instead of water. Brock's medium was chosen based on Fsk optimal growth results in different media derived from the previously described experiment.

Brock's medium supplemented with either no carbon source, or glucose/galactose/sucrose as sole carbon source were prepared. Quantities of supplemented carbon-containing compounds were adjusted to provide equal quantities (grammoatoms) of carbon.

A 5 mm Fsk plug cut with a cork borer from a previous Fsk culture on water agar was used as inoculum for each flask. Each flask consisted a biological replicate. 4 biological replicates were assessed for each medium. Cultures were placed on a rotary shaker and incubated for 5 days (180 rpm, 28 °C). The incubation temperature was chosen based on findings from experiment 2. At the end of the experimental period, conidia were harvested and their concentration was estimated using a haemocytometer. Mycelium was also collected, dried in an oven (70 °C. 2 days), and mycelium dry weight was determined.

Potassium phosphate buffer was prepared as described above.

Brock's medium was prepared as described above with the respective carbon-source substitution.

2.2.6 Effect of different nitrogen sources on Fsk conidia production and mycelium dry weight

0.1 M Potassium Phosphate buffer (pH=5.8) was used to prepare Brock's medium instead of water. Brock's medium was chosen based on Fsk optimal growth results in different media derived from the previously described experiment.

Brock's medium supplemented with either no nitrogen source, or NaNO₃, NaNO₂, NH₄Cl, Ammonium Tartrate, Urea, Peptone, L-asparagine as sole nitrogen source was prepared. Quantities of supplemented nitrogen-containing substances were adjusted to provide equal quantities (grammoatoms) of nitrogen.

A 5 mm Fsk plug cut with a cork borer from a previous Fsk culture on water agar was used as inoculum for each flask. Each flask consisted a biological replicate. 4 biological replicates were assessed for each medium. Cultures were placed on a rotary shaker and incubated for 5 days (180 rpm, 28 °C). The incubation temperature was chosen based on findings from experiment 2. At the end of the experimental

period, conidia were harvested and their concentration was estimated using a haemocytometer. Mycelium was also collected, dried in an oven (70 °C, 2 days), and mycelium dry weight was determined.

Potassium phosphate buffer was prepared as described above.

Brock's medium was prepared as described above with the respective nitrogen-source substitution.

2.2.7 Statistical analysis

One-way ANOVA (followed by Tukey's post-hoc test) was used in comparisons between three or more categorical variables.

Two-way ANOVA (followed by Tukey's post-hoc test) was used to examine the effect of two factors on a dependent variable.

Statistical analyses employed are indicated in detail in the corresponding Figures/Figure legends and in Appendix of Chapter 2.

2.3 Results

2.3.1 Effect of temperature on FsK mycelial colony growth

To determine the impact of various temperatures on FsK growth, PDA containing Petri dishes were inoculated with a constant fungal inoculum and the colony diameter was recorded for a maximal period of 15 days. FsK grew rapidly at temperatures 26, 28 and 30 °C and reached the maximal growth in the Petri dish (defined as when the colony reaches the edge of the plate) in ~8 days post fungal inoculation and incubation initiation. The fungus demonstrated a relatively delayed rate of growth at 22 °C, and reached maximal growth on plate at ~11 days post incubation initiation. FsK demonstrated a belated proliferation at relatively low and high temperatures (18 and 37 °C), as indicated by the fact that mycelium had not yet reached the edge of the Petri dish (Figure 2-2). Statistical significant differences were recorded among the various temperatures during the whole experimental period. At the 8th day of the experiment (final day of calculations of mycelia grown in all temperatures examined) differences were recorded among 3 groups of temperatures: group a (18, 37 °C), group b (22 °C), group c (26, 28, 30 °C).

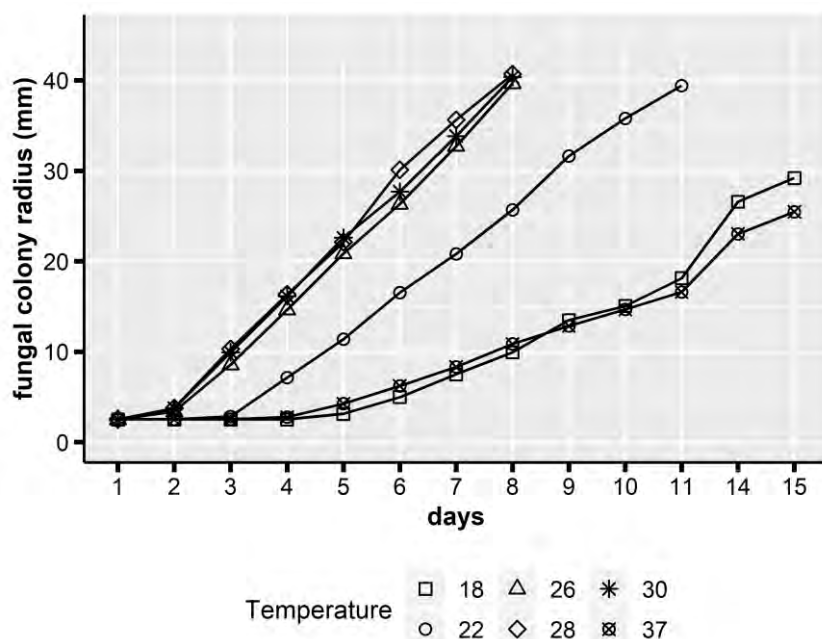


Figure 2-2 Effect of temperature on FsK mycelial growth. FsK was grown in Petri dishes containing PDA as substrate. Petri dishes were incubated in growth chambers set constantly at 18, 22, 26, 28, 30 and 37 °C. Fungal colony radius was determined approximately on a daily basis. The experiment ended when the fungal colony reached the edge of the Petri dish. Four (4) or 5 biological replicates were investigated for each temperature. Statistical significant differences between the temperatures investigated was recorded at the 8th day of the experiment (final day in which plates incubated in all temperatures examined are included in the calculations) (one way anova, Tukey's test at the 0.05 level).

To further assess the impact of the various temperatures in FsK growth, the linear velocity of fungal mycelial growth was calculated, as the mm of mycelial colony growth per day (Table 2-6). In accordance to the above results, the fungus demonstrated the maximal velocity of growth at 28, 30, 26 °C, respectively, followed by the temperature of 22 °C. The lowest growth velocity was observed at relatively low (18 °C) and relatively high (37 °C) temperatures. Statistical analysis revealed significant differences in all pairwise comparisons using mean linear velocity values, besides comparisons of linear velocity values among 30-26 and 30-28 °C.

Table 2-6 Impact of temperature on linear velocity of growth of FsK mycelium. FsK was grown in Petri dishes containing Potato Dextrose Agar as substrate. Petri dishes were incubated in growth chambers constantly set at 18, 22, 26, 28, 30 and 37 °C. Fungal colony radius was determined approximately on a daily basis. Four (4) or 5 biological replicates were assessed for each temperature. The linear relationship between time (x) and fungal colony radius (y) was generated. The coefficient variable corresponds to the mycelium linear velocity (mm/day). Statistically significant differences were recorded in all pairwise comparisons of linear velocity values corresponding to the temperatures investigated, besides comparisons among 30-26 and 30-28°C (one-way ANOVA, Tukey's post-hoc test at the 0.05 level) (see Appendix of Chapter 2).

Temperature	Linear velocity (mm/day)	sd
18	2.04	0.06
22	4.10	0.11
26	5.55	0.13
28	5.85	0.08
30	5.66	0.09
37	1.76	0.19

2.3.2 Effect of pH values on FsK sporulation and mycelial growth

Different growth medium (PDB) pH values were assessed for their impact on FsK conidiation capacity. The pH of the medium was adjusted prior to fungal inoculation by preparing the medium in phosphate solution with buffering capacity, allowing maintenance of the pH throughout fungal growth. FsK sporulates optimally when the medium pH value is adjusted at the acidic range (Figure 2-3). More specifically pH 5.7 gave the optimal results in terms of conidia production, followed by pH 5.45. pH values tested within the range 6.15 – 7.5 resulted in a statistically significantly lower number of conidia, in comparison to the optimal pH value 5.7.

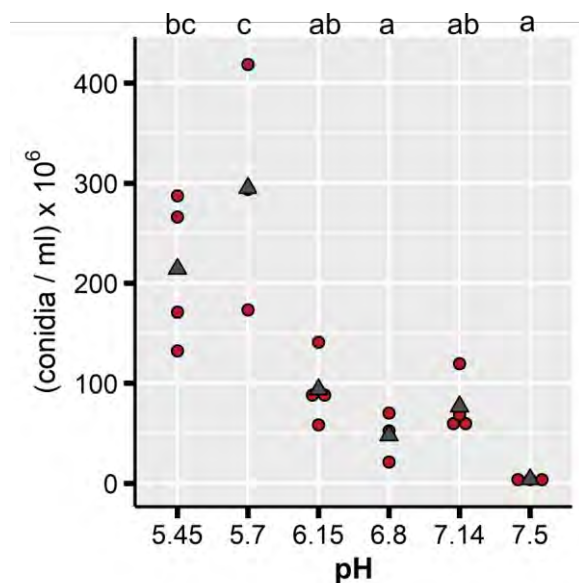


Figure 2-3 Effect of growth medium pH values on *FsK* conidia production. *FsK* was grown on PDB medium for 5 days (28 °C, 180 rpm). The growth medium pH was adjusted to the following values: 5.45, 5.7, 6.15, 6.8, 7.14, 7.5. Conidia production was investigated at the end of the experiment. 4 biological replicates were analyzed for each pH value adjustment. Statistical significant differences are indicated with different letters (one-way ANOVA, Tukey's test at the 0.05 level).

red dots, biological replicates; dark grey triangles, mean values at the different pH adjustment values.

From the same fungal cultures used above, mycelium was also collected on a cheesecloth, allowed to dry in an oven, and afterwards, dry mycelium weight was estimated. In contrast to the recorded impact of pH on conidia production, all pH values gave similar results in terms of dry mycelium weight. More specifically, values closer to the neutral range (6.15-7.14) yielded slightly higher mycelium weight, in comparison to more acidic or more basic values. No statistically significant difference was recorded in the dry weight of fungal mycelium produced in any of the different pH values.

In all, pH seems to affect conidia production but not the increase of the fungal mycelium mass. Acidic pH values favor sporulation, whereas mycelial growth is more tolerant and is supported in a wider range of pH values, from slightly acidic to basic, with a preference towards the neutral range.

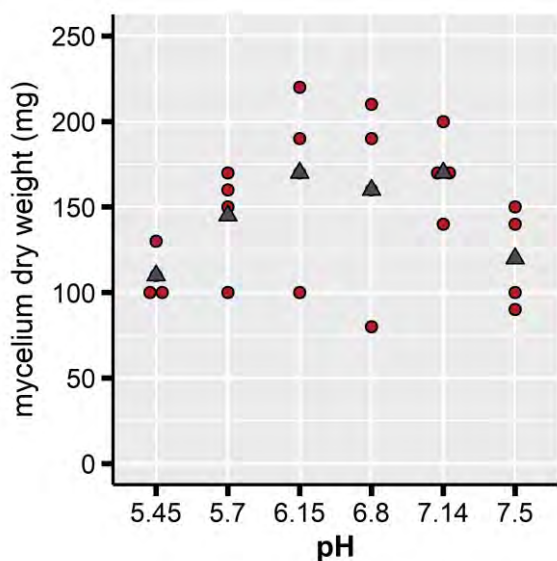


Figure 2-4 Effect of growth medium pH values on FsK mycelium dry weight. FsK was grown on PDB medium for 5 days (28 °C, 180 rpm). The growth medium pH was adjusted to the following values: 5.45, 5.7, 6.15, 6.8, 7.14, 7.5. At the end of the experiment mycelium was collected, allowed to dry in an oven (70 °C) and dry weight was estimated. Four (4) biological replicates were analyzed for each pH value adjustment. No statistically significant difference was recorded in FsK mycelium dry weight under the influence of growth medium pH values examined herein (one-way ANOVA). red dots, biological replicates; dark grey triangles, mean values at the different pH adjustment values.

2.3.3 Effect of different media on FsK mycelial growth

Two different media commonly used for fungal growth in laboratory conditions were assessed for their impact on colony diameter increase over time. More specifically, Brock's medium and Complete Yeast Medium were used and compared to fungal growth in Water Agar (absence of main carbon, nitrogen source). Potato Dextrose Agar was not included in the experiment, because it is a mixture of carbon and nitrogen sources provided in a powdery form, thus not allowing for substances separation and substitution with another source (performed in the subsequent experiments). Its preparation from potatoes in the laboratory also does not allow the substitution of specific substances. Both media examined contain glucose as their primary carbon source. Brock's medium contains less glucose per liter in comparison to Complete Yeast Medium. Agar, provided as a jellifying agent in all media, is a mixture of two components: the linear polysaccharide agarose, and a heterogeneous mixture of smaller molecules called agaropectin. Agarose makes up about 70% of the mixture.

In terms of nitrogen sources, Brock's medium contains inorganic nitrogen (NaNO_3), whereas Complete Yeast Medium contains organic nitrogen (peptone and yeast extract). Bacteriological peptone is dried powder containing amino acids, short chained peptides derived from enzymatic digestion of high quality protein. Yeast extract is a complex and widely used hydrolysate of yeasts. It provides nitrogenous compounds, carbon, sulfur, trace nutrients, vitamin B complex and other important growth factors, which are essential for the growth of diverse microorganisms. The two media used herein harbor also minor differences in metal containing substances. FsK growth measured as colony radius increase over time, was very similar in all media tested. Fungal growth was similar in all 3 media tested, despite the absence

of a primary carbon and nitrogen source in water agar medium (Figure 2-5). Brock's Medium and Complete Yeast Medium allowed for a slight faster growth (the fungus reached the maximum colony diameter approximately 1 day sooner in comparison to water agar). Statistical analysis at the 8th day of the experiment (comparisons of calculations derived from all 3 media tested) revealed differences in water agar media in comparison to Complete Yeast or Brock's medium. No difference was recorded between Complete Yeast and Brock's medium at the final day of the experiment.

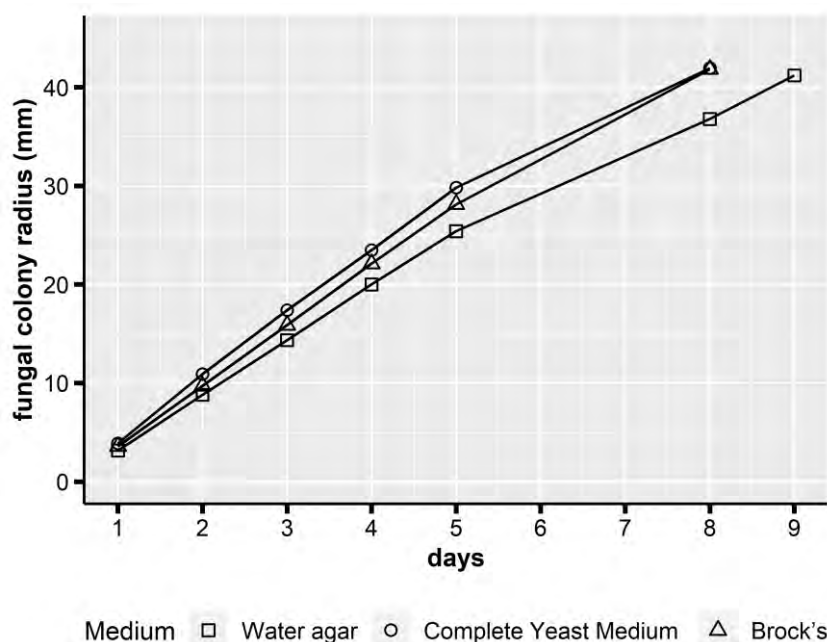


*Figure 2-5 Effect of different growth media on *FsK* mycelial growth. *FsK* was grown in Petri dishes containing: water agar, complete yeast medium, Brock's medium. Petri dishes were incubated in a growth chamber (28 °C). Fungal colony radius was determined approximately on a daily basis. The experiment ended when the fungal colony reached the edge of the Petri dish. 5 biological replicates were examined for each growth medium. Statistically significant difference was recorded in fungal colony radius between Water Agar and the other two media at the 8th day of the experiment (one-way ANOVA, Tukey's post-hoc test at the 0.05 level).*

The linear velocity of fungal growth in these media was furthermore calculated. More specifically the mm of colony growth per day was estimated. As expected, Complete Yeast Medium and Brock's medium demonstrated the higher velocity values (Table 2-7), with both media giving very similar results. Water agar demonstrated the lowest linear velocity value, as also easily observed from the graph of Figure 2-7. Statistical analysis in mean linear velocity values revealed differences only in pairwise comparisons between water agar – Brock's medium and water agar – Complete Yeast Medium. No differences were recorded in linear velocity values between Brock's and Complete Yeast Medium.

Table 2-7 Impact of different growth media on FsK mycelium linear velocity. FsK was grown in Petri dishes containing: water agar, complete yeast medium, Brock's medium. Petri dishes were incubated in a growth chamber (28 °C). Fungal colony radius was determined approximately on a daily basis. The experiment ended when the fungal colony reached the edge of the Petri dish. 5 biological replicates were examined for each growth medium. The linear relationship between time (x) and fungal colony radius (y) was generated. The coefficient variable corresponds to the mycelium linear velocity (mm/day). Statistically significant differences were recorded in pairwise comparisons among water agar and Brock's or Complete Yeast medium (one-way ANOVA, Tukey's post-hoc test at the 0.05 level). Statistical analysis is presented in Appendix of Chapter 2.

Medium	Linear velocity (mm/day)	sd
Water agar	4.68	0.10
Complete Yeast Medium	5.45	0.06
Brock's	5.50	0.02

2.3.4 Effect of various carbon sources on FsK sporulation and mycelial growth

The impact of different carbon sources on FsK ability to produce asexual propagules (conidia) was assessed, by supplementing the growth medium with different carbohydrates. Brock's medium was selected as the principal medium, due to the higher fungal growth linear velocity recorded in this medium (Table 2-7). The pH of the medium was adjusted to the optimal value supporting FsK mycelial growth presented in Figure 2-5 (pH 5.8). Brock's medium with no carbon source added was used as control. Two monosaccharides (glucose and galactose) and 1 disaccharide (sucrose) were assessed for their ability to support fungal sporulation. As demonstrated in Figure 2-6, all carbohydrates supplemented in the medium supported fungal conidia production. The monosaccharide glucose, enabled the highest conidia production (average value: 13.2×10^7 conidia/ml). Galactose and sucrose resulted in lower values of produced conidia. As expected, in the control medium, no conidia were produced, indicating the importance of the addition of a carbon source on asexual reproductive spores formation. Statistical analysis revealed differences among the conidia produced in the absence of a carbon source, and conidia produced in presence of glucose, or galactose, or sucrose. No differences were recorded in the conidia produced in the presence of the various carbon sources.

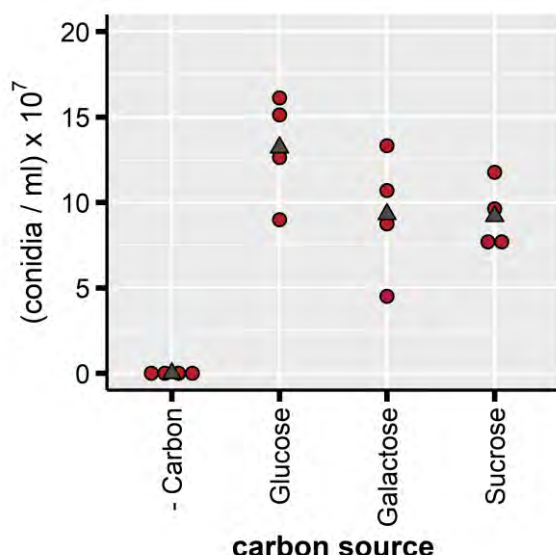


Figure 2-6 Effect of carbon sources on *FsK* conidia production. *FsK* was grown in Brock's broth medium supplemented with: no carbon source, glucose, galactose, sucrose. Liquid cultures were incubated in a growth chamber for 5 days (28 °C, 180 rpm). Conidia production was investigated at the end of the experiment. Four biological replicates were examined for each growth medium. All sources resulted in significantly higher values of conidia, in comparison with the control (one-way anova, Tukey's test at the 0.05 level). No differences were recorded among the 3 carbon sources (one-way ANOVA). See Appendix of Chapter 2.

red dots, biological replicates; dark grey triangles, mean values at the different carbon sources.

From the same biological replicates used for conidia production, mycelium was harvested with a cheesecloth and allowed to air dry for several days, and the mycelium dry weight was estimated. In contrast to the absence of mycelium production in the absence of a carbon source, all carbon sources well supported the mycelium production. We observed differences on mycelium mass production, which depended on the carbon source supplemented in the growth medium. When dry mycelium values in the presence of the various carbon sources were compared, sucrose and glucose gave similar results (Figure 2-7). These two carbohydrates resulted in statistically significantly higher values of mycelium dry weight in comparison to galactose, the epimer of glucose.

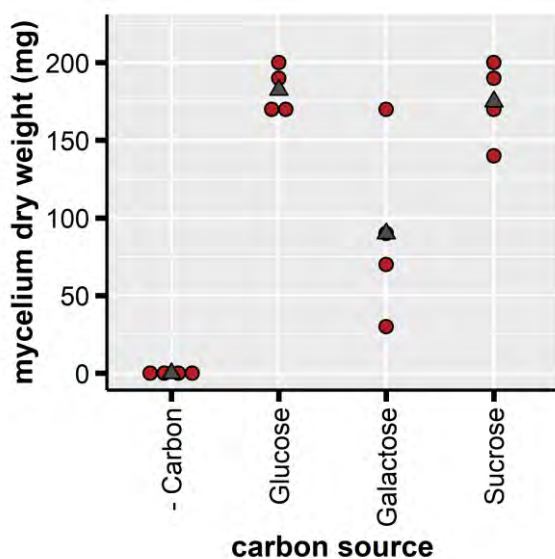


Figure 2-7 Effect of carbon sources on *FsK* mycelium weight. *FsK* was grown in Brock's broth medium supplemented with: no carbon source, glucose, galactose, sucrose. Liquid cultures were incubated in a growth chamber for 5 days (28 °C, 180 rpm). Mycelium was harvested at the end of the experiment, dried in an oven, and its dry weight was determined. Four (4) biological replicates were examined for each growth medium. All carbon sources resulted in statistically significantly higher values of mycelium weight in comparison to the mycelium weight in the absence of a carbon source (no mycelium produced). Among the carbon sources, statistically significant differences were recorded only in pairwise comparisons of galactose with glucose or sucrose. See Appendix of Chapter 2.

red dots, biological replicates; dark grey triangles, mean values at the different carbon sources.

2.3.5 Effect of various nitrogen sources on *FsK* sporulation and mycelial growth

The impact of various sources of nitrogen on *FsK* asexual spore production was assessed by supplementing the medium (Brock's medium with adjusted pH 5.8) with different nitrogenous substances. More specifically, we assessed both inorganic compounds (NaNO_3 , NaNO_2 , NH_4Cl) and organic compounds (ammonium tartrate, urea, peptone, L-asparagine). As control, Brock's medium with no addition of a nitrogenous source was employed. To our surprise only peptone allowed for high production of conidia in liquid culture. Only peptone and ammonium tartrate, and marginally NH_4Cl , resulted in significantly higher values of conidia in comparison to values recorded in the absence of a nitrogenous source. All other sources of nitrogen resulted to low/no production of conidia (Figure 2-8).

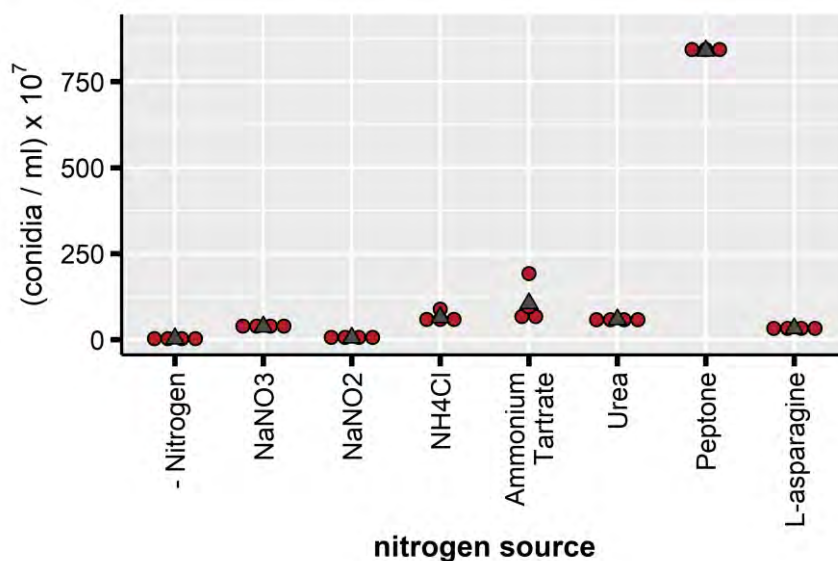


Figure 2-8 Effect of nitrogen sources on *FsK* conidia production. *FsK* was grown in Brock's broth medium supplemented with: no nitrogen source, NaNO₃, NaNO₂, NH₄Cl, Ammonium Tartrate, Urea, Peptone, L-asparagine. Liquid cultures were incubated in a growth chamber for 5 days (26 °C, 180 rpm). Conidia were harvested at the end of the experiment and their concentration was estimated. Four (4) biological replicates were examined for each growth medium. Statistical analysis (one-way ANOVA, Tukey's test) is presented in Appendix of Chapter 2. red dots, biological replicates; dark grey triangles, mean values at the different nitrogen sources.

From the same biological replicates used for conidia production, mycelium was collected at the end of the experimental period with a cheesecloth and allowed to dry. Afterwards, mycelium dry weight was determined. The impact of various nitrogen sources on mycelium dry weight was different from that recorded on asexual spore production. *FsK* is able to use a various range of nitrogenous substances that allow increase in its mycelium weight. Only NaNO₂ and NaNO₃ resulted in moderate mycelial mass values, as demonstrated in Figure 2-9. More specifically, the weight of the mycelium produced in the presence of NaNO₂ showed no significant difference to the weight of the mycelium produced in the absence of a nitrogen source. All other nitrogen sources (including NaNO₃) resulted in significantly higher values of mycelium weight produced in comparison to values recorded in the absence of a nitrogenous source. Peptone, and the amino acid L-asparagine gave optimum results.

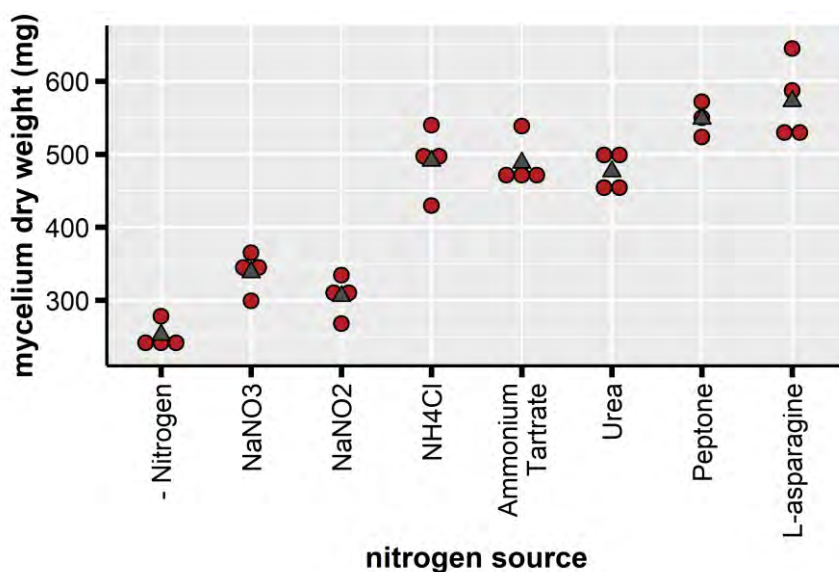


Figure 2-9 Effect of nitrogen sources on *FsK* mycelium weight. *FsK* was grown in Brock's broth medium supplemented with: no nitrogen source, NaNO₃, NaNO₂, NH₄Cl, Ammonium Tartrate, Urea, Peptone, L-asparagine. Liquid cultures were incubated in a growth chamber for 5 days (28 °C, 180 rpm). Conidia were harvested at the end of the experiment and their concentration was estimated. Four (4) biological replicates were examined for each growth medium. Statistical analysis (one-way ANOVA, Tukey's test at the 0.05 level) revealed significant differences in mycelium produced in the presence of all nitrogen sources (besides NaNO₂) in comparison to mycelium produced in the absence of a nitrogenous source. See also Appendix of Chapter 2.

red dots, biological replicates; dark grey triangles, mean values at the different nitrogen sources.

2.4 Discussion

Fungi are among the most important organisms in nature. They contribute essentially to the biogeochemical cycles, i.e. the recycling of various elements in the ecosystem. They are capable decomposers of organic matter. They decompose organic compounds into their simplest constituents via production and extracellular secretion of a vast array of enzymes. For example, fungi produce a variety of carbohydrate activity enzymes (CAZymes) responsible for the breakdown, biosynthesis, or modification of glycoconjugates, oligo- and polysaccharides. Plant cell wall degrading enzymes secreted by fungi are particularly important due to their contribution in fungal pathogenesis: they facilitate penetration and successful infection and therefore allow fungi to gain nutrition (Zhao et al., 2013). Fungi are heterotrophs, and therefore depend on nutrient assimilation for energy and growth. They have the ability though to produce their own amino acids, provided with a carbon source and a simple nitrogenous source, like ammonium. Fungi are well utilized in biotechnology, industry, and agriculture.

Knowledge concerning fungal optimal growth and reproduction parameters can provide insight into optimizing their manipulation, irrespective of the research field. The knowledge of the nutritional requirements of microbes is necessary for their cultivation using any cultivation technique (Mehta et al., 2012). The carbohydrates, proteins, lipids, nucleic acids, are composed of macroelements: carbon, hydrogen, nitrogen, sulfur, phosphorus. The acquisition of nutrients is, for example, the main driver of host-microbe interactions (either mutualistic, symbiotic, or pathogenic). Saprotrophic fungi utilize a wide range of nutrient sources in their natural environment, but for industrial purposes like mass production and commercialization, simple and cheap media are needed for fungal growth in the laboratory. Documentation of pH, temperature and other physiological traits of fungal growth is essential for development of reliable and suitable methods for routine cultivation and multiplication in the laboratory, and are prerequisite for advanced research (Mehta et al., 2012). Current knowledge is based on the extensive investigation of the most important fungal 'lab-pets' *Aspergillus nidulans*, *Neurospora crassa*, *Sacchromyces cerevisiae*. It is important to extend this knowledge in other fungal taxa as well.

A number of factors has been recorded to influence fungal physiology, with nutrient provision being among the most important ones, as fungi need to assimilate nutrients and essential metals from their environment. Abiotic factors associated with the niche of a fungus also influence its physiology. Various environmental factors have been reported to affect fungal growth and reproduction, among them pH, oxygen, light, temperature etc.

In the present study certain factors influencing the physiology of *Fusarium solani* strain K (Kavroulakis et al., 2007) were investigated under laboratory conditions. The aim was to investigate its growth and reproduction in order to optimize its routine culture in the laboratory for subsequent experiments presented in the present dissertation. To this respect, the influence of a range of factors in growth and asexual reproduction of FsK under in vitro conditions (in solid as well as in liquid media, depending on the factor investigated) was examined. Among abiotic factors, the two major ones influencing fungal growth in the laboratory were investigated: temperature and pH.

Based on results of this study, FsK is considered a mesophile, and therefore grows optimally at temperatures 26-30 °C, showing minimal differences in the three temperatures investigated within this

range. Growth, as measured via radial growth on Petri dishes, initiated relatively fast (with a lag phase of only 1 day) at this temperature, and was constant up to the last time point measured (7 days post substrate inoculation). FsK showed a delayed growth initiation at 22 °C (lag phase of ~ 2 days) and reached its maximum size on the Petri dish at a later time point in comparison to its growth at the optimum temperature range (26-28 °C). The fungus showed the least preference for lower/higher temperatures than the above mentioned, that is 18 and 37 °C, respectively. The lag phase until growth initiation lasted longer (~4 days) and the fungus did not reach its maximum size on the Petri dish up to the last time point of the experiment (15 days post inoculation and incubation initiation).

FsK has therefore the ability to grow in a variety of temperatures, ranging from 18-37 °C. Its optimal growth lies at temperatures characteristic for mesophilic fungi (10-40 °C), although its optimal temperature lies outside the upper optimum range of growth for these organisms (22-25 °C) (Deacon, 2006). It is of importance that the fungus can also grow (relatively slower) at the upper range of mesophilic temperature of growth (37 °C). FsK was isolated from tomato plants (Kavroulakis et al., 2007), which are known as warm season plants, and therefore its niche of isolation might partially explain its preference for temperatures slightly higher than the ambient temperature (25 °C). This is in accordance to other studies on *Fusarium* genus. The effect of temperature on *in vitro* growth of the tomato crown and root rot causing agent *Fusarium oxysporum* f. sp. *radicis-lycopersici* (FORL) was assessed, and the highest growth speed was recorded at 25 °C (Hibar et al., 2006). Interestingly, the growth speed recorded was much higher than what it was recorded herein for similar temperatures (>13 mm*day⁻¹ and ~5.5 mm*day⁻¹, respectively). Mycelial growth was maintained at 20 and 30 °C, and it was reduced at 15 and 35 °C, as also observed for FsK. Nonetheless, lower growth speed rates were recorded for FsK in all examined temperatures of similar range. *Fusarium oxysporum* f. sp. *glycines* grows also optimally at temperatures 22-28 °C, and can develop a colony in a relatively wide range of temperatures (8-36 °C). A temperature of 38 °C was lethal for this fungal strain (Balasu et al., 2015). (Suárez-Estrella et al., 2003) demonstrated the detrimental effect of high temperatures in growth of the wilt causing phytopathogen *Fusarium oxysporum* f. sp. *melonis*, which grows optimally at 30 °C. Exposure of the fungal strain in high temperatures (46-65 °C) had a drastic effect on fungal growth, which was significantly eliminated. (Farooq et al., 2005) results concerning the optimal temperature for growth of *F. oxysporum* f. sp. *ciceris* are in agreement to results presented here. The fungus is able to grow in the temperature range 10-35 °C. It demonstrates optimal growth at 25 and 30 °C, whereas temperature values below 15 and above 35 °C reduced fungal growth.

The effect of the pH regime in the physiology of FsK was furthermore investigated, measured as changes in mycelial mass or in the production of asexual propagules (conidia production). pH influences the physiology of FsK (both in terms of growth and reproduction). Differences were recorded when the fungus was grown on various pH values. Conidia production was enhanced when the pH of the medium was slightly acidic (maximum production was recorded at pH 5.7, followed by 5.4). The increased number of conidia recorded in the slightly acidic environment may be due to protection of conidia from cytolysis (de-plasmolysis). During conidiogenesis, usage of organic compounds to support the increased metabolic requirements of the process, perhaps leads to a decrease in the intracellular pH, and therefore increase in proton ions. When the extracellular pH is also slightly acidic, the fungal cell is

protected from turgidity (absorption of water after cells are placed in a hypotonic solution). A wide range of pH values is able to support FsK mycelial mass increase, from slightly acidic to slightly basic values, at least for the time period investigated herein (5 days). A preference was observed towards the neutral range of pH values (6.1-7.1), which might reflect the intracellular pH of the mycelium balanced at neutral pH, at this stage of fungal growth. To conclude, pH affects the physiology of FsK, expressed as differences on the net mycelial mass and fungal propagules (asexual spores) produced by the fungus. Conidiation occurs optimally at the acidic range, whereas the mycelium grows relatively well in a wider range of pH values, spanning the acidic to neutral and basic pH range. The impact of pH on the growth and reproduction of *Fusarium oxysporum* *in vitro* has been investigated. The authors reported 6.5 as the optimal pH value both for mycelium production and for sporulation of the fungus. While maximum production of macro and microconidia was achieved on this near-neutral pH range, production of chlamydospores was optimal at pH 4.5 (Tyagi and Paudel, 2014). The effect of pH in the physiology of *Fusarium* sp. grown *in vitro* in both solid and liquid cultures has also been assessed. The highest colony diameter and mycelial fresh weight was achieved at neutral pH (7.0), whereas both parameters were negatively affected at the acidic range (pH 5.0). The authors reported that colony color and conidia morphology also differ in relation to the different pH values. The characteristic conidia of the species (dolphin-like, swollen appearance) were produced at pH 7.0 (Sánchez-Rangel et al., 2018). (Balasu et al., 2015) studied the influence of pH on the development of *Fusarium oxysporum* f. sp. *glycines*, and found that the fungus is able to grow on a wide range of pH values. Optimal pH ranged from acidic to basic values (4.0-7.0). Alkalinization of the medium negatively affected the vegetative growth of the fungus, but not its sporulation capabilities. The influence of pH on the growth of three *Fusarium oxysporum* f. sp. *elaeidis* isolates (causal agent of oil palm vascular wilt) has been investigated not only in artificial media but also in soil samples. pH values of 5.0-7.0 were best for growth and survival of the pathogen as estimated via chlamydospore germination and number of *Fusarium* propagules/g of soil. The least favorable results were recorded at the highly acidic value of pH 3.0 (Oritsejafor, 1986). (Farooq et al., 2005) results concerning the optimal pH of growth of *F. oxysporum* f. sp. *ciceris* are in agreement to results presented herein. The authors report that pH values of 6-8 well supported fungal growth with pH 7 being the most favorable. Acidic and basic values below and above this range, respectively, decreased fungal growth. Unfortunately, acidic pH values (<5.45) were not assessed in the present work, as the primary goal was to assess optimum pH values for routine cultivations.

Two different microbiological culture media routinely used in the laboratory for growing fungi were used, in order to test the ability of FsK for growth. Brock's medium was chosen in order to proceed with further analysis concerning carbon and nitrogen sources, despite the fact that both media supported well the rate of growth of FsK in solid culture. Both media contained glucose as carbon source; the principal nitrogenous source differed (peptone and NaNO₃ for Complete Yeast and Brock's medium, respectively).

Afterwards, the influence of several nutrients in FsK physiology was investigated, focusing on basic nutrients available in the laboratory, commonly used for routine microbiology practices. More specifically the influence of three major carbon sources (glucose, galactose, sucrose) in the growth and conidiation of FsK was assessed. All carbon sources supported well the ability of the fungus to produce

conidia, whereas very low levels of conidiation were recorded in the absence of a carbon source, an indication that a source of energy is necessary for asexual reproduction initiation of the fungus. Carbon starvation is thus a limiting factor in FSK ability to reproduce asexually. The degree of complexity of the molecule, that is whether it is a monosaccharide (glucose or galactose) or a disaccharide (sucrose: disaccharide, composed of glucose and fructose) did not seem to play a significant role in that process. Most probably both mono- and di-saccharides are well assimilated and support the needs of the fungus for energy during sporogenesis. On the other hand, differences were recorded when the net mycelial mass production was estimated. The monosaccharide glucose and the disaccharide sucrose were well used and supported the growth of the mycelium. It is not known though if the carbon sources contributed to increase in the mass of the cells that constitute the mycelium, or whether they contributed to an increase in the number of mycelial cells. Nonetheless, the epimer of glucose at C-4, galactose, contributed to a lesser extent in fungal mass increase, an indication that the stereochemistry of sugar substances plays a role in their assimilation and/or their further utilization within the fungal cell. It should be noted that FSK was routinely cultured on Potato Dextrose Agar prior to this experiment (despite the fact that for inoculations a previous culture of FSK on water agar was used), which contains dextrose (a form of glucose, D-glucose) as primary carbon source. Taking this into consideration, FSK was adapted in the uptake of glucose-based molecules for energy and for obtaining carbon skeletons. Perhaps this enabled the fungus to quickly assimilate and utilize the carbon sources provided in the experiment, with a preference over the monosaccharide glucose and the disaccharide sucrose (Mehta et al., 2012) assessed the influence of certain carbon sources on the total biomass production of isolates of the biofungicide *Trichoderma viride* (Ascomycota; Hypocreaceae), and isolates of the entomopathogenic fungus *Beauveria bassiana* (Ascomycota; Cordycipitaceae). Dextrose and fructose resulted in the highest total biomass production of *T. viride* and *B. bassiana*, respectively. The mycelial growth of *F. oxysporum* f. sp. *passiflorae* isolates, obtained from yellow passion fruit plants with fusariosis symptoms, in various carbon sources has been assessed. Starch was the optimal carbon source, resulting in the highest mycelial growth (Catarino et al., 2018). The influence of carbon sources on colony growth of *F. oxysporum* f. sp. *ciceris* has also been assessed. Maximum colony growth was recorded in medium containing dextrose and sucrose (Maitlo et al., 2017). Sucrose supported well the net mycelial mass of FSK as well. From the nine carbon sources examined, maltose, starch, glucose, xylose, lactose and fructose were most favorable for the growth of the pathogenic fungus *Fusarium oxysporum* f. sp. *ciceri*, whereas galactose was unfavorable. The absence of a carbon source resulted in absence of growth (Khilare and Ahmed, 2011). This is in agreement to present findings, as FSK did not grow in the absence of a carbon source in the growing medium, an indication that carbon constitutes the major structural component of fungal cells required for their growth and development. (Farooq et al., 2005) investigated the effect of carbon sources on *F. oxysporum* f. sp. *ciceri* and found that glucose, sucrose and starch supported well the fungal growth, with the monosaccharide glucose giving the best results.

The effect of various nitrogenous sources on FSK physiology (mycelial growth and reproduction) was furthermore investigated, by using a range of resources of nitrogen either organic or inorganic. As far as the production of conidia is concerned, peptone was the only compound that resulted in the highest

yield of asexual spores. This can be attributed to the properties of peptone: it is a mixture of small peptides and amino acids, most probably easily degradable by secreted proteases and therefore easily assimilated by the fungal cell for further usage within the fungal apoplast for growth. All other sources of N both organic and inorganic resulted in very low to lack of production of asexual spores.

In terms of net mycelial mass production, peptone and the amino acid L-asparagine gave optimum results. The amino acid L-asparagine can be utilized directly after its uptake for protein synthesis, or cleaved by proteases to form the easily utilized amino acid glutamate, which is the precursor of other amino acids synthesized by it by transamination reactions. Inorganic nitrogenous sources were proven less capable of supporting mycelial mass, besides NH_4Cl . The latter as well as all rest organic nitrogenous sources led to increase in dry mycelium weight. From inorganic N sources, NaNO_2 and NaNO_3 resulted in the lowest production of conidia by FSK. The absence of N in the medium resulted in very low mycelial growth and absence of conidia production, an indication that nitrogen starvation has a negative effect both in the growth and the reproduction of the fungus. It is important to address that organic nitrogenous sources (like FSK favorite sources, peptone and L-asparagine) also contribute to carbon assimilation further contributing as energy sources or as carbon skeletons for synthesis of organic substances such as amino acids. The simultaneous provision of carbon in the fungal cell might act synergistically to the provided nitrogen source leading to a further increase in the net mycelial growth and or in the conidiation process. (Mehta et al., 2012) assessed the influence of certain inorganic nitrogen sources on the total biomass production of isolates of the biofungicide *T. viride*, and isolates of the entomopathogenic fungus *B. bassiana*. Ammonium sulphate and sodium nitrate gave the highest mass values for *T. viride* and *B. bassiana*, respectively. (Khilare and Ahmed, 2011) investigated the effect of ten different N sources on the colony growth of *F. oxysporum* f. sp. *Ciceris*, the causing agent of chickpea wilt, and found that calcium nitrate, magnesium nitrate, potassium nitrate and urea were most favorable for fungal growth. The maximum colony growth of *F. oxysporum* f. sp. *ciceris* in the presence of various N sources has also been assessed by other research groups. (Maitlo et al., 2017) showed that potassium nitrate followed by peptone gave optimum results. (Farooq et al., 2005) showed that peptone was the best source of nitrogen for *F. oxysporum* f. sp. *ciceri*, followed by potassium nitrate. Results on peptone were in accordance to results concerning FSK growth.

2.5 References

- Allen JW, Shachar-Hill Y. 2009.** Sulfur Transfer through an Arbuscular Mycorrhiza. *Plant Physiology* **149**: 549–560.
- Anderson JB, Kohn LM. 1998.** Genotyping, gene genealogies and genomics bring fungal population genetics above ground. *Trends in Ecology and Evolution* **13**: 444–449.
- Balasu AG, Stelica C, Relu ZC, Orpea M. 2015.** The biological growth parameters of the *Fusarium oxysporum* f. sp. *glycines* fungus. *Romanian Biotechnological Letters* **20**: 10921–10928.
- Betina V. 1995.** Photoinduced conidiation in *Trichoderma viride*: A study with inhibitors. *Folia Microbiologica* **40**: 219–224.
- Buée M, Courty PE, Mignot D, Garbaye J. 2007.** Soil niche effect on species diversity and catabolic activities in an ectomycorrhizal fungal community. *Soil Biology and Biochemistry* **39**: 1947–1955.
- Cai L, Hyde K, Taylor P, Weir B, Waller J, Abang M, Zhang J, Yang Y, Phoulivong S, Liu Z, et al. 2009.** A polyphasic approach for studying *Colletotrichum*. *Fungal Diversity* **39**: 183–204.
- Catarino A de M, Rodrigues AAC, Silva LLS, de Oliveira L de JMG, Sardinha DHS, da Costa MG. 2018.** Morphological aspects and effect of carbon sources in the physiology of *Fusarium oxysporum* f. sp. *passiflorae*. *Emirates Journal of Food and Agriculture* **30**: 77–84.
- Chalot M, Brun A. 1998.** Physiology of organic nitrogen acquisition by ectomycorrhizal fungi and ectomycorrhizas. *FEMS Microbiology Reviews* **22**: 21–44.
- Child JJ, Knapp C, Eveleigh DE. 1973.** Improved pH Control of Fungal Culture Media. *Mycologia* **65**: 1078–1086.
- Cochrane VW. 1958.** *Physiology of Fungi*. John Wiley & Sons, New York & Chapman & Hall, London.
- Crous PW, Slippers B, Wingfield M, Rheeder J, Marasas WFO, Philips AJL, Alves A, Burgess T, Barber P, Groenewald JZ. 2006.** Phylogenetic lineages in the Botryosphaeriaceae. *Mycologia* **55**: 235–253.
- Dahlberg KR, Etten JL V. 1982.** Physiology and Biochemistry of Fungal Sporulation. *Annual Review of Phytopathology* **20**: 281–301.
- Deacon JW. 2006.** *Fungal Biology*. Blackwell Publishing.
- Divon HH, Fluhr R. 2007.** Nutrition acquisition strategies during fungal infection of plants. *FEMS Microbiology Letters* **266**: 65–74.
- Edwards MC, Bowling DJF. 1986.** The growth of rust germ tubes towards stomata in relation to pH gradients. *Physiological and Molecular Plant Pathology* **29**: 185–196.
- Farooq S, Iqbal SM, Rauf CA. 2005.** Physiological Studies of *Fusarium oxysporum* f. sp. *ciceri*. *International Journal of Agriculture & Biology* **7**: 275–277.
- Fernandez J, Marroquin-Guzman M, Wilson RA. 2014.** Mechanisms of Nutrient Acquisition and Utilization During Fungal Infections of Leaves. *Annual Review of Phytopathology* **52**: 155–174.
- Fleck CB, Schöbel F, Brock M. 2011.** Nutrient acquisition by pathogenic fungi: Nutrient availability, pathway regulation, and differences in substrate utilization. *International Journal of Medical Microbiology* **301**: 400–407.
- Giraldo MC, Valent B. 2013.** Filamentous plant pathogen effectors in action. *Nature reviews. Microbiology* **11**: 800–814.

- Gow NAR, Latge J-P, Munro CA. 2017.** The Fungal Cell Wall: Structure, Biosynthesis, and Function. *Microbiol Spectrum* **5**: FUNK-0035-2016.
- Griffin DM. 1985.** A comparison of the roles of bacteria and fungi. In: Leadbetter E.R. PJS, ed. *Bacteria in Nature*. Springer, Boston, MA, 221–255.
- Hanson MA, Marzluf GA. 1975.** Control of the synthesis of a single enzyme by multiple regulatory circuits in *Neurospora crassa*. *Proceedings of the National Academy of Sciences* **72**: 1240–1244.
- Hibar K, Daami-Remadi M, Jabnoun-Khiareddine H, Majhoub El M. 2006.** Temperature effect on mycelial growth and on disease incidence of *Fusarium oxysporum* f. sp. *radicis-lycopersici*. *Plant Pathology Journal* **5**: 233–238.
- Hung L-L, Trappe JM. 1983.** Growth Variation between and within Species of Ectomycorrhizal Fungi in Response to pH in Vitro. *Mycologia* **75**: 234–241.
- Ito ZA, Reshi ZA. 2014.** Effect of different nitrogen and carbon sources and concentrations on the mycelial growth of ectomycorrhizal fungi under in-vitro conditions. *Scandinavian Journal of Forest Research* **29**: 619–628.
- Jennings DH. 1990.** Nutrient acquisition by fungi-the relation between physiological understanding and ecological reality. *Proceedings: Plant Sciences* **100**: 153–163.
- Kavroulakis N, Ntougias S, Zervakis GI, Ehaliotis C, Haralampidis K, Papadopoulou KK. 2007.** Role of ethylene in the protection of tomato plants against soil-borne fungal pathogens conferred by an endophytic *Fusarium solani* strain. *Journal of Experimental Botany* **58**: 3853–3864.
- Khilare VC, Ahmed R. 2011.** Effect of nutritional sources on the growth of *Fusarium oxysporum* f. sp. *ciceris* causing chick pea wilt. *International journal of science and nature* **2**: 524–528.
- Klein DA, Paschke MW. 2004.** Filamentous fungi: The indeterminate lifestyle and microbial ecology. *Microbial Ecology* **47**: 224–235.
- Linder T. 2018.** Assimilation of alternative sulfur sources in fungi. *World Journal of Microbiology and Biotechnology* **34**: 51.
- Maitlo S, Rajput AQ, Syed RN, Khanzada MA, Rajput NA, Lodhi AM. 2017.** Influence of physiological factors on vegetative growth and sporulation of *Fusarium oxysporum* f. sp. *ciceris*. *Pakistan Journal of Botany* **49**: 311–316.
- Maldonado-Mendoza IE, Dewbre GR, Harrison MJ. 2007.** A Phosphate Transporter Gene from the Extra-Radical Mycelium of an Arbuscular Mycorrhizal Fungus *Glomus intraradices* Is Regulated in Response to Phosphate in the Environment. *Molecular Plant-Microbe Interactions* **14**: 1140–1148.
- Marzluf GA. 1997.** Molecular Genetics of Sulfur Assimilation in Filamentous Fungi and Yeast. *Annual Review of Microbiology* **51**: 73–96.
- Masurkar P, Bajpai R, Sahu V, Kumar M, Rajput RS. 2018.** Invasion and Nutrient Acquisition Strategies of Phytopathogens: Fungi, Bacteria and Viruses. *International Journal of Current Microbiology and Applied Sciences* **7**: 3132–3146.
- Mehta J, Jakhetia M, Choudhary S, Mirza J, Sharma D, Khatri P, Gupta P, Nair MM. 2012.** Impact of carbon & nitrogen sources on the *Trichoderma viride* (Biofungicide) and *Beauveria bassiana* (entomopathogenic fungi). *European Journal of Experimental Biology* **2**: 2061–2067.
- Nehls U, Hampp R. 2000.** Carbon allocation in ectomycorrhizas. *Physiological and Molecular Plant*

Pathology **57**: 95–100.

Oritsejafor JJ. 1986. Influence of moisture and pH on growth and survival of *Fusarium oxysporum* f.sp. *elaeidis* in soil. *Transactions - British Mycological Society* **87**: 511–517.

Paietta J V. 2004. Regulation of Sulfur Metabolism in Mycelial Fungi. In: *The Mycota (A Comprehensive Treatise on Fungi as Experimental Systems for Basic and Applied Research)*. Springer, Berlin, Heidelberg, 369–383.

Paietta J V. 2010. Sulfur, Phosphorus, and Iron Metabolism. In: Borkovich KA, Ebbole DJ, eds. *Cellular and Molecular Biology of Filamentous Fungi*. American Society for Microbiology, Washington.

Plassard C, Louche J, Ali MA, Duchemin M, Legname E, Cloutier-Hurteau B. 2011. Diversity in phosphorus mobilisation and uptake in ectomycorrhizal fungi. *Annals of Forest Science* **68**: 33–43.

Rangel-Castro JI, Danell E, Taylor AFS. 2002. Use of different nitrogen sources by the edible ectomycorrhizal mushroom *Cantharellus cibarius*. *Mycorrhiza* **12**: 131–137.

Rennenberg H. 1999. The significance of ectomycorrhizal fungi for sulfur nutrition of trees. *Plant and Soil* **215**: 115–122.

Roberson RW, Abril M, Blackwell M, Letcher P, McLaughlin DJ, Mourino-Perez RR, Riquelme M, Uchida M. 2010. Hyphal Structure. In: Borkovich KA, Ebbole DJ, eds. *Cellular and Molecular Biology of Filamentous Fungi*. American Society for Microbiology, Washington.

Sánchez-Rangel D, Hernández-Domínguez EE, Pérez-Torres CA, Ortiz-Castro R, Villafán E, Rodríguez-Haas B, Alonso-Sánchez A, López-Buenfil A, Carrillo-Ortiz N, Hernández-Ramos L, et al. 2018. Environmental pH modulates transcriptomic responses in the fungus *Fusarium* sp. associated with KSHB *Euwallacea* sp. near *forficatus*. *BMC Genomics* **19**: 1–21.

Solomon PS, Tan K-C, Oliver RP. 2003. The nutrient supply of pathogenic fungi; a fertile field for study. *Molecular Plant Pathology* **4**: 203–210.

Su YY, Noireung P, Liu F, Hyde KD, Moslem MA, Bahkali AH, Abd-Elsalam KA, Cai L. 2011. Epitypification of *Colletotrichum musae*, the causative agent of banana anthracnose. *Mycoscience* **52**: 376–382.

Su Y-Y, Qi Y-L, Cai L. 2012. Induction of sporulation in plant pathogenic fungi Yuan-Ying. *Fungal Ecology* **3**: 195–200.

Suárez-Estrella F, Vargas-García MC, Elorrieta MA, López MJ, Moreno J. 2003. Temperature effect on *Fusarium oxysporum* f.sp. *melonis* survival during horticultural waste composting. *Journal of Applied Microbiology* **94**: 475–482.

Tyagi S, Paudel R. 2014. Effect of different pH on the growth and sporulation of *Fusarium oxysporum*: the causal organism of wilt disease of tomato. *International Journal of Basic and Applied Biology* **2**: 103–106.

Vance CP, Uhde-Stone C, Allan DL. 2003. Phosphorus acquisition and use : critical adaptations by plants for securing a nonrenewable resource. *New Phytologist* **157**: 423–447.

Walker GM, White NA. 2017. Introduction to Fungal Physiology. In: *Fungi: Biology and Applications*. John Wiley & Sons, New York, 1–36.

Watkinson SC. 2016. *Physiology and Adaptation*. Elsevier Ltd.

Weber RWS, Pitt D. 2001. Filamentous fungi - growth and physiology. *Applied Mycology and*

Biotechnology 1: 13–54.

Webster J, Weber R. 2007. *Introduction to Fungi*. Cambridge: Cambridge University Press.

Zhao Z, Liu H, Wang C, Xu JR. 2013. Comparative analysis of fungal genomes reveals different plant cell wall degrading capacity in fungi. *BMC Genomics* 14: 274.

2.6 Appendix of Chapter 2: Statistical analysis

2.6.1 Effect of temperature on FsK mycelial growth

Table 2-8 Table summarizing Tukey's post-hoc test investigating significant differences in fungal colonies linear growth velocity (slope) values among the different temperatures.

comparison	p value
22-18	2.020606e-14
26-18	1.920686e-14
28-18	1.920686e-14
30-18	1.920686e-14
37-18	1.950159e-02
26-22	1.429745e-12
28-22	3.486100e-14
30-22	3.537171e-13
37-22	1.931788e-14
28-26	9.715892e-03
30-26	7.750554e-01
37-26	1.920686e-14
30-28	1.635289e-01
37-28	1.920686e-14
37-30	1.920686e-14

2.6.2 Effect of different growth media on FsK mycelial growth.

Table 2-9 Table summarizing Tukey's post-hoc test investigating differences in fungal colonies linear growth velocity (slope) values among the different media.

comparison	p value
Complete Yeast Medium -Water agar	1.277912e-09
Brock's-Water agar	6.139198e-10
Brock's-Complete Yeast Medium	4.625503e-01

2.6.3 Effect of different carbon sources in FsK conidia production

Table 2-10 Tukey's post hoc test investigating significant differences in fungal conidia production among the different carbon sources supplemented in the growth medium.

comparison	p-value
Glucose-- Carbon	6.365639e-05
Galactose-- Carbon	1.499027e-03
Sucrose-- Carbon	1.664773e-03
Galactose-Glucose	2.091020e-01
Sucrose-Glucose	1.897786e-01
Sucrose-Galactose	9.999011e-01

2.6.4 Effect of different carbons sources in FsK mycelium dry weight

Table 2-11 Tukey's post hoc test investigating significant differences in fungal mycelium dry weight among the different carbon sources supplemented in the growth medium.

comparison	p-value
Glucose-- Carbon	2.552694e-05
Galactose-- Carbon	1.089189e-02
Sucrose-- Carbon	3.886148e-05
Galactose-Glucose	9.043822e-03
Sucrose-Glucose	9.880812e-01
Sucrose-Galactose	1.582045e-02

2.6.5 Effect of different nitrogen sources in FsK conidia production

Table 2-12 Tukey's post hoc test investigating significant differences in FsK conidia production among the different nitrogen sources supplemented in the growth medium.

comparison	p-value
NaNO ₃ -- Nitrogen	5.730409e-01
NaNO ₂ -- Nitrogen	9.999999e-01
NH ₄ Cl-- Nitrogen	4.758053e-02
Ammonium Tartrate-- Nitrogen	2.758862e-04
Urea-- Nitrogen	9.246349e-02
Peptone-- Nitrogen	1.287859e-14
L-asparagine-- Nitrogen	7.505072e-01
NaNO ₂ -NaNO ₃	6.639222e-01
NH ₄ Cl-NaNO ₃	8.188351e-01
Ammonium Tartrate-NaNO ₃	2.362239e-02
Urea-NaNO ₃	9.402154e-01
Peptone-NaNO ₃	1.287859e-14
L-asparagine-NaNO ₃	9.999871e-01
NH ₄ Cl-NaNO ₂	6.491906e-02
Ammonium Tartrate-NaNO ₂	3.918442e-04
Urea-NaNO ₂	1.233806e-01
Peptone-NaNO ₂	1.287859e-14
L-asparagine-NaNO ₂	8.275795e-01
Ammonium Tartrate-NH ₄ Cl	3.845948e-01
Urea-NH ₄ Cl	9.999769e-01
Peptone-NH ₄ Cl	1.287859e-14
L-asparagine-NH ₄ Cl	6.529465e-01
Urea-Ammonium Tartrate	2.340060e-01
Peptone-Ammonium Tartrate	1.287859e-14
L-asparagine-Ammonium Tartrate	1.208168e-02
Peptone-Urea	1.287859e-14
L-asparagine-Urea	8.314712e-01
L-asparagine-Peptone	1.287859e-14

2.6.6 Effect of different nitrogen sources in FsK mycelium dry weight

Table 2-13 Tukey's post hoc test investigating significant differences in fungal mycelium dry weight among the different nitrogen sources supplemented in the growth medium.

comparison	p-value
NaNO ₃ -- Nitrogen	3.684309e-02
NaNO ₂ -- Nitrogen	4.215919e-01
NH ₄ Cl-- Nitrogen	3.862806e-08
Ammonium Tartrate-- Nitrogen	4.732625e-08
Urea-- Nitrogen	1.207730e-07
Peptone-- Nitrogen	2.761581e-09
L-asparagine-- Nitrogen	1.238107e-10
NaNO ₂ -NaNO ₃	8.788201e-01
NH ₄ Cl-NaNO ₃	6.330768e-05
Ammonium Tartrate-NaNO ₃	8.099976e-05
Urea-NaNO ₃	2.499527e-04
Peptone-NaNO ₃	1.414477e-06
L-asparagine-NaNO ₃	5.261754e-08
NH ₄ Cl-NaNO ₂	3.125850e-06
Ammonium Tartrate-NaNO ₂	3.939115e-06
Urea-NaNO ₂	1.141482e-05
Peptone-NaNO ₂	1.116031e-07
L-asparagine-NaNO ₂	4.443819e-09
Ammonium Tartrate-NH ₄ Cl	1.000000e+00
Urea-NH ₄ Cl	9.987861e-01
Peptone-NH ₄ Cl	4.137283e-01
L-asparagine-NH ₄ Cl	5.200245e-02
Urea-Ammonium Tartrate	9.996675e-01
Peptone-Ammonium Tartrate	3.607691e-01
L-asparagine-Ammonium Tartrate	4.149137e-02
Peptone-Urea	1.752712e-01
L-asparagine-Urea	1.428950e-02
L-asparagine-Peptone	9.821284e-01

Colonization of legumes by an endophytic *Fusarium solani* strain K reveals common features to symbionts and pathogens

A manuscript containing this work was published in 'Fungal Genetics and Biology'.

Experiments described in the manuscript were performed by Vasiliki Skiada.

The GFP-expressing FsK strain (strain F9a) was previously constructed by Nektarios Kavroulakis and Kalliope Papadopoulou.

Fixation of samples and sectioning prior to TEM observations was performed by Antonella Faccio.

TEM observations were performed by Paola Bonfante.

Fungal Genetics and Biology 127 (2019) 60–74



Contents lists available at ScienceDirect

Fungal Genetics and Biology

journal homepage: www.elsevier.com/locate/yfgbi



Regular Articles

Colonization of legumes by an endophytic *Fusarium solani* strain FsK reveals common features to symbionts or pathogens



Vasiliki Skiada^a, Antonella Faccio^b, Nektarios Kavroulakis^c, Andrea Genre^b, Paola Bonfante^b, Kalliope K. Papadopoulou^{a,*}

^a Department of Biochemistry and Biotechnology, University of Thessaly, Biopolis, Larissa 41500, Greece

^b Department of Life Sciences and Systems Biology, University of Torino, Torino 10125, Italy

^c Hellenic Agricultural Organization "Demeter", Institute for Olive Tree, Subtropical Plants and Viticulture, Agrokipo-Souda, 73100 Chania, Greece

3 Colonization of legumes by an endophytic *Fusarium solani* strain K reveals common features to symbionts or pathogens

Abstract

Plant cellular responses to endophytic filamentous fungi are scarcely reported, with the majority of described colonization processes in plant-fungal interactions referring to either pathogens or true symbionts. *Fusarium solani* strain K (FsK) is a root endophyte of *Solanum lycopersicum*, which protects against root and foliar pathogens. Here, we investigated the association of FsK with two legumes (*Lotus japonicus* and *Medicago truncatula*) and report on colonization patterns and plant responses during the establishment of the interaction. *L. japonicus* plants colonized by FsK complete their life cycle and exhibit no apparent growth defects under normal conditions. We followed the growth of FsK within root-inoculated plants spatiotemporally and showed the capability of the endophyte to migrate to the stem. In a bipartite system comprising of the endophyte and either whole plants or root organ cultures, we studied the plant sub-cellular responses to FsK recognition, using optical, confocal and transmission electron microscopy. A polarized reorganization of the root cell occurs: endoplasmic reticulum/cytoplasm accumulation and nuclear placement at contact sites, occasional development of papillae underneath hyphopodia and membranous material rearrangements towards penetrating hyphae. Fungal hyphae proliferate within the vascular bundle of the plant. Plant cell death is involved in fungal colonization of the root.

Our data suggest that the establishment of FsK within legume tissues requires fungal growth adaptations and plant cell-autonomous responses, known to occur during both symbiotic and pathogenic plant-fungal interactions. We highlight the overlooked plasticity of endophytic fungi upon plant colonization, and introduce a novel plant-endophyte association.

Abbreviations:

AMF, arbuscular mycorrhizal fungi; CA, cytoplasmic aggregation; CB, chlorazol black; CFUs, colony forming units; CWAs, cell wall appositions; dpi, days post inoculation; ER, endoplasmic reticulum; FsK, *Fusarium solani* strain K; FSSC, *Fusarium solani* species complex; GFP, green fluorescent protein; *Lj*, *Lotus japonicus*; LSCM, laser scanning confocal microscopy; *Mt*, *Medicago truncatula*; MVBs, multi-vesicular bodies; PI, propidium iodide; PM, plasma membrane; ROCs, root organ cultures; ROI, region of interest; TEM, transmission electron microscopy; TB, trypan blue; wt, wild-type

Keywords

Fusarium, *Lotus japonicus*, *Medicago truncatula*, symbiosis, pathogenesis, endophyte

3.1 Introduction

Endophytism is a symptomless association of other living organisms that grow within living plant tissues (Wilson, 1995) (Stone et al., 2000) (Brundrett, 2004) and can have profound impacts on plant communities. All known classes of fungal endophytes are primarily represented by ascomycetous fungi, whereas basidiomycetous fungi are less dominant (Rodriguez et al., 2009). The definition of endophytes does not address a specific functional relationship. To this respect, endophytes can be commensalistic symbionts, mutualists, or even latent pathogens/saprotrophs (Fesel and Zuccaro, 2016). Certain endophytic lifestyles have been described, like the case of the growth promoting fungus *Serendipita indica* (Varma et al., 1999) (Peškan-Berghöfer et al., 2004), which expresses alternative lifestyle strategies in a host-dependent manner (Lahrmann et al., 2013), exploits the host's cell death machinery (Deshmukh et al., 2006) (Zuccaro et al., 2011) (Jacobs et al., 2011) (Qiang et al., 2012a), depends on a functional mitogen-activated protein kinase (MPK6) for successful *A. thaliana* colonization (Daneshkhah et al., 2018), and secretes an ecto-nucleotidase to manipulate host eATP perception/signaling and affect colonization (Nizam et al., 2019).

Similarities in recognition of pathogenic and symbiotic fungi point out a partially common model of initial sub-cellular plant responses to these microorganisms. For example, cytoplasmic aggregation (CA), i.e. a cytoskeleton-driven accumulation of organelles, including the nucleus, at contact sites is a general plant cell response to an encounter with a compatible fungus (Genre et al., 2009). It occurs upon contact with pathogenic fungi (Tomiya, 1957) (Gross et al., 1993) (Takemoto et al., 2003) (Koh et al., 2005b) (Genre et al., 2009) or with symbionts, such as Arbuscular Mycorrhizal Fungi (AMF) (Genre et al., 2005) (Genre et al., 2009). While these responses are well characterized in plant-pathogen and plant-symbiont systems, little attention has been paid on the initial cell-autonomous responses and the sub-cellular rearrangements required for the accommodation of filamentous endophytic fungi in plant tissues.

The ascomycete *Fusarium solani* is the anamorph state of *Nectria haematococca* and a member of a monophyletic clade that currently contains at least 60 phylogenetically distinct species, known as '*F. solani* species complex (FSSC)' (Coleman et al., 2009) (Coleman, 2016). Members of the FSSC are medically important human pathogens and agriculturally important plant pathogens, endophytes and saprotrophs (Zhang et al., 2006) (Coleman et al., 2009) (Shweta et al., 2010). Their ability to adapt to a plethora of environments reflects their genetic plasticity and metabolic diversity (Coleman et al., 2009). *Fusarium solani* strain K (FsK) is an endophytic, non-pathogenic strain, previously isolated from the roots of tomato plants (Kavroulakis et al., 2007). FsK is effective in protecting tomato plants against root and foliar pathogens and in increasing plant tolerance to water stress (Kavroulakis et al., 2007) (Kavroulakis et al., 2018).

Here, we describe the association of FsK with two legumes, *Lotus japonicus* (Lj) and *Medicago truncatula* (Mt). Our aim was to shed light on cellular and sub-cellular plant responses upon recognition and accommodation of a fast growing, filamentous endophyte. Initially, classical and molecular approaches were used in order to follow spatiotemporally the fungal progression in plant tissues and we show that the endophyte has the ability to colonize root, stem and leaf tissues. The association was, also, studied in detail at the cellular level. An axenic dual culture system, engaging either whole plants

or Root Organ Cultures (ROCs) was developed, and optical, confocal and transmission electron microscopy (TEM) were used to record cellular responses to fungal accommodation. Our results demonstrate the so far overlooked plasticity of endophytic fungi upon colonization. We, furthermore, show that legume plant cell responses to colonization by FSK resemble features reported for both mycorrhizal fungi and other endophytes, as well as for pathogens.

3.2 Materials and methods

3.2.1 Plant and fungal material

Lotus japonicus (ecotype 'Gifu') seeds were chemically scarified with a 12-min sulfuric acid treatment, washed thoroughly with deionized water, surface sterilized for 20 min in a 20% NaOCl solution and washed 6x with sterile deionized water. Seeds were kept in water at 4°C overnight, to promote seed germination, placed afterwards on half strength MS medium (Murashige & Folke 1962), and grown in a growth chamber with a 16h light/8h dark photoperiod at 22°C.

For confocal microscopy observations, *L. japonicus* wild type (wt) plants (ecotype 'Gifu') as well as previously constructed *Agrobacterium rhizogenes*-transformed root cultures derived from *Medicago truncatula* Jemalong A17 (Genre et al., 2005) (Genre et al., 2008) (Sieberer et al., 2009) (Chabaud et al., 2011) were used for the interaction. Two lines of *M. truncatula* ROCs (Root Organ Cultures), with different cellular compartments labelled, were used. The first line carries a GFP-HDEL tag (Haseloff et al. 1997), driven by the cauliflower mosaic virus 35S (CaMV35S). HDEL signal retains the protein in the lumen of the ER and nuclear envelope (Haseloff et al., 1997), which aids monitoring ER and nuclear cellular dynamics upon fungal invasion and furthermore provides general information on cytoplasm distribution (Genre et al., 2005) (Genre et al., 2009). The second line carries a nucleoplasmin-Yellow Cameleon YC2.1 (NupYC2.1) fusion protein, driven by the CaMV35S promoter (Sieberer et al., 2009) (Chabaud et al., 2011), that allows visualization of the nuclear positioning.

Fungal inoculum was prepared as follows: Fsk was routinely cultured on potato dextrose broth (PDB) at 26 °C for 5 d in the dark. Following removal of mycelium fragments by sieving through sterile cheesecloth, conidia were recovered from the filtrate by centrifugation at 6500 rpm, counted using a haemocytometer and suspended in an appropriate volume of 0.85% NaCl to achieve the desired inoculum concentration. For fluorescent microscopy a GFP-transformed isolate of Fsk (strain F9a, produced as described below) was used.

3.2.2 *Agrobacterium tumefaciens* mediated transformation of Fsk

Agrobacterium tumefaciens strain AGL1 containing the Ti binary vector pCAMBgfp (Sesma and Osbourn, 2004) was kindly provided by A. Osbourn (John Innes Centre, UK). Ti vector pCAMBgfp contains the *egfp* gene under the control of the *Pyrenophora tritici-repentis toxA* promoter as well as the hygromycin phosphotransferase (*hph*) gene under the control of the *Aspergillus nidulans trpC* promoter. Transformation was carried out as described in (Sesma and Osbourn, 2004). Fsk transformed colonies appeared within 3-6 d of incubation at 25°C, and were transferred to selection dishes (PDA plus 50µg/ml hygromycin B). Both the wt and hygromycin B-resistant strains were cultured in PDB and chromosomal DNA was extracted. The presence of the *hph* gene was verified by PCR amplification using specific primers (Supplementary Table 3-2) and the wt DNA as negative control. The presence of the *egfp* gene was verified by fluorescence microscopy (filter system I 3: BP 450-490 nm, LP 515 nm). Two single conidia were obtained from each transformant and placed on a PDA selection dish (PDA supplemented with 50µg/ml hygromycin B). After sporulation, two single conidia were picked from each of the two cultures and placed on PDA dishes in the absence of hygromycin.

This procedure was repeated for five generations. Subsequently, the isolated conidia were placed on PDA selection dishes. Twenty-one gfp-tagged isolates were further tested comparatively with the wt Fsk strain for their hyphal growth characteristics both in liquid cultures and in solid media. Conidia production was also estimated. Strain F9a, which exhibited very similar growth traits as the wt Fsk, was selected to study the plant colonization process.

3.2.3 Quantification of fungal colonization by qPCR

Fsk colonization of root tissues was assessed via qPCR by using primers specific either for a ca 100 bp fragment of *Fusarium solani* ITS region or for a ca 170 bp fragment of the *Nectria haematococca translation elongation factor 1a (TEF1a)* gene (Supplementary Table 3-1). An external standard curve was generated as follows: ITS/TEF1a gene was amplified using Fsk genomic DNA as template, the PCR product was ligated into pGEM-T Easy vector (Promega, Madison, USA) and its concentration was determined via Qubit 2.0 Fluorometer. The copy number of the targeted gene was calculated directly from the concentration of the extracted plasmid DNA (Whelan et al., 2003). Serial 10-fold dilutions of the recombinant plasmid ranging from 6×10^0 to 6×10^7 copies/ μ l for ITS and 4×10^0 to 4×10^7 copies/ μ l for TEF1a were subjected in triplicate to qPCR to construct the standard curve. More specifically, CT (cycle threshold) values in each dilution were measured in triplicate using a real-time qPCR to generate the standard curves for ITS and TEF1a gene, respectively. The CT values were plotted against the logarithm of their initial template copy numbers. Each standard curve was generated by a linear regression of the plotted points. From the slope of each standard curve, PCR amplification efficiency was calculated (Lee et al 2005). For each experiment, amplification of each sample (standards - unknowns) occurred in a 10 μ l reaction mixture containing Kapa SYBR FAST qPCR Master Mix Universal (1x), 200nM of each primer, and 1 μ l of DNA, using a thermocycling protocol of 3 min at 95 °C; 45 cycles of 15 s at 95 °C, 20 s at 58 °C, followed by a melting curve to check the specificity of the products. Absolute quantification of unknown samples was estimated as the exact copy concentration of the target gene by relating the CT value to the standard curve. The fungal gene copy numbers of all samples are normalized by ng of total DNA isolated. Agarose gel (1.5% w/v) electrophoresis of qPCR products was routinely performed, to verify the amplification of a single fragment of the desired length.

3.2.4 Monitoring the life cycle of *L. japonicus* during its interaction with Fsk

Nine days old seedlings were transferred to pots containing a sterile sand:vermiculite mixture (3:1). Plants were alternately watered with full strength Hoagland Medium (Hoagland and Arnon, 1950) or water, until the end of the life cycle. Thirteen days old plants were inoculated with 10^4 Fsk conidia directly on each plant root. Control plants received no inoculum. During their growth, plants were monitored for plant growth phenotypes and first flowering date was recorded. At the end of the life cycle 18 control and 19 Fsk-inoculated plants were examined for the following growth/developmental parameters: root/shoot fresh weight, root/shoot length, root crown diameter; seedpod production and

seed weight were recorded. Differences in the biological parameters examined between control and FsK-inoculated plants, were analyzed by Student's t-test, at the 0.05 level.

A few individual plants from both treatments were harvested randomly at distinct time points (6, 24, 60 dpi) in order to verify and estimate the fungal colonization within the collected tissues. Tissues were washed thoroughly and DNA was extracted using the CTAB method (Doyle and Doyle, 1987). DNA was also extracted from seeds. DNA concentration was determined via Qubit 2.0 fluorometer (Thermo Scientific). Quantification of fungal colonization in the plant tissues was estimated as described above. qPCR amplification efficiencies were 94.66 % with r^2 value of 0.996 and a slope of -3.457 for *Fusarium solani* ITS gene fragment.

3.2.5 Monitoring of asexual structures formation (conidiation) in the rhizosphere

Lotus japonicus wt seeds (ecotype 'Gifu') were surface sterilized and germinated as described above. Ten days old plants were transplanted into magenta boxes (3 plants per magenta) containing ~250 g of sterile sand:vermiculite (3:1) mixture and directly inoculated with 100 FsK conidia per root. Control substrate received the same amount of fungal inoculum (3 x 100 conidia per magenta) in the absence of plants. The substrate was watered with ~35 ml of M medium (Boisson-Dernier et al., 2001) prior to transplantation/inoculation, in both treatments. Magenta boxes were transferred in a growth chamber (16h light/8h dark photoperiod, 22°C). Each magenta box was considered one biological replicate and 5 biological replicates were assessed for each treatment. At 2, 12, 35 and 50 dpi, ~1g of substrate sample was removed and added to 4 ml of sterile solution (0.85% w/v NaCl containing surfactant Tween 80 0.05% v/v). The suspension was mixed by vortexing (~30s), diluted appropriately and plated on water agar plates in triplicate. Plates were incubated at 26° C for ~48 hrs and CFUs were counted on each plate.

To quantify fungal growth within plant tissues, root/stem/leaf tissues were harvested at the same time points as follows: plants were explanted from the magenta boxes used above for substrate measurements, surface-sterilized (1 min in 1% NaOCl), washed 6x with sterile deionized water, blotted dry onto sterile filter paper, and root/stem/leaf tissues were separated and kept at -80°C until DNA isolation. DNA extraction and DNA concentration quantification were performed as described above. 5 biological replicates were assessed for each treatment, with each replicate consisting of 3 individual plants. Absolute quantification of two fungal genes (ITS and TEF1a) was performed. qPCR amplification efficiencies for ITS gene were 88.89%% with r^2 value of 0.995 and a slope of -3.620, whereas for TEF1a gene were 97.78 % r^2 value of 0.994 and a slope of -3.376.

Differences in CFU measurements between the control substrate (P-) and the plant-containing substrate (P+), in the various time points examined, were analyzed using Student's t-test.

Temporal differences in TEF/ITS gene copy numbers were analyzed for each tissue separately, using one-way ANOVA at the 0.05 level (Tukey's test).

Temporal differences in CFU values were analyzed for each substrate (P- or P+) separately, using one-way ANOVA at the 0.05 level (Tukey's test).

3.2.6 *Lotus japonicus* root inoculation with F_sK for microscopy

To meet the requirements of a targeted inoculation technique for filamentous fungi, the targeted AM inoculation technique for studying early stages of the symbiotic association between *Gigaspora* species and transformed root cultures, developed by (Chabaud et al., 2002) and adapted for confocal microscopy observation by (Genre et al., 2005), was furthermore modified and adapted. *L. japonicus* (ecotype 'Gifu') seeds were germinated as described above, and seedlings 9-12 days old were then transferred to M medium. Plants were inoculated with F_sK hyphal tips as follows: 50-100 conidia were placed on water agar plates, incubated at 26 °C at a 45° inclination for 2-3 d. One or two emerging hyphal tips from a germinated conidium were removed with the use of a sterile needle under a stereomicroscope and placed close to the root tip (~0.5cm distance). The inoculum was then fixed under a drop of a low melting agarose solution (0.4% w/v). The agarose was left to solidify and roots were covered with a thin (25-μm) gas-permeable plastic film (Biofolie 25™; Lumox, Sarstedt), as described in (Genre et al., 2005). Plants were grown by placing the Petri dishes vertically after the lower part of the dish was wrapped in aluminum foil, in order to protect the root tissues from light. Petri dishes were kept in a growth chamber (16h light/8h dark photoperiod, 22°C) until microscopic observation. For examination of fungal colonization in root/stem transverse sections via confocal microscopy, tissues were mounted on agarose and sectioned by hand.

Root cell viability was assessed by staining root tissues with 10μg/ml PI solution (81845 Sigma-Aldrich) for 5 min. PI stains the nuclei of cells lacking intact PM (Truernit and Haseloff, 2008). To assess putative plant-derived membrane invagination events upon fungal accommodation, plants were stained with 3 μM Synaptored C2 (FM4-64) solution (70027 Biotium) for 5 min (Zuccaro et al., 2011), a lipophilic dye previously used to demonstrate membrane invagination events upon appressorium formation (Genre et al., 2005). All staining techniques were performed directly on the Petri dish where the bipartite interaction was taking place. Excess stain was removed for both dyes but no washing with water was performed afterwards.

3.2.7 *Medicago truncatula* ROCs inoculation with F_sK for microscopy

The targeted inoculation technique used to follow the colonization process in whole *Lj* plants was also followed for *M. truncatula* ROCs. Apical segments of GFP-HDEL or NupYC2.1 *Mt* ROCs were transferred to M medium plates (one segment per Petri dish) and grown in the dark in a vertical position, to favor the development of a regular, fishbone-shaped root system (Chabaud et al., 2002). Vertically oriented root segments were inoculated with an F_sK hyphal tip and covered with Biofolie as described above for *L. japonicus* whole plants.

3.2.8 Confocal microscopy

Time-lapse observations following the early stages of *L. japonicus*-F_sK interaction in Petri dishes were performed under a confocal laser scanning microscope (Nikon Eclipse C1; EZ - C1 3.20 software), using the following objectives: 20X Plan Apochromat objective [numerical aperture (NA) 0.75], 40X Plan Achromat (NA 0.65), or 40X Plan Fluor oil objective (NA 1.30).

The interaction was monitored at 2, 3, 4 days post inoculation with a fungal hyphal tip. Physical plant-fungal contact was estimated under a stereoscope, prior to confocal observations, and occurred ~1.5 dpi. A 488 nm Ar laser was used to excite GFP, root cell- wall autofluorescence, PI and FM4-64 stain. Emission signals were discriminated via specific filter settings: 515/30 filter set for GFP and 630 LP filter set for plant autofluorescence and PI or FM4-64 stain.

Time-lapse observations following the early stages of *M. truncatula*-FsK interaction were performed under a Leica TCS SP2 confocal microscope fitted with a long distance 40X water-immersion objective (HCX Apo 0.80), at 1, 2, 3, 4 dpi. Physical plant-fungal contact was estimated under a stereoscope, prior to confocal observations, and occurred 1-1.5 dpi. The *M. truncatula* GFP-HDEL/FsK interaction was imaged using the Ar laser band at 488 nm, and a 500 to 525 nm emission window for GFP and 620-830 nm for root cells autofluorescence. The *M. truncatula* NupYC2.1/FsK interaction was imaged using the Ar laser band at 488 nm and a 490 to 515 nm emission window for GFP, 525 to 570 for YFP and 620 to 830 for plant cell autofluorescence.

Quantification of the (%) ratio of 'PI-positive FsK-colonized cells vs total cells colonized' was calculated as follows: Image stacks (all optical sections) from 6 independent sites originating from 2-3 individual plants were analysed, by marking ROIs (Regions Of Interest) of (a) PI-positive colonized cells and of (b) total colonized cells separately, using the multi-point tool of ImageJ software (Schneider et al., 2012). Relative coordinates of each ROI, as well as ROIs total number were extrapolated in a spreadsheet and ratios were calculated.

3.2.9 Electron microscopy

M. truncatula NupYC2.1 ROCs colonized by FsK were initially examined under the confocal microscope at 2 and/or 3 dpi. They were then excised under a stereomicroscope and rapidly fixed at room temperature for 2 h in 0.1M phosphate-saline buffer, pH 6.8, containing 2% glutaraldehyde, 0.1 mM EGTA, 2 mg/mL tannic acid, and 0.1 mM MgCl₂. Samples were then rinsed three times with phosphate buffer for 30 min and post fixed in 1% OsO₄ in phosphate buffer for 2 h at 48°C. After several washes with phosphate buffer, followed by 1 h in distilled water, en-bloc staining with aqueous 0.5% uranyl acetate was performed for 2 h at room temperature. Samples were then washed in distilled water, dehydrated progressively in an ethanol series, incubated two times in absolute acetone, infiltrated in Epon-Araldite resin (Hoch, 1986), and flat-embedded in a thin resin layer between Teflon-coated glass slides (Howard and O'Donnell, 1987). The resin was polymerized for 24 h at 60 °C. Fungal colonization sites within flat-embedded samples were selected under an optical microscope, excised using a razor blade, and mounted on resin stubs prior to ultramicrotomy. Semithin sections of 0.5 µm were stained with 1% toluidine blue to check the sample contents using optical microscopy. Based on these observations, ultrathin (70 nm) sections were cut, counterstained with uranyl acetate and lead citrate (Reynolds, 1963), and then viewed with a Philips CM10 transmission electron microscope.

3.2.10 Light microscopy

Images of semithin sections derived from resin embedded samples of FsK-inoculated ROCs were taken using a Leica DM2000 microscope mounted with a QImaging optiMOS digital camera.

For examination of fungal colonization in *Lotus japonicus* root/stem/leaves, tissues were cleared with 10% w/v KOH for 10-30 minutes at 95°C in a water bath (clearing time varied depending on the tissue processed; stem tissues required a longer clearing step), washed 4x with distilled water, acidified with 1N HCl for 20 min at RT, and subsequently stained either with 0.05% w/v Trypan blue (TB), or 0.05% Chlorazol black (CB) for 3-4 min at 95 °C and for ~20 min more at RT. Tissues were washed 4-5x with distilled water and kept at 4°C in water overnight in order to remove the excess dye (<https://invam.wvu.edu>). The stain was prepared by mixing the appropriate quantity of TB or CB with water, glycerol and lactic acid (1:1:1 by volume). Part of the collected tissues was stained with the ink and vinegar method (Vierheilig et al., 1998) (Kosuta et al., 2005). Tissues were mounted on microscope slides in Polyvinyl-Lacto-Glycerol (PVLG). Images were taken using a Novex microscope mounted with a CMEX DC.5000 Digital camera.

3.3 Results

3.3.1 FsK colonizes *L. japonicus* without adversely affecting its growth

We inoculated *L. japonicus* plants with FsK conidia and we monitored phenotypic traits throughout their life cycle in a pot experiment. Inoculation with FsK caused no apparent effects on plant growth under the optimal conditions we applied in this experiment (Figure 3-1A). No significant difference was recorded for the parameters measured, i.e. root/shoot fresh weight, root/shoot length, root crown diameter and seed setting, for inoculated and non-inoculated plants throughout the whole period examined (Supplementary Figure 3-9). Flowering time varied among plants but was initiated, for both treatments, at approximately the same period (50 ± 5 days).

In order to follow the progression of the endophyte in *L. japonicus* tissues, we quantified fungal colonization in plant tissues by qPCR by extrapolating gene copy numbers for two different fungal genes (*ITS* and *TEF1a* gene). Both fungal genes tested gave similar results (results are shown only for *ITS* gene; Figure 3-1B). The endophyte was detected in root tissues of *L. japonicus* at early stages of the interaction (6 days post inoculation, dpi). FsK was detected in the shoot of all explanted plants at later stages of the interaction (60 dpi) (Figure 3-1B). The fungus was never detected in the seeds of inoculated plants (data not shown).

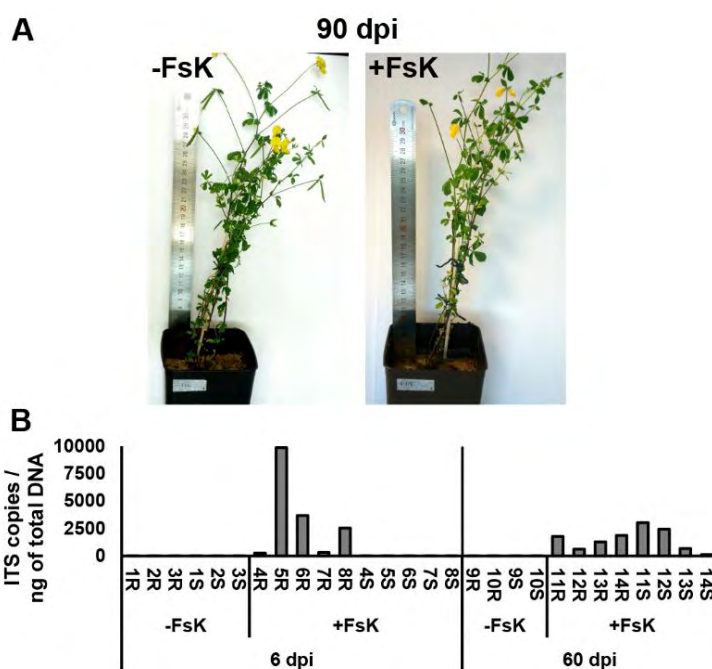


Figure 3-1 Monitoring the life cycle of FsK-inoculated *Lotus japonicus* plants.

Control and *Fusarium solani* strain K (FsK) inoculated plants 90 dpi. (A) *L. japonicus* plants exhibit no apparent phenotypic differences in comparison to controls. (B) Quantification of FsK colonization within *L. japonicus* tissues at distinct time points (6 and 60 dpi), using primers specific for *Fusarium ITS* gene. Values are normalized to ng of

total DNA isolated. Individual plants were subtracted and investigated at each time point. Root and shoot tissues were examined. The fungus has migrated to the upper part of the plant at 60 dpi.

1R-14R and 1S-14S, roots and shoots collected from individual plants.

Identical numbering in both abbreviations indicates the same explanted plant.

3.3.2 FsK progressively colonizes *L. japonicus* root system and subsequently migrates to the stem

To monitor FsK entry in plant tissues spatio-temporally, we inoculated *L. japonicus* plants with FsK and we allowed the interaction to take place for 50 days in magenta boxes. In our closed system, the plant remained alive, with no apparent defects in its growth, during the whole experimental period (Supplementary Figure 3-10A). Tissues (root/stem/leaves) were harvested at 2, 12, 35 and 50 dpi and fungal colonization was estimated via qPCR. Under these gnotobiotic conditions, fungal gene copy numbers in root tissues remained approximately the same from 12 dpi and on. In the stem, the fungus exhibited a major proliferation at 35 dpi, and a decline afterwards, probably either due to arrested proliferation and/or a simultaneous biomass increment of the tissue investigated. Fungal gene copy numbers in leaf tissues were hardly detectable (Supplementary Figure 3-10B).

Microscopic observations of whole-mounted stained tissues were performed to follow fungal progression in plant tissues. In the root system, fungal hyphae were found extraradically (Figure 3-2A). Fungal cells linked in chains were repeatedly observed inside plant cells (Figure 3-2B, 35 dpi). Spore-like structures were recorded in the proximity of root epidermis or attached to root hairs, especially at late time points of our experimental period (Figure 3-2C-D; 50 dpi). Epiphytic hyphae were recorded on the stem surface (Figure 3-2E, 12 dpi); spore-like structures in continuity to hyphal growth (Figure 3-2F-G) as well as intracellular hyphal colonization (Figure 3-2H) were also recorded in stem tissues. In few cases, leaf tissues were also colonized by FsK: cells in catenate series and in continuity to hyphal growth were recorded intracellularly (Figure 3-2I, K). As depicted in Figure 3-2J, fungal proliferation in leaf tissues occurred in certain instances via a secondary infection through the epidermis. A small number of FsK colonized leaves was detected via microscopy, so we attribute the very low detection of FsK in leaf tissues via qPCR to a DNA dilution effect.

We also monitored conidiation in the rhizosphere by counting Colony Forming Units (CFUs) on agar plates, obtained by serial dilutions of an aqueous extract derived from the potting substrate in the absence/presence of the plant (P-/P+ substrate). CFUs in the presence of the plant increased up to 12 dpi and remained at similar levels for the whole duration of the experiment (50 dpi). Statistical analysis gave no significant differences between P+ and P- samples, in any of the sampling dates (Supplementary Figure 3-10B).

Our findings indicate that FsK migrates to the aerial parts of the plant, which is able to withstand and support this migration. A constant presence of fungal propagules is recorded in the rhizospheric substrate, indicating that extraradical fungal propagule formation is independent of the presence of the plant, and that the fungus continues to grow within *Lotus* plant tissues up to the last time point examined (50 dpi).

3.3.3 Fsk exhibits plasticity in its colonization mode of *L. japonicus* root tissues

To visualize the colonization of *L. japonicus* root by Fsk in further detail, we used a Green Fluorescent Protein (GFP)-tagged isolate of Fsk, constitutively expressing cytoplasmic GFP, for live-cell imaging using Laser Scanning Confocal Microscopy (LSCM) at 16-24 h intervals. Propidium iodide (PI) stain was used to assess plant cell viability. A non-contacted root is illustrated in Figure 3-3A. In this experimental set up in petri dishes, the fungus established contact at ~ 2 dpi. Root hairs did not play a pivotal role in colonization process. In most cases, the fungus embraces the root hair, but no penetration of the root hair cell occurs during this process. Afterwards, normal fungal growth takes place on root epidermis. During the first days of the plant-fungal association (up to 2 dpi) epidermal and/or upper cortical cells were preferentially colonized, whereas localization in the inner cortex was mostly observed at later stages of the interaction (3 dpi, Figure 3-3B). Colonization began with the formation of a hyphopodium: a swollen, differentiated hyphal lobe that adheres to the root surface and from which a penetration hypha extends and penetrates the epidermal cell layer (Supplementary Figure 3-11A, B). Hyphae traversed the wall of epidermal cells either directly or by prior formation of an adhering surface (Figure 3-3C). We observed penetration events with single (Figure 3-3C) or multiple hyphae (Supplementary Figure 3-11C) crossing the plant cell wall. Hyphal stenosis was required for the fungus to traverse the cell wall (Figure 3-3D, E). Plasticity in hyphal morphology was observed intracellularly and filamentous hyphae occasionally became lobed and bulbous (Supplementary Figure 3-11D). At 4 dpi, hyphal swellings were observed intracellularly in epidermal and cortical cells. These structures were round in shape, formed singly (Supplementary Figure 3-11E) or in catenate series (Supplementary Figure 3-11F), seemed unicellular and remained attached to the main fungal hypha, from which they seemed to be delimited by a septum. Therefore, these structures differed from the irregular-shaped, bulbous hyphae mentioned above and resembled chlamydospores: thick walled, spore-like resting cells, borne singly, in pairs, in clumps or in chains (Nelson et al., 1994), ostensibly rising from intraradical sporulation events in our system.

To investigate whether Fsk enters the vasculature during colonization of *L. japonicus* root system, we observed cross sections from the uppermost part of the root, under the confocal microscope. Indeed, the fungus colonizes the root cortex and furthermore extends to the vascular bundle (7 dpi; Figure 3-3F), as was previously reported for tomato plants (Kavroulakis et al., 2007). Fsk was also recorded to colonize root tissues through lateral roots (Supplementary Figure 3-11G). The fungus was also recorded to colonize stem tissues (Figure 3-3G) where fungal structures of round shape are observed in the epidermis (stem cross section at a site close to the root crown, 7 dpi). This is in accordance to our optical microscope observations (Figure 3-2E-G).

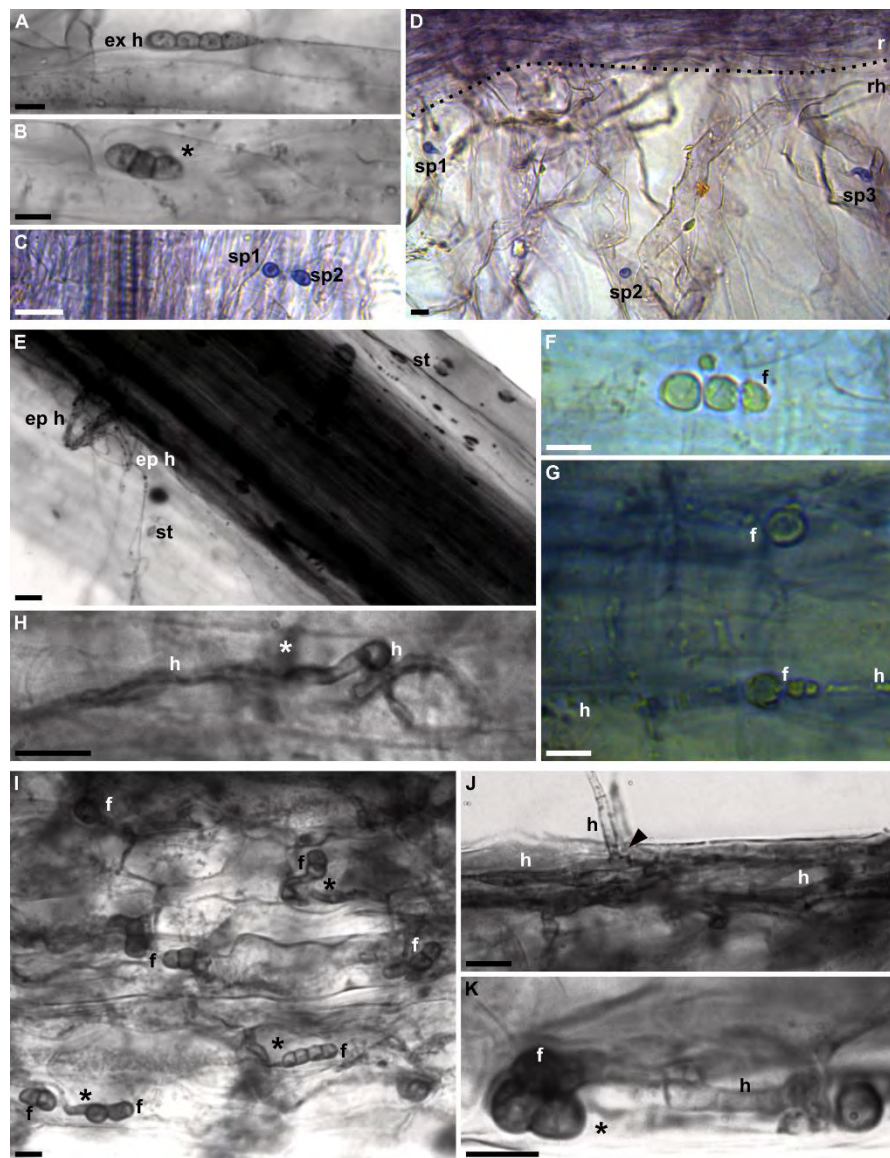


Figure 3-2 Growth of FsK in *L. japonicus* root-stem-leaf tissues. Light microscope images of whole mounted (not sectioned) tissues derived from wt *L. japonicus* whole plants colonized by FsK (12-50 dpi).

(A-D) Root tissues associated with FsK. (A) Growth on root epidermis, 35 dpi. (B) Intracellular growth in root tissues, 35 dpi. (C) Fungal spores in the proximity of root epidermis, 50 dpi. (D) Fungal spores formed in the proximity of root hairs, 50 dpi.

(E-H) Stem tissues associated with FsK. (E) Epiphytic hyphae on stem tissues, 12 dpi. (F and G) Fungal structures formed in stem tissues, 12dpi. (H) Intracellular hyphae in stem cells, 35 dpi.

(I-K) Leaf tissues associated with FsK, 35 dpi. (I) Leaf cells colonized by FsK. Various fungal structures are formed. (J) Fungal entrance point and colonization of leaf tissues. (K) A colonized leaf cell.

Tissues were stained as follows: (A, B, H-K), trypan blue; (C, D, F, G), ink; (E), chlorazol black.

ex h, extraradical hyphae; asterisk, intracellular growth; sp, fungal spore; r, main root; rh, root hair zone; ep h, epiphytic hyphae; st, stoma; f, structures of fungal origin; h, hyphae.

Bars = 10 µm

During the early stages of *Lotus*-FsK interaction, occasional plant cell death takes place. Certain fluorescent plant cell nuclei denoted loss of cell viability at various time points of the interaction (Figure 3-3B). However, this phenomenon was not tightly associated with penetration occurrence and fungal proliferation inside the cells, since non-colonized cells also showed signs of nuclear staining with PI (Supplementary Figure 3-11A, B). At late stages of the interaction, where intense fungal growth is recorded within plant tissues, cells with both positive and negative PI staining are observed (Figure 3-3B). Negative PI staining, at this time point though does not necessarily advocate for cell integrity maintenance, since cell viability could have already been lost earlier. Using the confocal microscope images, the percentage of dead colonized cells (positive PI stain) versus the total number of colonized

cells was estimated between 0-50% (ratios: 0.00%, 5.71%, 16.13%, 17.39%, 22.22%, 50%; calculations on z-stack series derived from 6 independent sites from 2-3 plants).

Nevertheless, our observations indicate that the integrity of colonized cells is preserved for some time upon fungal penetration, deserving more detailed investigation. Thus, we decided to search for more direct evidence of cell integrity in FSK-legumes system by following membrane and ER dynamics.

3.3.4 Membrane dynamics at penetration sites

Stable biotrophic plant-fungal interactions are generally characterized by an exclusion of the accommodating fungus from the plant cell cytoplasm via formation of peri-microbial compartments established by the plant (Harrison, 2012) (Leborgne-Castel and Bouhidel, 2014). To examine whether membrane trafficking plays a role during FSK accommodation within *L. japonicus* root cells, we used the vital dye FM4-64, which is inserted into the outer leaflet of the Plasma Membrane (PM) and passed to the intracellular membrane compartments, reportedly via endocytosis. It is assumed that the dye localizes in the inner membrane leaflet of the endocytic compartments: endocytic vesicles, endosomes, Golgi bodies, pre-vacuolar compartments and the tonoplast (Bolte et al., 2004) (van Gisbergen et al., 2008).

We visualized root tissues of FSK-inoculated plants after 5 min of incubation with the dye, using LSCM. Figure 3-4A-C shows a growing hypha on an epidermal cell. A focal accumulation of FM4-64-stained materials is demonstrated in the vicinity of the hyphopodium. Similar accumulations were observed at the tip of hyphae attempting penetration, as shown in Figure 3-4D-F. These observations are compatible with a local accumulation of endocytic vesicles, likely related to intense plant cell membrane dynamics at the penetration site (Fischer-Parton et al., 2000).

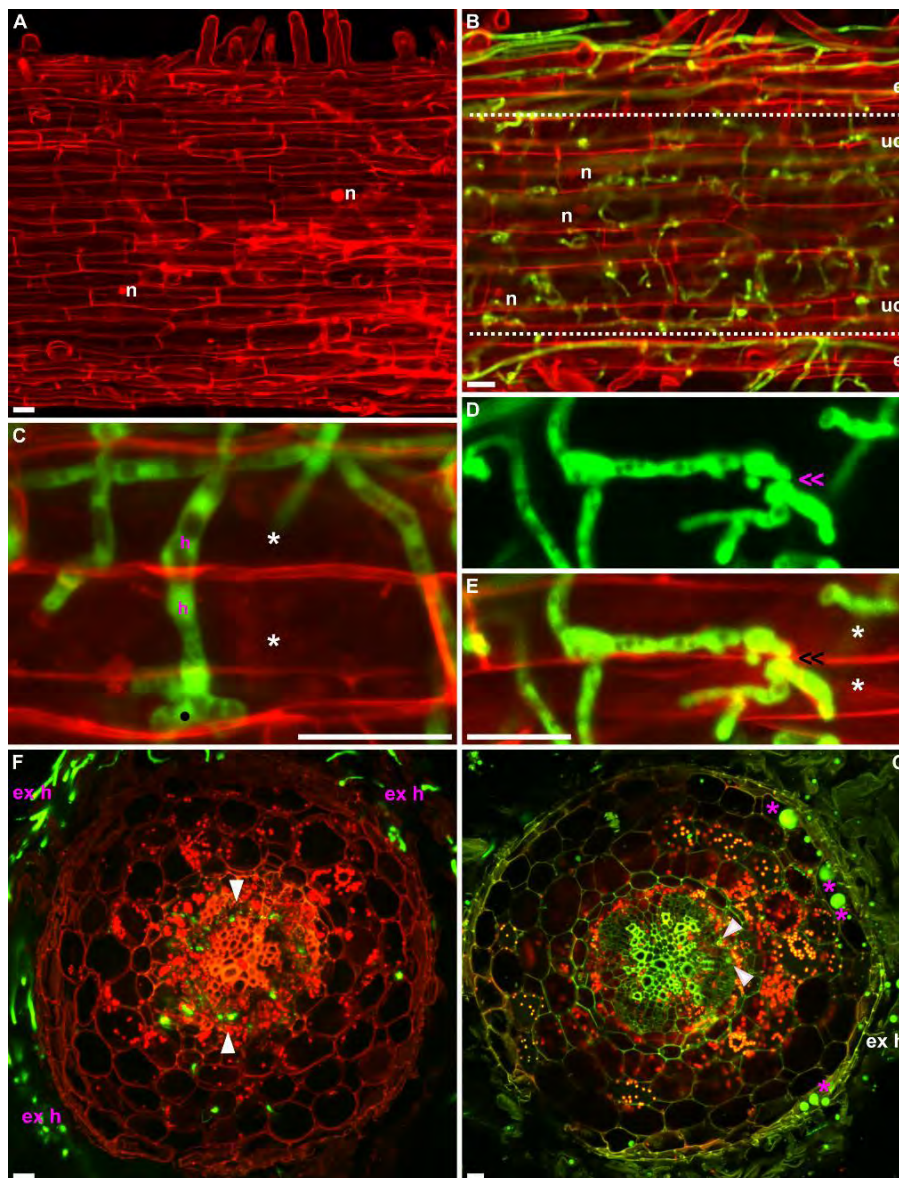


Figure 3-3 Colonization of *Lotus japonicus* root and stem tissues by *Fusarium solani* strain K.

Confocal microscope images of FsK expressing cytoplasmic GFP and wild-type *Lotus japonicus* root tissues from whole plants. Root tissues were stained with Propidium Iodide (A-E).

(A) Control root tissues (not infected). Certain nuclei are PI stained. (B) Extensive intracellular growth 3dpi, in the upper part of the root system. The fungus colonizes epidermal and cortical cells. Certain nuclei are PI stained. Dashed lines separate approximate positions of epidermal and upper cortical cells in the optical section. (C) A single hypha (h) crosses adjacent epidermal cells (asterisks). An adhering

surface is formed at the cell wall of the cell at the lower part of the image (dot). (D and E) Colonizing adjacent cells. Stenosis is required for hyphal crossing (arrow). The main hypha branches to several lobes on the colonized cell to the lower part of the image. (D) GFP channel. (E) GFP and red (plant cell autofluorescence/PI) channel merged image.

(F and G) FsK progression in roots and stems. Confocal microscope images of cross sections of wt *L. japonicus* whole plants colonized by FsK (7 dpi). Plant-fungal interaction took place in Petri dishes. (F) Cross section of the root at a site close to root crown. Fluorescence is detected in the vascular system of the root (arrows). Extraradical mycelium is also recorded. (G) Cross section of the stem, at a site very close to the root crown. Fungal structures of round shape are formed in epidermal/upper cortical cells (asterisks). Green fluorescence close to xylem cells, presumably of fungal origin is also observed (arrows).

Confocal microscope images are z axis projections of serial optical sections (A, C-G) or single optical sections (B). n, nucleus; e, epidermis; uc, upper cortex; h, hypha; dot, fungal adhesion surface; white asterisk, intracellular growth; double arrow, hyphal stenosis at penetration sites; single arrow, intraradical colonization; ex h, extraradical hyphae and hyphae on the space surrounding the stem; magenta asterisk, round shaped fungal structures.

Bars = 20 μ m.

An example of a hypha crossing the cell wall of an upper cortical cell is shown in Figure 3-4G-H. FM4-64-stained materials are recorded adjacent to the hypha at the entrance point. These presumably membranous materials could serve the vesicular supply to developing Cell Wall Appositions (CWAs, syn. papillae), i.e. local appositions of material to the cell wall, underneath hyphopodium contact sites. Additionally, we cannot exclude the possibility that the recorded signal is due and/or enhanced by autofluorescence emitted by CWAs themselves. In certain colonized epidermal cell, the fungal hypha exhibited an FM4-64 stained red contour, indicating cases of the presence of a perifungal membrane (Figure 3-4I).

Our data suggest that Fsk entrance into *L. japonicus* cells entails rearrangements of plant membranous materials and possible papillae-like formation at hyphopodium contact sites. Vesicular trafficking may be implicated in the process.

3.3.5 Fsk colonizes the root system of *Medicago truncatula* and promotes distinct sub-cellular responses

To analyze in further detail plant cell responses to Fsk colonization, we took advantage of the previously developed experimental system of ROCs of the model legume *M. truncatula* (Genre et al., 2005) (Genre et al., 2008) (Genre et al., 2009) (Genre et al., 2012), which allows live cell imaging in confocal microscopy, in addition to bright field imaging of fixed samples (Figure 3-5 to 3-6, Supplementary Figure 3-12, Supplementary Figure 3-13 to 3-16).

Fsk was able to colonize *M. truncatula* ROCs as fast as we observed for the root system of whole *L. japonicus* plants. Significant similarities in plant cell responses were observed during fungal progression, and in the structures formed by the endophyte in both interaction systems. The fungus contacted the root epidermis by the formation of a hyphopodium (Figure 3-5B, Supplementary Figure 3-12A, B, Supplementary Figure 3-13B) and proceeded towards the inner part of the root either intercellularly across openings between epidermal cells (Figure 3-5A), or by intracellular hyphal extension Supplementary Figure 3-13D).

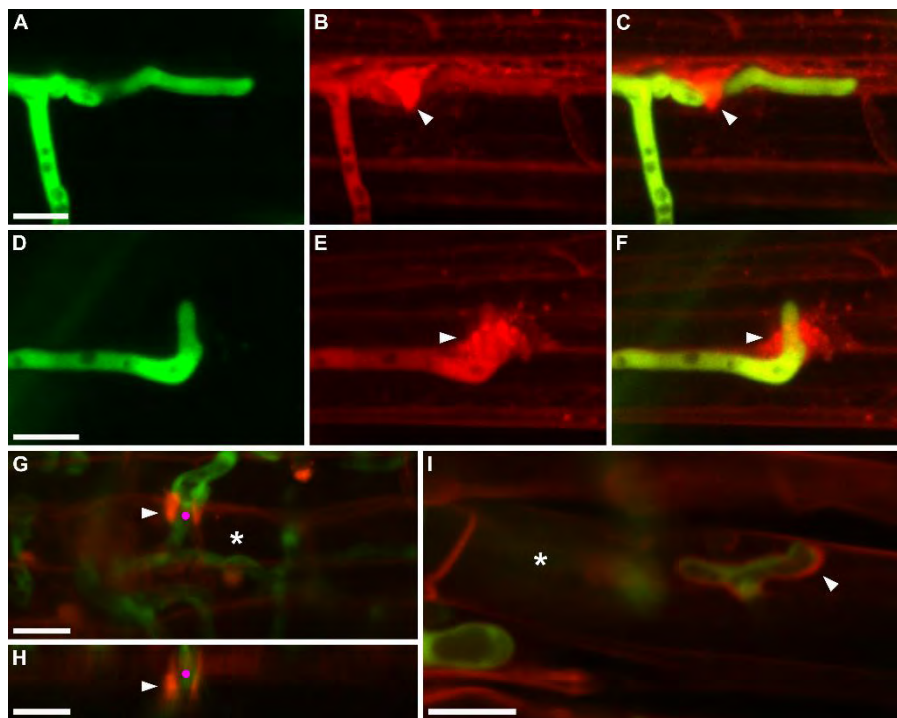


Figure 3-4 Membrane dynamics in the epidermis/upper cortex of wt *L. japonicus* roots upon FsK accommodation. Confocal microscope images of FsK expressing cytoplasmic GFP, and wt *L. japonicus* stained with the lipophilic dye FM4-64. (A-C) Intracellular growth in an epidermal cell. Localized materials, stained with FM4-64, accumulate as the hypha proceeds (arrow). (D-F) A hyphal tip attempts to enter an epidermal cell.

Localized, vesicle-like, FM4-64 stained materials accumulate around the hyphal tip (arrow). (G) A growing hypha penetrates the cell wall of an upper cortical cell and grows intracellularly. FM4-64 stained materials accumulate in close proximity to the fungal hypha (dot), intracellularly. (H) Orthogonal view of (G).

(I) A colonized epidermal cell. The fungal hypha exhibits an FM4-64 stained outline.

Images are z axis projections of serial optical sections (A-H) or single optical sections (I).

(A-C) and (D-F) image sets (from left to right): GFP channel; FM4-64 channel; merge.

Arrow, FM4-64 stained materials at contact/penetration sites; asterisk, colonized cell; dot, fungal hypha.

Bars = 10 μ m.

At penetration sites, single or multiple hyphae crossed the plant cell wall (Figure 3-5E; Supplementary Figure 3-13D; Supplementary Figure 3-12D, E, H). A significant amount of time was sometimes required between hyphopodium formation and full penetration of the cell. For instance, Supplementary Figure 3-13E-F demonstrates a colonization event that lasted ~7hrs. Intense plant cell autofluorescence was recorded at the site of imminent penetration, an indication of deposition of plant cell materials (Supplementary Figure 3-13B, E, G).

Intracellular growth varied and highly resembled the cell colonization pattern observed in whole *L. japonicus* plants. Single hyphae crossed the cell wall, traversed the plant cell cytoplasm and reached the opposite cell wall (Figure 3-5E; Supplementary Figure 3-12G; Supplementary Figure 3-13D) or, in other cases, hyphae ramified and filled the entire cell volume (Figure 3-5F; Supplementary Figure 3-13C). Based on calculations from our images, a single intracellular hypha grew approximately 0.15 μ m/min when inside the cell (Supplementary Figure 3-14). Fungal hyphae could change from thin to thicker structures intracellularly (Figure 3-5F; Supplementary Figure 3-13C; Supplementary Figure 3-13G). Hyphal stenosis was observed at cell-to-cell passages (Figure 3-5E; Supplementary Figure 3-13C, D; Supplementary Figure 3-14C). In Supplementary Figure 3-14C the hypha constricted at least

4-fold in order to cross the cell wall. Besides intracellular movement, cortical cells were, also, reached intercellularly (Supplementary Figure 3-12F).

Our observations in both legumes reveal the plasticity of the endophyte prior to and after penetration of the plant cell. Hyphal morphology is molded depending on the cell colonization strategy: hyphal constriction is mandatory for traversal of the cell wall; thin hyphae become thicker and bulbous; ramification of hyphae occurs intracellularly.

In the case of ROCs *in vitro* system, we recorded clear plant responses to endophyte entry attempts, which are compatible to our membrane dynamics observations in whole *L. japonicus* plants: a papilla-like structure was occasionally formed at the hypha-plant cell contact site (Figure 3-5C, D; Supplementary Figure 3-13B). The papilla was preserved for a while and its occurrence was linked to arrested penetration (Figure 3-5C, D). In other recorded cases, papilla formation at one site of a cell co-occurred with successful penetration at another site, located just a few μm away (Figure 3-7G). In all images derived from LSCM, papillae-like structures were easily identified due to their intense autofluorescence.

Endoplasmic Reticulum (ER) accumulation, associated to cytoplasmic aggregation (CA), was observed as a plant reaction towards encounter of FsK, as has been reported for compatible pathogenic and symbiotic fungi (Genre et al., 2009). Epidermal cells from non-contacted control roots exhibited a normal distribution of a lace-like network of lamellar and tubular ER cisternae across the cytoplasm (Figure 3-6A), as revealed by ER fluorescence imaging. In the presence of FsK hyphopodia, several roots displayed areas of epidermis, where the ER appeared disintegrated into small spherical bodies or completely disappeared from the cell lumen (Figure 3-6B). The most common plant cell reaction to hyphopodium formation, was the assembly of a dense accumulation of the ER underneath the contact site (Figure 3-6C-E, G, Supplementary Figure 3-15). It is noteworthy that not only the contacted cell but, also, the cells surrounding it exhibited ER accumulation. Figures 3-6C-E demonstrate an example for this reaction: a hyphopodium attaches the root surface (Figure 3-6C); the contacted epidermal cell responds with cytoplasm/ER accumulation (Figure 3-6D); the upper cortical cells respond with cytoplasm/ER accumulation as well (Figure 3-6E). The nuclei of the contacted and of the neighboring cells are positioned towards the contact site (Figure 3-6D, E).

It is of interest that the cytoplasm accumulation observed in the upper cortical cell of Figure 3-6E, has the shape of a column. In accordance, Figure 3-6F illustrates a section from a resin embedded sample, showing cytoplasm accumulation in the shape of a column, which started right underneath the hyphopodium and ended at the inner periclinal wall of the same cell. In the same image, the abutting cortical cell demonstrated cytoplasmic column formation as well.

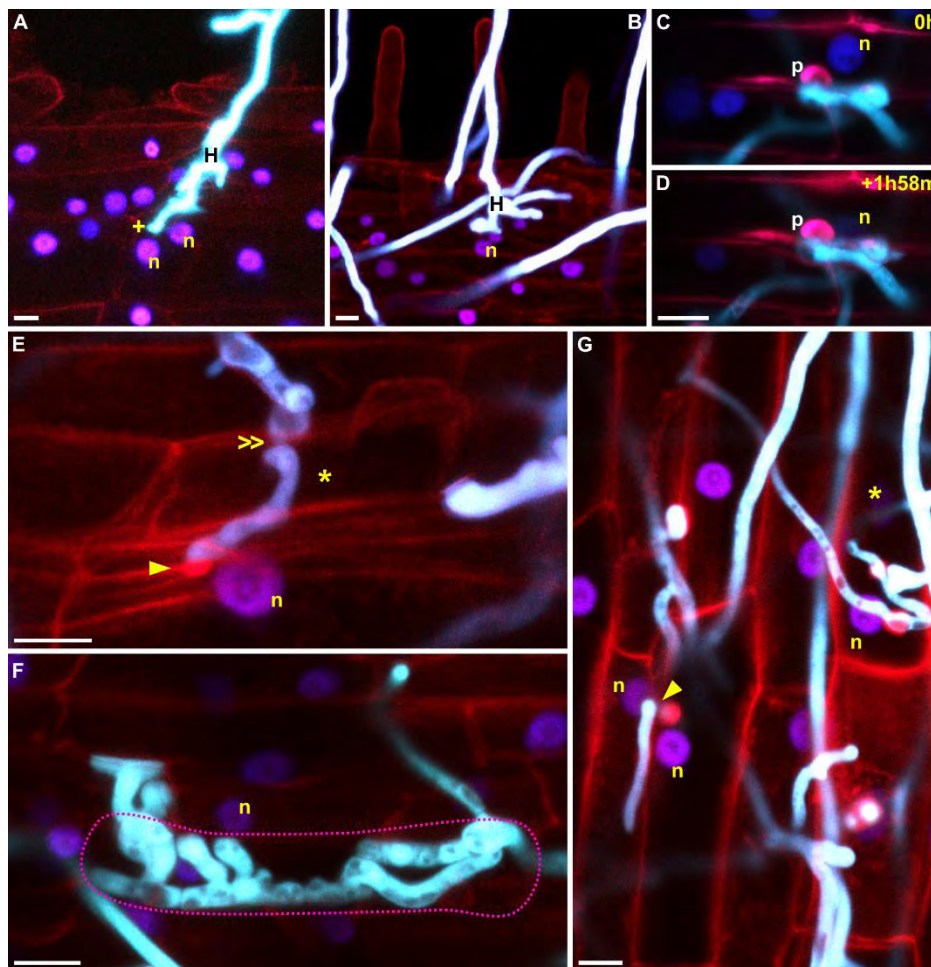


Figure 3-5 Nuclear dynamics and live cell penetration in wild type *Medicago truncatula* root cells upon interaction with FSK. Mt root organ cultures expressing the nuclear localized cameleon reporter NupYC2.1. Plant nuclei are pseudocolored in blue. (A) On a lateral root. Intercellular entrance (plus sign, +) towards the cortical tissue, 3dpi. (B) Hyphopodium formation upon contact with epidermal cells. Note the position of the nuclei of the contacted plant cells. (C) An attempted penetration event. An

autofluorescent accumulation, resembling a papilla, is visible in the inner part of the cell. The nucleus is positioned underneath the contacted hypha. (D) Same site as in (C), 1h58m later. The papilla-like structure is preserved. Penetration has not yet occurred, while the nucleus changed position. (E) Typical intracellular crossing (asterisk) requiring hyphal stenosis (double arrow). An autofluorescent accumulation precedes the traversing hypha (single arrow). (F) Ramifying hyphae completely fill an epidermal cell (dashed line), 4 dpi. (G) Attempted penetration (arrow) and live cell penetration (asterisk) on epidermis. Autofluorescent accumulations of round shape precede the hypha in both cases.

Images are z axis projections of serial optical sections.

Plus sign (+), intercellular growth; n, nucleus; H, hyphopodium; p, papilla-like structure; asterisk, intracellular growth; double arrow, hyphal stenosis at penetration sites; single arrow, contact sites.

Bars = 10 μ m.

Nucleus movement and positioning underneath the hyphopodium contact site was also among the first reactions of the contacted root cell (Figure 3-5A-E). This was confirmed by our observations of GFP-ER roots, where the GFP, also, highlighted the nuclear envelope (Figure 3-6D, E; Supplementary Figure 3-14B). Furthermore, nucleus migration was observed in epidermal and outer cortical cells across the root, in cells before penetration, and in cells adjacent to an already invaded one (Figure 3-5E, F). Lastly, this response was also observed in the vicinity of intercellular hyphae (Figure 3-6H, Supplementary Figure 3-15D), possibly related to penetration attempts.

In our experimental set-up, some cells lost ER fluorescence upon contact with Fsk (Supplementary Figure 3-14B, Supplementary Figure 3-16B-D), an indication of loss of cell viability. Loss of cell viability, also, occurred independently of a subsequent penetration event (Figure 3-6B, Supplementary Figure 3-16D) and many cells remained intact (Supplementary Figure 3-16A), even after intracellular penetration (Figure 3-5G), and particularly at the root cortex (Supplementary Figure 3-16E) at advanced stages of the interaction.

To summarize, Fsk induces a range of responses during its interaction with *M. truncatula* ROCs: focal accumulation of cytoplasm and nuclear placement at the site of imminent penetration (indications of a plant cell polarized reaction towards the fungal invasion site); deposition of papilla underneath the hyphopodium; live cell penetration and partial cell death induction (as indicated by the cessation of cytoplasmic streaming and/or the dismantled ER at distinct sites).

3.3.6 Ultrastructural evidence for membrane trafficking and defence activation during the fungal penetration attempts

To validate the events described when Fsk colonizes *M. truncatula* ROCs, we used TEM focusing on the early contact between the interaction partners (Figure 3-7A). The observations of 70-nm ultrathin sections for TEM revealed that a loose fibrillar network surrounded the extraradical hyphae and connected the fungus with the plant (Figure 3-7B). When the walls of the two partners came in direct contact, different levels of reactions were detected in *M. truncatula* epidermal cells. Figure 3-7C-D illustrate how the plant membrane stays adhered to the plant cell wall, even if some membrane pockets were already present. These contained membrane remnants and were surrounded by actively rough ER membranes. In some cases the contact between the interacting hypha and the epidermal cell was very tight (Figure 3-7E-F). In Figure 3-7E the plant plasma membrane responded with a detachment from the wall. Under this situation, which suggests a plasmolysis event, extense multivesicular bodies (MVBs) were observed. As seen under the confocal and optical microscope, the contact between the hyphae and the epidermal cells led to the deposition of the papillae. Papillae were detected during the penetration attempts (Figure 3-7G).

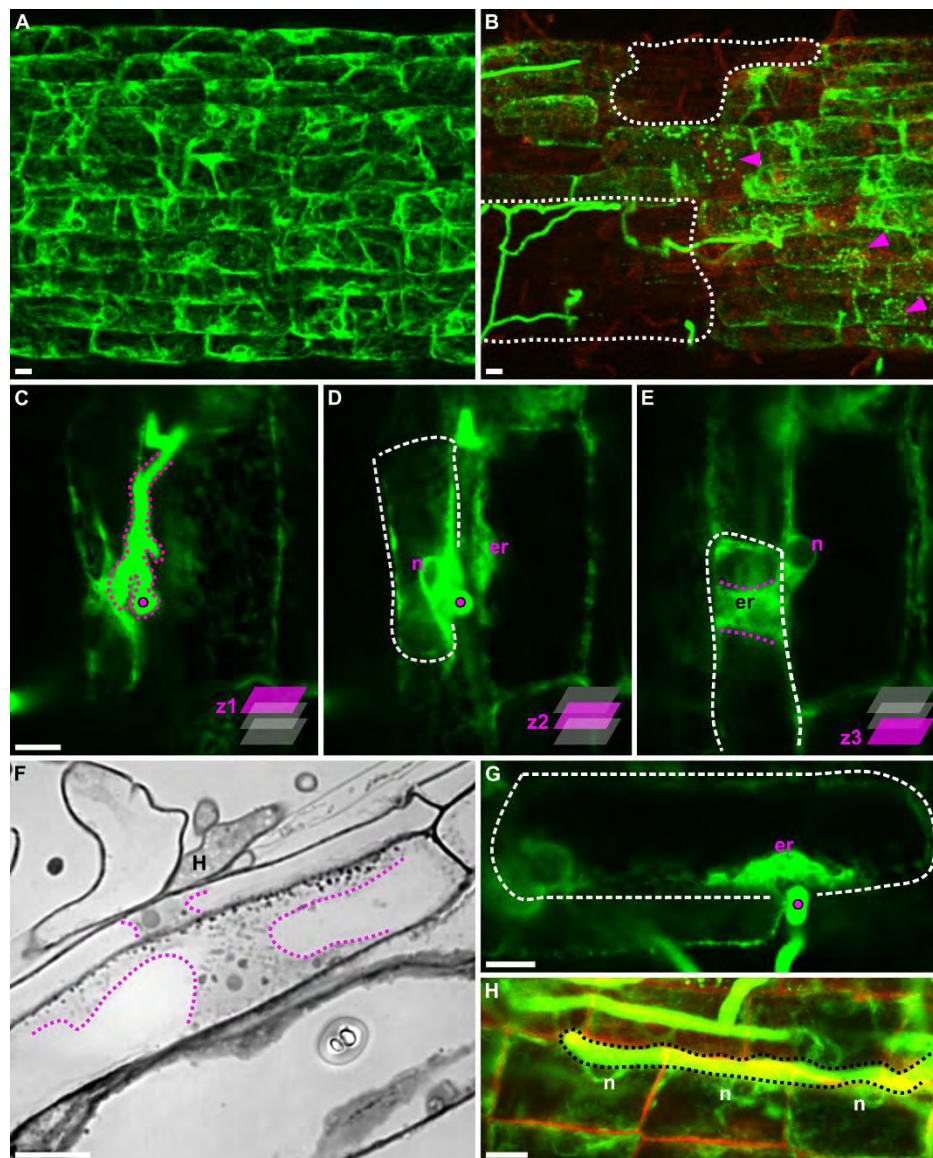


Figure 3-6
Endoplasmic Reticulum, nuclear and cytoplasmic responses of wild-type *M. truncatula* root organ cultures upon FsK inoculation. Confocal (A-E, G, H) and light microscope (F) images. *Mt* root organ cultures in confocal images are expressing GFP-HDEL. (A) Control roots (non-contacted by FsK). (B) Epidermal cells interacting with FsK lack of fluorescence, 1 dpi. Certain non-contacted epidermals also lack of fluorescence (dashed lines). ER disintegrates into spherical bodies (arrows). (C-E) Selected single optical sections

showing FsK establishing contact with *Mt* epidermis, 2 dpi. The relative z position of each section is denoted in magenta at the lower part of each image. (C) An epidermal interacts with a hypha (dashed line in magenta). (D) The epidermal (denoted with a white dashed line) responds with ER accumulation and nuclear positioning underneath the contact site. The adjacent cell also responds with ER accumulation. (E) The underneath upper cortical cell (denoted with a white dashed line) responds with ER aggregation in a type of column (magenta dashed lines).

(F) Light microscope image of a semithin section. A hyphopodium adheres to an epidermal. The contacted epidermal cell and the adjacent to it, respond with cytoplasmic accumulation. (G) Hyphal adhesion (magenta dot) on epidermis. The adjacent cell (white dashed line) reacts with ER accumulation. (H) Nuclei face a hypha traversing intercellularly (black dashed line).

Confocal images are z axis projections of serial optical sections (A, B, H) or single optical sections (C-E, G).

Arrow, ER disintegration; dot, hypha; n, nucleus; H, hyphopodium; er, endoplasmic reticulum.

Bars = 10 μ m.

When hyphae contact the host wall, MVBs of different size were observed moving towards the cell periphery to enlarge the papilla (Figure 3-7H, I). Image III-7I illustrates the heterogenous structure of

the papilla consisting of membranes and cell wall materials. Notwithstanding these defense attempts, many hyphae entered the epidermal and outer cortex cells. They were usually detected in senescing cells, while the fungus is always active and surrounded by membrane remnants (Figure 3-7J, K). During the first step of intracellular colonization, many vesicles aggregated around the hypha but they did not seem to fuse to produce an organized perifungal membrane, as seen in biotrophic interactions.

In conclusion, these ultrastructural observations highlight the cellular reorganization of the epidermal *Medicago* cells when contacted by FSK. In agreement with our confocal images, intense membrane dynamics are required and in particular the development of a machinery for a membrane trafficking.

3.4 Discussion

In the present study, an endophytic *Fusarium solani* strain (FsK) was studied in association with legumes. The latter were chosen as a plant associate since legumes consist an excellent tool for studying plant-microbe interactions due to their capacity to form symbiosis both with rhizobia and AMF. The genetic factors that mediate these interactions are well-known and can be used to provide insight on the establishment of other endophytic associations. Striking similarities as regards the molecular and cellular biology that govern the various types of plant-microbe interactions, including symbiosis, pathogenesis, and to a lesser extent endophytism, have been repeatedly reported (Tomiya, 1957) (Kobayashi et al., 1992) (Gross et al., 1993) (Takemoto et al., 2003) (Güimil et al., 2005) (Koh et al., 2005b) (O'Connell and Panstruga, 2006) (Gao and Mendgen, 2006) (Hardham et al., 2007) (Hardham, 2007) (Qingliang et al., 2008) (Genre et al., 2009) (Lu et al., 2012) (Lace and Ott, 2018).

FsK is a novel endophytic fungal isolate, thus far investigated only in association with *Solanum lycopersicum*. In tomato root tissues the endophyte profoundly proliferates intracellularly from epidermis to cortex, reaches the vascular tissues and proceeds lengthwise through the root system. Here we provide evidence that *L. japonicus* can also serve as host for FsK. Although no apparent beneficial effect to plant growth was obvious under the normal conditions examined in this study, *L. japonicus* plants were able to fully complete their life cycle. (Takeuchi et al., 2007b) investigated a pathosystem, comprising of *Lotus japonicus* and a pathogenic *Fusarium solani*, isolated from root lesions of diseased *Lotus japonicus*. The pathogenic *Fusarium solani* strain caused root rot in the model legume, necrotic lesions to stems and leaves, and eventually plant death. The comparative study of the two different strains in legumes may give insight in the molecular mechanisms resulting in endophytism or pathogenicity for members of the *F. solani* complex.

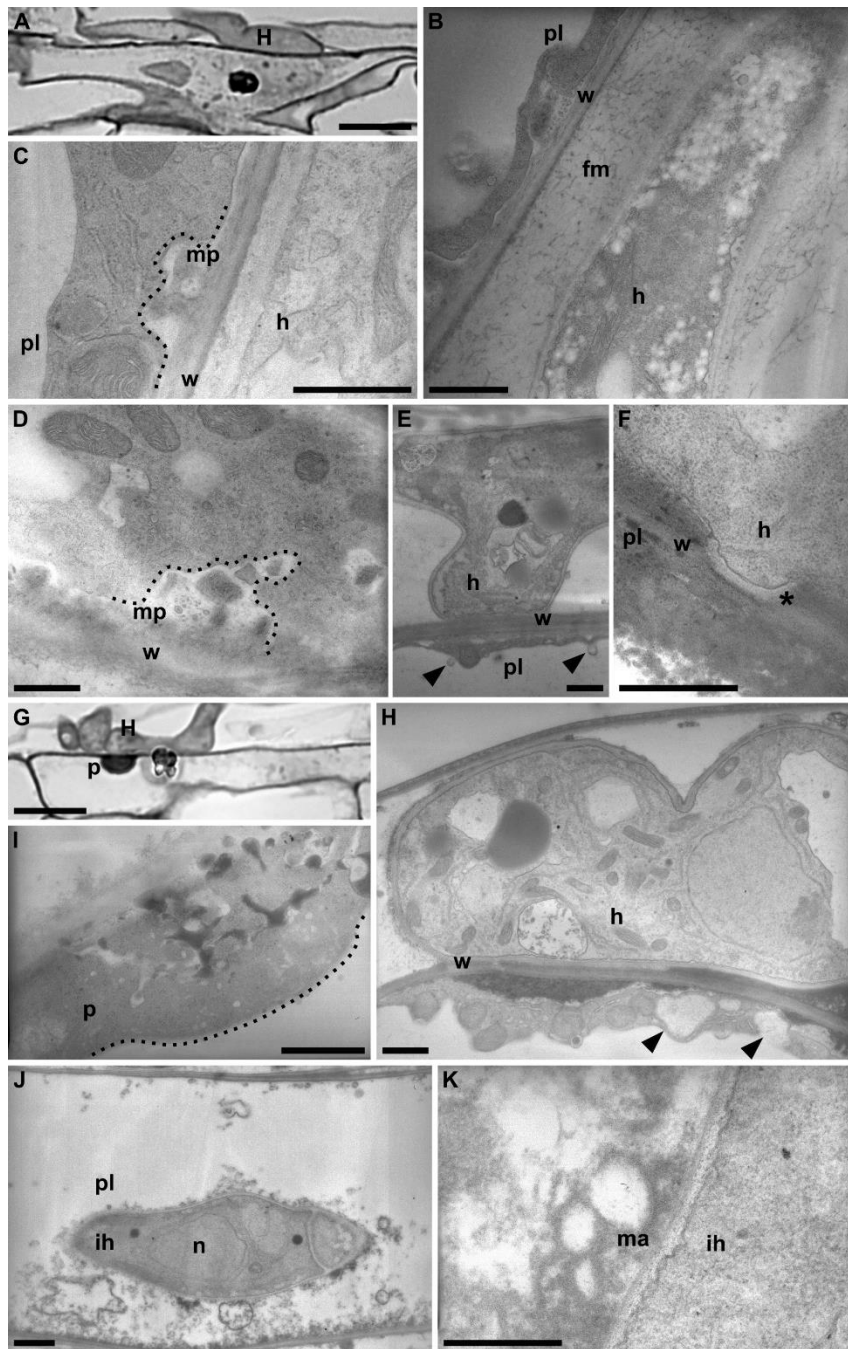


Figure 3-7 TEM and optical microscope images of *M. truncatula* ROCs interacting with Fsk.

(A) A hyphopodium contacts an epidermal cell. (B) A fungal hypha (h) approaches an epidermal cell. Extracellular fibrillar material (fm) surrounds the fungus and connects it with the plant.

(C and D) The plant cell reacts with membrane pockets (mp) formation in its plasma membrane in response to contact with the fungal hypha.

(E) The fungus has established tight contact with the plant cell wall. Extense multivesicular bodies (arrows) are observed.

(F) A penetration attempt (asterisk). (G) Hyphopodium formation on epidermis. A papilla is formed at one site of the cell; the fungus penetrates the same cell from another site.

(H) The fungus has established contact with the plant cell, which responds with papilla initiation. Multivesicular bodies move towards the cell periphery (arrows). (I) Heterogeneous structure of a

papilla. (J) A senescent colonized plant cell. The fungus is alive. (K) Membrane remnants surround an intracellular hypha.

Optical microscope images (A, G); TEM images (B-F, H-K).

H, hyphopodium; pl, plant cell; w, wall; fm, fibrillar material; h, hypha; mp, membrane pockets; arrow, multivesicular body; asterisk, penetration attempt; p, papilla; ih, intracellular hyphae; n, nucleus; ma, membranous aggregates. Bars = 10 μ m (A, G), 1 μ m (B-F, H-J), 0.5 μ m (K).

In tomato, Fsk growth is restricted to the root, and has not been detected in shoot tissues, even at very late stages of plant development (Kavroulakis et al., 2007) (Kavroulakis et al., 2018) (Papadopoulou et al, unpublished results). In this work, despite other similarities in the colonization pattern with the one in tomato, we clearly show that the endophyte is capable of colonizing the aerial parts of *L. japonicus*.

In our experimental set up, the fungus moves into the stem as early as 4 dpi *in vitro*. These results point out that the endophyte uses various lifestyles, which depend on the host plant. Fungal propagules were present in all plant tissues and CFUs in the rhizospheric substrate remained at steady numbers for a period of 50 dpi, an indication that the fungus benefits from the plant and proliferates, at least for the time period investigated here. An even longer period of interaction or possibly a different approach may allow further insight to the extent of the fungus dependency to the host plant. In the root system, there is an apparent absence of an orchestrated plant-fungus developmental pattern and we recorded no specialized intracellular fungal structures. In the stem of *L. japonicus* we recorded intracellular hyphae as well as spore-like fungal structures in epidermal cells.

3.4.1 FSK exhibits plasticity upon engagement with legumes

During colonization of legumes, various types of plant cell penetration are observed, i.e. from single to multiple hyphae penetrating the same cell. Nonetheless, in the majority of cases, no massive cell wall disruption is recorded when the fungus enters the cell, which suggests that a mechanism for plant cell integrity maintenance exists. In most cases, intracellular passage as well as transcellular movement occur at defined sites of the plant cell wall and are associated to a characteristic hyphal constriction. It would be interesting to examine whether FSK uses plasmodesmata to enter the cell lumen, as illustrated for the hemibiotrophic fungus *Magnaporthe oryzae* in its association with rice (Kankanala et al., 2007a). Intracellularly, fungal hyphae appear morphologically different at certain sites, depending on whether the entire cell is filled with the fungus or just individual hyphae occupy the cell. Differentiation of *M. oryzae* filamentous primary hyphae to thicker, bulbous invasive hyphae that fill the first-invaded cell and then move into neighboring cells has been previously reported (Heath et al., 1990) (Kankanala et al., 2007a). Heath et al (1990) correlated this dimorphic nature of the infection hypha of *M. grisea* with successful infection, since in cases where primary thin hyphae continue to grow undifferentiated, the invaded cell rapidly died and fungal growth was restricted to one thin unbranched hypha.

In *M. truncatula* root organ lines, our laser scanning confocal observations, verified by bright-field and TEM imaging, clearly show that papilla formation is among the first reactions of *Mt* ROC epidermal cells upon attempted fungal penetration at various sites. Papillae are among the earliest defense mechanisms of plants against microbial invasion. They are CWAs built in both compatible and incompatible interactions of plants and fungi. They are deposited at sites of microbial attack and differ in chemical and mechanical features from the normal cell wall (Hückelhoven, 2007). Classes of compounds commonly found in papillae are phenolics, reactive oxygen species, cell wall proteins and cell wall polymers; with (1,3)- β -glucan callose being the most abundant of the latter (Voigt, 2014). Papilla formation can, also, by retarding microbial invasion, gain time for an induction of additional defense responses that perhaps require gene activation and expression (Voigt, 2014). In our system, not all cells exhibited papilla formation upon contact, and when papillae were formed, colonization was not prevented. Papilla formation may indicate a-controlled-by-the-plant restriction of fungal proliferation, which is 'expressed' as the reinforcement of the cell wall in specific cells. When we employed whole *L. japonicus* plants, in certain cases we recorded FM4-64 stained material (seemingly in the form of vesicles), accumulating in the vicinity of contacting/penetrating hyphae. These accumulations are

compatible with a local accumulation of endocytic vesicles, likely related to intense plant cell membrane dynamics at the penetration site. We do not know whether these FM4-64 stained materials serve the supply for construction of a rather ephemeral membrane interface, which is not maintained for a long time post penetration or whether they serve the vesicular delivery of materials to developing CWAs (Hardham et al., 2007). In all, we can argue that intense endo/exocytic activity occurs in FSK-legumes association.

Differences regarding the time period needed to achieve cell penetration corroborate the hypothesis that symbionts and pathogens are recognized during this time frame via specific signals, which define responses, with symbionts achieving a faster entry than pathogens (Genre and Bonfante, 2007). FSK spores germinate relatively fast (within 2-3 h on water agar plates in the absence of the plant; Papadopoulou et al. unpublished results). Its growth rate outside and inside plant tissues is fast and we have recorded cases, where FSK needed only ~7hrs from papilla formation to subsequent cell penetration. Papillae form but are not sufficient to keep the fungal hyphae outside the cell. The type of signals (secreted molecules at contact site or diffusible signals) that orchestrate this interaction and allow the fungus to successfully and systemically colonize its host is an intriguing question for future work.

Cell integrity is maintained in some cases, while lost in others, upon FSK penetration and intracellular growth. Epidermal cells are, at least to a certain extent, the first line of cells 'sacrificed' upon fungal encounter. Direct guest-host contact and plant cell entry, play a critical role in biotrophic interactions. In these associations, plant cell integrity maintenance is of highest importance and this is achieved via the engulfment of the invader in plant-derived membranous materials (Genre and Bonfante, 2007). In AM symbiosis, the fungus is nicely membrane-confined and cytosol-excluded in all cases and the plant 'catches up' the demands for synthesis of an intracellular compartment. But in the case of filamentous fungi (pathogenic or beneficial) this task is more challenging (Genre and Bonfante, 2007). FSK is a filamentous, fast growing endophytic fungus, whose intracellular hyphae, as recorded in this study, may fully occupy the plant cell lumen. By and large, the plant faces difficulties to accommodate such a perplexing eukaryotic organism. We argue that the growth rate of the fungus is higher than what the plant can safely encapsulate within its cells and that, in the FSK-legume system, occasional cell death may be employed to limit fungal proliferation and prevent massive loss of cell viability.

Loss of plant cell integrity upon fungal accommodation has been previously reported for growth-promoting beneficial fungi. One of the most well-known cases is *Serendipita indica*. The fungus exploits the host's cell death machinery and a spatial association of dead root tissue with strong mycelial growth is recorded in barley (Deshmukh et al., 2006). In *A. thaliana*, a biphasic lifestyle has been recorded with the fungus swinging from biotrophy to necrotrophy within the root system (Jacobs et al., 2011) (Qiang et al., 2012a). Recently, *Colletotrichum tofieldiae*, a plant growth promoting fungus under low Pi conditions, was reported to establish a transient early biotrophic phase with *A. thaliana* epidermal cells, and a more stable biotrophic interaction in the cortex, since colonized cortical cells remain intact for longer periods (Hiruma et al., 2016). Lace et al (2015) observed necrotic lesions in a *M. truncatula*-*Trichoderma atroviride* association and advocate that in more natural conditions, local root lesions would be more tolerated by the plant. We support this view, since plants colonized by FSK complete

their life cycle and do not exhibit apparent phenotypic differences in comparison to controls. Thus, in more natural conditions, a-controlled-by-the host restriction of fungal proliferation within plant tissues could be expected. We, furthermore, argue that under our *in vitro* conditions an accelerated plant-fungal association develops and that the association would require a greater time frame in nature.

3.4.2 Assigning common sub-cellular responses to plant-fungal interactions

Previous studies have identified common plant cell responses upon microbial stimulation, among them being CA as well as nuclear migration at contact sites (Takemoto et al. 2003). Nuclear translocation in response to a stimulus is an expected phenomenon if we take into consideration the layout of a plant cell. By moving closer to the stimulus, the nucleus overcomes the obstacle posed by the large vacuole to rapid signal transduction. Thus, plant cell responses such as gene activation are accelerated (Genre et al., 2009). ER accumulation associated to CA at the stimulated area may also facilitate faster plant cell responses such as protein and/or lipid synthesis and transport at penetration site. Cytoplasmic movements and migration of the nucleus towards the infected part are known to occur in response to pathogens (Tomiya, 1957) (Gross et al., 1993). (Koh et al., 2005b) reported cellular dynamics involving ER and nucleus movement closer to the penetration site and developing haustorial complex for the *Arabidopsis thaliana*-*Erysiphe cichoracearum* interaction. Genre and colleagues (Genre et al., 2009) demonstrated that CA formation relates to contact by compatible fungi (symbiotic or pathogenic), whereas nuclear movement is considered a general, non-specific response of plant cells to physical stimuli that precedes a live cell penetration.

Our approach, in order to follow ER dynamics and nuclear movements upon FSK stimulation in legumes, was to use the previously constructed *M. truncatula* ROCs, which are labeled for specific cell compartments. Our results demonstrate that the first response of the plant to FSK stimulation is ER remodeling. At certain sites, cells respond with ER disintegration into small spherical bodies. Some cells lose viability, as indicated by cessation of ER streaming and/or fluorescence, though this occurs independently of subsequent penetration at certain sites. We have shown that at other sites, though, cells respond with a clear ER accumulation at contact site. We assume that this polarized ER accumulation in FSK-*Mt* interaction is associated to localized accumulation of the cytoplasm.

The nucleus of the plant cell is positioned at most cases underneath the penetrating hypha. This phenomenon was observed in numerous root tissues and in multiple sites. We demonstrate that this reaction occurs at the first contacted cell and extends to the adjacent cells, an indication that either fungal/plant cell (via perhaps a diffusible signal) and/or plant cell/plant cell communication occurs to prepare the surrounding cells for fungal presence and/or potential penetration. In addition, nuclear movement occurs even when FSK hyphae simply explore the apoplast, a reaction possibly related to penetration attempts.

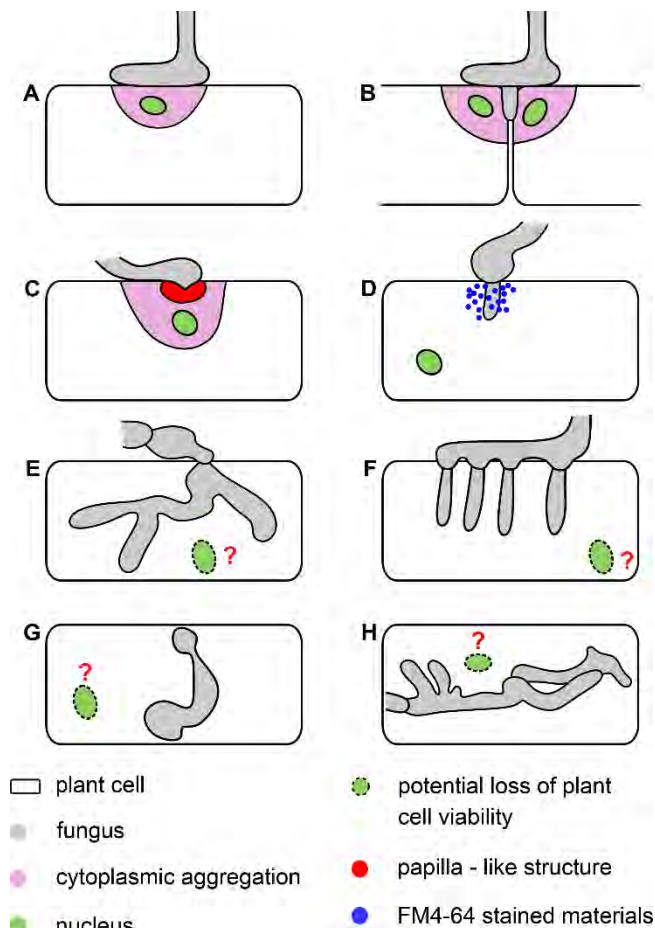


Figure 3-8 Schematic summary of main features of FsK root colonization and subcellular responses for *L. japonicus* and *M. truncatula*.

Structures are represented with the following colours: grey, fungus; green, nucleus; pink, cytoplasmic aggregation; red, papilla; blue, FM4-64 positive materials.

(A) A hyphopodium is formed on the root epidermis. This activates cytoplasmic aggregation (pink) associated to ER accumulation (not shown) and nuclear translocation underneath the hyphopodium contact site. (B) This reaction occurs in all contacted by the fungus cells, and even when the fungus proceeds intercellularly towards the root upper cortex. (C) The plant cell occasionally reacts with papilla formation underneath the site of imminent penetration. The nucleus is located underneath the contact site. (D) Local accumulations of FM4-64 positive materials are observed at attempted penetration/penetration sites.

(E and F) FsK penetrates the contacted cell either by single (E), or multiple hyphal lobes (F). Stenosis

is required to cross the cell wall in both cases. Cell viability is not maintained in all cases.

(G and H) FsK demonstrates plasticity inside the legume cell. A single hypha crosses the cell (G) or hyphae may ramify intracellularly and fill the entire cell lumen (H). Not all colonized cells remain alive.

Drawings are based on the following figures: (A) Figure 3-5B, Figure 3-6F-G, Supplementary Figure 3-11A-B; (B) Figure 3-5A; (C) Figure 3-5C, Supplementary Figure 3-13B; (D) Figure 3-4A-F; (E) Figure 3-3D; (F) Supplementary Figure 3-11C; (G) Supplementary Figure 3-12G, Supplementary Figure 3-13D; (H) Figure 3-5F.

3.4.3 Conclusions

In the present study we have shown that the endophytic tomato fungal isolate, *Fusarium solani* strain K, is able to colonize *L. japonicus* root tissues and to translocate to the aerial parts of the plant. Significant commonalities arose in the mode of root colonization in both model legume-hosts examined, *L. japonicus* and *M. truncatula*, which may be briefly summarized as: (a) hyphopodium formation upon contact with epidermal cells, (b) plant cell ER accumulation towards the contact site, (c) plant cell nuclear positioning towards the site of imminent penetration, (c) CWAs underneath the hyphopodium contact site, (d) FM4-64 stained materials surrounding hyphae at contact/penetration sites, (e) plasticity and versatility during colonization process, (f) vasculature colonization, (g) migration to the stem and formation of fungal structures, (h) partial loss of cell viability (graphically presented in Figure 3-8). FsK grows endophytically within legumes acting half-way between a symbiont and a pathogen. Its investigation is challenging, at least in whole plants where the multilayers of cells are simultaneously contacted and colonized by the fungus. FsK-legumes association represents an original plant-

endophyte system, which can be exploited to fill in existing gaps in our understanding of the mechanisms that endophytes use to ensure their entry in host plants and establish a reciprocal relationship.

Funding

This work was partially supported by the Postgraduate Programs 3817 & 3439 of the Department of Biochemistry and Biotechnology, University of Thessaly and COST Action FA1206 and FA1405 (STSM Grants to VS).

Competing interests

Fusarium solani FsK is patented (20070100563/1006119, issued by the Industrial Property Organization to KKP and NK).

Acknowledgments

The authors are grateful to Constantine Garagounis and Daniela Tsikou for fruitful comments in text revision; to Catalina Stedel for advices in plant care; to Marianna Avramidou for her assistance with the sporulation experiment; to Georgios C. Papadopoulos and Chryssa Bekiari for access to CLSM (Laboratory of Anatomy, Histology & Embryology, Veterinary School, Aristotle University of Thessaloniki, Greece).

3.5 References

- Boisson-Dernier A, Chabaud M, Garcia F, Bécard G, Rosenberg C, Barker DG. 2001.** *Agrobacterium rhizogenes*-transformed roots of *Medicago truncatula* for the study of nitrogen-fixing and endomycorrhizal symbiotic associations. *Molecular Plant-Microbe Interactions* **14**: 695–700.
- Bolte S, Talbot C, Boutte Y, Catrice O, Read ND, Satiat-Jeunemaitre B. 2004.** FM-dyes as experimental probes for dissecting vesicle trafficking in living plant cells. *Journal of Microscopy* **214**: 159–173.
- Brundrett M. 2004.** Diversity and classification of mycorrhizal associations. *Biol. Rev.* **79**: 473–495.
- Chabaud M, Genre A, Sieberer BJ, Faccio A, Fournier J, Novero M, Barker DG, Bonfante P. 2011.** Arbuscular mycorrhizal hyphopodia and germinated spore exudates trigger Ca²⁺ spiking in the legume and nonlegume root epidermis. *New Phytologist* **189**: 347–355.
- Chabaud M, Venard C, Defaux-Petras A, Becard G, Barker DG. 2002.** Targeted inoculation of *Medicago truncatula* in vitro root cultures reveals *MtENOD11* expression during early stages of infection by arbuscular mycorrhizal fungi. *New Phytologist* **156**: 265–273.
- Coleman JJ. 2016.** The *Fusarium solani* species complex: ubiquitous pathogens of agricultural importance. *Molecular Plant Pathology* **17**: 146–158.
- Coleman JJ, Rounsley SD, Rodriguez-Carres M, Kuo A, Wasmann CC, Grimwood J, Schmutz J, Taga M, White GJ, Zhou S, et al. 2009.** The Genome of *Nectria haematococca*: Contribution of Supernumerary Chromosomes to Gene Expansion. *PLoS Genetics* **5**: e1000618.
- Deshmukh S, Hüchelhoven R, Schäfer P, Imani J, Sharma M, Weiss M, Waller F, Kogel K-H. 2006.** The root endophytic fungus *Piriformospora indica* requires host cell death for proliferation during mutualistic symbiosis with barley. *Proceedings of the National Academy of Sciences of the United States of America* **103**: 18450–18457.
- Doyle JJ, Doyle JL. 1987.** A rapid DNA isolation procedure for small quantities of fresh leaf tissue. *Phytochemical Bulletin* **19**: 11–15.
- Fesel PH, Zuccaro A. 2016.** Dissecting endophytic lifestyle along the parasitism/mutualism continuum in *Arabidopsis*. *Current Opinion in Microbiology* **32**: 103–112.
- Fischer-Parton S, Parton RM, Hickey PC, Dijksterhuis J, Atkinson HA, Read ND. 2000.** Confocal microscopy of FM4-64 as a tool for analysing endocytosis and vesicle trafficking in living fungal hyphae. *Journal of Microscopy* **198**: 246–259.
- Gao K, Mendgen K. 2006.** Seed-transmitted beneficial endophytic *Stagonospora* sp. can penetrate the walls of the root epidermis, but does not proliferate in the cortex, of *Phragmites australis*. *Canadian Journal of Botany* **84**: 981–988.
- Genre A, Bonfante P. 2007.** Check-in procedures for plant cell entry by biotrophic microbes. *MPMI* **20**: 1023–1030.
- Genre A, Chabaud M, Faccio A, Barker DG, Bonfante P. 2008.** Prepenetration apparatus assembly precedes and predicts the colonization patterns of Arbuscular Mycorrhizal Fungi within the root cortex of both *Medicago truncatula* and *Daucus carota*. *The Plant Cell* **20**: 1407–1420.
- Genre A, Chabaud M, Timmers T, Bonfante P, Barker DG. 2005.** Arbuscular mycorrhizal fungi elicit a novel intracellular apparatus in *Medicago truncatula* root epidermal cells before infection. *The Plant*

Cell **17**: 3489–3499.

Genre A, Ivanov S, Fendrych M, Faccio A, Zarsky V, Bisseling T, Bonfante P. 2012. Multiple exocytotic markers accumulate at the sites of perifungal membrane biogenesis in arbuscular mycorrhizas. *Plant and Cell Physiology* **53**: 244–255.

Genre A, Ortu G, Bertoldo C, Martino E, Bonfante P. 2009. Biotic and abiotic stimulation of root epidermal cells reveals common and specific responses to Arbuscular Mycorrhizal Fungi. *Plant physiology* **149**: 1424–1434.

van Gisbergen PAC, Esseling-Ozdoba A, Vos JW. 2008. Microinjecting FM4 – 64 validates it as a marker of the endocytic pathway in plants. *Journal of Microscopy* **231**: 284–290.

Gross P, Julius C, Schmelzer E, Hahlbrock K. 1993. Translocation of cytoplasm and nucleus to fungal penetration sites is associated with depolymerization of microtubules and defence gene activation in infected, cultured parsley cells. *The EMBO Journal* **12**: 1735–1744.

Güimil S, Chang H-S, Zhu T, Sesma A, Osbourn A, Roux C, Ioannidis V, Oakeley EJ, Docquier M, Descombes P, et al. 2005. Comparative transcriptomics of rice reveals an ancient pattern of response to microbial colonization. *Proc Natl Acad Sci USA* **102**: 8066–8070.

Hardham AR. 2007. Cell biology of plant – oomycete interactions. *Cellular Microbiology* **9**: 31–39.

Hardham AR, Jones DA, Takemoto D. 2007. Cytoskeleton and cell wall function in penetration resistance. *Current Opinion in Plant Biology* **10**: 342–348.

Harrison MJ. 2012. Cellular programs for arbuscular mycorrhizal symbiosis. *Current Opinion in Plant Biology* **15**: 691–698.

Haseloff J, Siemering KR, Prasher DC, Hodge S. 1997. Removal of a cryptic intron and subcellular localization of green fluorescent protein are required to mark transgenic Arabidopsis plants brightly. *Proc Natl Acad Sci USA* **94**: 2122–2127.

Heath MC, Valent B, Howard RJ, Chumley FG. 1990. Interactions of two strains of *Magnaporthe grisea* with rice, goosegrass, and weeping lovegrass. *Canadian Journal of Botany* **68**: 1627–1637.

Hiruma K, Gerlach N, Sacristán S, Nakano RT, Hacquard S, Kracher B, Neumann U, Ramírez D, Bucher M, O’Connell RJ, et al. 2016. Root endophyte *Colletotrichum tofieldiae* confers plant fitness benefits that are phosphate status dependent. *Cell* **165**: 464–474.

Hoagland DR, Arnon DI. 1950. The water-culture method for growing plants without soil. *Circular. California Agricultural Experiment Station* **347**: 1–32.

Hoch HC. 1986. Freeze-substitution of fungi. In: Aldrich HC, Todd WJ, eds. *Ultrastructure Techniques of Microorganisms*. New York: Plenum Press, 183–211.

Howard RJ, O’Donnell KL. 1987. Freeze substitution of fungi for cytological analysis. *Experimental Mycology* **11**: 250–269.

Hückelhoven R. 2007. Cell wall-associated mechanisms of disease resistance and susceptibility. *Annu. Rev. Phytopathol.* **45**: 101–127.

Jacobs S, Zechmann B, Molitor A, Trujillo M, Petutschnig E, Lipka V, Kogel K-H, Schäfer P. 2011. Broad-spectrum suppression of innate immunity is required for colonization of Arabidopsis roots by the fungus *Piriformospora indica*. *Plant physiology* **156**: 726–740.

Kankanala P, Czymmek K, Valent B. 2007. Roles for rice membrane dynamics and plasmodesmata

during biotrophic invasion by the blast fungus. *The Plant Cell* **19**: 706–724.

Kavroulakis N, Doupis G, Papadakis IE, Ehaliotis C, Papadopoulou KK. 2018. Tolerance of tomato plants to water stress is improved by the root endophyte *Fusarium solani* FsK. *Rhizosphere* **6**: 77–85.

Kavroulakis N, Ntougias S, Zervakis GI, Ehaliotis C, Haralampidis K, Papadopoulou KK. 2007. Role of ethylene in the protection of tomato plants against soil-borne fungal pathogens conferred by an endophytic *Fusarium solani* strain. *Journal of Experimental Botany* **58**: 3853–3864.

Kobayashi I, Kobayashi Y, Yamaoka N, Kunoh H. 1992. Recognition of a pathogen and a nonpathogen by barley coleoptile cells. III. Responses of microtubules and actin filaments in barley coleoptile cells to penetration attempts. *Canadian Journal of Botany* **70**: 1815–1823.

Koh S, Andre A, Herb E, Ehrhardt D, Somerville S. 2005. *Arabidopsis thaliana* subcellular responses to compatible *Erysiphe cichoracearum* infections. *The Plant Journal* **44**: 516–529.

Kosuta S, Winzer T, Parniske M. 2005. Arbuscular mycorrhiza. *Lotus Japonicus Handbook*: 87–95.

Lace B, Ott T. 2018. Commonalities and differences in controlling multipartite intracellular infections of legume roots by symbiotic microbes. *Plant and Cell Physiology* **59**: 661–672.

Lahrmann U, Ding Y, Banhara A, Rath M, Hajirezaei MR, Döhlemann S, von Wirén N, Parniske M, Zuccaro A. 2013. Host-related metabolic cues affect colonization strategies of a root endophyte. *Proc Natl Acad Sci USA* **110**: 13965–13970.

Leborgne-Castel N, Bouhidel K. 2014. Plasma membrane protein trafficking in plant-microbe interactions: a plant cell point of view. *Frontiers in Plant Science* **5**: 1–13.

Lu YJ, Schornack S, Spallek T, Geldner N, Chory J, Schellmann S, Schumacher K, Kamoun S, Robatzek S. 2012. Patterns of plant subcellular responses to successful oomycete infections reveal differences in host cell reprogramming and endocytic trafficking. *Cellular Microbiology* **14**: 682–697.

Murashige T, Folke S. 1962. A revised medium for rapid growth and bio assays with tobacco tissue cultures. *Physiologia Plantarum* **15**: 473–497.

Nelson PE, Dignani CM, Anaissie EJ. 1994. Taxonomy, biology, and clinical aspects of *Fusarium* species. *Clinical microbiology reviews* **7**: 479–504.

O’Connell RJ, Panstruga R. 2006. Tête à tête inside a plant cell: establishing compatibility between plants and biotrophic fungi and oomycetes. *New Phytologist* **171**: 699–718.

Peškan-Berghöfer T, Shahollari B, Pham HG, Hehl S, Markert C, Blanke V, Kost G, Varma A, Oelmüller R. 2004. Association of *Piriformospora indica* with *Arabidopsis thaliana* roots represents a novel system to study beneficial plant-microbe interactions and involves early plant protein modifications in the endoplasmic reticulum and at the plasma membr. *Physiologia Plantarum* **122**: 465–477.

Qiang X, Weiss M, Kogel KH, Schäfer P. 2012. *Piriformospora indica*—a mutualistic basidiomycete with an exceptionally large plant host range. *Molecular Plant Pathology* **13**: 508–518.

Qingliang D, Yanping X, Qingqiang L, Guohong W, Minhe Y. 2008. Distribution and characteristics of *Colletotrichum* sp. as an endophyte in tea plants *Camelia sinensis*. *Scientia Silvae Sinicae* **44**: 84–89.

Reynolds ES. 1963. The use of lead citrate at high pH as an electron-opaque stain in electron-microscopy. *The Journal of Cell Biology* **17**: 208–212.

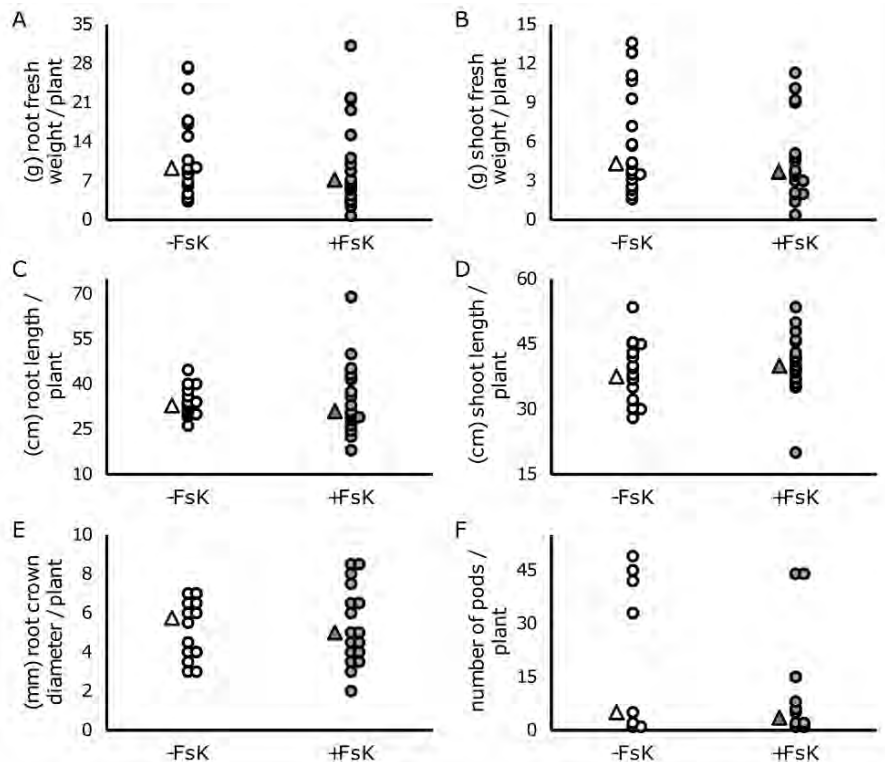
- Rodriguez RJ, White Jr JF, Arnold AE, Redman RS. 2009.** Fungal endophytes: diversity and functional roles. *New Phytologist* **182**: 314–330.
- Samils N, Elfstrand M, Lindner Czederpiltz DL, Fahleson J, Olson Å, Dixelius C, Stenlid J. 2006.** Development of a rapid and simple *Agrobacterium tumefaciens*-mediated transformation system for the fungal pathogen *Heterobasidion annosum*. *FEMS Microbiology Letters* **255**: 82–88.
- Schneider CA, Rasband WS, Eliceiri KW. 2012.** NIH Image to ImageJ: 25 years of image analysis. *Nature Methods* **9**: 671–675.
- Sesma A, Osbourn AE. 2004.** The rice leaf blast pathogen undergoes developmental processes typical of root-infecting fungi. *Nature* **431**: 582–586.
- Shweta S, Zuehlke S, Ramesha BT, Priti V, Mohana Kumar P, Ravikanth G, Spiteller M, Vasudeva R, Uma Shaanker R. 2010.** Endophytic fungal strains of *Fusarium solani*, from *Apodytes dimidiata* E. Mey. ex Arn (Icacaceae) produce camptothecin, 10-hydroxycamptothecin and 9-methoxycamptothecin. *Phytochemistry* **71**: 117–122.
- Sieberer BJ, Chabaud M, Timmers AC, Monin A, Fournier J, Barker DG. 2009.** A nuclear-targetedameleon demonstrates intranuclear Ca^{2+} spiking in *Medicago truncatula* root hairs in response to rhizobial nodulation factors. *Plant Physiology* **151**: 1197–1206.
- Stone JK, Bacon CW, White Jr JF. 2000.** An overview of endophytic microbes: endophytism defined. In: Bacon CW, White JFJ, eds. *Microbial Endophytes*. Marcel Decker Inc, New York, 3–29.
- Takemoto D, Jones DA, Hardham AR. 2003.** GFP-tagging of cell components reveals the dynamics of subcellular re-organization in response to infection of *Arabidopsis* by oomycete pathogens. *The Plant Journal* **33**: 775–792.
- Takeuchi K, Tomioka K, Kouchi H, Nakagawa T, Kaku H. 2007.** A novel pathosystem to study the interactions between *Lotus japonicus* and *Fusarium solani*. *Journal of General Plant Pathology* **73**: 336–341.
- Tomiyama K. 1957.** Cell physiological studies on the resistance of potato plant to *Phytophthora infestans*. *Japanese Journal of Phytopathology* **22**: 129–133.
- Truernit E, Haseloff J. 2008.** A simple way to identify non-viable cells within living plant tissue using confocal microscopy. *Plant Methods* **4**: 15.
- Varma A, Verma S, Sudha, Sahay N, Bütehorn B, Franken P. 1999.** *Piriformospora indica*, a cultivable plant-growth-promoting root endophyte. *Applied and Environmental Microbiology* **65**: 2741–2744.
- Vierheilig H, Coughlan AP, Wyss U, Piche Y. 1998.** Ink and vinegar, a simple staining technique for Arbuscular-Mycorrhizal Fungi. *Applied and Environmental Microbiology* **64**: 5004–5007.
- Voigt CA. 2014.** Callose-mediated resistance to pathogenic intruders in plant defense-related papillae. *Frontiers in Plant Science* **5**: 1–6.
- Whelan JA, Russell NB, Whelan MA. 2003.** A method for the absolute quantification of cDNA using real-time PCR. *Journal of Immunological Methods* **278**: 261–269.
- Wilson D. 1995.** Endophyte - the evolution of a term, and clarification of its use and definition. *Oikos* **73**: 274–276.
- Zhang N, Donnell KO, Sutton DA, Nalim FA, Summerbell RC, Padhye AA, Geiser DM. 2006.**

Members of the *Fusarium solani* species complex that cause infections in both humans and plants are common in the environment. *Journal of Clinical Microbiology* **44**: 2186–2190.

Zuccaro A, Lahrmann U, Güldener U, Langen G, Pfiffi S, Biedenkopf D, Wong P, Samans B, Grimm C, Basiewicz M, et al. 2011. Endophytic life strategies decoded by genome and transcriptome analyses of the mutualistic root symbiont *Piriformospora indica*. *PLoS Pathogens* **7**: e1002290.

3.6 Appendix of Chapter 3

3.6.1 Supplementary material

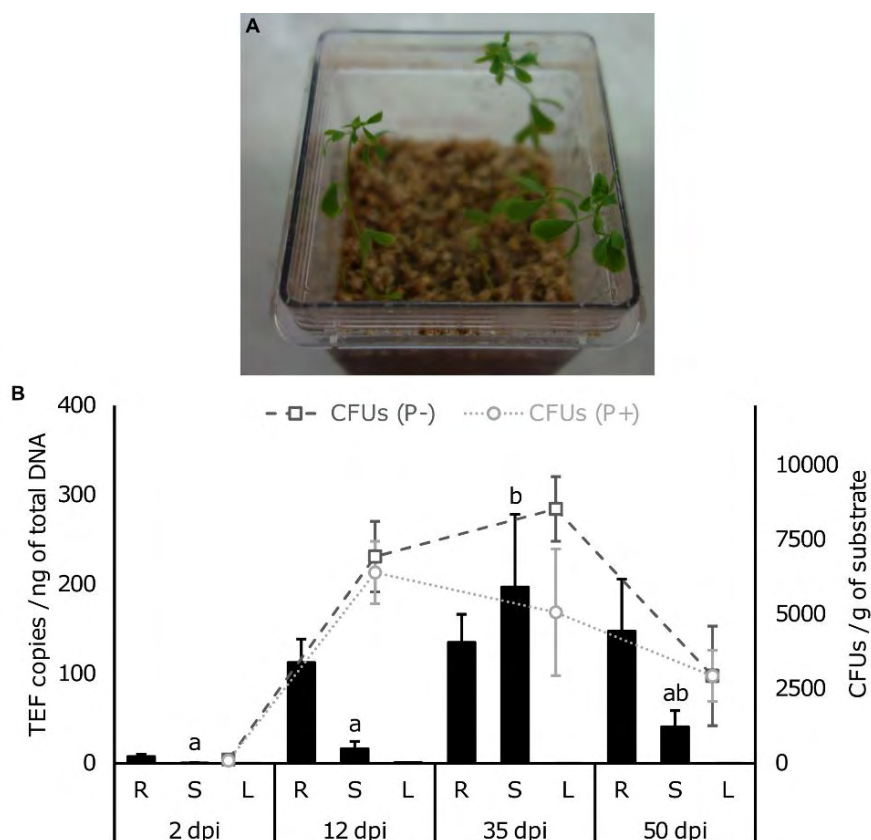


Supplementary Figure 3-9 Effect of Fsk in growth/developmental parameters of *L. japonicus* plants. Plants were grown in pots on a soilless sterile substrate. Dot-plots represent the following parameters:

(A and B) root/shoot fresh weight. (C and D) root/shoot length. (E) root crown diameter. (F) number of pods. Parameters were measured on ca. 18 plants per treatment at the last time point examined (122 dpi).

Open circles, control plants; grey circles, inoculated with Fsk plants; white and grey triangles, median values for control and Fsk-inoculated plants, respectively.

Statistical analysis (Student's *t*-test) showed no statistically significant difference between treatments, in any of the parameters examined.



Supplementary Figure 3-10 Temporal quantification of fungal colonization within *L. japonicus* tissues and monitoring of sporulation in the substrate.

(A) Experimental system at 35 dpi.

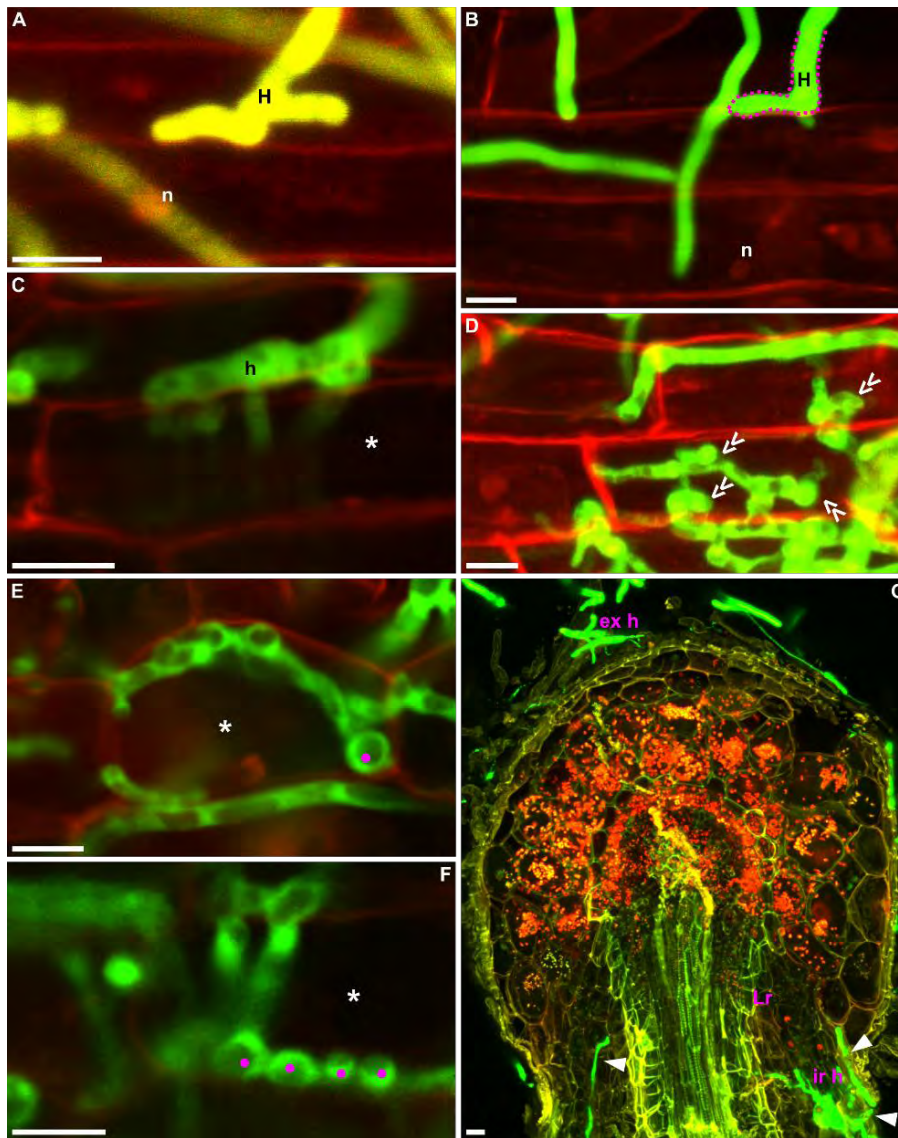
(B) Absolute quantification of fungal colonization within root/stem/leaf tissues by qPCR, using primers specific for *Fusarium* TEF1a gene (primary axis). Tissues were collected at 2, 12, 35, 50 dpi. Values are normalized to ng of total DNA isolated. Data are presented as means and standard errors of 5 biological replicates ($n=5$). Each biological replicate consists of 3 plants. *FsK* CFUs per g of surrounding substrate are presented in the secondary axis. Data are presented as means and standard errors of 5 biological replicates ($n=5$). 3 technical repetitions were averaged for each biological replicate.

Black bars, TEF1a gene copies; dark grey dashed line with square nodes, CFUs in the absence of the plant (P-); light grey dotted line with circular nodes, CFUs in the presence of the plant (P+); R, root; S, stem; L, leaves.

In the case of TEF1a gene copy numbers, statistics were performed separately for each tissue. Therefore, different letters (when present) indicate significant differences among the time points investigated, for the same tissue, at the 0.05 level (One-way anova, Tukey's test).

No statistically significant differences were recorded, when comparing CFUs in the P- versus the P+ samples (Student's t-test), at any of the time points investigated.

Temporal differences in CFU values were analyzed separately for each substrate (One way anova, Tukey's test). The P- substrate exhibited statistical significant differences at 2 and 35 dpi. The P+ substrate exhibited statistical significant differences at 2 and 12 dpi.



Supplementary Figure 3-11 Main features of *L. japonicus* root tissue colonization by *FsK*.

Confocal microscope images of *FsK* expressing cytoplasmic GFP and wild-type *Lotus japonicus* root tissues from whole plants. Root tissues were stained with Propidium Iodide (A-D) or FM4-64 (E, F).

(A and B) Hyphopodium formation on root epidermis, 2 dpi. Certain nuclei are PI stained but this is not tightly correlated to fungal accommodation events.

(C) Intracellular growth, 3 dpi. An upper cortical is penetrated by several hyphal lobes.

(D) Hyphal differentiation into bulbous shape in colonized epidermal cells (arrows).

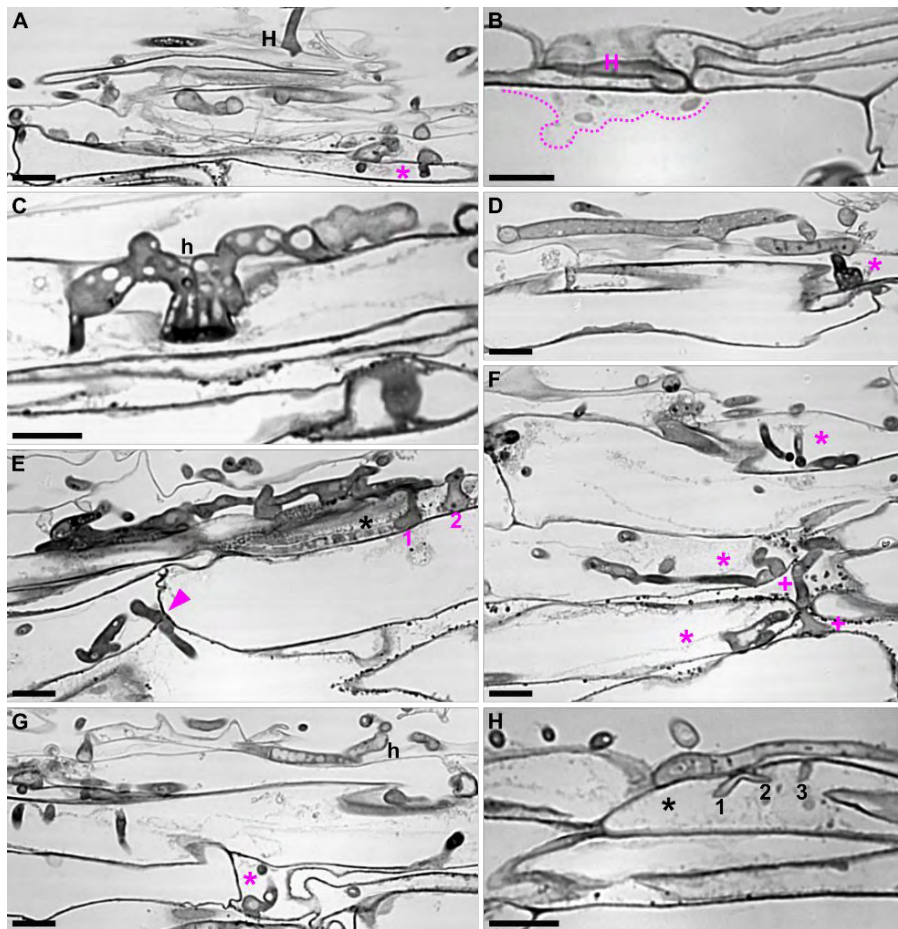
(E) FM4-64 stained root tissue, 4 dpi. A chlamyospore-like structure (magenta dot) is formed intracellularly.

(F) FM4-64 stained root tissue, 4 dpi. Hyphal swellings resembling chlamyospores are formed in chains, intracellularly (magenta dots).

(G) Colonization of a lateral root, 7 dpi.

Images are z axis projections of serial optical sections (A, D, F, G) or single optical sections (B, C, E).

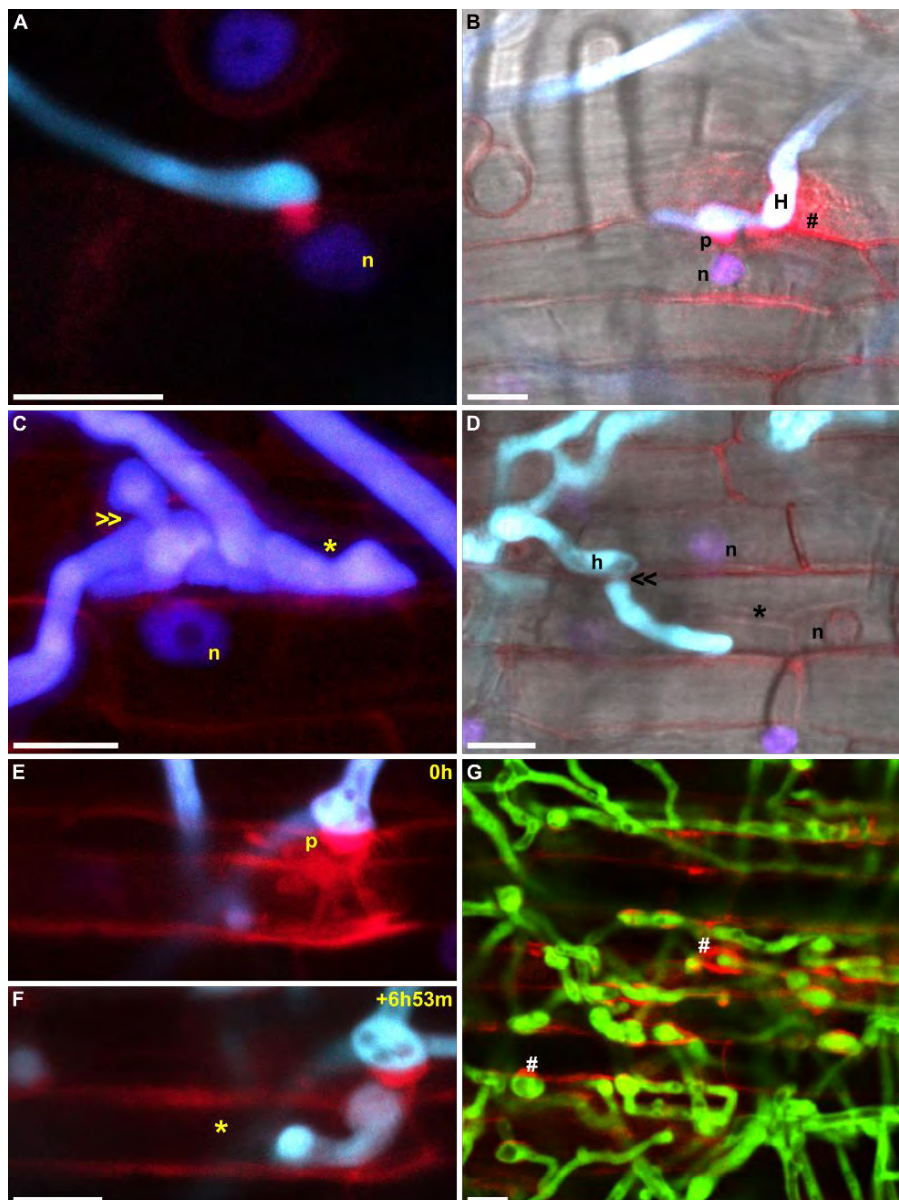
n, nucleus; H, hyphopodium; h, hypha; asterisk, intracellular growth; double arrow, hyphal differentiation; dot, chlamyospore-like structure; arrow, fungal hyphae; ex h, extraradical hyphae; Lr, lateral root; ir h, intraradical hyphae. Bars = 10 µm (A-F), 20 µm (G).



Supplementary Figure 3-12 Hyphopodium formation, cytoplasmic accumulation and epidermal/cortical cell wall crossings in *FsK* - *wt* *Mt* roots interaction. Light microscope images of semi-thin sections of *wt* *Mt* root organ culture tissues 2-3 days post *FsK* inoculation. Root tissues are stained with toluidine blue.

(A) Hyphopodium formation on an epidermal cell. Two sites of intracellular penetration (asterisk) in a cortical cell. (B) Hyphal contact leads to cytoplasmic accumulation (dashed line in magenta) in the plant cell. (C) A modified bulbous hypha with presumably enlarged vacuolar compartments is attached on an epidermal cell. (D) Hyphal growth on the epidermis and intracellular growth (asterisk). (E) Hyphae traverse the epidermis and break into a cell (asterisk) at two distinct sites (1, 2). Crossing the cell wall of a cortical cell (arrow). (F) Intracellular growth, in upper cortical and cortical cells (asterisks). Intercellular passage (plus sign, +) and attachment in a cortical cell. (G) Hyphal growth on the epidermis and intracellular growth (asterisk). (H) The fungus penetrates an epidermal cell (asterisk) through multiple sites (1, 2, 3).

H, hyphopodium; asterisk, intracellular growth; *h*, hypha; arrow, site of cell wall crossing; plus sign (+), intercellular growth; numbers, different hyphal lobes penetrating the same plant cell. Bars = 10 μ m.

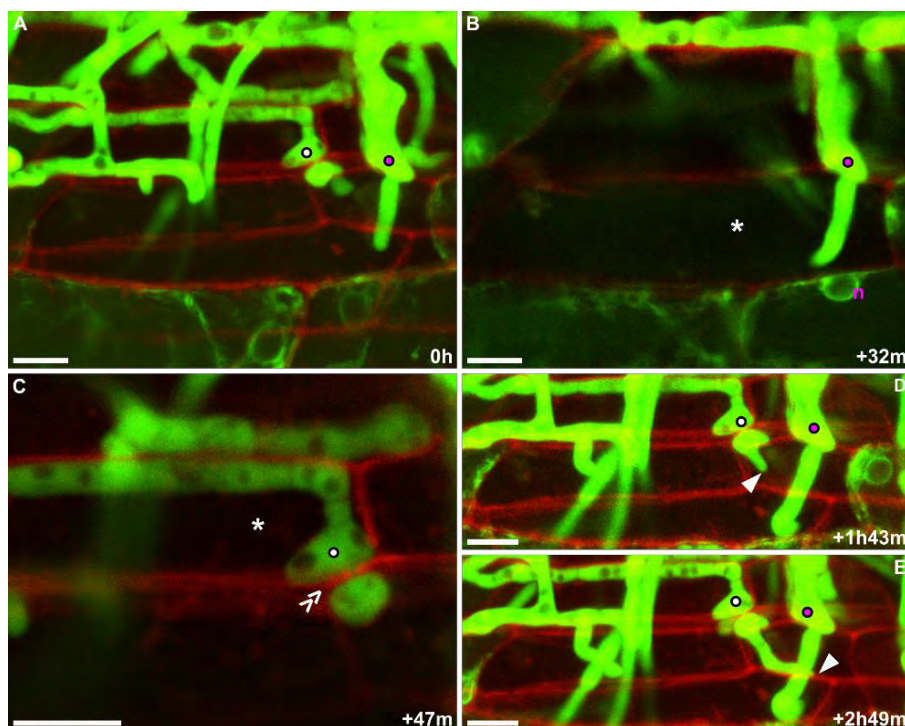


Supplementary Figure 3-13 Plant cell responses upon interaction with *FvK*. *Mt* root organ cultures expressing the nuclear localized cameleon reporter NupYC2.1. Plant nuclei are pseudocolored in blue.

(A) An epidermal cell is contacted by the fungus. A fluorescent deposition of round shape precedes the hyphal tip. (B) Overlaid transmitted light and fluorescent image. Papilla formation associated to a hyphopodium contact site. Intense plant autofluorescence is recorded at contact site. (C) Fully penetrated epidermal cell, 2 dpi. Hyphal stenosis is required to cross the plant cell wall (double arrow). (D) A single hypha is constricted (double arrow), and penetrates an epidermal cell, 4 dpi (asterisk). The plant cell is presumably dead, since the nucleus lacks of fluorescence. (E) Contact associated with papilla formation, 3 dpi. (F) Same site as in (E). The penetration and fungal growth lasted ~7h. (G) Extensive intracellular growth, 2 dpi. Colonized epidermal and cortical cells. Plant autofluorescence in red is observed at contact sites (hash sign, #).

Images are z axis projections of serial optical sections (C, E, F) or single optical sections (A, B, D, G).

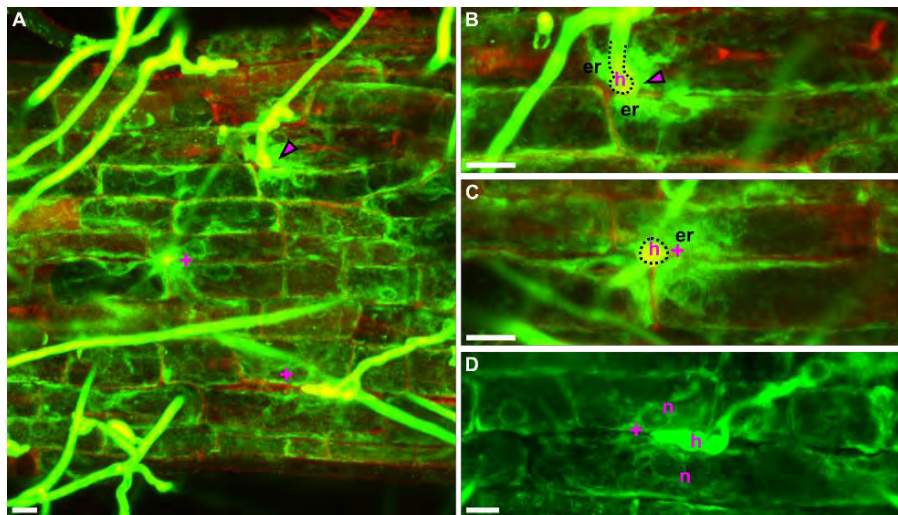
n, nucleus; H, hyphopodium; p, papilla-like structure; hash sign (#), plant cell autofluorescence; double arrow, hyphal stenosis at penetration sites; asterisk, intracellular growth; h, hypha. Bars = 10 μ m.



Supplementary Figure 3-14 Fsk intracellular growth in wt ROCs of *M. truncatula*.

Mt ROCs are expressing GFP-HDEL. (A-E) Time-lapse images demonstrating sites of intracellular growth and crossing to the next cell, 4 dpi. (A) Two types of intracellular hyphae on epidermis (white dot) and upper cortex (magenta dot). Colonized cells are presumably dead. (B) Single optical section of the growing hypha shown in A (magenta dot). Note the position of the nucleus in the adjacent cell. (C) Higher magnification, at a later time point, of the intracellular crossing demonstrated in (A) (white dot). Constriction is required to cross the cell wall (double arrow). (D and E) Time lapse images showing the intracellular growth of the hyphae shown in (A). Images are z axis projections of serial optical sections (A, D, E) or single optical sections (B, C).

Dots, hyphae; asterisk, intracellular growth; n, nucleus; double arrow, hyphal stenosis for intracellular penetration; single arrow, position of the hyphal tip. Bars = 10 μ m.

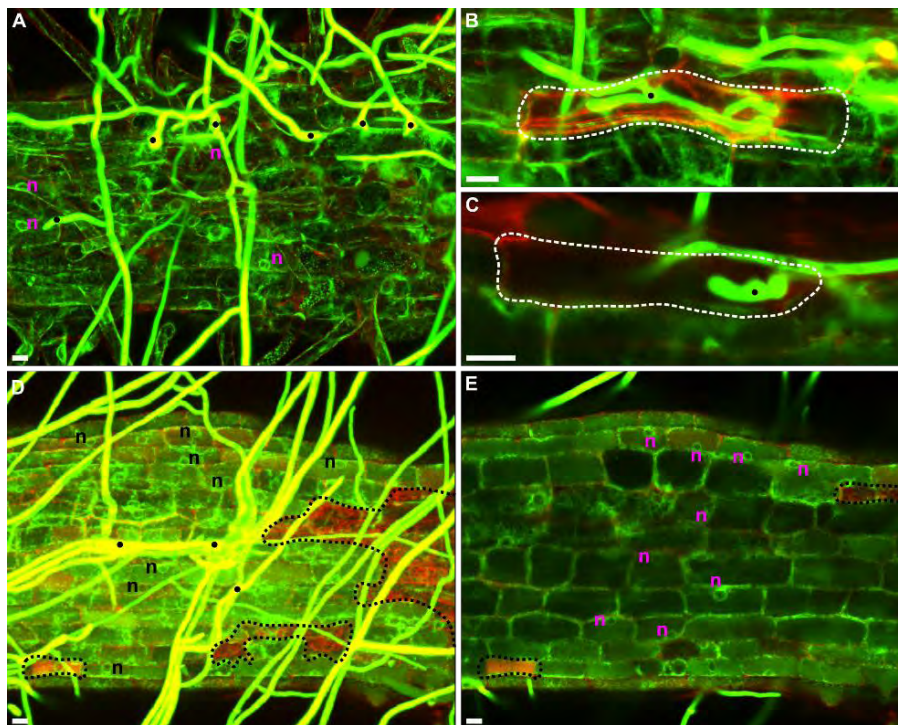


respectively). (B) A hyphopodium (dashed line) adheres on epidermal cells. Contacted cells respond with ER accumulation. (C) A hypha (dashed line) tries to enter intercellularly. Adjacent cells respond with ER aggregation. (D) A hypha proceeds intercellularly. Nuclei of adjacent cells face the traversing hypha.

All images are z axis projections of serial optical sections.

Arrow, contact site; plus sign (+), intercellular growth; h, hypha; er, endoplasmic reticulum; n, nucleus.

Bars = 10 μ m.



root cells, 3 dpi. Certain cells (epidermals – upper corticals) undergo cell death (dashed lines), while others retain their viability, as indicated by their intact nucleus. (E) Single optical section of (D) z series stack, showing mainly cortical cells maintaining viability. A few cells have undergone cell death (dashed lines), irrespectively of FsK presence.

Images are z axis projections of serial optical sections (A, B, D) or single optical sections (C, E).

Dots, fungal hyphae; n, nucleus; dashed line, dead plant cells. Bars = 10 μ m.

Supplementary Table 3-1 Primers used for fungal quantification within plant tissues

Primer name	Use in this study	Sequence (5'-3')	Reference(s)
<i>ITS-F</i>	qPCR	TGGTCATTTAGAGGAAGTAA	This study
<i>ITS-R</i>	qPCR	GGTATGTTACAGGGTTGATG	This study
<i>TEF1A-F</i>	qPCR	CCCCTCCAGGATGTCTACAA	This study
<i>TEF1A-R</i>	qPCR	GGAAGACCCTCAGTGAGCTG	This study

Supplementary Table 3-2 Primers used for amplification of the *hph* gene in *Agrobacterium* mediated fungal transformation experiments

Primer name	Use in this study	Sequence (5'-3')	Reference(s)
<i>HPH-F</i>	PCR	AAGCCTGAACTCACC GCGAC	(Samils et al., 2006)
<i>HPH-R</i>	PCR	CTATTCCTTTGCCCTCGGAC	(Samils et al., 2006)

Supplementary Table 3-3 M medium recipe

Macro elements stock solution	
MgSO ₄ .7H ₂ O	7.31 g/l
KNO ₃	0.80 g/l
KCl	0.65 g/l
KH ₂ PO ₄	0.048 g/l
Ca(NO ₃) ₂ .4H ₂ O stock solution	
Ca(NO ₃) ₂ .4H ₂ O	2.88 g/l
NaFeEDTA stock solution	
NaFeEDTA	0.24 g in 150 ml
Vitamins stock solution (keep at -20°C)	
Glycine	0.09 g in 150 ml
Thiamine HCl	0.003 g in 150 ml
Pyridoxine HCl	0.003 g in 150 ml
Nicotinic Acid	0.015 g in 150 ml
Myo-inositol	1.5 g in 150 ml
KI stock solution	
KI	0.015 g in 20 ml

Microelements stock solution	
MnCl ₂ .4H ₂ O	0.24 g in 5ml dH ₂ O
ZnSO ₄ .7H ₂ O	0.118 g in 5ml dH ₂ O
H ₃ BO ₃	0,0375 g in 5ml dH ₂ O
Mix the 3 solutions to obtain Solution A	
Dissolve 0,033g of CuSO ₄ .5H ₂ O in 2.5ml dH ₂ O, take 0.5 ml of this solution and add it to solution A	

Chapter 3

Dissolve 0,0058 g $(\text{NH}_4)_6\text{Mo}_7\text{O}_{24} \cdot 4\text{H}_2\text{O}$ in 5ml dH_2O , take 0.1 ml of this solution and add to solution A
Bring the volume to 25ml with H_2O

To prepare 1L of M medium:

Macro elements	100 ml
$\text{Ca}(\text{NO}_3)_2 \cdot 4\text{H}_2\text{O}$	100 ml
NaFeEDTA	5 ml
Vitamins	5 ml
Micronutrients	1 ml
KI	1 ml
Sucrose (addition only in ROCs)	10 g
Control pH to 5.5 (NaOH or HCl)	
Bring volume to 1L	
Phytigel 0.4%	
Sterilize 120°, 20 min	

Supplementary Table 3-4 Hoagland nutrient solution recipe

Stock solutions	Stock solutions	Hoagland solution 100%
MgSO_4	1 M	2 ml/L
KH_2PO_4	1 M	1 ml/L
NaFeEDTA	0.1 M	1 ml/L
Micro elements		1 ml/L
KNO_3	20 g / 100 ml	5 ml/L
$\text{Ca}(\text{NO}_3)_2 \cdot 4\text{H}_2\text{O}$	2.36 g / 100 ml	5 ml/L

Micro elements stock solution	
H_3BO_3	2.86 g/L
$\text{MnCl}_2 \cdot 4\text{H}_2\text{O}$	1.81 g/L
ZnCl_2	0.11 g/L
$\text{CuCl}_2 \cdot \text{H}_2\text{O}$	0.05 g/L
H_2MoO_4	0.02 g/L

Chapter 4

Symbiotic signaling is at the core of an endopytic *Fusarium solani*- legume association

A manuscript containing this work has been submitted for peer review

4 Symbiotic signaling is at the core of an endophytic *Fusarium solani*-legume association

Abstract

Legumes interact with a wide range of microbes in their root system, ranging from beneficial symbionts to pathogens. Symbiotic rhizobia and arbuscular mycorrhizal glomeromycetes trigger a so-called common symbiotic signaling pathway (CSSP), including the induction of nuclear calcium spiking in the root epidermis. In our study, the recognition of an endophytic *Fusarium solani* strain K in *Lotus japonicus* induced the expression of *LysM* receptors for chitin-based molecules, CSSP members and CSSP-dependent genes in *L. japonicus*. In *LysM* and CSSP mutant/RNAi lines, root penetration and fungal intraradical progression is either stimulated or restricted, while FsK exudates are perceived in a CSSP-dependent manner, triggering nuclear calcium spiking in epidermal cells of *Medicago truncatula* Root Organ Cultures. Our results corroborate that the CSSP is a more shared pathway than previously envisaged, involved in the perception of signals from other microbes beyond the restricted group of symbiotic interactions *sensu stricto*.

Abbreviations:

AM, Arbuscular Mycorrhizal; AU, airy units; CLSM, Confocal Laser Scanning Microscopy; CO5, pentameric chito-oligosaccharide; CSSP, Common Symbiosis Signaling Pathway; dpi, days post inoculation; Fom, *Fusarium oxysporum* f. sp. *medicaginis*; FsK, *Fusarium solani* strain K; LCOs, lipo-chitooligosaccharides; Lj, *Lotus japonicus*; Lysin-motif, *LysM*; Mt, *Medicago truncatula*; NF, Nod Factor; PM, plasma membrane; RLK, receptor-like kinase; RLS, rhizobium - legume symbiosis; ROCs, Root Organ Cultures; wt, wild-type

4.1 Introduction

Plants encounter diverse microorganisms at the root-soil interface, some of which invade the root system and establish detrimental or beneficial associations (Zipfel and Oldroyd, 2017). In this scenario, legumes are unique in their ability to establish two types of mutualistic symbioses: the arbuscular mycorrhizal (AM) and rhizobium-legume (RL) symbiosis. For both interactions, a few plant-directed microbial signals have been characterized so far, and all of them are water soluble chitin-based molecules. Rhizobia produce Nod Factors (NFs), lipo-chitoooligosaccharides (LCOs) that are recognized by specific receptor-like kinases (RLKs) (Amor et al., 2003) (Limpens et al., 2003) (Madsen et al., 2003) (Murakami et al., 2018) (Radutoiu et al., 2003), whereas AM fungi release both Nod factor-like Myc-LCOs (Maillet et al., 2011) and short-chain chitin oligomers (Myc-COs) (Genre et al., 2013). The perception of chitin-related molecules in plants is mediated by Lysin-motif (LysM)-RLKs (Antolín-Llovera et al., 2014). This is also the case for Nod factors and Myc-LCOs (Fliegmann et al., 2013) (Maillet et al., 2011), whereas specific receptors for Myc-COs remain to be characterized.

Downstream of receptor activation, the intracellular accommodation of both types of symbionts is mediated by a so-called common symbiosis signaling pathway (CSSP) that in *Lotus japonicus* includes eight genes: the plasma membrane-bound RLK *LjSYMRK* (*MtDMI2* in *Medicago truncatula*), three nucleoporins (NUP85, NUP133, NENA), the nuclear envelope located cation channels *LjCASTOR*, and *LjPOLLUX* (*MtDMI1*, orthologous to *POLLUX*), the nuclear calcium and calmodulin-dependent protein kinase *LjCCaMK* (*MtDMI3*), the CCaMK phosphorylation substrate *LjCYCLOPS* (Kistner et al., 2005) (Charpentier et al., 2008) (Genre and Russo, 2016). Downstream the CSSP lie nodulation/mycorrhization specific transcription factors such as *LjNSP1* and *LjNSP2* (Catoira et al., 2000) (Delaux et al., 2013) (Kalo et al., 2005) (Maillet et al., 2011), and early nodulin genes, like *LjENOD2* and *LjENOD40* (Glyan'ko, 2018) (Ferguson and Mathesius, 2014) (Takeda et al., 2005). A central element of the CSSP is the triggering of repeated oscillations in nuclear calcium concentration (spiking). In fact, mutants in all CSSP members acting upstream of CCaMK are defective for calcium spiking (Harris et al., 2003) (Miwa et al., 2006b) (Parniske, 2008), and the nuclear-localized CCaMK is considered to act as a decoder of the calcium signal, which is translated into phosphorylation events (Yano et al., 2008). Consequently, the induction of nuclear calcium spiking has become of common use as a reliable reporter of CSSP activation by symbiotic microbes or their isolated signals (Wais et al., 2000) (Sieberer et al., 2009) (Chabaud et al., 2011) (Genre et al., 2013) (Charpentier and Oldroyd, 2013). In particular, this approach has been used for the study of AM fungal signaling in both legume and non-legume hosts, using either whole plants or root organ cultures (ROCs) expressing nuclear-localized calcium-sensing reporters, such as cameleon proteins (Chabaud et al., 2011) (Genre et al., 2013) (Sun et al., 2015) (Carotenuto et al., 2017).

A role for the CSSP in non-symbiotic interactions, has been investigated by many research groups: some propose an (at least partial) involvement (Sanchez et al., 2005) (Weerasinghe et al., 2005) (Fernandez-Aparicio et al., 2010) (Wang et al., 2012) (Zgad Zaj et al., 2015) (Zgad Zaj et al., 2019), while others do not (Banhara et al., 2015) (Huisman et al., 2015). Nevertheless, little is known about the triggering of nuclear calcium oscillations in such associations, whereas compromised colonization phenotypes by a non-symbiont has not been reported, thus far, for a CSSP mutant.

FsK is a beneficial endophytic isolate of tomato, protecting the plant against root and foliar pathogens (Kavroulakis et al., 2007), spider mites (Pappas et al., 2018), zoophytophagous insects (Garantonakis et al., 2018), and drought (Kavroulakis et al., 2018). We have recently shown that FsK efficiently colonizes legume roots and demonstrates great plasticity throughout colonization (Skiada et al., 2019). Commonalities in the host cell responses between legumes-FsK, and to both symbiotic and pathogenic interactions (Genre et al., 2009) (Skiada et al., 2019), prompted us to investigate the role of the CSSP in this endophytic legume association.

We herein used gene expression analysis and phenotypic screening of mutant/RNAi lines to investigate the role of certain *LysM* receptors in the *Lotus*-FsK interaction. We furthermore demonstrate that the expression of *L. japonicus* markers of AM and/or RL symbiosis is partially altered in the presence of FsK, while two CSSP mutants, *ccamk* and *cyclops*, display a delay in fungal colonization. Lastly, we show that the endophyte exudates triggered CSSP-dependent nuclear calcium spiking in the outer root tissues of *M. truncatula* ROCs, which is also observed for exudates from other root-interacting fungi. Overall, our results show that multiple *LysM* receptors participate in FsK recognition and suggest that the core of the CSSP is also involved in the perception of diffusible signals from non-mycorrhizal fungi.

4.2 Materials and methods

4.2.1 Plant materials

L. japonicus wt plants and the CSSP mutant lines *symrk-1*, *castor-1*, *sym15-1* (*ccamk-1*), *sym6-1* (*cyclops-1*) as well as the *LysM* mutant lines *lys6-1*, *lys7*, *lys12-3* and the triple mutant *nfr1nfr5lys11* were used for phenotypic screening of Fsk intraradical abundance. All mutant lines were kindly provided by Associate Prof Simona Radutoiu (Department of Molecular Biology and Genetics - Plant Molecular Biology, Aarhus, Denmark). The plants were chemically scarified and grown in Petri dishes as described previously [chapter 3 (Skiada et al., 2019)] until seedlings transplantation to magenta boxes.

L. japonicus wt plants (ecotype 'Gifu') were used for gene expression analysis experiments.

M. truncatula ROC lines and the CSSP mutant ROC lines *dmi2-2* and *dmi3-1*, expressing the 35S:NupYC2.1 construct (Sieberer et al., 2009) were obtained previously (Chabaud et al., 2011). An apical segment deriving from each ROC line was routinely transferred to square Petri dishes containing M medium (Bécard and Fortin, 1988) and placed in a vertical position at 26°C in the dark, to favour the development of a regular, fishbone-shaped root system (Chabaud et al., 2002). Segments derived from ROCs were used for calcium spiking bioassays upon fungal exudates and chitooligosaccharide treatment.

4.2.2 Fungal materials

Fusarium solani strain K (Fsk) (Kavroulakis et al., 2007) was routinely cultured in Potato Dextrose Agar (PDA) medium and conidia were isolated as previously described [chapter 3 (Skiada et al., 2019)]. Fungal conidia were used as inoculum for phenotypic profiling of all mutant lines and for gene expression analysis experiments. *Fusarium oxysporum* f. sp. *medicaginis* (Fom, BPIC 2561) (Snyder and Hansen, 1940) was kindly provided by Benaki Phytopathological Institute (Benaki phytopathological Institute Collection, BPIC), Attiki, Greece. *Piriformospora indica* (MUT00004176) was kindly provided by Mycotheca Universitatis Taurinensis, Turin, Italy. Fom and *P. indica* were routinely cultured in PDA medium. Fsk, Fom and *P. indica* hyphal propagules were used for preparation of fungal exudates for calcium spiking analyses.

4.2.3 Experimental setup for gene expression analysis and phenotypic screening of *L. japonicus* mutants

L. japonicus seedlings (7-11 days old) were transplanted into magenta boxes (3 plants per magenta) containing sterile sand:vermiculite (3:1) and directly inoculated on the root with 10² conidia per plant. Control plants received the same volume of sterile water. The substrate was watered with 30 ml of M medium (Boisson-Dernier et al., 2001) prior to transplantation, in both treatments. Magenta boxes were transferred in a growth chamber (16h light/8h dark photoperiod, 22°C).

For gene expression analysis, plants were harvested at 1, 2, 4, 6, 12 days post inoculation (dpi), washed 5x with sterile water to remove the excess extraradical mycelium, root tissues were collected, flash frozen under liquid nitrogen and kept at -80°C until subsequent DNA/RNA isolation. Four (4) biological

replicates were assessed for each treatment, with each replicate consisting of 3 individual plants. Estimation of intraradical abundance and gene expression analysis were performed as described below.

For phenotypic profiling, wt and CSSP mutants were harvested at 4 and 8 dpi and *LysM* mutants were harvested at 4 dpi. Different batches of wt *L. japonicus* plants were assessed for CSSP or for *LysM* mutants. Harvested plants were surface sterilized (1% v/v NaOCl), washed 5x with sterile water, root tissues were collected, frozen under liquid nitrogen and kept at -20 until subsequent DNA isolation. Five (5) biological replicates were assessed for each treatment, with each replicate consisting of 3 individual plants. Estimation of intraradical fungal abundance was performed as described below. The experiment was performed twice with similar results, both for CSSP and *LysM* mutants.

4.2.4 DNA isolation

L. japonicus root tissues were grounded with a pestle, under the presence of liquid nitrogen, and total DNA was isolated using the CTAB method (Doyle and Doyle, 1987). For quantification of intraradical fungal abundance, the weight of the plant tissue was determined prior to DNA isolation. DNA concentration was determined using Qubit 2.0 fluorometer. 1µl of the eluted DNA was used as template in qPCR reaction for estimation of intraradical fungal abundance in *L. japonicus* wt, CSSP and *LysM* mutant/RNAi lines.

4.2.5 RNA isolation

Total RNA was extracted using the Isolate II RNA Plant Kit (BIO-52077, BIOLINE) according to manufacturer's instructions. To eliminate genomic DNA carry-over in subsequent reactions, samples were treated with DNase I (18047019, Invitrogen) at 37°C for 1h. Elimination of genomic DNA contamination was verified by PCR, using primers specific for *LjUBIQUITIN* gene (Supplementary Table 4-2) and subsequent agarose gel electrophoresis of the PCR products.

4.2.6 Gene expression analysis

First strand cDNA was synthesized from DNase treated total RNA, using the PrimeScript™ 1st strand cDNA Synthesis Kit (6110A, Takara). Quantitative real-time RT-PCR (qPCR) was performed using gene-specific primers (Supplementary Table 4-2) and the fluorescent intercalating dye Kapa SYBR Green (Kapa SYBR FAST qPCR Master Mix Universal, Kapa Biosystems) in a BIORAD CFX Connect™ Real-Time PCR Detection System. All quantifications were normalized to *Lj UBIQUITIN* housekeeping gene. Data were analysed according to (Pfaffl, 2001). Reaction efficiencies were estimated through the free software program LinRegPCR (Ramakers et al., 2003).

4.2.7 Quantification of fungal colonization in *L. japonicus* wt, CSSP, *LysM* mutant lines

To estimate fungal abundance within root tissues, absolute quantification of *F. solani ITS* or *TEF1a* gene was performed by using a previously constructed standard curve (Skiada et al., 2019). For each experiment, amplification of each sample (standards - unknowns) occurred in a 10 µl reaction mixture containing Kapa SYBR FAST qPCR Master Mix Universal (1x), 200 nM of each primer, and 1 µl of DNA, using a thermocycling protocol of 3 min at 95 °C; 45 cycles of 15 s at 95 °C, 20 s at 58 °C, followed by a melting curve to check the specificity of the products. Absolute quantification of unknown samples was estimated as the exact copy concentration of the target gene by relating the CT value to the standard curve. The fungal gene copy numbers of all samples were normalized by ng of total DNA isolated, or by mg of tissue used to extract DNA, or both. Agarose gel (1.5% w/v) electrophoresis of qPCR products was routinely performed, to verify the amplification of a single fragment of the desired length. Intraradical fungal colonization of *L. japonicus* control/FsK inoculated plants was estimated by quantification of *TEF1a* fungal gene. qPCR amplification efficiencies were 100.91 % with r^2 value of 0.991 and a slope of -3.300. Intraradical fungal colonization in *L. japonicus* wt-CSSP mutants, and in wt-*LysM* mutants was estimated by quantification of *ITS* fungal gene. qPCR amplification efficiencies were 91.82 % with r^2 value of 0.997 and a slope of -3.535 for the *CSP* mutants, and 95.46 % with r^2 value of 0.995 and a slope of -3.436 for *LysM* mutants.

4.2.8 Preparation of fungal exudates and root treatment

Exudates of FsK, Fom and *P. indica* were prepared as previously described (Lace et al., 2015). Briefly, 1ml of water was distributed in eppendorf tubes and inoculated with fungal hyphae obtained by slightly scrapping with a sterile scalpel the surface of a previous culture of the fungus on Potato Dextrose Agar (PDA). Tubes were incubated for 7 days at 26°C, the exudate was afterwards recovered with a sterile syringe, filter sterilized (0.2 µm filters), concentrated 10-fold using a lyophilizer, and stored at -20°C until further use. Exudates of *Gigaspora margarita* were prepared as described in (Chabaud et al., 2011). Segments of primary *Mt* wild type and *dmi2-2/dmi3-1* mutant ROCs carrying one or two young laterals were placed in a microchamber and treated with 100 µl of fungal exudate as described in (Chabaud et al., 2011). For CO5 treatment, aqueous solutions at a final concentration of 10^{-6} M were prepared from a concentrated stock of purified chitin pentamer solution and root explants were treated as above. As negative control, sterile water was used. As positive control, *G. margarita* germinated spore exudate, or purified COs (degree of polymerization, $n=5$) were used.

4.2.9 Assays performed on fungal exudates and COs

Chitinase treatment of the *G. margarita* GSE was performed using 1 mg ml⁻¹ chitinase from *Streptomyces griseus* (ref C6137; Sigma-Aldrich) in sterile H₂O for 16 h at room temperature. Autoclave treatment was performed by autoclaving the exudates (121 °C, 1 atm) for 20 min or for 1 h.

Chitinase treated exudates of FsK and Fom were tested for their ability to generate calcium spiking responses on wt NupYC2.1 *Mt* ROCs epidermis. Autoclave treated exudates of FsK were tested for their ability to generate calcium spiking responses on wt NupYC2.1 *Mt* ROCs epidermis.

4.2.10 Confocal microscopy for calcium spiking measurements in *M. truncatula* ROC epidermis

A FRET-based ratiometric approach (Sieberer et al., 2009) was used to record the relative changes of nuclear calcium concentrations corresponding to Yellow Fluorescent Protein (YFP) to Cyan Fluorescent Protein (CFP) fluorescence intensity changes over time (Miyawaki et al., 1997). Analysis was performed using a Leica TCS SP2 confocal microscope fitted with a long distance x40 water-immersion objective (HCX Apo 0.80). Measurements were performed and settings were set as previously described (Chabaud et al., 2011). The pinhole diameter was set at 6 airy units. YFP and CFP fluorescence intensities were calculated for each region of interest (each nucleus) using Leica LCS software. Values were then exported to a Microsoft Excel spreadsheet, the YFP/CFP ratio for each time frame was calculated, and ratio values were plotted over time. A graphical representation of FRET ratio was finally generated, which indicated the relative calcium concentration changes in the nucleus over time. Nuclear spiking was examined in all cases in an atrichoblast/low-trichoblast zone located 10-20 mm from the root tip.

Calcium spiking measurements were furthermore analyzed using CaSA software (Russo et al., 2013). The generation of at least 3 peaks was the threshold for discrimination between responding and non-responding cells. The total number of epidermal cell nuclei and independent root segments analyzed for each test are reported in the corresponding Figures/Figure legends. CaSA output PNG image files indicating spike initiation and end points, were used to manually calculate peak width and lag phases prior to calcium spiking response initiation in responding nuclei. CaSa output waiting time autocorrelation values were used to generate the corresponding histogram.

4.2.11 Statistical analysis

Two-way ANOVA followed by Tukey's post-hoc test was used in gene expression analysis data. Student's t-test was used in all pairwise comparisons. One-way ANOVA was used in comparisons between 3 or more independent (unrelated) groups (i.e. analysis of calcium spiking results obtained after plant cells elicitation with the three investigated fungal exudates). The non-parametric Kolmogorov-Smirnov (K-S) two-sample test was used to assess whether data corresponding to a) number of peaks, b) lag phase prior to spiking initiation, c) width of peaks, generated in *Mt* nuclei by the 3 elicitors, are drawn from the same distribution (pairwise comparisons among results from the 3 elicitors). Pearson's chi squared test was used to test whether the frequency distribution of waiting times autocorrelation values of peaks generated by the 3 fungal exudates are independent. Statistical analyses used are indicated in detail in the corresponding Figures/Figure legends.

4.3 Results

4.3.1 Fsk inoculation affects the expression of CSSP members and CSSP-regulated genes

Early Fsk colonization of legume roots triggers a number of host cell responses (cytoplasm/ER accumulation, nuclear movement and membrane trafficking at contact site) that are also known to occur in both symbiotic and pathogenic interactions (Skiada et al., 2019). This prompted us to investigate potential similarities with symbiosis-related plant gene expression. We, therefore, analyzed the expression of key CSSP components, such as *LjCASTOR*, *LjCCaMK* and *LjCYCLOPS*, as well as CSSP-regulated symbiosis markers, namely *LjNSP1*, *LjNSP2*, *LjIPN2*, *LjENOD40* and *LjENOD2*. Their regulation was investigated at specific time points during *Lotus*-Fsk interaction, alongside fungal colonization levels (Supplementary Figure 4-6, 4-14). The expression of *LjCCaMK* was marginally but significantly upregulated upon Fsk inoculation at very early stages of the interaction (1 dpi), reaching a 2.2-fold upregulation compared to controls at 12 dpi. By contrast, no significant difference was recorded in the expression of *LjCASTOR* and *LjCYCLOPS*, or the transcription factors *LjNSP1* and *LjNSP2*, or *LjIPN2* (Interacting Protein of NSP2) acting downstream the CSSP, in control and inoculated plants at any time point (Supplementary Figure 4-6, 4-14).

We then tested whether the expression of the symbiosis marker gene *LjENOD40* was altered in our *Lotus*-Fsk interaction system. We focused on *LjENOD40-1* gene, which is strongly upregulated at very early stages of rhizobium infection, in contrast to the mature nodule marker *LjENOD40-2* (Kumagai et al., 2006). A statistically significant induction of *LjENOD40-1* was observed at 2, 4 and 6 dpi (1.6-, 1.9-, 1.7-fold, respectively) in inoculated compared to non-inoculated plants. *ENOD40* expression coincides with maximum levels of intraradical fungal accommodation (recorded at 4 dpi) (Supplementary Figure 4-14). By contrast, we recorded no differences between control and inoculated plants in the expression levels of our second nodulation marker gene, *ENOD2*, which is expressed in legumes during rhizobial and AM infection and nodule morphogenesis, but not upon fungal pathogen infection (Franssen et al., 1987) (van de Wiel et al., 1990) (van Rhijn et al., 1997).

To summarize, our analyses revealed that Fsk colonization was associated with the upregulation of a subset of known symbiosis markers over the course of 12 days post inoculation.

4.3.2 Fsk colonization is reduced in CSSP mutants compared to wt plants

Based on our gene expression results, we investigated the phenotypic differences in Fsk colonization of *L. japonicus* CSSP mutants compared to wt plants (Figure 4-1). We selected mutant lines impaired in CSSP genes acting upstream (*symRK-1*, *castor-1*) and downstream of nuclear calcium spiking (*ccamk-1*, *cyclops-1*). Fsk intraradical colonization was quantified via qPCR at 4 and 8 dpi (Figure 4-1B), when roots are well-colonized by the fungus under our experimental conditions (Supplementary Figure 4-14). The colonization of *symRK-1* and *castor-1* mutants was similar to that of wt plants. By contrast, a significant reduction in fungal colonization was observed in both *ccamk-1* (75.17%) and *cyclops-1* (68.82%) compared to wt plants at 4 dpi. A comparable reduction in fungal intraradical colonization persisted at 8 dpi only in *cyclops-1* plants (45.77%).

In conclusion, our phenotypic analysis revealed a significant reduction in FsK colonization only for CSSP mutants for genes that act downstream of nuclear calcium spiking, and the reduction was more evident at earlier time points of the interaction.

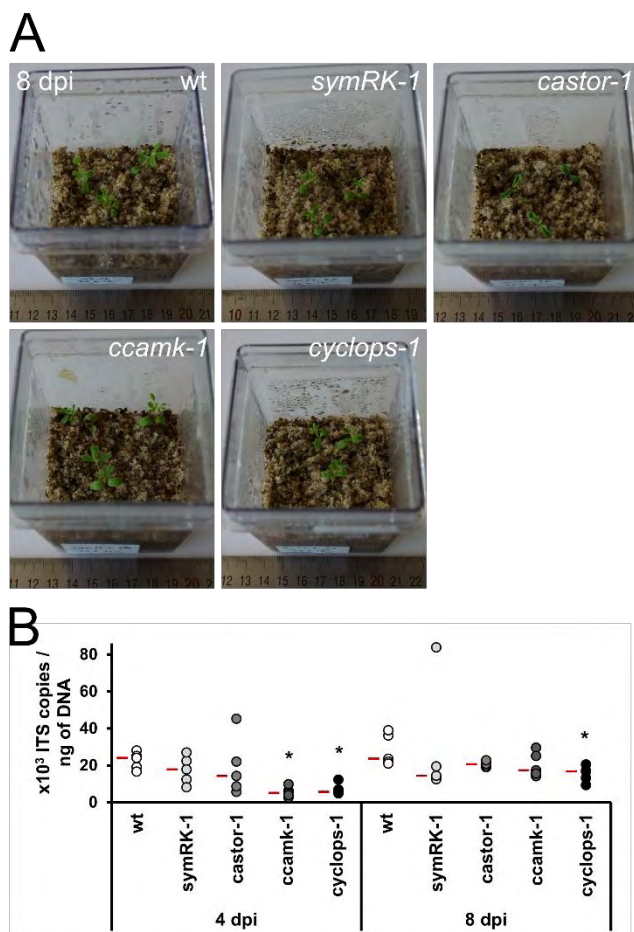


Figure 4-1 Quantification of FsK colonization in *L. japonicus* CSSP mutants.

(A) FsK inoculated *Lotus japonicus* wt and CSSP mutants at the last time point of the experiment (8 dpi).

(B) Absolute quantification of FsK ingress within *L. japonicus* root tissues in wt and CSSP mutants (*symRK-1*, *castor-1*, *ccamK-1*, *cyclops-1*), via qPCR, using primers specific for a fragment of *Fusarium* ITS gene. Tissues were harvested at 4 and 8 dpi. ITS gene copy numbers are normalized to ng of total DNA extracted from the root tissue. Data are presented as a dotplot. Each dot represents a single biological replicate. 5 biological replicates were assessed for each genotype. Each replicate consists of 3 individual plants. Median values are presented in red. The experiment was repeated twice with similar results.

Asterisks represent statistically significant differences between wt and the respective mutant line at the 0.05 level (Student's *t*-test).

4.3.3 Fungal exudates trigger nuclear calcium spiking in wt *M. truncatula* ROC epidermis

Based on the colonization phenotype in CSSP mutant lines, we then investigated nuclear calcium signals in response to FsK exudate treatment. To this aim, we used wt *Medicago truncatula* ROCs expressing the nuclear localizedameleon reporters (NupYC2.1), thus allowing FRET based imaging analysis of nuclear calcium responses (Chabaud et al., 2011) (Carotenuto et al., 2019).

We focused on epidermal cells in an area 1-2 cm above the root tip harboring few trichoblasts, because this root zone in model legumes is susceptible to colonization by FsK (Skiada et al., 2019) and is also reported to show the strongest calcium spiking responses to AM fungal exudate (Chabaud et al., 2011). As additional controls, we extended our analysis to include other compatible legume colonizers: the pathogenic *Fusarium oxysporum* f.sp. *medicaginis* (Fom) (Snyder and Hansen, 1940), and *Piriformospora* (*Serendipita*) *indica* (Hayes et al., 2014) (Ramírez-Suero et al., 2010), an endophytic fungus with a versatile lifestyle (Verma et al., 1998) (Deshmukh et al., 2006) (Lahrmann et al., 2013).

Exudates from all tested fungi triggered nuclear calcium oscillations in wt *M. truncatula* epidermal cells (Figure 4-2, Supplementary Figure 4-7; details about the biological replicates and nuclei screened are presented in Supplementary Table 4-1). A higher number of cells responded to FsK (70.11%) or Fom (80.95%), compared to *P. indica* exudate (43.59%; Figure 4-3A). In addition, although the median number of spikes generated in active cells over 30 minutes of recording was comparable for all exudates (5 peaks for FsK and Fom; 4 peaks for *P. indica*; *p*-value 0.245) (Figure 4-3B), when we analysed the distribution of peak numbers among the fungal exudates tested in all cells, we recorded differences among peak numbers generated by *P. indica* and FsK or Fom, respectively (*p*-value <0.005 for each pairwise comparison). Thus, differences in the pattern of calcium spikes, expressed as the number of spikes per cell over a period were present.

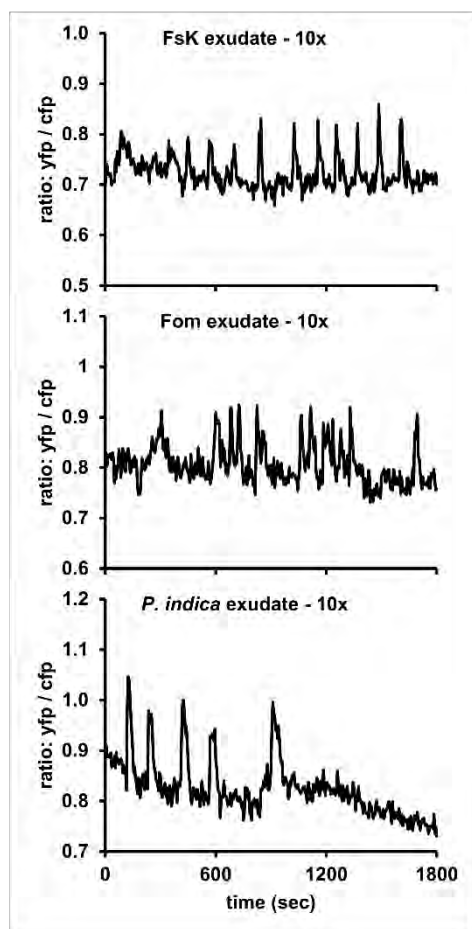


Figure 4-2 Exudates produced by fungi induce changes in nuclear calcium levels imaged using cameleon Mt ROCs.

Calcium spiking responses were recorded in a low-trichoblast-region located 10-20 mm from the root tip. *M. truncatula* wt ROCs expressing the NupYC2.1 cameleon were used for the bioassay. Fungal exudates derived from FsK, Fom, or *P. indica* were used as elicitors.

Representative plots showing changes in nuclear calcium levels after treatment with 10x concentrated FsK, Fom, or *P. indica* exudate, in a 30 min (1800 sec) recording. Graphs show ratios of YFP:CFP fluorescence over time. The respective changes in fluorescence over time are presented in graphs of Supplementary Figure 4-2.

It has been postulated that information in calcium-mediated signals can be encoded in the amplitude and frequency of the spiking, duration of the response as well as tissue specificity, and this information is responsible for the induction of specific responses (McAinsh and Hetherington, 1998b) (Vadassery et al., 2009). Thus, we analyzed (Figure 4-3C) the oscillatory responses generated by our fungal exudates (Figure 4-2) by manually calculating the interval between the treatment and the occurrence of the first spike in active cells (lag phase). Differences in median lag phase values of active cells examined per exudate were sharp (127.96 sec for *P. indica*, 290.32 sec for FsK and 273.12 sec for

Fom), and the distribution of lag phase values were statistically different for induced calcium spiking between *P. indica*-FsK and *P. indica*-Fom (p-value <0.005 and p-value <0.05, respectively).

We also measured the width of each spike in all active cells, estimated as the difference in seconds between the first time point of the upward phase (elevation from the baseline - steady state) and the last time point of the downward phase (return to the baseline – steady state) for each spike. Spikes generated by the 3 fungal exudates had comparable median values (60.22 sec for FsK, 63.38 sec for Fom, 66.47 sec for *P. indica*; as calculated in the total number of active cells). Analysis of the distribution of spike width values recorded in response to the three exudates, revealed differences among FsK and *P. indica* (p-value <0.005).

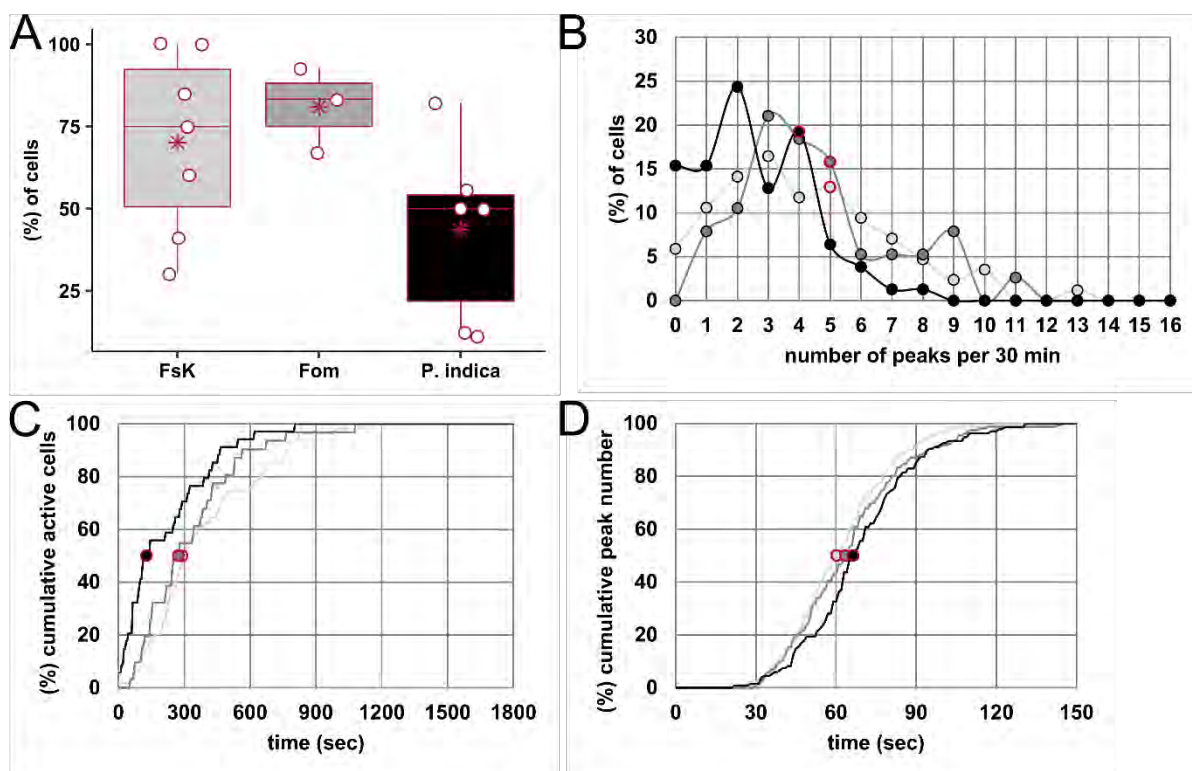


Figure 4-3 Analysis of fungal exudate-triggered nuclear calcium responses in *Mt wt* ROCs epidermis.

Calcium spiking responses were recorded in a low-trichoblast-region located 10-20 mm from the root tip. *M. truncatula* wt (ROCs) expressing the NupYC2.1 cameleon were used for the bioassay. Fungal exudates derived from FsK, Fom, or *P. indica* were used as elicitors.

(A) Percentage of responsive cells (peak number > 2), in 30 min recordings post fungal exudate application. Data are presented as a dotplot in combination with a boxplot for each exudate. Each dot represents a single biological replicate (individual lateral root segments derived from ROCs). Median values are presented as red line within the boxplot, whereas average values are presented as a red asterisk. No statistically significant difference was recorded in average percentages of cells showing calcium spikes in response to FsK/FoM/*P. indica* exudate elicitation (one-way anova).

(B) Histogram exhibiting the distribution of fungal exudate-induced calcium spiking responses in all nuclei examined (active and non-active cells). Dots represent the frequency of peak number (presented in continuous intervals of 1

peak) in a 30 min recording period. Median peak number values calculated only in active cells are also presented in red.

Two-sample Kolmogorov Smirnov (K-S) test was performed to compare the distribution of peak numbers generated in response to the three exudates. Distributions were compared in a pairwise manner, under the null hypothesis that populations are drawn from the same distribution. When all cells (active and non-active) were included in the analysis: *FsK-P. indica* and *Fom-P. indica* comparison showed that data are drawn from different distributions ($p < 0.005$ for both comparisons).

(C) Cumulative probability line plots showing, for each exudate (depicted by different line colour), the percentage of active cells as functions of the delay time (in sec) recorded prior to spiking initiation. Lag phases were measured manually for all active nuclei examined per elicitor. Lag phase represents the time intervening between the recording initiation and the first recorded spike for each responsive nucleus. Median delay time values are also presented in red.

Two-sample K-S test was then performed to compare the distribution of lag phases recorded in response to each elicitor. Distributions were compared in a pairwise manner, under the null hypothesis that populations are drawn from the same distribution. Pairwise comparisons among *FsK-P. indica* and *Fom-P. indica* showed that data are drawn from different distributions ($p < 0.005$ and $p < 0.05$, respectively).

(D) Cumulative probability line plots showing, for each elicitor (depicted by different line colour), the percentage of active cells as functions of the spike width (in sec). Spike widths were measured manually for all peaks recorded and for each fungal exudate applied. Median spike width values are also presented in red.

Two-sample K-S test was then performed to compare the distribution of spike width values recorded in response to each elicitor. Distributions were compared in a pairwise manner, under the null hypothesis that populations are drawn from the same distribution. Pairwise comparisons among *FsK-P. indica* showed that data are drawn from different distributions ($p < 0.005$).

Light grey/dark grey/black lines in panels B, C, D: frequencies for *FsK/FoM/P. indica* exudate-elicited calcium spiking responses, respectively.

The number of biological replicates/nuclei/peaks assessed for each elicitor and for each analysis is indicated in Supplementary Table 4-1.

Lastly, we analysed the waiting time, i.e. the interval between subsequent peaks. The histogram in Supplementary Figure 4-9 illustrates the distribution of waiting time autocorrelation values in our populations of spiking profiles. A high number of cells in all treatments demonstrated negative autocorrelation values, indicating that spiking responses to all fungal exudates are in most cases irregular, in analogy to what was described for AM fungal-induced spiking profiles and in contrast with the mostly regular rhizobium-induced calcium spiking signals in the same experimental system (Russo et al., 2013). Statistical analysis showed no dependency between the distribution of waiting time autocorrelation values and the fungal exudate tested.

Altogether our analysis revealed that the conditions (i.e. constituents of the exudates) that determined the distribution of a) peak number generated over a certain period of time, b) lag phase prior to spiking initiation, and, c) peak width of individual traces in response to the 3 elicitors examined, were not the same. More specifically, *P. indica*- induced calcium spiking had the most profound differences in comparison to *Fusaria*-induced calcium spiking. Pairwise comparison among the two *Fusaria* examined, revealed no differences in any of the parameters examined herein.

4.3.4 Nuclear calcium spiking is abolished in *Mtdmi2-2* but not in *Mtdmi3-1* epidermis

We then extended our investigation of nuclear calcium signals in ROC epidermal cells of mutants for either *MtDMI2* (*dmi2-2*) and *MtDMI3* (*dmi3-1*), homologs to *LjSYMRK* and *LjCCAMK*, respectively (Figure 4-4, Supplementary Figure 4-10). In *dmi2-2*, very few cells were active in any treatment (10.26% for FsK, 15% for Fom, 3.92 % for *P. indica* exudate). By contrast, nuclear calcium spiking was retained in *dmi3-1* upon stimulation by the fungal exudates tested (Figure 4-4A). Furthermore, FsK exudate induced nuclear spiking in a higher percentage of *dmi3-1* cells (81.68%) compared to wt (70.11%). The opposite was observed for Fom exudate (69.70% for *dmi3-1* vs 80.95% for wt), whereas approximately the same percentage of responding cells was recorded in *dmi3-1* and wt treated with *P. indica* exudate (43.50% for *dmi3-1* vs 43.59% for wt) (Figure 4-4A).

We then analysed the distribution of peak number in *dmi3-1* cells generated by the three fungal exudates (Figure 4-4B). The median number of spikes for active cells was within similar ranges in all exudates (similar median values to those obtained in the wt lines) (Figure 4-4B). On the other hand, a significant association was recorded in the peak distribution in total cells (active and non-active) among FsK and *P. indica* exudate (p-value <0.001), indicating again differences in the number of spikes per cell over a period as observed in wt.

In conclusion, all fungal exudates examined generated intense and repeated nuclear calcium oscillations (spiking). Their activation was dependent on *DMI2* (a member of the CSSP acting upstream of calcium oscillations) but not on *DMI3* (acting downstream of calcium signaling), suggesting that the core of the CSSP that transduces AM fungal, rhizobial and actinorrhizal signals (Barker et al., 2017) is also involved in the perception of signals from all three non-mycorrhizal fungi.

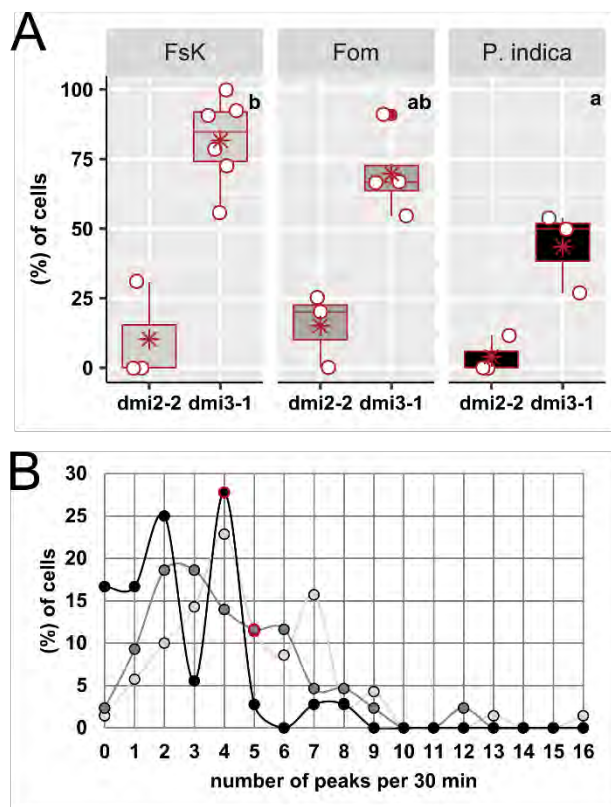


Figure 4-4 Analysis of fungal exudate-triggered nuclear calcium responses in *Mt dmi2-2* and *dmi3-1* ROCs epidermis.

Calcium spiking responses in a low-trichoblast-region located 10-20 mm from the root tip. *M. truncatula dmi2-2* and *dmi3-1* mutant lines (ROCs) expressing the NupYC2.1 cameleon were used for the bioassay. Fungal exudates derived from FsK, Fom, or *P. indica* were used as elicitors.

(A) Percentage of responsive cells (peak number > 2) in the *dmi2-2* and *dmi3-1* mutant background, in 30 min recordings. Data are presented as a dotplot in combination with a boxplot for each mutant line/exudate. Each dot represents a single biological replicate (individual lateral root segments derived from ROCs). Median values are presented as red line within the boxplot, whereas average values are presented as a red asterisk. Note that an outlier is presented in *dmi3-1* lines for Fom exudate (presented as a red dot).

The outlier value was not excluded from subsequent analysis as we consider it a result of biological variation within our system.

Different letters indicate statistically significant differences in percentages of *dmi3-1* responding cells to each elicitor (one-way anova performed in biological replicates, followed by Tukey's post-hoc test).

(B) Histogram exhibiting the distribution of fungal exudate-induced calcium spiking responses in nuclei of *dmi3-1* ROC segments (active and non-active cells). Dots represent the frequency of peak number (presented in continuous intervals of 1 peak) in a 30 min recording period. Median peak number values calculated only in only active cells are presented in red.

Two-sample (K-S) test was then performed to compare the distribution of peak numbers generated in response to fungal exudates. Distributions were compared in a pairwise manner, under the null hypothesis that populations are drawn from the same distribution. When all cells (active and non-active) were included in the analysis, *FsK-P. indica* comparison showed that data are drawn from different distributions ($p < 0.001$).

Light grey/dark grey/black lines: frequencies of peak number values of *FsK/FoM/P. indica* exudate-elicited calcium spiking responses in panel B, respectively.

The number of biological replicates/nuclei assessed for each elicitor/ROC line is indicated in Supplementary Table 4-1.

4.3.5 The biological activity of *Fusarium* exudates is affected by chitinase and heat treatment

In an attempt to determine the nature of the factors that triggered nuclear calcium spiking by *FsK*, we hypothesized that if the triggering compounds were chitin-based molecules, their enzymatic cleavage with chitinase would lead to a decrease in the spiking response (Genre et al., 2013) (Chabaud et al., 2016). For this quest, we also included in the analysis the exudates of *Fom*, since it belongs in the *Fusarium* genus, and the two fungal strains produced similar calcium spiking responses in wt and *dmi3-1* cells. Supplementary Figure 4-11 shows that the percentage of epidermal cells responding to chitinase-treated *FsK* exudate dropped significantly by 62.86%, and an analogous 44.68% reduction was observed upon chitinase treatment of *Fom* exudate, compared to their respective control experiments with untreated exudates. As a control for the enzymatic activity of the chitinase solution, we used short-chain COs that are known to elicit calcium spiking in atrichoblasts (Genre et al., 2013). Pre-treatment of 10^{-6} M CO5 with chitinase resulted in partial abolishment of nuclear calcium oscillatory response in our experiments (32.12% reduction; Supplementary Figure 4-12).

As a second step, we examined the stability of the two exudates under heat treatment. To this aim, we autoclaved *FsK* and *Fom* exudates at 120°C for 20 min. Again, the reduction in the percent of cells responding to heat-treated exudates as compared to the non-treated ones was more severely affected for *FsK* (55.92 %) than *Fom* (14.22 %). A prolonged heat treatment of 60 min did not reduce further the activity of *FsK* exudates (56.70 % reduction in responding epidermal cells).

In short, our tests suggested that the active molecules present in *FsK* and *Fom* exudates include both chitinase- and heat-sensitive compounds. Furthermore, the observed differences in the reduction of the activity between heat-treated *FsK* and *Fom* exudates suggests that the molecules that trigger a comparable nuclear calcium spiking pattern are different in the two fungal species.

4.3.6 Reaching the pathway backwards: involvement of LysM-RLKs in *Lotus japonicus* response

Our results on FRET-based analysis of nuclear calcium changes in wt ROC cells upon chitinase- treated FsK exudate, prompted us to investigate the role of members of the *LysM* RLK gene family in *Lotus*-FsK interaction. We focused on genes that are regulated upon chitin/fungal treatment (Fuechtbauer et al., 2018) (Lohmann et al., 2010) (Rasmussen et al., 2016), and followed their transcriptional regulation over time during *Lotus* root colonization by FsK. More specifically, we investigated the transcript levels of 7 *LjLys* genes: *Lys6*, *Lys7*, *Lys11*, *Lys12*, *Lys13*, *Lys14*, *Lys20* (Supplementary Figure 4-13, 4-14). Four *LysM* genes were transcriptionally regulated during the interaction with FsK: *Lys6* had a statistically significant upregulation (1.5-fold) at 4 dpi, which correlates with maximal fungal presence within plant tissues at this time point (Supplementary Figure 4-14); *Lys7* showed a >2-fold upregulation at very early stages of the interaction (1 dpi); *Lys13* was upregulated from 2 dpi onwards, and *Lys14* is upregulated only at late stages of the interaction (12 dpi). *Lys12* and *Lys20* expression was not altered in the presence of FsK, while *Lys11* transcript levels were very low in both control and inoculated tissues, under our experimental conditions.

To further investigate the possible role of differentially expressed *LysM* genes in *Lotus*-FsK interaction, we compared FsK colonization levels between wt and mutant lines impaired in *LysM* genes that were also, transcriptionally affected. *Ljlys6-1* and *Ljlys7* displayed significantly higher FsK colonization levels at 4dpi compared to wt plants. Finally, two more available mutant lines, *Ljlys12-3* and the triple mutant *Ljnfr1nfr5lys11*, were included for comparison, since *Lys12* and *Lys11* expression levels were not affected by the presence of the endophyte. The defect in *NF* receptors in the triple mutant was not expected to have an effect on FsK colonization. *Ljlys12-3* displayed significantly higher FsK colonization levels at 4dpi, whereas the triple mutant was colonized to levels similar to those recorded in wt plants (Figure 4-5B).

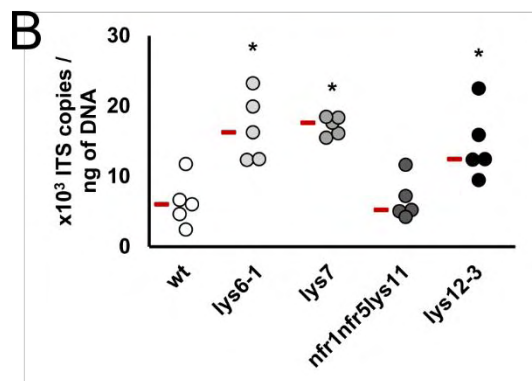
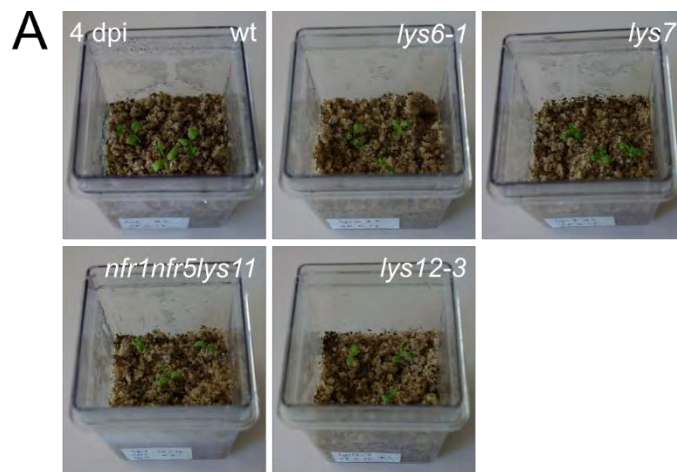


Figure 4-5 Quantification of FsK abundance in roots of *L. japonicus* mutants impaired in LysM receptors, and in LysM13/14 RNAi lines.

(A) FsK inoculated *L. japonicus* wt and LysM mutants at the last time point of the experiment (4 dpi).

(B) Absolute quantification of FsK ingress within *L. japonicus* root tissues in wt and LysM mutants (*lys6-1*, *lys7*, *nfr1nfr5lys11*, *lys12-3*), via qPCR, using primers specific for a fragment of *Fusarium* ITS gene. Tissues were harvested at 4 dpi. ITS gene copy numbers are normalized to ng of total DNA extracted from wt and mutant root tissues, respectively. Data are presented as a dotplot. Each dot represents a single biological replicate. Median values are presented in red. 5 biological replicates were assessed for each genotype. Each replicate consists of 3 individual plants.

Asterisks represent statistically significant differences between wt and the respective

mutant lines at the 0.05 level (Student's *t*-test). The experiment was repeated twice with similar results.

4.4 Discussion

4.4.1 Intraradical accommodation of an endophytic fungus is controlled by multiple LysM receptors

Chitin represents the most ancestral structural polysaccharide in the fungal cell wall (Gow et al., 2017), and most fungi possess chitin synthase enzymes. This was recently, also, shown for oomycetes (Fuechtbauer et al., 2018) (Gibelin-Viala et al., 2019), even though their cell walls primarily consist of β -glucans (Mélida et al., 2013). Chitosaccharides of variable degree of polymerization, produced either by enzymatic cleavage of the long crystalline chitin, or synthesized anew, are considered as Microbe Associated Molecular Patterns (MAMPs), able to trigger symbiotic signaling (as is the case of short chain COs) (Genre et al., 2013), or immune responses (as is the case of longer-chain COs, dp = 6–8 N-acetyl glucosamine) (Stacey and Shibuya, 1997) (Kouzai et al., 2014) (Liang et al., 2014). As regards the receptors of chitinaceous signal molecules from symbionts, highly specific ones have been identified for the NF and Myc LCOs (Amor et al., 2003) (Radutoiu et al., 2003) (Limpens et al., 2003) (Madsen et al., 2003) (Maillet et al., 2011) (Fliegmann et al., 2013) (Murakami et al., 2018). Recent work on structurally related molecules from pathogenic fungi has shown that very similar LysM-RLKs in legumes enable discrimination between chitin perception and perception of NFs (Bozsoki et al., 2017).

FsK exudates comprise of, at least partially, chitin-based molecules of unknown degree of polymerization, while heat-labile molecules must also be present. Characterization of the nature of FsK triggering compounds will require substantially additional research but it is notable that heat treatment did not affect the AM fungal exudate activity (Navazio et al., 2007). As anticipated, certain *LysM* genes (*Lys6*, *Lys7*, *Lys13*, *Lys14*) are regulated in *Lotus*-FsK interaction, further implying that chitin-based molecules produced by the fungus are recognized by the plant. LjLYS6, LYS7 and perhaps LYS12 may act as balancing receptors, controlling fungal intraradical proliferation, at the post initial infection stages. This role has already been assigned to LYS6 and LYS12 receptors, in interaction of legumes with pathogenic fungi (Bozsoki et al., 2017) (Fuechtbauer et al., 2018).

In the *Lotus*-FsK system, we could detect a phenotype in terms of fungal intraradical accommodation in available plant lines mutated in *LysM* genes, which are, also, transcriptionally affected by FsK. These RLKs could play a role at both early and late stages of the interaction. Assessing the spatial expression of these genes during FsK progression as well as a putative triggering of immune responses will provide further insight in such roles for the accommodation of the endophytic fungus.

4.4.2 A very common symbiosis signaling pathway

Structural similarities between chitin-based elicitors from either symbiotic or non-symbiotic microbes raise questions about how plants distinguish friend from foe (Zipfel and Oldroyd, 2017). We investigated the role of the CSSP in establishing an endophytic association, making use of the *Lotus*-FsK system (Skiada et al., 2019). Our results indicate an unparalleled involvement of the CSSP in *Lotus*-FsK association.

Transcriptional reprogramming of CSSP genes, as well as genes acting downstream of it, have been originally described for RL and AM symbiosis. Apart from symbiotic associations in legumes, the

involvement of the CSSP in plant associations has been studied in non-symbiotic bacteria in legumes (Sanchez et al., 2005); in legume-parasitic root-knot nematodes (Weerasinghe et al., 2005); and in the successful nodulation of the actinorrhizal plant *Casuarina glauca* by its symbiont, *Frankia sp.*, in which a functional *LjSYMRK* (Gherbi et al., 2008) as well as a functional *CCaMK* (Svistoonoff et al., 2013) are required. Recently, *L. japonicus* symbiosis genes were shown to structure the root microbiota, as revealed by CSSP mutant analysis (Zgadzaaj et al., 2019). In our experimental system, among the genes examined, those acting upstream *CCaMK* had no effect on FSK accommodation in *Lotus* roots and were dispensable for determination of FSK colonization levels. In fact, the non-nodulating and non-mycorrhizal *symRK-1* and *castor-1* mutants (Schauser et al., 1998) (Wegel et al., 1998) (Bonfante et al., 2000) (Novero et al., 2002) (Stracke et al., 2002), displayed a wt-like phenotype in terms of intraradical FSK colonization.

Downstream the nuclear envelope cation channel in the CSSP lies symbiotic calcium spiking (Genre and Russo, 2016). The calcium ion is a universal second messenger in numerous plant signaling pathways. On one hand, cytoplasmic calcium oscillations constitute a general plant cell response to abiotic and biotic stimulation (Knight et al., 1997) (Aldon et al., 2018). More specifically, cytosolic calcium signals have been reported upon perception of symbiotic signals (Navazio et al., 2007), fungal elicitors like chitin and β -glucans (Mithöfer et al., 1999), cell wall fractions and exudates of endophytic fungi (Vadassery et al., 2009) (Johnson et al., 2018). On the other hand, the generation of nuclear and perinuclear calcium oscillations have been shown to trigger specific plant responses. They occur upon abiotic stimulation (Lachaud et al., 2010) (van der Luit et al., 1999), rhizobial and AM fungi perception (Ehrhardt et al., 1996) (Chabaud et al., 2011), perception of *Frankia* signals by actinorrhizal plants (Chabaud et al., 2016), and perception of flagellin (*flg22*), oligosaccharides and proteins leading to necrosis in *Nicotiana* sp cells (Lecourieux et al., 2005). Our results show that FSK exudates trigger periodic calcium oscillations in the nucleus of *M. truncatula* ROCs harbouring nuclear-targetedameleon reporters (Sieberer et al., 2009). The suppression of this response in *dmi2-2* and its persistence in *dmi3-1* mutants, strongly suggests that FSK-triggered calcium signals are acting within the CSSP, in analogy to what has been observed for the response to AM fungi and rhizobia (Wais et al., 2000) (Chabaud et al., 2011) (Genre et al., 2013). To the best of our knowledge, there are no previous reports of nuclear calcium oscillations upon compatible, non-symbiotic legume-microbe interactions that are CSSP-dependent. *M. truncatula* epidermal cells respond to oomycete cell wall fractions by nuclear calcium oscillations but only in a CSSP-independent manner (Nars et al., 2013). This unprecedented conclusion opens a broad field of discussion about the role of the CSSP outside the restricted group of symbiotic interactions *sensu stricto*.

Indeed, a comparison of nuclear calcium oscillations as a response to FSK exudate with calcium signatures in response to symbiotic factors revealed possible analogies: the patterns recorded in our study resemble those triggered by CO4/AM fungal exudate for their relatively irregular peak distribution. In addition, the average peak width of ~60 sec recorded for FSK, is closer to the 71-100 sec interval for significant peaks as response to Nod factors than to the much shorter 24-36 sec interval observed for mycorrhizal factors (Kosuta et al., 2008). Furthermore, by employing the exudates from two additional fungal species as external controls - the pathogenic *Fusarium oxysporum* f. sp. *medicaginis* and the

non-mycorrhizal mutualist *P. indica* - we observed comparable nuclear calcium spiking profiles that are CSSP-dependent.

Generation of nuclear calcium oscillations by multiple fungal strains should not be a surprise. Chitin-based molecules are secreted and/or deposited by fungi at the proximity of the interacting plant cell surface. These molecules are structurally related to rhizobial LCOs, as well as Myc COs/LCOs, which are able to activate nuclear calcium spiking in host plants (Ehrhardt et al., 1996) (Sieberer et al., 2009) (Chabaud et al., 2011). Reported symbiotic calcium spiking inducing signals are therefore primarily chitinaceous and the only currently known exception, to our knowledge, is the case of *Frankia* symbiotic factors able to elicit *NIN* (Nodule Inception) gene activation and nuclear calcium spiking on roots of the actinorrhizal plant *Casuarina glauca*. *Frankia* factors are composed of hydrophilic compounds that are resistant to chitinase digestion (Chabaud et al., 2016).

The placement of nuclear calcium spiking at the core of *Lotus*-FsK signaling pathway(s) is supported by CSSP gene expression and phenotyping of mutants impaired in genes acting downstream the nuclear calcium spiking response. *LjCCaMK* (*MtDMI3*), the gene encoding the kinase responsible for deciphering nuclear calcium signals (Lévy et al., 2004), was marginally upregulated both at early and relatively late time points of the interaction. *CCaMK* activation at very early stages of the interaction is of interest, because this gene acts at the core of the signal transduction process. Induction of *CCaMK* at late stages of the interaction, is perhaps associated to fungal progression within host tissues at these stages. Interestingly, *LjCCaMK* expression is only marginally affected by *M. loti* inoculation (Tirichine et al., 2006), suggesting that this calcium-activated enzyme is differentially involved in the two interactions. An impaired phenotype with lower colonization levels was recorded in both *ccamk-1* and *cyclops-1* mutants, genes acting downstream the calcium spiking response. Interestingly, a comparable delay in nodulation and the occasional and late colonization by AMF (delayed and reduced arbuscule formation) has been reported for the *ccamk-1* weak allele (Schauser et al., 1998) (Demchenko et al., 2004), suggestive of a partial functioning of the truncated protein. Alternatively, at these later time points, and possibly due to fungal overload, the necessity for signal deciphering through *CCaMK*, and signal transduction through *CYCLOPS*, may be bypassed by redundant proteins acting in parallel and/or alternative signaling routes that allow the progression of fungal accommodation even in the absence of key components of the CSSP. In this latter case, colonization proceeds fast and reaches wt levels belatedly.

Summarizing the above, we propose that FsK produces at least two different types of molecules to activate the CSSP: chitosaccharides of unknown degree of polymerization and heat sensitive molecules. FsK colonizes the root of legumes at least via three alternative routes: a) When all CSSP components are functional, FsK utilizes the pathway by generating nuclear calcium spiking and activating *CCaMK*, which lies at the core of FsK recognition towards intraradical accommodation; b) When *SYMRK* is impaired, calcium spiking does not occur, but FsK is still capable of effectively colonizing the root, possibly by activating *CCaMK* through a *SYMRK*- and calcium spiking-independent route. c) When the calcium spiking response is generated but cannot be perceived or transmitted (impaired *CCaMK* or *CYCLOPS*) the CSSP is completely abolished, and yet FsK is still able to colonize

the legume root, though with less efficiency. We assume that in this case, an unexplored third route allows a belated intraradical fungal accommodation.

By moving 'deeper' into symbiotic signaling, the nodulation- and mycorrhization- specific transcription factors acting downstream the calcium spiking response, *LjNSP1* and *NSP2* (Maillet et al., 2011) (Delaux et al., 2013) were not affected in our system. Nevertheless, CSSP-regulated genes that act early in nodulation process were induced upon Fsk interaction. The constant mild induction of *ENOD40* from 4dpi onwards suggest a possible implication of this nodulin gene in Fsk accommodation process. *ENOD40* is an early nodulin gene induced in legume tissues upon NF/chitin pentamer treatment (Minami et al., 1996), during AM infection (van Rhijn et al., 1997) and it is linked to symbiotic (nodule formation) and non-symbiotic organogenetic processes (i.e. lateral root formation) in legumes (Papadopoulou et al., 1996). *ENOD40* is also regulated by cytokinin (van Rhijn et al., 1997). One can speculate that the rapid and sustained expression of *ENOD40* is linked to the preparation of root tissues for Fsk accommodation: as a filamentous fungus that grows rapidly within plant tissues, Fsk intracellular growth varies from partial to full occupation of the host cell, involving the rearrangement of plant membranous materials and vesicular activity at infection sites and possibly the assembly of a perifungal membrane system that preserves host cell integrity for a limited time (Skiada et al., 2019). In this frame, plant cells may have to expand, and perhaps divide. Cortical cell division was also recently linked to AM symbiosis (Russo et al., 2018). Analysing the hormonal balance in Fsk-legume system during such initial events is expected to shed light on the establishment of this legume-endophyte association.

4.4.3 Conclusion

In the present study we have shown that multiple LysM receptors that perceive chitin molecules play a role during FSK recognition by the legume plant, and act balancing regulators of fungal progression within the root. We furthermore show that the CSSP, so far known to be triggered upon microbial symbiont/symbiotic factor perception to allow intracellular accommodation in legume roots, is also utilized by fungal legume-interacting microbes, as exemplified by the endophytic *Fusarium solani* strain K. This conclusion suggests that alternative upstream routes - specific to FSK and possibly other microbes - are involved in the activation of the CSSP central core beside rhizobial, mycorrhizal and actinorrhizal factor receptors. The positive regulation of fungal accommodation may be further controlled at steps downstream the calcium spiking response. Our results contribute to the emerging notion that the CSSP is not solely a feature of symbiotic interactions of legumes. It is intriguing and far more perplexing that the CSSP should be viewed as a multi-triggered response module rather than as a discriminative mechanism between microbes.

4.5 References

- Aldon D, Mbengue M, Mazars C, Galaud JP. 2018.** Calcium signalling in plant biotic interactions. *International Journal of Molecular Sciences* **19**: 1–19.
- Amor B Ben, Shaw SL, Oldroyd GED, Maillet F, Penmetsa RV, Cook D, Long SR, Dénarié J, Gough C. 2003.** The NFP locus of *Medicago truncatula* controls an early step of Nod factor signal transduction upstream of a rapid calcium flux and root hair deformation. *Plant Journal* **34**: 495–506.
- Antolín-Llovera M, Petutsching EK, Ried MK, Lipka V, Nürnberger T, Robatzek S, Parniske M. 2014.** Knowing your friends and foes - plant receptor-like kinases as initiators of symbiosis or defence. *New Phytologist* **204**: 791–802.
- Banhara A, Ding Y, Kühner R, Zuccaro A, Parniske M. 2015.** Colonization of root cells and plant growth promotion by *Piriformospora indica* occurs independently of plant common symbiosis genes. *Frontiers in Plant Science* **6**: 667.
- Barker DG, Chabaud M, Russo G, Genre A. 2017.** Nuclear Ca²⁺ signalling in arbuscular mycorrhizal and actinorhizal endosymbioses: on the trail of novel underground signals. *New Phytologist* **214**: 533–538.
- Bécard G, Fortin JA. 1988.** Early events of vesicular-arbuscular mycorrhiza formation on Ri T-DNA transformed roots. *New Phytologist* **108**: 211–218.
- Bonfante P, Genre A, Faccio A, Martini I, Schauser L, Stougaard J, Webb J, Parniske M. 2000.** The *Lotus japonicus* *LjSym4* gene is required for the successful symbiotic infection of root epidermal cells. *Molecular plant-microbe interactions : MPMI* **13**: 1109–20.
- Bozsoki Z, Cheng J, Feng F, Gysel K, Vinther M, Andersen KR, Oldroyd G, Blaise M, Radutoiu S, Stougaard J. 2017.** Receptor-mediated chitin perception in legume roots is functionally separable from Nod factor perception. *Proceedings of the National Academy of Sciences* **114**: E8118–E8127.
- Carotenuto G, Chabaud M, Miyata K, Capozzi M, Takeda N, Kaku H, Shibuya N, Nakagawa T, Barker DG, Genre A. 2017.** The rice LysM receptor-like kinase OsCERK1 is required for the perception of short-chain chitin oligomers in arbuscular mycorrhizal signaling. *New Phytologist* **214**: 1440–1446.
- Carotenuto G, Volpe V, Russo G, Politi M, Sciascia I, de Almeida-Engler J, Genre A. 2019.** Local endoreduplication as a feature of intracellular fungal accommodation in arbuscular mycorrhizas. *New Phytologist* **223**: 430–446.
- Catoira R, Galera C, de Billy F, Penmetsa RV, Journet E-P, Maillet F, Rosenberg C, Cook D, Gough C, Denarie J. 2000.** Four Genes of *Medicago truncatula* Controlling Components of a Nod Factor Transduction Pathway. *The Plant Cell* **12**: 1647–1665.
- Chabaud M, Genre A, Sieberer BJ, Faccio A, Fournier J, Novero M, Barker DG, Bonfante P. 2011.** Arbuscular mycorrhizal hyphopodia and germinated spore exudates trigger Ca²⁺ spiking in the legume and nonlegume root epidermis. *New Phytologist* **189**: 347–355.
- Chabaud M, Gherbi H, Pirolles E, Vaissayre V, Fournier J, Moukouanga D, Franche C, Bogusz D, Tisa LS, Barker DG, et al. 2016.** Chitinase-resistant hydrophilic symbiotic factors secreted by *Frankia* activate both Ca²⁺ spiking and *NIN* gene expression in the actinorhizal plant *Casuarina glauca*. *New Phytologist* **209**: 86–93.
- Chabaud M, Venard C, Defaux-Petras A, Becard G, Barker DG. 2002.** Targeted inoculation of

Medicago truncatula in vitro root cultures reveals *MtENOD11* expression during early stages of infection by arbuscular mycorrhizal fungi. *New Phytologist* **156**: 265–273.

Charpentier M, Bredemeier R, Wanner G, Takeda N, Schleiff E, Parniske M. 2008. *Lotus japonicus* CASTOR and POLLUX are ion channels essential for perinuclear calcium spiking in legume root endosymbiosis. *The Plant Cell* **20**: 3467–79.

Charpentier M, Oldroyd GED. 2013. Nuclear Calcium Signaling in Plants. *Plant Physiology* **163**: 496–503.

Delaux P-M, Becard G, Combier J-P. 2013. NSP1 is a component of the Myc signaling pathway. *New Phytologist* **199**: 59–65.

Demchenko K, Winzer T, Stougaard J, Parniske M, Pawlowski K. 2004. Distinct roles of *Lotus japonicus* SYMRK and SYM15 in root colonization and arbuscule formation. *New Phytologist* **163**: 381–392.

Deshmukh S, Hückelhoven R, Schäfer P, Imani J, Sharma M, Weiss M, Waller F, Kogel K-H. 2006. The root endophytic fungus *Piriformospora indica* requires host cell death for proliferation during mutualistic symbiosis with barley. *Proceedings of the National Academy of Sciences of the United States of America* **103**: 18450–18457.

Doyle JJ, Doyle JL. 1987. A rapid DNA isolation procedure for small quantities of fresh leaf tissue. *Phytochemical Bulletin* **19**: 11–15.

Ehrhardt DW, Wais R, Long SR. 1996. Calcium spiking in plant root hairs responding to rhizobium modulation signals. *Cell* **85**: 673–681.

Ferguson BJ, Mathesius U. 2014. Phytohormone Regulation of Legume-Rhizobia Interactions. *Journal of Chemical Ecology* **40**: 770–790.

Fernandez-Aparicio M, Rispaill N, Prats E, Morandi D, Garcia-Garrido JM, Dumas-Gaudot E, Duc G, Rubiales D. 2010. Parasitic plant infection is partially controlled through symbiotic pathways. *Weed Research* **50**: 76–82.

Flemetakis E, Kavroulakis N, Quaedvlieg NE, Spaink HP, Dimou M, Roussis A, Katinakis P. 2000. *Lotus japonicus* contains two distinct ENOD40 genes that are expressed in symbiotic, nonsymbiotic, and embryonic tissues. *Molecular plant-microbe interactions : MPMI* **13**: 987–94.

Fliegmann J, Canova S, Lachaud C, Uhlenbroich S, Gasciolli V, Pichereaux C, Rossignol M, Rosenberg C, Cumener M, Pitorre D, et al. 2013. Lipo-chitooligosaccharidic Symbiotic Signals Are Recognized by LysM Receptor-Like Kinase LYR3 in the Legume *Medicago truncatula*. *ACS Chemical Biology* **8**: 1900–1906.

Franssen HJ, Nap J-P, Gloudemans T, Stiekema W, Van Dam H, Govers F, Louwerse J, Van Kammen A, Bisseling T. 1987. Characterization of cDNA for nodulin-75 of soybean: A gene product involved in early stages of root nodule development. *Proceedings of the National Academy of Sciences* **84**: 4495–4499.

Fuechtbauer W, Yunusov T, Bozsóki Z, Gavrin A, James EK, Stougaard J, Schornack S, Radutoiu S. 2018. LYS12 LysM receptor decelerates *Phytophthora palmivora* disease progression in *Lotus japonicus*. *Plant Journal* **93**: 297–310.

Garantonakis N, Pappas ML, Varikou K, Skiada V, Broufas GD, Kavroulakis N, Papadopoulou

- KK. 2018.** Tomato Inoculation With the Endophytic Strain *Fusarium solani* K Results in Reduced Feeding Damage by the Zoophytophagous Predator *Nesidiocoris tenuis*. *Frontiers in Ecology and Evolution* **6**: 126.
- Genre A, Chabaud M, Balzergue C, Puech-Pagès V, Novero M, Rey T, Fournier J, Rochange S, Bécard G, Bonfante P, et al. 2013.** Short-chain chitin oligomers from arbuscular mycorrhizal fungi trigger nuclear Ca²⁺ spiking in *Medicago truncatula* roots and their production is enhanced by strigolactone. *New Phytologist* **198**: 190–202.
- Genre A, Ortu G, Bertoldo C, Martino E, Bonfante P. 2009.** Biotic and abiotic stimulation of root epidermal cells reveals common and specific responses to Arbuscular Mycorrhizal Fungi. *Plant physiology* **149**: 1424–1434.
- Genre A, Russo G. 2016.** Does a common pathway transduce symbiotic signals in plant-microbe interactions? *Frontiers in Plant Science* **7**: 96.
- Gherbi H, Markmann K, Svistoonoff S, Estevan J, Aufran D, Gabor G, Auguy F, Peret B, Laplaze L, Franche C, et al. 2008.** SymRK defines a common genetic basis for plant root endosymbioses with arbuscular mycorrhiza fungi, rhizobia, and Frankia bacteria. *PNAS* **105**: 4928–4932.
- Gibelin-Viala C, Amblard E, Puech-Pages V, Bonhomme M, Garcia M, Bascaules-Bedin A, Fliegmann J, Wen J, Mysore KS, le Signor C, et al. 2019.** The *Medicago truncatula* LysM receptor-like kinase LYK9 plays a dual role in immunity and the arbuscular mycorrhizal symbiosis. *New Phytologist* **0**.
- Glyan'ko AK. 2018.** Phytohormones and Morphogenesis of Root Nodules and Lateral Roots of a Legume Plant. *Journal of Stress Physiology & Biochemistry* **14**: 12–26.
- Gow NAR, Latge J-P, Munro CA. 2017.** The Fungal Cell Wall: Structure, Biosynthesis, and Function. *Microbiol Spectrum* **5**: FUNK-0035-2016.
- Harris JM, Wais R, Long SR. 2003.** Rhizobium-Induced calcium spiking in *Lotus japonicus*. *Molecular plant-microbe interactions : MPMI* **16**: 335–341.
- Hayashi M, Tansengco ML, Suganuma N, Szczyglowski K, Krusell L, Ott T, Udvardi MK. 2005.** *Lotus japonicus* handbook. In: Marquez AJ, Stougaard J, Udvardi MK, Parniske M, Spaink H, Saalbach G, Webb J, Chiurazzi M, eds. *Lotus japonicus Handbook*. Springer, 53–82.
- Hayes MW, Stutte GW, Mckeen-bennett M, Murray PG. 2014.** Mutualism Within a Simulated Microgravity Environment -*Piriformospora indica* Promotes the Growth of *Medicago truncatula*. *Gravitational and Space Research* **2**: 21–33.
- Huisman R, Bouwmeester K, Brattinga M, Govers F, Bisseling T, Limpens E. 2015.** Haustorium Formation in *Medicago truncatula* Roots Infected by *Phytophthora palmivora* Does Not Involve the Common Endosymbiotic Program Shared by Arbuscular Mycorrhizal Fungi and Rhizobia. *Molecular Plant-Microbe Interactions* **28**: 1271–1280.
- Imaizumi-Anraku H, Takeda N, Charpentier M, Perry J, Miwa H, Umehara Y, Kouchi H, Murakami Y, Mulder L, Vickers K, et al. 2005.** Plastid proteins crucial for symbiotic fungal and bacterial entry into plant roots. *Nature* **433**: 527–531.
- Johnson JM, Ludwig A, Furch ACU, Mithöfer A, Scholz S, Reichelt M, Oelmüller R. 2018.** The Beneficial Root-Colonizing Fungus *Mortierella hyalina* Promotes the Aerial Growth of Arabidopsis and

Activates Calcium-Dependent Responses That Restrict *Alternaria brassicae*-Induced Disease Development in Roots. *Molecular Plant-Microbe Interactions* **32**: 351–363.

Kalo P, Gleason C, Edwards A, Marsh J, Mitra RM, Hirsch S, Jakab J, Sims S, Long SR, Rogers J, et al. 2005. Nodulation Signaling in Legumes Requires NSP2, a Member of the GRAS Family of Transcriptional Regulators. *Science* **308**: 1786–1789.

Kavroulakis N, Doupis G, Papadakis IE, Ehaliotis C, Papadopoulou KK. 2018. Tolerance of tomato plants to water stress is improved by the root endophyte *Fusarium solani* FsK. *Rhizosphere* **6**: 77–85.

Kavroulakis N, Ntougias S, Zervakis GI, Ehaliotis C, Haralampidis K, Papadopoulou KK. 2007. Role of ethylene in the protection of tomato plants against soil-borne fungal pathogens conferred by an endophytic *Fusarium solani* strain. *Journal of Experimental Botany* **58**: 3853–3864.

Kistner C, Winzer T, Pitzschke A, Mulder L, Sato S, Kaneko T, Tabata S, Sandal N, Stougaard J, Webb KJ, et al. 2005. Seven *Lotus japonicus* Genes Required for Transcriptional Reprogramming of the Root during Fungal and Bacterial Symbiosis. *The Plant Cell* **17**: 2217–2229.

Knight H, Trewavas AJ, Knight MR. 1997. Calcium signalling in *Arabidopsis thaliana* responding to drought and salinity. *Plant Journal* **12**: 1067–1078.

Kosuta S, Hazledine S, Sun J, Miwa H, Morris RJ, Downie JA, Oldroyd GED. 2008. Differential and chaotic calcium signatures in the symbiosis signaling pathway of legumes. *Proceedings of the National Academy of Sciences of the United States of America* **105**: 9823–8.

Kouzai Y, Nakajima K, Hayafune M, Ozawa K, Kaku H, Shibuya N, Minami E, Nishizawa Y. 2014. CEBiP is the major chitin oligomer-binding protein in rice and plays a main role in the perception of chitin oligomers. *Plant Mol Biol* **84**: 519–528.

Kumagai H, Kinoshita E, Ridge RW, Kouchi H. 2006. RNAi knock-down of ENOD40s leads to significant suppression of nodule formation in *Lotus japonicus*. *Plant and Cell Physiology* **47**: 1102–1111.

Lace B, Genre A, Woo S, Faccio A, Lorito M, Bonfante P. 2015. Gate crashing arbuscular mycorrhizas: In vivo imaging shows the extensive colonization of both symbionts by *Trichoderma atroviride*. *Environmental Microbiology Reports* **7**: 64–77.

Lachaud C, Da Silva D, Cotellet V, Thuleau P, Xiong TC, Jauneau A, Brière C, Graziana A, Bellec Y, Faure J, et al. 2010. Nuclear calcium controls the apoptotic-like cell death induced by D-erythro-sphinganine in tobacco cells. *Cell Calcium* **47**: 92–100.

Lahrman U, Ding Y, Banhara A, Rath M, Hajirezaei MR, Döhlemann S, von Wirén N, Parniske M, Zuccaro A. 2013. Host-related metabolic cues affect colonization strategies of a root endophyte. *Proc Natl Acad Sci USA* **110**: 13965–13970.

Lecourieux D, Lamotte O, Bourque S, Wendehenne D, Mazars C, Ranjeva R, Pugin A. 2005. Proteinaceous and oligosaccharidic elicitors induce different calcium signatures in the nucleus of tobacco cells. *Cell Calcium* **38**: 527–538.

Lévy J, Bres C, Geurts R, Chalhoub B, Kulikova O, Duc G, Journet E-P, Ané J-M, Lauber E, Bisseling T, et al. 2004. A Putative Ca²⁺ and Calmodulin-Dependent Protein Kinase Required for Bacterial and Fungal Symbioses. *Science* **303**: 1361 LP – 1364.

Liang Y, Tóth K, Cao Y, Tanaka K, Espinoza C, Stacey G. 2014. Lipochitooligosaccharide

recognition: an ancient story. *The New phytologist* **204**: 289–296.

Limpens E, Franken C, Smit P, Willemse J, Bisseling T, Geurts R. 2003. LysM Domain Receptor Kinases Regulating Rhizobial Nod Factor-Induced Infection LysM Domain Receptor Kinases Regulating Rhizobial Nod Factor – Induced Infection. *Science* **302**: 630–633.

Lohmann GV, Shimoda Y, Nielsen MW, Jørgensen FG, Grossmann C, Sandal N, Sørensen K, Thirup S, Madsen LH, Tabata S, et al. 2010. Evolution and Regulation of the *Lotus japonicus* LysM Receptor Gene Family. *Molecular Plant-Microbe Interactions* **23**: 510–521.

Lopez-Gomez M, Sandal N, Stougaard J, Boller T. 2012. Interplay of flg22-induced defence responses and nodulation in *Lotus japonicus*. *Journal of Experimental Botany* **63**: 393–401.

van der Luit AH, Olivari C, Haley A, Knight MR, Trewavas AJ. 1999. Distinct Calcium Signaling Pathways Regulate Calmodulin Gene Expression in Tobacco. *Plant Physiology* **121**: 705 LP – 714.

Madsen EB, Madsen LH, Radutoiu S, Olbryt M, Rakwalska M, Szczygłowski K, Sato S, Kaneko T, Tabata S, Sandal N, et al. 2003. A receptor kinase gene of the LysM type is involved in legume perception of rhizobial signals. *Nature* **425**: 637–640.

Maillet F, Poinot V, André O, Puech-Pagès V, Haouy A, Gueunier M, Cromer L, Giraudet D, Formey D, Niebel A, et al. 2011. Fungal lipochitooligosaccharide symbiotic signals in arbuscular mycorrhiza. *Nature* **469**: 58–63.

McAinsh MR, Hetherington AM. 1998. Encoding specificity in Ca²⁺ signalling systems. *Trends in Plant Science* **3**: 32–36.

Mélida H, Sandoval-Sierra J V., Diéguez-Urbeondo J, Bulone V. 2013. Analyses of Extracellular Carbohydrates in Oomycetes Unveil the Existence of Three Different Cell Wall Types. *Eukaryotic Cell* **12**: 194–203.

Minami E, Kouchi H, Cohn JR, Ogawa T, Stacey G. 1996. Expression of the early nodulin, ENOD40, in soybean roots in response to various lipo-chitin signal molecules. *Plant Journal* **10**: 23–32.

Mithöfer A, Ebel J, Bhagwat AA, Boller T, Neuhaus-Url G. 1999. Transgenic aequorin monitors cytosolic calcium transients in soybean cells challenged with β -glucan or chitin elicitors. *Planta* **207**: 566–574.

Miwa H, Sun J, Oldroyd GED, Downie JA. 2006. Analysis of Nod-Factor-Induced Calcium Signaling in Root Hairs of Symbiotically Defective Mutants of *Lotus japonicus*. *Molecular plant-microbe interactions : MPMI* **19**: 914–923.

Miyawaki A, Llopis J, Heim R, McCaffery JM, Adams JA, Ikura M, Tsien RY. 1997. Fluorescent indicators for Ca²⁺ based on green fluorescent proteins and calmodulin. *Nature* **388**: 882–887.

Murakami E, Cheng J, Gysel K, Bozsoki Z, Kawaharada Y, Hjuler CT, Sørensen KK, Tao K, Kelly S, Venice F, et al. 2018. Epidermal LysM receptor ensures robust symbiotic signalling in *Lotus japonicus*. *eLife* **7**: e33506.

Nars A, Lafitte C, Chabaud M, Drouillard S, Melida H, Danoun S, Le Costaouec T, Rey T, Benedetti J, Bulone V, et al. 2013. Aphanomyces euteiches Cell Wall Fractions Containing Novel Glucan-Chitosaccharides Induce Defense Genes and Nuclear Calcium Oscillations in the Plant Host *Medicago truncatula*. *PLoS ONE* **8**: e75039.

Navazio L, Moscatiello R, Genre A, Novero M, Baldan B, Bonfante P, Mariani P. 2007. A Diffusible

Signal from Arbuscular Mycorrhizal Fungi Elicits a Transient Cytosolic Calcium Elevation in Host Plant Cells. *Plant Physiology* **144**: 673 LP – 681.

Novero M, Faccio A, Genre A, Stougaard J, Webb KJ, Mulder L, Parniske M, Bonfante P. 2002. Dual requirement of the *LjSym4* gene for mycorrhizal development in epidermal and cortical cells of *Lotus japonicus* roots. *New Phytologist* **154**: 741–749.

Papadopoulou K, Roussis A, Katinakis P. 1996. *Phaseolus* ENOD40 is involved in symbiotic and non-symbiotic organogenetic processes: Expression during nodule and lateral root development. *Plant Molecular Biology* **30**: 403–417.

Pappas ML, Liapoura M, Papantoniou D, Avramidou M, Kavroulakis N, Weinhold A, Broufas GD, Papadopoulou KK. 2018. The Beneficial Endophytic Fungus *Fusarium solani* Strain K Alters Tomato Responses Against Spider Mites to the Benefit of the Plant. *Frontiers in Plant Science* **9**: 1603.

Parniske M. 2008. Arbuscular mycorrhiza: the mother of plant root endosymbioses. *Nature Reviews Microbiology* **6**: 763.

Pfaffl MW. 2001. A new mathematical model for relative quantification in real-time RT-PCR. *Nucleic Acids Research* **29**: e45.

Radutoiu S, Madsen LH, Madsen EB, Felle HH, Umehara Y, Grønlund M, Sato S, Nakamura Y, Tabata S, Sandal N, et al. 2003. Plant recognition of symbiotic bacteria requires two LysM receptor-like kinases. *Nature* **425**: 585–592.

Ramakers C, Ruijter JM, Lekanne Deprez RH, Moorman AFM. 2003. Assumption-free analysis of quantitative real-time polymerase chain reaction (PCR) data. *Neuroscience Letters* **339**: 62–66.

Ramírez-Suero M, Khanshour A, Martinez Y, Rickauer M. 2010. A study on the susceptibility of the model legume plant *Medicago truncatula* to the soil-borne pathogen *Fusarium oxysporum*. *European Journal of Plant Pathology* **126**: 517–530.

Rasmussen SR, Füchtbauer W, Novero M, Volpe V, Malkov N, Genre A, Bonfante P, Stougaard J, Radutoiu S. 2016. Intraradical colonization by arbuscular mycorrhizal fungi triggers induction of a lipochitooligosaccharide receptor. *Scientific Reports* **6**: 1–12.

van Rhijn P, Fang Y, Galili S, Shaul O, Atzmon N, Wininger S, Eshed Y, Lum M, Li Y, To V, et al. 1997. Expression of early nodulin genes in alfalfa mycorrhizae indicates that signal transduction pathways used in forming arbuscular mycorrhizae and *Rhizobium*-induced nodules may be conserved. *Proceedings of the National Academy of Sciences of the United States of America* **94**: 5467–5472.

Russo G, Carotenuto G, Fiorilli V, Volpe V, Chiapello M, Van Damme D, Genre A. 2018. Ectopic activation of cortical cell division during the accommodation of arbuscular mycorrhizal fungi. *New Phytologist* **221**: 1036–1048.

Russo G, Spinella S, Sciacca E, Bonfante P, Genre A. 2013. Automated analysis of calcium spiking profiles with CaSA software: two case studies from root-microbe symbioses. *BMC plant biology* **13**: 224.

Sanchez L, Weidmann S, Arnould C, Bernard AR, Gianinazzi S, Gianinazzi-Pearson V. 2005. *Pseudomonas fluorescens* and *Glomus mosseae* Trigger DMI3-Dependent Activation of Genes Related to a Signal Transduction Pathway in Roots of *Medicago truncatula*. *Plant Physiology* **139**: 1065 LP – 1077.

Schauser L, Handberg K, Sandal N, Stiller J, Thykjaer T, Pajuelo E, Nielsen A, Stougaard J. 1998.

Symbiotic mutants deficient in nodule establishment identified after T-DNA transformation of *Lotus japonicus*. *Mol Gen Genet* **259**: 414–423.

Sieberer BJ, Chabaud M, Timmers AC, Monin A, Fournier J, Barker DG. 2009. A nuclear-targetedameleon demonstrates intranuclear Ca^{2+} spiking in *Medicago truncatula* root hairs in response to rhizobial nodulation factors. *Plant Physiology* **151**: 1197–1206.

Skiada V, Faccio A, Kavroulakis N, Genre A, Bonfante P, Papadopoulou KK. 2019. Colonization of Legumes by an Endophytic *Fusarium solani* strain FsK Reveals Common Features to Symbionts or Pathogens. *Fungal Genetics and Biology* **127**: 60–74.

Snyder WC, Hansen HN. 1940. The Species Concept in *Fusarium*. *American Journal of Botany* **27**: 64–67.

Stacey G, Shibuya N. 1997. Chitin recognition in rice and legumes. *Plant and Soil* **194**: 161–169.

Stracke S, Kistner C, Yoshida S, Mulder L, Sato S, Kaneko T, Tabata S, Sandal N, Stougaard J, Szczyglowski K, et al. 2002. A plant receptor-like kinase required for both bacterial and fungal symbiosis. *Nature* **417**: 959–962.

Sun J, Miller JB, Granqvist E, Wiley-Kalil A, Gobbato E, Maillet F, Cottaz S, Samain E, Venkateshwaran M, Fort S, et al. 2015. Activation of symbiosis signaling by arbuscular mycorrhizal fungi in legumes and rice. *The Plant cell* **27**: 823–38.

Svistoonoff S, Benabdoun FM, Nambiar-Veetil M, Imanishi L, Vaissayre V, Cesari S, Diagne N, Hoher V, de Billy F, Bonneau J, et al. 2013. The Independent Acquisition of Plant Root Nitrogen-Fixing Symbiosis in Fabids Recruited the Same Genetic Pathway for Nodule Organogenesis. *PLOS ONE* **8**: e64515.

Takeda N, Okamoto S, Hayashi M, Murooka Y. 2005. Expression of *LjENOD40* genes in response to symbiotic and non-symbiotic signals: *LjENOD40-1* and *LjENOD40-2* are differentially regulated in *Lotus japonicus*. *Plant and Cell Physiology* **46**: 1291–1298.

Tirichine L, Imaizumi-Anraku H, Yoshida S, Murakami Y, Madsen LH, Miwa H, Nakagawa T, Sandal N, Albrechtsen AS, Kawaguchi M, et al. 2006. Deregulation of a Ca^{2+} /calmodulin-dependent kinase leads to spontaneous nodule development. *Nature* **441**: 1153–6.

Vadassery J, Ranf S, Drzewiecki C, Mithofer A, Mazars C, Scheel D, Lee J, Oelmu R. 2009. A cell wall extract from the endophytic fungus *Piriformospora indica* promotes growth of Arabidopsis seedlings and induces intracellular calcium elevation in roots. *The Plant Journal* **59**: 193–206.

Verma S, Varma A, Rexer K, Hassel A, Kost G, Sarbhoy A, Bisen P, Butehorn B, Franken P. 1998. *Piriformospora indica*, gen. et sp. nov., a new root-colonizing fungus. *Mycologia* **90**: 896–903.

Wais RJ, Galera C, Oldroyd G, Catoira R, Penmetza R V, Cook D, Gough C, Denarié J, Long SR. 2000. Genetic analysis of calcium spiking responses in nodulation mutants of *Medicago truncatula*. *Proceedings of the National Academy of Sciences of the United States of America* **97**: 13407–13412.

Wang E, Schornack S, Marsh JF, Gobbato E, Schwessinger B, Eastmond P, Schultze M, Kamoun S, Oldroyd GED. 2012. A common signaling process that promotes mycorrhizal and oomycete colonization of plants. *Current Biology* **22**: 2242–2246.

Weerasinghe RR, Bird DM, Allen NS. 2005. Root-knot nematodes and bacterial Nod factors elicit common signal transduction events in *Lotus japonicus*. *Proceedings of the National Academy of*

Sciences **102**: 3147–3152.

Wegel E, Schauser L, Sandal N, Stougaard J, Parniske M. 1998. Mycorrhiza Mutants of *Lotus japonicus* Define Genetically Independent Steps During Symbiotic Infection. *Molecular Plant-Microbe Interactions* **11**: 933–936.

van de Wiel C, Scheres B, Franssen H, van Lierop MJ, van Lammeren A, van Kammen A, Bisseling T. 1990. The early nodulin transcript ENOD2 is located in the nodule parenchyma (inner cortex) of pea and soybean root nodules. *The EMBO Journal* **9**: 1–7.

Yano K, Yoshida S, Mueller J, Singh S, Banba M, Vickers K, Markmann K, White C, Schuller B, Sato S, et al. 2008. CYCLOPS, a mediator of symbiotic intracellular accommodation. *Proceedings of the National Academy of Sciences of the United States of America* **105**: 20540–20545.

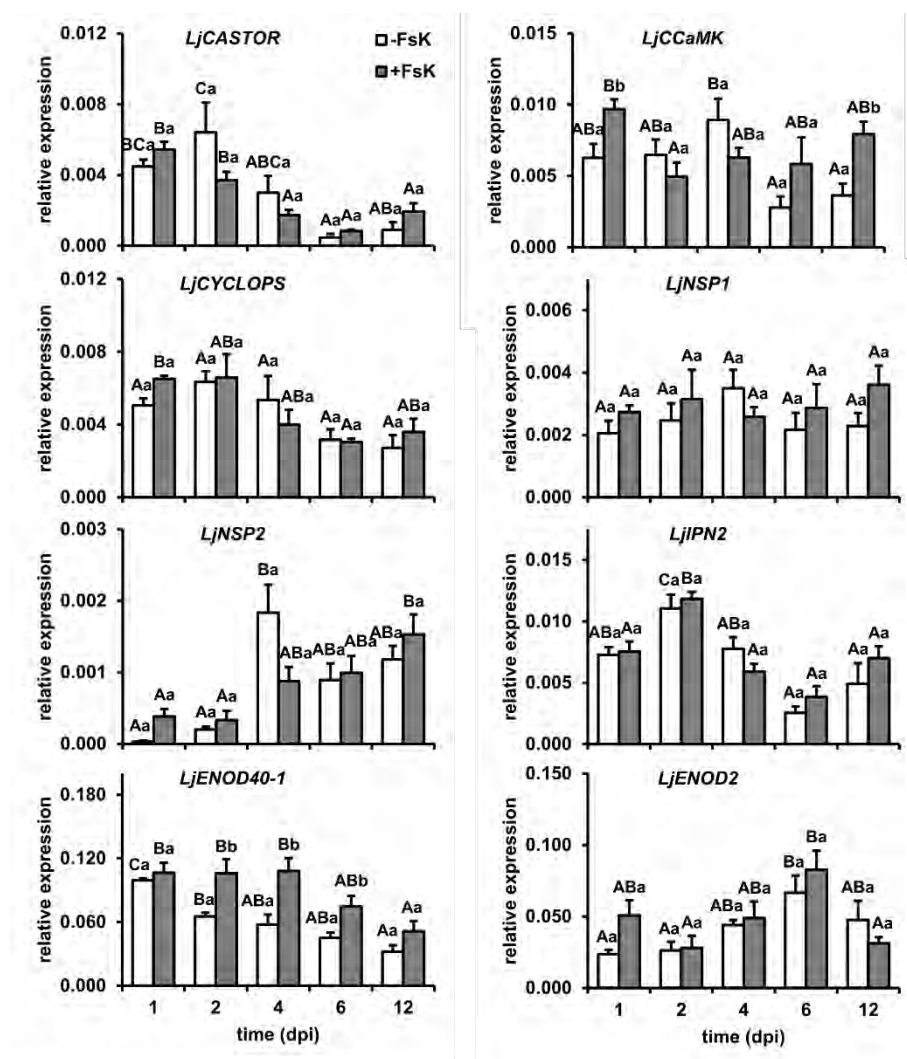
Zgad Zaj R, James EK, Kelly S, Kawaharada Y, de Jonge N, Jensen DB, Madsen LH, Radutoiu S. 2015. A Legume Genetic Framework Controls Infection of Nodules by Symbiotic and Endophytic Bacteria. *PLoS Genetics* **11**: 1–21.

Zgad Zaj R, Thiergart T, Bozsoki Z, Garrido-Oter R, Radutoiu S, Schulze-Lefert P. 2019. *Lotus japonicus* symbiosis signaling genes and their role in the establishment of root-associated bacterial and fungal communities. *bioRxiv* **547687**.

Zipfel C, Oldroyd GED. 2017. Plant signalling in symbiosis and immunity. *Nature* **543**: 328.

4.6 Appendix of Chapter 4

4.6.1 Supplementary material

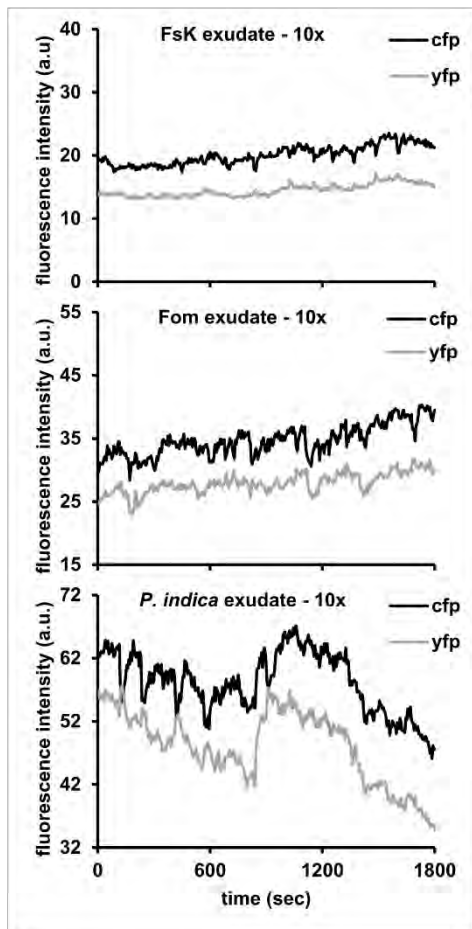


Supplementary Figure 4-6 Relative expression of *L. japonicus* genes acting within and downstream the CSSP, upon FSK treatment.

Temporal quantitative gene expression analysis of *L. japonicus* CSSP genes: *CASTOR*, *CCaMK*, *CYCLOPS*, and genes acting downstream the CSSP: *NSP1*, *NSP2*, *IPN2*, *ENOD40-1* and *ENOD2*, in control and FSK-inoculated *L. japonicus* root tissues. Expression levels are normalized to *Lj UBIQUITIN* housekeeping gene. Data are presented as means and standard errors of 3-4 biological replicates of 3 plants.

Different upper case letters denote significant differences within the same treatment at the 0.05 level, whereas different lower case letters, significant differences within the same time at the 0.05 level (two-Way Anova, Tukey's test).

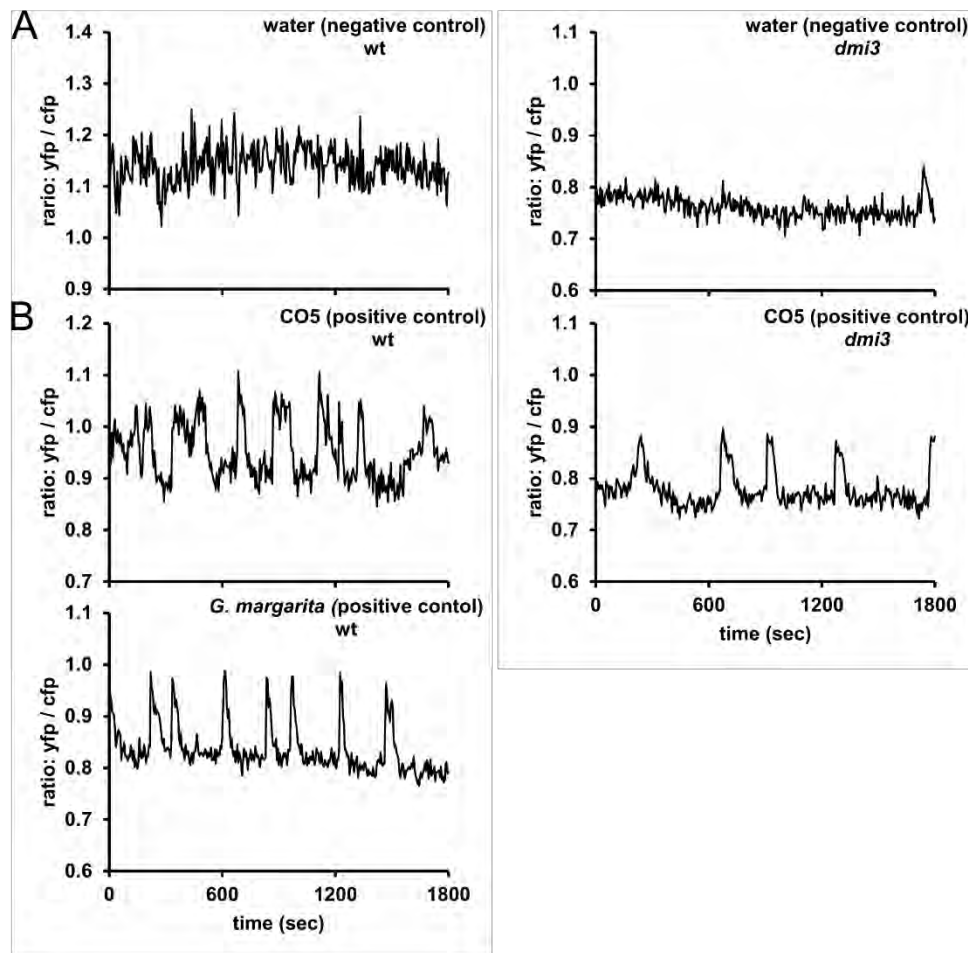
White/grey bars, expression in control/FsK inoculated tissues



Supplementary Figure 4-7 Changes in CFP, YFP fluorescence over time obtained from Mt wt ROC epidermal cells upon elicitation with fungal exudates.

Calcium spiking responses were recorded in a low-trichoblast-region located 10-20 mm from the root tip. *M. truncatula* wt ROCs expressing the NupYC2.1 cameleon were used for the bioassay. Fungal exudates derived from *FsK*, *Fom*, or *P. indica* were used as elicitors.

Graphs show the changes in CFP and YFP fluorescence (in arbitrary units) following addition of *FsK*, *Fom* or *P. indica* exudate, respectively. The presented plotted changes in fluorescence correspond to YFP:CFP ratios presented in Figure 4-2.



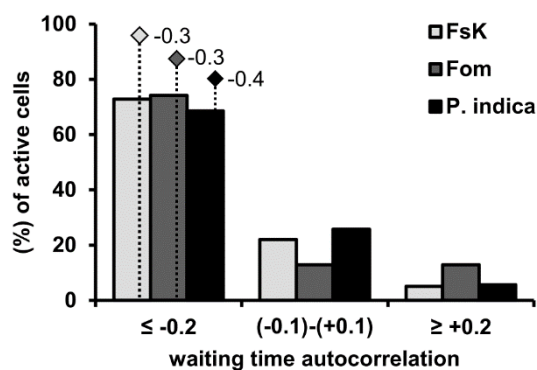
Supplementary Figure 4-8 Absence of calcium spiking in response to mock treatment, and generation of calcium spiking in response to CO5 and *G. margarita* germinated spore exudate treatment.

Calcium spiking responses were recorded in a low-trichoblast-region located 10-20 mm from the root tip. *M. truncatula* wt and *dmi3-1* ROCs expressing the NupYC2.1 cameleon were used for the bioassay.

A - B Graphs show ratios of YFP:CFP fluorescence over time obtained from epidermal cells.

A Plots showing absence of changes in nuclear calcium levels in wt or *dmi3-1* ROC lines upon (mock) treatment with sterile water.

B Plots showing nuclear calcium spiking induced in wt ROC lines after treatment with chito-oligosaccharides (CO5) or *G. margarita* germinated spore exudate, and in *dmi3-1* ROC lines after treatment with CO5.



Supplementary Figure 4-9 Distribution of waiting time autocorrelation values in the spiking profiles induced by fungal exudates.

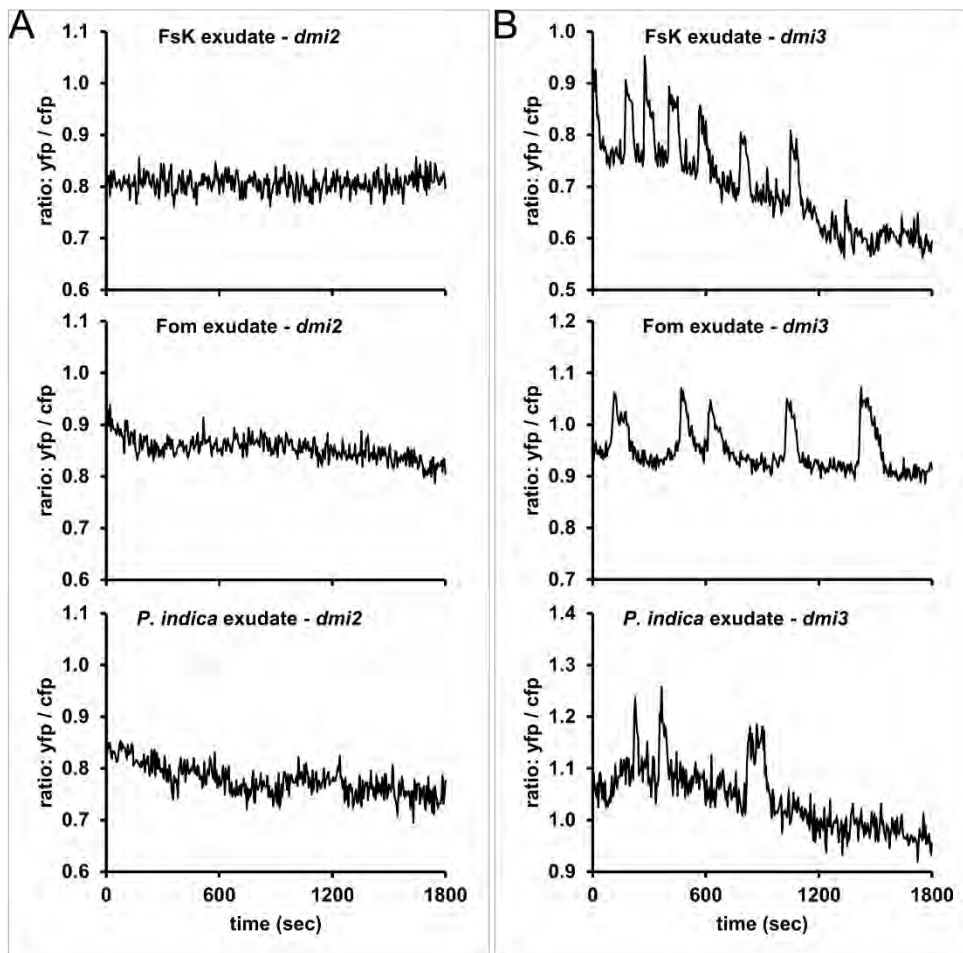
Histogram illustrating the waiting time autocorrelation values in the spiking profiles induced by FsK, Fom, or *P. indica* fungal exudate. The majority of nuclei demonstrate negative autocorrelation values (≤ -0.2) in all fungal exudates tested.

Statistical analysis showed no dependence between the fungal exudate tested and the frequency distribution of waiting time autocorrelation values, at the 0.05 level (Pearson's chi-squared test).

Light grey/dark grey/black bars: frequency of waiting time autocorrelation values intervals in response to FsK/FoM/*P. indica* exudate, respectively.

Waiting time autocorrelation values correspond to peaks derived from active plant cell nuclei of biological replicates, as presented in Supplementary Table 1.

Rhomboid shapes, waiting time autocorrelation median values of peaks generated in response to FsK/FoM/*P. indica* exudate, respectively.



Supplementary Figure 4-10 Nuclear calcium spiking is abolished in the *Mt dmi2-2*, but maintained in the *Mt dmi3-1* mutant lines.

Calcium spiking responses were recorded in a low-trichoblast-region located 10-20 mm from the root tip. *M. truncatula dmi2-2* and *dmi3-1* ROCs expressing the NupYC2.1 cameleon were used for the bioassay. Fungal exudates derived from *FsK*, *FoM*, or *P. indica* were used as elicitors.

(A) – (B) Graphs show ratios of YFP:CFP fluorescence obtained from epidermal cells in a low-trichoblasts-zone.

(A) Representative plots showing absence of changes in calcium levels in the nucleus of *dmi2-2* lines post treatment with 10x concentrated *FsK*, *FoM*, or *P. indica* exudate.

(B) Representative plots showing the induced changes in calcium levels in the nucleus of *dmi3-1* lines post treatment with 10x concentrated *FsK*, *FoM*, or *P. indica* exudate. All graphs show the plotted changes in the ratio of YFP:CFP fluorescence.

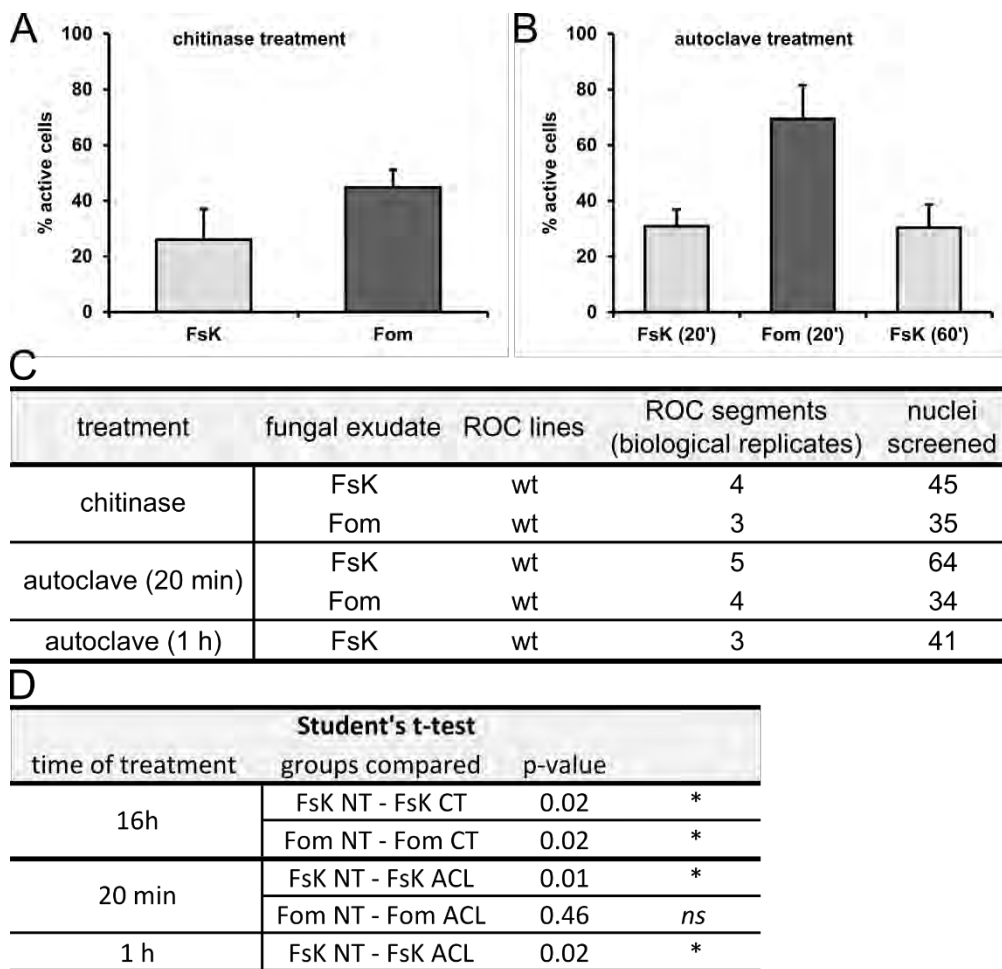


Figure 4-11 Nuclear calcium spiking responses in Mt wt ROCs elicited by FsK/FoM fungal exudate pretreated with chitinase or heat.

Calcium spiking responses were recorded in a low-trichoblast-region located 10-20 mm from the root tip. *M. truncatula* wt ROCs expressing the NupYC2.1 cameleon were used for the bioassay. Fungal exudates derived from FsK or Fom were used as elicitors.

(A) Chitinase pretreated FsK or FoM exudate elicits nuclear calcium spiking in a statistically significant lower number of cells.

(B) Heat treatment of the fungal exudates, elicits nuclear calcium spiking in a statistically significant lower number of cells only in the FsK fungal exudate. Extending the period of heat treatment from 20 min to 1 h does not further affect the number of cells showing calcium spiking upon treatment with FsK fungal exudate.

Light/dark grey bars: percentages of cells responding with calcium spiking to FsK/Fom treated exudate, respectively.

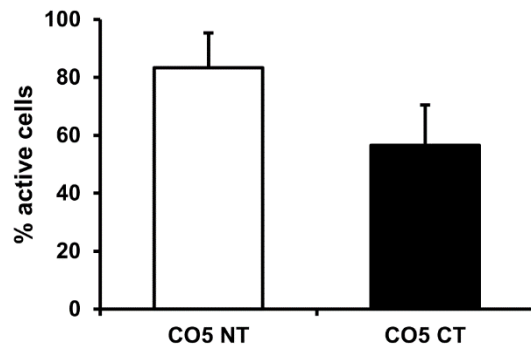
Data for panel A and B are presented as means and standard errors of biological replicates (individual lateral root segments derived from ROCs) as indicated in panel C.

(C) Summary of ROC segments (biological replicates), and total nuclei screened upon application of the treated with chitinase or heat FsK/FoM fungal exudate.

(D) Summary of p-values estimated based on Student's t-test (0.05 level). Comparisons were conducted in % of cells responding to untreated versus treated fungal exudates.

% of cells responding to untreated fungal exudates are shown in Figure 4-3A.

NT, non-treated exudate; CT, chitinase treatment; ACL, autoclave treatment



Supplementary Figure 4-12 Partial abolishment of nuclear calcium spiking in *Mt* wt ROC epidermis upon chitinase treatment of chitooligosaccharides.

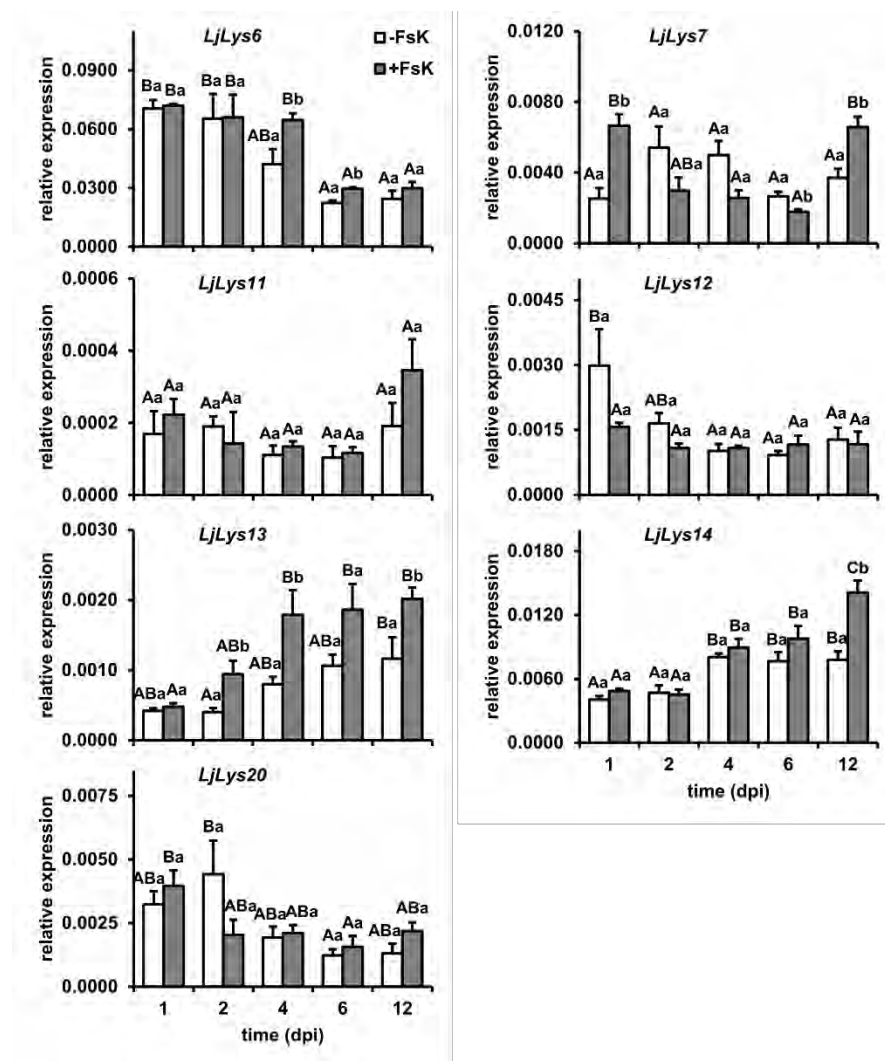
Calcium spiking responses were recorded in a low-trichoblast-region located 10-20 mm from the root tip. *M. truncatula* wt ROCs expressing the NupYC2.1 cameleon were used for the bioassay. Untreated CO5 solution and CO5 solution enzymatically treated with *S. griseus* chitinase were used as elicitors.

Percentage of responsive cells (peak number > 2), in 30 min recordings post CO5 (non-treated and chitinase-treated) elicitation.

Data are presented as means and standard errors of 3 biological replicates (individual lateral root segments derived from ROCs).

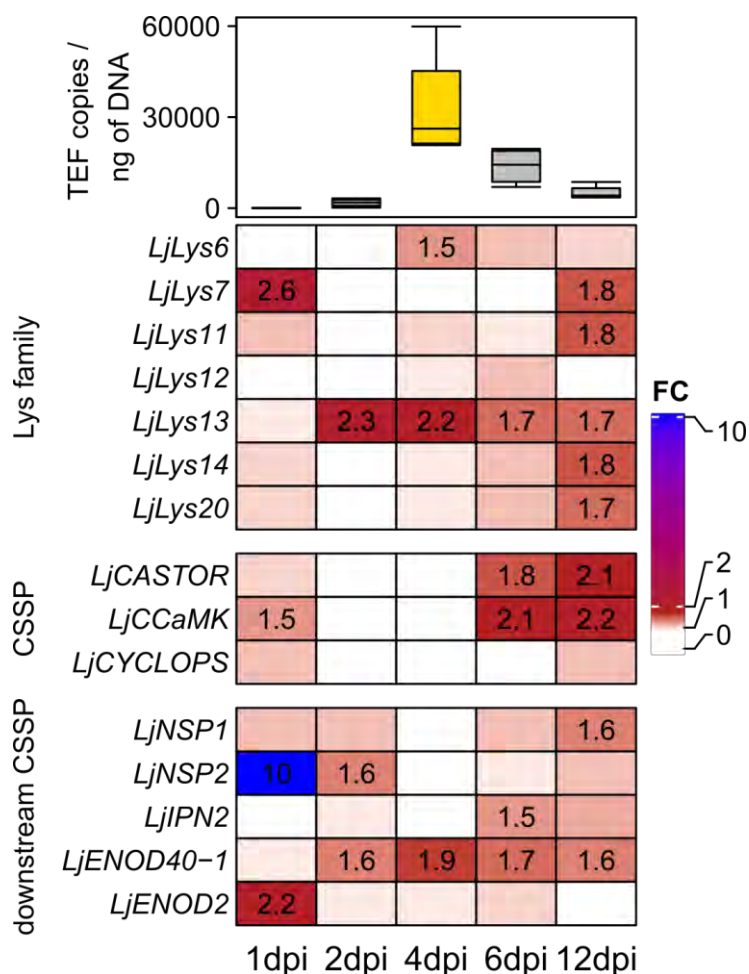
Statistical analysis showed no statistically significant difference in the % of cells responding to non-treated versus chitinase-treated CO5 solution at the 0.05 level (Student's *t*-test).

White/black bars: % of responsive cells upon non-treated (CO5 NT) or chitinase-treated (CO5 CT) elicitation, respectively.



Supplementary Figure 4-13 Temporal gene expression analysis of *L. japonicus* *LysM* genes upon *FsK* treatment. Temporal quantitative RT-PCR analysis of *Lj Lys6*, *Lys7*, *Lys11*, *Lys12*, *Lys13*, *Lys14*, and *Lys20* transcripts in control and *FsK*-inoculated *L. japonicus* root tissues. Expression levels are normalized to *Lj UBIQUITIN* housekeeping gene. Data are presented as means and standard errors of 3-4 biological replicates of 3-4 plants. Different uppercase letters denote significant differences within the same treatment at the 0.05 level, whereas different lowercase letters, significant differences within the same time at the 0.05 level (two-Way Anova, Tukey's test).

White/grey bars, expression in control/*FsK* inoculated tissues, respectively.



Supplementary Figure 4-14 Heatmap summarizing fold-changes in relative transcript levels of genes examined in the present study

Temporal fold-changes in transcript levels of all genes investigated in the present study are summarized and presented as a heatmap. Fold-change values are indicated within each cell, only $FC > 1.45$ are presented. Gene expression analysis is also presented in detail in Supplementary Figures 4-1 and 4-8.

Colour code: $0 < FC < 1$, white; $1 < FC < 2$, firebrick; $2 < FC < 11$, blue.

Top annotation of the heatmap: Box-plots represent the temporal quantification of fungal abundance within *FsK*-inoculated *L. japonicus* roots tissues, via qPCR, using primers specific for a fragment of *TEF1a* gene. Tissues were collected at 1, 2, 4, 6, 12 dpi. Values are normalized to ng of total DNA isolated.

Boxplots are created using the values of 4 biological replicates per time point; each biological replicate consisting of 3 plants. Boxplots extend from the 25th to 75th percentile, respectively; the midline indicates the median of the distribution; whiskers go down to the smallest value and up to the largest, thus showing all data points.

Different box colours indicate significant differences in fungal abundance (gene copy number average values), among the different time points investigated, at the 0.05 level (one-way Anova, Tukey's test).

Supplementary Table 4-1 Summary of individual Mt ROC segments (biological replicates), total plant cell nuclei, and total number of peaks screened for the measurements presented.

(A) Summary of individual ROC segments (biological replicates), and total plant cell nuclei screened upon application of fungal exudates

(B) Summary of total plant cell nuclei used to calculate delay time, and total peaks used to calculate spike width upon application of fungal exudates. Only responsive cells (peak number>2) were used for the analysis.

(C) Summary of the total number of dmi2-2 and dmi3-1 ROC segments (biological replicates), and total nuclei screened upon FsK/FoM/P. indica exudate treatment. The total number of cells (active and non-active) was used in the analysis and is presented.

A. Total nuclei screened upon elicitation of <i>Mt</i> wt ROC lines with fungal exudates			
Fungal exudate	ROC lines	ROC segments (biological replicates)	Nuclei screened
FsK	wt	7	85
Fom	wt	3	38
P. indica	wt	6	78
B. Total nuclei screened for calculations of delay time and total peak number screened for calculations of peak width			
Fungal exudate	ROC lines	Nuclei screened for initial delay time	Peaks screened for width
FsK	wt	59	316
Fom	wt	31	156
P. indica	wt	34	135
C. Total nuclei screened upon elicitation of <i>Mt dmi2-2</i> and <i>dmi3-1</i> with fungal exudates			
Fungal exudate	ROC lines	ROC segments (biological replicates)	Nuclei screened
FsK	dmi2-2	3	42
	dmi3-1	6	70
Fom	dmi2-2	3	28
	dmi3-1	4	43
P. indica	dmi2-2	3	37
	dmi3-1	3	36

Supplementary Table 4-2 Primer sequences used in the present work

Target	Sequence (5'-3'), (F, forward; R, reverse)	Reference
Check for genomic DNA contamination in DNase treated RNA		
<i>LjUBIQUITIN</i>	F: ATGCAGATCTTTTGTGAAGAC	(Flemetakis et al., 2000)
	R: ACCACCACGGAAGACGGAG	(Flemetakis et al., 2000)
Expression analysis (qPCR)		
<i>LjUBIQUITIN</i>	F: TTCACCTTGTGCTCCGTCTTC	(Hayashi et al., 2005)
	R: CCAGAAGAGGCCACAACAAAC	
<i>LjLys6</i>	F: TTCAGTTGCGAAGATGGCCC	(Lohmann et al., 2010)
	R: AACATCCCAGTCGTCAGTGG	(Lohmann et al., 2010)
<i>LjLys7</i>	F: TACCCTCTTGACTCCGTATTTAAGGTGTC	(Lohmann et al., 2010)
	R: TCCAGACATTAGATGCACCAAAGCTTGA	(Lohmann et al., 2010)
<i>LjLys11</i>	F: AGCCTCTGTCAAGACCAACC	(Lohmann et al., 2010)
	R: CCCACAAGTCCATGATCTCTC	(Lohmann et al., 2010)
<i>LjLys12</i>	F: ATGGACCCCTTGAGTGAGTGG	(Lohmann et al., 2010)
	R: TGGATGTGAGGAGGAGAAGTG	(Lohmann et al., 2010)
<i>LjLys13</i>	F: GTTGAACGCTCCAGATCTGTTAGC	(Lohmann et al., 2010)
	R: GTGTAGTGAGGGTGAAAATGATCC	(Lohmann et al., 2010)
<i>LjLys14</i>	F: GGGATCCATCTGATGAACTC	(Lohmann et al., 2010)
	R: CACAGAATTTATTATGGCTTCAG	(Lohmann et al., 2010)
<i>LjLys20</i>	F: CCACATCCTTCTAAGTACATGTTAGG	(Lohmann et al., 2010)
	R: ACCATGATTATTGCGCCGCCAG	(Lohmann et al., 2010)
<i>LjCASTOR</i>	F: ATGGTGGCCTTGACATAAG	(Imaizumi-Anraku et al., 2005)
	R: AGTGACGACGTATAACAGCA	(Imaizumi-Anraku et al., 2005)
<i>LjCCaMK</i>	F: TCCCTCTTAGCAACCGCGTATA	
	R: AGCACAAACGGAGAGCATCA	
<i>LjCYCLOPS</i>	F: GCTGGCAGATGAAAAAGAGC	(Yano et al., 2008)
	R: GCGTGTTTGAGCACAAACATT	(Yano et al., 2008)
<i>LjNSP1</i>	F: ATTCCCATCCAGCTTCCAC	(Lopez-Gomez et al., 2012)
	R: GAGGTCGAGCTTTGTTGAGG	(Lopez-Gomez et al., 2012)
<i>LjNSP2</i>	F: CATCGACTCCATGATTGACG	(Lopez-Gomez et al., 2012)
	R: GGTTGTTGTTGTCGTGGTTG	(Lopez-Gomez et al., 2012)
<i>LjIPN2</i>	F: GAGCCCTTTGATGTGGAGTGA	
	R: GCTCTTCTTGGTGATGGCCT	
<i>LjENOD40-1</i>	F: GGAGGTATGCTCAAACATTC	(Flemetakis et al., 2000)
	R: CCTACTCATCTGCAGAAACTG	(Flemetakis et al., 2000)
<i>LjENOD2</i>	F: CAGGAAAAACCAACACCTGT	(Radutoiu et al., 2003)
	R: ATGGAGGCGAATACACTGGTG	(Radutoiu et al., 2003)
Quantification of Fsk colonization within <i>Lotus japonicus</i> root tissues		
<i>Fusarium-ITS</i>	F: TGGTCATTTAGAGGAAGTAA	(Skiada et al., 2019)
	R: GGTATGTTACAGGGTTGATG	(Skiada et al., 2019)
<i>Fusarium-TEF1a</i>	F: CCCCTCCAGGATGTCTACAA	(Skiada et al., 2019)
	R: GGAAGACCCTCAGTGAGCTG	(Skiada et al., 2019)

Chapter 5
Activation of chitin-induced, defense genes in *L. japonicus*-Fsk
interaction

5 Activation of chitin-induced, defense genes in *L. japonicus*-Fsk interaction

5.1 Introduction

Plant-interacting microbes secrete MAMPs, acting as elicitors of plant defense, at the microbe-host interface. Perception of MAMPs (including chitin) by plant cells leads to induced defense responses: production of reactive oxygen species (ROS), production of reactive nitrogen species (such as nitric oxide), alterations in the plant cell wall, induction of antimicrobial compounds (such as phytoalexins), and the synthesis of pathogenesis-related (PR) proteins (Newman et al., 2013). Chitin is a long-chain polymer of N-acetylglucosamine and is the second most abundant fiber of fungal cell wall. Chitooligosaccharides, the fragments of chitin, are ligands of LysM domain containing proteins.

Symbiotic signals are primarily chitinaceous, though evidence arise for chitinase-resistant molecules acting as symbiotic signals in non-legume symbiotic associations (Chabaud et al., 2016). While suppression of plant defense responses occurs during establishment of the LRS (Mithöfer, 2002), defense responses have also been reported. In alfalfa-*R. meliloti* system, after the successful establishment of the first nodule primordia, the plant eliminates further infection, by eliciting a hypersensitive-like response (aborted infection threads in cortical cells where both symbionts undergo necrosis, phenolics and phytoalexins accumulation, defense proteins accumulation) (Vasse et al., 1993).

Chitin receptors in *A. thaliana* (CERK1 or LysM RLK1) and rice (CEBiP) are LysM motif containing proteins. CERK1 possesses a kinase domain (Miya et al., 2007) (Wan et al., 2008), whereas CEBiP necessitates an additional component for signaling through the PM into the cytoplasm, since it lacks intracellular domains (Kaku et al., 2006). In rice, chitin signaling has been linked to symbiosis, as the OsCERK1 receptor forms a complex with the LysM protein OsCEBiP in the presence of chitin, serves both chitin and AM COs perception, and is required for mycorrhization (Zhang et al., 2015a) (Carotenuto et al., 2017).

Chitin perception in plants leads to changes in expression levels of certain genes, within minutes after exposure to the polysaccharide (Hamel and Beaudoin, 2010). These Chitin Responsive Genes (CRGs) include *Wrkys*, a super family of TFs, so far only identified in plant kingdom (Eulgem et al., 1999). *Wrkys* encode for TFs that recognize W-box elements in promoters of defense related genes. *Wrky33* and *Wrky53* are two TFs previously found to be regulated by chitin both in *Arabidopsis thaliana* and *Lotus japonicus* (Wan et al., 2004) (Wan et al., 2008) (Lohmann et al., 2010), and are considered important components of the pathway involved in chitin signaling in *Arabidopsis* (Wan et al., 2004).

(Liu et al., 2003) used cDNA arrays and expression profiling to obtain insights into the transcriptional alterations associated with the development of a mycorrhizal symbiosis between *M. truncatula* and an AM fungus. A set of defense-related genes was recorded to be induced at early stages of the interaction. These genes showed a subsequent decrease as the symbiosis developed. *Wrkys* differential regulation seems to be a general plant response to colonization by fungi. *Wrky* TFs have been recorded to be induced during root colonization both by symbiotic (Güimil et al., 2005) (Gallou et al., 2012) and by pathogenic fungi (Güimil et al., 2005).

5.2 Materials and methods

5.2.1 Plant materials

L. japonicus wt plants (ecotype 'Gifu') were used for gene expression analysis experiments.

Fusarium solani strain K was routinely cultured, and conidia were isolated for inoculation of *L. japonicus* plants, as described in the corresponding Materials and methods section of Chapter 4.

5.2.2 Experimental setup for gene expression analysis

Experimental procedures are described in the corresponding sections of Chapter 4 ('Experimental setup for gene expression analysis', 'RNA isolation', 'Gene expression analysis')

5.2.3 Statistical analysis

Two-way ANOVA followed by Tukey's post-hoc test was used in gene expression analysis data.

5.3 Results

By searching the publicly available genomic database of *Nectria haematococca* (anamorph state: *Fusarium solani*) (<https://genome.jgi.doe.gov/Necha2/Necha2.home.html>) (Coleman et al., 2009) 15 genes with putative chitin synthase activity were identified. It was anticipated that FsK produces chitin-based molecules potentially acting as elicitors of plant defense responses. The involvement of chitin-induced, defense related genes during FsK-*Lotus* interaction was therefore examined.

qPCR analysis was used to determine the expression pattern of genes regulated upon chitin perception. The following genes were examined: the TFs *LjWrky33* and *Wrky53*, *LjCP40* involved in antimicrobial compounds biosynthesis, and the pathogenesis related protein *LjPRp27b* (Figure 5-1).

Both *Wrky* genes showed an induction upon FsK presence in root tissues. *Wrky33* transcript levels show no significant difference in FsK treated roots in comparison to controls up to 6dpi. At the relatively advanced stage of 12dpi though, a >5-fold upregulation is recorded. *Wrky53* showed a ~2-fold induction at 4dpi. Statistically significantly elevated transcript levels are also observed at 6 and 12 dpi. Both *Wrky* genes examined are induced at late stages of *FsK-Lotus* interaction. It should be noted that *LjLys13* and *Lys14* are also regulated at relatively late stages of the interaction system (Chapter 4, Supplementary Figure 4-14). Increased induction of both *Wrky* genes at late stages of the plant-fungal interaction (12 dpi) coincides with arrested fungal intraradical progression at this time point (Chapter 4, Supplementary Figure 4-14).

Temporal analysis of *LjCP450* transcripts upon FsK-*Lotus* interaction, revealed that *LjCP450* transcripts increase 11-fold in at 4 dpi in comparison to control plants. Afterwards, a decline in transcript levels is observed. Increased *CP450* transcript levels at 4 dpi coincides to the increased intraradical fungal levels at that specific time point. The induction in expression of *CP450* precedes the induction of *Wrkys* transcript levels.

The transcript levels of the pathogenesis related (PR) protein *LjPRp27b* were also examined. *LjPRp27b* is highly induced (>25-fold of induction) 4-6 dpi. Transcript levels in FsK-inoculated plants remain high up to the last time point investigated (12 dpi), indication that defense-related gene expression takes place in this plant-fungal system. This is in accordance to *Wrky* and phytoalexin synthesis (*CP450*) - related gene expression recorded from 4dpi and on. It is of interest that defense-related gene expression (PR and phytoalexin biosynthesis genes) coincided with the time point of maximal recorded intraradical fungal progression (4dpi). At later time points (6 dpi and on), the reduced intraradical levels of fungal abundance coincided with chitin-related gene induction.

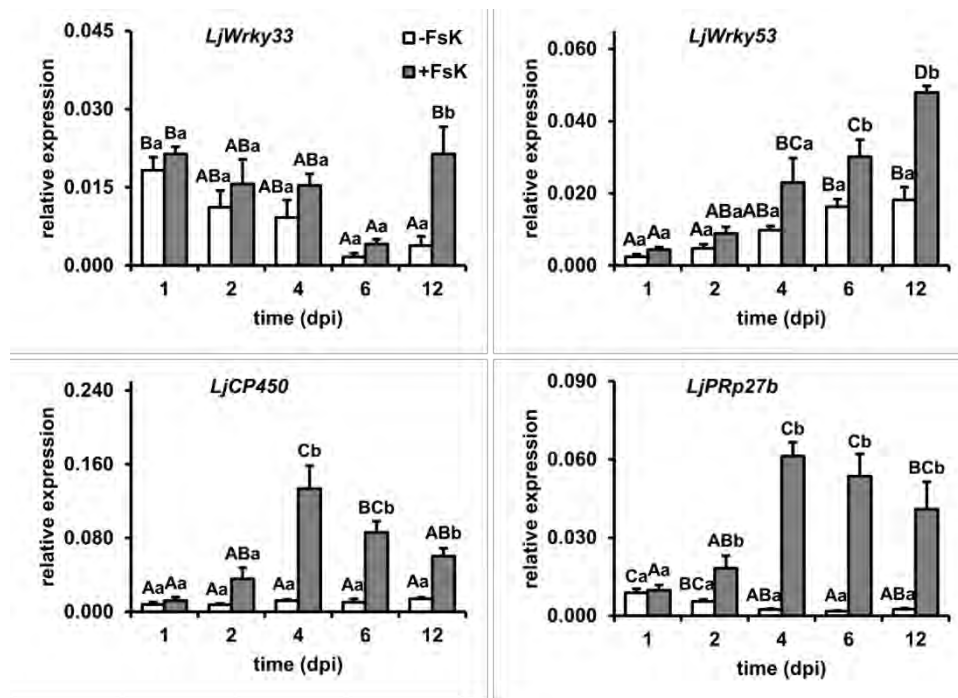


Figure 5-1 Relative expression analysis of *Wrky33*, *Wrky53*, *LjPRp27b* and *LjCP450* transcripts in roots of *FsK* inoculated *L. japonicus* plants.

Temporal quantitative RT-PCR analysis of *Lj Wrky33*, *Wrky53*, *PRp27b*, *CP450* transcripts in control and *FsK*-inoculated *L. japonicus* root tissues. Expression levels are normalized to *Lj UBIQUITIN* housekeeping gene. Data are presented as means and standard errors of 3 to 4 biological replicates of 3-4 plants.

Different upper case letters denote significant differences within the same treatment at the 0.05 level, whereas different lower case letters, significant differences within the same time at the 0.05 level (2-Way Anova, Tukey's test).

White bars, expression in control tissues; grey bars, expression in inoculated tissues.

To summarise, chitin-related, antimicrobial-compounds-synthesis-associated gene expression takes place in *FsK-Lotus* interaction. It is of interest that major expression levels of defense-related genes such as *Wrky* TFs coincides with *LysM*-gene expression and lower levels of fungal intraradical ingress.

5.4 Discussion

Nectria haematococca possesses multiple chitin synthase genes responsible for synthesis of chitosaccharidic molecules. Chitosaccharides of varying degree of polymerization can be secreted in the proximity of the plant epidermis. Such molecules can be perceived by LysM RLKs at the plant cell surface leading to defense gene activation. In the FsK-legumes system, defense genes and chitin induced TFs are activated, at relatively late stages of the interaction, as verified by gene expression analysis. The genes examined via qPCR were not regulated at early stages, a mechanism that may allow initial establishment of colonization. Defense gene activation coincides to maximal intraradical fungal representation, maybe as a plant mechanism to limit further fungal progression. FsK is a fast growing filamentous fungus. Cell death and plant cell wall strengthening via papilla deposition at penetration sites is implicated in FsK colonization process of *Lotus japonicus* (discussed in Chapter 2). These processes may be associated to retardation or restriction of fungal proliferation. Synthesis of antimicrobial compounds such as phytoalexins can create an unfriendly host environment that can confine microbial progression. *LjCP450* primers (Lopez-Gomez et al., 2012), used herein, amplify the previous designated *LjCYP-2* clone (belonging to the CYP81E family). *LjCYP-2*, as well as *A. thaliana CP450* encode for enzymes essential for phytoalexins biosynthesis (Shimada et al., 2000) (Nafisi et al., 2007).

Wrkys differential regulation is a general plant response to colonization by fungi: they are induced during root colonization by symbiotic, and by pathogenic fungi (Güimil et al., 2005) (Gallou et al., 2012). *LjPRp27b* is induced 1h post NF, chitin or the flg22 treatment in wt *L. japonicus* roots. *nfr1* mutants show no increase in transcript levels of *LjPRp27b* (Nakagawa et al., 2011).

Wrkys gene activation occurs at late time points of the interaction and coincides with a decline in FsK intraradical abundance. On the other hand, activation of the gene coding for the PR protein 27b occurs at 4dpi, and coincides with the highest levels of FsK ingress in the root system.

Together, these results point out that activation of defense genes and CRGs takes place in FsK-*Lotus* interaction, in parallel to utilization of the CSSP (as discussed in Chapter 4), but at late stages. This could act as a plant mechanism for restriction of fungal progression, though this requires further investigation.

5.5 References

- Carotenuto G, Chabaud M, Miyata K, Capozzi M, Takeda N, Kaku H, Shibuya N, Nakagawa T, Barker DG, Genre A. 2017.** The rice LysM receptor-like kinase OsCERK1 is required for the perception of short-chain chitin oligomers in arbuscular mycorrhizal signaling. *New Phytologist* **214**: 1440–1446.
- Chabaud M, Gherbi H, Pirolles E, Vaissayre V, Fournier J, Moukouanga D, Franche C, Bogusz D, Tisa LS, Barker DG, et al. 2016.** Chitinase-resistant hydrophilic symbiotic factors secreted by *Frankia* activate both Ca²⁺ spiking and *NIN* gene expression in the actinorhizal plant *Casuarina glauca*. *New Phytologist* **209**: 86–93.
- Coleman JJ, Rounsley SD, Rodriguez-Carres M, Kuo A, Wasmann CC, Grimwood J, Schmutz J, Taga M, White GJ, Zhou S, et al. 2009.** The Genome of *Nectria haematococca*: Contribution of Supernumerary Chromosomes to Gene Expansion. *PLoS Genetics* **5**: e1000618.
- Eulgem T, Rushton P, Schmelzer E, Hahlbrock K, Somssich IE. 1999.** Early nuclear event in plant defence: rapid gene activation by WRKY transcription factors. *The EMBO Journal* **18**: 4689–4699.
- Flemetakis E, Kavroulakis N, Quaedvlieg NE, Spaink HP, Dimou M, Roussis A, Katinakis P. 2000.** *Lotus japonicus* contains two distinct ENOD40 genes that are expressed in symbiotic, nonsymbiotic, and embryonic tissues. *Molecular plant-microbe interactions : MPMI* **13**: 987–94.
- Gallou A, Declerck S, Cranenbrouck S. 2012.** Transcriptional regulation of defence genes and involvement of the WRKY transcription factor in arbuscular mycorrhizal potato root colonization. *Functional and Integrative Genomics* **12**: 183–198.
- Güimil S, Chang H-S, Zhu T, Sesma A, Osbourn A, Roux C, Ioannidis V, Oakeley EJ, Docquier M, Descombes P, et al. 2005.** Comparative transcriptomics of rice reveals an ancient pattern of response to microbial colonization. *Proc Natl Acad Sci USA* **102**: 8066–8070.
- Hamel L-P, Beaudoin N. 2010.** Chitooligosaccharide sensing and downstream signaling: contrasted outcomes in pathogenic and beneficial plant – microbe interactions. *Planta* **232**: 787–806.
- Hayashi M, Tansengco ML, Suganuma N, Szczyglowski K, Krusell L, Ott T, Udvardi MK. 2005.** *Lotus japonicus* handbook. In: Marquez AJ, Stougaard J, Udvardi MK, Parniske M, Spaink H, Saalbach G, Webb J, Chiurazzi M, eds. *Lotus japonicus Handbook*. Springer, 53–82.
- Kaku H, Nishizawa Y, Ishii-minami N, Akimoto-tomiyama C, Dohmae N, Takio K, Minami E, Shibuya N. 2006.** Plant cells recognize chitin fragments for defense signaling through a plasma membrane receptor. : 1–6.
- Liu J, Blaylock LA, Endre G, Cho J, Town CD, Vandenbosch KA, Harrison MJ. 2003.** Transcript Profiling Coupled with Spatial Expression Analyses Reveals Genes Involved in Distinct Developmental Stages of an Arbuscular Mycorrhizal Symbiosis. *The Plant Cell* **15**: 2106–2123.
- Lohmann GV, Shimoda Y, Nielsen MW, Jørgensen FG, Grossmann C, Sandal N, Sørensen K, Thirup S, Madsen LH, Tabata S, et al. 2010.** Evolution and Regulation of the *Lotus japonicus* LysM Receptor Gene Family. *Molecular Plant-Microbe Interactions* **23**: 510–521.
- Lopez-Gomez M, Sandal N, Stougaard J, Boller T. 2012.** Interplay of flg22-induced defence responses and nodulation in *Lotus japonicus*. *Journal of Experimental Botany* **63**: 393–401.
- Mithöfer A. 2002.** Suppression of plant defence in rhizobia–legume symbiosis. *Trends in Plant Science* **7**: 440–444.

- Miya A, Albert P, Shinya T, Desaki Y, Ichimura K, Shirasu K, Narusaka Y, Kawakami N, Kaku H, Shibuya N. 2007.** CERK1 , a LysM receptor kinase , is essential for chitin elicitor signaling in *Arabidopsis*. **104**.
- Nafisi M, Goregaoker S, Botanga CJ, Glawischnig E, Olsen CE, Halkier BA, Glazebrook J. 2007.** *Arabidopsis* cytochrome P450 monooxygenase 71A13 catalyzes the conversion of indole-3-acetaldoxime in camalexin synthesis. *Plant Cell* **19**: 2039–2052.
- Nakagawa T, Kaku H, Shimoda Y, Sugiyama A, Shimamura M, Takanashi K, Yazaki K, Aoki T, Shibuya N, Kouchi H. 2011.** From defense to symbiosis : limited alterations in the kinase domain of LysM receptor-like kinases are crucial for evolution of legume – *Rhizobium* symbiosis. *Plant Journal* **65**: 169–180.
- Newman M-A, Sundelin T, Nielsen JT, Erbs G. 2013.** MAMP (microbe-associated molecular pattern) triggered immunity in plants. *Frontiers in Plant Science* **4**: 1–14.
- Shimada N, Akashi T, Aoki T, Ayabe S. 2000.** Induction of isoflavonoid pathway in the model legume *Lotus japonicus*: Molecular characterization of enzymes involved in phytoalexin biosynthesis. *Plant Science* **160**: 37–47.
- Vasse J, de Bily F, Truchet G. 1993.** Abortion of infection during the *Rhizobium meliloti*-alfalfa symbiotic interaction is accompanied by a. *The Plant Journal* **4**: 555–566.
- Wan J, Zhang X, Neece D, Ramonell KM, Clough S, Kim S, Stacey MG, Stacey G. 2008.** A LysM Receptor-Like Kinase Plays a Critical Role in Chitin Signaling and Fungal Resistance in *Arabidopsis*. *The Plant Cell* **20**: 471–481.
- Wan J, Zhang S, Stacey G. 2004.** Activation of a mitogen-activated protein kinase pathway in *Arabidopsis* by chitin. *Molecular Plant Pathology* **5**: 125–135.
- Zhang X, Dong W, Sun J, Feng F, Deng Y, He Z, Oldroyd GED, Wang E. 2015.** The receptor kinase *CERK1* has dual functions in symbiosis and immunity signalling. *Plant Journal* **81**: 258–267.

5.6 Appendix of Chapter 5

Table 5-1 List of primers used in this the present chapter

Target	Sequence (5'-3'), (F, forward; R, reverse)	Reference
Check for genomic DNA contamination in DNase treated RNA		
<i>LjUBIQUITIN</i>	F: ATGCAGATCTTTTGTGAAGAC	(Flemetakis et al., 2000)
	R: ACCACCACGGAAGACGGAG	(Flemetakis et al., 2000)
Expression analysis (qPCR)		
<i>LjUBIQUITIN</i>	F: TTCACCTTGTGCTCCGTCTTC	(Hayashi et al., 2005)
	R: CCAGAAGAGGCCACAACAAAC	
<i>LjWrky33</i>	F: AATGAGGGTATATCAGCCCCTGG	(Lohmann et al., 2010)
	R: GGGTGTGTGCATTTATAGTAACTCCTTG	(Lohmann et al., 2010)
<i>LjWrky53</i>	F: GGAACCTCCCTCTCATGCTAGTTAAG	(Lohmann et al., 2010)
	R: CTCTTGCTATTGCTTGAGCCAGAAG	(Lohmann et al., 2010)
<i>LjCP450</i>	F: TAATGCTTGGGCCCTTCATAGGGA	(Lopez-Gomez et al., 2012)
	R: ATGCTGATTGCACGAATCGCCAAG	(Lopez-Gomez et al., 2012)
<i>LjPRp27b</i>	F: CATGGTTATGATGTTACTGCTCGT	(Nakagawa et al., 2011)
	R: GATCACTATAACCAGTCCTCATCT	(Nakagawa et al., 2011)

Chapter 6

Differential expression analysis of *Lotus japonicus* genes at early stages of *Lotus*-FsK interaction using an RNA sequencing approach

Bioinformatic analysis was conducted by Sotirios Vasileiadis

Analysis of the generated data was performed by Vasiliki Skiada

6 Differential expression analysis of *Lotus japonicus* genes at early stages of *Lotus*-FsK interaction using an RNA sequencing approach

6.1 Introduction

6.1.1 Background on transcriptomics analysis

With the term transcriptomics we refer to those techniques used to study an organism's transcriptome, that is the complete set of its RNA transcripts in a given developmental stage of the organism or a physiological condition (Wang et al., 2009). The information content of an organism is recorded in the DNA of its genome and expressed through transcription. mRNA serves as a transient intermediary molecule in the pipeline of genetic information, whilst non-coding³⁴ RNAs perform additional diverse functions (Lowe et al., 2017). Gene expression is the fundamental level at which the result of genetic and regulatory programs is observable (Berge et al., 2019). Understanding the transcriptome is necessary for interpreting the functional elements of the genome, as well as reveal the molecular constituents of cells and tissues. The key aims of transcriptomics are: a) to catalogue all species of transcript, including mRNAs, non-coding RNAs, and small RNAs, b) to determine the transcriptional structure of genes in terms of their start sites, 5' and 3' ends, splicing patterns and other post-transcriptional modifications, c) to quantify the changing expression levels of each transcript during development and under different conditions (Wang et al., 2009).

Different technologies have been developed to deduce and quantify the transcriptome:

- *Hybridization based gene expression technologies.* These include technologies such as DNA microarrays³⁵. Hybridization based approaches are high throughput³⁶ and relatively inexpensive. They have a series of limitations though: they rely on a pre-existing genomic sequence and they have high background levels owing to cross-hybridization. Their detection power is hindered by the fact that probe collection on a chip relies on the coverage and accuracy of both the genomic sequences and the clone libraries. Despite the above drawbacks, they require a lower workload and cost.
- *Sequencing-based gene expression technologies.* In contrast to microarrays, sequence-based approaches determine directly the cDNA sequence. They are based on a different strategy compared

³⁴ Non-coding RNA: an RNA molecule that is not translated into protein. Examples are: transfer RNAs (tRNAs), ribosomal RNAs (rRNA), small RNAs such as microRNAs, siRNAs etc.

³⁵ A microarray is a laboratory tool used to detect the expression of thousands of genes at the same time. DNA microarrays are microscope slides that are printed with thousands of tiny spots in defined positions, with each spot containing a known DNA sequence or gene. These slides are referred to as gene chips or DNA chips. The DNA molecules attached to each slide act as probes to detect gene expression. The process in which the cDNA molecules bind to the DNA probes on the slide is called hybridization. Following hybridization, the microarray is scanned to measure the expression of each gene printed on the slide. The expression levels of each transcript are obtained by reading out intensities of hybridization signals (basically fluorescently labelled cDNA hybridized to DNA probes) (<https://www.nature.com/scitable/definition/microarray-202>).

³⁶ A microarray assays large amounts of biological material and is considered a high-throughput technology. High-throughput sequencing refers to sequencing techniques that allow sequencing of thousands of strands at once.

to microarray technologies. Initially, Sanger sequencing³⁷ of cDNA or EST libraries³⁸ was used. This approach is relatively low throughput, expensive and generally not quantitative. Tag-based methods were developed to overcome limitations, including: serial analysis of gene expression (SAGE)³⁹, cap analysis of gene expression (CAGE)⁴⁰, massively parallel signature sequencing (MPSS)⁴¹. SAGE and MPSS do not require a pre-existing mRNA library, but instead, they use restriction endonucleases (i.e. tagging enzymes), to collect short tags (typically 10-22 bases) from each mRNA molecule, if a recognition site exists on the mRNA molecule. These tag-based sequencing approaches are high throughput and can provide precise, digital gene expression levels. Most of them are based though on the expensive Sanger sequencing technology, and a significant portion of the short tags cannot be uniquely mapped to the reference genome. Moreover, only a portion of the transcript is analyzed and isoforms cannot be distinguished from each other. These disadvantages limit the use of traditional sequencing technology in annotating the structure of transcriptomes. The tag-and-count methodologies allow though sampling of exhaustive amounts of transcripts, and allow identification of novel mRNAs (Wang et al., 2009) (Liu et al., 2007).

³⁷ Sanger sequencing: DNA polymerase incorporates deoxynucleotides at each step of template DNA strand extension. When a dideoxynucleotide is added, DNA extension terminates. Sanger dideoxy sequencing results in the formation of extension products of various lengths terminated with dideoxynucleotides at the 3' end. The extension products are then separated by electrophoresis. The speed at which a DNA fragment moves through the medium is inversely proportional to its molecular weight. This process of electrophoresis can separate the extension products by size at a resolution of one base. Fluorescence-based cycle sequencing system is an extension and refinement of Sanger dideoxy sequencing. Unlike Sanger's method, which uses radioactive material, cycle sequencing uses fluorescent dyes to label the extension products (<https://www.thermofisher.com>).

³⁸ Expressed sequence tags (ESTs) are fragments of mRNA sequences derived through single sequencing reactions performed on randomly selected clones from complementary DNA (cDNA) libraries.

³⁹ Serial Analysis of Gene Expression (SAGE): mRNA is extracted, reverse transcribed into stable double stranded-cDNA, the ds-cDNA is cleaved by restriction endonuclease enzymes, to produce ~11-nucleotide 'tag' fragments, the tags are ligated together to produce concatenated tags. The latter are sequenced using long-read Sanger sequencing. The sequences are de-convoluted to find the frequency of the tag. The tag frequency is used to report on transcription of the gene that the tag came from (Lowe et al., 2017).

⁴⁰ Cap Analysis of Gene Expression (CAGE): this method is a variant of SAGE that sequences tags from the 5' end of an mRNA transcript only. Therefore, the transcriptional start site of genes can be identified when the tags are aligned to a reference genome. It is a useful technique when aiming for promoter analysis and for the cloning of full-length cDNAs (Lowe et al., 2017).

⁴¹ Massively Parallel Signature Sequencing (MPSS): mRNA is isolated, reverse transcribed to cDNA, the cDNA is fused to a small oligonucleotide tag which allows the cDNA to be PCR amplified and then coupled to microbeads. The DNA templates on each microbead is hybridized to fluorescently labelled probes, sequenced for several rounds by repeated cycles of enzymatic cleavage with restriction endonucleases, and a signature sequence of 16-20 bases is obtained. Fluorescent imaging captures the signal from all of the beads, while affixed to a 2D surface, so DNA sequences are determined from all the beads in parallel. The templates on the beads are simultaneously analyzed using a fluorescence-based sequencing method (on a 2D surface) that does not require DNA separation. In a single operation, hundreds of thousands of sequences can be acquired simultaneously (Brenner et al., 2000).

Table 6-1 Comparison of contemporary transcriptomics methods. From (Lowe et al., 2017).

Method	RNA seq	Microarray
Throughput	High	Higher
Input RNA amount	Low ~ 1 ng of total RNA	Low ~ 1 µg of total RNA
Labor intensity	High (sample preparation and data analysis)	Low
Prior knowledge	None required, though genome sequence is useful	Reference transcripts required for probes
Quantitation accuracy	~90% (limited by sequence coverage)	>90% (limited by fluorescence detection accuracy)
Sequence resolution	Can detect SNPs and splice variants (limited by sequence accuracy of ~99%)	Dedicated arrays can detect splice variants (limited by probe design and cross-hybridization)
Sensitivity	10^{-6} (limited by sequence coverage)	10^{-3} (limited by fluorescence detection)
Dynamic range	$>10^5$ (limited by sequence coverage)	10^3 - 10^4 (limited by fluorescence saturation)
Technical reproducibility	>99%	>99%

RNA sequencing (RNA seq) is a novel, high-throughput⁴² DNA sequencing method for mapping and quantifying transcriptomes. It is a tool for profiling transcriptomes using deep-sequencing⁴³ technologies. It has advantages over existing approaches, which are briefly introduced in Table 6-1.

6.1.2 RNA sequencing technology and benefits

The power of sequencing RNA lies in the fact that both discovery and quantification can be combined in a single high-throughput sequencing assay (Conesa et al., 2016). RNA seq provides a quantitative system for profiling the transcriptome of organisms on a large scale (Berge et al., 2019). As mentioned above, RNA seq uses recently developed deep-sequencing technologies.

The general approach can be described in brief as follows (Figure 6-2): isolation of total RNA from a sample is followed by enrichment of target RNAs, which are fragmented to molecules of appropriate size, reverse-transcribed to cDNA (first strand), the RNA is degraded, and the first-strand cDNA is complemented to a double strand. Adapter sequences are ligated to the double-stranded cDNA. The cDNA library is amplified by PCR using parts of the adapter sequences as primers. Each molecule, is sequenced in a high-throughput manner to obtain short sequences from one end (single-end sequencing) or both ends (pair-end sequencing). Following sequencing, the resulting reads are either aligned to a reference genome, or to reference transcripts, or assembled *de novo*⁴⁴ without the genomic sequence. A genome-scale transcription map is reconstructed that provides information for both the

⁴² High-throughput sequencing technologies: they produce millions of short sequence reads and are routinely being applied to genomes, epigenomes, and transcriptomes (Oshlack et al., 2010).

⁴³ Deep-sequencing technologies aim for high number of unique reads of each region of a sequence.

⁴⁴ *De novo* assembly: assembling a transcriptome without the aid of a reference genome (genome that has already been sequenced and assembled).

transcriptional structure (discovery) and/or the level of expression (quantification) for each gene (Wang et al., 2009) (Berge et al., 2019).

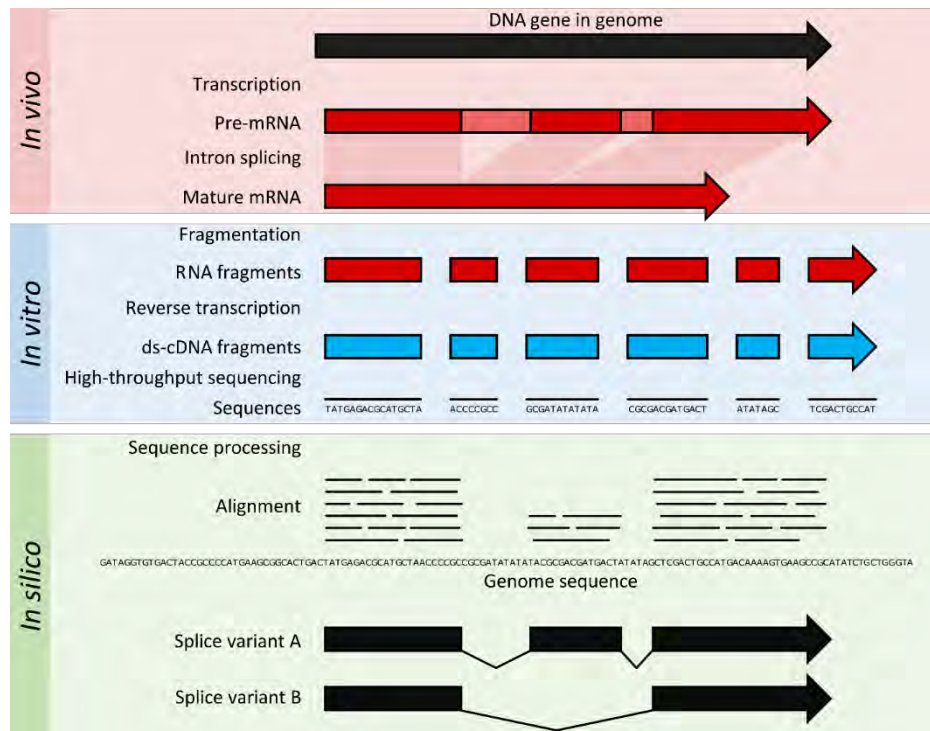


Figure 6-1 Summary of RNA sequencing. From (Lowe et al., 2017).

RNA seq offers several advantages over existing technologies:

- It allows identification of novel transcripts, as it is not limited to detecting transcripts that correspond to an already existing genomic sequence, unlike hybridization-based approaches. It is therefore ideal for non-model organisms.
- It is free of limitations that exist for other technologies (e.g. microarrays, PCR), such as the dependence on previous knowledge of the organism.
- It can reveal the precise location of transcription boundaries, to a single-base resolution.
- The short reads from RNA seq can provide information about how two exons are connected.
- It can reveal sequence variations (e.g., single nucleotide polymorphisms, SNPs) in the transcribed regions.
- It is useful for studying complex transcriptomes.
- It has a low background signal because DNA sequences can unambiguously be mapped to unique regions of the genome.
- Basically, there is no upper limit for transcript quantification, so the dynamic range for detection of gene expression levels is large. In contrast, DNA microarrays lack sensitivity for genes expressed either at low or very high levels and therefore have a much smaller dynamic range.
- RNA seq is highly accurate for quantifying expression levels, as determined using qPCR and spike-in RNA controls of known concentration.
- It produces results with high levels of reproducibility, for both technical and biological replicates.

- Since there are no cloning steps, it requires less RNA sample.
- It allows exploring inaccessible fields such as allele-specific expression⁴⁵, novel promoters and isoforms.

6.1.3 Main steps in an RNA sequencing experiment

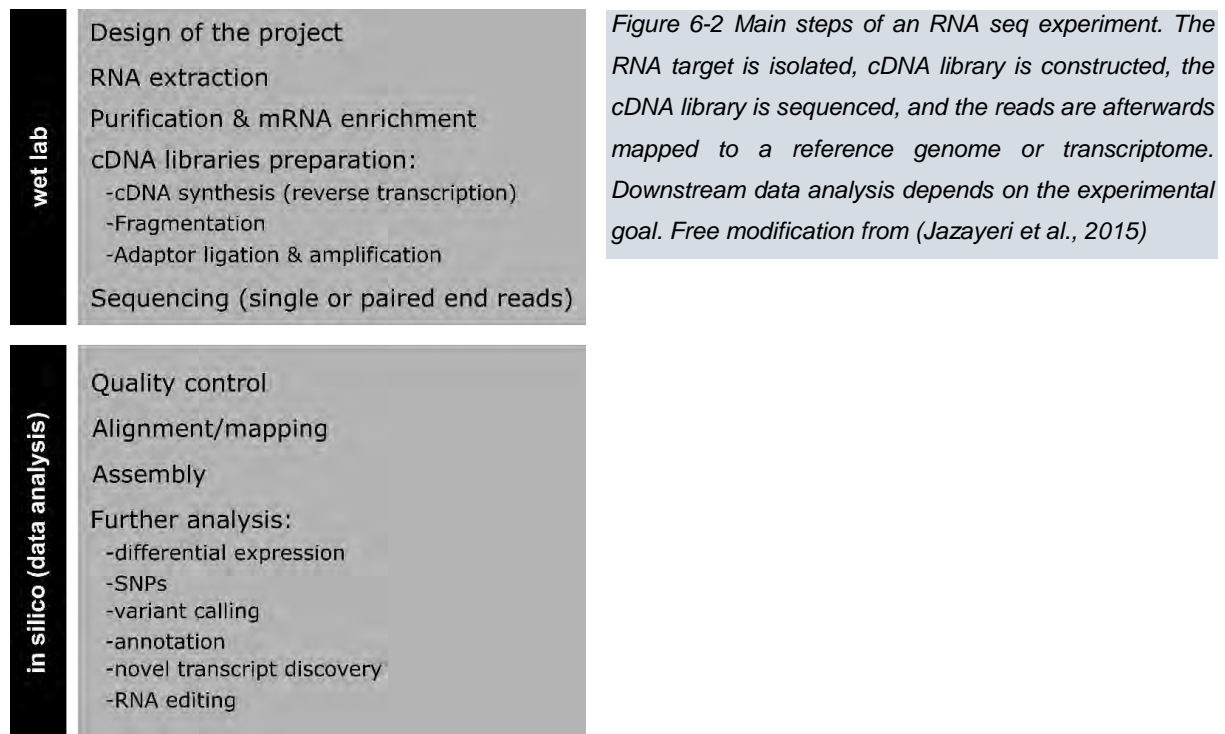
The main steps of a typical RNA experiment can be described as follows (Figure 6-3):

- RNA is isolated and purified from the samples of interest.
- Target RNAs are enrichment. In that way the sensitivity of the experiment is increased by enriching classes of RNA that are of interest, and depleting abundant RNAs. Enrichment methods are: a) mRNA enrichment via polyA⁴⁶ tail selection, or b) ribo-depletion to remove abundant but uninformative ribosomal RNAs (rRNAs) (~95% of total RNA). Small RNAs such as microRNAs, can be purified based on their size by gel electrophoresis and extraction.
- mRNAs are longer than the read-lengths of typical high-throughput sequencing methods. Therefore, selected RNAs are chemically or enzymatically fragmented prior to sequencing to fragments of the appropriate size (300-500 bp for Illumina TruSeq).
- Single stranded RNAs are reverse transcribed to cDNA. Therefore, DNA sequencing technologies apply to RNA seq. Direct sequencing of RNA can be also performed using nanopore sequencing which is able to detect modified bases that would otherwise be masked when sequencing cDNA, and also eliminates amplification steps that can otherwise introduce bias.
- Adapter sequences are either ligated to the 3' and 5' end of the double stranded cDNA or used as primers in the reverse transcription reaction.
- The final cDNA library consists of cDNA inserts flanked by an adapter sequence on each end, and is amplified by PCR using parts of the adapter sequences as primers, to enrich for fragments that contain the expected 5' and 3' adapter sequences. Amplification is also used to allow sequencing of low-input amounts of RNA (Berge et al., 2019) (Lowe et al., 2017).
- The library is loaded onto a flow cell where the cDNAs bind to short oligonucleotides complementary to the adapter sequence. A process known as 'sequencing by synthesis' follows. Single stranded templates are read as the complementary strand is generated. A single, fluorescently labelled deoxynucleoside triphosphate (dNTP) is added in each step. The label acts as a terminator and prevents the incorporation of more than one dNTP at the same time. After the fluorescently label has been imaged, it is enzymatically cleaved and the next dNTP can bind to the chain. Base calls are inferred directly from the measured fluorescent signal intensity. cDNA libraries can be sequenced in one of two modes: single-end or paired-

⁴⁵ Allele-specific expression refers to the differential abundance of the allelic copies of a transcript. It requires accurate determination of the prevalence of transcribed single nucleotide polymorphisms (SNPs) (Oshlack 2010).

⁴⁶ The polyA tail is a long chain of adenine nucleotides that is added to the 3' end of a messenger RNA molecule during RNA processing. The process is called polyadenylation, and makes the RNA molecule more stable and prevents its degradation. The polyA tail allows the mature mRNA molecule to be exported from the nucleus to the cytoplasm where it will be translated into protein by ribosomes.

end. In single-end mode, only one end of the cDNA insert is sequenced whereas in paired-end mode, both ends are sequenced, yielding two reads in opposite orientation, one from each end. There are cases that demand preservation of the coding strand information, for example when expressed RNAs originate from opposite strand of the same genomic locus. In these cases, specific protocols (unstranded vs stranded RNA seq) can be used that allow discrimination of the two strands. A stranded library can be generated by incorporation of dUTPs in the generation of the 2nd strand cDNA, the dUTP labeled cDNA is degraded before PCR amplification. Another approach is to use alternative adapter to distinguish between 5' and 3' ends of the RNA.



Most RNA seq experiments proceed with generation of 50 bp (single-end) or 100 bp (paired-ends), and comprise between 10 and 100 million reads, with a trend towards deeper sequencing over time. Progress in sequencing technology have enabled longer read lengths (e.g. Illumina MiSeq⁴⁷ at 250-300 bp) and much higher throughput for the same cost, but also much lower amounts of required starting material. Single-cell RNA seq is a rapidly emerging technique that can be used to sequence the sparse transcriptome of individual cells van (Berge et al., 2019).

6.1.4 RNA seq data analysis (pipeline for DE analysis)

A typical RNA seq pipeline for differential expression (DE) analysis entails the following steps:
Quality control. Sequence reads are not perfect, so the accuracy of each base in the sequence needs to be estimated prior to downstream analyses. Raw data are examined for: quality scores for base calls,

⁴⁷ Illumina MiSeq, HiSeq: The chemistry behind both systems is the same. One of the main differences is that HiSeq can generate more reads in comparison to MiSeq.

GC-content, over representation of short sequence motifs (k-mers), and for unexpected high read duplication rate.

Alignment. The first step in the RNA seq pipeline is the read mapping or alignment, that is the process to find the unique location where a short read is identical to the reference. There are certain things to consider when mapping to a genome or transcriptome: single nucleotide polymorphisms (SNPs), indels (insertions or deletions), mapping of reads that span exon boundaries, multimapping (reads that map equally well to several locations). Paired-end reads reduce the problem of multi-mapping. Both ends of the cDNA fragment from which the short reads were generated should map nearby the transcriptome, allowing resolving of the ambiguity in some cases. Alignment of primary transcript mRNA sequences derived from eukaryotes to a reference genome requires specialized handling of intron sequences, which are absent from mature mRNA. Assembly is the process in which mapped reads for each sample are assembled into gene, exon, or transcript level expression summaries. Assembly can be performed *de novo* or using a reference genome, transcriptome. De novo assembly can be used to align reads to one another to construct full-length transcript sequences without the use of a reference genome. Once assembled *de novo*, the assembly can be used as a reference for subsequent sequence alignment methods and quantitative gene expression analysis.

Quantification (summarizing mapped reads). After having obtained genomic locations for as many reads as possible, the next task is to summarize and aggregate reads over some biologically meaningful unit, such as exons, transcripts or genes. Reads that align equally well to multiple locations must be identified and either removed, aligned to one of the possible locations, or aligned to the most probable location.

Normalization. The summarized data are normalized in concert with the statistical testing of DE, leading to a ranked list of genes with associated p-values and fold changes (FC). Normalization enables accurate comparisons of expression levels between and within samples. Normalization methods differ for between- and within-library comparisons. When examining individual genes for DE between samples, technical biases, such as gene length and nucleotide composition, are not an issue, because the sequence used for comparison between samples is practically the same.

Between sample normalization is still essential for comparing counts from different libraries relative to each other. The simple and most commonly used normalization adjusts by the total number of reads in the library, accounting for the fact that reads assigned to each gene depends on the sequencing depth of the sample (more reads will be assigned to a gene if a sample is sequenced to a greater depth).

The most frequently used normalization methods are: RPM/CPM (reads or counts per million, respectively), RPKM (reads per kilobase of exon model per million mapped reads), RPKs (reads per kilobase), TPM (transcripts per million). Normalization methods are explained in Box 2 of this chapter.

Differential expression. This refers basically to the process of highlighting genes that have changed significantly in abundance across experimental conditions. Differential gene expression analysis requires that gene expression values should be compared among samples. This practically means, taking a table of summarized count data for each library and performing statistical testing between the samples of interest (Oshlack et al., 2010) (Conesa et al., 2016) (Lowe et al., 2017) (Chatterjee et al., 2018).

6.1.5 Packages used for analysis of RNA sequencing data

In RNA sequencing experiments, the expression level of each RNA unit (transcript) is a measure of the number of sequenced fragments that map (correspond) to that specific transcript, which is expected to directly correlate with the transcript's abundance level. The expression signal of a transcript is limited though by the sequencing depth⁴⁸ and is dependent on the expression levels of other transcripts. The main purpose of RNA seq analysis process is the identification of differentially expressed genes (DEGs) as accurately as possible. 3 main steps are performed in a differential gene expression analysis of such data: normalization of counts, parameter estimation of the statistical model, and tests for DE. Many statistical algorithms have been developed to implement different approaches for normalization and DE detection. Typical approaches use Poisson⁴⁹ or negative binomial distributions⁵⁰ to model the gene count data and a variety of normalization procedures (Rapaport et al., 2013). Among the most cited computational methods used for RNA seq data analysis are: cufflinks/cuffdiff2, edgeR, DESeq, PoissonSeq, bayseq, NOISeq, SAMseq, EBSeq, limma. Concerning the statistical models used by the various packages for DE detection, edgeR, DESeq and bayseq, cufflinks use negative binomial models, NOISeq and SAMseq use non-parametric approaches. Some methods (like edgeR) work directly on the count data. One of the most popular RNA seq tools, cufflinks, does not use matrices. Cufflinks takes BAM⁵¹ files as input and makes comparisons. This constitutes cufflinks more cumbersome due to the large file sizes and binary⁵² formats. Methods such as DESeq and edgeR that use count matrices as input are easier to handle and simulate for comparative evaluations Transcript based detection methods, like cuffdiff2 and EBSeq, also enable gene level DE reports (Seyednasrollah et al., 2013) (Soneson and Delorenzi, 2013). (Zhang et al., 2014).

A number of studies have conducted comparisons among the most widely used RNA seq analysis computational methods. It is widely accepted that increasing the number of replicate samples gives the most accurate results in terms of accurate identification of DEGs. Results based on sequencing depth and replication analysis demonstrate that the number of sample replicates is the most significant factor, especially in studies focusing on detecting differential expression among lowly expressed genes (Rapaport et al., 2013). This is also supported by (Schurch et al., 2015) who suggest that increasing replication gives a large increase in true positive rate⁵³ (TPR) when considering all DEGs but only a

⁴⁸ Sequencing depth: number of reads per sample

⁴⁹ A Poisson Distribution is a model for a series of discrete events where the average time between events is known, but the exact timing of events is random. The arrival of an event is independent of the event before. A Poisson process meets the following criteria: (a) events are independent of each other. The occurrence of one event does not affect the probability another event will occur, (b) the average rate (events per time period) is constant, (c) two events cannot occur at the same time. From: <https://towardsdatascience.com>

⁵⁰ Negative binomial distribution: the negative binomial experiment is almost the same as a binomial experiment with one difference: a binomial experiment has a fixed number of trials. If the following five conditions are met the experiment is negative binomial: (a) non-fixed number of n trials, (b) each trial is independent, (c) only two outcomes are possible (success and failure), (d) probability of success for each trial is constant, (e) a random variable Y= the number of trials needed to make r successes.

From: <https://www.statisticshowto.datasciencecentral.com>

⁵¹ BAM files: the binary version of sequence alignment data

⁵² Binary format: a format in which file information is stored in the form of ones and zeros, or in some other binary (two-state) sequence.

⁵³ True positive rate: explained in Box 1.

small increase for high fold-change genes. The authors suggest a $n > 6$ for biological replicates, rising to $n > 12$ when attempting to identifying differential gene expression irrespective of FC.

An important characteristic of the Poisson distribution is that the variance is equal to the mean, which equals λ , that is a real number equal to the expected number of reads from transcript fragments. In reality the variance of gene expression across multiple biological replicates is larger than its mean expression values. To address the over-dispersion problem⁵⁴, methods such as edgeR used the negative binomial distribution, where the relation between the variance and mean is calculated via a dispersion factor α . edgeR estimates α as a weighted combination of two components: a gene-specific dispersion effect and a common dispersion effect calculated from all genes. Cuffdiff computes a separate variance model for single-isoform genes and multi-isoform genes (Rapaport et al., 2013).

As mentioned above, many studies have performed comparisons among RNA seq analysis packages. We will focus on findings concerning edgeR and cufflinks/cuffdiff2 packages, to assist further reading, since these packages were used for analysis of *Lotus*-FsK interaction data.

edgeR (Robinson et al., 2009) uses a negative binomial statistical model. The package was developed to enable analysis of experiments with small numbers of replicates. An empirical Bayes⁵⁵ procedure is used to moderate the degree of over-dispersion across genes by borrowing information between genes. An exact test (analogous to Fisher's exact test)⁵⁶ but adapted to over-dispersed data is used to assess DE for each gene. The TMM normalization⁵⁷ procedure is carried out to account for the different sequencing depths between the samples, whereas the Benjamini-Hochberg procedure is used to control the false discovery rate⁵⁸ (FDR) (Robinson 2010) (Seyednasrollah et al., 2013). (Rapaport et al., 2013) report that methods based on negative binomial modelling (like edgeR) have improved specificity and sensitivities as well as good control of false positive errors with comparable performance. (Schurch et al., 2015) proposed edgeR as a good package of choice when replicate number is less than 12 per condition (they recommend edgeR even when the number of replicates is less than 3 and the fold-change threshold is 0.5 or 2). (Zhang et al., 2014) found that edgeR performs slightly better than cuffdiff2 in terms of the ability to uncover true positives. The package performed well when a dataset with no replicates was used. edgeR is a better choice than cuffdiff2 for DE analysis when sequencing depth is low (number of reads less than 10M). For edgeR, the correlation between the number of DEGs and the number of biological replicates is almost linear (the proposed number of replicates is 3 or 4, but for edgeR the number of DEGs increases almost linearly as the number of replicates increases).

⁵⁴ Over-dispersion: in statistics, over-dispersion is when a data set exhibits higher variability (statistical dispersion) than what would be expected based on a given statistical model.

⁵⁵ Bayes procedure: relies on incorporating prior probability distributions in order to generate posterior probabilities. Prior probability, is the probability of an event before new data are collected.

⁵⁶ Fisher's exact test: a test of significance that is used in the place of chi square test in 2 by 2 tables, especially in cases of small samples. The test is used when we have two nominal variables and we want to know if the proportions of one variable are different depending on the value of the other variable.

From <http://www.biostathandbook.com>

⁵⁷ TMM normalization, stands for trimmed mean of M values. It is the normalization method used in edgeR package. Since sequencing depth might differ between samples, a per-sample library size normalization must be performed before samples can be compared.

⁵⁸ False discovery rate: explained in Box 1.

Cuffdiff2 (Trapnell et al., 2010) uses a negative binomial distribution model (Schurch et al., 2016). It estimates expression at transcript-level resolution and controls for variability and read mapping ambiguity by using a beta negative binomial model for fragment counts. It is part of the cufflinks package developed for identification of DEGs and transcripts and revealing differential splicing and promoter-preference changes. The package enables to analyze signals at the transcript level, it reports DE also at the gene level. It uses an FPKM normalization procedure to account for the different sequencing depths and the Benjamini-Hochberg⁵⁹ procedure to control the FDR. A t-test is used to assess DE for each gene. The cuffdiff2 method specifically addresses the uncertainties in counts owing to ambiguous reads that easily result in false DE calls of genes especially with several similar isoforms (Seyednasrollah et al., 2013). (Rapaport et al., 2013) report that cuffdiff introduced a high number of false positives. This might relate to its normalization procedure, which attempts to account for both alternative isoform expression and length of transcripts. (Zhang et al., 2014) report that the number of DEGs detected by cuffdiff2 increases steadily with the number of replicates but with an obvious drop in the number of detected DEGs with 5 biological replicates. The authors mention that the differences in the statistical significance testing for the identification of DEGs between edgeR and cuffdiff are expected, since cuffdiff2 is designed to detect DE at the transcript level on different underlying models and assumptions compared to edgeR. They conclude that cuffdiff2 is not recommended for DE analysis at gene level resolution, particularly if sequencing depth is low (<10 million reads per individual sample). To summarize, there is no single package suitable for analysis of an RNA sequencing experiment. Most authors recommend the use of an increased number of replicates when designing RNA seq experiments and concerning the data analysis process, the use of more than one packages and the identification of the intersection of their DEGs list, are advisable methods to achieve accurate results (Zhang et al., 2014).

6.1.6 Applications of RNA seq technology

The applications of RNA sequencing technology are numerous. Genome annotation is the principal application. Many transcriptomes are still incomplete, even those of well-studied organisms such as humans, or model organisms such as mice, zebrafish, or fruit flies. Another important application area is that of gene regulation. RNA seq enables the comparison of gene/transcript/exon expression between different tissues, cell types, genotypes, experimental conditions, time points, etc. The ultimate purpose is identification of the set of genes that change in expression, in order to understand the molecular pathways that are used or altered, or the regulatory components that are utilized (Berge et al., 2019). Further RNA seq application areas include: spatial transcriptomics, where cellular positional information is maintained in the preparation of cDNA fragments; host-pathogen interactions via 'dual RNA seq', where the transcriptomes of both host and pathogen are simultaneously assayed; the analysis of

⁵⁹ Benjamini-Hochberg procedure: a tool that decreases the false discovery rate. Adjusting the rate helps to control for the fact that sometimes small p-values (less than 5%) happen by chance, which could lead to incorrectly reject the true null hypotheses. In other words, the B-H Procedure helps to avoid Type I errors (false positives). From <https://www.statisticshowto.datasciencecentral.com>

genetic variation among expressed genes; RNA editing⁶⁰ events; characterization of long intergenic non-coding RNAs⁶¹; meta-transcriptomics⁶²; single-cell⁶³ transcriptomics (Berge et al., 2019). Other current RNA usages include: developmental biology, genome diversity, cancer and diseases in human, phylogenetic studies, functional genomics, abiotic and biotic stress responses in plants, SNPs (Jazayeri et al., 2015).

6.1.7 Gene expression analysis and RNA sequencing techniques application in studying PMIs

Transcriptomics approaches have allowed the development of 'dual RNA seq', that is the investigation and determination of changes in gene expression in two organisms simultaneously (for example, a pathogen and the host). Eukaryotic host cells are subject to infection by various agents, from viruses to bacteria to eukaryotic parasites such as fungi and protozoa. Understanding the transcriptomes of both organisms can provide new insights into these complex interaction systems, e.g. by identifying new virulence factors in the pathogen, or new pathways in the host cell that respond to the exposure to specific pathogens, microbes in general, or Pathogen- or Microbe-Associated Molecular Patterns (PAMPs or MAMPs). RNA seq technique allows in parallel analysis on both transcriptomes. The major benefit of this approach is the potential to monitor changes in expression levels of genes in two different organisms to a high level of accuracy and depth (Westermann et al., 2012).

The last two decades a large number of studies have investigated the transcriptome changes in plant microbe interactions, with a primary focus on symbiotic ones. Interest has been paid into identifying a core set of genes common in Arbuscular Mycorrhiza (AM) and Legume Rhizobium (LR) symbiosis, while also searching for commonalities/differences with pathogenic interactions. Various studies have used microarrays and oligoarrays for identifying genes induced in a number of PMIs, whereas the use of high throughput technologies (RNA seq) is more recent.

A great attention has been given into the transcriptional changes occurring in AM and LR symbiosis in the model legumes *Lotus japonicus* and *Medicago truncatula* (Liu et al., 2003) (Manthey et al., 2004) (Frenzel et al., 2005) (Güimil et al., 2005) (Hohnjec et al., 2005) (Deguchi et al., 2007) (Gomez et al., 2009) (Guether et al., 2009) (Benedito et al., 2010) (Hogekamp et al., 2011) (Czaja et al., 2012) (Gallou et al., 2012) (Hogekamp and Küster, 2013). These analyses have identified a number of genes up and down regulated specifically during AM development. From the plant side of view, genes for plant lectins, blue copper proteins, peptide transporters, proteases, annexin, glutathione S transferases, Myb transcription factors have been identified as AM specific (Handa et al., 2015). Other studies have

⁶⁰ RNA editing: a process through which the nucleotide sequence specified in the genomic template is modified to produce a different nucleotide sequence in the transcript. It is an important mechanism of genetic regulation that amplifies genetic plasticity by allowing the production of alternative protein products from a single gene.

From <https://www.sciencedirect.com/topics/neuroscience/rna-editing>

⁶¹ Long intergenic non coding RNAs: autonomously transcribed non-coding RNAs (> 200 nucleotides) that do not overlap annotated coding genes.

⁶² Meta-transcriptomics: the study of the function and activity of the complete set of transcripts (RNA seq) from environmental samples. While metagenomics gives information about which microbes are present, metatranscriptomics gives information about their activity.

⁶³ Single-cell transcriptomics (scRNA seq): it enables working with very small amounts of starting mRNA, that can hypothetically be obtained from just a single cell (Conesa et al., 2016).

analyzed the transcriptome of isolated infected cells by using laser microdissection⁶⁴, and demonstrated the expression of genes for plant transporters, TFs, and lipid metabolism in arbusculated cortical cells (Gomez et al., 2009) (Guether et al., 2009) (Hogekamp et al., 2011) (Gaude et al., 2012) (Hogekamp and Küster, 2013). From the fungal side of view, transcriptome analysis of AM fungal genes was until recently relatively limited, but EST analysis and the genome sequencing of the AM fungus *Rhizophagus irregularis* (Tisserant et al., 2012) (Tisserant et al., 2013) (Lin et al., 2014) have advanced and contributed to the field.

Concerning LR symbioses, studies have used microarrays to identify genes specifically regulated during colonization of legumes by rhizobia (Kouchi et al., 2004) (Lohar et al., 2006). (Kelly et al., 2018) revealed distinct symbiotic transcriptomic responses of *L. japonicus* to its compatible symbiont *M. loti* R7A and a spectrum of interacting bacteria (from semi-compatible symbionts to pathogenic bacteria), by performing RNA seq analysis experiments. The authors did not record elicitation of defense responses by compatible rhizobia during the establishment of symbiosis, as recorded by previous studies (Kouchi et al., 2004).

Several studies have proceeded with comparative analysis among the two well-known symbiotic associations. (Manthey et al., 2004) used cDNA microarrays and *in silico* screening to identify *M. truncatula* genes induced in both root nodules and mycorrhized roots. (Deguchi et al., 2007) used cDNA microarrays to analyze the transcriptome of *L. japonicus* AM roots and compared results with those obtained from *M. loti* induced *L. japonicus* mature nodules. The authors found that phenylalanine ammonia lyase genes (PAL) and other phenylpropanoid biosynthesis related genes were moderately induced on the initiation of infection by the two symbionts and afterwards repressed upon establishment of the symbiosis. Defense genes were initially upregulated and afterwards repressed. In the more recent study of (Handa et al., 2015) RNA seq technology was used to compare transcriptome profiles of the two interactions, and found that the co-upregulated genes were not abundant, but transcripts encoding for membrane traffic related proteins, transporters and iron-transport related proteins were found to be highly co-up regulated.

Stepping away from the two well-studied symbiotic associations of legumes, many studies have analyzed plant transcriptome responses in endophytic, biocontrol, mutualistic, beneficial, pathogenic plant-microbe associations (Zuccaro et al., 2011) (Dupont et al., 2015) (Morán-Diez et al., 2012) (Plett et al., 2014) (Hiruma et al., 2016) (Güimil et al., 2005).

⁶⁴ Laser microdissection: a technology that allows the rapid procurement of selected cell populations from a section of heterogeneous tissues. It allows extraction of DNA, RNA, proteins and even metabolites from these cell populations (Balestrini et al., 2009).

BOX 1: RNA seq Glossary

p-value: The p-value takes into account the mean difference, the variance, and also the sample size. It is a measure of how likely we are to obtain a set data if no real difference existed. Usually, the cut-off used for p-value is 0.05.

False discovery rate (FDR): the expected proportion of false positives among the tests found to be significant. Another way to look at the difference between p-value and FDR is that a p-value of 0.05 implies that 5% of all tests will result in false positives. An FDR adjusted p-value (or q-value) of 0.05 implies that 5% of significant tests will result in false positives. The latter will result in fewer false positives.

q-value: the q-value is an adjusted p-value, taking into account the false discovery rate (FDR). Applying FDR becomes necessary when we are measuring thousands of variables (e.g. gene expression levels) from a small sample set.

False positives: a positive is a significant result, i.e. the p-value is less than the cut off value set, normally 0.05. A false positive is when there is a significant difference recorded where, in reality, none exists.

Multiple testing problem: the potential increase in Type I error (false positives) that occurs when statistical tests are used repeatedly (i.e. taking into consideration that a large number of DEGs are tested for significance in an RNA seq experiment). For example, if we have found 2000 DEGs in a dataset, and we apply an anova or t-test to each, then we would expect to get (2000*5%) 100 false positives by chance alone (with a p-value set at 0.05). This is known as the multiple testing problem.

From: <http://www.nonlinear.com/support/progenesis/comet/faq/v2.0/pq-values.aspx>

BOX 2: RNA seq normalization units

The concept of counting is the same with either type of read (single-end or paired-end, as each read represents a fragment that was sequenced).

A 'feature' is an expression feature, that is a genomic region containing a sequence that can normally appear in an RNA seq experiment (gene, isoform, exon).

Counts are the number of reads that align to a particular feature. The number of counts is heavily dependent on two things: a) the amount of fragments sequenced, b) the length of the feature.

Since counts are not scaled by the length of the feature, all units in this category are not comparable within a sample without adjusting for the feature length.

Within sample normalization: The number of fragments corresponding to a feature depends on its length. To compare features of different length we should normalize counts by the length of the feature. These methods of normalization allow for comparison of features with different length within a sample but not between samples.

Common normalization methods include:

- RPM, reads per million

$RPM = \text{read counts} / (\text{total reads} / 10^6)$

- CPM, counts per million. Normalization method used in edgeR, it does not allow normalization by transcript length and therefore is not reliable for comparing transcript abundance from different experiments.

The formula for CPM is the same as the one used for RPM

- RPKM, reads per kilobase of exon model per million reads, is a within sample normalization method that will remove the feature-length and library-size effects.

$RPKM = RPM / [\text{gene length (bp)} / 10^3] =$

$[\text{read counts} / (\text{total reads} / 10^6)] / [\text{gene length (bp)} / 10^3] =$

$[\text{read counts} / (\text{total reads} \times \text{gene length})] \times 10^9$

- FPKM, fragments per kilobase of exon model per million mapped reads, a within sample normalized transcript expression. It is calculated similarly to RPKM, but instead of reads, the cDNA fragments are counted and normalized.

The formula for FPKM is the same as for RPKM

- RPKs, reads per kilo base (of transcripts)

$$\text{RPK} = \text{Read counts} / [\text{gene length (bp)} / 10^3]$$

- TPM (Transcripts per Kilobase Million)

$$\text{TPM} = \text{RPK} / 10^6 = \Sigma[(\text{read counts}/\text{gene length (bp)} \times 10^3) / 10^6]$$

Where, read counts = number of reads mapped to a gene (or transcript) sequence; gene length = length of the gene sequence;
total reads = total number of mapped reads of a sample

RPKM and FPKM are equivalent for SE reads. Correcting for gene length is not necessary when comparing changes in gene expression within the same gene across samples, but it is necessary for correctly calculating gene expression levels within a sample taking into consideration the fact that longer genes accumulate more reads.

From: (Chatterjee et al., 2018)

6.2 Materials and methods

6.2.1 Plant and fungal material

Lotus japonicus wt (ecotype GIFU) plants were used in all experiments.

Fusarium solani strain K (Kavroulakis et al., 2007) was routinely cultured on PDA medium (26 °C, 5 d in the dark). FSK hyphal propagules were used for inoculations of *Lotus japonicus* plants by slightly scrapping with a sterile needle the surface of a fresh FSK culture on PDA.

6.2.2 Experimental setup and sample collection for RNA sequencing analysis.

Lotus japonicus wt seeds (ecotype Gifu) were chemically scarified with a 12-min sulfuric acid treatment, washed thoroughly with deionized water, surface sterilized for 20 min in a 20% NaOCl (v/v) solution and washed 6× with sterile deionized water. Seeds were kept in water at 4 °C overnight, to promote seed germination, placed afterwards on half strength MS medium (Murashige and Folke, 1962), and grown in a growth chamber with a 16 h light/8h dark photoperiod at 22 °C. 11 day old plants were transferred to M medium plates (Bécard and Fortin, 1988) and inoculated on the same day with FSK hyphal propagules at a distance ~1 cm beneath the root tip. Control plants received no inoculum. As a second control, M medium plates were also inoculated with fungal hyphae, in the absence of the plant. Plant and fungal growth was allowed to take place in a growth chamber (16 h light/8h dark photoperiod at 22 °C) until contact between the two partners occurred (4 dpi; fungal hyphae had sufficiently contacted the lower part of the root). Contact between the two partners was verified via stereomicroscopical examination. At this time point, control and inoculated plants, were harvested, washed thoroughly with distilled water sterile to eliminate the extraradical fungal mycelium, root tissues were collected, flash frozen on liquid nitrogen and kept at -80 °C until subsequent RNA extraction. Fungal mycelium growing alone was also harvested, flash frozen, and kept for RNA extraction.



Figure 6-3 Experimental setup for RNA experiment on M medium containing plates.

From left to right: *L. japonicus* control, non-inoculated plants; *L. japonicus* FSK inoculated plants; FSK growing alone.

6.2.3 RNA isolation

L. japonicus root tissues were grounded with a pestle, under the presence of liquid nitrogen, and total RNA was extracted using the Isolate II RNA Plant Kit (BIO-52077, BIONE) according to manufacturer's instructions. RNA concentration and integrity were assessed after isolation using Qubit Fluorometer 2.0 and gel electrophoresis (2% agarose gel), respectively. 3 biological replicates for each treatment were prepared for subsequent RNA sequencing analysis. Each biological replicate comprised a pooled sample of 5 individual RNA extraction events for plant samples and 2 individual RNA extraction events for fungal samples. Roots belonging to 3 individual plants were used as starting material for a single RNA extraction event. RNA concentration and integrity were also assessed at the sequencing center using the Bioanalyzer 2100 (Agilent Technologies).

6.2.4 Library construction and Illumina sequencing

Three (3) biological replicates for each treatment were subjected to RNA sequencing. Briefly, libraries were prepared with the KAPA stranded RNA-Seq Library Preparation kit (KAPA Biosystems, Wilmington, MA, USA), and ~10 million paired-end reads of 250 nucleotides each were obtained using an Illumina HiSeq 2500 in Rapid mode. Library preparation and sequencing protocols were performed by the Brigham Young University DNA Sequencing Center (Provo, Utah, USA).

6.2.5 Mapping of sequenced reads, assessment of gene expression and differential gene expression analysis

RNA sequencing analysis was carried out using a transcript read mapping approach. In brief, paired reads were mapped on the previous genome assembly of the sequenced strain using the STAR v2.5 software (Dobin and Gingeras 2015) using the default parameters.

Following, the Cufflinks v2.2.1 software suit (Trapnell et al., 2010) modules were used for quantifying the fragment per kilo-base pair per million reads (FPKM) normalized expression, and performing the differential expression tests between the treatments.

Transcript counts were assessed with HTSeq v0.11.2 (Anders et al., 2015).

Differential expression analysis with EdgeR v3.27.12 (McCarthy et al., 2012) was performed by setting a minimum cutoff of 10 transcripts per million (TPM) for considering transcript counts, followed by the read normalization method of trimmed means of M (TMM) (Robinson and Oshlack, 2010), dispersal estimation, and Fischer's exact test performance.

6.2.6 Gene annotation

The *Fusarium solani* genome was annotated as follows. The Funannotate v0.6.2 software suit (<https://funannotate.readthedocs.io/en/latest/>) was used for searching closest hits against a collection of databases (in a pairwise comparison manner with the basic local alignment search tool - BLAST - (Altschup et al., 1990) and the hidden Markov model - HMM - search based with tools like HMMER (Eddy, 2011) as described at the software manual. Further searches were performed against the *Nectria*

haematococca v2.0 genome with BLAST and the EggNOG v4.5 database (Huerta-Cepas et al., 2016) with the database provided search tool emapper v1.0.3 (<https://github.com/eggnogdb/eggnog-mapper/releases>).

Lotus japonicus genome annotation was downloaded from <http://www.plantgdb.org/LjGDB/>.

6.3 Results and discussion

6.3.1 Input data and preparations

Nine (9) samples were originally sent for RNA sequencing analysis (3 biological replicates of FsK-inoculated *L. japonicus* root tissues, 3 biological replicates of control non-inoculated *L. japonicus* plants, and 3 biological replicates of FsK growing alone). Results were received from all biological replicates except for the *L. japonicus* FsK samples, for which results from only 2 biological replicates were received, due to a mistake of the sequencing provider. Reads were mapped to *Fusarium solani* strain K assembled genome (results of FsK genome analysis are not part of the present thesis), and *L. japonicus* genome (MG20 v3.0, *Lotus* base), in order to discriminate among transcripts of plant and fungal origin. The number of reads mapped to each genomic feature of interest were recorded and extracted to an excel spreadsheet. Differential expression results were furthermore filtered by taking out the low abundance transcripts (transcripts with no more than 1 count in the samples examined).

The set of gene wise counts for each sample makes up the expression profile or library for that sample. The expected size of each count is the product of the library size and the relative abundance of that gene in each specific sample (Gonzalez, 2014).

In the present thesis, only the plant transcriptome profiling is analyzed and presented, in line with results from previous chapters. In the spreadsheet analyzed, there were gene identifiers (IDs) with zero counts in all samples (control and treated biological replicates). These were removed prior to subsequent assessment of the data.

6.3.2 Data exploration and quality assessment

This part of the analysis refers to quality assessment (QA) and exploration of data. These steps are usually performed early in the analysis of the data set, preceding the normalizations step, and DE testing. The purpose is the detection of DEGs, and perhaps the detection of samples whose experimental treatment suffered from an abnormality that may render the data points obtained from these particular samples not suitable for our purpose. The best way for QA of the data is visual (Gonzalez, 2014).

6.3.2.1 Data transformation

For data exploration and visualization, it is useful to work with transformed versions of the count data. As the count values distribution is highly skewed⁶⁵, the log2 transformation helps to approximately normalize the distributions (Gonzalez, 2014).

When the histogram of raw counts is plotted (i.e. the distribution of raw counts for the gene IDs identified in each sample investigated), it is observed that a large proportion of raw count values are close to zero, and therefore data are skewed to the left side of the histogram. If raw values are transformed

⁶⁵ Skewed are the data that are not symmetric around the mean. Skewness in statistics, is the degree of distortion from the symmetrical bell curve, or normal distribution, in a set of data. Skewness can be negative, positive, zero or undefined. A normal distribution has a skew of zero, while a lognormal distribution would exhibit some degree of right-skew. A symmetric distribution is one where the left and right hand sides of the distribution are roughly equally balanced around the mean. For a right skewed distribution, the mean is typically greater than the median.

using the logarithmic scale, it is ensured that values display a more even distribution. By converting to the logarithmic scale we respond to skewness towards large values, i.e. cases in which one or a few points are much larger than the bulk of the data.

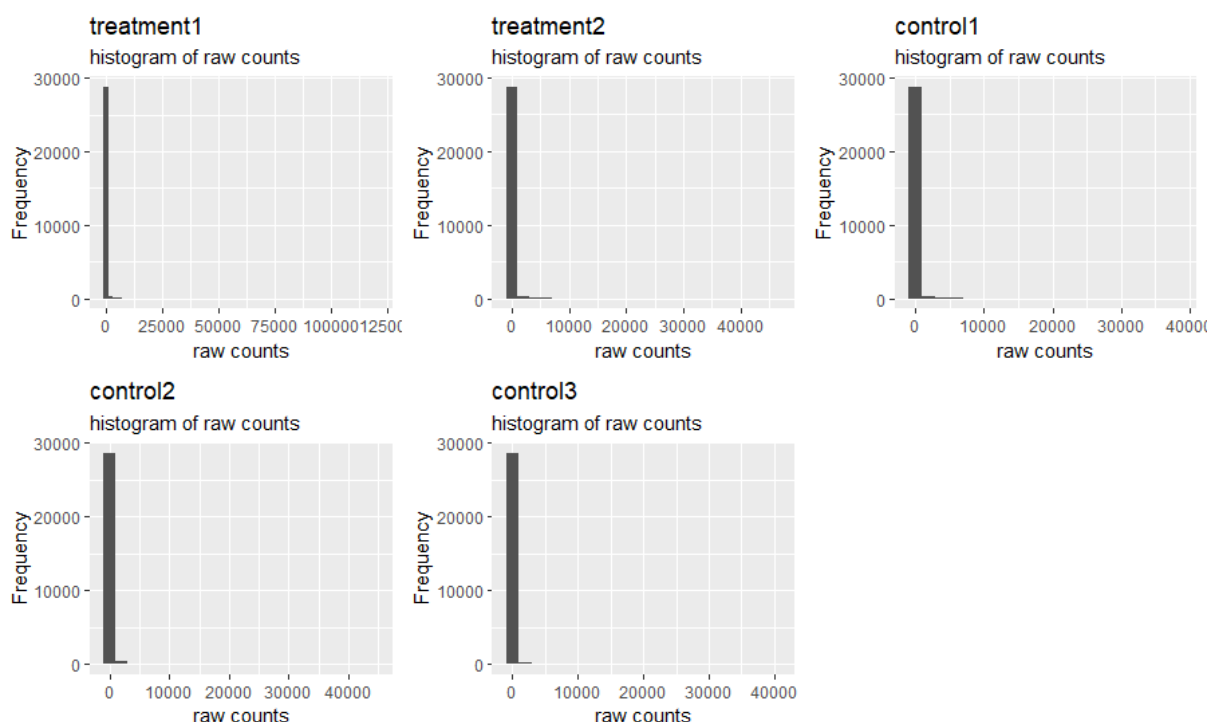


Figure 6-4 Histograms showing the distribution of raw counts for the gene IDs identified in each sample investigated (individual biological replicates). The data set contains 5 individual samples: 2 treated *L. japonicus* root samples with *FsK*, and 3 control root samples (non-inoculated). Note that most of the raw counts are gathered within bin1: 0-2000 raw counts.

Treatment 1-2, FsK-inoculated Lj root samples; control 1-3, non-inoculated Lj root samples

Log base 2 is typically used as it facilitates the conversion back to the original scale: a difference of 1 on the log base 2 scale corresponds to a fold change of 2 on the original count scale. Since count values for a gene can be zero in some conditions (and non-zero in others), the use of pseudocounts is preferable, i.e. transformations of the form

$$y = \log_2(K + 1) \text{ or more generally, } y = \log_2(K + k_0);$$

where K represents the count values and k_0 is a positive constant (Gonzalez, 2014).

So, to calculate pseudocounts the following formula was used:

$$\text{pseudocounts} = \log_2(\text{raw counts} + 1)$$

Following log-transformation of raw counts, if the histogram of the distribution of pseudocounts (i.e. \log_2 -transformed count data) is plotted, for the gene IDs identified in each sample, plots are as follows:

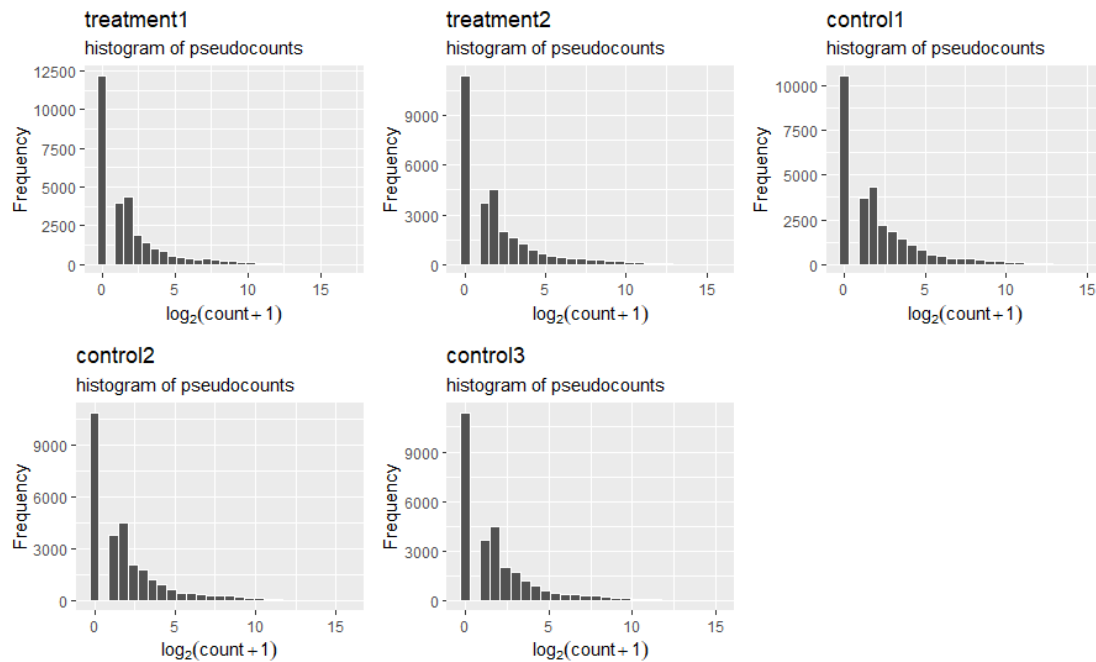


Figure 6-5 Histograms showing the distribution of pseudo counts for the gene IDs identified in each sample investigated (individual biological replicates). The data set contains 5 individual samples: 2 treated *L. japonicus* root samples with *FsK*, and 3 control root samples (non-inoculated). Note that most of the pseudo counts are now dispersed among the bins of the histogram (bin size = 0.6).

Treated 1-2, *Lj* roots inoculated with *FsK*; control 1-3: *Lj* roots non-inoculated.

6.3.2.2 Exploring the between sample distribution

Visualizing the between-sample distribution of counts is useful to contrast the distribution of gene-level expression values on different samples. It can for example be used to display the effects of between-samples before and after filtering and/or normalization (Gonzalez, 2014). The following plots are representative ways of demonstrating the between-sample distribution.

○ Boxplot

The boxplot method provides an easy way to visualize the distribution of pseudocounts in each sample. Note that all samples demonstrate a similar visual pattern with low count values representing the 25th to 75th percentile of the distribution, whereas high count values are drawn as whiskers/points. The black line within each boxplot represents the median value of the data.

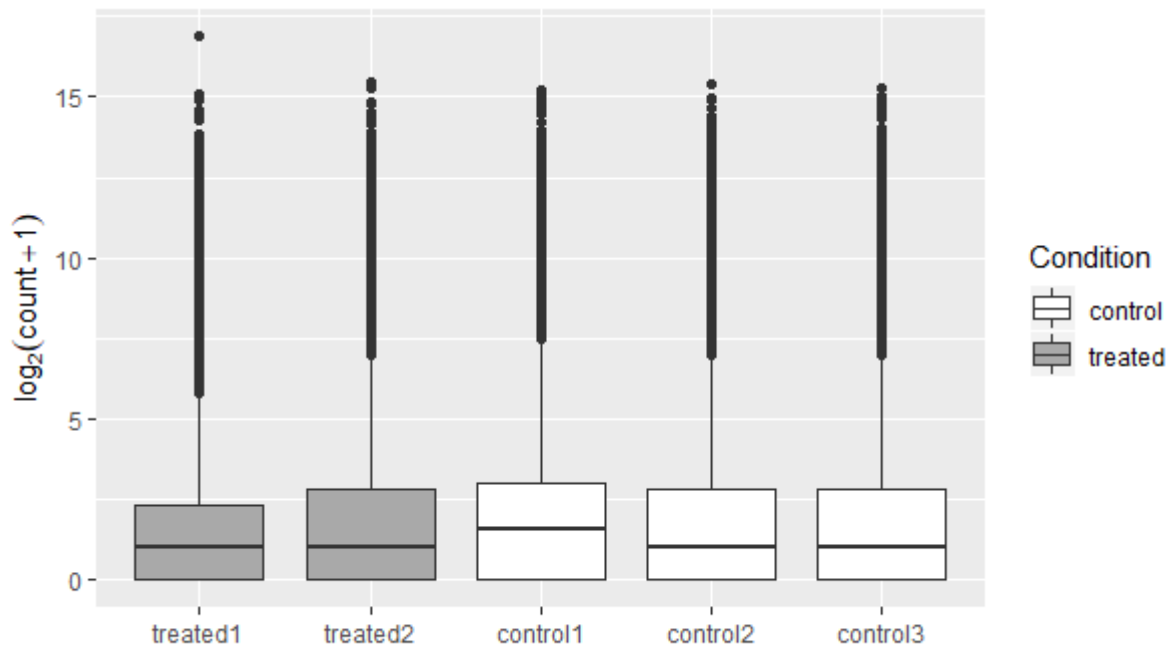


Figure 6-6 Parallel boxplots from pseudocounts data. The median value of log transformed raw counts is also presented with a black line within the box. Whiskers and dot points extending above the boxes represent genes with high count values, possibly representing outliers.

Treated 1-2, *Lj* roots inoculated with *FsK*; control 1-3: *Lj* roots non-inoculated.

○ Density plot

Pseudocounts distributions can also be summarized by means of a density plot. Density plots provide more detail by enabling, for example, the detection of a secondary mode in the distribution.

Figure 6-7 shows the densities of pseudocounts for the samples displayed in Figure 6-6. As there is evidence of bi-modality, these displays provide additional information (what is not captured by boxplots). In the density plot, the x-axis represents the value of the variable just like in a histogram (e.g. in the histogram of Figure 6-5). The y-axis in a density plot is the probability density function for the kernel density estimation. The Kernel density plot makes it clear that for all the samples the distribution is distinctly skewed, not normal.

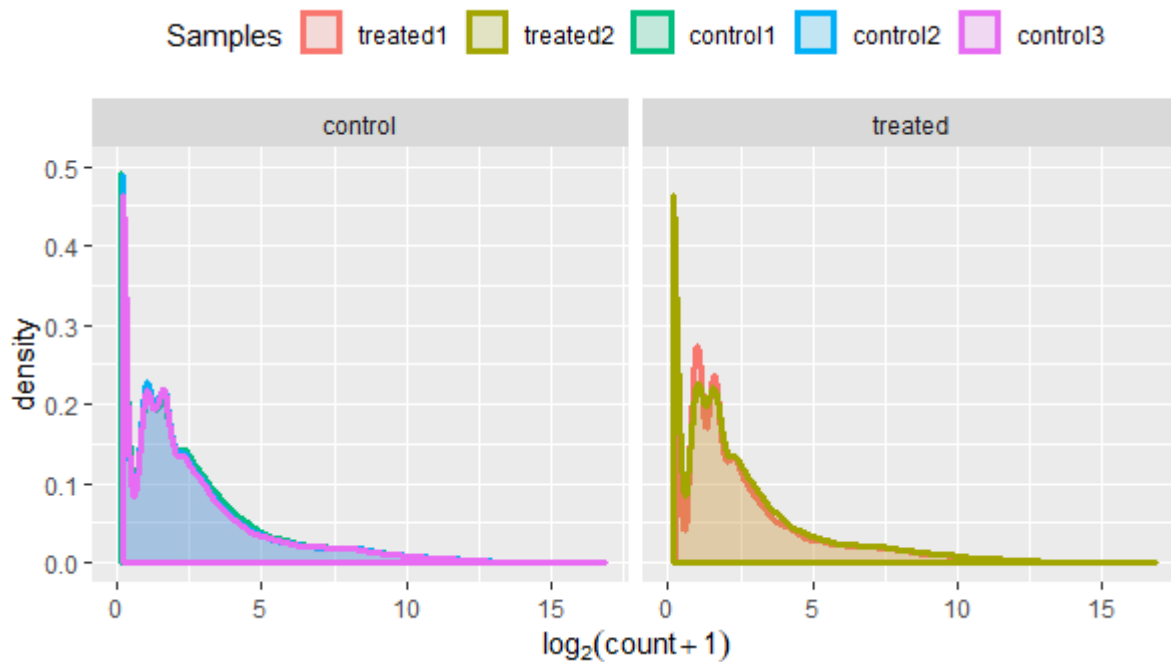


Figure 6-7 Density plot demonstrating the distribution of pseudocounts for samples examined. The smooth curve displayed estimates the probability density function of the pseudocounts variable. 'Density' y-axis is displayed in arbitrary units.

Treated 1-2, FSK-inoculated *Lj* root tissues; control 1-3, non-inoculated *Lj* root tissues.

A density plot visualizes the distribution of data over a continuous interval. This chart is a variation of a histogram that uses kernel smoothing to plot values, allowing for smoother distributions by smoothing out the noise. The peaks of a density plot help display where values are concentrated over the interval. An advantage density plots have over histograms is that they are better at determining the distribution shape because they are not affected by the number of bins used. The density plot shows the smooth distribution of points along the numeric axis. The peaks of the density plot are at the locations where there is the highest concentration of points.

The area under the curve of a density function represents the probability of getting a y value between a range of x values.

From the density plot we can observe that pseudocounts 'gather' (main peaks) at values 0-2 (x-axis values), therefore the majority of raw count values are relatively small (as also indicated by the boxplots of Figure 6-6). The same distribution is observed for all samples examined (treated – controls).

○ MA plots between samples

An MA-plot is a plot of log-fold change (M-values, i.e. the log of the ratio of level counts for each gene between two samples) against the log-average (A-values, i.e. the average level counts for each gene across the two samples). The MA-plot is a useful way to visualize reproducibility between samples of an experiment. From an MA-plot one can see if normalization is needed. In MA plot, genes with similar expression levels in two samples will appear around the horizontal line $y = 0$. A line in red is also plotted underlying a possible trend in the bias related to the mean expression (Gonzalez, 2014).

An MA plot concludes how different the two samples compared are in terms of read counts in an RNA seq experiment. If for example we plot a sample versus itself, we will notice that data points converge to zero at y-axis, because $\log(x/x)$ is zero.

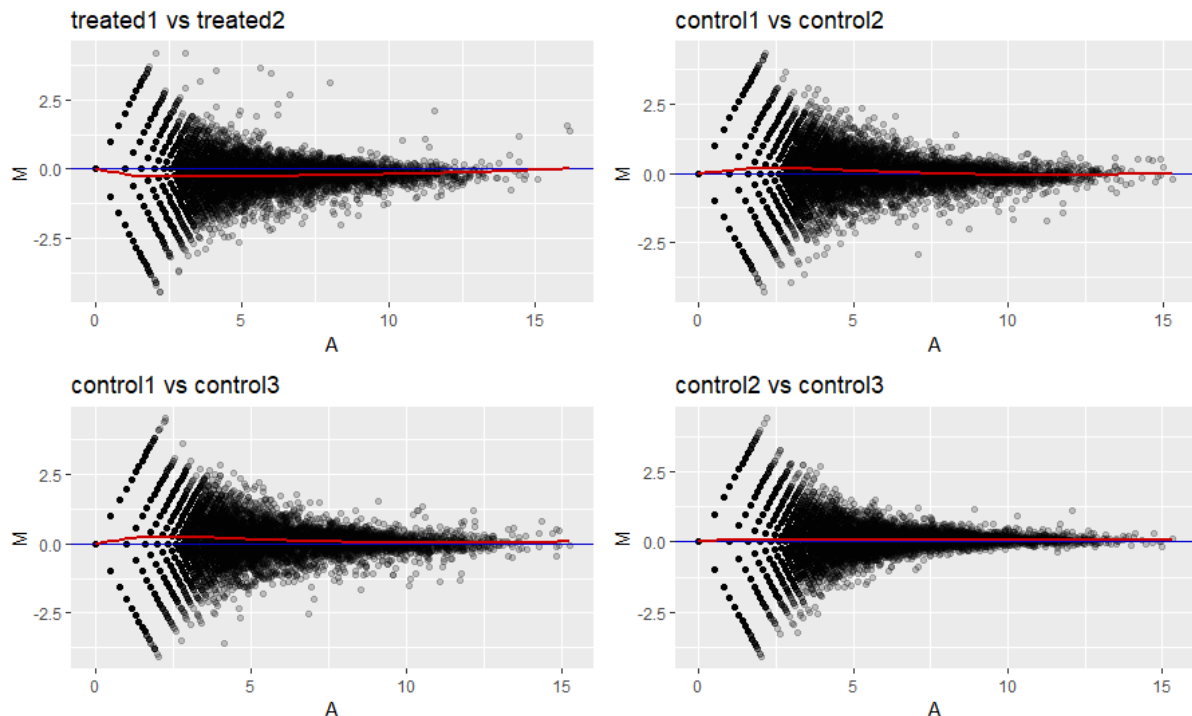


Figure 6-8 MA plot between treated and control samples. There is a good reproducibility of samples as indicated by their placement on the graph around horizontal line $x=0$.

Treated 1-2, FSK-inoculated *L. japonicus* root tissues; control 1-3, non-inoculated *L. japonicus* root tissues

The MA plot allows to look at the relationship between intensity and difference between two samples for the under analysis gene list. It creates a 2D plot with each point representing a feature (gene, transcript). The x-axis represents the average quantified values across the data stores (samples), and the y-axis shows the difference between them.

In all pairwise comparisons, all points corresponding to features identified in the data set are distributed around the $x=0$ horizontal red line. This indicates the good reproducibility of the samples.

○ Clustering of the sample to sample distances

To explore the similarities and dissimilarities between samples, it is often instructive to look a clustering image map (CIM) or heatmap of sample-to-sample distance matrix. A heatmap is a two-dimensional, rectangular, colored grid. The rows and columns of the matrix are rearranged independently according to a hierarchical clustering method (Euclidean distance⁶⁶), so that similar rows and columns are placed next to each other, respectively (Gonzalez, 2014).

⁶⁶ Euclidean distance method: The Euclidean distance between two points in either the plane or a 3D space in the length of the straight line connecting the two points. From <http://rosalind.info/glossary/euclidean-distance/>

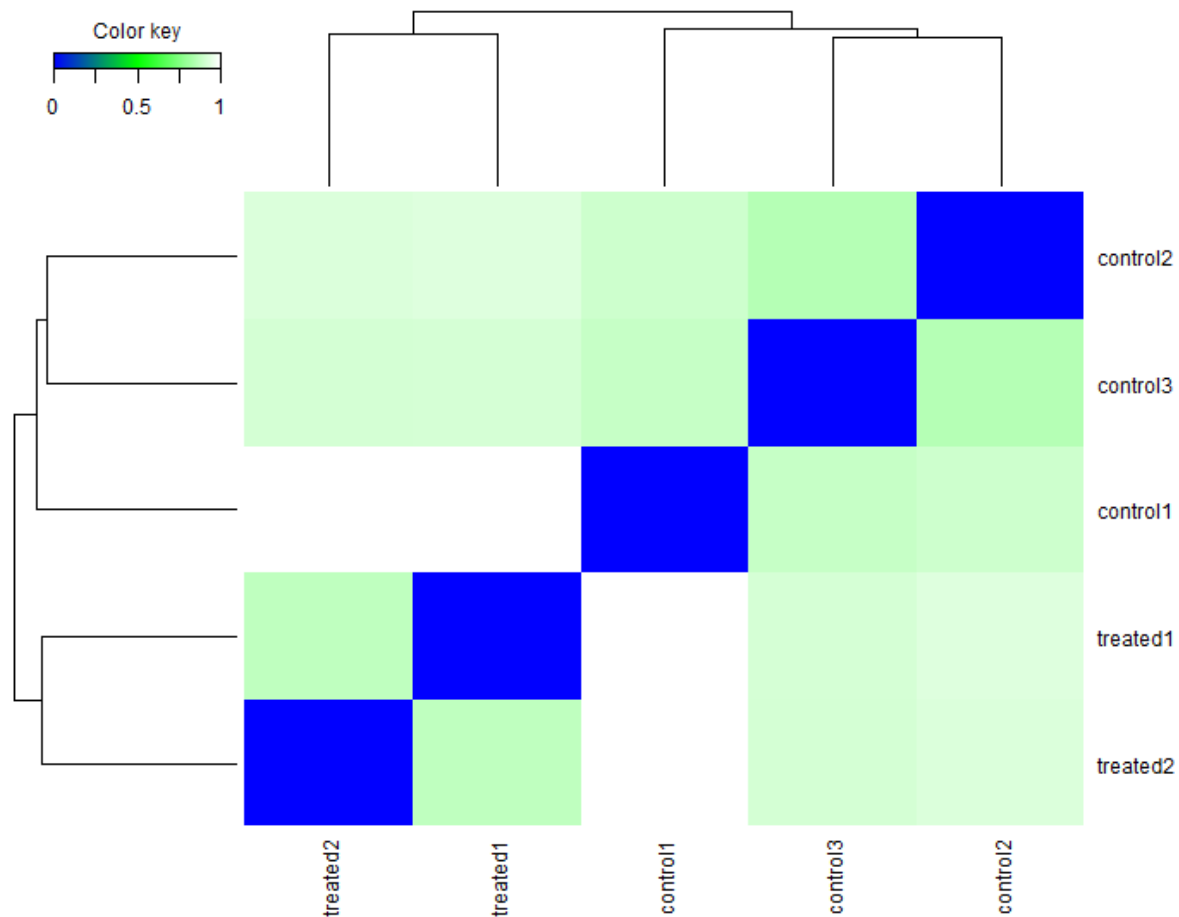


Figure 6-9 Correlation matrix showing the Euclidean distance between control and treated samples. Note that treated samples and control samples, respectively, cluster together. Coloring key towards blue (zero values) indicates stronger correlation.

Treated1-2, *FsK*-inoculated *Lj* root tissues; control 1-3, non-inoculated *Lj* root tissues

A clustering of samples exposed to the same treatment is seen in the CIM image. Treated samples and controlled samples are clustered together, respectively. Control 2 and 3 are closely clustered together in comparison to control 1. Pseudocounts were entered as a matrix. Color values close to 0 (towards blue colors) indicate that there is a strong correlation among samples compared. Color values close to 1 (towards white colors) indicate that there is low to no correlation among samples compared.

Principal component plot of the samples

This type of plot is useful for visualizing the overall effect of experimental covariates and batch effects. The plot is produced from the output of principal component analysis (PCA) on the transposed of the given counts matrix. PCA is used to reduce multidimensional datasets to lower dimensions for analysis; it is a technique that can determine the key features of high-dimensional datasets. In the context of RNA seq analysis, PCA essentially clusters samples by groups of the most significantly dysregulated genes. Clustering first by the most significant group, then by progressively less significant groups.

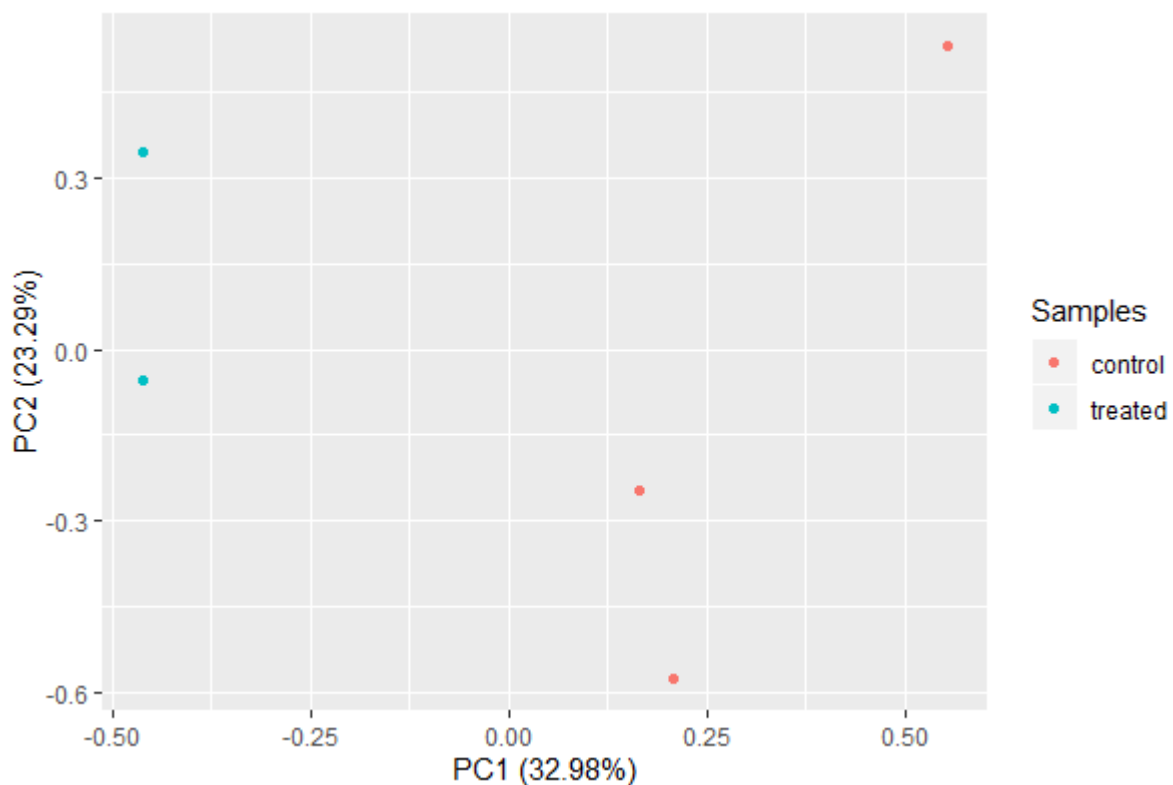


Figure 6-10 PCA plot. The 5 samples are shown in the 2D plane spanned by their first two principal components. K-means clustering was applied to the data set. Note that treated samples and control samples, respectively, cluster together. The observations included in the data set (pseudocounts) were portioned into $k=2$ clusters, in which each observation belongs to the cluster with the nearest mean, serving as the prototype to the cluster. Treated, FSK-inoculated Lj root tissues; control, non-inoculated Lj root tissues

Given the experimental design of the dataset that is analyzed here (i.e., samples belong to only two distinct groups), a control group and a treatment group, there should be a clear separation of both groups of samples by the first component. PCA is performed on the top genes selected by highest row variance.

The score plot displays each sample in the data set with respect to the first two principal components and can therefore be used to interpret the relations among the samples. This information can be used to identify outliers.

In the plot displayed above, the replicate samples show a high similarity with respect to the first two principal components, a small within group variance and a good separation of groups. Note that control 1 is more distant in the matrix in comparison to control 2 and 3, as is also indicated by the correlation matrix shown as a heatmap in Figure 6-9.

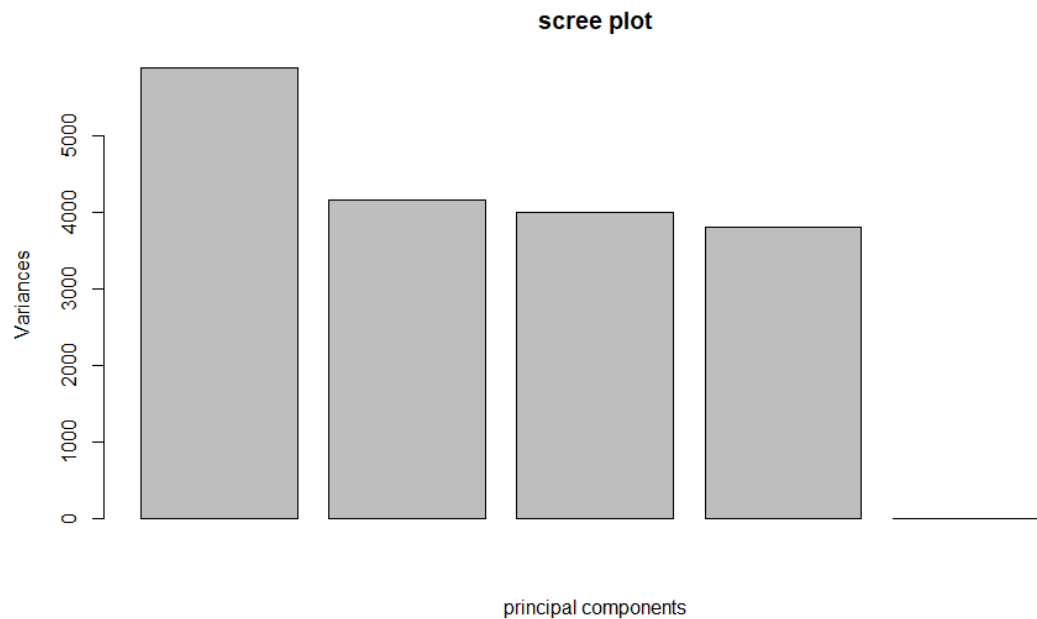


Figure 6-11 Scree plot demonstrating the Principal Components contributing in the variance within the data set.

A scree plot is a plot of the eigenvalues of factors or principal components in an analysis. The scree plot is used to determine the principal components to keep in a PCA. A scree plot displays the eigenvalues in order from largest to smallest.

From the scree plot we can see that the amount of variation explained drops dramatically after the 4th component. For simplification the first two components are presented in the PCA plot of Figure 6-10.

The contribution to the amount of variance explained is as follows: PC1: 32.98%, PC2: 23.29%, PC3: 22.40%, PC4: 21.32%.

In order to test whether the pattern shown in PCA plot of Figure 6-10 changes if we demonstrate the 5 samples in the 3D plane spanned by the 3 first principal components a second PCA plot is plotted and shown below. The pattern does not change: control samples are grouped together and treated samples are grouped together.

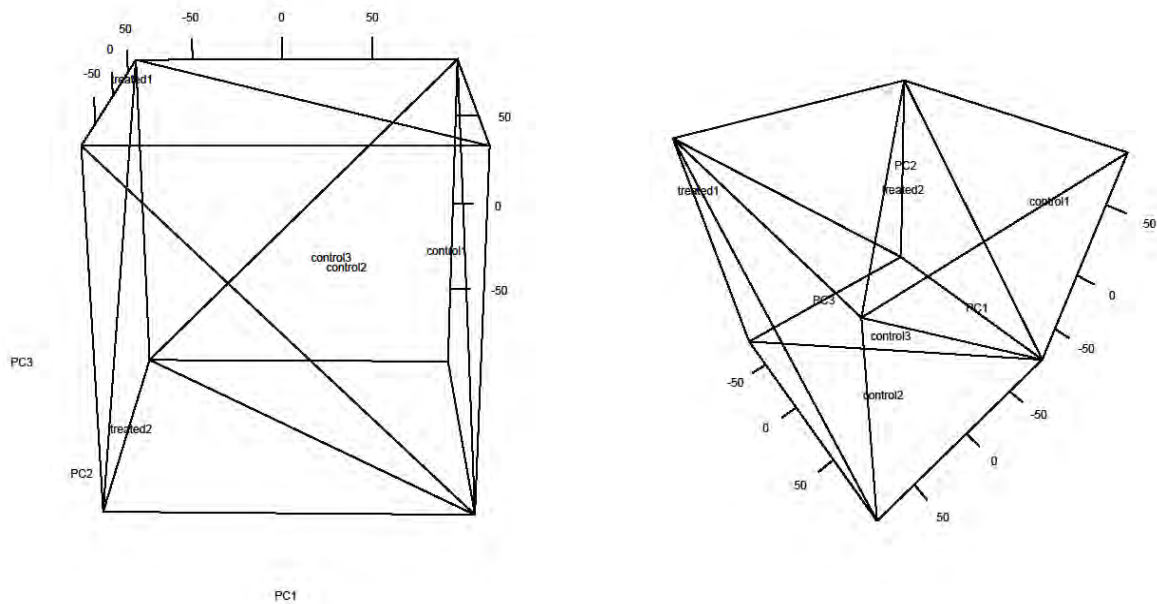


Figure 6-12 PCA plot. The 5 samples are shown in the 3D plane spanned by their first three principal components. Panels show different rotations of the plot.
Treated 1-2, Fsk-inoculated Lj root tissues; control 1-3, non-inoculated Lj root tissues

6.3.2.3 Investigating the normalized data

From this point on, analysis is performed on normalized counts. As mentioned in the materials and methods section, data were analyzed via two different computational methods, to achieve more accurate results in terms of DE analysis. More specifically, the cufflinks software, and edgeR software were used. Normalized data as provided by the software, were used for further analysis of the data.

○ Plotting the histogram of p values

The distribution of p -values of gene IDs as identified based on cufflinks analysis is presented in Figure 6-13. More specifically, the p -values are divided in bins, with bin size = 0.05. The frequency of each bin size is calculated and displayed. The bin containing p -values < 0.05 is indicated in red. Note the large size of the last bin ($0.95 < p\text{-value} < 1$). Interestingly, the total number of gene IDs identified via cufflinks and edgeR analysis differs (29055 vs 13158 gene IDs for cufflinks and edgeR analysis, respectively). The difference is also reflected in the gene IDs with p -values below the 0.05 cutoff (3139 vs 1674 gene IDs for cufflinks and edgeR analysis, respectively).

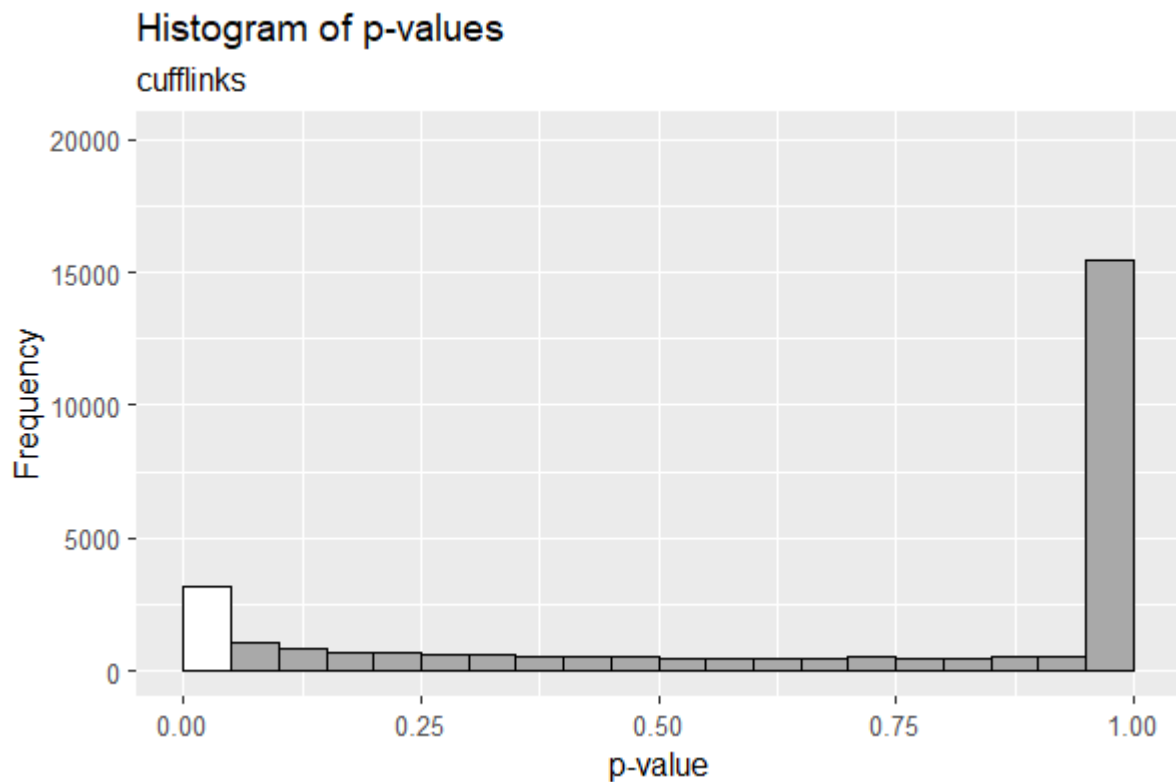


Figure 6-13 Histogram of the p-values corresponding to 29055 gene IDs derived from the unfiltered Lotus-FsK dataset analysed via cufflinks software. Histogram bin size was set to 0.05. The y-axis values are shown on the non-transformed (natural) scale. The first bin (in white) indicates p-values that are below the 0.05 cutoff (3139 transcripts).

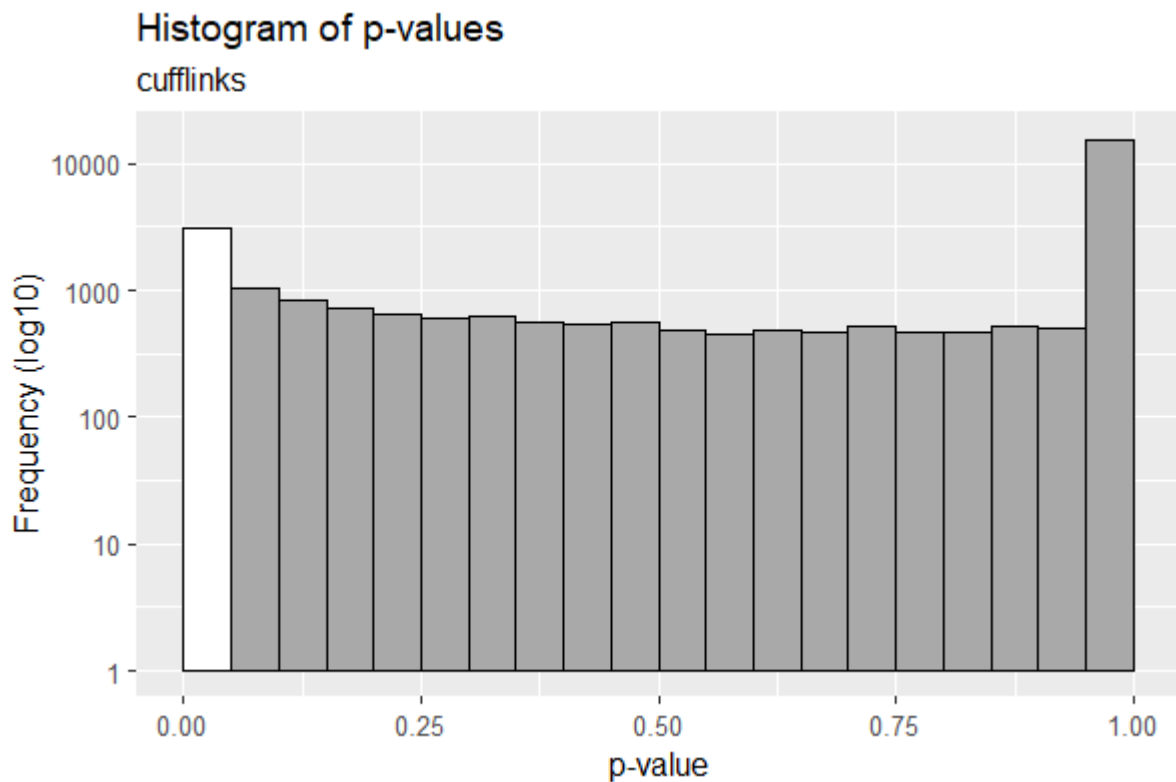


Figure 6-14 Histogram of the p-values corresponding to 29055 gene IDs derived from the unfiltered Lotus-FsK dataset analysed via cufflinks software. Histogram bin size was set to 0.05. The y-axis values are shown on the log10 transformed scale. The first bin (in white) indicates p-values that are below the 0.05 cutoff (3139 transcripts).

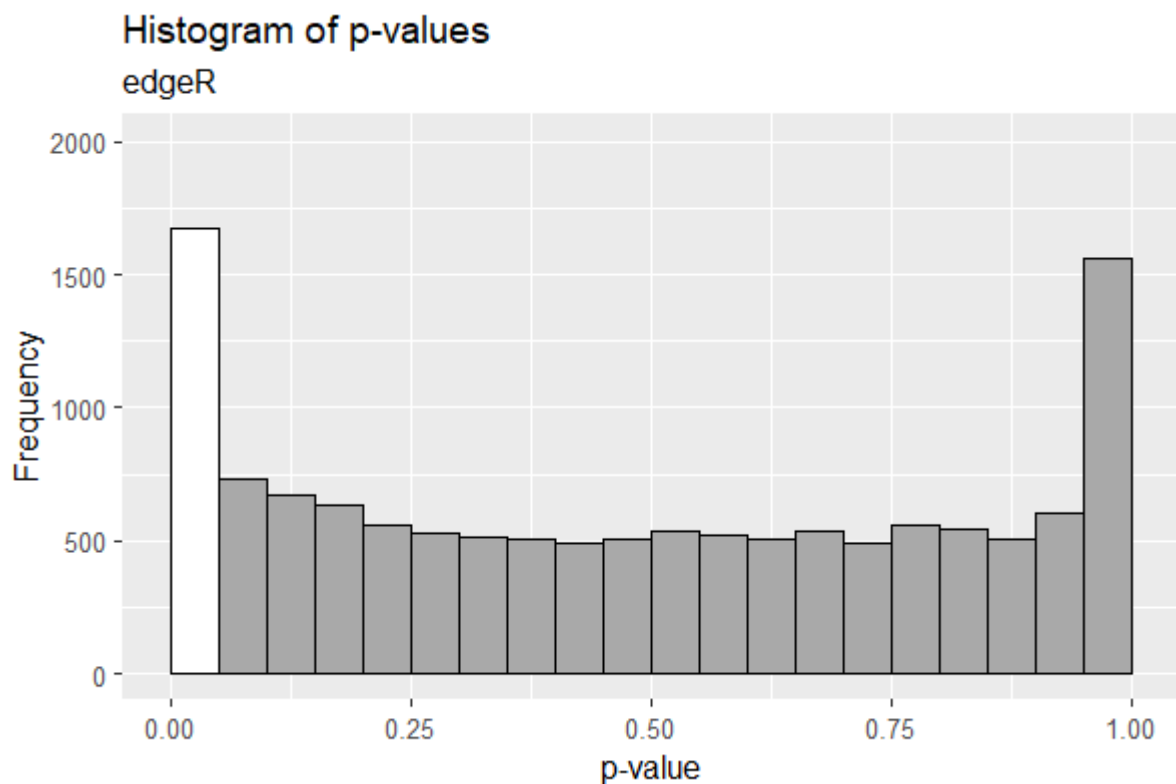


Figure 6-15 Histogram of the p-values corresponding to 13158 gene IDs derived from the unfiltered Lotus-FsK dataset analyzed via edgeR software. Histogram bin size was set to 0.05. The y-axis values are shown on the non-

transformed (natural) scale. The first bin (in white) indicates p-values of genes below the 0.05 cutoff (1674 transcripts).

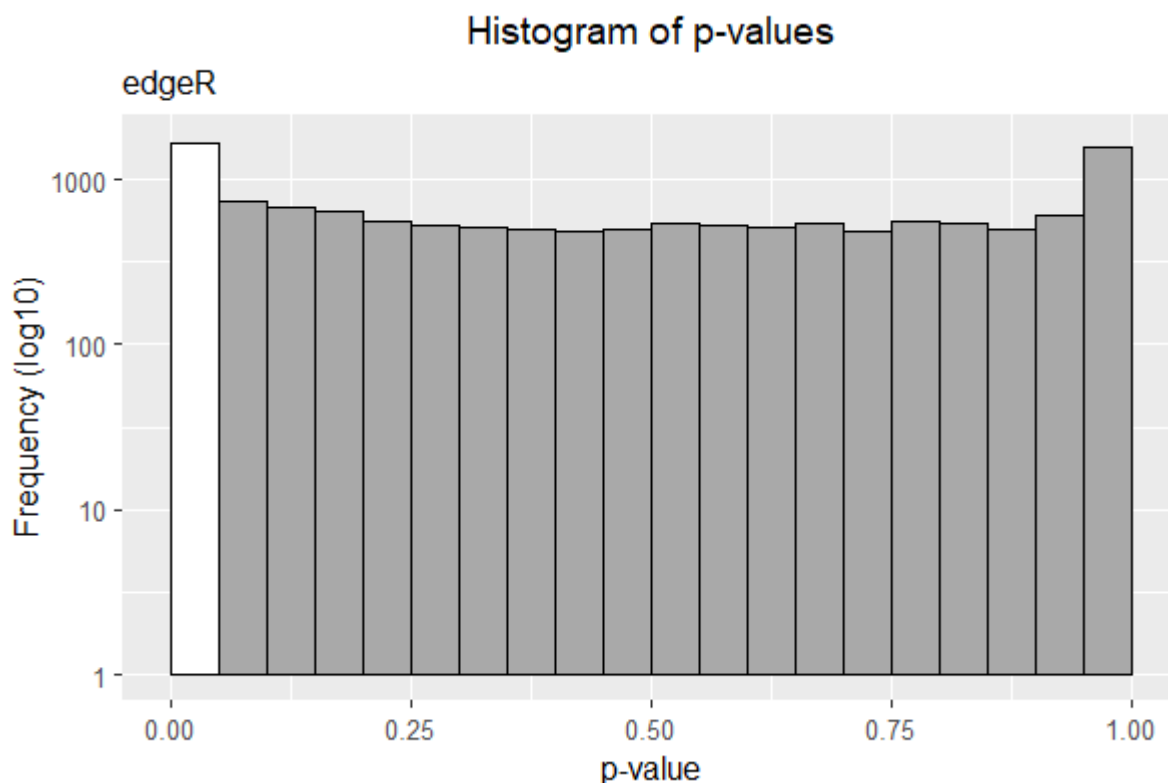


Figure 6-16 Histogram of the p-values corresponding to 13158 gene IDs derived from the unfiltered Lotus-FsK dataset analyzed via edgeR software. Histogram bin size was set to 0.05. The y-axis values are shown on the log10 transformed (natural) scale. The first bin (in white) indicates p-values of genes below the 0.05 cutoff (1674 transcripts).

○ Plotting an MA plot

As mentioned above, an MA plot is a visual representation of the differences between measurements taken in two samples. The data are transformed onto M (log ratio) and A (mean average) scales, and then these values are plotted. MA plots are used to visualize high-throughput sequencing analysis.

For cufflinks analysis the following filtering steps and calculations were performed prior to construction of the graph:

1. q-value ≤ 0.05 .
2. Gene IDs with infinite log2FC values were removed (4 entries were removed).
3. The mean value of log2 FPKM value of control and treated samples was calculated

$$\log_2 \text{FPKM} = \log_2 \left[\frac{1}{2} * (\text{FPKM}_{\text{control}} + \text{FPKM}_{\text{treatment}}) \right]$$

The x-axis of the MA plot represents the log2FPKM as calculated with the above formula for each gene ID identified after filtering steps.

The y-axis of the MA plot represents the log2FC for each gene ID identified.

Each point represents a feature identified (gene IDs). Points above the $x=0$ line (in grey) represent upregulated genes. Points below the $x=0$ line (in yellow) represent downregulated genes.

Justification for the filtering steps performed:

The p-value is commonly used for performing a single significant test. The q-value is useful for assigning a measure of significance to each of many tests performed simultaneously. Therefore q-value is proposed as a well suited measure of significance for genome-wide tests of significance (Storey and Tibshirani, 2003). To this respect, in the present analysis q-values were used instead of p-values to take into consideration corrections for multiple hypothesis testing. A stricter cut-off is therefore set, in terms of the significance and accuracy of the results.

Infinite \log_2FC values occur due to zero counts in either average value of control sample (infinite values) or average value of treated with FsK sample (minus infinite sample). Zero counts might represent absence of expression in one of the two conditions, and enhancement on the other. These results were removed from the present analysis as they were not considered accurate, although should be regarded, perhaps after validation via qPCR.

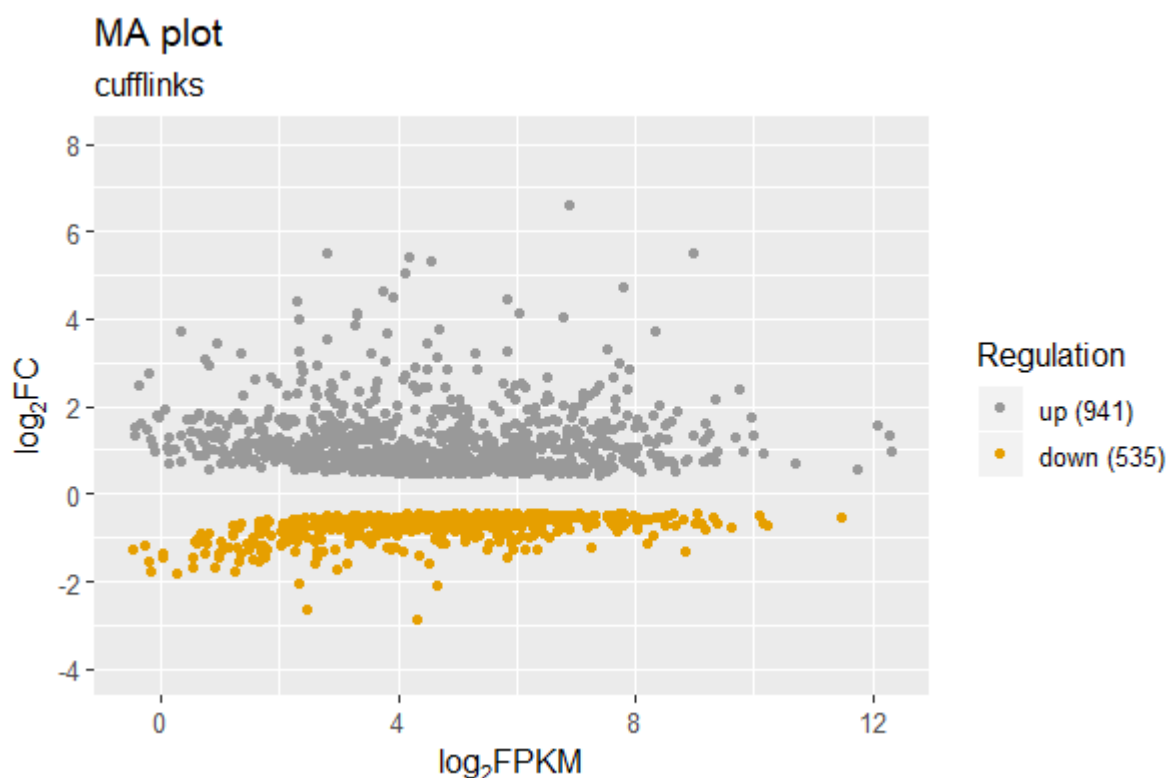


Figure 6-17 MA plot of the \log_2 fold change values versus average \log_2 FPKM values for all genes with q -values ≤ 0.05 , based on cufflinks analysis. Grey points indicate DEGs showing upregulation, whereas yellow points indicate DEGs demonstrating downregulation. x-axis represents average \log_2 FPKM values, whereas y-axis represents \log_2 fold change values. The number of up- and down-regulated genes is shown at the right of the plot. FPKM, Fragments Per Kilobase Million.

For edgeR analysis the following steps were performed prior to construction of the MA plot:

1. $FDR \leq 0.05$
2. There were no samples with infinite \log_2FC values in edgeR analysis, so no samples were removed
3. edgeR calculates the log average abundance of control and treatment, that is:

$$\log_2\left[\frac{1}{2} * (CPM_{control} + CPM_{treatment})\right]$$

The x-axis of the MA plot represents the \log_2CPM as calculated via edgeR for each gene ID.

The y-axis of the MA plot represents the \log_2FC for each gene ID identified.

Each point represents a feature identified (gene IDs). Points above the $x=0$ line (in grey) represent upregulated genes. Points below the $x=0$ line (in yellow) represent downregulated genes.

Justification of the filtering steps used:

An FDR cut-off was set at 0.05. The false discovery rate implies a concern on the false positives among the tests found to be significant. FDR also takes into consideration the performance of multiple tests (correction for multiple hypothesis testing). A more stringent cut-off is also set in results of edgeR analysis, in an attempt to obtain more accurate results.

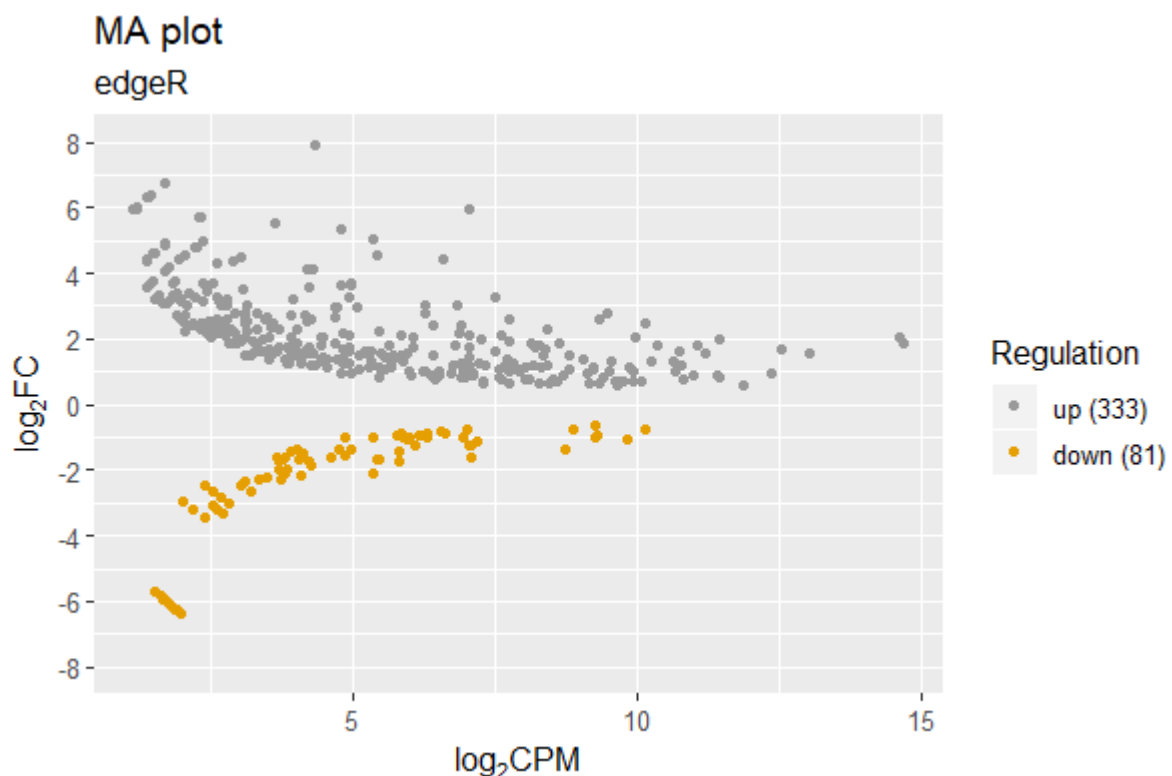


Figure 6-18 MA plot of the \log_2 fold change values versus average \log_2 CPM values for all genes with q -values ≤ 0.05 , based on edgeR analysis. Grey points indicate DEGs showing upregulation, whereas yellow points indicate DEGs demonstrating downregulation. x-axis represents average \log_2 CPM values, whereas y-axis represents \log_2 fold change values. The number of up- and down-regulated genes is shown at the right of the plot. CPM, Counts Per Million.

○ *Plotting a heatmap*

A generic heatmap is plotted demonstrating the abundance of the log₂FC of DEGs identified either with cufflinks or edgeR analysis, to obtain an overview of the regulation of genes IDs identified.

For cufflinks analysis results the following filtering steps prior to heatmap construction were performed:

1. q-value ≤ 0.05
2. Samples with infinite log₂FC values were removed (4 entries were removed)
3. Absolute(log₂FC) ≥ 1 (therefore FC ≥ 2 , either up- or down-regulation)

For edgeR analysis results the following filtering steps prior to heatmap construction were performed:

1. FDR ≤ 0.05
2. Absolute(log₂FC) ≥ 1 (therefore FC ≥ 2 , either up-, or down-regulation)

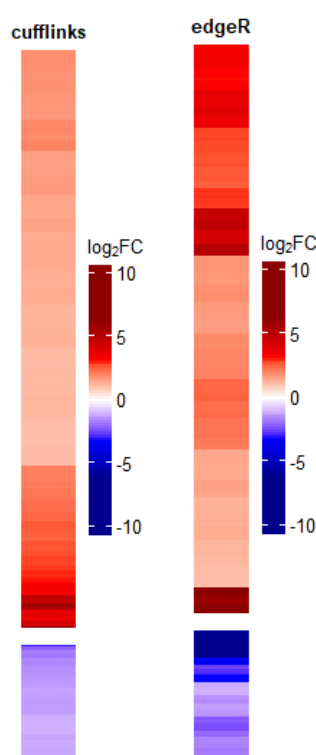


Figure 6-19 Heatmap showing an overview of the log₂ fold changes of DEGs in Lotus-FsK data set analysed either with cufflinks or edgeR tool. Heatmaps are clustered by rows and split based on positive/negative log₂ fold change values (up- or downregulation of the identified genes).

Filtering steps of the initial data set prior to heatmap generation: 1) q-value or FDR value cut-off at 0.05 (for cufflinks and edgeR, respectively), 2) absolute log₂ fold change ≥ 1 .

Colour scale towards red indicates highly upregulated genes, whereas colour scale towards blue indicates highly downregulated genes. The heatmap is split based on positive or negative log₂FC values, thus in the upper part of the heatmap upregulated genes are shown, whereas in the lower part of the heatmap downregulated genes are shown.

A total of 528 genes is presented for cufflinks analysis (439 upregulated and 89 downregulated), whereas a total of 355 genes is presented for edgeR analysis (288 upregulated and 67 downregulated).

Note that in both analyses, the number of upregulated genes identified is higher than that of the downregulated genes (83.1 and 81.1%, respectively for cufflinks and edgeR analysis).

- *Plotting pie charts*

The percentage of up- and down-regulated genes identified via cufflinks or edgeR analysis are presented with a pie chart (Figure 6-20) for a simplified visualization of the results.

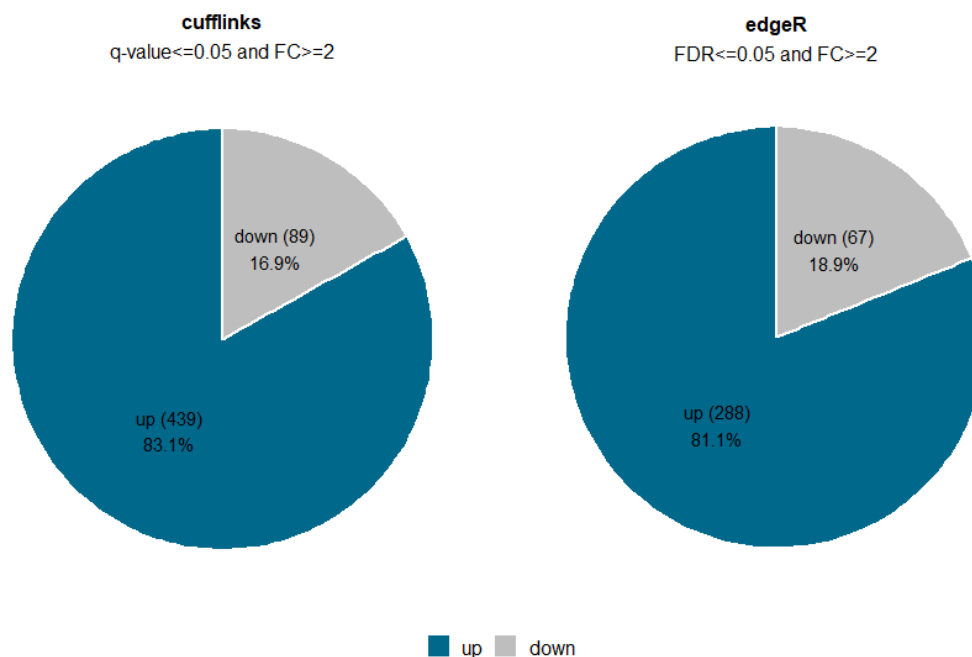


Figure 6-20 Pie charts demonstrating number and percent distribution of uniquely expressed upregulated and downregulated genes in Lotus-FsK data set when analysis is performed either with cufflinks or edgeR software. Filtering steps: 1) q-value and FDR cutoff at 0.05 for cufflinks and edgeR analysis, respectively, 2) FC ≥ 2

For cufflinks analysis, after filtering for significantly regulated genes, 83.1% of total DEGs were identified as upregulated in the treated samples in comparison to controls, and only 16.9% were identified as down-regulated. For edgeR analysis, after filtering for significantly regulated genes, 81.1% of total DEGs were identified as upregulated in the treated samples in comparison to controls, and only 18.9% were identified as down-regulated. It is of interest that the majority of differentially *L. japonicus* regulated genes, responds to FsK presence with upregulation.

- *Identifying and plotting the annotated in public databases *L. japonicus* transcripts regulated upon FsK presence*

The number of annotated versus non-annotated identified transcripts is presented in Figure 6-21. Cufflinks analysis led to identification of 464 (87.88%) annotated versus 64 (12.12%) non-annotated in public databases transcripts. edgeR analysis led to identification of 148 (41.69%) annotated versus 207 (58.31%) non-annotated transcripts.

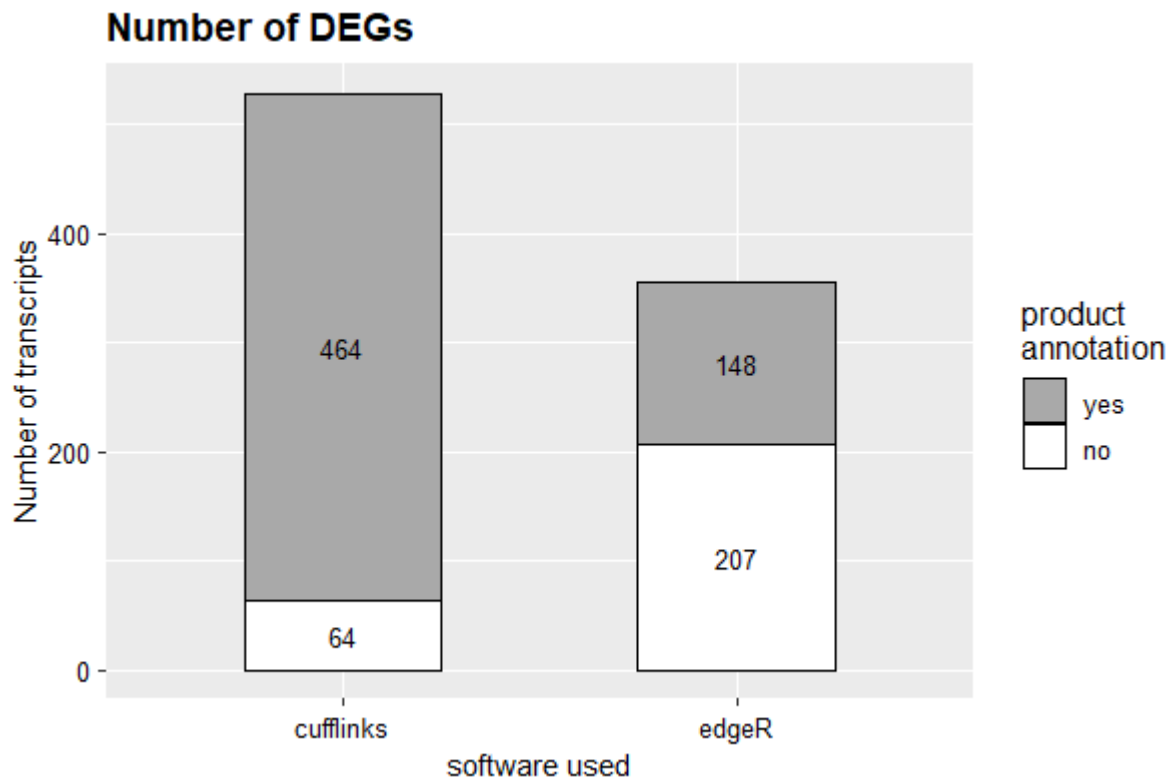


Figure 6-21 DEGs in the filtered Lotus-FsK data set divided into 2 categories on the basis of their annotation status. DE gene IDs identified via the two software packages were ordered on the basis of their total number of detections after performing the following filtering steps: 1) q-value, FDR cut-off at 0.05 level for cufflinks and edgeR software respectively, 2) absolute log2 fold change ≥ 1 . Grey and white bar, annotated and non-annotated DEGs based on blast results against public databases.

It is of interest that more than half of the DEGs identified via edgeR analysis are non-annotated transcripts. Only a small fraction of DEGs identified via cufflinks analysis received no annotation when 'blasted' against public databases.

- Plotting a Venn diagram to demonstrate the common DEGs identified via cufflinks/edgeR analysis

The intersect of DEGs identified via cufflinks / edgeR analysis was determined and results were plotted as a Venn diagram. It is of interest that only 20 DEGs were found as common in the DEGs output of the two computational analysis methods. The common list of DEGs is presented at the end of the chapter (Appendix of chapter 6):

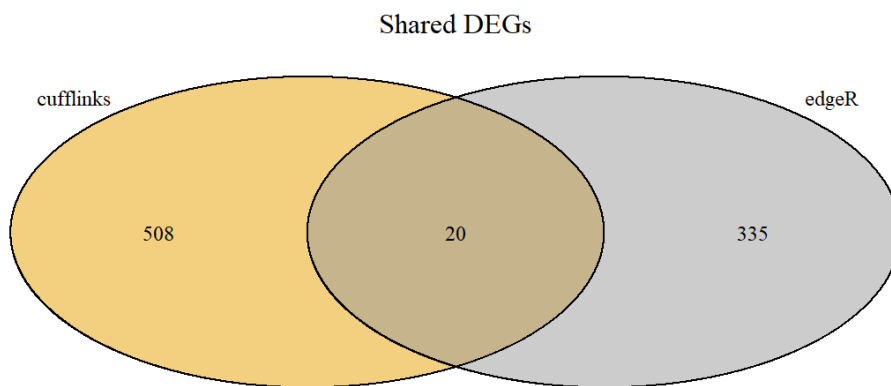


Figure 6-22 Venn diagram showing the intersection of DEGs identified by the two software used to analyze the Lotus-FsK dataset. Filtering steps prior to Venn diagram, construction: 1) q-value and FDR cut-off at 0.05, 2) absolute log2 fold change ≥ 1 .

6.3.2.4 Analysis of the DEGs identified

- Using Lotus base and WEGO web based tool to obtain a 'reader friendly' overview of the results

The process followed for the analysis is described below:

The primary goal was to achieve a reader friendly, relatively generic overview of results. To this respect, it was firstly attempted to match the gene IDs identified via cufflinks analysis with a corresponding Gene Ontology term. Gene IDs were extrapolated from the original spreadsheet file and introduced into the web based tool 'Lotus Base Transcript Explorer' (TREX) (<https://lotus.au.dk/tools/trex>). A total number of 494 gene IDs (these were the gene IDs with a provided sequence in the original spreadsheet file) was 'pasted' on Lotus base TREX interface, and a file providing information on GO terms as well as a description of each gene was downloaded. A .txt file was then generated with each row containing a gene descriptor (the gene ID) and the various GO terms matching the gene ID.

The .txt file was introduced into the WEGO web tool. WEGO (Web Gene Ontology Annotation Plot) is a simple tool useful for visualizing, comparing and plotting GO annotation results. WEGO uses the GO annotation results as an input. Based on GO's standardized DAG (Directed Acyclic Graph) structured vocabulary system, the number of genes corresponding to each GO ID is calculated and shown in a graphical format. WEGO provides the reference data of nine model species: baker's yeast (*Saccharomyces cerevisiae*), *Caenorhabditis elegans*, *Escherichia coli*, house mouse, human, fruit fly, brown rat, rice and zebrafish. The graph output of WEGO is a traditional histogram. The x-axis displays the GO terms selected from the GO trees. The right y-axis shows the gene numbers of selected GO terms, while the left y-axis shows the percentages (Ye et al., 2018). For the purposes of the analysis, the choice for reference statement at the WEGO interface was set to 'none'.

The main results of the analysis as shown in WEGO site is shown in the desktop capture of Figure 6-23. It should be noted that duplicate gene ID values were removed from the analysis, as identification of potential gene isoforms was not a priority at this point of the analysis (this explains the lower number of input genes 488 over 494). Two histograms were generated matching GO terms to gene IDs. The

first histogram is more generic (Figure 6-27), and shows how many genes matched to GO terms of level 2. A more detailed histogram was generated and is shown in Figure 6-25, by using GO terms of level 3.

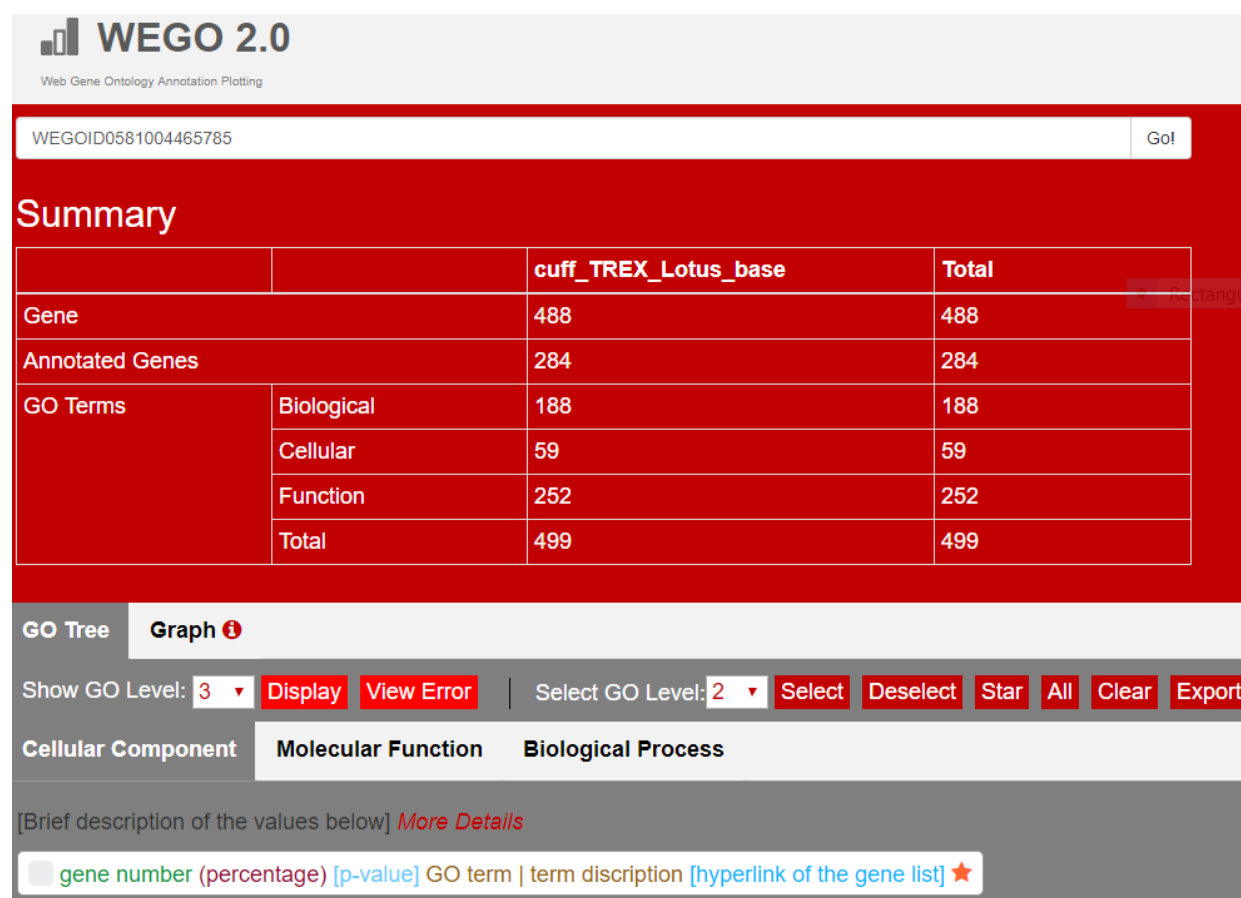


Figure 6-23 Desktop capture showing summary of results of WEGO analysis (web based tool for ontology visualization). 488 gene IDs (cufflinks analysis) were introduced into WEGO interface.

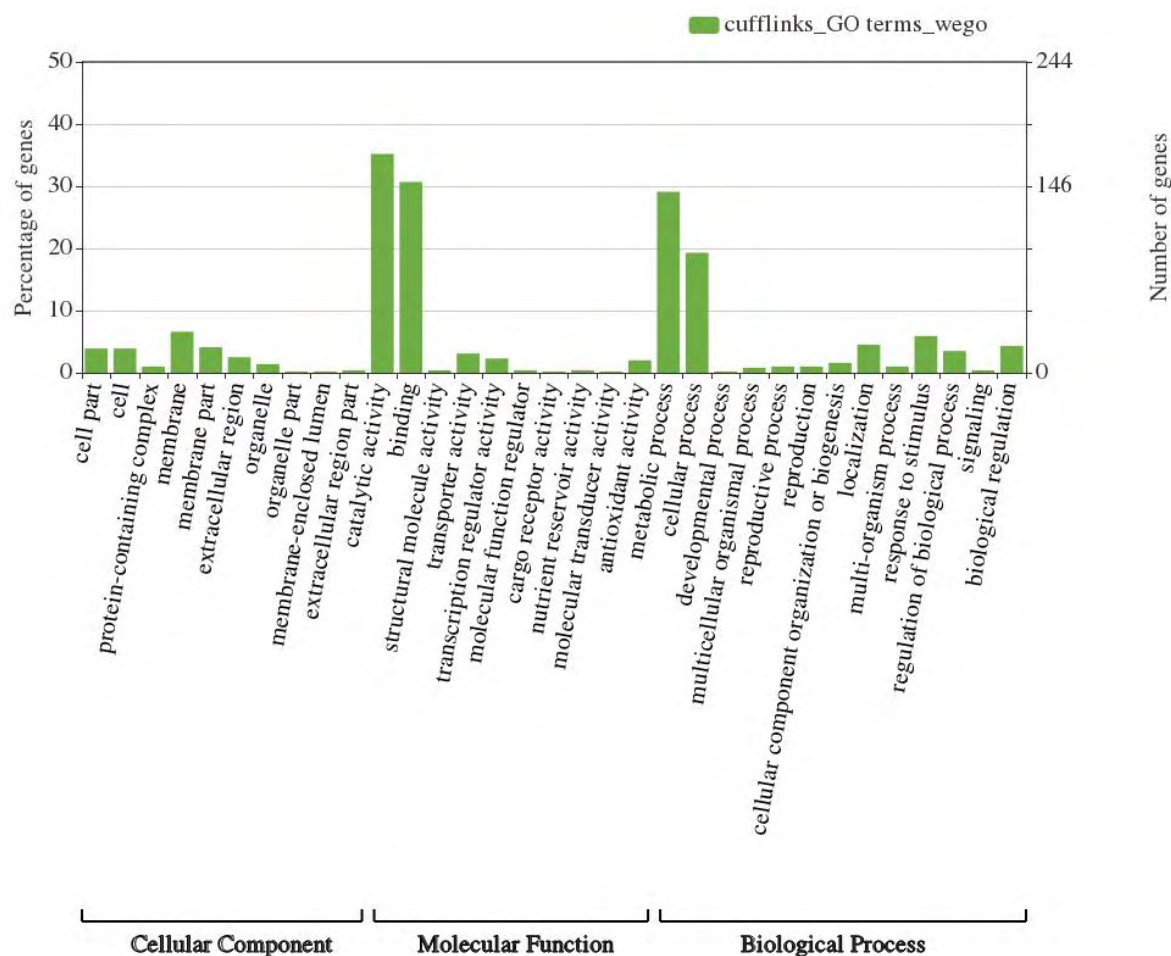


Figure 6-24 Histogram showing the list of GO terms (level 2) matching the gene IDs identified as DE via cufflinks analysis. DE gene IDs were first introduced to Lotus base and matched to multiple GO terms. The GO terms retrieved were entered as input into WEGO web based tool for visualization. Level 2 of GO terms is shown for simplification purposes. The y-axis on the left shows percentages of genes corresponding to each GO term. The y-axis on the right shows the exact number of genes matching to each GO term. All 3 Gene Ontology Aspects (Biological Process, Molecular Function, Cellular Component) are shown.

At the generic GO term level 2, overrepresented GO terms are: catalytic activity, binding, metabolic process, cellular process.

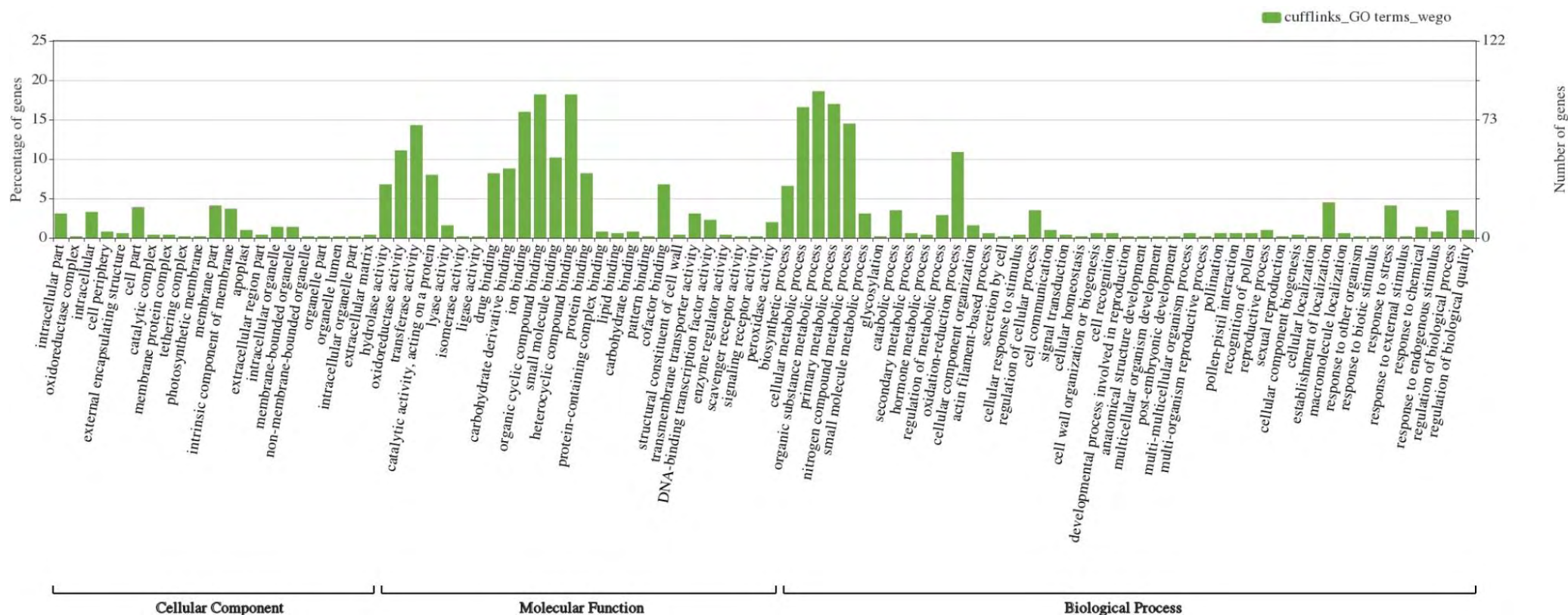


Figure 6-25 Histogram showing the list of GO terms (level 3) matching the gene IDs identified as DE via cufflinks analysis. DE gene IDs were first introduced to Lotus base and matched to multiple GO terms. The GO terms retrieved were entered as input into WEGO web based tool for visualization. Level 3 of GO terms is shown for simplification purposes. The y-axis on the left shows percentages of genes corresponding to each GO term. The y-axis on the right shows the exact number of genes matching to each GO term. All 3 Gene Ontology Aspects (Biological Process, Molecular Function, Cellular Component) are shown.

At the less generic GO terms level 3, overrepresented GO terms are: hydrolase activity, oxidoreductase activity, transferase activity, catalytic activity-binding on a protein, drug binding, carbohydrate derivative binding, ion binding, organic cyclic compound binding, small molecule binding, heterocyclic compound binding, protein binding, cofactor binding, biosynthetic process, cellular metabolic process, organic substance metabolic process, primary metabolic process, nitrogen compound metabolic process, oxidation-reduction process.

Gene ontology, terms are divided into different levels based on the specificity of a given term. The higher the level, the more specific the GO term is. The usefulness of levels is limited though in a GO term analysis, because different GO branches might have different levels. For example, a term can belong to a specific level in one branch, and to a different level in another branch. Undeniably, graphs comprising GO terms of higher levels would be much more informative, but such graphs were difficult to be presented, due to the large amount of GO terms they include. A more simplified version of GO terms matching the gene IDs identified is presented later in the present section.

The same procedure was followed for edgeR analysis. A total of 168 genes (those were the genes provided with a nucleic acid sequence in the original spreadsheet file) were introduced in the interface of WEGO web tool. The main results of the analysis as shown in WEGO site is shown in the desktop capture of Figure 6-26. Two histograms were generated, showing the GO terms matching the identified gene IDs. The first histogram is more generic (Figure 6-27), and shows how many genes matched to GO terms of level 2. A more detailed histogram was generated and is shown in Figure 6-28, by using GO terms of level 3.

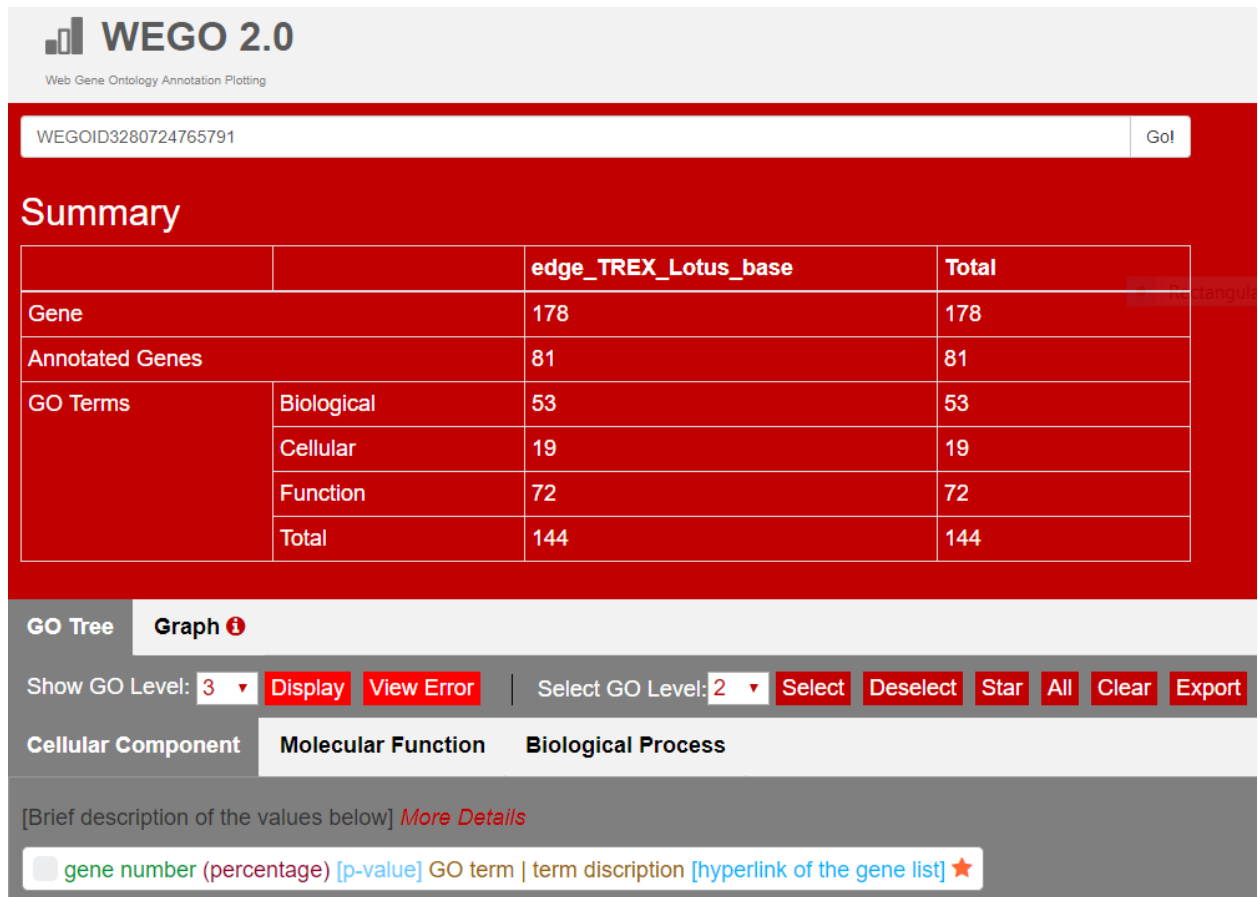


Figure 6-26 Desktop capture showing summary of results of WEGO analysis (web based tool for ontology visualization). 178 gene IDs (edgeR analysis) were introduced into WEGO interface.

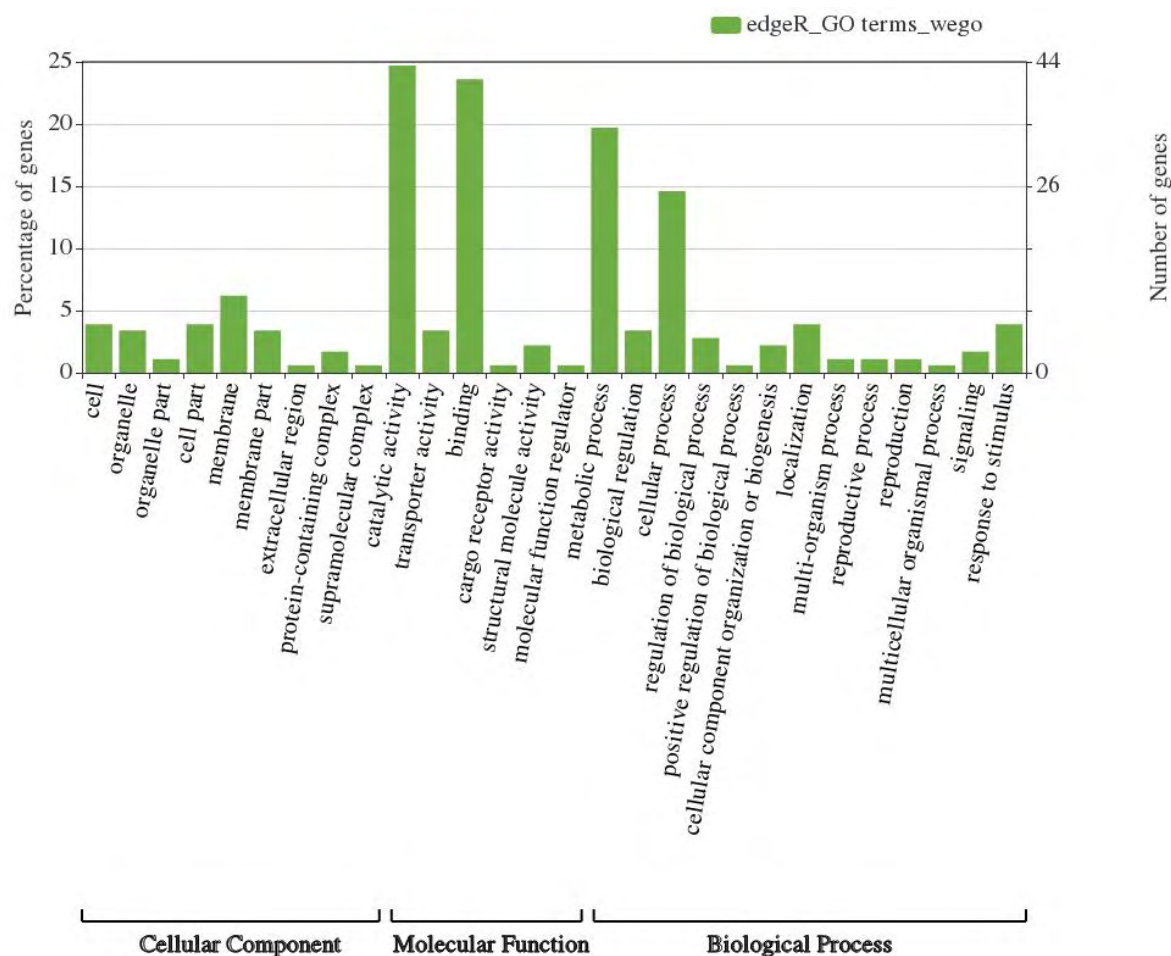


Figure 6-27 Histogram showing the list of GO terms (level 2) matching the gene IDs identified as DE via edgeR analysis. DE gene IDs were first introduced to Lotus base and matched to multiple GO terms. The GO terms retrieved were entered as input into WEGO web based tool for visualization. Level 2 of GO terms is shown for simplification purposes. The y-axis on the left shows percentages of genes corresponding to each GO term. The y-axis on the right shows the exact number of genes matching to each GO term. All 3 Gene Ontology Aspects (Biological Process, Molecular Function, Cellular Component) are shown.

At the generic GO term level 2, overrepresented GO terms are: catalytic activity, binding, metabolic process, cellular process.

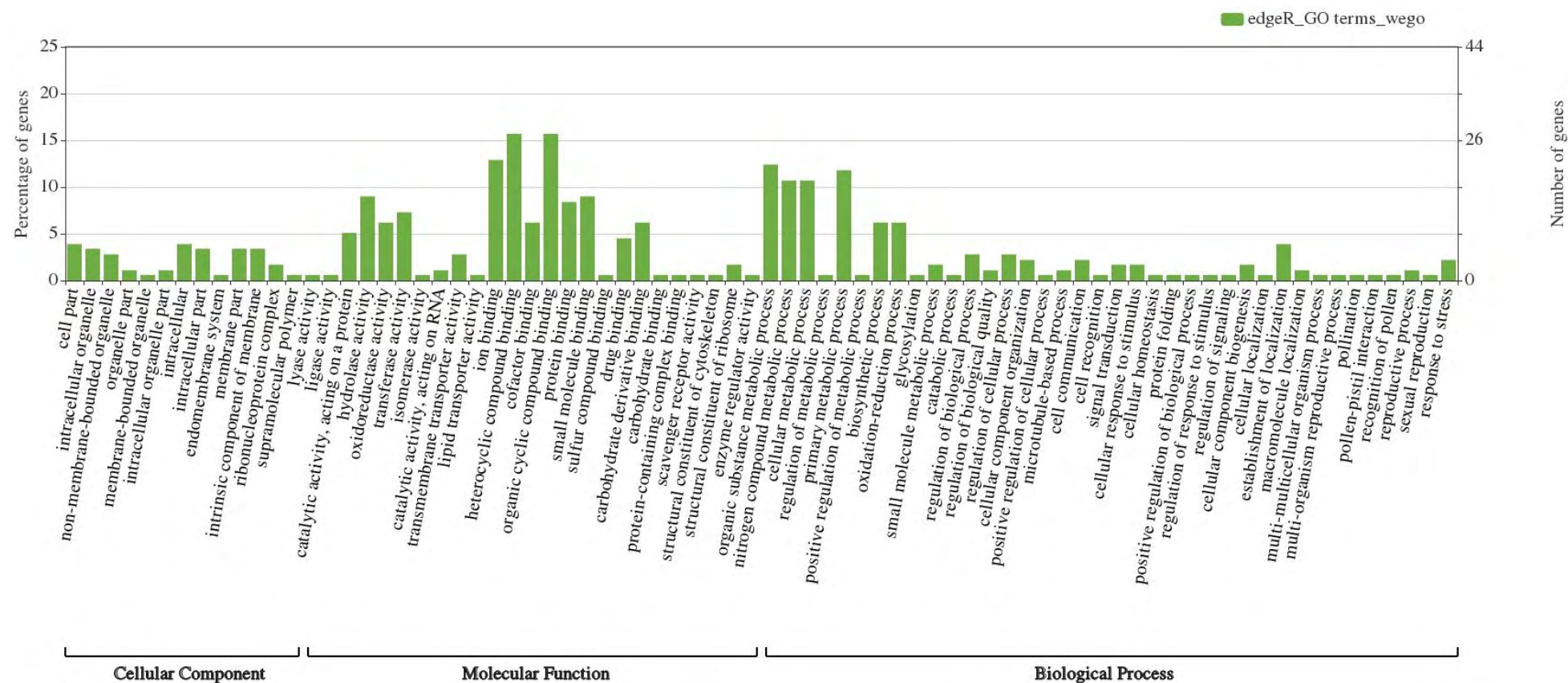


Figure 6-28 Histogram showing the list of GO terms (level 3) matching the gene IDs identified as DE via cufflinks analysis. DE gene IDs were first introduced to Lotus base and matched to multiple GO terms. The GO terms retrieved were entered as input into WEGO web based tool for visualization. Level 3 of GO terms is shown for simplification purposes. The y-axis on the left shows percentages of genes corresponding to each GO term. The y-axis on the right shows the exact number of genes matching to each GO term. All 3 Gene Ontology Aspects (Biological Process, Molecular Function, Cellular Component) are shown.

At the less generic GO terms level 3, overrepresented GO terms are: catalytic activity-acting on a protein, hydrolase activity, oxidoreductase activity, transferase activity, ion binding, heterocyclic compound binding, cofactor binding, organic cyclic compound binding, protein binding, small molecule binding, carbohydrate derivative binding, organic substance metabolic process, nitrogen compound metabolic process, cellular metabolic process, primary metabolic process, biosynthetic process, oxidation-reduction process

○ *Analysis of up- and downregulated GO terms using Lotus base*

The process used to assign GO terms to the identified *L. japonicus* DEGs is described below:

The list of DEGs identified via cufflinks analysis was filtered as follows:

1. q-value ≤ 0.05
2. the DEGs corresponding to infinite \log_2FC values (plus or minus) were filtered out
3. Only DEGs with $FC \geq 2$ (and therefore absolute $\log_2FC \geq 1$) were kept for subsequent analysis

The list of DEGs identified via edgeR analysis was filtered as follows:

1. FDR ≤ 0.05
2. Only DEGs with $FC \geq 2$ (and therefore absolute $\log_2FC \geq 1$) were kept for subsequent analysis

The following steps were the same for both DEG lists (edgeR and cufflinks).

DEGs remaining after filtering were matched to *Lotus japonicus* annotation file based on identified gene ID. In that way, each gene ID was matched to a GO term. Gene IDs that did not match a GO term were filtered out. Note that in this step, gene IDs might correspond to multiple GO terms aspects. The gene ID column was ordered based on the following Ontology aspect order: Biological Process > Molecular Function > Cellular Component. Gene IDs that correspond to multiple Gene Ontology aspects were removed in the above mentioned order. For example, if a gene ID corresponded to a Biological Process Aspect GO term and simultaneously in a Molecular Function GO term, then the Molecular Function term was removed and only the Biological Process was kept. GO terms generated were uploaded to Princeton Uni slimmer tool (<https://go.princeton.edu/cgi-bin/GOTermMapper>) by using *Arabidopsis thaliana* as annotation organism (TAIR) and by choosing the appropriate Ontology aspect (BP, MF, CC) in order to retrieve generic GO annotations for each term that will be used for simplification reasons and for visualization of results. The slim GO annotations were exported into a spreadsheet and the generated file was used to match gene IDs, GO terms identified via *Lotus* base and generic GO annotations retrieved via the above mentioned slimmer tool. In cases where a slimmer GO annotation was not assigned to a GO term, the GO annotation was identified via the 'Gene Ontology Resource' (<http://geneontology.org/>) and was assigned manually.

GO annotations were used to generate the barplots presented below, which give an overview of annotations corresponding to up- and downregulated genes.

It should be noted that this is just a way of visualization of results. A gene usually corresponds to multiple GO terms, since genes have more than one roles/functions. In the plots presented, only one GO term (the most representative one, wherever that was possible) was kept for each gene ID. To this respect, a number of GO terms is not shown due to space limitations within the plots.

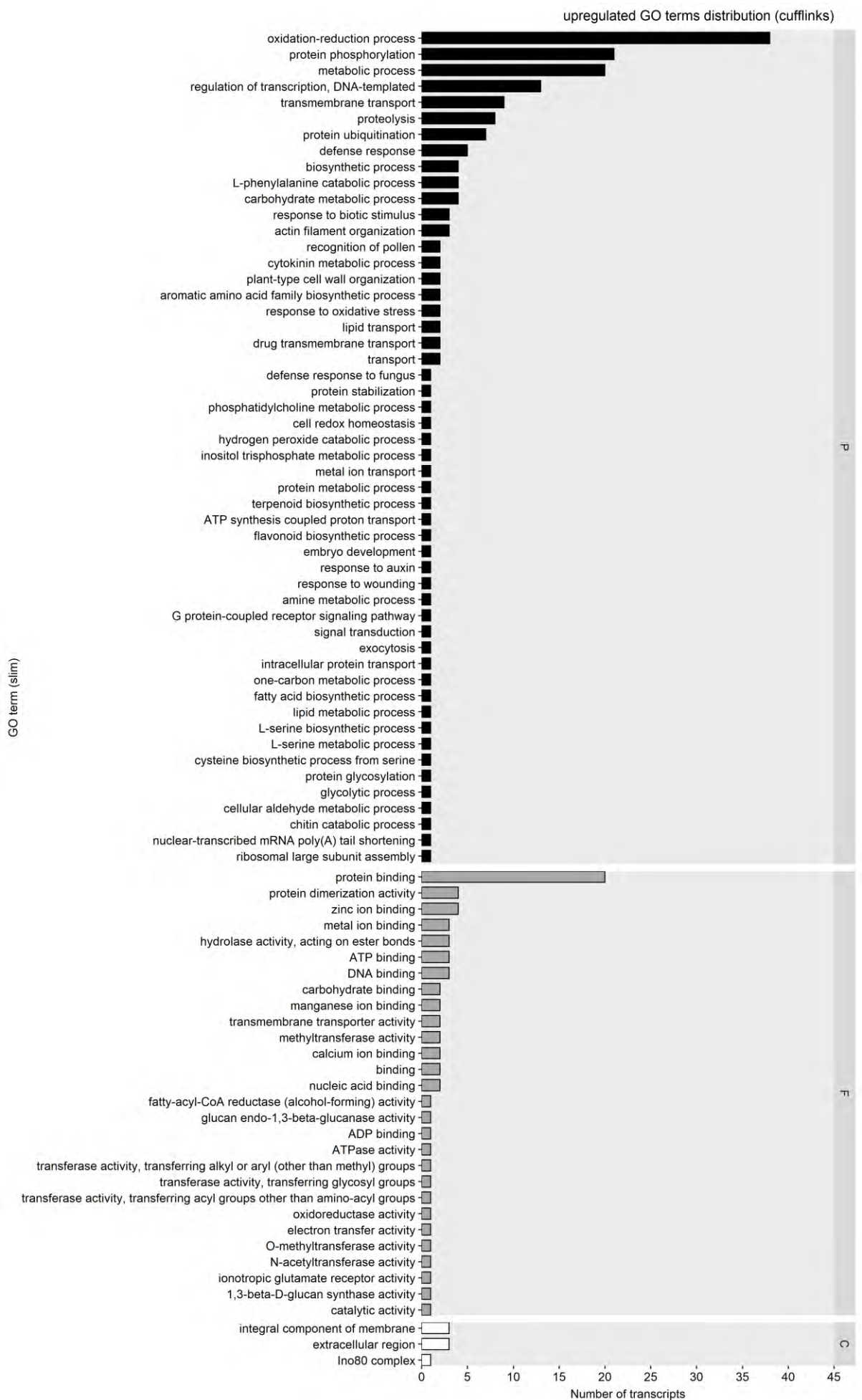


Figure 6-29 GO annotations of DEGs in FsK colonized *L. japonicus* roots identified via cufflinks analysis. GO term annotation of upregulated DEGs in FsK-colonized roots as identified by performing the appropriate filtering steps: 1) q-value cut-off at 0.05, 2) absolute log₂ fold change ≥ 1 .

Only Lotus DEGs matching a GO prediction were included in the analysis. DEGs are summarized in 3 main categories: biological process (P), molecular function (F), and cellular component (C). The DE analysis was performed via cufflinks software. The Gene Ontology analysis was performed using the 'Lotus japonicus MG20 v3.0 gene ontology (GO) annotation file' (<https://lotus.au.dk/data/download>). DEG IDs as provided via cufflinks analysis were compared and matched to GO annotations assigned to Lotus japonicus genome gene IDs. For simplification, GO categories were kept for presentation by respecting the following order: B > F > C (i.e. if a GO term matched both a BP and a MF aspect, only the BP process aspect was kept). GO annotations were furthermore mapped to more generic terms by using the 'Generic Gene Ontology (GO) Term Mapper' web tool of Princeton University (<https://go.princeton.edu/cgi-bin/GOTermMapper>), by using *Arabidopsis thaliana* (TAIR) as annotation organism, and by choosing the appropriate Ontology Aspect (Process, Function, Component). All transcripts matching GO annotations are shown in the plot. The y-axis indicates the GO sub-categories and the x-axis indicates the frequency distribution of each category in the DEG list.

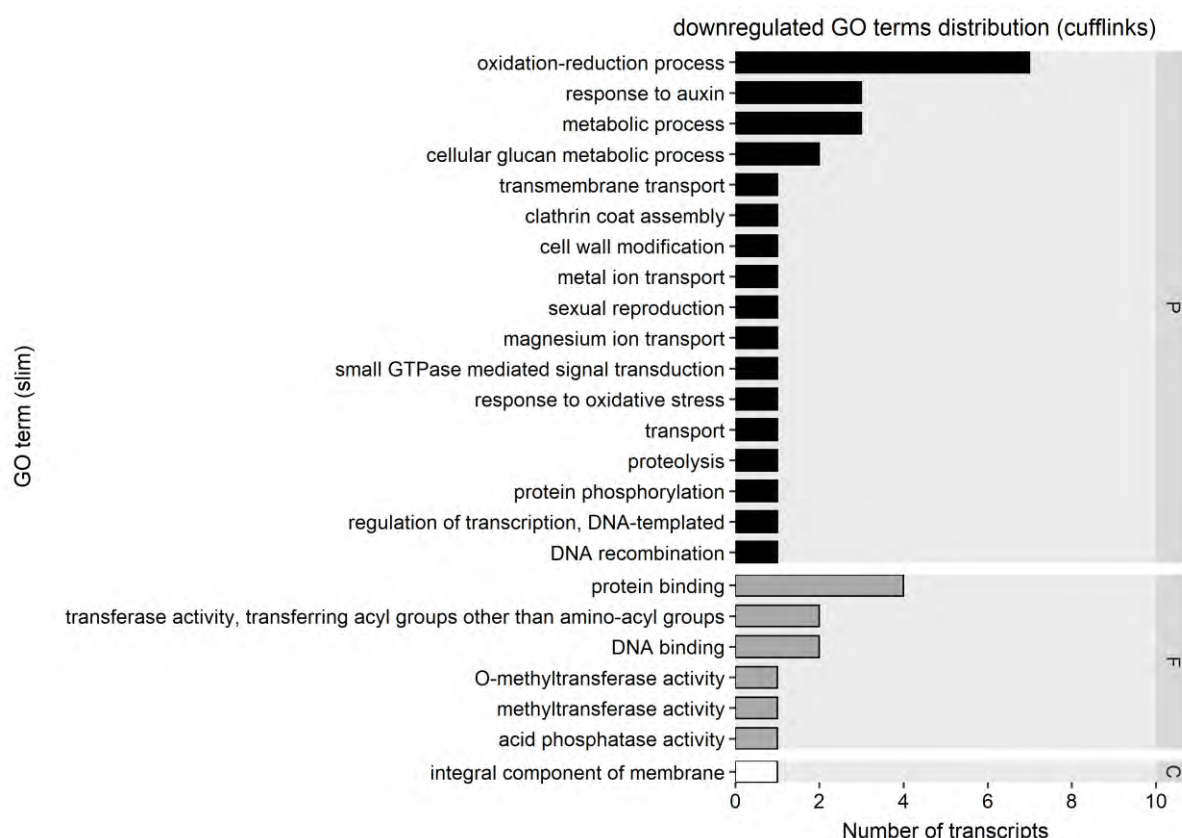


Figure 6-30 GO annotations of DEGs in FsK colonized *L. japonicus* roots identified via cufflinks analysis. GO term annotation of downregulated DEGs in FsK-colonized roots as identified by performing the appropriate filtering steps: 1) q-value cut-off at 0.05, 2) absolute log₂ fold change ≥ 1 .

Only Lotus DEGs matching a GO prediction were included in the analysis. DEGs are summarized in 3 main categories: biological process (P), molecular function (F), and cellular component (C). The DE analysis was performed via cufflinks software. The Gene Ontology analysis was performed using the 'Lotus japonicus MG20 v3.0 gene ontology (GO) annotation file' (<https://lotus.au.dk/data/download>). DEG IDs as provided via cufflinks analysis were compared and matched to GO annotations assigned to Lotus japonicus genome gene IDs. For

simplification, GO categories were kept for presentation by respecting the following order: $B > F > C$ (i.e. if a GO term matched both a BP and a MF aspect, only the BP process aspect was kept). GO annotations were furthermore mapped to more generic terms by using the 'Generic Gene Ontology (GO) Term Mapper' web tool of Princeton University (<https://go.princeton.edu/cgi-bin/GOTermMapper>), by using *Arabidopsis thaliana* (TAIR) as annotation organism, and by choosing the appropriate Ontology Aspect (Process, Function, Component). All transcripts matching GO annotations are shown in the plot. The y-axis indicates the GO sub-categories and the x-axis indicates the frequency distribution of each category in the DEG list.

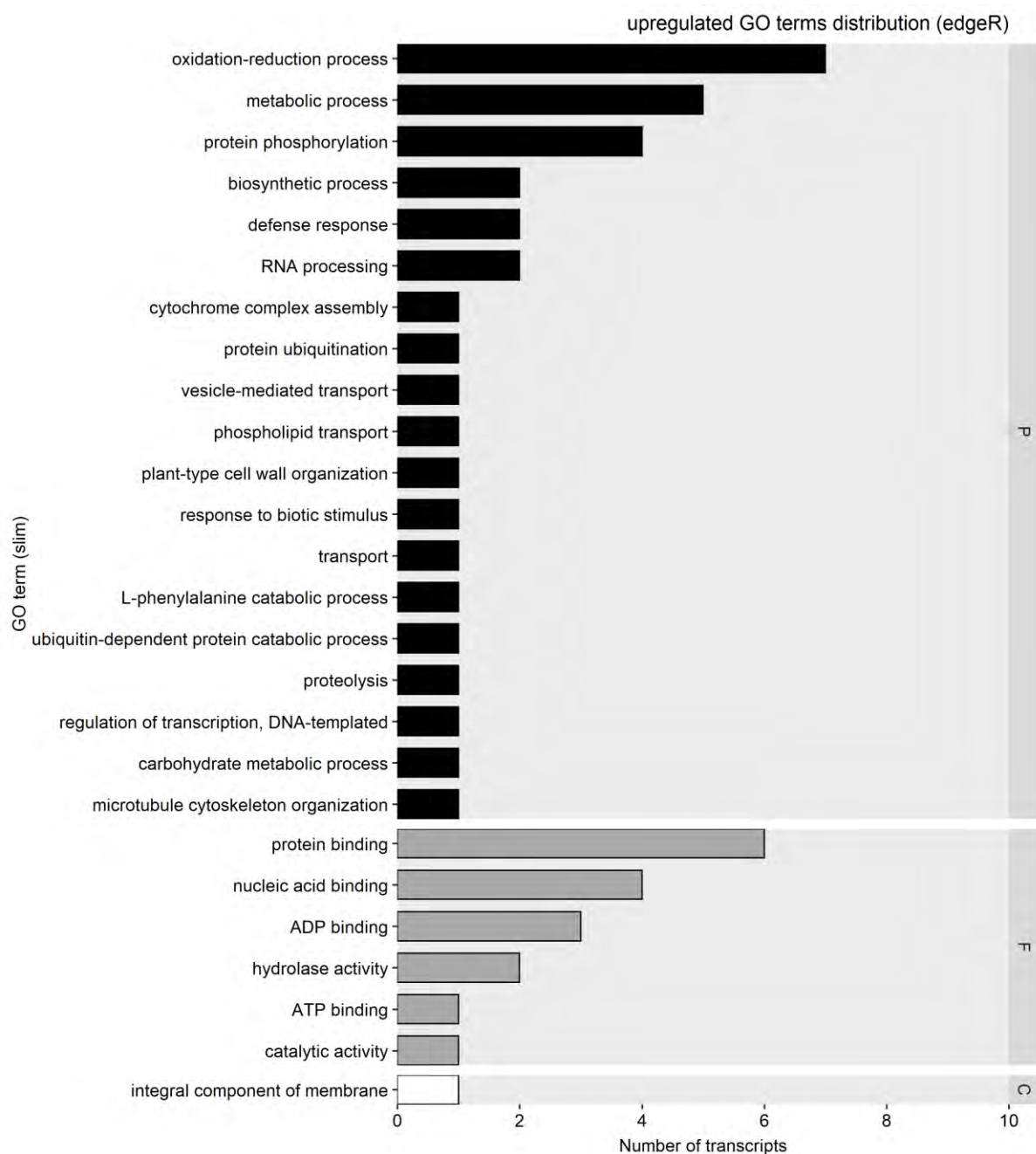


Figure 6-31 GO annotations of DEGs in FSK colonized *L. japonicus* roots identified via edgeR analysis. GO term annotation of upregulated DEGs in FSK-colonized roots as identified by performing the appropriate filtering steps: 1) FDR cut-off at 0.05, 2) absolute log2 fold change ≥ 1 .

Only Lotus DEGs matching a GO prediction were included in the analysis. DEGs are summarized in 3 main categories: biological process (P), molecular function (F), and cellular component (C). The DE analysis was performed via edgeR software. The Gene Ontology analysis was performed using the 'Lotus japonicus MG20 v3.0 gene ontology (GO) annotation file' (<https://lotus.au.dk/data/download>). DEG IDs as provided via cufflinks analysis were compared and matched to GO annotations assigned to Lotus japonicus genome gene IDs. For simplification, GO categories were kept for presentation by respecting the following order: B > F > C (i.e. if a GO term matched both a BP and a MF aspect, only the BP process aspect was kept). GO annotations were furthermore mapped to more generic terms by using the 'Generic Gene Ontology (GO) Term Mapper' web tool of Princeton University (<https://go.princeton.edu/cgi-bin/GOTermMapper>), by using *Arabidopsis thaliana* (TAIR) as annotation organism, and by choosing the appropriate Ontology Aspect (Process, Function, Component). All transcripts matching GO annotations are shown in the plot. The y-axis indicates the GO sub-categories and the x-axis indicates the frequency distribution of each category in the DEG list.

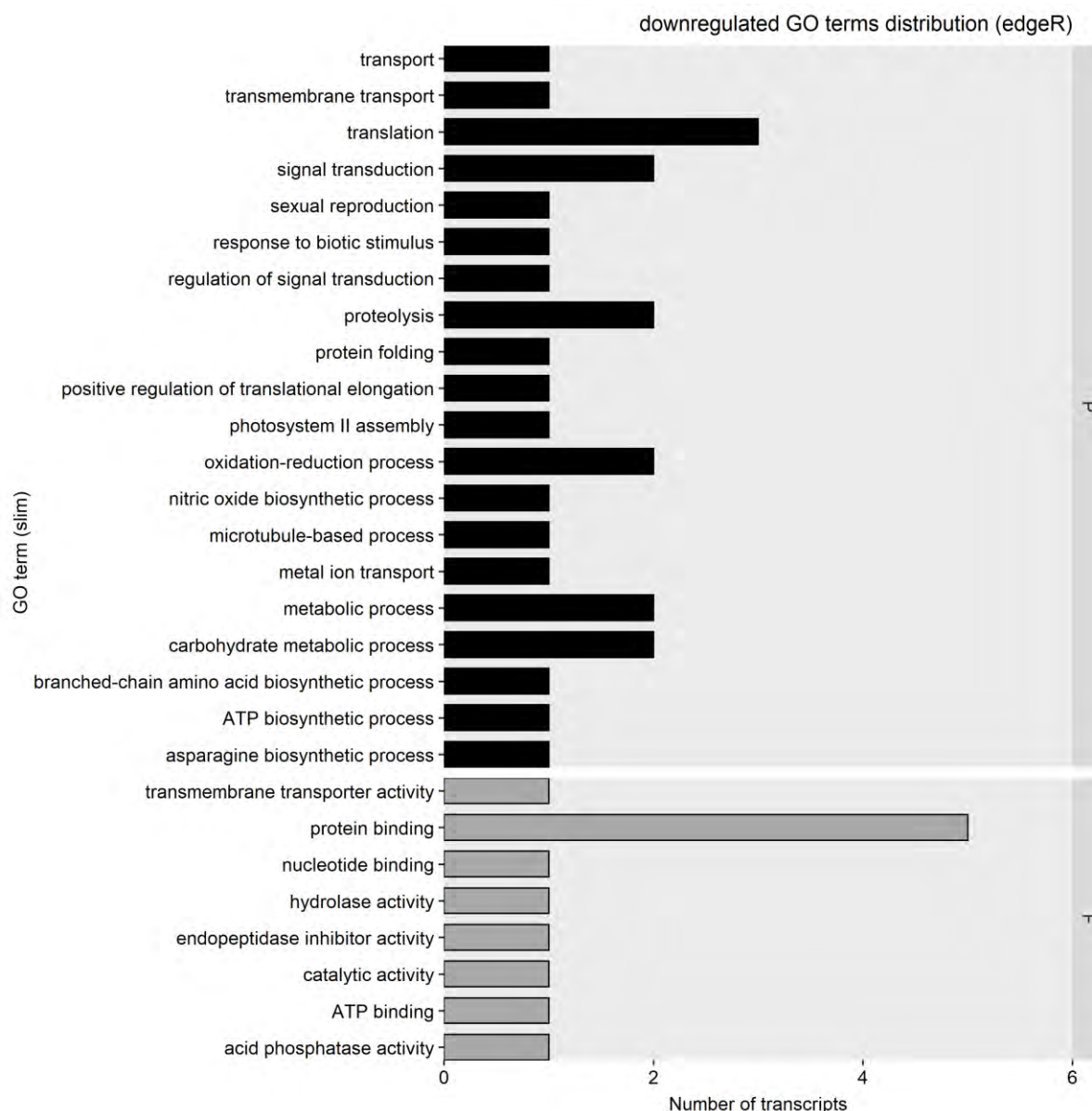


Figure 6-32 GO annotations of DEGs in FsK colonized *L. japonicus* roots identified via edgeR analysis. GO term annotation of downregulated DEGs in FsK-colonized roots as identified by performing the appropriate filtering steps: 1) FDR cut-off at 0.05, 2) absolute log₂ fold change ≥ 1 .

Only Lotus DEGs matching a GO prediction were included in the analysis. DEGs are summarized in 3 main categories: biological process (P), molecular function (F), and cellular component (C). The DE analysis was performed via edgeR software. The Gene Ontology analysis was performed using the 'Lotus japonicus MG20 v3.0 gene ontology (GO) annotation file' (<https://lotus.au.dk/data/download>). DEG IDs as provided via cufflinks analysis were compared and matched to GO annotations assigned to Lotus japonicus genome gene IDs. For simplification, GO categories were kept for presentation by respecting the following order: B > F > C (i.e. if a GO term matched both a BP and a MF aspect, only the BP process aspect was kept). GO annotations were furthermore mapped to more generic terms by using the 'Generic Gene Ontology (GO) Term Mapper' web tool of Princeton University (<https://go.princeton.edu/cgi-bin/GOTermMapper>), by using Arabidopsis thaliana (TAIR) as annotation organism, and by choosing the appropriate Ontology Aspect (Process, Function, Component). All transcripts matching GO

annotations are shown in the plot. The y-axis indicates the GO sub-categories and the x-axis indicates the frequency distribution of each category in the DEG list.

- Using Function Annotator web based tool to gain insight on the DEGs identified via cufflinks analysis

Function Annotator (FA) is a web based tool (Chen et al., 2017), which offers annotations, including GO term assignment, enzyme annotation, domain/motif identification, and predictions for subcellular localization. FA also provides the distribution of species from best hits at different taxonomic levels. Users upload a FASTA file format containing the nucleotide sequences on FA interface, and proceed with the desired analysis.

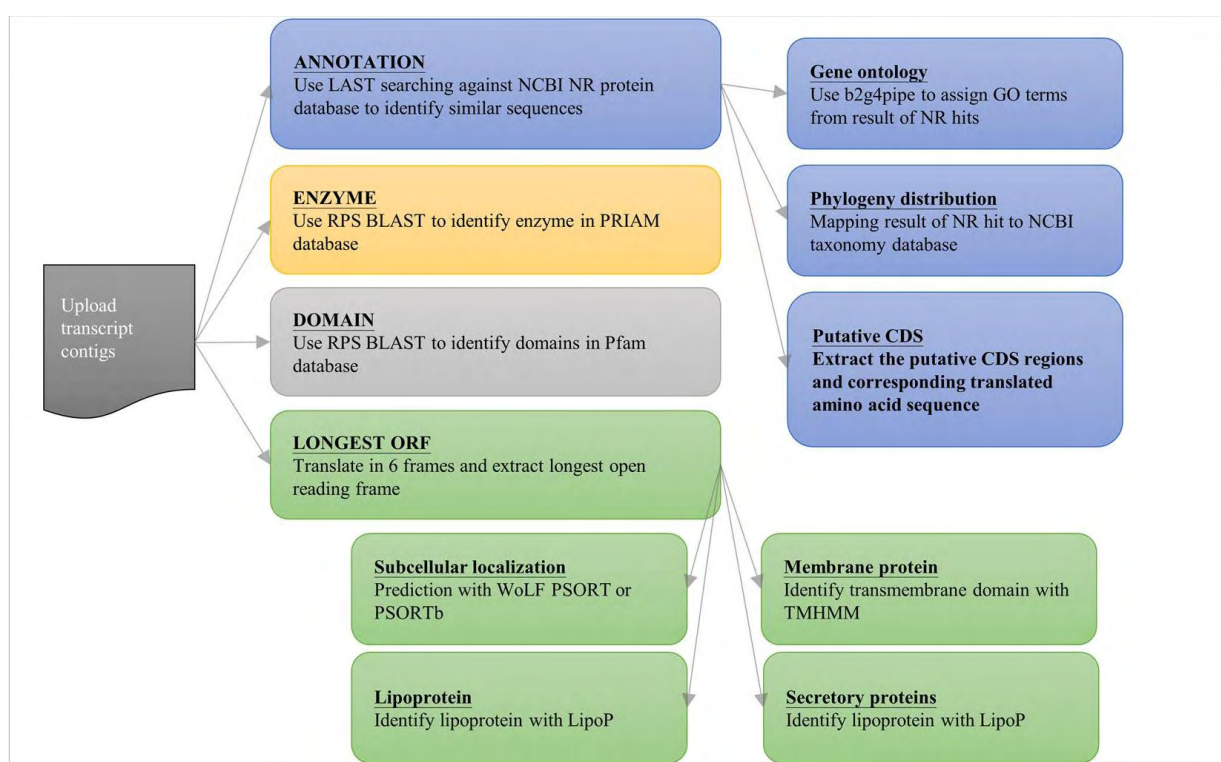


Figure 6-33 Overview of the annotation system implemented in Function Annotator web based tool.

FA provided a file containing predictions on the subcellular localization of proteins corresponding to the DE genes identified via cufflinks/edgeR in *Lotus*-FsK system. FA uses the WoLF PSORT protein subcellular localization prediction tool (<https://wolfpsort.hgc.jp/>). Using these results, barplots were constructed (Figure 6-34, 6-35) that indicate the number of plant proteins corresponding to a specific subcellular compartment.

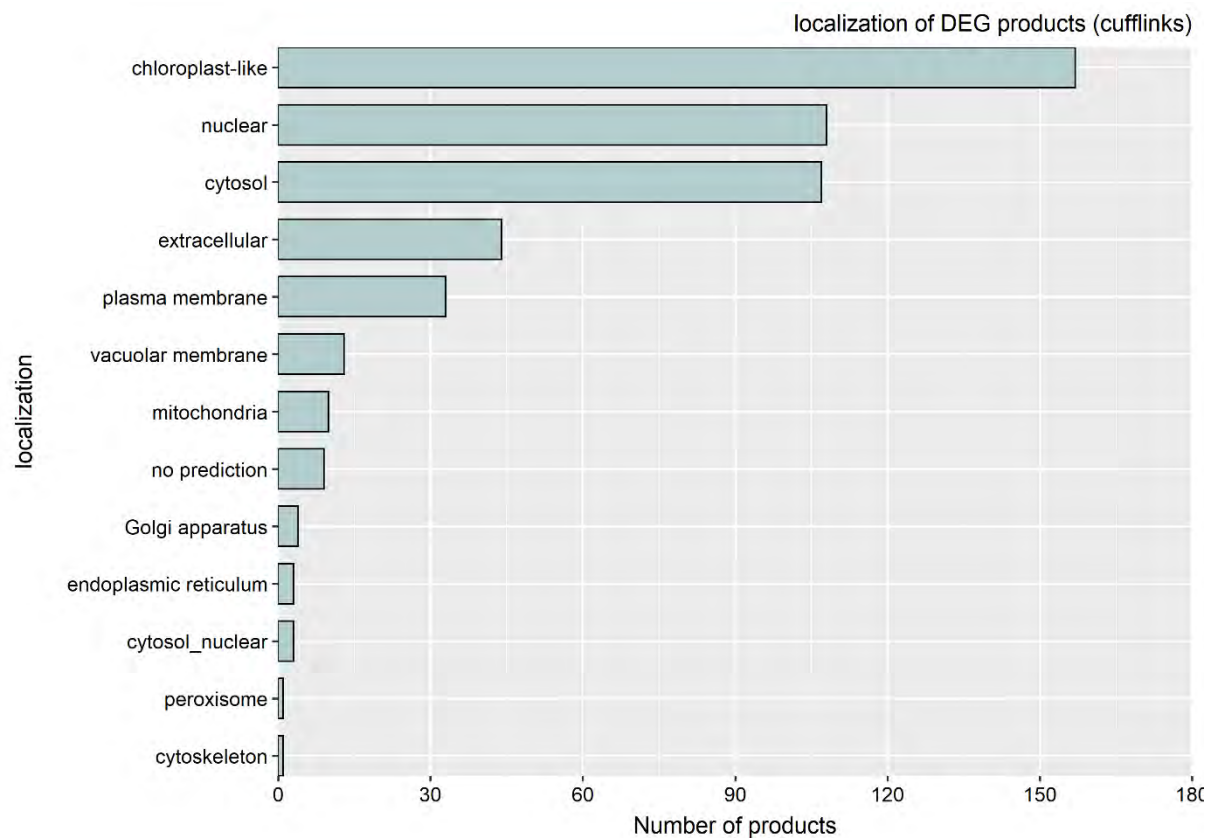


Figure 6-34 Barplot demonstrating the number of proteins matching a certain subcellular localization prediction. DE genes coding for the proteins were identified via cufflinks analysis.

Subcellular compartments matching the higher percentages of DEG products were: chloroplast, nucleus, cytosol, extracellular region, plasma membrane.

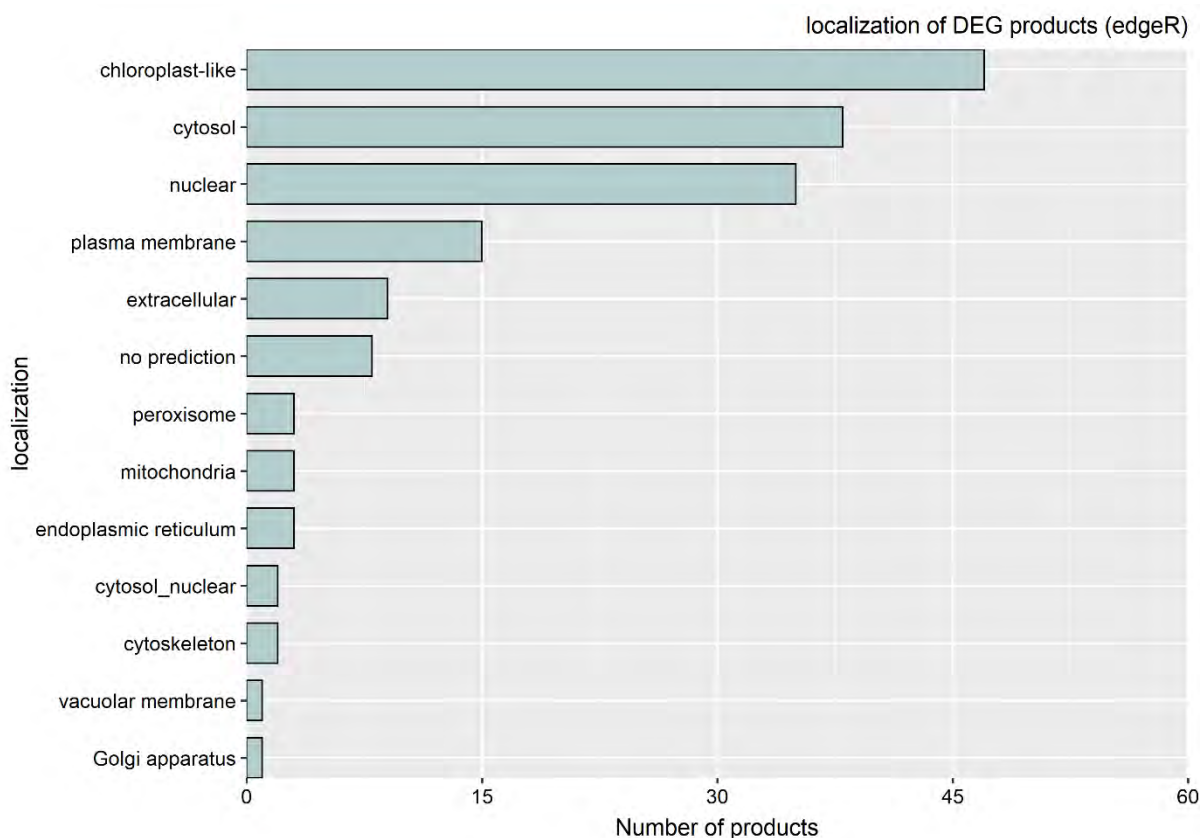


Figure 6-35 Barplot demonstrating the number of proteins matching a certain subcellular localization prediction. DE genes coding for the proteins were identified via edgeR analysis.

Subcellular compartments matching the higher percentages of DEG products were: chloroplast, cytosol, nucleus, plasma membrane, extracellular region.

6.3.2.5 Analysis of DE genes identified with cufflinks analysis

Based on the literature, the most accurate way to proceed would be to analyze the intersection of the gene lists provided via cufflinks and edgeR analysis, but since this intersection comprised only 20 genes, it was assumed that both software analyses provided to some extent accurate identification of DEGs, but for a yet unknown reason, results obtained differ. It should be noted that both analyses resulted in more or less the same generic GO terms enriched, despite differences in the gene ID level. For example, among the common main categories enriched are: hydrolase activity, oxidoreductase activity, transferase activity, catalytic activity-binding on a protein, carbohydrate derivative binding, ion binding, organic cyclic compound binding, small molecule binding, heterocyclic compound binding, protein binding, cofactor binding, biosynthetic process, cellular metabolic process, organic substance metabolic process, primary metabolic process, nitrogen compound metabolic process, oxidation-reduction process. Almost all these GO terms are highly enriched in both cufflinks and edgeR analysis, as indicated via exploration of the data with the WEGO web based tool (described above).

It is hypothesized that both software accurately identified DEGs of the *Lotus*-FsK dataset, but differences lie in the detection power of the two. The reason behind the differences might not lie in the

FC of differential expression, since a filtering based on the same FC cut-off has been performed. Differences might be attributed on low counts in one of the two treatments or in some replicates of both treatments. For example, from a visual examination of results after filtering steps, there is the impression that cufflinks identified as DE more transcripts at the low count level, whereas edgeR identified as DE transcripts exhibiting high count levels. In that respect, edgeR might have filtered out gene IDs with very low count levels (despite the actual FC difference between the two treatments). This might also reflect on the statistical analysis used by the two software (exact test vs t-test, based on the literature).

Another factor contributing to the differences could be the lack of many biological replicates in our system. The number of biological replicates is among the most important factors determining the outcome of an RNA seq experiment, with edgeR software performing well with a small number to none biological replicates (Zhang et al., 2014). In an attempt to compensate for the lack of a high number of biological replicates per treatment due to cost limitations, each biological replicate sent for analysis (3 per condition, except the Fsk-inoculated plant sample where 2 biological replicates were processed due to a mistake of the sequencing provider) comprised of multiple individual biological replicates (see Materials and methods section of this chapter).

This might indicate that despite suggestions by researchers that the DEGs intersection derived by multiple software analyses contributes to accurate identification of differential expression in RNA seq experiments, there might be cases where their union might reflect the reality. Of course this necessitates further investigation.

For the purposes of the present thesis, only genes identified via cufflinks analysis are furthermore processed and discussed. At any rate, since DEGs identified were strictly filtered ($q\text{-value} \leq 0.05$ and $FC \geq 2$) the accuracy of the results is ensured at some level. On the contrary, due to the strict filtering set, a high number of genes is not included, and which perhaps show some level of regulation during *Lotus*-Fsk interaction. Of course, the accuracy of the results will be verified by qPCR analysis of both high and low DE genes identified, an aim of future work.

A manual classification of DEGs into functional groups was attempted, based on the groups presented in (Hogekamp et al., 2011), which were furthermore modified and others were included in order to serve the purpose of the analysis and to best characterize the set of transcripts identified herein. Each individual gene ID-corresponding-annotation was 'searched' against the UniProt database (<https://www.uniprot.org/>) to retrieve information based on findings from other well-annotated plant systems (*Arabidopsis thaliana*, *Medicago truncatula*, *Glycine max*). This search into UniProt database aided classification of genes into the 25 categories: 1) Proteins involved in signaling 2) Proteins related to carbohydrate metabolism, 3) Lectins, 4) Germin-like proteins, 5) Proteins related to endo-/exocytosis (including those related to vesicular trafficking), 6) Proteins involved in defense, 7) Proteins related to abiotic stress, 8) Proteins related to cell wall synthesis and modifications, 9) Proteins involved in cell modifications, 10) Proteins related to transmembrane transport (including proteins involved in general transport mechanisms), 11) Proteins related to ion binding, 12) Putative secreted proteins, 13) Proteins involved in nucleotide metabolism (DNA and RNA), 14) Proteins involved in gene expression (transcription), 15) Proteins involved in protein biosynthesis, 16) Proteins involved in protein processing,

17) Proteins involved in protein degradation (including protease inhibitors), 18) Proteins related to primary metabolism, 19) Proteins related to secondary metabolism, 20) Lipid metabolism, 21) Proteins related to hormone metabolism, 22) Proteins responding to hormones, 23) Proteins related to redox metabolism, 24) Proteins involved in other physiological processes, 25) Unknown and uncharacterized proteins.

Functional categories and gene IDs corresponding to them are presented below in separate tables. The annotation as well as a more generic term corresponding to each gene ID were retrieved from *Lotus* base and are also presented. The log2FC of each transcript is also given in a separate column.

To complement the analysis, gene IDs identified in *Lotus*-FsK dataset were searched against the (Handa et al., 2015) RNA seq dataset. The latter describes the transcriptomic profile of the plant and the fungus in a *L. japonicus*-*R. irregularis* association, and a comparison of this profile with the transcriptome profile of the plant in association with rhizobia. (Handa et al., 2015) processed in their analysis the following *L. japonicus* root samples: a) AMF 15dpi, b) AMF 27dpi, c) no AMF 15 dpt (days post transplantation), d) rhizobia 3 dpi, e) rhizobia 12 dpi, f) no rhizobia 3 dpt. We chose for comparisons the samples: 'AMF 15dpi' and 'rhizobia 3dpi' since these correspond to relatively initial stages of AM and LR symbiosis, and the respective controls comprise plants of the same age as the treated samples. So, two extra columns are included in each table, demonstrating for each gene ID identified in *Lotus*-FsK dataset, the log2FC of the same gene ID in *Lotus* roots associated with AMF or rhizobia. To this respect, a direct comparison among the 3 plant-microbe associations can be performed, also complementing results presented in Chapter 3 of the present thesis regarding CSSP and CSSP-dependent gene expression analysis.

The functional categories of main DEGs identified are presented below:

1. Proteins involved in signaling

Gene ID	Annotation (hit)	Lotus base annotation	log2FC	q value	log2FC_Rh	log2FC_AMF
Lj4g3v1085080	PREDICTED: cysteine-rich receptor-like protein kinase 3-like [Glycine max] gi 356567656 ref XP_003552033.1	Cysteine-rich receptor-like protein kinase 3-like	2.6	0.001	-	-1
Lj0g3v0346649	PREDICTED: probable leucine-rich repeat receptor-like serine/threonine-protein kinase At3g14840-like isoform X1 [Cicer arietinum] gi 502089237 ref XP_004488850.1	Probable leucine-rich repeat receptor-like serine/threonine-protein kinase At3g14840-like isoform X1	2.2	0.001	2.3	-2.3
Lj2g3v1560870	PREDICTED: proline-rich receptor-like protein kinase PERK2-like [Cicer arietinum] gi 502142195 ref XP_004504838.1		2.2	0.001	-	-
Lj0g3v0107979	Plastid movement impaired 2 [Theobroma cacao] gi 508712106 gb EOY04003.1		2	0.001	1.3	-
Lj2g3v1155520	PREDICTED: IgA FC receptor-like [Glycine max] gi 356552286 ref XP_003544499.1		1.9	0.001	1.4	-3.8
Lj0g3v0176959	histidine kinase [Rivularia sp. PCC 7116] gi 427739404 ref YP_007058948.1		1.7	0.001	-	-
Lj0g3v0314389	PREDICTED: wall-associated receptor kinase 5-like [Glycine max] gi 356551203 ref XP_003543967.1	Wall-associated receptor kinase 5-like	1.7	0.001	-	-
Lj4g3v0496530	PREDICTED: glutamate receptor 2.7-like [Glycine max] gi 356519637 ref XP_003528477.1	Glutamate receptor 2.7-like	1.7	0.001	-	-1
Lj2g3v0852090	PREDICTED: receptor-like protein kinase HSL1-like [Glycine max] gi 356497583 ref XP_003517639.1	Receptor-like protein kinase HSL1-like	1.7	0.001	2.2	-1.9

Chapter 6

Lj2g3v1880820	PREDICTED: mitogen-activated protein kinase kinase 1-like [Glycine max] gi 356496902 ref XP_003517304.1	Mitogen-activated protein kinase kinase kinase 1-like	1.7	0.011	6.2	-6.5
Lj6g3v2193570	PREDICTED: proline-rich receptor-like protein kinase PERK2-like [Cicer arietinum] gi 502142195 ref XP_004504838.1		1.7	0.001	-	-
Lj1g3v1798860	Ankyrin repeat domain-containing protein [Medicago truncatula] gi 357465949 ref XP_003603259.1	Ankyrin repeat domain-containing protein	1.6	0.045	1	
Lj0g3v0250199	PREDICTED: cysteine-rich receptor-like protein kinase 29-like [Glycine max] gi 356574368 ref XP_003555320.1	Cysteine-rich receptor-like protein kinase 29-like	1.4	0.001	1	-1.4
Lj0g3v0295619	beta-glucan-elicitor receptor [Glycine max] gi 1752734 dbj BAA11407.1	Beta-glucan-elicitor receptor	1.4	0.001	1.2	-
Lj0g3v0089049	Pheromone receptor-like protein [Medicago truncatula] gi 357465437 ref XP_003603003.1		1.3	0.001	1.3	-
Lj0g3v0173689	PREDICTED: wall-associated receptor kinase 5-like [Glycine max] gi 356551203 ref XP_003543967.1	Wall-associated receptor kinase 5-like	1.3	0.001	-1.6	-
Lj0g3v0182159	PREDICTED: LOW QUALITY PROTEIN: serine/threonine-protein kinase ATM-like [Cicer arietinum] gi 502133902 ref XP_004501929.1	Serine/threonine-protein kinase ATM-like	1.3	0.002	-	-
Lj0g3v0258629	PREDICTED: protein KIAA0664 homolog [Glycine max] gi 356508390 ref XP_003522940.1		1.3	0.004	-	-
Lj0g3v0271569	PREDICTED: ankyrin repeat-containing protein At5g02620-like [Glycine max] gi 356546390 ref XP_003541609.1		1.3	0.001	2.6	-3.3
Lj0g3v0321459	Cysteine-rich receptor-like protein kinase [Medicago truncatula] gi 357490335 ref XP_003615455.1	Cysteine-rich receptor-like protein kinase	1.3	0.001	-	-
Lj3g3v3337420	Extra-large G-protein 1 [Theobroma cacao] gi 508699367 gb EOX91263.1	Extra-large G-protein 1	1.3	0.001	-	-
Lj1g3v2910560	PREDICTED: probable LRR receptor-like serine/threonine-protein kinase At4g08850-like isoform X1 [Cicer arietinum] gi 502106329 ref XP_004492917.1	Probable LRR receptor-like serine/threonine-protein kinase At4g08850-like isoform X1	1.3	0.012	1.6	-
Lj4g3v1477230	inositol phosphate kinase [Glycine max] gi 351721472 ref NP_001237466.1	Inositol phosphate kinase	1.3	0.001	-1.2	1.1
Lj0g3v0207799	Receptor-like protein kinase [Medicago truncatula] gi 357458061 ref XP_003599311.1		1.2	0.047	1.1	-
Lj0g3v0234429	Nuclear receptor corepressor [Medicago truncatula] gi 357443347 ref XP_003591951.1		1.2	0.003	-	1
Lj0g3v0241709	PREDICTED: receptor-like serine/threonine-protein kinase At4g25390-like [Cicer arietinum] gi 502119504 ref XP_004496642.1	Receptor-like serine/threonine-protein kinase At4g25390-like	1.2	0.001	-	1.1
Lj1g3v1687840	Cysteine-rich receptor-like protein kinase [Medicago truncatula] gi 357465633 ref XP_003603101.1	Cysteine-rich receptor-like protein kinase	1.2	0.001	-	1
Lj3g3v0392830	Cysteine-rich receptor-like protein kinase [Medicago truncatula] gi 357515961 ref XP_003628269.1	Cysteine-rich receptor-like protein kinase	1.2	0.01	1.9	-1.1
Lj1g3v0526480	PREDICTED: probable LRR receptor-like serine/threonine-protein kinase At1g74360-like [Glycine max] gi 356519088 ref XP_003528206.1	Probable LRR receptor-like serine/threonine-protein kinase At1g74360-like	1.2	0.001	-	-1
Lj6g3v2116920	PREDICTED: receptor-like serine/threonine-protein kinase SD1-8-like [Cicer arietinum] gi 502077540 ref XP_004485681.1	Receptor-like serine/threonine-protein kinase SD1-8-like	1.2	0.001	-	-1.9
Lj0g3v0099729	Plastid movement impaired 2 [Theobroma cacao] gi 508712106 gb EOY04003.1		1.1	0.001	-	-
Lj0g3v0144159	PREDICTED: ankyrin repeat-containing protein At5g02620-like [Glycine max] gi 356546390 ref XP_003541609.1		1.1	0.001	1.3	-2.4
Lj2g3v0636320	PREDICTED: receptor-like protein 12-like [Glycine max] gi 356495069 ref XP_003516403.1	Receptor-like protein 12-like	1.1	0.001	2.6	-2.5
Lj0g3v0324409	PREDICTED: serine/threonine-protein kinase CTR1-like [Glycine max] gi 356554074 ref XP_003545374.1		1	0.005	-	-
Lj2g3v0852080	PREDICTED: receptor-like protein kinase HSL1-like [Glycine max] gi 356495853 ref XP_003516786.1	Receptor-like protein kinase HSL1-like	1	0.001	-	-
Lj6g3v1088860	Receptor-like protein kinase [Medicago truncatula] gi 358345048 ref XP_003636596.1	Receptor-like protein kinase	1	0.025	2.7	-
Lj1g3v0052300	Formin-like protein 18 [Theobroma cacao] gi 508723716 gb EOY15613.1		-1.1	0.001	-	-

Lj0g3v0115159	PREDICTED: probable receptor-like protein kinase At4g39110-like [Glycine max] gi 356542359 ref XP_003539634.1	Probable receptor-like protein kinase At4g39110- like	-1.5	0.001	-	1
---------------	---	---	------	-------	---	---

2. Proteins related to carbohydrate metabolism

Gene ID	Annotation	Lotus base annotation	log2FC	q value	log2FC_Rh	log2FC_AMF
Lj0g3v0106789	PREDICTED: glucan 1,3-beta-glucosidase A-like [Glycine max] gi 356548252 ref XP_003542517.1	Glucan 1,3-beta-glucosidase A-like		0.001	-	1.2
Lj0g3v0213009	beta-1,3-glucanase [Sesbania rostrata] gi 82949442 dbj BAE53382.1	Beta-1,3-glucanase	2	0.001	-	1.7
Lj0g3v0285709	PREDICTED: laccase-5-like [Glycine max] gi 356540011 ref XP_003538485.1	Laccase-5-like	1.8	0.021	1	-
Lj0g3v0202539	PREDICTED: glucan endo-1,3-beta-glucosidase-like [Cicer arietinum] gi 502084830 ref XP_004487771.1	Glucan endo-1,3-beta-glucosidase-like	1.6	0.001	-	-
Lj0g3v0318099	PREDICTED: glucan 1,3-beta-glucosidase A-like [Glycine max] gi 356548252 ref XP_003542517.1	Glucan 1,3-beta-glucosidase A-like	1.4	0.001	-	-
Lj5g3v1961260	Chitinase [Medicago truncatula] gi 357443753 ref XP_003592154.1	Chitinase	1.4	0.001	3.1	-3.4
Lj0g3v0361989	PREDICTED: probable glucan 1,3-beta-glucosidase A-like [Glycine max] gi 356548266 ref XP_003542524.1	Probable glucan 1,3-beta-glucosidase A-like	1.3	0.001	-	-
Lj0g3v0316509	PREDICTED: laccase-8-like [Cicer arietinum] gi 502103902 ref XP_004492390.1	Laccase-8-like	1.2	0.001	-	-
Lj6g3v1078670	chitinase-related agglutinin [Robinia pseudoacacia] gi 119721188 gb ABL98074.1		1.2	0.013	-2	-
Lj2g3v2833010	PREDICTED: laccase-5-like [Glycine max] gi 356551363 ref XP_003544045.1	Laccase-5-like	1.2	0.001	-	-
Lj0g3v0362579	PREDICTED: chitotriosidase-1-like [Glycine max] gi 356556606 ref XP_003546615.1	Chitotriosidase-1-like	1	0.001	-	-
Lj4g3v1709670	PREDICTED: glucan endo-1,3-beta-glucosidase-like protein 3-like [Glycine max] gi 356516859 ref XP_003527110.1		-1	0.001	-	-
Lj5g3v2060690	PREDICTED: probable xyloglucan endotransglucosylase/hydrolase protein 8-like [Glycine max] gi 356575805 ref XP_003556027.1	Probable xyloglucan endotransglucosylase/hydrolase protein 8-like	-1	0.001	-	-
Lj2g3v0824780	PREDICTED: probable xyloglucan endotransglucosylase/hydrolase protein 26-like [Glycine max] gi 356496414 ref XP_003517063.1	Probable xyloglucan endotransglucosylase/hydrolase protein 26-like	-1.1	0.001	-	-
Lj0g3v0147469	PREDICTED: polygalacturonase-like [Glycine max] gi 356498258 ref XP_003517970.1		-1.2	0.003	-	-

3. Lectins

Gene ID	Annotation (hit)	Lotus base annotation	log2FC	q value	log2FC_Rh	log2FC_AMF
Lj0g3v0304439	RecName: Full=Seed lectin; AltName: Full=LECSJASG; Flags: Precursorgi 1755064 gb AAB51441.1 lectin precursor [Sophora japonica] gi 3122340 sp P93535.1 LECS_SOPJA	RecName: Full=Seed lectin; AltName: Full=LECSJASG; Flags: Precursorgi 1755064 gb AAB51441.1 lectin precursor	1.5	0.001	-2.6	3.5
Lj1g3v4994140	PREDICTED: pro-hevein [Glycine max] gi 356573103 ref XP_003554704.1	Pro-hevein	1.5	0.001	-	-
Lj0g3v0356899	PREDICTED: G-type lectin S-receptor-like serine/threonine-protein kinase At4g27290-like [Cicer arietinum] gi 502084183 ref XP_004487641.1	G-type lectin S-receptor-like serine/threonine-protein kinase At4g27290-like	1.4	0.001	-	-1.1
Lj1g3v5010640	PREDICTED: L-type lectin-domain containing receptor kinase IX.1-like [Glycine max] gi 356546735 ref XP_003541778.1	L-type lectin-domain containing receptor kinase IX.1-like	1.4	0.001	1.1	-
Lj0g3v0134279	lectin [Robinia pseudoacacia] gi 4115547 dbj BAA36415.1	Lectin	1.3	0.001	-2.4	3.3

Lj0g3v0321389	PREDICTED: G-type lectin S-receptor-like serine/threonine-protein kinase At2g19130-like [Cicer arietinum] gi 502083045 ref XP_004487351.1	G-type lectin S-receptor-like serine/threonine-protein kinase At2g19130-like	1.3	0.034	2	-1.7
Lj0g3v0138509	PREDICTED: G-type lectin S-receptor-like serine/threonine-protein kinase At1g11330-like [Vitis vinifera] gi 359496523 ref XP_003635255.1		1.2	0.045	1	
Lj0g3v0136559	PREDICTED: G-type lectin S-receptor-like serine/threonine-protein kinase At1g11330-like [Glycine max] gi 356560807 ref XP_003548678.1		1.1	0.004	-	-
Lj2g3v0663780	PREDICTED: G-type lectin S-receptor-like serine/threonine-protein kinase RLK1-like [Glycine max] gi 356555135 ref XP_003545892.1	G-type lectin S-receptor-like serine/threonine-protein kinase RLK1-like	1	0.001	2.5	-1.7

4. Germin-like proteins

Gene ID	Annotation (hit)	Lotus base annotation	log2FC	q value	log2FC_Rh	log2FC_AMF
Lj2g3v0946290	Germin-like protein [Medicago truncatula] gi 357495757 ref XP_003618167.1	Germin-like protein	4.4	0.001	-	-
Lj1g3v3833760	Germin-like protein subfamily 1 member [Medicago truncatula] gi 357468889 ref XP_003604729.1	Germin-like protein subfamily 1 member	1.8	0.001	-2.8	5

5. Proteins related to endo-/exocytosis (including those related to vesicular trafficking)

Gene ID	Annotation (hit)	Lotus base annotation	log2FC	q value	log2FC_Rh	log2FC_AMF
Lj0g3v0264849	Vacuolar protein sorting-associated protein [Medicago truncatula] gi 357445545 ref XP_003593050.1		1.4	0.003	1.3	-
Lj0g3v0313429	Exocyst complex component [Medicago truncatula] gi 357472627 ref XP_003606598.1	Exocyst complex component	1.1	0.001	-	-
Lj0g3v0324319	PREDICTED: vacuolar protein sorting-associated protein 8 homolog [Glycine max] gi 356560233 ref XP_003548398.1	Vacuolar protein sorting-associated protein 8 homolog	1.1	0.001	-	1.2
Lj0g3v0114299	PREDICTED: Vacuolar protein sorting-associated protein [Glycine max] gi 356577865 ref XP_003557042.1	8-hydroxyquercetin 8-O-methyltransferase-like	-1	0.001	-	-
Lj4g3v2401050	ENTH/VHS/GAT family protein [Arabidopsis thaliana] gi 15222535 ref NP_173895.1	ENTH/VHS/GAT family protein	-1.1	0.001	-	-
Lj4g3v2786890	PREDICTED: ras-related protein Rab7-like [Cicer arietinum] gi 502140003 ref XP_004504012.1	Ras-related protein Rab7-like	-1.2	0.017	-	-

6. Proteins involved in defense

Gene ID	Annotation (hit)	Lotus base annotation	log2FC	q value	log2FC_Rh	log2FC_AMF
Lj0g3v0286359	PREDICTED: disease resistance response protein DRRG49-C-like [Cicer arietinum] gi 502084966 ref XP_004487804.1	Disease resistance response protein DRRG49-C-like	5.5	0.001	divided by zero (in control)	
Lj1g3v4383290	PREDICTED: disease resistance response protein 206-like [Glycine max] gi 356572142 ref XP_003554229.1		3.7	0.001	-1.6	-
Lj6g3v1513550	PREDICTED: pathogenesis-related protein STH-2-like [Cicer arietinum] gi 502084988 ref XP_004487809.1	Pathogenesis-related protein STH-2-like	3.3	0.001	2.4	-2.9
Lj0g3v0144569	NBS-containing resistance-like protein [Medicago truncatula] gi 357459929 ref XP_003600246.1		3.2	0.006	-	-
Lj2g3v2470450	PREDICTED: protein NDR1-like [Cicer arietinum] gi 502096464 ref XP_004490745.1		2.9	0.001	5.1	-4.6
Lj6g3v1513720	Pathogenesis-related protein PR10 [Medicago truncatula] gi 357449105 ref XP_003594829.1	Pathogenesis-related protein PR10	2.4	0.001	-	-
Lj0g3v0348489	Pathogenesis-related protein PR10 [Medicago truncatula] gi 357449115 ref XP_003594834.1	Pathogenesis-related protein PR10	2.2	0.001	-	-
Lj4g3v2618270	tau class glutathione S-transferase [Glycine soja] gi 330687254 gb AEC32486.1	Tau class glutathione S-transferase	2	0.001	1.3	-1.8

Lj0g3v0303509	PREDICTED: glutathione S-transferase F9-like [Cicer arietinum] gi 502128459 ref XP_004499970.1	Glutathione S-transferase F9-like	1.9	0.001	1.3	-
Lj4g3v0510200	PREDICTED: (+)-neomenthol dehydrogenase-like [Cicer arietinum] gi 502142909 ref XP_004505149.1		1.9	0.001	-	-
Lj0g3v0340389	PREDICTED: disease resistance protein RPM1-like [Cicer arietinum] gi 502162289 ref XP_004512454.1		1.7	0.006	-	-
Lj0g3v0348509	pathogenesis-related protein class 10 [Oxytropis splendens] gi 359754795 gb AEV59587.1	Pathogenesis-related protein class 10	1.7	0.001	-1.8	1.7
Lj2g3v1694190	PREDICTED: thaumatin-like protein 1-like [Cicer arietinum] gi 502126365 ref XP_004499280.1		1.7	0.001	-	-
Lj3g3v0128220	PREDICTED: pleiotropic drug resistance protein 1-like [Glycine max] gi 356555825 ref XP_003546230.1	Pleiotropic drug resistance protein	1.7	0.001	-	-
Lj0g3v0124019	PREDICTED: callose synthase 2-like isoform X3 [Cicer arietinum] gi 502087187 ref XP_004488455.1	Callose synthase 2-like isoform X3	1.6	0.001	-	1
Lj0g3v0140429	Pathogenesis-related protein PR10 [Medicago truncatula] gi 357449105 ref XP_003594829.1		1.6	0.001	-	-
Lj0g3v0363519	Sigma factor binding protein [Medicago truncatula] gi 357456359 ref XP_003598460.1		1.6	0.012	divided by 0 (in control)	
Lj1g3v2609230	PREDICTED: BON1-associated protein 2-like [Glycine max] gi 356566868 ref XP_003551648.1	BON1-associated protein 2-like	1.5	0.001	5.1	-5.3
Lj5g3v2183850	Protein MKS1 [Medicago truncatula] gi 357444747 ref XP_003592651.1		1.5	0.001	-	-
Lj0g3v0216469	pathogenesis-related protein class 10 [Oxytropis splendens] gi 359754793 gb AEV59586.1	Pathogenesis-related protein class 10	1.4	0.001	-	-
Lj0g3v0288349	tau class glutathione S-transferase [Glycine soja] gi 406716690 gb AFS51729.1	Tau class glutathione S-transferase	1.4	0.001	-	-
Lj5g3v2112200	PRp27-like protein [Olea europaea subsp. europaea] gi 396318181 gb AFN85535.1		1.4	0.001	-1.2	-
Lj0g3v0134919	NB-LRR type disease resistance protein Rps1-k-2 [Glycine max] gi 62632825 gb AAx89383.1	NB-LRR type disease resistance protein Rps1-k-2	1.3	0.021	1.3	-1.2
Lj0g3v0150409	PREDICTED: disease resistance response protein 206-like [Cicer arietinum] gi 502147529 ref XP_004506818.1		1.3	0.001	-	-
Lj0g3v0213289	PREDICTED: BON1-associated protein 2-like [Cicer arietinum] gi 502157374 ref XP_004510853.1	BON1-associated protein 2-like	1.3	0.001	5.8	-6.2
Lj0g3v0312429	PREDICTED: callose synthase 10-like [Cicer arietinum] gi 502133618 ref XP_004501831.1		1.3	0.001	1.5	-
Lj2g3v0634890	Disease resistance-like protein [Medicago truncatula] gi 357499675 ref XP_003620126.1	Disease resistance-like protein	1.3	0.001	3.5	
Lj3g3v2983920	nematode resistance HS1pro1 protein [Glycine max] gi 351726303 ref NP_001236610.1	Nematode resistance HS1pro1 protein	1.3	0.001	3.6	-2.8
Lj6g3v1513840	Pathogenesis-related protein PR10 [Medicago truncatula] gi 357449105 ref XP_003594829.1	Pathogenesis-related protein PR10	1.2	0.001	-	-
Lj0g3v0268649	stress induced protein [Morella rubra] gi 427199330 gb AFY26888.1		1.1	0.001	4.5	-3.9
Lj2g3v1155180	Protein MKS1 [Medicago truncatula] gi 357444747 ref XP_003592651.1		1.1	0.001	2.4	-2.3
Lj0g3v0327439	disease resistance protein/LRR protein-related protein precursor [Glycine max] gi 351724553 ref NP_001235526.1	Disease resistance protein/LRR protein-related protein precursor	1	0.001	2.4	-1.3
Lj4g3v0109430	pollen Ole e 1 allergen and extensin family protein [Arabidopsis thaliana] gi 18422820 ref NP_568686.1		1	0.002	-	-
Lj5g3v1696980	PREDICTED: probable glutathione S-transferase-like [Cicer arietinum] gi 502118048 ref XP_004496075.1	Probable glutathione S-transferase-like	-1.1	0.001	-	-1.7
Lj1g3v3441360	PREDICTED: probable glutathione S-transferase-like [Glycine max] gi 356520951 ref XP_003529123.1	Probable glutathione S-transferase-like	-1.3	0.001	-	-1
Lj1g3v3441490	glutathione S-transferase GST 8 [Glycine max] gi 351726820 ref NP_001238675.1	Glutathione S-transferase GST 8	-1.3	0.001	-	-

7. Proteins related to abiotic stress

Gene ID	Annotation (hit)	Lotus base annotation	log2FC	q value	log2FC_Rh	log2FC_AMF
---------	------------------	-----------------------	--------	---------	-----------	------------

Lj0g3v0250919	Late embryogenesis abundant hydroxyproline-rich glycoprotein family [Theobroma cacao] gi 508717952 gb EOY09849.1		1.8	0.001	-	-
Lj3g3v0566040	SAB [Medicago truncatula] gi 357465183 ref XP_003602873.1		1	0.001	-	1.1
Lj6g3v2017530	Late embryogenesis abundant protein [Medicago truncatula] gi 357446653 ref XP_003593602.1		-1	0.017	-	-1.1
Lj0g3v0346569	Late embryogenesis abundant (LEA) protein-related [Theobroma cacao] gi 508720930 gb EOY12827.1		-1.7	0.001	-	-
Lj6g3v1629690	late embryogenesis abundant protein-like protein [Arabidopsis thaliana] gi 30685319 ref NP_188574.2		-2.6	0.001	-1.2	1.4

8. Proteins related to cell wall synthesis and modifications

Gene ID	Annotation (hit)	Lotus base annotation	log2FC	q value	log2FC_Rh	log2FC_AMF
Lj4g3v1614580	PREDICTED: expansin-like B1-like [Glycine max] gi 356563391 ref XP_003549947.1	Expansin-like B1-like	5.3	0.001	-1.2	-
Lj4g3v1176640	PREDICTED: expansin-like B1-like [Cicer arietinum] gi 502152576 ref XP_004508990.1		4.5	0.001	-	-1.3
Lj0g3v0066909	PREDICTED: expansin-like B1-like [Glycine max] gi 356563391 ref XP_003549947.1	Expansin-like B1-like	4.4	0.002	-	-
Lj4g3v1213510	PREDICTED: expansin-like B1-like [Glycine max] gi 356563391 ref XP_003549947.1	Expansin-like B1-like	4.1	0.001	1.4	-3.8
Lj0g3v0130759	PREDICTED: expansin-like B1-like [Glycine max] gi 356563391 ref XP_003549947.1		2.4	0.001	1.5	-1.9
Lj2g3v0264280	hydroxyproline-rich glycoprotein [Solanum tuberosum] gi 24745591 dbj BAC23028.1	Hydroxyproline-rich glycoprotein	1.4	0.009	2.9	-
Lj2g3v0777220	PREDICTED: arabinogalactan peptide 22-like [Glycine max] gi 356520575 ref XP_003528937.1		1.3	0.001	4.2	-4.6
Lj2g3v0264020	hydroxyproline-rich glycoprotein [Solanum tuberosum] gi 24745591 dbj BAC23028.1	Hydroxyproline-rich glycoprotein	1.2	0.001	1.3	-
Lj0g3v0135039	PREDICTED: epidermis-specific secreted glycoprotein EP1-like [Glycine max] gi 356549665 ref XP_003543212.1		1.1	0.001	-	-
Lj0g3v0284229	plant cell wall protein SITFR88 [Solanum lycopersicum] gi 350534998 ref NP_001233914.1		1.1	0.001	2.7	-3.2
Lj6g3v2203710	PREDICTED: classical arabinogalactan protein 1-like [Cicer arietinum] gi 502079397 ref XP_004486247.1		1.1	0.001	1.3	-1.5
Lj0g3v0341889	PREDICTED: probable pectinesterase/pectinesterase inhibitor 41-like [Glycine max] gi 356533561 ref XP_003535331.1	Probable pectinesterase/pectinesterase inhibitor 41-like	-1.1	0.001	-	1.2
Lj3g3v3556010	PREDICTED: expansin-like A1-like [Glycine max] gi 356543973 ref XP_003540432.1	Expansin-like A1-like	-1.2	0.001	-	-1.5
Lj0g3v0140179	PREDICTED: expansin-A8-like [Glycine max] gi 356500942 ref XP_003519289.1		-1.4	0.03	-	-

9. Proteins involved in cell modifications

Gene ID	Annotation (hit)	Lotus base annotation	log2FC	q value	log2FC_Rh	log2FC_AMF
Lj0g3v0237409	EXORDIUM like 2 [Theobroma cacao] gi 508724068 gb EOY15965.1		-1.1	0.001	-	-
Lj3g3v1203500	casparian strip membrane protein 5 [Glycine max] gi 351725825 ref NP_001236338.1		-1.1	0.001	-	-
Lj0g3v0217659	PREDICTED: casparian strip membrane protein 1-like [Cicer arietinum] gi 502178620 ref XP_004516297.1		-1.2	0.001	-	-
Lj3g3v2809710	Cortical cell-delineating protein [Medicago truncatula] gi 357476911 ref XP_003608741.1		-1.3	0.001	-	-
Lj3g3v2809690	Cortical cell-delineating protein [Medicago truncatula] gi 357476911 ref XP_003608741.1		-1.6	0.001	-1	-

10. Proteins related to transmembrane transport (including proteins involved in general transport mechanisms)

Gene ID	Annotation (hit)	Lotus base annotation	log2FC	q value	log2FC_Rh	log2FC_AMF
Lj3g3v1314810	PREDICTED: LOW QUALITY PROTEIN: protein TRANSPARENT TESTA 12-like [Glycine max] gi 356544808 ref XP_003540839.1	Protein TRANSPARENT TESTA 12-like	2.9	0.001	-	-
Lj5g3v2288960	PREDICTED: ABC transporter G family member 1-like [Glycine max] gi 356576859 ref XP_003556547.1	ABC transporter G family member 1-like	2.5	0.001	-	-
Lj0g3v0075999	Multidrug and toxin extrusion protein [Medicago truncatula] gi 357481725 ref XP_003611148.1	Multidrug and toxin extrusion protein	2.2	0.001	3.9	-5.4
Lj1g3v0116440	PREDICTED: non-specific lipid-transfer protein-like protein At5g64080-like isoform X1 [Cicer arietinum] gi 502159097 ref XP_004511392.1		2.2	0.001	-	-
Lj0g3v0341429	PREDICTED: sugar transport protein 13-like [Cicer arietinum] gi 502158979 ref XP_004511353.1	Sugar transport protein 13-like	2	0.001	1.2	-1
Lj3g3v0139630	PREDICTED: coatomer subunit beta'-2-like [Cicer arietinum] gi 502080953 ref XP_004486721.1	Coatomer subunit beta'-2-like	1.9	0.001	-	-
Lj6g3v1880060	PREDICTED: glucose-6-phosphate/phosphate translocator 2, chloroplastic-like [Glycine max] gi 356548981 ref XP_003542877.1	Glucose-6-phosphate/phosphate translocator 2, chloroplastic-like	1.9	0.001	-4.9	3.7
Lj5g3v2057350	PREDICTED: sugar transport protein 13-like [Glycine max] gi 356541627 ref XP_003539275.1	Sugar transport protein 13-like	1.8	0.029	-	-1.6
Lj3g3v1063670	PREDICTED: ABC transporter G family member 10-like [Cicer arietinum] gi 502089871 ref XP_004489046.1	ABC transporter G family member 10-like	1.8	0.001	-	-
Lj5g3v0999920	PREDICTED: non-specific lipid-transfer protein-like protein At2g13820-like isoform X2 [Cicer arietinum] gi 502115364 ref XP_004495186.1	Non-specific lipid-transfer protein-like protein At2g13820-like isoform X2	1.8	0.001	-	-
Lj1g3v2141030	PREDICTED: LOW QUALITY PROTEIN: S-type anion channel SLAH1-like [Glycine max] gi 356518004 ref XP_003527674.1	S-type anion channel SLAH1-like	1.7	0.001	-1.1	1.3
Lj5g3v0528770	PREDICTED: lipid transfer-like protein VAS-like [Glycine max] gi 356559508 ref XP_003548041.1	Lipid transfer-like protein VAS-like	1.6	0.015	-	-1.2
Lj0g3v0300329	Phosphate transporter 3,1 [Theobroma cacao] gi 508711024 gb EOY02921.1		1.5	0.001	1.2	-3.5
Lj0g3v0315079	White-brown-complex ABC transporter family [Medicago truncatula] gi 357476291 ref XP_003608431.1		1.5	0.001	-	-2.4
Lj1g3v4692980	Sulfite exporter TauE/SafE family protein isoform 2 [Theobroma cacao] gi 508716173 gb EOY08070.1	Sulfite exporter TauE/SafE family protein isoform 2	1.4	0.001	-	-
Lj0g3v0066539	PREDICTED: lysine histidine transporter-like 8-like [Cicer arietinum] gi 502161666 ref XP_004512243.1		1.4	0.001	-	-
Lj0g3v0295969	Solute carrier family 22 member [Medicago truncatula] gi 357515127 ref XP_003627852.1	Solute carrier family 22 member	1.3	0.001	-	1.6
Lj0g3v0315069	PREDICTED: ABC transporter G family member 11-like [Cicer arietinum] gi 502142153 ref XP_004504817.1		1.3	0.001	-	-
Lj0g3v0200159	PREDICTED: organic cation/carnitine transporter 4-like [Cicer arietinum] gi 502084151 ref XP_004487632.1		1.2	0.009	-1.2	2
Lj0g3v0234389	PREDICTED: ABC transporter C family member 3-like [Glycine max] gi 356553519 ref XP_003545103.1		1.2	0.005	1.6	-1.6
Lj5g3v0841020	Syntaxin-121 [Medicago truncatula] gi 357440101 ref XP_003590328.1	Syntaxin-121	1.2	0.001	2.6	-2.5
Ljmitog3v0000450	ATPase subunit 1 (mitochondrion) [Lotus japonicus] gi 372450305 ref YP_005090487.1	ATPase subunit 1 (mitochondrion)	1.2	0.001	-	-
Lj2g3v1589590	Auxin efflux carrier family protein isoform 1 [Theobroma cacao] gi 508698726 gb EOX90622.1	Auxin efflux carrier family protein isoform 1	1.1	0.001	1.7	-2.1

Lj5g3v0133240	Transmembrane protein [Medicago truncatula] gi 357438093 ref XP_003589322.1	Transmembrane protein	1.1	0.001	-	-
Lj5g3v1630010	PREDICTED: ABC transporter C family member 4-like [Glycine max] gi 356536723 ref XP_003536885.1	ABC transporter C family member 4-like	1.1	0.001	divided by zero (in control)	divided by zero (in control)
Lj0g3v0114899	PREDICTED: protein spinster-like [Glycine max] gi 356552876 ref XP_003544788.1	Protein spinster-like	1	0.001	-	-
Lj1g3v0605120	PREDICTED: sugar transport protein 5-like [Glycine max] gi 356515798 ref XP_003526585.1	Sugar transport protein 5-like	1	0.001	-	-
Lj0g3v0326139	PREDICTED: phosphoenolpyruvate/phosphate translocator 2, chloroplastic [Vitis vinifera] gi 225457009 ref XP_002282424.1	Phosphoenolpyruvate/phosphate translocator 2, chloroplastic	1	0.001	-	-
Lj5g3v2169440	Protein TRANSPARENT TESTA [Medicago truncatula] gi 357444623 ref XP_003592589.1	Protein TRANSPARENT TESTA	1	0.001	-	-1
Lj1g3v0948550	PREDICTED: bidirectional sugar transporter SWEET3-like [Cicer arietinum] gi 502124125 ref XP_004498397.1	Bidirectional sugar transporter SWEET3-like	-1	0.001	-3	2.8
Lj3g3v3500150	PREDICTED: magnesium transporter NIPA2-like [Cicer arietinum] gi 502144837 ref XP_004505767.1	Magnesium transporter NIPA2-like	-1	0.001	-	-1.5
Lj1g3v4287660	PREDICTED: oligopeptide transporter 5-like [Glycine max] gi 356503458 ref XP_003520525.1	Oligopeptide transporter 5-like	-1.1	0.001	-	-
Lj1g3v3381390	PREDICTED: patellin-3-like [Glycine max] gi 356509557 ref XP_003523514.1	Patellin-3-like	-1.1	0.001	-	-
Lj1g3v1991510	PREDICTED: probable cyclic nucleotide-gated ion channel 14-like [Cicer arietinum] gi 502132108 ref XP_004501229.1		-1.4	0.008	-	-
Lj0g3v0290599	PREDICTED: heavy metal-associated isoprenylated plant protein 26-like [Cicer arietinum] gi 502123961 ref XP_004498327.1	Heavy metal-associated isoprenylated plant protein 26-like	-1.6	0.004	3.3	-5.7

11. Proteins related to ion binding

Gene ID	Annotation (hit)	Lotus base annotation	log2FC	q value	log2FC_Rh	log2FC_AMF
Lj5g3v0614880	Zinc finger protein [Medicago truncatula] gi 357510467 ref XP_003625522.1	Zinc finger protein	5.1	0.014	divided by zero (in control)	-
Lj1g3v0562680	PREDICTED: RING-H2 finger protein ATL3-like [Glycine max] gi 356506122 ref XP_003521836.1	RING-H2 finger protein ATL3-like	2.6	0.001	3.3	-3.7
Lj0g3v0311049	PREDICTED: probable calcium-binding protein CML45-like [Glycine max] gi 356531760 ref XP_003534444.1	Probable calcium-binding protein CML45-like	1.6	0.001	1.8	-1.9
Lj4g3v3112860	PREDICTED: protein PLANT CADMIUM RESISTANCE 2-like [Glycine max] gi 356511317 ref XP_003524373.1		1.3	0.001	1.3	-2.3
Lj0g3v0084599	Calcium-dependent lipid-binding family protein isoform 4 [Theobroma cacao] gi 508714946 gb EOY06843.1		1.2	0.041	1	-
Lj0g3v0355229	RING finger family protein [Medicago truncatula] gi 357463473 ref XP_003602018.1	RING finger family protein	1.2	0.001	2.8	-2.2
Lj1g3v1720190	PREDICTED: zinc finger protein ZAT10-like [Glycine max] gi 356514469 ref XP_003525928.1	Zinc finger protein ZAT10-like	1.2	0.001	2.4	-1.7
Lj1g3v3019860	PREDICTED: probable calcium-binding protein CML45-like [Glycine max] gi 356531760 ref XP_003534444.1	Probable calcium-binding protein CML45-like	1.2	0.001	2	-2.4
Lj0g3v0154819	RING finger family protein [Medicago truncatula] gi 357441591 ref XP_003591073.1		1.1	0.001	1.8	-2.6
Lj5g3v0614980	PREDICTED: zinc finger protein ZAT11-like [Cicer arietinum] gi 502114591 ref XP_004494993.1	Zinc finger protein ZAT11-like	1.1	0.001	4	-4
Lj5g3v2099610	PREDICTED: zinc finger protein ZAT10-like [Glycine max] gi 356575726 ref XP_003555988.1	Zinc finger protein ZAT10-like	1.1	0.001	2.1	-1.6
Lj4g3v2704690	Basic blue protein [Medicago truncatula] gi 357519409 ref XP_003629993.1	Basic blue protein	1	0.001	2.9	-3.4

Lj2g3v0635660	PREDICTED: ZF-HD homeobox protein At4g24660-like [Cucumis sativus] gi 449439493 ref XP_004137520.1	ZF-HD homeobox protein At4g24660-like	-1.2	0.042	-	-
---------------	--	---------------------------------------	------	-------	---	---

12. Putative secreted proteins

Gene ID	Annotation (hit)	Lotus base annotation	log2FC	q value	log2FC_Rh	log2FC_AMF
Lj3g3v1342650	Cysteine-rich repeat secretory protein [Medicago truncatula] gi 357453525 ref XP_003597040.1		1.8	0.001	1.8	-2.2

13. Proteins involved in nucleotide metabolism (DNA and RNA)

Gene ID	Annotation (hit)	Lotus base annotation	log2FC	q value	log2FC_Rh	log2FC_AMF
Lj0g3v0342229	PREDICTED: chromatin structure-remodeling complex protein SYD-like isoform X2 [Cicer arietinum] gi 502151178 ref XP_004508316.1	Chromatin structure-remodeling complex protein SYD-like isoform X2	2	0.001	-	1
Lj0g3v0077789	PREDICTED: DNA polymerase theta-like [Glycine max] gi 356554501 ref XP_003545584.1	DNA polymerase theta-like	1.9	0.002	-	1
Lj0g3v0110029	endonuclease [Flavobacterium sp. CF136] gi 495079196 ref WP_007804020.1		1.9	0.001	-	-
Lj0g3v0269349	chromatin remodeling complex subunit [Populus trichocarpa] gi 224122872 ref XP_002318937.1		1.8	0.001	-	1.2
Lj0g3v0196139	Helicase/SANT-associated, DNA binding protein [Arabidopsis thaliana] gi 42565171 ref NP_189132.2		1.7	0.001	-	1.4
Lj0g3v0071459	PREDICTED: box C/D snoRNA protein 1-like isoform X1 [Cicer arietinum] gi 502085927 ref XP_004488052.1		1.7	0.001	-	-
Lj1g3v0118820	PREDICTED: U5 small nuclear ribonucleoprotein 200 kDa helicase-like [Glycine max] gi 356525813 ref XP_003531516.1		1.5	0.033	-	-
Lj0g3v0325869	Nuclear factor related to kappa-B-binding protein [Medicago truncatula] gi 357454025 ref XP_003597293.1	Nuclear factor related to kappa-B-binding protein	1.2	0.001	-	1.7
Lj0g3v0270019	PREDICTED: DNA ligase 1-like [Cicer arietinum] gi 502155808 ref XP_004510199.1	DNA ligase 1-like	1.1	0.037	-	-
Lj0g3v0336359	DNA polymerase [Medicago truncatula] gi 357459413 ref XP_003599987.1		1.1	0.001	-	-
Lj2g3v2183350	PREDICTED: DNA double-strand break repair Rad50 ATPase-like [Cicer arietinum] gi 502136692 ref XP_004502790.1		-1.2	0.047	-1.8	-
Lj4g3v2526040	PREDICTED: ATP-dependent DNA helicase Q-like 5-like isoform X1 [Cicer arietinum] gi 502141185 ref XP_004504477.1	ATP-dependent DNA helicase Q-like 5-like isoform X1	-1.2	0.007	-	-
Lj0g3v0333259	PREDICTED: acid phosphatase 1-like [Glycine max] gi 356575237 ref XP_003555748.1	Acid phosphatase 1-like	-1.4	0.001	-	-

14. Proteins involved in gene expression (transcription)

Gene ID	Annotation (hit)	Lotus base annotation	log2FC	q value	log2FC_Rh	log2FC_AMF
Lj1g3v4483640	PREDICTED: ethylene-responsive transcription factor 15-like [Glycine max] gi 356503610 ref XP_003520600.1	Ethylene-responsive transcription factor 15-like	3.5	0.001	1.5	-1.7
Lj4g3v2214780	Ethylene-responsive transcription factor RAP2-9 [Medicago truncatula] gi 357450169 ref XP_003595361.1	Ethylene-responsive transcription factor RAP2-9	3	0.001	4.8	-3.2
Lj3g3v2960740	PREDICTED: probable CCR4-associated factor 1 homolog 9-like [Glycine max] gi 356542778 ref XP_003539842.1	Probable CCR4-associated factor 1 homolog 9-like	2.2	0.001	4.7	-4.8

Lj0g3v0298769	PREDICTED: probable WRKY transcription factor 41-like [Glycine max] gi 356509299 ref XP_003523388.1	Probable WRKY transcription factor 41-like	2	0.001	4.7	-4.6
Lj1g3v1222700	Ethylene-responsive transcription factor ERF110 [Medicago truncatula] gi 357464465 ref XP_003602514.1	Ethylene-responsive transcription factor ERF110	1.9	0.001	2	-
Lj0g3v0283799	PREDICTED: LOW QUALITY PROTEIN: midasin-like [Cicer arietinum] gi 502156332 ref XP_004510421.1	Midasin-like	1.8	0.001	1.3	-
Lj1g3v4241070	PREDICTED: LOW QUALITY PROTEIN: heat stress transcription factor B-3-like [Cicer arietinum] gi 502108702 ref XP_004493479.1	Heat stress transcription factor B-3-like	1.7	0.001	1	-
Lj6g3v1239580	Transcription factor MYC4 [Medicago truncatula] gi 357449849 ref XP_003595201.1	Transcription factor MYC4	1.6	0.001	2.7	-2.6
Lj0g3v0332559	PREDICTED: ethylene-responsive transcription factor 1B-like [Glycine max] gi 356536967 ref XP_003537003.1	Ethylene-responsive transcription factor 1B-like	1.5	0.001	-	-
Lj2g3v1495100	PREDICTED: transcription factor MYB39-like [Glycine max] gi 356529726 ref XP_003533439.1	Transcription factor MYB39-like	1.5	0.001	2.1	-2
Lj3g3v2477670	MYB transcription factor MYB92 [Glycine max] gi 351722536 ref NP_001238271.1	MYB transcription factor MYB92	1.5	0.001	1.6	-1.6
Lj4g3v2963430	bHLH transcription factor [Lotus japonicus] gi 300117045 dbj BAJ10680.1	Bhlh transcription factor	1.5	0.001	1.3	-1.4
Lj2g3v1981820	VQ motif-containing protein [Arabidopsis lyrata subsp. lyrata] gi 297802170 ref XP_002868969.1		1.4	0.001	2.2	-3.1
Lj0g3v0101299	PREDICTED: heat shock factor protein HSF24-like [Cicer arietinum] gi 502152898 ref XP_004509144.1		1.3	0.001	-	-1.4
Lj1g3v3847230	PREDICTED: probable WRKY transcription factor 56-like [Glycine max] gi 356561712 ref XP_003549123.1	Probable WRKY transcription factor 56-like	1.3	0.001	3.4	-3.3
Lj2g3v3341870	VQ motif-containing protein [Phaseolus vulgaris] gi 396582359 gb AFN88222.1		1.3	0.001	2.6	-1.8
Lj3g3v0397240	PREDICTED: transcription factor JUNGBRUNNEN 1-like [Cicer arietinum] gi 502088387 ref XP_004488808.1	Transcription factor JUNGBRUNNEN 1-like	1.3	0.001	1	-1.6
Lj3g3v2477660	MYB transcription factor MYB92 [Glycine max] gi 351722536 ref NP_001238271.1		1.3	0.001	1.3	-1.7
Lj1g3v3948170	transcriptional factor NAC11 [Glycine max] gi 351727585 ref NP_001236142.1	Transcriptional factor NAC11	1.2	0.001	4.8	-2.9
Lj3g3v0478050	PREDICTED: transcription factor bHLH130-like [Glycine max] gi 356548947 ref XP_003542860.1	Transcription factor bHLH130-like	1.2	0.001	-	-
Lj0g3v0165839	MYB29 protein [Glycine max] gi 359807202 ref NP_001241360.1	MYB29 protein	1.1	0.001	1.8	-1.9
Lj3g3v1393570	PREDICTED: probable WRKY transcription factor 33 [Glycine max] gi 356495083 ref XP_003516410.1	Probable WRKY transcription factor 33	1.1	0.001	1.3	-
Lj4g3v0451130	PREDICTED: heat stress transcription factor B-2a-like [Glycine max] gi 356495198 ref XP_003516466.1	Heat stress transcription factor B-2a-like	1.1	0.001	-	-
Lj5g3v1167370	transcription factor AP2-EREBP [Lotus japonicus] gi 193237553 dbj BAG50053.1	Transcription factor AP2-EREBP	1.1	0.001	-	-
Lj1g3v2114700	PREDICTED: ethylene-responsive transcription factor ERF026-like [Cicer arietinum] gi 502119418 ref XP_004496613.1	Ethylene-responsive transcription factor ERF026-like	-1	0.001	2.4	-3.1
Lj0g3v0330909	transcription factor [Glycine max] gi 351725863 ref NP_001237619.1		-1.1	0.001	1.4	-1
Lj1g3v4851620	calcineurin transcriptional regulator CRZ1, partial [Zymoseptoria tritici IPO323] gi 398389072 ref XP_003847997.1		-1.3	0.001	-	-
Lj1g3v3751720	PREDICTED: myb-related protein 315-like [Glycine max] gi 356560528 ref XP_003548543.1	Myb-related protein 315-like	-1.4	0.001	-	-

15. Proteins involved in protein biosynthesis

Gene ID	Annotation (hit)	Lotus base annotation	log2FC	q value	log2FC_Rh	log2FC_AMF
Lj0g3v0214539	PREDICTED: eukaryotic translation initiation factor 4G-like [Cucumis sativus] gi 449442451 ref XP_004138995.1		2	0.001	-	2
Lj0g3v0304609	Eukaryotic translation initiation factor 4G [Medicago truncatula] gi 357512923 ref XP_003626750.1		1.3	0.001	-	1.9
Lj2g3v3085370	60S ribosomal protein L18a [Medicago truncatula] gi 357494221 ref XP_003617399.1	60s ribosomal protein L18a	1	0.001	2.9	-2.8

16. Proteins involved in protein processing

Gene ID	Annotation (hit)	Lotus base annotation	log2FC	q value	log2FC_Rh	log2FC_AMF
Lj3g3v2385390	PREDICTED: chaperone protein dnaJ 20, chloroplastic-like [Cicer arietinum] gi 502142064 ref XP_004504775.1		2.5	0.001		
Lj4g3v0340640	PREDICTED: chaperone protein dnaJ 20, chloroplastic-like [Cicer arietinum] gi 502142064 ref XP_004504775.1		2.3	0.001	3.6	-3
Lj3g3v2385400	PREDICTED: chaperone protein dnaJ 20, chloroplastic-like [Cicer arietinum] gi 502142064 ref XP_004504775.1		2.2	0.001		
Lj0g3v0297749	PREDICTED: beta-1,3-galactosyltransferase 7-like [Glycine max] gi 356548603 ref XP_003542690.1	Beta-1,3-galactosyltransferase 7-like	1.3	0.001	-	-
Lj1g3v1032230	Mitochondrial chaperone BCS1 [Medicago truncatula] gi 357464059 ref XP_003602311.1	Mitochondrial chaperone BCS1	1.3	0.001	-	-
Lj2g3v0039390	PREDICTED: saccin-like [Glycine max] gi 356530237 ref XP_003533689.1		1.2	0.001	-	1
Lj0g3v0184659	PREDICTED: chaperone protein ClpB-like [Glycine max] gi 356551867 ref XP_003544294.1	Chaperone protein ClpB-like	1.1	0.015	-1.3	1.7
Lj1g3v4921040	Heat shock protein 70 (Hsp 70) family protein [Theobroma cacao] gi 508719590 gb EOY11487.1		1.1	0.041	-2	3.7
Lj0g3v0258139	Chaperone protein dnaJ [Medicago truncatula] gi 357438881 ref XP_003589717.1		-1.5	0.014	-1.6	-

17. Proteins involved in protein degradation (including protease inhibitors)

Gene ID	Annotation (hit)	Lotus base annotation	log2FC	q value	log2FC_Rh	log2FC_AMF
Lj2g3v0636850	PREDICTED: U-box domain-containing protein 21-like [Glycine max] gi 356522898 ref XP_003530079.1	U-box domain-containing protein 21-like	3.7	0.001	5.7	-7
Lj5g3v1174410	protease inhibitor [Medicago truncatula] gi 357494051 ref XP_003617314.1	Protease inhibitor	3	0.001	2.6	-
Lj3g3v2995720	subtilase [Lotus japonicus] gi 163914235 dbj BAF95887.1	Subtilase	2.8	0.01	2.3	2.3
Lj2g3v2794440	PREDICTED: U-box domain-containing protein 13-like [Glycine max] gi 356499213 ref XP_003518436.1	U-box domain-containing protein 13-like	2.7	0.001	1.9	-
Lj6g3v1880250	PREDICTED: basic 7S globulin-like [Glycine max] gi 356548993 ref XP_003542883.1	Basic 7S globulin-like	2.3	0.001	-	-
Lj6g3v0408370	PREDICTED: U-box domain-containing protein 21-like [Cicer arietinum] gi 502137539 ref XP_004503116.1	U-box domain-containing protein 21-like	2.2	0.001	3.7	-2.9
Lj0g3v0296999	Protein tolB [Medicago truncatula] gi 358347274 ref XP_003637684.1	Protein tolB	2.1	0.001	2.3	-2.2
Lj6g3v1849460	PREDICTED: probable F-box protein At4g22030-like [Glycine max] gi 356532291 ref XP_003534707.1		2.1	0.001	5.3	-4.1
Lj5g3v0963160	PREDICTED: basic 7S globulin-like [Glycine max] gi 356500210 ref XP_003518926.1	Basic 7S globulin-like	1.8	0.001	1.8	-2.1

Lj6g3v1849450	PREDICTED: probable F-box protein At4g22030-like [Glycine max] gi 356532295 ref XP_003534709.1		1.8	0.001	divided by zero (in control)	-1
Lj0g3v0267019	PREDICTED: U-box domain-containing protein 20-like [Glycine max] gi 356553261 ref XP_003544976.1	U-box domain-containing protein 20-like	1.7	0.001	3.6	-3.5
Lj4g3v2803800	U-box domain-containing protein [Medicago truncatula] gi 357519575 ref XP_003630076.1	U-box domain-containing protein	1.7	0.001	-	1.6
Lj4g3v1534900	PREDICTED: U-box domain-containing protein 19-like [Glycine max] gi 356565018 ref XP_003550742.1	U-box domain-containing protein 19-like	1.5	0.001	2.3	-2.6
Lj6g3v1880370	PREDICTED: basic 7S globulin-like [Glycine max] gi 356557887 ref XP_003547241.1	Basic 7S globulin-like	1.5	0.001	3	-2.1
Lj0g3v0200149	Calpain-like protein [Medicago truncatula] gi 357519297 ref XP_003629937.1		1.4	0.001	-	-
Lj3g3v2938470	PREDICTED: E3 ubiquitin-protein ligase PUB24-like [Glycine max] gi 356544768 ref XP_003540819.1	E3 ubiquitin-protein ligase PUB24-like	1.4	0.001	-	-1.8
Lj0g3v0014579	PREDICTED: E3 ubiquitin-protein ligase PUB24-like [Cicer arietinum] gi 502122252 ref XP_004497654.1	E3 ubiquitin-protein ligase PUB24-like	1.3	0.001	2.6	-2
Lj0g3v0163939	PREDICTED: E3 ubiquitin-protein ligase BRE1-like 1-like isoform X2 [Cicer arietinum] gi 502103046 ref XP_004492186.1		1.3	0.001	-	-
Lj1g3v2728130	PREDICTED: E3 ubiquitin-protein ligase RHA1B-like [Glycine max] gi 356568413 ref XP_003552405.1	E3 ubiquitin-protein ligase RHA1B-like	1.3	0.001	1.9	-
Lj0g3v0200139	F-box/LRR-repeat protein [Medicago truncatula] gi 357468013 ref XP_003604291.1	F-box/LRR-repeat protein	1.2	0.001	-	-
Lj0g3v0245049	PREDICTED: E3 ubiquitin-protein ligase RING1-like [Cicer arietinum] gi 502081845 ref XP_004486987.1	E3 ubiquitin-protein ligase RING1-like	1.2	0.001	1.8	-1.7
Lj4g3v0816700	PREDICTED: F-box protein SKIP2-like [Glycine max] gi 356514260 ref XP_003525824.1	F-box protein SKIP2-like	1.2	0.001	2.4	-2.2
Lj0g3v0322949	F-box protein PP2-B3 [Medicago truncatula] gi 357441795 ref XP_003591175.1	F-box protein PP2-B3	1.1	0.001	2.3	-1.4
Lj1g3v4944910	PREDICTED: E3 ubiquitin-protein ligase ATL6-like [Cicer arietinum] gi 502113388 ref XP_004494634.1	E3 ubiquitin-protein ligase ATL6-like	1.1	0.001	1.3	-
Lj2g3v1472950	PREDICTED: E3 ubiquitin-protein ligase RING1-like [Cicer arietinum] gi 502148453 ref XP_004507169.1	E3 ubiquitin-protein ligase RING1-like	1.1	0.001	2.3	-1.9
Lj2g3v2001600	PREDICTED: metalloendoproteinase 1-like [Glycine max] gi 356540528 ref XP_003538740.1	Metalloendoproteinase 1-like	1.1	0.002	-	-
Lj3g3v0966710	PREDICTED: metalloendoproteinase 1-like [Cicer arietinum] gi 502154901 ref XP_004509890.1	Metalloendoproteinase 1-like	1.1	0.001	1.4	-1.4
Lj5g3v1203340	PREDICTED: basic 7S globulin-like [Glycine max] gi 356576537 ref XP_003556387.1	Basic 7S globulin-like	1	0.001	2.8	-2.6
Lj0g3v0164769	Protease inhibitor/seed storage/LTP family protein [Medicago truncatula] gi 357505755 ref XP_003623166.1		-1.2	0.001	-2.4	1.3

18. Proteins related to primary metabolism

Gene ID	Annotation (hit)	Lotus base annotation	log2FC	q value	log2FC_Rh	log2FC_AMF
Lj0g3v0121549	phenylalanine ammonia-lyase [Lotus japonicus] gi 118142392 dbj BAF36971.1	Phenylalanine ammonia-lyase	2.3	0.001	-	-2.6
Lj1g3v4590710	PREDICTED: phenylalanine ammonia-lyase 2-like isoform X1 [Cicer arietinum] gi 502118418 ref XP_004496257.1		1.9	0.001	3	-2.7
Lj6g3v0527170	PREDICTED: bifunctional aspartate aminotransferase and glutamate/aspartate-prephenate aminotransferase-like [Cicer arietinum] gi 502140078 ref XP_004504047.1	Bifunctional aspartate aminotransferase and glutamate/aspartate-prephenate aminotransferase-like	1.9	0.001	-	-1
Lj1g3v4590850	phenylalanine ammonia-lyase [Lotus japonicus] gi 118142392 dbj BAF36971.1	Phenylalanine ammonia-lyase	1.8	0.001		
Lj1g3v2682510	Cysteine synthase [Medicago truncatula] gi 357507415 ref XP_003623996.1	Cysteine synthase	1.6	0.001	-	1.2

Chapter 6

Lj1g3v4590840	phenylalanine ammonia-lyase [Lotus japonicus] gi 118142384 dbj BAF36967.1	Phenylalanine ammonia-lyase	1.6	0.001	1.7	-1.7
Lj2g3v3339740	PREDICTED: phenylalanine ammonia-lyase class 3-like [Cicer arietinum] gi 502100067 ref XP_004491627.1	Phenylalanine ammonia-lyase class 3-like	1.5	0.001	1.3	-1
Lj2g3v1645510	PREDICTED: phosphoserine aminotransferase, chloroplastic-like [Cicer arietinum] gi 502153680 ref XP_004509428.1	Phosphoserine aminotransferase, chloroplastic-like	1.4	0.001	-	-
Lj0g3v0129059	NADH glutamate synthase precursor [Phaseolus vulgaris] gi 62177687 gb AAL26865.2 AF314925_1	NADH glutamate synthase precursor	1.1	0.001	-	1.1
Lj4g3v2592460	serine hydroxymethyltransferase [Glycine max] gi 389548688 gb AFK83582.1	Serine hydroxymethyltransferase	1.1	0.001	-	-
Lj1g3v4226900	PREDICTED: glycerol-3-phosphate dehydrogenase [NAD(P)+] gi 356572006 ref XP_003554161.1	Glycerol-3-phosphate dehydrogenase	1	0.018	-	-

19. Proteins related to secondary metabolism

Gene ID	Annotation (hit)	Lotus base annotation	log2FC	q value	log2FC_Rh	log2FC_AMF
Lj4g3v0486150	2-hydroxyisoflavanone synthase [Lotus japonicus] gi 148839039 dbj BAF64284.1	2-hydroxyisoflavanone synthase	4.7	0.001	2.3	-1
Lj0g3v0315869	PREDICTED: R-linalool synthase, chloroplastic-like [Glycine max] gi 356543756 ref XP_003540326.1	R-linalool synthase, chloroplastic-like	4	0.001	1	-1.6
Lj0g3v0207649	PREDICTED: 7-ethoxycoumarin O-deethylase-like [Glycine max] gi 356576337 ref XP_003556289.1	7-ethoxycoumarin O-deethylase-like	3.3	0.001	2.2	-2
Lj1g3v2093260	PREDICTED: NADP-dependent malic enzyme-like [Cicer arietinum] gi 502131779 ref XP_004501098.1	NADP-dependent malic enzyme-like	3.2	0.001	-	-1.8
Lj0g3v0297459	PREDICTED: cytochrome P450 71A1-like [Cicer arietinum] gi 502101155 ref XP_004491826.1	Cytochrome P450 71A1-like	2.9	0.002	1.2	-2.6
Lj0g3v0214389	PREDICTED: hydroquinone glucosyltransferase-like [Glycine max] gi 356527181 ref XP_003532191.1	Hydroquinone glucosyltransferase-like	2.8	0.001	-	-
Lj3g3v0681370	chalcone synthase [Dictamnus albus] gi 54311699 emb CAH61575.1	Chalcone synthase	2.8	0.001	2.9	-3
Lj4g3v2574990	chalcone synthase CHS4 [Glycine max] gi 34148079 gb AAQ62588.1	Chalcone synthase CHS4	2.8	0.001	3.2	-4.2
Lj1g3v0116650	PREDICTED: chalcone synthase [Glycine max] gi 356538729 ref XP_003537853.1	Chalcone synthase	2.7	0.001		
Lj2g3v2051190	PREDICTED: 1-aminocyclopropane-1-carboxylate synthase-like [Glycine max] gi 356539620 ref XP_003538294.1	1-aminocyclopropane-1-carboxylate synthase-like	2.7	0.001	-	-2.4
Lj6g3v0672170	PREDICTED: hydroquinone glucosyltransferase-like [Glycine max] gi 356527183 ref XP_003532192.1	Hydroquinone glucosyltransferase-like	2.7	0.001	-	-1.3
Lj0g3v0353399	alcohol dehydrogenase [Lotus japonicus] gi 356582742 gb AET21261.1	Alcohol dehydrogenase	2.4	0.001	-1.1	-1.8
Lj2g3v2124320	chalcone synthase 1 [Astragalus membranaceus] gi 325911190 gb ADZ45299.1	Chalcone synthase 1	2.4	0.001		
Lj1g3v0579600	PREDICTED: UDP-glycosyltransferase 89B1-like [Cicer arietinum] gi 502181677 ref XP_004516861.1	UDP-glycosyltransferase 89B1-like	2.3	0.001	1.6	divided by zero (in control)
Lj2g3v2124310	chalcone synthase [Glycyrrhiza uralensis] gi 122725488 gb ABM66532.1	Chalcone synthase	2.3	0.001	2.9	-3.6
Lj0g3v0082139	PREDICTED: homogentisate phytyltransferase 1, chloroplastic-like [Glycine max] gi 356546073 ref XP_003541456.1	Homogentisate phytyltransferase 1, chloroplastic-like	2.2	0.028	divided by zero (in control)	-1.3
Lj1g3v0116620	RecName: Full=Chalcone synthase; AltName: Full=Naringenin-chalcone synthase gi 19593 emb CAA48227.1 naregenin-chalcone synthase [Medicago sativa] gi 1705839 sp P51080.1 CHS7_MEDSA	RecName: Full=Chalcone synthase; AltName: Full=Naringenin-chalcone synthase gi 19593 emb CAA48227.1 naregenin-chalcone synthase	2.2	0.001	2.2	-3.1

Chapter 6

Lj1g3v4691550	Flavonol synthase/flavanone 3-hydroxylase [Medicago truncatula] gi 357510917 ref XP_003625747.1	Flavonol synthase/flavanone 3-hydroxylase	2	0.001	-1.6	-
Lj0g3v0105319	PREDICTED: phospho-2-dehydro-3-deoxyheptonate aldolase 2, chloroplastic-like [Fragaria vesca subsp. vesca] gi 470127404 ref XP_004299659.1	Phospho-2-dehydro-3-deoxyheptonate aldolase 2, chloroplastic-like	2	0.001	-	-
Lj2g3v1267160	PREDICTED: anthocyanidin 5,3-O-glucosyltransferase-like [Glycine max] gi 356561808 ref XP_003549170.1	Anthocyanidin 5,3-O-glucosyltransferase-like	2	0.001	-	-
Lj2g3v1483000	PREDICTED: bifunctional dihydroflavonol 4-reductase/flavanone 4-reductase-like [Glycine max] gi 356531429 ref XP_003534280.1		2	0.001	-	-
Lj6g3v1934030	PREDICTED: cytochrome P450 710A1-like [Cicer arietinum] gi 502078717 ref XP_004486033.1	Cytochrome P450 710A1-like	1.9	0.001	-	2.5
Lj2g3v1022330	PREDICTED: probable galacturonosyltransferase-like 9-like [Glycine max] gi 356572000 ref XP_003554158.1	Probable galacturonosyltransferase-like 9-like	1.8	0.001	3	-2.9
Lj0g3v0001739	NAD(P)H-dependent 6'-deoxychalcone synthase [Medicago truncatula] gi 357462577 ref XP_003601570.1	NAD(P)H-dependent 6'-deoxychalcone synthase	1.7	0.001	1	-1
Lj1g3v0098420	Acyl-CoA N-acyltransferases superfamily protein isoform 1 [Theobroma cacao] gi 508713827 gb EOY05724.1	Acyl-CoA N-acyltransferases superfamily protein isoform 1	1.7	0.001	3.9	-4.2
Lj1g3v0838120	Aldehyde dehydrogenase family 3 member H1 [Medicago truncatula] gi 357463521 ref XP_003602042.1	Aldehyde dehydrogenase family 3 member H1	1.7	0.001	-	-1.5
Lj1g3v05060470	3-ketoacyl-CoA synthase [Medicago truncatula] gi 357512625 ref XP_003626601.1	3-ketoacyl-CoA synthase	1.7	0.001	-	-
Lj4g3v1514840	PREDICTED: UDP-glycosyltransferase 71D1-like [Cicer arietinum] gi 502095991 ref XP_004490590.1	UDP-glycosyltransferase 71D1-like	1.7	0.001	-	-
Lj2g3v1925640	PREDICTED: isoflavone 2'-hydroxylase-like [Cicer arietinum] gi 502160756 ref XP_004511882.1	Isoflavone 2'-hydroxylase-like	1.6	0.017	-	-
Lj0g3v0184099	Cytochrome P450 [Medicago truncatula] gi 357496145 ref XP_003618361.1	Cytochrome P450	1.6	0.001	divided by zero (in control)	
Lj0g3v0354359	PREDICTED: isoliquiritigenin 2'-O-methyltransferase-like [Glycine max] gi 356532221 ref XP_003534672.1	Isoliquiritigenin 2'-O-methyltransferase-like	1.6	0.001	1.1	-1.7
Lj2g3v1455360	PREDICTED: probable 1-deoxy-D-xylulose-5-phosphate synthase, chloroplastic-like [Glycine max] gi 356529695 ref XP_003533424.1	Probable 1-deoxy-D-xylulose-5-phosphate synthase, chloroplastic-like	1.6	0.001	-	-
Lj2g3v1691110	PREDICTED: thiosulfate sulfurtransferase, chloroplastic-like [Glycine max] gi 356496631 ref XP_003517169.1		1.6	0.001	-	-
Lj4g3v0484930	RecName: Full=Isoflavone 4'-O-methyltransferase; Short=LjJH4'OMT; AltName: Full=2,7,4'-trihydroxyisoflavanone 4'-O-methyltransferase; AltName: Full=S-adenosyl-L-methionine: 2,7,4'-trihydroxyisoflavanone 4'-O-methyltransferasegi 28804596 dbj BAC58013.1 S-adenosyl-L-methionine: 2,7,4'-trihydroxyisoflavanone 4'-O-methyltransferase [Lotus japonicus] gi 75146881 sp Q84KK4.1 4OMT_LOTJA	RecName: Full=Isoflavone 4'-O-methyltransferase; Short=LjJH4'OMT; AltName: Full=2,7,4'-trihydroxyisoflavanone 4'-O-methyltransferase; AltName: Full=S-adenosyl-L-methionine: 2,7,4'-trihydroxyisoflavanone 4'-O-methyltransferasegi 28804596 dbj BAC58013.1 S-adenosyl-L-methionine: 2,7,4'-trihydroxyisoflavanone 4'-O-methyltransferase	1.6	0.001	-	-
Lj4g3v2800440	PREDICTED: cytochrome P450 71A1-like [Glycine max] gi 356511127 ref XP_003524281.1	Cytochrome P450 71A1-like	1.6	0.002	-	-
Lj0g3v0088989	PREDICTED: UDP-glycosyltransferase 71D1-like [Cicer arietinum] gi 502095988 ref XP_004490589.1	UDP-glycosyltransferase 71D1-like	1.5	0.001	-1	-

Chapter 6

Lj1g3v0130090	Cytochrome P450 [Medicago truncatula] gi 357481083 ref XP_003610827.1	Cytochrome P450	1.5	0.001	-	-
Lj0g3v0001769	NAD(P)H-dependent 6'-deoxychalcone synthase [Medicago truncatula] gi 357462577 ref XP_003601570.1	NAD(P)H-dependent 6'-deoxychalcone synthase	1.4	0.001	-	-
Lj1g3v1168690	PREDICTED: chalcone--flavonone isomerase-like [Cicer arietinum] gi 502136777 ref XP_004502829.1	Chalcone--flavonone isomerase-like	1.4	0.001	-	-
Lj1g3v4037150	Dihydrofolate reductase [Medicago truncatula] gi 357509019 ref XP_003624798.1		1.4	0.001	-	-
Lj5g3v0711180	PREDICTED: fructose-bisphosphate aldolase, cytoplasmic isozyme-like [Cicer arietinum] gi 502122153 ref XP_004497605.1	Fructose-bisphosphate aldolase, cytoplasmic isozyme-like	1.4	0.001	-	-
Lj0g3v0248079	PREDICTED: omega-hydroxypalmitate O-feruloyl transferase-like [Glycine max] gi 356571583 ref XP_003553956.1	Omega-hydroxypalmitate O-feruloyl transferase-like	1.3	0.001	-	-
Lj0g3v0254229	Cytochrome b5 [Medicago truncatula] gi 357469369 ref XP_003604969.1		1.3	0.001	-	-1
Lj4g3v0485090	cytochrome P450 [Lotus japonicus] gi 7415992 dbj BAA93632.1	Cytochrome P450	1.3	0.001	1.3	-
Lj5g3v0670150	PREDICTED: bifunctional monodehydroascorbate reductase and carbonic anhydrase nectarin-3-like [Glycine max] gi 356533269 ref XP_003535188.1	Bifunctional monodehydroascorbate reductase and carbonic anhydrase nectarin-3-like	1.3	0.001	-	-1.6
Lj1g3v3218110	PREDICTED: carnitiny-CoA dehydratase-like [Glycine max] gi 356568988 ref XP_003552689.1	Carnitiny-CoA dehydratase-like	1.2	0.001	-	-
Lj6g3v1985690	PREDICTED: anthocyanidin 3-O-glucosyltransferase 5 [Vitis vinifera] gi 225458362 ref XP_002281768.1	Anthocyanidin 3-O-glucosyltransferase 5	1.2	0.002	-1.3	1.3
Lj0g3v0161909	PREDICTED: primary amine oxidase-like [Glycine max] gi 356557184 ref XP_003546898.1	Primary amine oxidase-like	1.1	0.032	-	1.4
Lj0g3v0202109	PREDICTED: cellulose synthase-like protein E1-like [Glycine max] gi 356527159 ref XP_003532180.1		1.1	0.001	2.3	-
Lj1g3v1648930	PREDICTED: patatin group A-3-like [Glycine max] gi 356518083 ref XP_003527713.1	Patatin group A-3-like	1.1	0.001	-	-
Lj1g3v3023790	RecName: Full=Isoflavone 7-O-methyltransferase; AltName: Full=Daidzein 7-O-methyltransferasegi 28804594 dbj BAC58012.1 S-adenosyl-L-methionine: daidzein 7-O-methyltransferase [Glycyrrhiza echinata] gi 75146882 sp Q84KK5.1 D7OMT_GLYEC	RecName: Full=Isoflavone 7-O-methyltransferase; AltName: Full=Daidzein 7-O-methyltransferasegi 28804594 dbj BAC58012.1 S-adenosyl-L-methionine: daidzein 7-O-methyltransferase	1.1	0.001	2	-1.7
Ljmitog3v0000540	Cytochrome c biogenesis [Medicago truncatula] gi 357436015 ref XP_003588283.1		1.1	0.001	-	-1.1
Lj1g3v0263110	PREDICTED: phospho-2-dehydro-3-deoxyheptanate aldolase 1, chloroplastic-like [Cicer arietinum] gi 502177864 ref XP_004516132.1	Phospho-2-dehydro-3-deoxyheptanate aldolase 1, chloroplastic-like	1	0.001	-	-
Lj2g3v1455170	PREDICTED: UDP-glycosyltransferase 85A3-like [Glycine max] gi 356497681 ref XP_003517688.1	UDP-glycosyltransferase 85A3-like	1	0.001	1.2	-2.5
Lj4g3v2107220	cytochrome P450 reductase [Lotus japonicus] gi 197209812 dbj BAG68945.1	Cytochrome P450 reductase	1	0.001	-2	divided by zero (in control)
Lj1g3v4690420	PREDICTED: UDP-glycosyltransferase 73C2-like [Glycine max] gi 356572494 ref XP_003554403.1	UDP-glycosyltransferase 73C2-like	-1	0.024	-	divided by zero (in control)
Lj1g3v4690460	PREDICTED: UDP-glycosyltransferase 73C3-like [Cicer arietinum] gi 502111561 ref XP_004494094.1	UDP-glycosyltransferase 73C3-like	-1	0.001	3.4	-4.9
Lj0g3v0273599	PREDICTED: isoliquiritigenin 2'-O-methyltransferase-like [Glycine max] gi 356532221 ref XP_003534672.1	Isoliquiritigenin 2'-O-methyltransferase-like	-1.1	0.001	2.6	-3
Lj3g3v0718740	PREDICTED: cytochrome P450 82C2-like [Glycine max] gi 356560747 ref XP_003548649.1	Cytochrome P450 82C2-like	-1.1	0.001	-1.8	1.7

Lj6g3v1077640	PREDICTED: serine carboxypeptidase 24-like isoform 1 [Glycine max] gi 356500663 ref XP_003519151.1	Serine carboxypeptidase 24-like isoform 1	-1.1	0.008	-	-
Lj0g3v0363569	PREDICTED: benzyl alcohol O-benzoyltransferase-like [Glycine max] gi 356500043 ref XP_003518844.1	Benzyl alcohol O-benzoyltransferase-like	-1.2	0.001	4.4	-5.2
Lj2g3v0561120	PREDICTED: abietadienol/abietadienol oxidase-like [Glycine max] gi 356559993 ref XP_003548280.1	Abietadienol/abietadienol oxidase-like	-1.4	0.001	-	1.5
Lj0g3v0315379	PREDICTED: benzyl alcohol O-benzoyltransferase-like [Glycine max] gi 356500043 ref XP_003518844.1	Benzyl alcohol O-benzoyltransferase-like	-1.8	0.015	5.1	-5

20. Lipid metabolism

Gene ID	Annotation (hit)	Lotus base annotation	log2FC	q value	log2FC_Rh	log2FC_AMF
Lj0g3v0335279	PREDICTED: GDSL esterase/lipase At5g03610-like [Cicer arietinum] gi 502178206 ref XP_004516199.1	GDSL esterase/lipase At5g03610-like	4.2	0.001	-	-
Lj6g3v0750030	PREDICTED: 4-coumarate--CoA ligase-like 1-like [Cicer arietinum] gi 502177503 ref XP_004516098.1	4-coumarate--CoA ligase-like 1-like	3.7	0.015	1.8	-1.1
Lj0g3v0326489	PREDICTED: probable carboxylesterase 1-like [Cicer arietinum] gi 502178720 ref XP_004516320.1	Probable carboxylesterase 1-like	2.8	0.001		-
Lj5g3v0085060	PREDICTED: elongation of fatty acids protein A-like [Cicer arietinum] gi 502131616 ref XP_004501043.1	Elongation of fatty acids protein A-like	2.3	0.001	2.1	-2.4
Lj3g3v2995750	PREDICTED: fatty acyl-CoA reductase 3-like [Glycine max] gi 356539286 ref XP_003538130.1	Fatty acyl-CoA reductase 3-like	1.6	0.001	-1	-
Lj6g3v1966630	PREDICTED: GDSL esterase/lipase At1g29670-like [Cicer arietinum] gi 502079509 ref XP_004486282.1	GDSL esterase/lipase At1g29670-like	1.6	0.001	1.2	-
Lj4g3v0855360	PREDICTED: GDSL esterase/lipase At2g23540-like [Glycine max] gi 356498499 ref XP_003518088.1	GDSL esterase/lipase At2g23540-like	1.5	0.001	-	-
Lj6g3v1491480	PREDICTED: phospholipase D p1-like [Glycine max] gi 356556110 ref XP_003546370.1	Phospholipase D p1-like	1.5	0.001	-	1
Lj0g3v0243489	PREDICTED: GDSL esterase/lipase At2g23540-like [Glycine max] gi 356498499 ref XP_003518088.1		1.4	0.001	-	-
Lj2g3v2003100	PREDICTED: phospholipase D gamma 1-like isoform 1 [Glycine max] gi 356497199 ref XP_003517450.1	Phospholipase D gamma 1-like isoform 1	1.4	0.001	-	1.3
Lj0g3v0268829	PREDICTED: acetyl-CoA carboxylase 1-like [Cicer arietinum] gi 502130304 ref XP_004500605.1	Acetyl-CoA carboxylase 1-like	1.2	0.001	-	-
Lj5g3v1015360	PREDICTED: phospholipase A1-lgamma1, chloroplastic-like [Glycine max] gi 356500145 ref XP_003518894.1	Phospholipase A1-lgamma1, chloroplastic-like	1.1	0.001	-	-

21. Proteins related to hormone metabolism

Gene ID	Annotation (hit)	Lotus base annotation	log2FC	q value	log2FC_Rh	log2FC_AMF
Lj2g3v2879460	ACC-oxidase [Vigna angularis] gi 1944152 dbj BAA19605.1	ACC-oxidase	5.5	0.001	-	-1.9
Lj0g3v0075119	PREDICTED: 12-oxophytodienoate reductase 3-like [Glycine max] gi 356547929 ref XP_003542357.1	12-oxophytodienoate reductase 3-like	4.1	0.001	2.2	-5.5

Chapter 6

Lj3g3v0421660	PREDICTED: gibberellin 2-beta-dioxygenase 1-like [Glycine max] gi 356549549 ref XP_003543155.1	Gibberellin 2-beta-dioxygenase 1-like	2.6	0.001	3.3	-1
Lj0g3v0219159	PREDICTED: zeatin O-glucosyltransferase-like [Cicer arietinum] gi 502123235 ref XP_004498042.1	Zeatin O-glucosyltransferase-like	2.5	0.001	-	-
Lj1g3v0115350	12-oxophytodieneate reductase [Lotus japonicus] gi 283132371 dbj BAI63591.1	12-oxophytodieneate reductase	2.4	0.001	1.2	-1.5
Lj0g3v0219149	PREDICTED: zeatin O-glucosyltransferase-like [Glycine max] gi 356537475 ref XP_003537252.1	Zeatin O-glucosyltransferase-like	1.9	0.001	1.2	-1.2
Lj2g3v3222870	PREDICTED: indole-3-acetate O-methyltransferase 1-like [Glycine max] gi 356567094 ref XP_003551758.1	Indole-3-acetate O-methyltransferase 1-like	1.6	0.001	3	-
Lj4g3v2253520	PREDICTED: gibberellin 2-beta-dioxygenase 2-like [Cicer arietinum] gi 502150760 ref XP_004508110.1	Gibberellin 2-beta-dioxygenase 2-like	1.3	0.001	1.5	-1.2
Lj3g3v3500200	PREDICTED: gibberellin 2-beta-dioxygenase 8-like [Cicer arietinum] gi 502144822 ref XP_004505762.1	Gibberellin 2-beta-dioxygenase 8-like	1.2	0.001	3.5	-4.3
Lj0g3v0300579	9-cis-epoxycarotenoid dioxygenase [Caragana korshinskii] gi 256561143 gb ACU86971.1	9-cis-epoxycarotenoid dioxygenase	1.1	0.001	1.7	-
Lj4g3v0484780	PREDICTED: LOW QUALITY PROTEIN: gibberellin 20 oxidase 1-like [Glycine max] gi 356515486 ref XP_003526431.1	Gibberellin 20 oxidase 1-like	1.1	0.001	-1.1	-
Lj3g3v3650360	PREDICTED: cytokinin dehydrogenase 6-like [Glycine max] gi 356542934 ref XP_003539919.1	Cytokinin dehydrogenase 6-like	1	0.001	1	-1.2
Lj2g3v3341900	Cytokinin-O-glucosyltransferase [Medicago truncatula] gi 357495617 ref XP_003618097.1	Cytokinin-O-glucosyltransferase	-1.3	0.001	-	-2.3

22. Proteins responding to hormones

Gene ID	Annotation (hit)	Lotus base annotation	log2FC	q value	log2FC_Rh	log2FC_AMF
Lj4g3v0336110	PREDICTED: auxin-induced protein 5NG4-like [Glycine max] gi 356528066 ref XP_003532626.1	Auxin-induced protein 5NG4-like	4.6	0.001	-	-2.7
Lj0g3v0288689	Auxin-induced protein 5NG4 [Medicago truncatula] gi 357445675 ref XP_003593115.1	Auxin-induced protein 5NG4	3.4	0.005	-	-
Lj0g3v0268999	PREDICTED: chitin-inducible gibberellin-responsive protein 1-like [Glycine max] gi 356514974 ref XP_003526176.1		2.2	0.001	-	-2.3
Lj0g3v0160899	PREDICTED: auxin-induced protein 5NG4-like [Glycine max] gi 356528066 ref XP_003532626.1		1.6	0.005	-2.1	1.9
Lj5g3v1315640	RmIC-like cupins superfamily protein [Theobroma cacao] gi 508718920 gb EOY10817.1		1.4	0.001	-	-
Lj4g3v0119950	PREDICTED: auxin-induced in root cultures protein 12-like [Glycine max] gi 356532614 ref XP_003534866.1		1.2	0.001	-	-
Lj5g3v0198060	Gibberellin-regulated protein [Medicago truncatula] gi 357438421 ref XP_003589486.1		1.2	0.001	-	-
Lj1g3v3353990	PREDICTED: auxin-induced protein 10A5-like [Glycine max] gi 356517873 ref XP_003527610.1	Auxin-induced protein 10A5-like	1.1	0.001	5.2	-4.4
Lj1g3v4590920	PREDICTED: indole-3-acetic acid-induced protein ARG7-like [Glycine max] gi 356570761 ref XP_003553553.1	Indole-3-acetic acid-induced protein ARG7-like	-1.1	0.001	-3.1	2.2
Lj0g3v0040139	PREDICTED: indole-3-acetic acid-induced protein ARG7-like [Glycine max] gi 356545069 ref XP_003540968.1	Auxin-induced protein 10A5-like	-1.3	0.003	-1	-
Lj3g3v2576020	SAUR family protein [Populus trichocarpa] gi 224074081 ref XP_002304244.1	SAUR family protein	-1.6	0.001	-	-

23. Proteins related to redox metabolism

Gene ID	Annotation (hit)	Lotus base annotation	log2FC	q value	log2FC_Rh	log2FC_AMF
Lj3g3v3513660	PREDICTED: lignin-forming anionic peroxidase-like [Glycine max] gi 356576113 ref XP_003556178.1	Lignin-forming anionic peroxidase-like	5.4	0.001	divided by zero (in control)	
Lj0g3v0328269	polyketide reductase [Lotus japonicus] gi 121309832 dbj BAF44219.1	Polyketide reductase	4	0.001	1.8	-2.6
Lj1g3v4482330	formate dehydrogenase, selenocysteine-containing chain A [Desulfotalea psychrophila LSv54] gi 51245621 ref YP_065505.1		3.2	0.001	5.6	-3
Lj2g3v3339240	polyketide reductase [Lotus japonicus] gi 121309832 dbj BAF44219.1	Polyketide reductase	2.7	0.001	4.5	-4.8
Lj2g3v2412440	Peroxidase [Medicago truncatula] gi 357491415 ref XP_003615995.1	Peroxidase	2.5	0.001	-	-
Lj6g3v1249630	FAD linked oxidase, N-terminal [Medicago truncatula] gi 124360772 gb ABN08744.1	FAD linked oxidase, N-terminal	2.5	0.036	divided by zero (in control)	
Lj5g3v1925220	PREDICTED: peroxidase 12-like [Cicer arietinum] gi 502118925 ref XP_004496443.1	Peroxidase 12-like	1.9	0.001	-	1.4
Lj0g3v0246969	PREDICTED: protein SRG1-like [Glycine max] gi 356499960 ref XP_003518803.1	Protein SRG1-like	1.6	0.001	2.5	-1.6
Lj0g3v0272079	peroxidase [Vigna angularis] gi 218328 dbj BAA01950.1	Peroxidase	1.6	0.001	-	-
Lj2g3v3339350	polyketide reductase [Lotus japonicus] gi 121309832 dbj BAF44219.1		1.5	0.001	1.7	-1.8
Lj5g3v0626670	PREDICTED: peroxidase 21-like [Glycine max] gi 356537521 ref XP_003537275.1	Peroxidase 21-like	1.5	0.001	4.6	
Lj0g3v0261869	NADPH:quinone oxidoreductase [Medicago truncatula] gi 357456791 ref XP_003598676.1	NADPH:quinone oxidoreductase	1.3	0.001	-	-
Lj2g3v3339170	polyketide reductase [Lotus japonicus] gi 121309832 dbj BAF44219.1	Polyketide reductase	1.3	0.001	1.4	-1.9
Lj4g3v2817870	PREDICTED: L-ascorbate oxidase-like [Cicer arietinum] gi 502140076 ref XP_004504046.1	L-ascorbate oxidase-like	1.3	0.001	3	-2.7
Lj6g3v1162950	Flavin-dependent monooxygenase 1 [Theobroma cacao] gi 508782921 gb EOY30177.1	Flavin-dependent monooxygenase 1	1.3	0.001	-2.1	2.1
Lj0g3v0266939	glutaredoxin family protein [Arabidopsis lyrata subsp. lyrata] gi 297801614 ref XP_002868691.1	Glutaredoxin family protein	1.1	0.001	-	-
Lj3g3v3513680	PREDICTED: lignin-forming anionic peroxidase-like [Glycine max] gi 356576113 ref XP_003556178.1	Lignin-forming anionic peroxidase-like	1	0.001	1	-2.2
Lj4g3v0998940	PREDICTED: peroxidase 72-like [Cicer arietinum] gi 502153363 ref XP_004509315.1	Peroxidase 72-like	1	0.001	-	-
Lj4g3v2120580	PREDICTED: peroxidase 16-like [Cicer arietinum] gi 502150284 ref XP_004507879.1	Peroxidase 16-like	-1	0.001	-	-
Lj3g3v2889720	PREDICTED: peroxidase 3-like [Cicer arietinum] gi 502171701 ref XP_004515086.1	Peroxidase 3-like	-1.1	0.001	-	-
Lj2g3v1467700	Geraniol dehydrogenase 1 [Theobroma cacao] gi 508699991 gb EOX91887.1	Geraniol dehydrogenase 1	-1.2	0.032	-	-
Lj2g3v2411410	PREDICTED: peroxidase 4-like [Glycine max] gi 356500928 ref XP_003519282.1	Peroxidase 4-like	-1.2	0.001	-	1
Lj0g3v0074079	probable aldo-keto reductase 1 [Glycine max] gi 351723659 ref NP_001236007.1		-1.3	0.001	-	-
Lj6g3v2083620	PREDICTED: NAD(P)H dehydrogenase B2, mitochondrial-like [Cicer arietinum] gi 502079444 ref XP_004486261.1	NAD(P)H dehydrogenase B2, mitochondrial-like	-1.3	0.001	-	1
Lj2g3v1014110	PREDICTED: quinone oxidoreductase-like protein At1g23740, chloroplastic-like [Cicer arietinum] gi 502090613 ref XP_004489284.1	Quinone oxidoreductase-like protein At1g23740, chloroplastic-like	-2.9	0.001	-	-

24. Proteins involved in other physiological processes

Gene ID	Annotation (hit)	Lotus base annotation	log2FC	q value	log2FC_Rh	log2FC_AMF
Lj2g3v0739570	PREDICTED: LOB domain-containing protein 41-like [Glycine max] gi 356520597 ref XP_003528948.1		3.5	0.042	3.1	-4.5

Lj1g3v4317620	seed maturation protein LEA 4 [Glycine tomentella] gi 11612197 gb AAG37451.1	Seed maturation protein LEA 4	1.9	0.028	-4	-
Lj0g3v0230519	Photosystem I P700 chlorophyll a apoprotein [Medicago truncatula] gi 357463453 ref XP_003602008.1	Photosystem I P700 chlorophyll a apoprotein	1.9	0.001	-	1.4
Ljchlorog3v0010750	photosystem II protein H [Lotus japonicus] gi 13518467 ref NP_084826.1	Photosystem II protein H	1.4	0.001	-	-
Lj0g3v0202659	seed maturation protein PM39 [Glycine max] gi 5802248 gb AAD51627.1		1	0.027	1.6	-
Lj1g3v3477210	Male sterility 5 family protein [Medicago truncatula] gi 357505367 ref XP_003622972.1	Male sterility 5 family protein	-2	0.001	-1.5	-

25. Unknown/uncharacterized proteins

Gene ID	Annotation (hit)	Lotus base annotation	log2FC	q value	log2FC_Rh	log2FC_AMF
Lj2g3v0227070			3.8	0.001	-	-1
Lj4g3v3003940	Uncharacterized protein TCM_016469 [Theobroma cacao] gi 508777772 gb EOY25028.1		3.8	0.001	4.6	-3.6
Lj6g3v0958320	Uncharacterized protein TCM_040942 [Theobroma cacao] gi 508785660 gb EOY32916.1		3.1	0.001	4.2	-4.6
Lj3g3v2188220	Uncharacterized protein TCM_027159 [Theobroma cacao] gi 508778543 gb EOY25799.1		3	0.001	-	-4.9
Lj6g3v1126300	Uncharacterized protein TCM_015652 [Theobroma cacao] gi 508776642 gb EOY23898.1		2.6	0.001	-	-
Lj0g3v0211559	Uncharacterized protein TCM_000701 [Theobroma cacao] gi 508699663 gb EOX91559.1		2.5	0.001	2.1	-1.8
Lj1g3v3267760	Uncharacterized protein TCM_019359 [Theobroma cacao] gi 508712195 gb EOY04092.1		2.5	0.003	5.6	-5.3
Lj3g3v0349300	Uncharacterized protein TCM_019970 [Theobroma cacao] gi 508712893 gb EOY04790.1		2.5	0.001	1.6	-1.4
Lj4g3v1560500	F14D16.17 [Arabidopsis thaliana] gi 8778278 gb AAF79287.1 AC068602_10		2.5	0.001	6.6	-6.6
Lj0g3v0147659	Uncharacterized protein TCM_030216 [Theobroma cacao] gi 508781429 gb EOY28685.1		2.4	0.001	1.6	-
Lj2g3v2185510	Uncharacterized protein TCM_015546 [Theobroma cacao] gi 508776492 gb EOY23748.1		2.4	0.001	1.1	-1.1
Lj4g3v0975530	Uncharacterized protein TCM_000343 [Theobroma cacao] gi 508699138 gb EOX91034.1		2.3	0.001	3	-3.5
Lj3g3v2213510	JHL06P13.17 [Jatropha curcas] gi 317106740 dbj BAJ53236.1		2.2	0.001	1.6	-3.1
Lj4g3v0975500	Uncharacterized protein TCM_000343 [Theobroma cacao] gi 508699138 gb EOX91034.1		2.1	0.001	4.6	-4.1
Lj5g3v1853000	Uncharacterized protein TCM_043091 [Theobroma cacao] gi 508726672 gb EOY18569.1		2.1	0.001	-	-1.1
Lj1g3v3330040	NAD(P)-binding Rossmann-fold superfamily protein [Theobroma cacao] gi 508705586 gb EOX97482.1		2	0.001	-	-
Lj3g3v0931340	Uncharacterized protein TCM_040311 [Theobroma cacao] gi 508785151 gb EOY32407.1		1.9	0.001	2.2	-1.8
Lj4g3v0975490	Uncharacterized protein TCM_000343 [Theobroma cacao] gi 508699138 gb EOX91034.1		1.9	0.001	4.2	-3.7
Lj1g3v4998310	Uncharacterized protein TCM_026263 [Theobroma cacao] gi 508719103 gb EOY11000.1		1.8	0.001	2.8	-3.2
Lj5g3v2110890	Uncharacterized protein isoform 1 [Theobroma cacao] gi 508706532 gb EOX98428.1		1.8	0.001	-	-
Lj1g3v3754830			1.8	0.011	-	-
Lj5g3v1414150	MtN26 protein [Medicago truncatula] gi 357512267 ref XP_003626422.1		1.8	0.001	1.4	1
Lj0g3v0024519	pinorensin-laricresin reductase homolog [Lotus japonicus] gi 116077988 dbj BAF34845.1		1.7	0.001	1.2	-1.3
Lj0g3v0060449	Uncharacterized protein TCM_043094 [Theobroma cacao] gi 508726677 gb EOY18574.1		1.7	0.005	1.2	-

Chapter 6

Lj3g3v1421790	PREDICTED: centrosome-associated protein CEP250 isoform 1 [Pan paniscus] gi 397523781 ref XP_003831897.1		1.7	0.016	-	-1.7
Lj3g3v3360920	pterocarpan reductase [Lotus japonicus] gi 116077982 dbj BAF34842.1		1.7	0.001	-	-
Lj0g3v0127139	Uncharacterized protein TCM_010371 [Theobroma cacao] gi 508708593 gb EOY00490.1		1.6	0.001	1.7	-1.3
Lj5g3v0629110	Uncharacterized protein TCM_022156 [Theobroma cacao] gi 508715935 gb EOY07832.1		1.6	0.001	-	-1.5
Lj6g3v2193410	PREDICTED: mucin-2-like [Cicer arietinum] gi 502142197 ref XP_004504839.1		1.6	0.019	-	-
Lj0g3v0243359	Coiled-coil domain-containing protein [Medicago truncatula] gi 357498253 ref XP_003619415.1		1.5	0.001	-	-
Lj0g3v0328449	Uncharacterized protein TCM_034853 [Theobroma cacao] gi 508724034 gb EOY15931.1		1.5	0.001	3.5	-3.1
Lj2g3v1194190	Uncharacterized protein TCM_011355 [Theobroma cacao] gi 508709587 gb EOY01484.1		1.5	0.001	4.4	-4.2
Lj5g3v0529060	PREDICTED: vitellogenin-2-like [Cicer arietinum] gi 502125004 ref XP_004498757.1		1.4	0.001	1.2	-2
Lj0g3v0164069	PREDICTED: UPF0496 protein 4-like [Glycine max] gi 356502356 ref XP_003519985.1		1.3	0.001	2.1	-1.3
Lj6g3v1211950	Uncharacterized protein TCM_037603 [Theobroma cacao] gi 508783120 gb EOY30376.1		1.3	0.001	4.3	-4.2
Lj1g3v2253690	Syringolide-induced protein 14-1-1 [Medicago truncatula] gi 357467101 ref XP_003603835.1		1.3	0.001	2.8	-2.2
Lj1g3v4729290	syringolide-induced protein B13-1-9 [Glycine max] gi 351726220 ref NP_001237119.1		1.3	0.001	4.2	-4.2
Lj0g3v0101529	Uncharacterized protein TCM_043094 [Theobroma cacao] gi 508726677 gb EOY18574.1		1.2	0.006	2.2	-1.8
Lj1g3v1743570	Uncharacterized protein TCM_034673 [Theobroma cacao] gi 508723787 gb EOY15684.1		1.2	0.001	4	-3.5
Lj4g3v0654410			1.2	0.002		
Lj0g3v0082249	Uncharacterized protein TCM_020826 [Theobroma cacao] gi 508714071 gb EOY05968.1		1.1	0.001	-	-
Lj0g3v0140129	Uncharacterized protein TCM_035327 [Theobroma cacao] gi 508724633 gb EOY16530.1		1.1	0.001	-	-
Lj0g3v0208329	Uncharacterized protein TCM_000023 [Theobroma cacao] gi 508698699 gb EOX90595.1		1.1	0.001	2.6	-3.2
Lj0g3v0256929	expressed protein [Oryza sativa Japonica Group] gi 78707843 gb ABB46818.1		1.1	0.045	-	-1
Lj0g3v0279189	Uncharacterized protein TCM_017498 [Theobroma cacao] gi 508711176 gb EOY03073.1		1.1	0.026	-	-
Lj2g3v1294240	Uncharacterized protein TCM_011746 [Theobroma cacao] gi 508710070 gb EOY01967.1		1.1	0.001	1.8	-1.4
Lj3g3v0823570	PREDICTED: UPF0496 protein 4-like [Cicer arietinum] gi 502177279 ref XP_004516046.1		1.1	0.001	5.1	-3
Lj3g3v3236620	Uncharacterized protein isoform 1 [Theobroma cacao] gi 508786634 gb EOY33890.1		1.1	0.001	-	-
Lj4g3v2172960	Uncharacterized protein TCM_037603 [Theobroma cacao] gi 508783120 gb EOY30376.1		1.1	0.001	4.2	-3.6
Lj5g3v2167320	Uncharacterized protein TCM_010809 [Theobroma cacao] gi 508708993 gb EOY00890.1		1.1	0.001	2.7	-2.6
Lj6g3v1983300	Uncharacterized protein TCM_031992 [Theobroma cacao] gi 508721522 gb EOY13419.1		1.1	0.001	4	-3.6
Lj1g3v0415660	predicted protein [Naegleria gruberi] gi 290974341 ref XP_002669904.1		1	0.001	3.7	-4.2
Lj3g3v2705610	PREDICTED: dentin sialophosphoprotein-like [Cicer arietinum] gi 502156182 ref XP_004510347.1		1	0.011	-	-
Lj3g3v2235790	Uncharacterized protein TCM_028364 [Theobroma cacao] gi 508779312 gb EOY26568.1		-1	0.001	-	-
Lj3g3v3363100	CM0216.240.nc [Lotus japonicus] gi 164564729 dbj BAF98211.1		-1	0.004	-	-
Lj6g3v1878770	Uncharacterized protein TCM_030210 [Theobroma cacao] gi 508781419 gb EOY28675.1		-1	0.001	-	-1.5

Lj0g3v0232099	Uncharacterized protein TCM_034360 [Theobroma cacao] gi 508723320 gb EOY15217.1		-1.1	0.037	-	-1.1
Lj1g3v3466030	Uncharacterized protein isoform 1 [Theobroma cacao] gi 508702077 gb EOX93973.1		-1.1	0.001	-	-
Lj3g3v3363120	CM0216.210.nc [Lotus japonicus] gi 164564727 dbj BAF98210.1		-1.1	0.003	-	-1
Lj0g3v0250469	Uncharacterized protein TCM_002928 [Theobroma cacao] gi 508702033 gb EOX93929.1		-1.2	0.015	-1.5	1.8
Lj0g3v0268109	F12M16.8 [Arabidopsis thaliana] gi 7769852 gb AAF69530.1 AC008007_5		-1.3	0.003	-	-
Lj1g3v2114690	ST225 [Eutrema halophilum] gi 193872612 gb ACF23034.1		-1.3	0.001	2.9	-1.8
Lj3g3v3363260	CM0216.240.nc [Lotus japonicus] gi 164564729 dbj BAF98211.1		-1.3	0.009	-	-
Lj3g3v3363300	CM0216.280.nc [Lotus japonicus] gi 164564730 dbj BAF98212.1		-1.3	0.011	-	-
Lj5g3v1770490	PREDICTED: RAB6-interacting golgin-like [Cicer arietinum] gi 502118280 ref XP_004496189.1		-1.3	0.042	-	1
Lj5g3v1353010	Uncharacterized protein isoform 3 [Theobroma cacao] gi 508719023 gb EOY10920.1		-1.4	0.039	-	1.5
Lj1g3v1991560	skeleton-binding protein 1 [Plasmodium falciparum 3D7] gi 124505949 ref XP_001351572.1		-1.5	0.001	-	-
Lj6g3v0183450			-1.5	0.021	-1.6	2.2
Lj3g3v3363340	CM0216.330.nc [Lotus japonicus] gi 164564735 dbj BAF98217.1		-1.6	0.028	-	-
Lj4g3v2617140	Uncharacterized protein TCM_029650 [Theobroma cacao] gi 508780685 gb EOY27941.1		-1.7	0.038	-	-
Lj4g3v2789200	Uncharacterized protein TCM_000101 [Theobroma cacao] gi 508698815 gb EOX90711.1		-1.7	0.015	-	-
Lj0g3v0133149			-1.8	0.019	-	-
Lj0g3v0356039	Uncharacterized protein TCM_007253 [Theobroma cacao] gi 508706613 gb EOX98509.1		-1.8	0.003	-	-

A description of plant gene IDs identified as DE in the *Lotus*-FsK dataset follows:

1. Proteins involved in signaling

38 transcripts were grouped into this functional category. A highly diverse set of receptors was identified. Among them at least 5 are LRR (leucine rich repeat) motif containing receptors (Lj0g3v0346649, Lj2g3v0852090, Lj1g3v2910560, Lj1g3v0526480, Lj2g3v0852080), at least 5 are cysteine-rich receptors (Lj4g3v1085080, Lj0g3v0250199, Lj0g3v0321459, Lj3g3v0392830, Lj1g3v1687840) and at least 2 are proline rich receptors (Lj2g3v1560870, Lj6g3v2193570). 3 of them (one LRR, one cysteine-rich, and one proline-rich receptor) showed the highest expression (>4-fold) among the transcripts placed in this category. 2 of the LRR receptors and 4 more are serine/threonine protein kinases (Lj0g3v0346649, Lj1g3v2910560, Lj0g3v0182159, Lj6g3v2116920, Lj0g3v0241709, Lj1g3v0526480, Lj0g3v0324409). 2 transcripts were annotated as “Receptor-like protein kinase HSL1-like” and the *A. thaliana* homolog is predicted to contain an LRR motif. A ‘beta-glucan-elicitor receptor’ is also up regulated (Lj0g3v0295619) and a ‘mitogen-activated protein kinase’ (Lj2g3v1880820). It is of interest that from the 38 transcripts identified, only two (Lj1g3v0052300, Lj0g3v0115159) are repressed (>2-fold) in *Lotus* roots elicited by FsK at very early stages of the interaction. The first transcript is annotated as a putative formin-like protein. Formins are not very well studied in plants. In animals and fungi, formins are just one of the four major classes of poly-L-proline-containing proteins

that form part of the signal-transduction cascade that leads to rearrangement of the actin cytoskeleton (Deeks et al., 2002).

Signal perception through cell surface receptors is a common feature of both plants and animals. Plant protein kinases can be classified according to their primary sequences and the type of protein phosphorylation activity: serine/threonine (ser/thr), histidine, or tyrosine (Chevalier et al., 2005). Protein phosphorylation is a post-translational modification process in which an amino acid residue of a protein is covalently modified by addition of a phosphate group involving an enzyme known as protein kinase. The kinase domain of a serine/threonine protein harbors the ability to phosphorylate the OH group of serine or threonine (which have similar sidechains) residues to regulate various cellular functions and activities (Ho, 2015).

Leucine-rich repeat receptor kinases constitute the largest group of plant RLKs, which play crucial roles in development and stress responses. The ectodomain of these receptors comprises of a varying number of LRR repeats, and LRR diversity allows sensing of various ligands, including small molecules, peptides, and entire proteins. LRR-RLKs function in a wide array of plant processes: some play role in control of plant growth and development, BRI1 is involved in brassinosteroid signaling, some respond to abiotic and biotic stress, such as FLS2- and EFR-mediated plant resistance against bacterial pathogens, some have dual roles in development and defense. For example, BAK1 is involved in developmental regulation through interaction with the plant brassinosteroid receptor BRI1, and is also involved in innate immunity against pathogens through interaction with FLS2, which recognizes the flg22 peptide from bacterial flagellin (Liu et al., 2017).

Receptor proteins have also been identified in the *S. indica*-*A. thaliana* association, among them a receptor kinase with leucine-rich repeats and a serine/threonine kinase required for full activation of two mitogen activated protein kinases 3 and 6 (MPK3, MPK6). In *A. thaliana* MPK6 is involved in developmental processes and stress responses in which plant hormones (JA and ET) are also involved. MPK6 is necessary for proper colonization and growth promoting effects conferred by *S. indica* to the plant, which is dependent on JA/ET signaling pathways as shown by mutant analysis (Daneshkhah et al., 2018). Mitogen activated protein kinases are involved in stress and hormonal responses, the regulation of cell division, growth, differentiation, programmed cell death as well as in symbiotic and pathogenic interactions (Smékalová et al., 2014).

2. Proteins related to carbohydrate metabolism

15 enzymes related to the metabolism of carbohydrate molecules were identified, most of them related to carbohydrate breakdown. More specifically, at least 5 enzymes with glucosidase properties (Glucan 1,3-beta-glucosidase like molecule) (Lj0g3v0106789, Lj0g3v0202539, Lj0g3v0318099, Lj0g3v0361989, Lj4g3v1709670) were identified; all were upregulated and only the latter was 2-fold downregulated. One enzyme with glucanase properties (Beta-1,3-glucanase; Lj0g3v0213009) was identified, which showed ~4-fold upregulation. 2 enzymes with laccase properties were upregulated (>2-fold) (Lj0g3v0285709, Lj0g3v0316509, Lj2g3v2833010). 3 enzymes with chitinase properties were identified and all were upregulated (>2-fold) in our system (Lj5g3v1961260, Lj6g3v1078670, Lj0g3v0362579).

In contrast to the ligninolytic activity of fungal laccases, plant laccases are involved in plant lignin biosynthesis through catalysis of monolignols oxidation and polymerization. They are also involved in wound healing, maintenance of cell wall structure and integrity, and certain laccase members are predicted to take part in the polymerization of phenolic compounds (Wang et al., 2015).

3. Lectins

9 transcripts were grouped as lectins. At least 6 have also the properties of serine/threonine protein kinase (phosphorylation of serine or threonine residues) (Lj1g3v5010640, Lj0g3v0356899, Lj0g3v0321389, Lj0g3v0138509, Lj0g3v0136559, Lj2g3v0663780).

Lectins are proteins with a main feature: they selectively recognize and bind reversibly to specific mono- or oligosaccharides. Lectins and carbohydrates are linked by a number of relatively weak interactions that ensure specificity, yet permit unlinking if required. Also, to be defined as lectins carbohydrate binding proteins have to display no enzymatic activity towards the recognized sugars and should not belong to the immunoglobulin family. They are soluble or membrane proteins, present both inside and outside cells. In plants, lectins have been early described as important players in defense against pathogens. Most of them are secretory proteins routed either to the vacuole, or to the cell wall and the PM (Bellande et al., 2017). At the PM, LecRLKs (lectin receptor-like kinases) are considered important proteins for the perception of various effector molecules. Plants employ a multitude of different LecRLKs/RLPs to recognize and fight pathogens. PM located LecRLKs and cytoplasmic lectins have roles in plant immunity, symbiosis, development and growth. In addition to their carbohydrate-binding interactions, lectins can also be engaged in protein-protein interactions (Holle and Damme, 2018). An *OsLecRK* gene (in rice) and its homologue in *Arabidopsis* (*AtLecRK*) are upregulated in interaction of both plants with *S. indica*. The gene was also shown via mutant analysis to be important for colonization of *Arabidopsis* roots by the fungus (Nivedita et al., 2017).

4. Germin-like proteins

2 transcripts encoding germin-like proteins were identified (Lj2g3v0946290, Lj1g3v3833760). The first one is highly upregulated (>16-fold upregulation) in *Lotus*-FsK system.

Germins and germin-like proteins (GLPs) constitute a large and highly diverse family of ubiquitous plant proteins. The name germin was given because the 1st described member of the family, wheat germin, was discovered in germinating wheat grains. These proteins are found in all organs and developmental stages. Germins and GLPs participate in many processes important for plant development and defense. All germins and GLPs are glycoproteins somehow associated with the extracellular matrix. 3 classes of functions have been identified for these proteins: enzymatic activity, structural proteins, receptors (Bernier and Berna, 2001).

5. Proteins related to endo-/exocytosis (including those related to vesicular trafficking)

6 transcripts encoding for proteins related with vesicular trafficking, vacuolar protein sorting, endo-/exocytosis related processes were identified as either up- or down regulated. More specifically, 2 transcripts encoding for proteins related to vacuolar protein sorting showed upregulation and a member

of the exocyst complex (Lj0g3v0264849, Lj0g3v0324319, Lj0g3v0313429). One transcript coding for a protein related to vacuolar protein sorting (Lj0g3v0114299), two transcripts coding for a protein associated with protein transport (ENTH/VHS/GAT family protein; Lj4g3v2401050, and Ras-related protein Rab7-like; Lj4g3v2786890) were ~2-fold repressed in *Lotus*-FsK system.

In eukaryotic cells, polarized secretion mediated by exocytotic fusion of membrane vesicles with the PM is necessary for expansion of the PM at distinct and restricted sites and for the delivery of molecules to specific locations at the membrane and/or cell surface. The EXOCYST complex is central to this process. Intense polarized exocytosis occurs for example, during AM development. Deposition of the periarbuscular membrane, one of the most important alterations occurring in the colonized by AM fungi cell, is achieved via polarized exocytosis, which involves the EXOCYST complex. An EXO70I protein is present exclusively in plants engaging in AM symbiosis, and *M. truncatula* *exo70i* mutants do not form normal arbuscules (Zhang et al., 2015b).

6. Proteins involved in defense

A high number of transcripts showed moderate to high levels of regulation in *Lotus* FsK system. More specifically, from the 36 transcripts identified, 33 were upregulated and only 3 were repressed. Among them transcripts coding for disease resistance and pathogenesis related proteins were identified. 4 transcripts were identified as coding for isoforms of pathogenesis-related PR10 (Lj6g3v1513720, Lj0g3v0348489, Lj0g3v0140429, Lj6g3v1513840) and they showed ~2 to ~4 upregulation. A transcript coding for a pathogenesis related PR27-like protein (Lj5g3v2112200) was also upregulated (>2-fold). 6 transcripts were annotated as glutathione S transferases. 3 were upregulated (>2-fold) (Lj4g3v2618270, Lj0g3v0303509, Lj0g3v0288349) and the other three were downregulated (Lj5g3v1696980, Lj1g3v3441490, Lj1g3v3441360). At least 2 transcripts coding for MAP kinase proteins were identified (MKS1-like proteins; Lj5g3v2183850, Lj2g3v1155180), and two transcripts coding for callose synthases were upregulated in *Lotus*-FsK system (Lj0g3v0124019, Lj0g3v0312429).

Glutathione S transferase genes (GSTs) play a role in a wide range of stress conditions including biotic stress. GSTs are markedly induced in the early phase of bacterial, fungal, and viral infections. Multiple GST proteins accumulate in infected plants. GSTs play a role on the detoxification of toxic substances by their conjugation with glutathione facilitating their metabolism, sequestration, or removal, on the attenuation of oxidative stress, and in hormone transport. GSTs can detoxify toxic lipid hydroperoxides that accumulate during infections. They are involved in plant infections by biotrophic, hemibiotrophic, necrotrophic fungi (Gullner et al., 2018). GSTs have also been found in nodules of *Glycine max* (soybean), and downregulation of one of them (GST9) led to a decrease in nitrogenase activity and an increase in oxidatively damaged proteins, suggesting a role for GSTs in providing antioxidant defenses, which are important to support nitrogen fixation (Dalton et al., 2009). A Glutathione S transferase gene has been reported to be upregulated in AM roots (Deguchi et al., 2007).

7. Proteins related to abiotic stress

5 transcripts were identified as coding for proteins related to abiotic stress, among other functions. 2 of them were upregulated, one coding for a late embryogenesis glycoprotein (Lj0g3v0250919), and one

coding for a SAB protein (Lj3g3v0566040). The other 3 transcripts, all coding for late embryogenesis proteins were downregulated (Lj6g3v2017530, Lj0g3v0346569), one of them >4-fold (Lj6g3v1629690). A gene coding for a late embryogenesis abundant (LEA) protein was recorded as symbiosis upregulated in a cDNA array hybridization experiment aiming to identify genes induced in both mature root nodules and arbuscular mycorrhiza (3 weeks post AMF inoculation). The gene was induced in both interactions (Manthey et al., 2004). LEA proteins have been associated with a conserved cellular function in land plants involved in desiccation tolerance which is the ability to survive the removal of almost all cellular water without irreparable damage. These proteins were originally associated with the acquisition of desiccation tolerance in plant embryos due to their high gene expression and protein accumulation in the later stages of seed maturation. LEA genes also accumulate in vegetative tissues under abiotic stress such as drought, salinity, heat and freezing (Artur et al., 2019).

8. *Proteins related to cell wall synthesis and modifications*

14 transcripts associated to modification of the cell wall were identified as regulated in *Lotus*-FsK system. More specifically, 11 were upregulated and 3 were downregulated. From the upregulated transcripts, 4 were identified as coding for expansin-like proteins (Lj4g3v1614580, Lj4g3v1176640, Lj0g3v0066909, Lj4g3v1213510, Lj0g3v0130759); one of them was highly upregulated (>32-fold). 3 transcripts were glycoproteins, 2 of which were rich in proline (Lj2g3v0264280, Lj2g3v0264020). 2 other transcripts were annotated as coding for arabinogalactan proteins (Lj2g3v0777220, Lj6g3v2203710). The 3 repressed transcripts were identified as coding for a pectinesterase (Lj0g3v0341889), and the other 2 for expansin-proteins (Lj3g3v3556010, Lj0g3v0140179).

An expansin gene was reported to be repressed in *M. truncatula* arbuscule containing cells in a cDNA microarray hybridization experiment (Gaude et al., 2012). Expansins are cell wall proteins that mediate acid-induced growth by catalyzing loosening of plant cell walls without lysis of wall polymers. The plant cell grows in volume via selective loosening of the primary cell wall, which confines and shapes the cell, resulting in wall stress relaxation and subsequent water uptake and cell enlargement (Cosgrove, 2015). Extensins are arabinogalactan proteins and hydroxyproline- and proline-rich proteins, which are important components of cell wall proteins that play important roles in cell wall transduction cascades, plant development, and stress tolerance. Proline is an important source of cell wall matrix. Hydroxyproline-rich glycoproteins are expressed during wounding and pathogen attack, they are implicated in development in some tissues, nodule formation, fertilization, cytokinesis, apoptosis, senescence, cell wall lignification (Kishor et al., 2015).

9. *Proteins involved in cell modifications*

5 transcripts were grouped into this functional category, and all of them were repressed in our system. More specifically, 1 transcript was annotated as coding for 'exordium like 2' protein, 2 transcripts were identified as coding for 'casparian strip membrane' proteins (Lj3g3v1203500, Lj0g3v0217659), and the other 2 were identified as coding for 'cortical cell-delineating proteins' (Lj3g3v2809710, Lj3g3v2809690). All transcripts showed >2-fold downregulation.

In *Arabidopsis thaliana* the EXO (EXORDIUM) gene was identified as a mediator of brassinosteroid (BR)-promoted growth. Lack of expression of this gene results in diminished leaf and root growth and reduced biomass production. Overexpression promotes root and shoot growth. The EXO gene is essential for cell expansion in leaves. The EXO gene is a BR-regulated gene, and BR controls cell wall modifications, organization of microtubules and cellulose microfibrils, aquaporin activity, and photosynthesis (Schröder et al., 2009).

Casparian strip membrane domain proteins were identified in *Arabidopsis*; they are four transmembrane proteins that form a median domain referred to as the Casparian strip membrane domain (CSD). The CSD anchors the plasma membrane to the cell wall and recruits the enzymes necessary for lignin biosynthesis. It has been shown that membranous proteins cannot diffuse freely within this region. These proteins have an important role in the modification of the cell wall: they mediate the deposition of lignin and the building up of the Casparian strips (Roppolo et al., 2014).

10. *Proteins related to transmembrane transport (including proteins involved in general transport mechanisms)*

35 transcripts were assigned into the functional group of transmembrane transport (including transcripts involved in general cell transport mechanisms), among which 6 were repressed. Among the highly upregulated transcripts there were two coding for a 'protein transparent TESTA-like' (Lj3g3v1314810, Lj5g3v2169440) and a transcript coding for a protein of the MATE gene family of metabolite transporters (Lj0g3v0075999). Among the upregulated transcripts, 3 were identified as coding for proteins related to sugar transport (Lj0g3v0341429, Lj5g3v2057350, Lj1g3v0605120). A sulfite exporter was also identified (Lj1g3v4692980), 6 ABC transporters (Lj5g3v2288960, Lj3g3v1063670, Lj0g3v0315079, Lj0g3v0315069, Lj0g3v0234389, Lj5g3v1630010) one of which was >4-fold regulated, and an auxin efflux carrier (Lj2g3v1589590). A putative glucose-6-phosphate/phosphate translocator gene was also upregulated (Lj6g3v1880060).

Among the repressed transcripts, there was a bidirectional sugar transporter (Lj1g3v0948550), a probable cyclic nucleotide-gated ion channel (Lj1g3v1991510), and an oligopeptide transporter (Lj1g3v4287660).

MATE (Multidrug and Toxic Compound Extrusion or Multi-Antimicrobial Extrusion) transporters comprise a universal gene family of membrane effluxers. Most MATE transporters export primary and secondary metabolites out of the cytosol using electrochemical gradient across the membrane. They have prominent roles in cell detoxification. In plants, they implicate directly or indirectly in mechanisms of detoxification of heavy metals, disease resistance, transport of secondary metabolites, such as flavonoids and hormones (dos Santos et al., 2017). A transporter (solute flippase) of the MATE family has been identified as induced in both root nodules and mycorrhized roots in *M. truncatula* (Benedito et al., 2010).

ABC proteins (ATP-binding cassette proteins) are membrane-bound transporters and soluble proteins involved directly in the transport of a wide range of molecules across membranes. They can be categorized as importers or exporters, depending on the direction of transport relative to the cytoplasm (Verrier et al., 2008). ABC transporters play a significant role in AM symbiosis. (Zhang et al., 2010)

identified two *M. truncatula* ABC transporters, essential for arbuscule development in AM symbiosis. These transporters putatively form a heterotrimeric export pump located in the PAM and are involved in the export of signaling molecules into the peri-arbuscular space. In another study, a MtABC transporter showed increased transcript levels in arbusculated cells and in adjacent cells. The transporter may be involved in the transport of signaling molecules between plant cells during AM symbiosis (Gauze et al., 2012).

11. Proteins related to ion binding

13 transcripts were identified as coding for ion binding proteins, 12 of which were upregulated. 3 transcripts coding for calcium binding proteins were identified (Lj0g3v0311049, Lj0g3v0084599, Lj1g3v3019860), 5 transcripts coding for proteins with zinc binding domain(s) (Lj5g3v0614880, Lj1g3v1720190, Lj0g3v0355229, Lj5g3v0614980, Lj5g3v2099610, Lj0g3v0154819), and one transcript coding for a basic blue protein (Lj4g3v2704690).

A gene coding for a blue copper binding protein, *MtBcp1*, is induced in AMF-inoculated roots, and was demonstrated to be preferentially expressed in arbuscule-containing regions. Further proteomic analysis of mycorrhized *M. truncatula* PM fractions, suggested that the blue copper protein is located in the PAM. The protein is implicated in electron transfer reactions and is characterized by the presence of a copper binding site (Valot et al., 2006).

12. Putative secreted proteins

One transcript was annotated as encoding for a putative secreted protein rich in cysteine (Lj3g3v1342650). As we did not perform analysis searching for secretory proteins (searching for motifs in the amino acid sequence corresponding to DEGs) we cannot say that this is the only transcript identified coding for a secretory protein.

13. Proteins involved in nucleotide metabolism (DNA and RNA)

13 transcripts were matched to nucleotide metabolism group. 10 were upregulated whereas 3 were repressed. From the upregulated ones, only 1 transcript was annotated as coding for an endonuclease (Lj0g3v0110029), and 3 transcripts were identified as coding for proteins involved in chromatin remodeling (Lj0g3v0342229, Lj0g3v0269349, Lj0g3v0325869), 2 code for DNA polymerases (Lj0g3v0077789, Lj0g3v0336359), 2 for helicases (Lj0g3v0196139, Lj1g3v0118820) and 1 for a DNA ligase (Lj0g3v0270019). 1 transcript coding for a snoRNA-like protein was also upregulated (Lj0g3v0071459).

From the 3 repressed transcripts, 1 codes for an enzyme involved in DNA repair (Lj2g3v2183350), one for an ATP-dependent helicase (Lj4g3v2526040), and one for an acid phosphatase (Lj0g3v0333259). An acid phosphatase has been isolated from the root nodules of soybean. The enzyme shows high specificity for purine 5'-nucleotides and is developmentally regulated in a manner consistent with a role in the intermediate reactions of ureide biosynthesis, which is together with allantoin and allantoic acid, the chemical form that soybeans and other tropical legumes use to export fixed nitrogen (Penheiter et al., 1998).

14. Proteins involved in gene expression (transcription)

28 transcripts were predicted as transcription factors. 24 were upregulated, whereas only 4 were repressed. Among the upregulated genes were: 4 transcripts coding for ethylene-responsive TFs (Lj1g3v4483640, Lj4g3v2214780, Lj1g3v1222700, Lj0g3v0332559, Lj1g3v2114700), 2 of which showed the highest upregulation in the whole functional group (>8-fold), 3 transcripts coding for WRKY TFs (Lj0g3v0298769, Lj1g3v3847230, Lj3g3v1393570), 4 transcripts coding for MYB TFs (Lj2g3v1495100, Lj3g3v2477670, Lj3g3v2477660, Lj0g3v0165839).

Among the downregulated genes an ethylene responsive TF (Lj1g3v2114700), and a transcript coding for a MYB transcriptional regulator (Lj1g3v3751720) were identified.

Plant MYBs have been implicated in controlling many diverse processes, among them plant organ development. In a *L. japonicus* – *Gigaspora margarita* interaction, among the highly regulated TFs is a *LjMyb* TF gene (Guether et al., 2009). Homologs of a Myb-like protein have identified as TFs differentially expressed during early stages of *M. truncatula* – *S. meliloti* interaction (Lohar et al., 2006). Myb family TFs were among the most strongly induced in arbuscule containing and non-colonized cells of *M. truncatula* mycorrhized roots (Gaude et al., 2012).

WRKY are TFs implicated in transcriptional reprogramming during plant immune responses. They contain DNA-binding domains and they bind to promoters of defense-associated genes. They act as positive or negative regulators of plant defense (Eulgem and Somssich, 2007). Genes encoding WRKY TFs were induced in *L. japonicus* during mycorrhiza development and during nodulation (Deguchi et al., 2007).

15. Proteins involved in protein biosynthesis

3 transcripts were identified as involved in protein biosynthesis, all of them were upregulated in *Lotus*-FsK system. 2 transcripts are coding for translation initiation factors (Lj0g3v0214539, Lj0g3v0304609), and one for a ribosomal protein (Lj2g3v3085370).

16. Proteins involved in protein processing

9 transcripts were identified as coding for proteins involved in protein processing. 8 were upregulated, among them 6 transcripts coding for chaperons (Lj3g3v2385390, Lj4g3v0340640, Lj3g3v2385400, Lj1g3v1032230, Lj2g3v0039390, Lj0g3v0184659), one coding for a heat shock 70kDa protein (Lj1g3v4921040), and one coding for a putative 'beta-1,3-galactosyltransferase 7-like' (Lj0g3v0297749) responsible for protein glycosylation. One transcript coding for a chaperone protein was downregulated in *Lotus*-FsK system (Lj0g3v0258139).

Galactosyltransferases are enzymes that catalyze the transfer of galactose.

17. Proteins involved in protein degradation (including protease inhibitors)

29 transcripts were identified as coding for proteins involved in protein degradation. 28 were upregulated and one was downregulated, which was identified as a protease inhibitor (Lj0g3v0164769) and was classified in the group for simplification purposes. 7 proteases / proteinases / peptidases were

identified (Lj5g3v1174410, Lj3g3v2995720, Lj0g3v0200149, Lj2g3v2001600, Lj3g3v0966710, Lj0g3v0164769). Several ubiquitin ligases (Lj3g3v2938470, Lj0g3v0014579, Lj0g3v0163939, Lj1g3v2728130, Lj0g3v0245049, Lj1g3v4944910, Lj2g3v1472950), 6 transcripts coding for U-box containing proteins (Lj2g3v0636850, Lj2g3v2794440, Lj6g3v0408370, Lj0g3v0267019, Lj4g3v2803800, Lj4g3v1534900). A transcript coding for a subtilase was also identified (Lj3g3v2995720). 4 transcripts coding for 'basic 7S globulin' proteins with putative involvement in protein catabolic processes were also identified (Lj6g3v1880250, Lj5g3v0963160, Lj6g3v1880370, Lj5g3v1203340). 5 transcripts coding for proteins with F-box motifs with putative ubiquitin functions were also recorded (Lj6g3v1849460, Lj6g3v1849450, Lj0g3v0200139, Lj4g3v0816700, Lj0g3v0322949).

18. Proteins related to primary metabolism

11 transcripts were identified as involved in primary metabolic processes such as amino acid metabolism. All transcripts within this group were upregulated. 4 transcripts were identified as coding for PAL genes (phenylalanine-ammonia-lyase genes) (Lj0g3v0121549, Lj1g3v4590710, Lj1g3v4590850, Lj1g3v4590840, Lj2g3v3339740), 2 are coding for aminotransferases (Lj6g3v0527170, Lj2g3v1645510), a transcript is coding for a glutamate synthase precursor (Lj0g3v0129059), one transcript involved in the metabolism of glycerol (Lj1g3v2682510), one transcript codes for a protein involved in cysteine biosynthesis (Lj1g3v2682510), and one transcript codes for a protein involved in glycine biosynthetic process from serine (Lj4g3v2592460).

Phenylalanine ammonia-lyase (PAL) catalyzes the first step in the phenylpropanoid pathway; through the pathway phenylpropanoid compounds are synthesized from the amino acids phenylalanine and tyrosine. Formation of lignin, suberin, phytoalexins, coumarins and other flavonoids depends on PAL activity. PAL genes are involved in phenylpropanoid biosynthesis. They have been recorded to be moderately induced in *L. japonicus* initial infection stages by AMF, or rhizobia, and are afterwards repressed (in AM roots and nitrogen-fixing root nodules), concomitant with the establishment of the symbiosis (Deguchi et al., 2007)

Glutamine synthase is the key enzyme in charge of glutamine biosynthesis. The enzyme catalyzes the incorporation into one molecule of the amino acid glutamate of the ammonium derived from either primary (nitrate reduction, N_2 fixation), or secondary forms of nitrogen assimilation (Betti et al., 2012).

19. Proteins related to secondary metabolism

A high number of transcripts associated with primary metabolism processes was identified. 64 transcripts were classified into this group, 55 were upregulated in Lotus-FsK system and only 8 downregulated. Among the upregulated transcripts, 9 code for cytochrome P450s (Lj0g3v0297459, Lj6g3v1934030, Lj4g3v2800440, Lj0g3v0184099, Lj1g3v0130090, Lj4g3v0485090, Lj0g3v0254229, Ljmitog3v0000540, Lj4g3v2107220), 7 transcripts code for chalcone synthases (Lj4g3v2574990, Lj3g3v0681370, Lj1g3v0116650, Lj2g3v2124320, Lj2g3v2124310, Lj1g3v0116620, Lj1g3v1168690), 2 transcripts were annotated as coding for 'Isoliquiritigenin 2'-O-methyltransferase-like' (Lj0g3v0354359, Lj0g3v0273599).

Isoliquiritigenin 2'-O-methyltransferase is an enzyme that methylates the 2'-hydroxyl of isoliquiritigenin to form 4,4'-dihydroxy-2'-methoxychalcone, which is the most potent of the nod-gene-inducing flavonoid derivatives released from alfalfa roots (Maxwell et al., 1993).

20. Lipid metabolism

12 transcripts were identified as involved in lipid metabolism / biosynthesis, all of them were upregulated. More specifically, 5 transcripts are coding for esterases/lipases (Lj0g3v0335279, Lj0g3v0326489, Lj6g3v1966630, Lj4g3v0855360, Lj0g3v0243489), 3 transcripts are coding for phospholipases (Lj6g3v1491480, Lj2g3v2003100, Lj5g3v1015360), 5 transcripts are involved in metabolism/biosynthesis of fatty acids (Lj6g3v0750030, Lj0g3v0326489, Lj5g3v0085060, Lj3g3v2995750, Lj0g3v0268829).

Genes involved in lipid biosynthetic pathway are expressed in plant cells accommodating fungal arbuscules in a RAM1 gene dependent manner. Lipids are synthesized in the plant host, transferred from the plant to mycorrhizal fungi, which are fatty acid auxotrophs. It is suggested that this transfer has a nutritive purpose and lipids, in addition to sugars, play a role in carbon transfer between plants and AMF (Luginbuehl et al., 2017).

21. Proteins related to hormone metabolism

13 transcripts were identified as involved in hormone metabolism/biosynthesis. 12 of them were upregulated in *Lotus*-FsK system. 4 transcripts code for proteins related to gibberellin biosynthesis (Lj3g3v0421660, Lj4g3v2253520, Lj3g3v3500200, Lj4g3v0484780), 3 code for proteins involved in cytokinin biosynthesis (Lj0g3v0219159, Lj0g3v0219149, Lj3g3v3650360), one for a protein related to auxin biosynthesis (Lj2g3v3222870), one for a protein involved in abscisic acid biosynthesis (Lj0g3v0300579). The downregulated transcript of the category codes for a cytokinin glycosyltransferase (Lj2g3v3341900).

22. Proteins responding to hormones

11 transcripts belong to this category, 8 of them show upregulation. From the latter, 6 transcripts respond/interact with auxin (Lj4g3v0336110, Lj0g3v0288689, Lj0g3v0160899, Lj5g3v1315640, Lj4g3v0119950, Lj1g3v3353990), and 2 respond to gibberellin (Lj0g3v0268999, Lj5g3v0198060). Downregulated transcripts, putatively encode for auxin responding proteins (Lj1g3v4590920, Lj0g3v0040139, Lj3g3v2576020).

23. Proteins related to redox metabolism

25 transcripts were assigned to redox metabolism group. 18 were upregulated. Among the upregulated transcripts, 7 code for peroxidases (Lj3g3v3513660, Lj2g3v2412440, Lj5g3v1925220, Lj0g3v0272079, Lj5g3v0626670, Lj3g3v3513680, Lj4g3v0998940), and one codes for an SRG1-like protein with oxidoreductase activity involved in leaf senescence (Lj0g3v0246969).

24. Proteins involved in other physiological processes

6 transcripts were identified as involved in other physiological processes. 5 were upregulated and only 1 was downregulated. Among the upregulated transcripts, 2 were identified as involved in the process of photosynthesis (Lj0g3v0230519, Ljchlorog3v0010750), 2 were identified as coding for proteins involved in seed maturation and embryo development (Lj1g3v4317620, Lj0g3v0202659), and one transcript was annotated as coding for a protein containing a LOB (Lateral Organ Boundaries) motif (Lj2g3v0739570).

Lateral Organ Boundaries Domain (LBD) proteins are a family of plant specific TFs defined by a conserved Lateral Organ Boundaries (LOB) domain, which have essential roles in the regulation of lateral organ development, and metabolic processes, such as anthocyanin and nitrogen metabolism in higher plants. Besides lateral organ boundaries formation, they regulate other processes as well, like pollen development, plant regeneration, photomorphogenesis, pathogen response (Xu et al., 2016).

6.4 References

- Altschup SF, Gish W, Miller W, Myers E, Lipman D. 1990.** Basic Local Alignment Search Tool Stephen. *J Mol Biol* **215**: 403–410.
- Anders S, Pyl PT, Huber W. 2015.** HTSeq-A Python framework to work with high-throughput sequencing data. *Bioinformatics* **31**: 166–169.
- Artur MAS, Zhao T, Ligterink W, Schranz E, Hilhorst HWM. 2019.** Dissecting the genomic diversification of late embryogenesis abundant (LEA) protein gene families in plants. *Genome Biology and Evolution* **11**: 459–471.
- Bécard G, Fortin JA. 1988.** Early events of vesicular-arbuscular mycorrhiza formation on Ri T-DNA transformed roots. *New Phytologist* **108**: 211–218.
- Bellande K, Bono J, Savelli B, Jamet E, Canut H. 2017.** Plant Lectins and Lectin Receptor-Like Kinases: How Do They Sense the Outside? *International Journal of Molecular Sciences* **18**: 1164.
- Benedito VA, Li H, Dai X, Wandrey M, He J, Kaundal R, Torres-Jerez I, Gomez SK, Harrison MJ, Tang Y, et al. 2010.** Genomic Inventory and Transcriptional Analysis of *Medicago truncatula* Transporters. *Plant Physiology* **152**: 1716–1730.
- Bernier F, Berna A. 2001.** Germins and germin-like proteins: Plant do-all proteins. *Plant Physiol Biochem* **39**: 545–554.
- Betti M, García-Calderón M, Pérez-Delgado CM, Credali A, Estivill G, Galván F, Vega JM, Márquez AJ. 2012.** Glutamine synthetase in legumes: Recent advances in enzyme structure and functional genomics. *International Journal of Molecular Sciences* **13**: 7994–8024.
- Chen T-W, Gan R-C, Fang Y-K, Chien K-Y, Liao W-C, Chen C-C, Wu TH, Chang IY-F, Yang C, Huang P-J, et al. 2017.** FunctionAnnotator, a versatile and efficient web tool for non-model organism annotation. *Scientific Reports* **7**: 10430.
- Chevalier D, Walker JC, Chevalier D, Walker JC. 2005.** Functional genomics of protein kinases in plants. *Briefings in Functional Genomics and Proteomics* **3**: 362–371.
- Cosgrove DJ. 2015.** Plant expansins: diversity and interactions with plant cell walls. *Curr. Opin. Plant Biol.* **25**: 162–172.
- Dalton DA, Boniface C, Turner Z, Lindahl A, Kim HJ, Jelinek L, Govindarajulu M, Finger RE, Taylor CG. 2009.** Physiological Roles of Glutathione S-Transferases in Soybean Root Nodules. *Plant Physiology* **150**: 521–530.
- Daneshkhah R, Grundler FMW, Wieczorek K. 2018.** The Role of MPK6 as Mediator of Ethylene/Jasmonic Acid Signaling in *Serendipita indica* -Colonized *Arabidopsis* Roots. *Plant Molecular Biology Reporter* **36**: 284–294.
- Deeks MJ, Hussey PJ, Davies B. 2002.** Formins: Intermediates in signal-transduction cascades that affect cytoskeletal reorganization. *Trends in Plant Science* **7**: 492–498.
- Deguchi Y, Banba M, Shimoda Y, Chechetka SA, Suzuri R, Okusako Y, Ooki Y, Toyokura K, Suzuki A, Uchiumi T, et al. 2007.** Transcriptome profiling of *Lotus japonicus* roots during arbuscular mycorrhiza development and comparison with that of nodulation. *DNA Research* **14**: 117–133.
- Eddy SR. 2011.** Accelerated profile HMM searches. *PLoS Computational Biology* **7**.
- Eulgem T, Somssich IE. 2007.** Networks of WRKY transcription factors in defense signaling. : 366–

371.

Gaude N, Bortfeld S, Duensing N, Lohse M, Krajinski F. 2012. Arbuscule-containing and non-colonized cortical cells of mycorrhizal roots undergo extensive and specific reprogramming during arbuscular mycorrhizal development. *Plant Journal* **69**: 510–528.

Gonzalez I. 2014. Tutorial: Statistical analysis of RNA seq data.

Guether M, Balestrini R, Hannah M, He J, Udvardi MK, Bonfante P. 2009. Genome wide reprogramming of regulatory networks, transport, cell wall and membrane biogenesis during arbuscular mycorrhizal symbiosis in *Lotus japonicus*. *New Phytologist* **182**: 200–212.

Gullner G, Komives T, Király L, Schröder P. 2018. Glutathione S-Transferase Enzymes in Plant-Pathogen Interactions. *Frontiers in Plant Science* **9**: 1836.

Handa Y, Nishide H, Takeda N, Suzuki Y, Kawaguchi M, Saito K. 2015. RNA-seq Transcriptional Profiling of an Arbuscular Mycorrhiza Provides Insights into Regulated and Coordinated Gene Expression in *Lotus japonicus* and *Rhizophagus irregularis*. *Plant and Cell Physiology* **56**: 1490–1511.

Ho HL. 2015. Journal of Biodiversity , Bioprospecting Functional Roles of Plant Protein Kinases in Signal Transduction Pathways during Abiotic and Biotic Stress. *Journal of Biodiversity, Bioprospecting and Development* **2**: 147.

Hogekamp C, Arndt D, Pereira PA, Becker JD, Hohnjec N, Küster H. 2011. Laser Microdissection Unravels Cell-Type-Specific Transcription in Arbuscular Mycorrhizal Roots, Including CAAT-Box Transcription Factor Gene Expression Correlating with Fungal Contact and Spread. *Plant Physiology* **157**: 2023–2043.

Holle S Van, Damme EJM Van. 2018. Signaling through plant lectins: modulation of plant immunity and beyond. *Biochemical Society Transactions* **46**: 217–233.

Huerta-Cepas J, Szklarczyk D, Forslund K, Cook H, Heller D, Walter MC, Rattei T, Mende DR, Sunagawa S, Kuhn M, et al. 2016. EGGNOG 4.5: A hierarchical orthology framework with improved functional annotations for eukaryotic, prokaryotic and viral sequences. *Nucleic Acids Research* **44**: D286–D293.

Kavroulakis N, Ntougias S, Zervakis GI, Ehaliotis C, Haralampidis K, Papadopoulou KK. 2007. Role of ethylene in the protection of tomato plants against soil-borne fungal pathogens conferred by an endophytic *Fusarium solani* strain. *Journal of Experimental Botany* **58**: 3853–3864.

Kishor PBK, Hima Kumari P, Sunita MSL, Sreenivasulu N. 2015. Role of proline in cell wall synthesis and plant development and its implications in plant ontogeny. *Frontiers in Plant Science* **6**: 1–17.

Liu P, Du L, Huang Y, Gao S, Yu M. 2017. Origin and diversification of leucine-rich repeat receptor-like protein kinase (LRR-RLK) genes in plants. *BMC Evolutionary Biology* **17**: 47.

Lohar DP, Sharopova N, Endre G, Penuela S, Samac D, Town C, Silverstein KAT, VandenBosch KA. 2006. Transcript Analysis of Early Nodulation Events in. *Plant Physiology* **140**: 221–234.

Luginbuehl LH, Menard GN, Kurup S, Van Erp H, Radhakrishnan G V., Breakspear A, Oldroyd GED, Eastmond PJ. 2017. Fatty acids in arbuscular mycorrhizal fungi are synthesized by the host plant. *Science* **356**: 1175–1178.

Manthey K, Krajinski F, Hohnjec N, Firnhaber C, Pühler A, Perlick AM, Küster H, Genetik L, Biologie F, Bielefeld U, et al. 2004. Transcriptome Profiling in Root Nodules and Arbuscular

Mycorrhiza Identifies a Collection of Novel Genes Induced During *Medicago truncatula* Root Endosymbioses. *MPMI* **17**: 1063–1077.

Maxwell CA, Harrison MJ, Dixon RA. 1993. Molecular characterization and expression of alfalfa isoliquiritigenin 2'-O-methyltransferase, an enzyme specifically involved in the biosynthesis of an inducer of *Rhizobium meliloti* nodulation genes. *The Plant Journal* **4**: 971–981.

McCarthy DJ, Chen Y, Smyth GK. 2012. Differential expression analysis of multifactor RNA-Seq experiments with respect to biological variation. *Nucleic Acids Research* **40**: 4288–4297.

Murashige T, Folke S. 1962. A revised medium for rapid growth and bio assays with tobacco tissue cultures. *Physiologia Plantarum* **15**: 473–497.

Nivedita, Verma PK, Upadhyaya KC. 2017. Lectin Protein Kinase Is Induced in Plant Roots in Response to the Endophytic Fungus, *Piriformospora indica*. *Plant Mol Biol Rep* **35**.

Penheiter AR, Klucas R V., Sarath G. 1998. Purification and characterization of a soybean root nodule phosphatase expressed in *Pichia pastoris*. *Protein Expression and Purification* **14**: 125–130.

Robinson MD, Oshlack A. 2010. A scaling normalization method for differential expression analysis of RNA-seq data. *Genome Biology* **11**.

Roppolo D, Boeckmann B, Pfister A, Boutet E, Rubio MC, Dénervaud-Tendon V, Vermeer JEM, Gheyselinck J, Xenarios I, Geldner N. 2014. Functional and evolutionary analysis of the CASPARIAN STRIP MEMBRANE DOMAIN PROTEIN family. *Plant Physiology* **165**: 1709–1722.

dos Santos AL, Chaves-Silva S, Yang L, Maia LGS, Chalfun-Júnior A, Sinharoy S, Zhao J, Benedito VA. 2017. Global analysis of the MATE gene family of metabolite transporters in tomato. *BMC Plant Biology* **17**: 1–13.

Schröder F, Lisso J, Lange P, Müssig C. 2009. The extracellular EXO protein mediates cell expansion in *Arabidopsis* leaves. *BMC Plant Biology* **9**: 20.

Smékalová V, Dosko A, Komis G, Jozef Š. 2014. Crosstalk between secondary messengers, hormones and MAPK modules during abiotic stress signalling in plants. *Biotechnology Advances* **32**: 2–11.

Storey JD, Tibshirani R. 2003. Statistical significance for genomewide studies. *Proceedings of the National Academy of Sciences of the United States of America* **100**: 9440–9445.

Trapnell C, Williams B a, Pertea G, Mortazavi A, Kwan G, van Baren MJ, Salzberg SL, Wold BJ, Pachter L. 2010. Transcript assembly and abundance estimation from RNA-Seq reveals thousands of new transcripts and switching among isoforms. *Nature Biotechnology* **28**: 511–515.

Valot B, Negroni L, Zivy M, Gianinazzi S, Dumas-Gaudot E. 2006. A mass spectrometric approach to identify arbuscular mycorrhiza-related proteins in root plasma membrane fractions. *Proteomics* **6**: 145–155.

Verrier PJ, Bird D, Burla B, Dassa E, Forestier C, Geisler M, Klein M, Kolukisaoglu Ü, Lee Y, Martinoia E, et al. 2008. Plant ABC proteins - a unified nomenclature and updated inventory. *Trends in Plant Science* **13**: 151–159.

Wang J, Feng J, Jia W, Chang S, Li S, Li Y. 2015. Lignin engineering through laccase modification: a promising field for energy plant improvement. *Biotechnology for Biofuels* **8**: 145.

Xu C, Luo F, Hochholdinger F. 2016. LOB Domain Proteins: Beyond Lateral Organ Boundaries.

Trends in Plant Science **21**: 159–167.

Ye J, Zhang Y, Cui H, Liu J, Wu Y, Cheng Y, Xu H, Huang X, Li S, Zhou A, et al. 2018. WEGO 2.0: A web tool for analyzing and plotting GO annotations, 2018 update. *Nucleic Acids Research* **46**: W71–W75.

Zhang Q, Blaylock L a, Harrison MJ. 2010. Two *Medicago truncatula* half-ABC transporters are essential for arbuscule development in arbuscular mycorrhizal symbiosis. *The Plant cell* **22**: 1483–1497.

Zhang ZH, Jhaveri DJ, Marshall VM, Bauer DC, Edson J, Narayanan RK, Robinson GJ, Lundberg AE, Bartlett PF, Wray NR, et al. 2014. A comparative study of techniques for differential expression analysis on RNA-seq data. *PLoS ONE* **9**: e103207.

Zhang X, Pumplin N, Ivanov S, Harrison MJ. 2015. EXO70I Is Required for Development of a Sub-domain of the Periarbuscular Membrane during Report EXO70I Is Required for Development of a Sub-domain of the Periarbuscular Membrane during Arbuscular Mycorrhizal Symbiosis. *Current Biology* **25**: 2189–2195.

6.5 Appendix of Chapter 6

Table 6-2 Intersection of DEGs identified in via cufflinks / edgeR analysis. For simplification p-values, q-values, log2FC values derived from cufflinks analysis only are presented.

	Gene ID	Cufflinks analysis			Product description
		p-value	q-value	log ₂ FC	
1	Lj0g3v0001739.1	5x10 ⁻⁵	0.001	1.66	aldo/keto reductase
2	Lj0g3v0140429.1	5x10 ⁻⁵	0.001	1.59	pathogenesis related protein (bet v I-like)
3	Lj0g3v0286359.1	5x10 ⁻⁵	0.001	5.51	pathogenesis related protein (bet v I-like)
4	Lj1g3v2114690.1	5x10 ⁻⁵	0.001	-1.33	no annotation
5	Lj1g3v4383290.1	5x10 ⁻⁵	0.001	3.74	plant disease resistance response protein; nucleoporin related
6	Lj2g3v0852090.1	5x10 ⁻⁵	0.001	1.72	LRR (leucine-rich-repeat) protein
7	Lj2g3v1483000.1	5x10 ⁻⁵	0.001	1.98	cinnamoyl-CoA reductase
8	Lj2g3v2124320.1	5x10 ⁻⁵	0.001	2.41	chalcone/stilbene synthase
9	Lj2g3v2124320.2	5x10 ⁻⁵	0.001	2.41	thiolase-like; chalcone synthase
10	Lj2g3v3339170.1	5x10 ⁻⁵	0.001	1.25	aldo/keto reductase
11	Lj3g3v3556010.1	5x10 ⁻⁵	0.001	-1.24	barwin-like endoglucanases
12	Lj4g3v0486150.1	5x10 ⁻⁵	0.001	4.73	cytochrome P450
13	Lj5g3v0085060.1	5x10 ⁻⁵	0.001	2.32	fatty acid acyl transferase-related
14	Lj5g3v0841020.1	5x10 ⁻⁵	0.001	1.17	syntaxin; SNARE protein
15	Lj5g3v0963160.1	5x10 ⁻⁵	0.001	1.82	aspartyl proteases, peptidase
16	Lj6g3v0408370.1	5x10 ⁻⁵	0.001	2.19	ARM (armadillo) repeat containing protein
17	Lj6g3v0527170.1	5x10 ⁻⁵	0.001	1.86	pyridoxal phosphate-dependent transferase
18	Lj6g3v1162950.1	5x10 ⁻⁵	0.001	1.29	flavin monooxygenase-like protein
19	Lj6g3v1513720.1	5x10 ⁻⁵	0.001	2.37	no annotation
20	Ljmitog3v0000540.1	5x10 ⁻⁵	0.001	1.07	cytochrome c-type synthesis protein and pts transmembrane component

Chapter 7

Concluding remarks

7 Concluding remarks

Results of the present doctoral thesis are presented and discussed in the individual chapters of this dissertation. This last section is dedicated on general observations, remarks, concerns, and thoughts on future perspectives, developed during the period of my PhD, and especially during the last 2.5 years along with the writing of the publications, and after fruitful discussions first with my supervisor, Kalliope Papadopoulou, throughout this journey, and secondly with my two other advisors, Andrea Genre and Paola Bonfante, mainly on results concerning cellular modifications and Ca^{2+} spiking analysis.

The novelty of the work presented lies in the fact that FSK, a fungal isolate of the genus *Fusarium* (typically known as devastating plant pathogens) is able to colonize *L. japonicus* root tissues by (partially) utilizing the unique signaling pathway that is used by bacterial and fungal endosymbionts in legumes. This delineates the continuum that appears to be present in the host-microbe interactions and further extends the quest of the molecular means that are used by the plant to discriminate friends from foe in the complex rhizosphere environment. During FSK intracellular growth fungal and plant cell adaptations commonly described for symbionts and pathogens occur, but also unique features, worth of further investigation.

FSK grows relatively well (~5.8 mm/day) in a wide range of solid and liquid media, even in water agar plates with no extra supplement of a carbon source. It was, therefore, a challenge to set up an *in vitro* system to investigate the interaction with the model legume *L. japonicus*. FSK is also a free-living fungus, it can grow extremely well in the absence of a host; it possesses chitinases and cellulolytic enzymes, based on the genome annotation of its teleomorph state, *Nectria haematococca*. For legume nodulation, it has been nicely phrased that ‘the host controls the party’, referring to the -tightly regulated by the host- intracellular events leading to nodulation (Ferguson et al., 2019). During the time spent studying FSK-*Lotus* interaction under the microscope, I sometimes with surprise, realized that in the proximity of the root, the plant does not have control over fungal growth, at least in the *in vitro* system. Knowledge towards the plant control over intracellular events, originated from this work, is discussed below. The fungus grew fast extraradically, and was able to cover the root system within a few days, limiting the time available for observations to a few days. This time frame turned out to be sufficient, though, for observing early progression of the interaction and the cellular changes involved, presenting in a simplified two-organism cosmos fraction of what would perhaps occur in the real multi-organismal rhizosphere world. Gene expression and mutant analysis were nonetheless performed in the more ‘natural’ environment of magenta boxes, permitting a prolonged investigation of this plant-fungal system.

At the pre-contact level, FSK is recognized by members of the *LysM*-receptor family in *L. japonicus*. All receptors examined herein (Lys6, Lys7, Lys12) were shown to negatively control fungal progression, besides NF receptors and Lys11, that demonstrated no control over intraradical fungal accommodation. So, chitin based molecules, either fractionated products of the long, crystalline chitin, or synthesized anew are secreted by FSK at the proximity of plant cells and recognized by the extracellular LysM

domains of these receptors. It is of interest that RNA seq results in FsK-inoculated *Lotus* roots revealed differential expression of an 'Isoliquiritigenin 2'-O-methyltransferase' gene, an enzyme that catalyzes the formation of a nod-gene-inducing flavonoid derivative in alfalfa. It would be interesting to see the implication of this enzyme in chitosaccharidic-triggering-compounds produced by FsK.

FsK exudates putatively comprise at least two types of triggering compounds, heat labile and chitinase-sensitive. Both are able to induce Ca^{2+} spiking in the nucleus of *M. truncatula* epidermal cells, a hallmark of symbiotic associations of legumes. Similar findings on induction of nuclear Ca^{2+} spiking in symbiotic associations outside legumes, were published a few days before submission of the present thesis by another research group, further corroborating findings of this work. More specifically, it was reported that the ECM fungus *Laccaria bicolor* produces LCOs able to induce nuclear Ca^{2+} spiking in the roots of *Populus*, and fungal colonization proceeds in a *CASTOR/POLLUX* and *CCaMK* dependent manner (Cope et al., 2019). In FsK-*M. truncatula* association, induction of Ca^{2+} spiking is *DMI2* (*LjSYMRK*)-dependent, as verified by ROC mutant analysis. In terms of fungal colonization, all *L. japonicus* mutants acting upstream the Ca^{2+} spiking response were not affected. Mutants acting downstream the response showed reduced colonization levels, which was compensated at later stages, with colonization proceeding then fast and reaching wt levels. It was, therefore, assumed that *CCaMK* is indispensable for normal fungal progression. These observations led to an unusual speculation: when Ca^{2+} spiking is not an option (as in the case of *symrk* mutants), a Ca^{2+} spiking independent *CCaMK* activation may occur. Ca^{2+} -independent activation of CaMKs has been previously described in mammal cells, where activation occurred by ROS generation (Erickson et al., 2008). A limitation of the work presented on this topic is that while Ca^{2+} spiking and mutant analysis were performed on two different plants, *M. truncatula* and *L. japonicus*, respectively, Ca^{2+} spiking measurements were performed in ROCs instead of whole plants. It is important to verify Ca^{2+} spiking occurrence *in planta*, upon elicitation by the fungal exudates and perhaps identify the Ca^{2+} -responding cells when the fungus itself is present. Identifying the responsive cells might also shed light on the cells chosen by FsK for penetration. In addition, fungal progression in plant mutants affected in genes acting downstream the Ca^{2+} spiking response needs to be verified by microscopy (perhaps by measurement of successful infection sites). Based on findings of this work it is proposed that FsK uses at least three different routes to achieve colonization within legume tissues (summarized in scheme of Figure 7-1): a) when CSSP is fully functional, Ca^{2+} spiking occurs normally in the nucleus and fungal progression proceeds normally, b) when Ca^{2+} spiking does not occur (as in the *symrk* mutant), *CCaMK* is activated in a *DMI2*- and Ca^{2+} -spiking independent manner, and this activation allows for fungal progression as in the wt, c) when the signal is generated but cannot be perceived or transmitted (*ccamk* or *cyclops* mutants), a totally different, and yet unexplored pathway is used, allowing belated intraradical fungal accommodation.

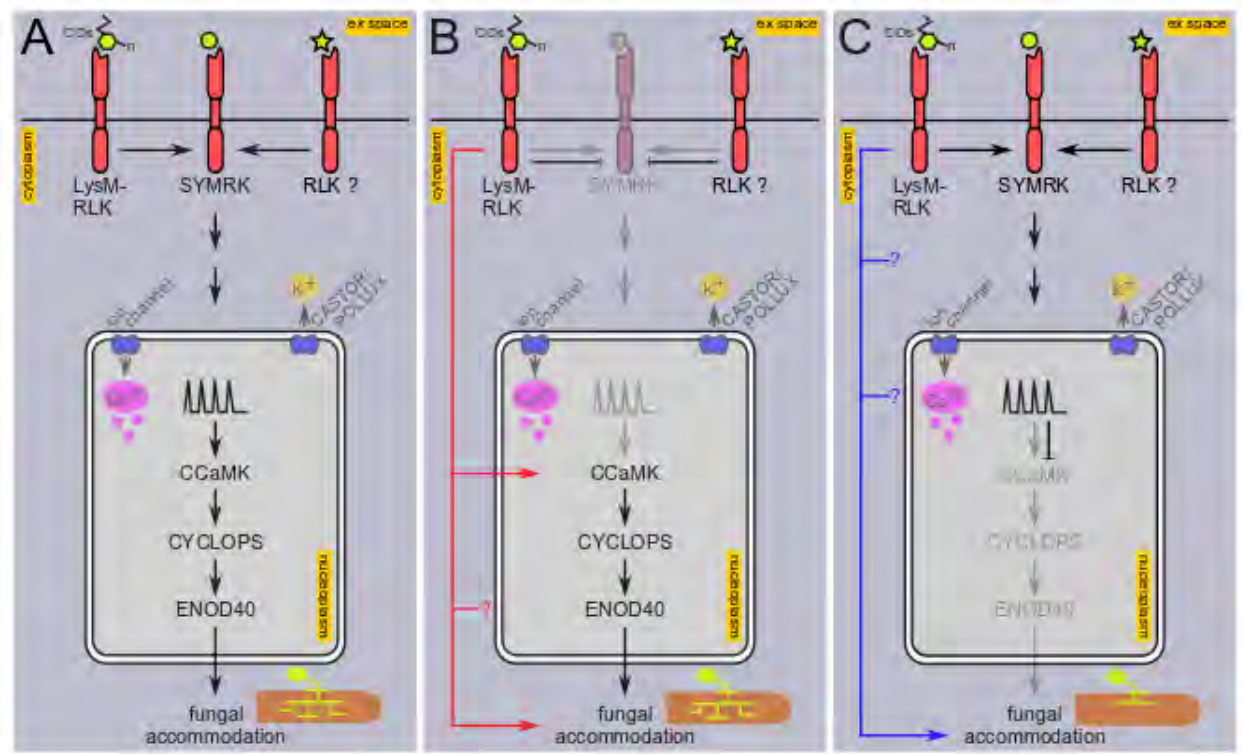


Figure 7-1 Schematic summary describing recognition of putative triggering molecules derived from FsK exudate by *L. japonicus*, subsequent signaling cascade and fungal accommodation (based on results from *L. japonicus* and *M. truncatula* ROCs).

(A) A chitin based molecule (perhaps COs of unknown degree of polymerization) is recognized by PM located LysM-RLK(s), or a heat labile molecule (asterisk) is recognized by an RLK. SYMRK is activated, and subsequent signaling through the CSSP leads to calcium influx in the nucleoplasm. Ionic balance is maintained through perhaps efflux of potassium ions through the cation channels CASTOR and/or POLLUX. Calcium spiking occurs in the nucleoplasm, the generated signal is perceived through CCaMK and transmitted through CYCLOPS phosphorylation. Downstream activation of symbiosis genes (like ENOD40) occurs. Fungal accommodation progresses normally.

(B) When SYMRK is impaired, calcium spiking does not occur in the nucleus. Recognition of triggering molecules by LysM-RLK(s) perhaps leads to a SYMRK- and therefore calcium- independent activation of CCaMK. This CSSP-independent activation of CCaMK allows an 'on time' fungal progression at wt levels. Activation of ENOD40 perhaps occurs as in the wt.

(C) Chitin based triggering molecules are recognized by LysM-RLK(s). Activation of SYMRK occurs normally, calcium influx occurs in the nucleus and calcium spiking is generated. When CCaMK is impaired, the calcium signal cannot be perceived or transmitted (e.g. when CYCLOPS is impaired). The pathway downstream CCaMK is not utilized. A different pathway is activated which perhaps employs certain components of the symbiosis pathway. Fungal accommodation progresses belatedly, indicating that CCaMK is at the core of FsK recognition pathway in legumes.

At the cellular level, common aspects in the colonization pattern of FsK in both *L. japonicus* roots and *M. truncatula* ROCs were revealed. Fungal hyphae reach the root epidermis, progress along it -perhaps through the intercellular pits formed in between cell borders- but often progression is arrested, and hyphopodia are developed. Microscopical observations revealed that hyphopodium formation is

associated with a penetration attempt. How FSK selects the root sites to differentiate its elongating hypha to a hyphopodium-like structure is still unknown. Fungal stenosis is required for plant cell penetration, further advocating for a mechanism of host cell protection. Nevertheless, despite the recorded development of papillae by the host plant, penetration occurs. Papilla formation is associated with callose deposition underneath the contact site, and accordingly, callose synthase genes were among the plant upregulated genes induced by FSK at very early stages (identified via RNA seq analysis). How FSK achieves cell to cell movement is also intriguing. Inspiring work on the rice hemibiotrophic fungus *M. oryzae* showed invasive hyphae scanning leaf sheath cell walls before crossing, seeking out for plasmodesmata to contact or cross cell walls (Kankanala et al., 2007a). If this is the case for FSK, it will partially explain its non-destructive mechanism for plant cell perforation. RNA seq analysis revealed plant laccase genes activated upon early stages of the interaction, which unlike their role in the fungal kingdom, in plants have a role in lignin biosynthesis, and are involved in wound healing, and in maintenance of cell wall structure and integrity. These enzymes might act in a plant cell protection/fortification mechanism during accommodation of another eukaryotic organism.

Cytoplasm, ER, nuclear movements were observed at contact sites, as recorded for other compatible plant-fungal associations. Observation of multiple sites revealed that this was not a sole feature of the plant cell awaiting penetration, but of other adjacent cells as well. In AM associations, it is known that penetration occurs only after full completion of PPA formation (Genre et al., 2005) (Genre et al., 2008). In *Lotus*-FSK association, evidence of a cytoplasm accumulation in the form of a column and perifungal membrane were recorded, but they were proven to be ephemeral. So a question is raised, as to how the fungus chooses the appropriate cell for penetration. Is a complete formation of a rather fragile cytoplasmic column a prerequisite for cell penetration, and if yes, how soon after penetration does it dismantle? Or, is it, that completion of the cytoplasmic column is not important, thus explaining the very few sites depicting a perifungal membrane enclosing it? The inability to create a steady biotrophic state, characterized by a persistent apoplastic interface, may be related with the observed loss of plant cell viability. Other questions concerning the role of plant cell death in FSK-*Lotus* interaction also rise. Is it a plant mechanism for further or excessive fungal progression restriction; does FSK feed on these cells during a stage of its lifecycle as shown for *P. indica*-barley association (Lahrmann et al., 2013), or does it progress and feeds on living ones? And is plant cell death involved in FSK association with tomato plants as well, the plant of FSK origin, or it is a sole feature of FSK association with legumes, further supporting its versatile lifestyle, depending on its host? Answering these questions will help to further characterize the nature of FSK associations with its various host plants.

FSK efficiently colonizes the interior of the plant cell by occasionally expanding to the whole cell volume. This would require an expansion/increase in the plant cell, perhaps by loosening/relaxation of its rigid cell wall. Also, at the tissue level, root tissues would have to expand, and divide in order to sustain the growth of the fast growing, filamentous fungus. Data obtained by the molecular approaches, support this hypothesis. Thus, cytokinin-induced genes, also involved in organogenetic processes like *LjENOD40* were mildly but constantly expressed throughout FSK-*Lotus* interaction (2-12 dpi). In addition, RNA seq analysis, revealed five genes coding for expansins, cell wall proteins catalyzing plant cell wall loosening without lysis of wall polymers, upregulated (> 4-fold). In addition, genes coding for

important cell wall scaffolding proteins like the extensins, hydroxyproline-rich glycoproteins, and arabinogalactan proteins, were also upregulated, an indication that alterations in plant cell architecture through modification of the rigid plant cell wall occurs in this plant-fungal association. If and how these scaffolding proteins enable cell wall alterations, and the timeframe in which they act is intriguing.

FsK proceeds intraradically from epidermis to cortex, and was clearly shown within the present work that it enters the vasculature system of the root. It, furthermore, colonizes the aerial part of the plants, unlike of what was previously reported for tomato plants (Kavroulakis et al., 2007). It was shown to grow on the stem not only endophytically but also epiphytically. The fungus was found close to xylem cells in *L. japonicus* stem sections at sites close to the root crown, but it was not determined whether migration to the stem occurs through the vascular system of the plant, or it is a result of secondary ingress through the epidermis. Experiments designed to prevent the epiphytic growth are necessary to decipher whether this migration also occurs through the vascular bundle. Nevertheless, four genes possibly implicated in fortification of the inner part of the root system, two ‘casparian strip membrane proteins’ and two ‘cortical cell-delineating proteins’ were recorded as downregulated via RNA seq analysis in early stages of FsK-*Lotus* association, and their potential involvement in FsK passage from the epidermis to the vasculature is intriguing. In the stem, FsK also forms round structures of unknown function in epidermal/upper cortical cells, and investigation of when/how and, adding a level of difficulty, why they are formed could be of interest.

As anticipated, FsK does not bypass the host plant surveillance system, eliciting defense gene expression throughout the course of the interaction. Gene expression analysis revealed a number of chitin induced, defense genes expressed mainly at late stages of intraradical fungal progression, among them *Wrky* TFs, pathogenesis related genes, and genes encoding for phytoalexins (*LjCP450*). Defense gene induction at earlier stages though, was also verified by RNA seq analysis where a large number of genes (33 induced and only 3 repressed) was identified as differentially expressed; among those induced is the gene encoding for the pathogenesis related protein 27b (PRp27b), which was initially recorded as highly regulated (>25-fold) at 4-6 dpi via qPCR. Differences in the time of defense gene expression initiation could be attributed to the experimental setup: the first experiment was set in magenta boxes, whereas the second one was set in Petri dishes. Induction of defense related genes is anticipated at least to some extent at early stages of the FsK-*Lotus* association. It is of interest that genes involved in cell detoxification, such as ‘glutathione S transferases’ were identified both as up- and down-regulated in RNA seq results, and these genes have also been described to play a role in nodulation and mycorrhization. Experiments involving comparative RNA seq results analysis of defense gene activation at early versus advanced stages of fungal progression, is the aim of future work. Furthermore, induction of a series of other defense reactions elicited in *L. japonicus* plants by the fungus/fungal exudates can be examined, like ROS accumulation, MAPK3/6 phosphorylation etc.

This work was complemented with recent findings via RNA seq results analysis, which offered identification of a series of DE genes, partially supporting observations obtained via microscopy and molecular biology, and allowing for future perspectives. RNA seq results offer new fields for investigation, by pinpointing an extensive reprogramming of the plant cell upon recognition and early accommodation of the fungus, at the transcriptome level. The extent of transcriptional reprogramming

is surprising if we consider that root tissues were collected just when the fungus had covered the root tip (Chapter 6, Figure 6-1). In addition, whole roots were sampled, allowing the assumption that reprogramming might not be limited to the root tip (in contact with the fungus at that specific time point), though spatial expression experiments have not been performed. CSSP and CSSP-dependent genes were not identified as DE in the analysis of RNA seq data presented herein. This could be attributed to the single timepoint studied. A promising field is that of nutrient exchange, which I envisage to be bidirectional, and analysis of the fungal transcriptome will additionally offer insight to that. From the plant side of view, at least twelve genes involved in lipid metabolism are upregulated, and it was recently shown that fatty acids are provided by the host plant in AM symbiosis (Luginbuehl et al., 2017). Furthermore, genes coding for proteins involved in transmembrane transport (ABC transporters, sugar transport proteins, lipid transfer proteins) were upregulated in F_sK-*Lotus* system. For (bidirectional) nutrient exchange to occur, a steady biotrophic interface must be preserved for at least some time, so additional experiments involving microscopy are required on that topic. Also, later stages of the interaction should be examined, as nutrient exchange is anticipated to take place after the fungus has settled within plant tissues. A large number of gene functional groups was identified, opening new routes for exploration, like hormonal balance, effector translocation, organogenesis, cell wall/cell modifications, nutrient exchange, transmembrane transport occurring at early stages of this interesting, novel plant-fungal association.

To conclude, the present thesis contributed to a re-evaluation of the current knowledge concerning the molecular mechanisms employed by plants to recognize and discriminate among microbes that they interact with. It seems that basic signalling/communication pathways evolved to aid the establishment of ancient types of symbiosis, were re-adjusted and employed by other microbes displaying a capacity for endophytic growth. In this concept, a shared pathway, perhaps through its basic core (nuclear Ca²⁺ spiking), acts as a multi-triggering module in response to microorganisms, while certain molecular players act to determine the outcome of each individual relationship.

7.1 References

- Cope KR, Bascaules A, Irving TR, Venkateshwaran M, Maeda J, Garcia K, Rush T, Ma C, Labbé J, Jawdy S, et al. 2019.** The ectomycorrhizal fungus *Laccaria bicolor* produces lipochitooligosaccharides and uses the common symbiosis pathway to colonize *Populus*. *The Plant cell* In Press.
- Erickson JR, Joiner M ling A, Guan X, Kutschke W, Yang J, Oddis C V., Bartlett RK, Lowe JS, O'Donnell SE, Aykin-Burns N, et al. 2008.** A Dynamic Pathway for Calcium-Independent Activation of CaMKII by Methionine Oxidation. *Cell* **133**: 462–474.
- Ferguson BJ, Mens C, Hastwell AH, Zhang M, Su H, Jones CH, Chu X, Gresshoff PM. 2019.** Legume nodulation: The host controls the party. *Plant Cell and Environment* **42**: 41–51.
- Genre A, Chabaud M, Faccio A, Barker DG, Bonfante P. 2008.** Prepenetration apparatus assembly precedes and predicts the colonization patterns of Arbuscular Mycorrhizal Fungi within the root cortex of both *Medicago truncatula* and *Daucus carota*. *The Plant Cell* **20**: 1407–1420.
- Genre A, Chabaud M, Timmers T, Bonfante P, Barker DG. 2005.** Arbuscular mycorrhizal fungi elicit a novel intracellular apparatus in *Medicago truncatula* root epidermal cells before infection. *The Plant Cell* **17**: 3489–3499.
- Kankanala P, Czymmek K, Valent B. 2007.** Roles for rice membrane dynamics and plasmodesmata during biotrophic invasion by the blast fungus. *The Plant Cell* **19**: 706–724.
- Kavroulakis N, Ntougias S, Zervakis GI, Ehaliotis C, Haralampidis K, Papadopoulou KK. 2007.** Role of ethylene in the protection of tomato plants against soil-borne fungal pathogens conferred by an endophytic *Fusarium solani* strain. *Journal of Experimental Botany* **58**: 3853–3864.
- Lahrman U, Ding Y, Banhara A, Rath M, Hajirezaei MR, Döhlemann S, von Wirén N, Parniske M, Zuccaro A. 2013.** Host-related metabolic cues affect colonization strategies of a root endophyte. *Proc Natl Acad Sci USA* **110**: 13965–13970.
- Luginbuehl LH, Menard GN, Kurup S, Van Erp H, Radhakrishnan G V., Breakspear A, Oldroyd GED, Eastmond PJ. 2017.** Fatty acids in arbuscular mycorrhizal fungi are synthesized by the host plant. *Science* **356**: 1175–1178.

Acknowledgments

The present dissertation would not have been possible without the influence, guidance, and contribution of the following people:

Firstly, of my supervisor/teacher Kalliope Papadopoulou, who has always been present and available whenever I needed her, and who has been generously guiding me both in a personal and in a scientific level over the last 6.5 years. I thank her for the valuable guidance on experimental planning and research aims, the influence, fruitful discussions, the constructive criticism, and the generous offer of opportunities.

Of Professor Paola Bonfante and Associate Professor Andrea Genre who were second advisors for me, and have generously guided me during my stage in Torino and afterwards. I thank Andrea Genre for teaching me laboratory techniques, confocal microscopy, and for transmitting me his passion for microscopical imaging. I also thank Professor Bonfante for all the influence, and I will keep what she once said to me: 'Science is like calcium spikes, sometimes it goes up, and sometimes it goes down'.

I would also like to express my appreciation and a big thank you to the following people:

To Professor Constantine Ehaliotis, and Professor Dimitrios Karpouzas for always been there whenever I needed them, for their guidance, offer of opportunities, discussions, and all the advice throughout my PhD studies, and for their participation in my advisory committee. I particularly thank Professor Constantine Ehaliotis for prompting me to initiate the present doctoral thesis.

To the Assistant Professor Daniela Tsikou for her guidance during my first steps in the laboratory as a PhD student, for the valuable discussions throughout my PhD studies, and her participation in my examination committee.

To Dr. Nektarios Kavroulakis, and Associate Professor Aikaterini Karamanoli for their participation in my examination committee.

To the Post-doctoral fellow Sotirios Vasileiadis, for the bioinformatic analysis of RNA sequencing data, for his comments, and generous help whenever I needed it, and friendship.

To Antonella Faccio for the preparation of samples prior to transmission electron microscopy.

To the present and former members of the Plant and Environmental Biotechnology laboratory for help in everyday lab-life, and friendship: PhD candidate Panagiota Plitsi, Post-doctoral fellow Chiara Perruchon, Post-doctoral fellow Panagiotis Karas, Post-doctoral fellow Marco Campos, MSc student Marili Anagnostou, PhD student Marianna Avramidou.

To the present and past members of the group from Orto Botanico, Torino, Italy (Mara, Antonella, Alessandra, Iolanda, Simone, Gennaro, Salvo, Valeria, Matteo, Francesco, Marco G, Valentina, Veronica, Luisa), who made me feel at home during my presence in their lab.

To the Post-Doctoral Fellow Catalina Stedel for the friendship, discussions, support in everyday 'plant group'-life, and to the Post-Doctoral Fellow Constantine Garagounis for the friendship, exchange of ideas, (scientific) discussions, and support/guidance in lab-life.

To Mrs Aleka Tsiropoulou and to Mr Kyriakos Papadopoulos for accommodating me in their home, whenever my experiments required so.

A special thank you to the Post-doctoral fellows Konstantina Roussidou, Evangelia Papadopoulou, and Athanasia Katsoula for their friendship, (scientific) discussions, their contribution in a nice and friendly lab environment, and their valuable company especially during late hours and weekends working in the lab.

A heartfelt thank you to my always supporting mother, Maria, to whom I owe a lot, and to my sister Ioanna.

A big thank you to my long-lasting friend Gerasimia (Memi) Tsasi, for her support, advice, (scientific) discussions, and encouraging words during this -at times- difficult period, and to my long-lasting friends Marina Triantafyllou, Eleni Xypolytakou, and Sophia Tsiropoulou.

I can find no words to thank Vasileios Kioussis for always believing in me, and for being supportive from day one until the end of this journey, despite our actual kilometric distance. Without his influence, contagious sense of humor, and -always at the right moment- encouraging words, I would have accomplished very few.

